The chronology of Late Glacial and Holocene dune development
in the northern Central European lowland reconstructed
by optically stimulated luminescence (OSL) dating

I n a u g u r a l – D i s s e r t a t i o n

zur

Erlangung des Doktorgrades

der Mathematisch-Naturwissenschaftlichen Fakultät

der Universität zu Köln

vorgelegt von

Alexandra Hilgers

aus Neuss

Köln, 2007

Berichterstatter :   Prof. Dr. U. Radtke
                        Prof. Dr. G. Schellmann
                        PD Dr. R. Zeese

Tag der mündlichen Prüfung: 6. November 2006

Contents

Appendix A: Dose rate data tables

Appendix B: Choice of measurement protocol and mineral fraction for dating

Appendix C: Luminescence measurement equipment and beta source calibration

Appendix D: Equivalent dose determination

Appendix E: Results of OSL dating and list of ^{14}C ages

Appendix F: Location of study sites and comparison of analytical results

Danksagung/Acknowledgements

List of tables

List of figures

Contents

Contents   12

Contents

Contents 14

1. Introduction

Sedimentological, palaeontological, morphological and geochemical evidence shows that climatic change is characteristic of geological time. The reasons suggested for these changes are many and varied. Contemporary observations and measurements show beyond doubt that climatic fluctuations are still in train. In light of the current discussion about global warming and the impacts of sea level rise, soil degradation and desertification on human well-being, a better understanding of climatic changes is of practical as well as of academic interest and importance. The question is to what extent they are merely a continuation and extension of the secular variations recognised in the past climatic record, or whether, and if so to what degree, they reflect human activities.

A thorough reconstruction and interpretation of past patterns of climatic change is considered essential for any rational discussion of any man-made changes in climate, especially as these will be superimposed on the background of natural climatic variations. This claim may or may not be valid. Factors as yet unrecognised may intervene or human activities may introduce new forces operating to neutralise others. But the possibility that the past may provide possible clues to future change nevertheless ought to be pursued.

Climatic change is global and must of necessity be complex with regional variations and differences in the response of individual proxy records[1]. Any record of regional climatic change is useful for it provides information about one piece of the global jigsaw puzzle of reconstruction of past environments. The study presented here is intended to shape and fit in another small part of that puzzle. It is concerned with the reconstruction of dune formation and reactivation by means of optically stimulated luminescence (OSL) dating of dunes developed throughout the last 20,000 years or so in the central part of the so-called 'European Sand Belt' (ESB) in northeast Germany and adjacent areas in Poland.

---

[1] Proxy record = any line of evidence that provides an indirect measure of former climates or environments, including diverse materials such as pollen records, tree rings, charcoal or bones; indirect 'proxy' indicators= natural archives that record past climate variations

2. Aims of the study

The aim of this study is to investigate the potential of an OSL record of dune formation as a proxy for Lateglacial climate change in the study area. Looming large is whether Holocene climatic oscillations can be identified in the aeolian record or whether they are completely masked by the effects of human activities on the landscape, leading to dune reactivation. If the latter holds true, the record of dune reactivation might represent periods of varying human impact related to the settlement history of the study area.

Phases of aeolian deposition are linked to specific climatic conditions (e.g. ample sand supply mobilised as a result of sparse vegetation cover, the latter caused by limited moisture or sufficient warmth in the environment and sufficient wind-velocities for sand transport). Thus each layer of dune sand preserves information on palaeoclimate. In order to use this terrestrial archive for a chronology of climatic change precise dating of the depositional events is crucial. This is also essential for regional correlation. A suitable number of comparable sequences are required to distinguish local catastrophic events from secular or long-term aeolian activity reflecting climate changes of sufficient larger amplitude and regional distribution. Twenty dune sequences located in five different areas were investigated and the results compared in this study.

To establish a chronology of aeolian deposition at the individual study sites the luminescence dating technique is applied. OSL is frequently the only procedure that permits age determination in non-carbon bearing sediments such as dune sands. Here the robustness of OSL dating techniques for aeolian deposits is first discussed. Quality criteria which are inherent to the OSL technique are measured and, where possible, OSL ages are cross-checked with independent age control (e.g. radiocarbon chronologies, palynological records, palaeosol horizons, a tephra chronomarker).

Once the OSL record of dune building phases has been shown to be reliable, the results are discussed in the context of other records of palaeoclimatic changes. Arctic ice-core records are of particular interest as they provide the most continuous high-resolution records of past climate variations in the North Atlantic region (e.g. BJÖRCK et al. 1998). Coincidence or systematic deviation between the ice-core and dune records could provide evidence as to whether the terrestrial archive reacts simultaneously or lags behind the atmospheric changes which are preserved in the ice-core records.

For various reasons the time span under consideration in this study is restricted to the last 20,000 years. This period comprises the termination of the Last Glacial Maximum through the Last Glacial-Interglacial Transition (also referred to as Termination I or, informally, 'Lateglacial', BJÖRCK et al. 1998) and the entire Holocene. To focus on a transition period from a cold - glacial mode to a warm – interglacial mode is advantageous in terms of the clarity of the record. During transition phases with episodes of drastic climatic changes, the contrast in response ought to be sharply defined. Furthermore, in the study area, the Weichselian Lateglacial records ought to provide the best preserved and most continuous terrestrial records, if only because no subsequent glaciations disturbed and destroyed the evidence.

The restriction of the study area to northeastern Germany and adjacent areas in northwestern Poland arises from the fact that most previous studies of dune development are based on results of radiocarbon dating (^{14}C). Unfortunately only phases of landscape stability are dated by ^{14}C, for it was only in such phases that dunes were stabilised by the vegetation, that provided enough organic material in the soil for dating. The event of aeolian sedimentation itself is only relatively dated. For any aeolian processes predating the onset of plant growth only minimum ages can be derived. By contrast, optically stimulated luminescence (OSL) dating allows the direct dating both of dune sand deposition and the environmental conditions under which dunes were formed. A further advantage of luminescence dating is that no calibration to calendar years is required as it is for radiocarbon dating, because luminescence dating is independent of ^{14}C variations in the atmosphere. However, despite this possible problem with accuracy, radiocarbon chronologies provide a higher precision compared to with OSL chronologies. A high precision is crucial for dating short-term climatic oscillations as those characterising the Lateglacial climate. Obviously a combination of radiocarbon and luminescence chronologies provides the most likely record of the alternation of dune formation and stabilisation by vegetation in the course of climate fluctuation. Therefore a special focus of this study is placed on the comparison and combination of OSL and ^{14}C chronologies. Furthermore, by cross-checking of OSL ages of dune deposits with ^{14}C results obtained for associated organic layers the robustness of the luminescence measurement protocol applied in this study can be tested.

A further shortcoming of the existing record of dune formation in the study area is that despite the large number of isolated studies carried out since the late 19th century, a summary of the dune record is still missing, most commonly because investigations focused not on the entire

record but on particular questions or time slices only. This problem combined with the use of various methods complicates a summary of the results (see discussion for example in SCHLAAK 1993, DE BOER 1995).

The reasons for the lack of a summarising study of the aeolian record preserved in inland dunes for the Lateglacial and Holocene in northeastern Germany becomes clearer with reference to the German research priority programme "*Changes of the Geo-Biosphere during the last 15,000 years – continental sediments as evidence for changing environmental conditions*" (reviewed in ANDRES & LITT 1999, LITT 2003). This multi-disciplinary long-term project concentrated on a broad variety of archives, including annually laminated lacustrine sediments, fluvial sediments, colluvial deposits, soils, speleothems, bogs and coastal sediments, but not on dune records in detail. The study presented here will contribute to eliminating this gap by investigating numerous and widely distributed dune sites within the north German plain and applying a consistent approach in sampling, sample preparation and experimental setting of the luminescence measurements.

Finally this study can be included in a wider context of palaeoclimate reconstruction. The relationship is illustrated in Fig. 1 showing an example for 'Multi-Proxy Databases' (MPDB). These are used in 'General Circulation Models' (GCM) for the simulation of past environmental conditions with the aim of modelling future scenarios of climate change (e.g ISARIN et al. 1998, KUTZBACH et al. 1998, WEBB & KUTZBACH 1998, RENSSEN & ISARIN 2001, VANDENBERGHE et al. 2001, RENSSEN et al. 2002,).

Fig. 1: Multi proxy database for palaeclimate reconstruction (MPDB).
The main data pools focussed on in this study are indicated by darker colouring and grey arrows indicate the data relation (redrawn from HUIJZER & ISARIN 1997: 516).
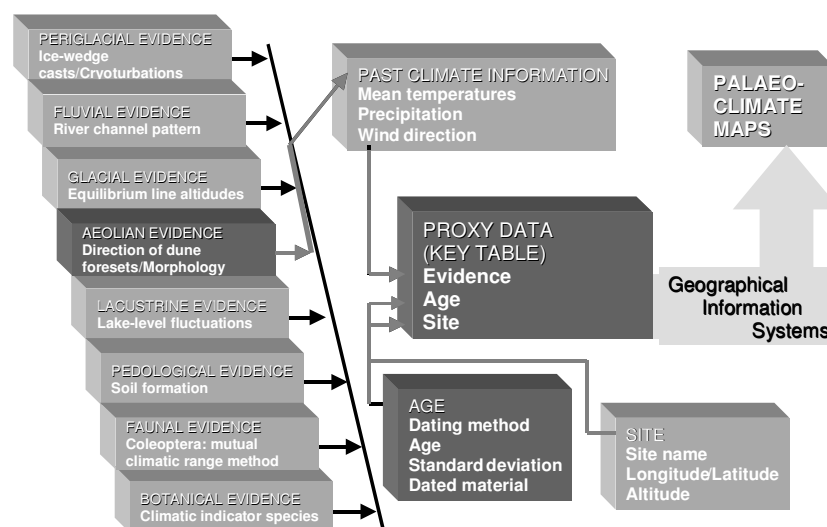
3. Luminescence dating of sediments

Optically stimulated luminescence (OSL) dating can be used to date quartz grains extracted from dune sands. By that a time frame is created for the information on climatic and environmental conditions which prevailed at the time of dune sand deposition. An accurate and precise chronology of dune formation is crucial to link this terrestrial archive to any other proxy record for palaeoenvironmental changes.

Optically stimulated luminescence dating is part of the family of trapped charge dating methods, which further includes thermoluminescence (TL), radiofluorescence (RF), electron spin resonance (ESR), and fission track dating. All these methods are based on the process of a time dependent accumulation of charge at structural defects in the crystal lattice of common minerals such as quartz or feldspars. Charge transfer is induced by ionising radiation resulting from naturally occurring radioactive processes.

This study focuses on OSL dating of sedimentary quartz, therefore the description of luminescence behaviour and dating procedures concentrate on the single-aliquot regenerative-dose protocol applied to coarse-grain quartz. For other approaches and protocols used for dating, for example, linear modulated luminescence (LM-OSL), infrared-stimulated luminescence (IRSL) or infrared-radiofluorescence (IR-RF) of feldspars, dating of fine-grained material etc. the reader is referred to the literature. The state of the art of luminescence dating techniques is regularly presented in the conference proceedings of the triennial International Conferences on Luminescence and ESR Dating (see e.g. Quaternary Science Reviews Vol. 13(5-7): 1994, 16(3-5): 1997, 20(5-9): 2001, 22(10-13): 2003; Radiation Measurements Vol. 23(2/3): 1994, 27(2): 1997, 32(5/6): 2000, 37: 2003). The most comprehensive account of luminescence dating is given in the books of AITKEN on thermoluminescence (1985) and optically stimulated luminescence (1998). Most recently the state of the art in OSL dosimetry is presented in the book of BØTTER-JENSEN et al. (2003) including detailed descriptions of the OSL properties of quartz and feldspars used as natural dosimeters and the application of OSL for geological dating.

3.1 Basic principle, history and current trends of luminescence dating

Luminescence phenomena in quartz or feldspar crystals are induced by charge transfer processes. Preconditions for creation of luminescence are, first, a source of ionising radiation,

which is given by the ubiquitous naturally radioactivity, and, second, possibilities for storage of this charge, which are provided by defects in the mineral crystal lattice, and, third, a mechanism to release trapped charge that gives rise to luminescence emission. To use the luminescence emission for dating purposes, a zeroing event is necessary, at which any previously stored trapped charge is released, thus, any luminescence signal is reset to zero or at least to a measurable residual signal. In the case of sediment dating, the zeroing mechanism is the optical stimulation by exposure to sunlight, the so-called 'bleaching' during sediment transport and deposition. This is valid no matter whether TL dating or OSL dating is finally used for age determination. In case of dating ceramics or flint artefacts from archaeological contexts, for example, the zeroing event is the last burning event (see Fig. 2 a). In general, the last resetting event is datable, e.g. the last exposure of quartz grains to sunlight. Consequently, sedimentary or depositional ages are obtained rather than mineralisation/crystallisation ages.

Fig. 2: Basic principles of luminescence dating.
a) The luminescence signal increases with the time provided for storage of energy. By exposing a sample to sufficient heat (burning of ceramics) or light energy (sunlight during sediment transport) the stored energy is released and by that the luminescence signal intensity set to zero, commonly referred to as 'bleaching' in case of light exposure. By subsequent shielding from severe heat or light the signal can increase again until sampling. The last zeroing event than is datable.
b) Determination of a dose, which is equivalent to the absorbed natural palaeodose, by irradiation with known radioactive doses and subsequent luminescence measurements in the laboratory.
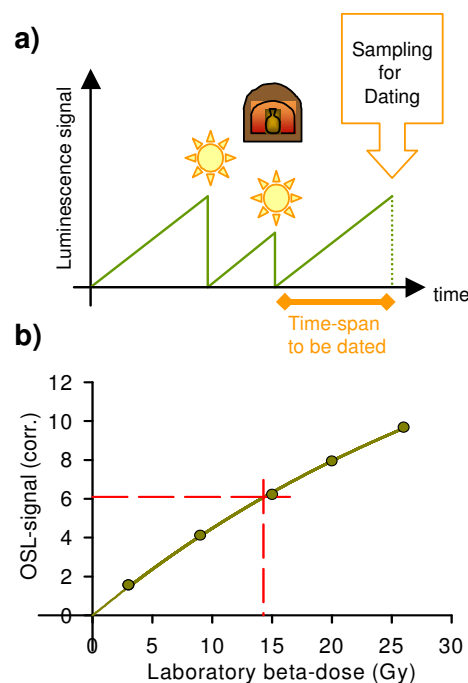
Exposure of a target-sample to natural irradiation gradually increases the number of trapped electrons and thus the absorbed dose. In proportion, the luminescence signal intensity

increases until the sampling –shielded from light - and measurement of the sample's luminescence emission in the laboratory. The intensity of this first measured luminescence signal is called 'natural luminescence intensity' (L_n). It is measured by exposing the sample to a light source with an appropriate wavelength and intensity to stimulate luminescence (OSL method) or by heating the sample up to about 500°C (TL method). The luminescence emission of the mineral grains is monitored as a function of stimulation time or temperature, respectively. The luminescence emission measured in the laboratory is in proportion to the radiation dose absorbed by the mineral since the last event of signal resetting. To make this luminescence intensity usable for age calculations it is translated into dose values through calibration of the response signals against known doses of radiation in the laboratory. Sub-samples are exposed to increasing laboratory irradiation of known defined doses and by plotting the corresponding luminescence intensities against the laboratory dose a so-called 'dose response curve' is obtained (see Fig. 2 b). Finally, the natural luminescence intensity L_n is translated into a dose value by projecting the L_n value onto the dose response curve. This experimentally determined dose value is an equivalent of the naturally received dose. While this so-called palaeodose (P) results from the absorption of the sum of alpha-, beta-, gamma- and cosmic radiation, the equivalent dose (D_e) determined by luminescence measurements results from laboratory irradiation with mono-energetic β- or γ-sources.

To translate the equivalent dose value into a luminescence age the factor of time has to be introduced by including the environmental dose rates which describe the strength of natural radioactivity per time unit. Ionising radiation in sediments results from the decay of lithogenic radionuclides, in particular uranium (U), thorium (Th), and potassium (K). The procedure of dose rate determination will be explained in detail in section 3.3. Finally, assuming the dose rate had been constant over burial time, the luminescence age is calculated by the following equation:

Age (ka) = Equivalent dose (D_e in Gy) : Dose rate (D_0 in Gy/ka)

The starting point for luminescence dating of minerals was the thermoluminescence process. DANIELS et al. (1953) were the first to describe the use of thermoluminescence emissions of limestone and ancient pottery to determine the time since the mineral was last crystallised or the pottery was heated during the fabrication process. When SHELKOPLYAS and MOROZOV (1965, in PRESCOTT & ROBERTSON 1997) discovered the light sensitivity of the electron traps, the basis was created for using TL to determine the time since sediments were last exposed to

sunlight. The first comprehensive studies on TL dating of sediments were carried out by WINTLE and HUNTLEY (1979, 1980). Over 30 years after the first descriptions of TL dating HUNTLEY et al. (1985) set the starting point for OSL dating with their study using a blue-green argon-ion laser beam to stimulate luminescence in quartz extracted from South Australian dune sands. HUNTLEY et al. used light in the visible wavelength range to free trapped electrons (generally summarised as optically stimulated luminescence OSL, or further specified according to the wavelength range in e.g. blue-light stimulated luminescence BLSL). HÜTT et al. (1988) were the first who stimulated luminescence from feldspars using near infra-red wavelengths around 880 nm (infra-red stimulated luminescence IRSL). For both techniques, OSL and IRSL, a light source with a constant wavelength and stimulation power (e.g. ~10 mW/cm²) is used and the OSL signal is monitored continuously throughout the stimulation period. This continuous monitoring is known as 'continuous wave-OSL' (CW-OSL[2], BØTTER-JENSEN et al. 2003). In contrast, if the intensity of the stimulation source is ramped linearly while the OSL is measured, e.g. from 0 to ~10 mW/cm², the corresponding OSL readout is called 'linear-modulation OSL' (LM-OSL). This technique was introduced by BULUR (1996). For more details and a summary of recent studies further reading of BØTTER-JENSEN et al. (2003) is suggested. Already in their pilot study on OSL dating HUNTLEY et al. (1985) mentioned, that "in principle, the discrimination of induced luminescence from scattered incident light can be made on the basis of wavelength or time" (p. 105). They decided to use the former by using appropriate optical filter sets to discriminate stimulation light from light due to luminescence emissions. The fairly recent method of 'pulsed optical stimulation' (POSL) takes up the latter point of discriminating induced luminescence by time. In POSL measurements emission and scattered stimulating light are separated in time. Time-resolved spectra are recorded by detecting the luminescence emission between the optical stimulation pulses with pulse width in the range of µs or ns. This method is predominantly used to study luminescence characteristics, such as luminescence lifetimes, and was applied to feldspars by CLARK et al. (1997) and CLARK and BAILIFF (1998) and first extended to quartz by CHITHAMBO and GALLOWAY (2000). In contrast to these new readout techniques with a special importance for basic research, the use of radioluminescence for dating of feldspars is a fairly new member in the family of luminescence dating techniques, which was pioneered by TRAUTMANN et al. (1998) and TRAUTMANN (1999) and further developed by ERFURT (2003)

---

[2] Instead of using CW-OSL in the following the abbreviation OSL is used in the sense of CW-OSL.

and ERFURT and KRBETSCHEK (2003). Radioluminescence dating is based on the reverse process which is responsible for the production of optically stimulated luminescence. The latter is dependent on the number of electrons released from light-sensitive traps during optical stimulation. In contrast, radioluminescence emission is caused by the radiative trapping of electrons into the traps, thus the radioluminescence signal decreases with the successive filling of traps during irradiation.

Optically stimulated luminescence is now widely used to date Quaternary deposits. In particular the introduction of so-called ‚single-aliquot'-protocols (DULLER 1991, 1994 and 1995) and the development of the ‚single-aliquot regenerative-dose protocol' for dating sand-sized quartz grains (MURRAY & WINTLE 2000) substantially improved the precision of OSL ages. This results in a much better resolution of age records based on luminescence dating. Furthermore, the single aliquot technique allows a more detailed investigation of the degree of signal resetting by sunlight exposure during sediment transport and deposition. Therefore OSL dating could be improved considerably for sediments which have been transported and deposited under restricted light conditions, such as fluvial sands, or which have been intermixed with older material after deposition, such as cave deposits (e. g. OLLEY et al. 1998, 1999, BATEMAN et al. 2003, DULLER 2004).

Recently the 'single-grain' approach was introduced (MURRAY & ROBERTS 1997). Although its use as a general dating tool is limited by the extremely time consuming measurements, single-grain studies are most valuable in terms of investigating luminescence properties of the dating material and resolving complex dose distributions in not fully bleached sand samples (THOMSEN et al. 2003, DULLER et al. 2003).

In the focus of current research in luminescence dating is also the expansion of the dating range. Due to optimised equipment features the lower dating limit could be successfully reduced to even a few tens of years (e.g. BALLARINI et al. 2003, MADSEN et al. 2005, FORMAN et al. 2005a). This is essential for dating recent or sub-recent dune activity in the study area.

Numerous luminescence studies are concerned with the development of protocols to increase the upper dating limit. The application of radiofluorescence (RF) dating of potassium-rich feldspar extracts, for example, provides a suitable tool for dating further back in time (about 500,000 years) (TRAUTMANN 2000, KRBETSCHEK et al. 2000, ERFURT 2003).

With regard to quartz extracted from sediments in most instances the upper dating limit is set to c. 350,000 years (MURRAY & OLLEY 2002). Nevertheless, HUNTLEY et al. (1993) dated an Australian fossil dune system to ~800 ka by TL of quartz in good agreement with oxygen isotope data. Their samples were characterised by very low radionuclide and hence by low annual doses.

However, a range of approaches has been tested for their potential for extending the dating range of quartz. The slow OSL component of quartz also has been used for dating of Quaternary sediments. SINGARAYER et al. (2000) calculated a slow component age of 735±71 ka and concluded a good potential of slow component measurements as a long-range dating tool for sediments deposited ~1 Ma ago, although the application might be restricted to aeolian sediments because of the slow optical resetting of the slow component. Recently, RHODES et al. (2006) reported single aliquot OSL ages for sedimentary quartz samples deposited around 500,000 years and even close to 1 Ma ago, which are in good agreement with independent chronological constraints (ESR ages and one U-series date). They improved the dating precision by using novel slow-component and component-resolved OSL techniques.

Measurements of the 'red' TL of quartz have been shown to provide a tool for extending the dating range for volcanic quartz to 1 Ma (e.g. FATTAHI & STOKES 2000). But the application to unheated quartz extracted from sediments is restricted due to the poor resetting of the 'red' TL signal by sunlight. LAI and MURRAY (2005), for example, observed high signal residual levels of up to 40% of the initial signal after sunlight exposure. WESTAWAY and ROBERTS (2006) illustrate the potential of a new measurement technique based on the 'red' TL signal of quartz, which might also extent the dating range for unheated quartz from sedimentary environments.

WANG and LU (2005) applied a modified measurement protocol to determine the equivalent dose from the recuperated OSL signal of fine-grain quartz. They obtained OSL ages for Chinese loess samples of 720-850 ka which are in agreement with palaeomagnetic age control.

3.2 Source and nature of ionising radiation in sediments

The interaction of ionising radiation with mineral crystals in sedimentary systems provides the background for luminescence dating. Therefore some information on the source and nature of radioactivity occurring in sediments is presented prior to the description of the various methods applied in this study to determine the strength of the radiation field in sediments.

Radioactivity is the result of spontaneous transformations of the nuclei of atoms. Atoms are subdivided into nuclides which are specified by the number of positively charged protons (Z) and neutrons (N) in the nucleus and the number of negatively charged electrons (e⁻) in the surrounding atomic shell. Nuclides with a nearly equal number of Z and N are stable. But most known nuclides are unstable and decompose spontaneously either directly or in several steps to a stable nuclear configuration. They are called radioactive nuclides or radionuclides and their spontaneous transformation gives rise to the phenomenon of radioactivity. Radioactive decay causes changes of Z and N in the nuclei and thus leads to the transformation of an atom of one element, known as mother, into that of another element, known as daughter. This daughter may itself be unstable and will in turn form an isotope of another element by its own radioactive decay. This process, illustrated in general by so-called decay chains, continues until a stable configuration is reached. The energy released in such transformations is emitted as alpha (α), beta (β) or gamma (γ) rays. The term ionising radiation is used to describe the interaction of these rays with a medium. Charged (e.g. electrons or protons) or uncharged particles (e.g. photons or neutrons) collide with atoms or molecules and liberate electrons from the atomic shell. An electrically neutral atom is transformed into a charged ion (ICRU 1998, SIEHL 1996). This process of ionisation is distinguished from that of excitation, which is a transfer of electrons to higher energy levels in atoms or molecules requiring generally less energy (see Fig. 3).

Fig. 3: Interaction of charged particles with atoms.
N= nucleus, K, L, M= atomic shells. **a)** ionisation: on collision of charged particles with an atom an electron is liberated from the atomic shell as a secondary electron. **b)** excitation: on collision of charged particles with the atom an electron is transferred to a higher energy level (after HARDER 1996: 33).

a) ionisation   **b)** excitation
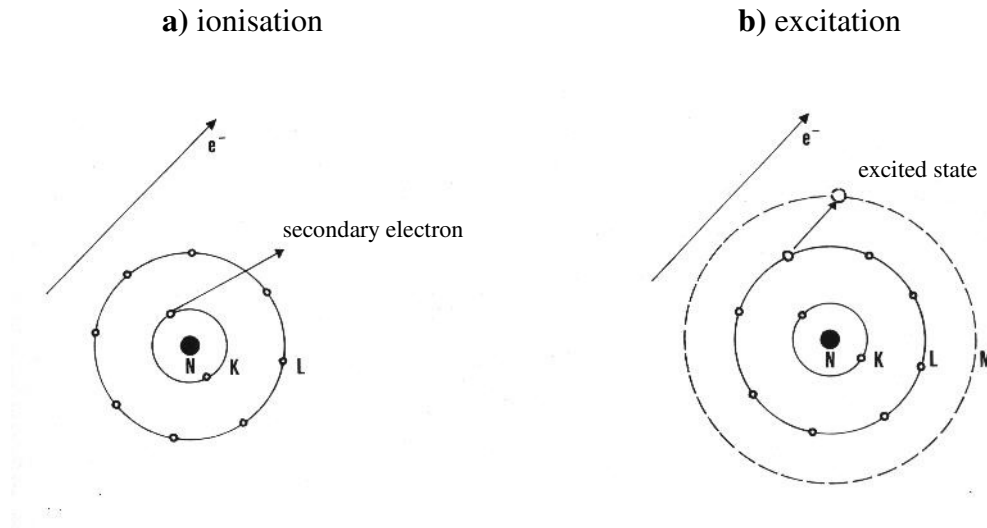
3.2.1 Types of radiation and their characteristics

The type of radiation, which is emitted by the decay of a particular radionuclide, is dependent on the decay process. The naturally occurring radionuclides relevant for luminescence dating dosimetry disintegrate via alpha, beta and electron capture decay. These decay processes result in the emission of alpha particles, beta particles (electrons), and gamma rays (gamma photons). Because all these types of radiation show a different behaviour concerning their interaction with solid matter (e.g. mineral crystals) their characteristics are summarised below.

Alpha decay and alpha particle emission:
An alpha particle consists of two neutrons and two protons and consequently has two units of positive charge (helium ion). This helium ion is emitted from the radioactive nuclei subject to alpha decay with high kinetic energies. Because of their appreciable mass and heavily ionising nature, alpha particles have only a very localised effect. They are absorbed in air already after a few centimetres (SIEHL 1996), and in matter, e.g. in sediments with a density of 2.5 g/cm³, already within ~ 20 µm distance from the decaying radionuclide (GRÜN 1989). Alpha particles travel in straight lines. Along its track into material an alpha particle ionises neighbouring atoms and hence loses its energy rapidly, but leaving a trail known as fission

track. Therefore alpha particles are less efficient in their ionisation of surrounding matter than beta and gamma rays, which are scattered after being released from the decaying nucleus. The ratio of alpha effectiveness in induction of luminescence compared to that of the same dose of β or γ radiation is expressed by the alpha efficiency factor. This is usually in the range of 0.05 to 0.2 (AITKEN 1985), and is highly dependent on the density of the absorbing matter. For quartz values have been presented in the range of 0.032 to 0.043 (REES-JONES 1995) or 0.035 (BELL & ZIMMERMAN 1978).

Beta decay and beta particle emission:
Beta rays are streams of particles identical to electrons. Beta decay occurs when a neutron in the nucleus is transformed into a proton and an electron. As a result of such beta decay electrons are expelled from the nucleus as negatively charged beta (β^-) particles, accompanied by neutrinos (FAURE 1986). By contrast with alpha particles, the much smaller beta particles are scattered after emission and considerably less ionising. Thus, beta particles show a different power of penetration; in air they are absorbed after several tenths of metres and in sediments with densities of 2.5 g/m³ after about 2 mm (GRÜN 1989, AITKEN 1998, SIEHL 1996).

Besides negatively charged beta particles emitted in beta negatron decay, positively charged beta particles (positrons, β^+) also exist. They have energy spectra similar to β^- particles. A positron is expelled from a radionuclide when a proton in the nucleus is transformed into a neutron, a positron, and a neutrino (FAURE 1986).

Electron capture decay:
A radionuclide can transform also by capturing one of its extranuclear electrons, predominantly from the K shell, which is the closest to the nucleus. By that the nucleus can increase its neutron number and decrease its proton number. Such electron capture decay is accompanied by the emission of a neutrino from the nucleus and, if the product nucleus is left in an excited state, by the emission of gamma radiation when the product returns to the ground state.

Gamma rays:
Gamma radiation consists of electromagnetic waves and can alternatively be regarded as a stream of discrete photons with, typically, energies in the range of >0.05 MeV (wavelength <0.025 nm). Compared with alpha and beta particles gamma rays show the least interaction

with the matter penetrated. In sediments gamma rays are absorbed after about 30 cm (SIEHL 1996, AITKEN 1998, 1985).

A nucleus which is transformed by alpha or beta decay remains in a short-lived excited state and then falls back into the ground state by the emission of gamma photons. Gamma rays are an accompaniment of alpha or beta particle emission and also of electron capture decay.

3.2.2 Radionuclides in sediments as radiation source

The term half-life describes the time which is required for half of the initial radioactive atoms to decay. Most known radioisotopes have very short half-lives. Therefore, the major part of ionising radiation in sediments is caused by only the few naturally occurring relatively long-lived radionuclides of uranium, thorium, and potassium, and the members of their respective decay chains. A minor contribution comes from rubidium-87. The radioisotopes ^{238}U, ^{235}U, ^{232}Th, and ^{40}K are so-called primordial radioelements. They were present at the formation of the Earth and, because their decay rates are very slow, are not yet completely disintegrated (see Table 1).

Table 1: Natural radioisotopes relevant for luminescence dating.
Potassium has three different isotopes: ^{39}K (93.2 %), ^{41}K (6.73 %), and ^{40}K (0.0117 %), the last-named being the only radioactive isotope (summarised from FAURE 1986 and KEMSKI et al. 1996) (α= alpha decay, β= beta decay, ec= electron capture decay).

Radionuclide	Half-life	Type of decay and daughter products	Isotopic abundances in %
^{40}K	1.28·10^9 a	^{40}Ca (β), ^{40}Ar (ec)	0.0117
^{238}U	4.47·10^9 a	decay chain to ^{206}Pb (α, β)	99.2672
^{235}U	7.04·10^8 a	decay chain to ^{207}Pb (α, β)	0.7202
^{234}U	2.45·10^5 a	daughter of the ^{238}U-decay chain	0.0056
^{232}Th	1.41·10^9 a	decay chain to ^{208}Pb (α, β)	100
^{228}Th	1.9 a	daughter of the ^{232}Th-decay chain	
^{234}Th	24.1 d	daughter of the ^{238}U-decay chain	
^{230}Th	7.54·10^3 a	daughter of the ^{238}U-decay chain	
^{231}Th	25.4 h	daughter of the ^{235}U-decay chain	
^{227}Th	18.2 d	daughter of the ^{235}U-decay chain	

In sediments the concentration of U, Th, and K varies, because the distribution of these elements during geological and pedogenic processes is determined by their specific geochemical behaviour. Both uranium and thorium occur in nature predominantly in the tetravalent oxidation state and both have large ionic radii (U^{4+}: 1.05 Å, Th^{4+}: 1.10 Å). Therefore they are geochemical incompatible and are incorporated in the common rock-forming minerals (e.g. quartz, feldspars) usually only in very low concentrations of typically only a few ppm (parts per million, equals mg per kg). Once segregated from the crystal lattice of a mineral by weathering processes, uranium forms the uranyl ion (UO_2^{+2}) under oxidising conditions in which U has a valence of +6. This uranyl ion builds compounds which are soluble in water. Therefore U is a mobile element in sedimentary systems characterised by an oxidising milieu (FAURE 1986, KEMSKI et al. 1996). On contrary, Th is an immobile element, because the compounds formed by Th^{4+} are generally insoluble in water. Compared to U and Th, potassium is a common element in nature and because of its comparatively small ionic radius it is easily incorporated into the crystal lattice. Thus K^{2+} is an important cation in rock-forming silicate minerals, especially in feldspars (KEMSKI et al. 1996).

In Fig. 4 the decay chains of ^{238}U and ^{232}Th are illustrated. According to Table 1 uranium-235 is parent nuclide of an individual decay series, but this is less important with respect to the isotopic abundance of only ~0.7% compared to that of uranium-238 of ~99.3%.

The energy which is release from the decay series of uranium and thorium can be summarised (see ADAMIEC & AITKEN 1998) (energies are given in MeV and represent the energy emitted per disintegration):

^{238}U$\rightarrow$ ^{206}Pb: 8 α (42.7)+ 6 β^- (2.28)+ γ (1.78)   in total 46.76 MeV/disintegrated nuclide

^{235}U$\rightarrow$ ^{207}Pb: 7 α (41.1)+ 4 β^- (1.27)+ γ (0.665)   in total 43.04 MeV/disintegrated nuclide

^{232}Th$\rightarrow$ ^{208}Pb: 6 α (35.7)+ 4 β^- (1.33)+ γ (2.32)   in total 39.35 MeV/ disintegrated nuclide

The processes involved in the disintegration of ^{40}K and the energies emitted by the decay process are shown in Fig. 5.

Fig. 4: Decay chains of uranium-238 and thorium-232.
The 'parent' nuclide ^{238}U is transformed into the 'daughter' product ^{234}Th by emission of alpha particles. Because the daughter product is unstable it decays in turn by emission of radiation (here beta particles) and the production of the next daughter nucleus and so on until a final stable configuration is reached. Several intermediate daughters, e.g. ^{214}Bi, undergo branched decay with an emission of either an alpha particle or a beta particle by the transformation to ^{214}Po or ^{210}Tl, respectively. Although the chain splits into separate branches ^{206}Pb is the stable end product of all the possible decay paths. (modified from SIEHL 1996: 9 & 7)

Element and decay chain with emitted particles		Half-life
^{238}U	α	4,47 Ga
^{234}Th	β	24,1 d
^{234}Pa	β	6,7 h
^{234}U	α	245 ka
^{230}Th	α	75,4 ka
^{226}Ra	α	1600 a
^{222}Rn	α	3,8 d
^{218}Po		3,1 min
^{218}At		1,6 s
^{214}Pb		27 min
^{214}Bi		19,9 min
^{214}Po		164 ms
^{210}Tl		1,3 min
^{210}Pb		22,3 a
^{210}Bi		5,0 d
^{210}Po		138,4 d
^{206}Tl		4,2 min
^{206}Pb		stable

Element and decay chain with emitted particles		Half-life
^{232}Th	α	14,1 Ga
^{228}Ra	β	5,8 a
^{228}Ac	β	6,1 h
^{228}Th	α	1,9 a
^{224}Ra	α	3,7 d
^{220}Rn	α	55,6 s
^{216}Po		150 ms
^{216}At		300 ms
^{212}Pb		10,6 h
^{212}Bi		60,5 min
^{212}Po		45 s
^{208}Tl		3.1 min
^{208}Pb		stable

Fig. 5: The radioactive decay of potassium-40.
a) Conversion of atoms of ^{40}K to ^{40}Ca through the emission of a $β^-$ particle (n= number of neutrons, p= number of protons). **b)** Conversion of ^{40}K to ^{40}Ar through electron capture (ec) by the nucleus. c) Probabilities of the decay types for ^{40}K and released energies. (a & b from LOWE & WALKER 1997: 249, c modified from SIEHL 1996: 10)
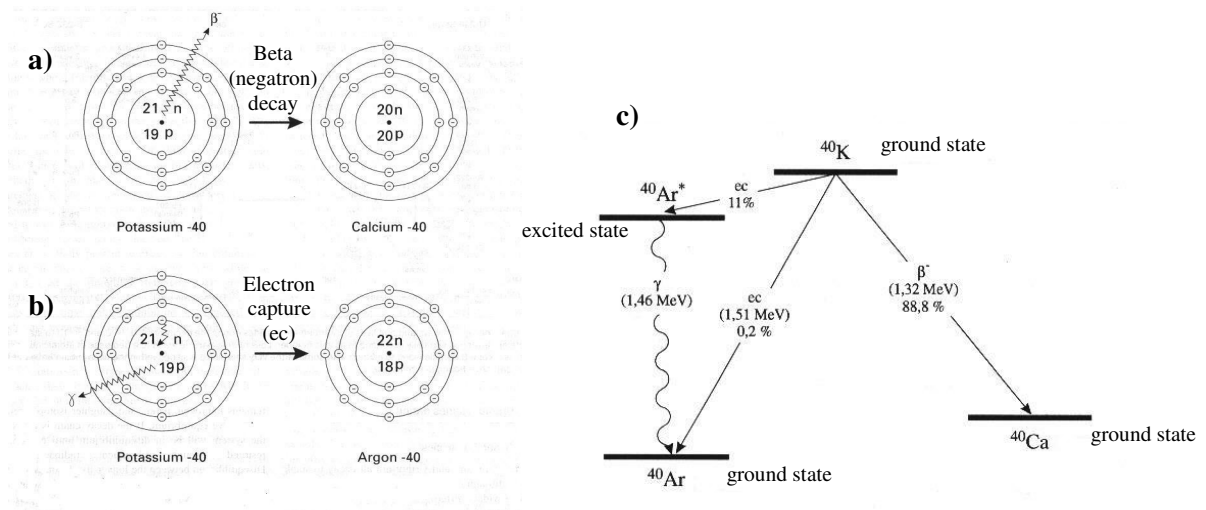
3.3 Dose rate determination

3.3.1 Conversion of energy emission into dose rates for quartz as absorbing matter

It has been shown that the radiation emitted during the decay of the different radionuclides carries energies of various intensities. Radiation interacts with matter in a series of processes in which this energy is converted and finally deposited in matter. The dose rate describes the amount of energy imparted to matter per unit mass (in J/kg=Gy) in a defined time interval (e.g. in a or ka). This parameter has to be determined for the calculation of luminescence ages (see section 3.1). A detailed report on the conversion of energy emission values into dose rates relevant for luminescence dating dosimetry is given by ADAMIEC and AITKEN (1998).

Various interaction processes occur between radiation and matter. In particular a radiation particle may be absorbed, or its energy and/or direction be altered. Besides the character of the interaction process, the type and energy of radiation, the density of the absorbing material, and the traversed distance in this material influence radiation attenuation. Furthermore, the concentration of radioactive elements within a mineral grain and its surrounds varies considerably. Bearing those facts in mind, an external and an internal dose rate has to be assessed independently. The external dose rate summarises the radiation dose in the sediment matrix and the internal dose rate the radiation dose resulting from radionuclides incorporated in the crystal lattice or in inclusions of the mineral grains finally used for luminescence measurements.

An important parameter in the calculation of the external dose rate is the grain size of the minerals exposed to environmental radiation, because of the different penetration power of the three types of radiation.

Alpha particles have average ranges in sediments of only a few tens of microns (see section 3.2.1). Therefore sediment grains used for luminescence dating, in this study predominantly in the grain size range of 100 to 200 µm, receive a substantial external alpha dose. With respect to luminescence dating of quartz the outer alpha-particle irradiated shell is removed during sample preparation by etching in concentrated hydrofluoric acid (HF) (for example removal of the outer 6-8 µm by immersion in 48% HF acid for 40 min according to SPOONER & QUESTIAUX 2000). However, etching may occur along dislocation lines in the crystal lattice structure. Therefore it remains questionable whether etching is isotropic and it has to be taken

in mind that any calculation of alpha dose removal is only an approximation (AITKEN 1985). In Table 2 the effect of an assumed effective etching on the dose rate data for sand-sized quartz is shown.

Table 2: Dose rates for the U and Th decay chains and K calculated for sand-sized grains of quartz as absorbing matter.
The water content is assumed to be zero and the cosmic dose contribution is included for a sampling depth of one metre. The values shown in parenthesis are calculated for quartz with the outer α-irradiated layer removed by HF etching (based on ADAMIEC & AITKEN 1998: 46).

Radionuclide content	Effective D_α (in µGy/a) [a]	D_β (in µGy/a) [b]	D_γ (in µGy/a)	D_0 coarse grain quartz (in µGy/a)	Percentage of total D_0
1 ppm Nat. U	218	131	113	462 (244)	27 (17) %
1 ppm ^{232}Th	61	25	48	134 (73)	8 (5) %
1 % K		704	243	947	55 (66) %
Cosmic			180	180	10 (12) %
Totals	279 (0)	860	584	**1723 (1444)**	
Percentage of total D_0	16 (0) %	50 (60) %	34 (40) %		

[a] The effective alpha dose rates are calculated using an α-value of 0.1 (see ADAMIEC & AITKEN 1998: 45).

[b] Here, an average correction factor of 0.9 is applied for the beta dose attenuation in coarse quartz grains (AITKEN 1985, 1998), (see also Table 3).

Beta particles penetrate matter with densities of c. 2.5 g/cm³ like sediments for about 2 mm before their energy is completely absorbed. Due to interaction of the particles along their pathways the beta radiation is attenuated within quartz grains in dependence on the grain diameter. Therefore, in calculations of the beta doses to quartz grains from internal and external sources a correction factor has to be applied that depends on the size of the grains (MEJDAHL 1979, BRENNAN 2003). Such beta dose absorption and attenuation factors as calculated for quartz grains are shown in Table 3 for the grain size fraction predominantly used in this study (100-200 µm).

Table 3: Beta dose absorption and attenuation factors for spherical, source-free quartz grains with a diameter of 100 or 200 µm in a uniform matrix containing 12 ppm Th, 3 ppm U, and 0.83 % K. (summarised from MEJDAHL 1979: 67, BRENNAN 2003: 302)

	grains	Attenuation factor for ∅ 100 µm	Attenuation factor for ∅ 200 µm
MEJDAHL 1979	unetched	0.921	0.875
BRENNAN 2003	unetched	0.922	0.872
BRENNAN 2003	etched[1]	0.913	0.863

[1]Attenuation factor for a grain with the outer 9µm layer etched away

Gamma rays have an average range in sediments of 30 cm. In the dose rate calculation for quartz grains in the range of 0.1 to 0.2 mm used in this study no radiation attenuation has to be considered.

3.3.2 Methods for dose rate determination

According to the data in Table 2 radionuclide concentrations can be converted into dose rates. Various methods are used in luminescence dating studies for elemental determination, for example inductively coupled plasma-mass spectrometry (ICP-MS), neutron activation analysis (NAA), atomic absorption spectrometry (AAS, for K determination), and gamma-ray spectrometry (for descriptions of the individual techniques see e.g. GEYH & SCHLEICHER 1990, GEYH 2005). Furthermore, individual dose rate components can be measured directly, e.g. via thick source ZnS alpha-counting or beta counting. In this study annual dose determination is based on NAA, which was carried out for all samples. But for some samples high-resolution gamma-spectrometry for radionuclide analysis and in-situ measurements of the total gamma dose rate have been carried out in order to check the reliability of the NAA results.

3.3.2.1 Neutron activation analysis (NAA)

For neutron activation analysis the several mg of the bulk sediment samples are irradiated in a reactor with neutrons. When neutrons interact with the nuclei of the atoms of the sample, radioisotopes are formed. These radioactive unstable isotopes decay by emitting gamma rays that are unique in energy and half-life and are measured by gamma ray spectrometry (see section 3.3.2.2). These distinct energy lines provide a signature to identify the targeted

elements present in the sample. The elements' concentration on the other hand is determined by the energy intensities (count rate). Further descriptions of the method itself can be found in GEYH (2005) and elsewhere.

All NAA measurements used in this study were carried out at the Becquerel Laboratories, Sydney, Australia. The laboratory gives the following analysis uncertainties dependent on the detection limits (pers. communication D. Garnett, 11.02.2000):

Element concentration exceeds the detection limit by ..*n*...times:	Relative standard deviation of the analysis in %:
10	5
8	6
6	8
4	11
3	15
2	25

3.3.2.2 High-resolution gamma-ray spectrometry

For a set of 48 samples high-resolution gamma-ray spectrometry was carried out in this study in addition to the NAA. Gamma rays originate from the decay of atomic nuclei. Gamma radiation does not form a continuous spectrum, but consists of one or more characteristic lines which can be used to identify the decaying nucleus. Potassium, for example, is determined using the single gamma line at 1.461 keV of ^{40}K (MEAKINS et al. 1979). The gamma rays used for uranium and thorium determination come from daughter isotopes. The high resolution (HR) gamma spectrometer at the Department of Geography in Cologne, for example, is able to detect the following energy peaks of daughter isotopes from the uranium decay chain (further details on the measurement facilities see PREUSSER & KASPER 2001):

^{214}Pb (E_γ=295.2 & 351.9 keV), ^{214}Bi (E_γ=609.3 & 1120.3 keV), ^{226}Ra (E_γ=186.0 keV)
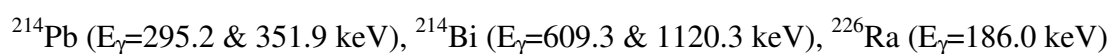
For the Th decay series the gamma lines of the following daughter nuclides were considered:

^{208}Tl (E$_\gamma$=583.2 & 2614.5 keV), ^{212}Pb (E$_\gamma$=238.6 & 300.1 keV),

^{212}Bi (E$_\gamma$=727.3 keV), ^{228}Ac (E$_\gamma$=338.3 & 911.1 keV)
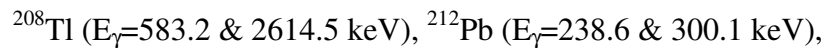
Provided that the decay chains are in equilibrium, thus the measured daughter gamma activities equal the parent nuclide activity, an equivalent U or Th concentration can be calculated.

Measurements in Cologne were carried out either on 800 g or 1600 g of the bulk, dried (105°C for 24 h) sediment samples, which were filled into Marinelli beakers. These were airtight sealed and stored for 28 days, by which time equilibrium is reached between ^{226}Ra and ^{214}Bi. The conversion of the gamma counts measured per channel in the gamma ray spectrum to element concentration requires calibrated standards known to be in secular equilibrium. Calibration of the detector in Cologne is based on home standards containing known quantities of added radioactive elements (IAEA). PREUSSER and KASPER (2001) give relative standard deviations for the measurement reproducibility including the uncertainty due to peak matching and the error caused by background variability of 2.1 % for K, 4.6 % for Th and 3.4 % for U. The overall error of the radionuclide contents based on the gamma spectrometry results includes this uncertainty and the standard deviation between the results from different energy peaks used for U or Th determination, respectively.

Further gamma-spectrometry measurements were carried out at the NLLD in Rosklide, Denmark, (Dr. A. Murray, Nordic Laboratory for Luminescence Dating, risø National Laboaorty) and at the MPI in Heidelberg (Dr. A. Kadereit, Forschungsstelle Archäometrie der Heidelberger Akademie der Wissenschaften, Max Planck Institut). About ~200 g (at R) or ~30 g (at HD), respectively, of each sediment sample was used for these measurements, which were carried out with low-background high-resolution gamma-ray spectrometers equipped with high purity germanium detectors. Therefore they allow assessing the equilibrium state in the Th and U decay series.

The results of laboratory gamma-ray spectrometry will be discussed and compared to the NAA results in section 3.3.4.2.

3.3.2.3 In-situ gamma-dose measurements

In-situ measurements were carried out at various sampling sites using a dose rate meter with a scintillator probe type "automess 6150AD-b" (for discussion of the results see section 3.3.4.3). The detector of the probe is suitable for measurements of photon radiation, thus measuring the total gamma- and cosmic-radiation in the sediments in the energy range of 23 keV to 7 MeV (www.automess.de/6150-AD-e.htm, 25.01.2006). The gamma ray interacting with a scintillator probe produces a pulse of light, which is converted to an electric pulse by a photomultiplier (PM) tube. The PM consists of a photocathode, a focusing electrode and 10 or more dynodes that multiply the number of electrons striking them several times each.

Measurements were carried out by placing the scintillator probe into the (widened) hole from which the tube for OSL sampling and the material for laboratory gamma-spectrometry and NAA measurements was taken. The major advantage of in-situ measurements is that being buried in the sediments the detector measures the radiation dose in a $4\,\pi$-geometry. By that more or less the entire gamma radiation field within a radius of about 30 cm around the sampling position is considered. Therefore, in heterogeneous sediment sequences, where samples were taken close to layer boundaries or where larger blocks of material varying from the sediment matrix composition were present, the in-situ measurements ought to yield the more reliable results for the total gamma dose, than the laboratory analysis of radionuclide contents of the sample material itself. This, of course, is only important for layers with significantly different radioisotope concentrations, densities and water contents.

3.3.3 Dose rate variation and sources of error

If the concentrations of potassium, uranium and thorium in the sediments have been determined by means of gamma-spectrometry measurements or other methods of element analysis (e.g. NAA), the dose rate for a specific sampling position can be calculated (see Table 2). This calculation is based on various assumptions, which may introduce a considerable source of error. These uncertainties have to be taken in mind when OSL ages are discussed in terms of 'absolute ages'. The different assumptions are outlined and discussed in the following.

3.3.3.1 Radioactive disequilibria

In dose rate determination it is usually assumed that the dose rate does not change over the period of burial. This implies, besides other parameters assumed to be constant throughout time, that the uranium and thorium decay series are in state of equilibrium. A decay chain is in equilibrium when the disintegration rate of each member equals that of the immediately preceding one. Thus, for each radioisotope of the chain the specific decay rates or activities, respectively, are the same, although the half lives may vary considerably. If the activities of individual chain members differ significantly disequilibrium is indicated. Mobility of individual nuclides in the decay chain can result in the disturbance of the decay chain, whereby a parent or daughter is moved into or out of a system. The different radioisotopes of a particular decay chain show different geochemical properties. Therefore they are affected by geochemical processes, such as solution, precipitation or gaseous diffusion, to varying extent (see Fig. 6 for the example of the ^{238}U decay chain). Furthermore, disequilibrium can only develop if the half-life of some daughter products is sufficient long to allow for significant fractionation. For a more general discussion of radioactive disequilibria it is referred to e.g. IVANOVICH & HARMON (1992). Numerous studies evaluate the impact of disequilibrium on luminescence dating results in more detail (READHEAD 1987, KRBETSCHEK et al. 1994, PRESCOTT & HUTTON 1995, OLLEY et al. 1996, 1997).

Disequilibrium in the ^{232}Th decay chain is unlikely to be important in sediments. First, the geochemical mobility of thorium is limited, because Th complexes are not soluble in water (see section 3.2.2). Second, the ability of fractionation is limited due to the very short half-lives of the ^{232}Th daughters (only up to 5.8 years, see Fig. 4). Therefore, the ^{232}Th decay chain is expected to be in equilibrium in sediments which are older than ~20 years and have been chemically closed since deposition (OLLEY et al. 1996, GEYH et al. 1997, GEYH & TECHMER 1997).

Serious disequilibria are known to occur in the ^{238}U decay chain due to the geochemical mobility of several nuclides. Furthermore, the half-lives of many ^{238}U daughters are long enough to allow the persistence of any established disequilibria for millennia.

Fig. 6: Likely causes for disequilibrium in the ^{238}U decay chain.
A decay chain is in equilibrium when the disintegration rate of each daughter is equal to that of the parent or the preceding member, respectively. Disequilibrium results from geochemical sorting according to different geochemical properties of the radioisotopes, whereby a process can act either to move a parent or daughter into or out of a system. Hence, an excess or deficit of the affected radionuclide can result.

Element and decay chain with emitted particle	Half-life
^{238}U α	4,47 Ga
^{234}Th β	24,1 d
^{234}Pa β	6,7 h
^{234}U α	245 ka
^{230}Th α	75,4 ka
^{226}Ra α	1600 a
^{222}Rn α	3,8 d
^{218}Po β / α	3,1 min
^{218}At α	1,6 s
^{214}Pb β	27 min
^{214}Bi β / α	19,9 min
^{214}Po α	164 ms
^{210}Tl β	1,3 min
^{210}Pb β	22,3 a
^{210}Bi β / α	5,0 d
^{210}Po α	138,4 d
^{206}Tl β	4,2 min
^{206}Pb	

☐ affected by dissolution
☐ affected by diffusion
→ measured by gamma ray spectrometry (Cologne lab.)

The mobility of the nuclides that are indicated in Fig. 6 can result in parts of the uranium chain being broken. The gaseous diffusion of ^{222}Rn results in a reduced activity of the lower part of the decay chain. Another important reason for the build up of disequilibria is the solubility of ^{226}Ra and of the radioisotopes of uranium (KRBETSCHEK et al. 1994, MEAKINS et al. 1979).

As mentioned already in section 3.2.2 uranium is mobilised in oxygen-rich aqueous solutions when U^{6+} ions form easily soluble uranyl-compounds. These compounds remove parent or daughter nuclei from the decay chain and into the environment, e.g. by percolating water into the groundwater. In such instances disequilibria result which are characterised by a loss of uranium. In sediments, where uranyl-compounds are precipitated again, an U uptake can also

cause a disequilibrium. The latter problem can affect carbonate-rich deposits in arid environments, when secondary carbonates are precipitated from uranium-rich groundwater and by that cause a post-sedimentary disequilibrium in the U decay series due to an excess of U.

In more temperate and humid climate organic matter plays an important role for the enrichment of uranium in sediments. Humic substances are able to adsorb U from uranium-rich groundwater under reducing conditions, because of its high ion exchange capacity. Soluble 6-valent uranyl-compounds are immobilised by reduction to insoluble 4-valent compounds. Uranium concentration in peat layers of up to 20 ppm has been found which can be ascribed to immobilisation of uranly-compounds by adsorption at humic acids under reducing conditions (GEYH & TECHMER 1997, GEYH et al. 1997).

With respect to the depositional context disequilibria most likely are to be expected at sampling sites showing wet conditions (e.g. current groundwater flow) or which probably have been wet for a significant time in its past history. In fact, numerous luminescence studies reporting on the occurrence of disequilibria in the U decay chain are concerned with the investigation of fluvial or lacustrine sediments (e.g. KRBETSCHEK et al. 1994, PRESCOTT & HUTTON 1995, OLLEY et al. 1996). Disequilibria related to the precipitation of secondary carbonates in arid environments are not relevant with respect to the sediments investigated in this study area. But samples derived from fluvial or glacio-lacustrine deposits or sediments close to peat layers should be treated with suspicion. In general, there is only little or no evidence for disequilibrium in dune sand deposits (KRBETSCHEK et al. 1994, PRESCOTT & HUTTON 1995). Thus, radioactive disequilibrium is considered to be a minor problem for most of the samples dated in this study as the majority of samples was taken from comparably dry dune sites without significant affection of groundwater fluctuation.

However, tests for radioactive disequilibrium should be carried out, in particular for samples from wet environments. Such checks can be carried out by making measurements of dose rates and/or element concentrations by independent methods. High-resolution alpha-spectrometry allows measurement of ^{238}U, ^{234}U and ^{230}Th and by that identification of disequilibria in the upper part of the ^{238}U decay chain (compare Fig. 6). But this method is too time-consuming to be applied routinely in luminescence dating studies. Measurements of the low energy region with low-level gamma-spectrometers provide a possibility to identify radon loss and U/Ra disequilibria in the upper part of the uranium decay series.

Several tests on the presence of disequilibria have been carried out in this study; the results will be presented and discussed in section 3.3.4.2.

3.3.3.2 Variation in the radiation field by inhomogeneities

A common assumption in dose rate determination is that the distribution of radionuclides, thus the distribution of radiation sources, in sediments sampled for luminescence dating is homogeneous. But the radiochemical composition of the sediments can vary spatially. For example, large, source-free blocks, e.g. of calcite, can be found embedded in a sandy, source-rich matrix. Or, layers of clay, with a significant higher radionuclide content compared to sandy deposits, alternate with sand layers with their thickness smaller than the range of gamma-photons (30 cm) (see Fig. 7 a). Different minerals represent different sources of radiation strength due to their content of radionuclides incorporated in their crystal structure, for example K-rich feldspars or zircons. By that variations in the radiation field on the grain-to-grain scale are present (so-called microdosimetry effects, see Fig. 7 b).

Fig. 7: Variations in environmental radiation field.
a) The gamma radiation field at sampling position 'A' is homogeneous. Provided that the blocks at the bottom of the section are source-free, the gamma dose at position 'B' is lower compared to the homogeneous radiation field at position 'A'. Higher radionuclide concentrations in the clay layer compared to the sand unit results in an increased gamma dose rate at sampling position 'C'. The circle indicates the range of γ radiation.
b) Grey shaded areas represent grains with a higher content of radionuclides (e.g. zircons, K-rich feldspars), thus representing stronger radioactive sources than the grains represented by white areas (e.g. source-free quartz grains). A grain sampled from position 'A' would have accumulated less radiation dose compared to the grain at position 'B'. The circle indicates the range of β particles.

a) Variations in the gamma radiation field   **b)** Variations in the beta radiation field
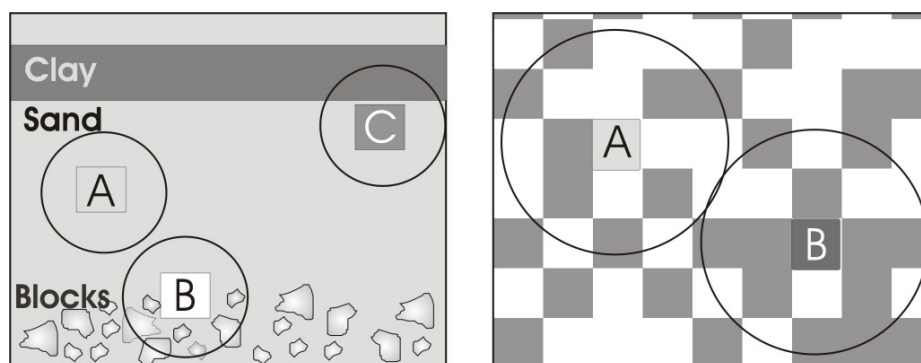
To summarize, any heterogeneity in the sediment cause a heterogeneous radiation field in the space surrounding the point of sampling, but at various scales. The impact of dose heterogeneity depends on the radii of the irradiating particles. Inhomogeneous distribution of the radioactivity at a scale of 30 µm, for example, cause an inhomogeneous alpha radiation field but radiation would be homogeneous regarding β-particles and gamma photons with a range of ~2 mm and ~30 cm in sediments, respectively (see e.g. WAGNER 1995).

In luminescence dating of sand sized quartz any problems in dose rate determination caused by variability in the external alpha radiation field can be circumvented by the removal of the outer alpha-irradiated layer of the grains. Variations of the accumulated dose from one grain to another caused by heterogeneities in β radiation generally can be compensated for by use of a large number of grains (multigrain aliquots) to average out the dose heterogeneity (see Fig. 7 b). If the gamma radiation field is spatially inhomogeneous, in-situ measurements of the gamma dose provide a suitable tool to assess the strength of gamma sources relevant at the sampling point. Furthermore, the gamma irradiating environment of a sample can be reconstructed by computer simulation. These calculations require the determination of the radionuclide concentration of all lithologic components of the γ irradiating environment, for example, the U, Th, and K content of the matrix and embedded blocks (e.g. BRENNAN et al. 1997, GUIBERT et al. 1998).

3.3.3.3 Influence of uncertainty in water content variations

The interstices of sediment can be filled with either water or air, which have different radiation attenuation characteristics. As water present in pore voids attenuates the radiation dose to the individual grains, the overall dose rate is reduced with rising moisture content in the sediments. Therefore, for the dose rate calculation the water content in the interstices of the sediment to be dated has to be taken into account. The 'as collected' water content of a sample can be measured and its influence on the radiation attenuation calculated by applying the appropriate attenuation factors, as described below. But in terms of dose rate assessment for dating, the variation in wetness over the whole time span of burial has to be considered (see factor F in the equation). This is the only parameter in the dose rate moisture correction procedure which cannot be measured or calculated directly.

Transformation of 'dry dose rates' into 'wet dose rates' (for etched quartz only the beta and gamma dose rates are regarded) (see AITKEN 1985, 1998):

$$D_\beta \text{ wet} = D_\beta \text{ dry } /1+H \, W \, F \quad D_\gamma \text{ wet} = D_\gamma \text{ dry } /1+H \, W \, F$$

H = attenuation factors for radiation (after ZIMMERMAN 1971): $H_\alpha = 1.50$
                                                                                                                          $H_\beta = 1.25$
                                                                                                                          $H_\gamma = 1.14$

W = saturation water content = (saturation wet weight – dry weight) / dry weight
F = average water content during burial / saturation water content W

The estimation of the average wetness of the sediment since deposition is fraught with problems. The water content of a sediment changes seasonally in response to the natural variations in precipitation. Furthermore, it may change significantly if the sediment layers are influenced temporarily by groundwater. Also variations of the climate conditions induced by global climate change in the geological past have to be regarded. Over the last several thousands and ten-thousands years periods drier than today or permafrost conditions may have prevailed. The latter would imply different radiation attenuation because ice and water have different densities. Furthermore, variations of water contents throughout the period of burial can result from alternation of the porosity due to significant post-sedimentary compaction of sediment layers by increased loading. Soil development with an increase in fine grained sediments and/or organic material can also affect the overall ability of a particular sediment layer to hold moisture compared to the unweathered sediments.

This brief summary underlines the uncertainties related to the water content estimation in luminescence dating studies. Quantification of the range of variations in moisture is almost impossible. Qualification or identification of all the processes involved is all that can be achieved and allowed for. In these terms sediments being constantly saturated with water should be the easiest to handle together with samples from arid areas which are known to be arid since the deposition of the target sediment. The uncertainty in water content estimation "is usually a fundamental limitation in reducing error limits on the age to below the level of about ±5 %" (AITKEN 1998: 43-44).

3.3.3.4 Internal dose rate

Besides the external dose rate resulting from the exposure of a mineral grain to environmental radioactivity in the surrounding sediment, there is also an internal dose rate resulting from alpha and beta particles emitted from radioelements within the grain. In potassium feldspars, for example, K contents of about 12.5±0.5 % (HUNTLEY & BARIL 1997) and Rb contents of 400±100 µg/g (HUNTLEY & HANCOCK 2001) give rise to considerable internal dose rates. In contrast, the internal dose rate of quartz is commonly assumed to be negligible. MEJDAHL (1987), for example, reports internal uranium contents of 39 quartz samples with most of them showing concentrations of less than 0.3 ppm. He further presents beta dose rates for 1 ppm internal contents of U and Th in quartz and feldspar grains of 0.1 mm grain diameter of 0.014 and 0.004 Gy/ka, concluding that since the total dose rate is usually about 1 Gy/ka or more, the internal beta dose rate from U and Th ought to be negligible in most cases. However, SUTTON and ZIMMERMAN (1978) found a contribution of up to 5 % to the total annual dose from alpha radiation emitted by uranium incorporated in the crystal lattice of their quartz samples. VANDENBERGHE et al. (2004) determined internal dose rates in etched quartz grains which were in the range of 4.7 to 7.9 % of the external dose rates. Finally checking the amount of internal radioactivity in quartz seems important in particular if the external dose rate is low.

3.3.3.5 Variation of the cosmic ray dose contribution

In contrast to the so-called terrestrial natural radioactivity explained above there is also a contribution of cosmic radiation to the overall dose rate in sediments, which has to be considered in the luminescence dating procedure. This cosmic radiation is differentiated into primary cosmic radiation arriving at the earth's surface unaltered from outer space and secondary cosmic radiation, which results from various reactions of cosmic rays with the earth's atmosphere. Sources of the primary component are the sun and radiation from the galaxy, presumably caused by supernova eruptions in the Milky Way system. Solar radiation, in the form of solar winds and radiation released by sun eruptions, is predominantly composed of protons and electrons (DÖRSCHEL et al. 1992). Galactic radiation contains protons (85 %), α-particles (12.5 %), heavy nuclei (1.5 %) and electrons (1 %) (ALLKOFER & SIMON 1970 in DÖRSCHEL et al. 1992). Close to the earth charged particles of the primary cosmic radiation are diverted by the earth's magnetic field. As the influence of the magnetic

field is stronger at the magnetic poles than in equatorial regions, the cosmic radiation dose depends on the geographic latitude. From the equator to 40° latitude the radiation intensity rises by 7 % and remains more or less constant from there on to the poles measured at sea-level (PRESCOTT & STEPHAN 1982, AITKEN 1998). The influence of variations in the earth's magnetic field is negligible in the time span of interest for the application of luminescence dating techniques of about 500,000 years (PRESCOTT & HUTTON 1994).

As soon as the primary cosmic radiation finally enters the atmosphere of the earth, photons and particles of the secondary cosmic radiation are produced by the collision of primary particles with nuclei in the atmosphere. Alpha particles and other heavy ions are split into individual nuclei. Further interaction and reaction of those nuclei produce the 'soft' component of the secondary cosmic radiation: electrons, positrons and photons. In contrast, the 'hard' component consists of protons, muons, neutrons, and neutrinos, with nearly exclusively the latter three reaching the earth's surface, because charged particles are absorbed in the atmosphere (DÖRSCHEL et al. 1992). This explains the dependence of the cosmic radiation dose on altitude. For samples taken from an altitude exceeding 1 km, the contribution of cosmic rays to the overall dose rate increases substantially (AITKEN 1985, 1998).

When the cosmic dose contribution to the overall dose rate of a sediment sample is determined, the relevant parameter controlling the intensity of cosmic radiation is the thickness and density of the overburden material. The 'soft' component is already absorbed in the top half-metre of sediment with a density of approximately 2 g/cm³, and is of minor influence on the cosmic dose contribution. The 'hard' component is more penetrating and is attenuated with increasing depth due to ionising reactions with the surrounding material (see Fig. 8).

Fig. 8: Cosmic dose variation with depth below surface.
Within the upper 50 cm of sampling depth the contribution of the cosmic dose decreases much slower than in greater depths due to the contribution of the hard component (see inset graph).
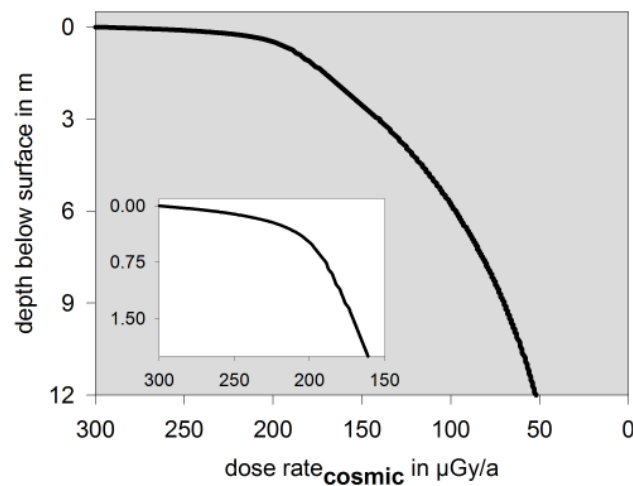
The contribution of cosmic radiation to the total dose rate is usually calculated according to the sampling depth and geographical position of the sampling site following PRESCOTT and HUTTON (1988, 1994). The dynamic character of sedimentary systems with repeated events of erosion and accumulation results in variations of the thickness of the overburden experienced by a buried sediment sample. Therefore the contribution of cosmic rays to the total dose rate of this sample is not constant over the entire period of burial time, but may vary significantly. Such fluctuations in the overburden thickness are less significant in sedimentary environments where the contribution of cosmic rays to the total dose is generally low. Frequently the proportion measures less than 10 %. But in aeolian dune sand systems with sediments predominantly consisting of more or less source-free quartz grains with only low feldspar and heavy mineral content, the dose rate resulting from radioactive decay of lithogenic radionuclides tends to be low. In these environments the cosmic ray contribution to the annual dose can be a major component to the total dose rate. In such cases a substantial error in the total dose rate calculation and finally in luminescence ages can be introduced if the cosmic dose contribution is calculated in correspondence to the present sampling depth. To improve the dose rate results the burial history of a sample should be taken into account, as far as this can be reconstructed (MUNYIKWA 2000). The impact of variations in the overburden thickness on the luminescence dating results of this study will be discussed in detail in section 3.3.4.6.

3.3.4 Results of dose rate (D$_0$) determination

3.3.4.1 Results of neutron activation analysis (NAA)

All element concentrations determined by NAA are summarised in Table A 1 Appendix A. For a set of 21 samples the NAA was carried out twice. These samples were chosen, either because the first analysis yielded U contents of below the detection limit (which was improved in the second run), or the first results were suspected to be erroneous by comparison with adjacent samples in the same sediment unit; or simply to check the reproducibility of the NAA results in general. A list of the samples included in this comparison is presented in Appendix A, Table A 2 (Fig. 9 illustrates the results). With ratios of 0.99±0.08 for the duplicate analysis of thorium and 1.02±0.09 for potassium the reproducibility of the NAA is reasonably good. The results for uranium are not as good: the ratio is only 0.86±0.48. As shown in Fig. 9, the best agreement was found in the lowest content range of less than 0.5 ppm, which is already close to the detection limit. The detection limit was, dependent on the sample characteristics and the varying influence of the measurement background, 0.1 or 0.5 ppm.

To evaluate the impact of the uncertainties regarding the accurate U determination by neutron activation analysis, the actual contribution of uranium to the total dose rates for the average radionuclide contents of the samples investigated here was calculated based on the data given in Table 4. The average concentration values of 179 NA analyses of sand samples were used (see Appendix A, Table A 1).

Fig. 9: Comparison of the duplicate neutron activation analysis results.
The individual data and samples investigated are listed in Appendix A, Table A 2. In total 21 samples were analysed. But regarding the uranium determination only 12 comparative data sets are available, because several results were below the detection limit. One potassium analysis was excluded. With a potassium concentration being several times lower than all the values obtained for dune sand samples in this study in general it was considered to be unreliable. All NA analyses were carried out at the Becquerel Laboratories in Sydney, Australia. The dashed line indicates the 1:1 ratio.
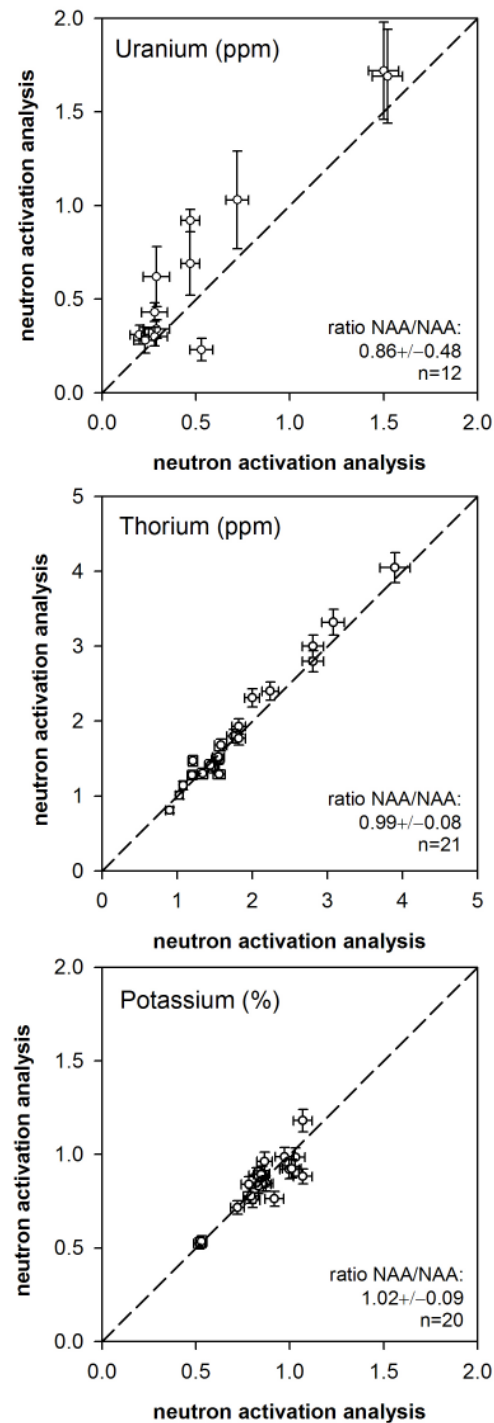
Table 4: Dose rates for the U and Th decay chains and K calculated for sand-sized grains of HF etched quartz grains based on the data summarised in Table 4.
The average radionuclide contents are based on NAA results obtained for 179 sand samples (see Appendix A, Table A 1). The water content is assumed to be zero.

Average radionuclide content of 179 sand samples	D_β (in µGy/a) [a]	D_γ (in µGy/a)	D_0 coarse grain quartz (in µGy/a)	Percentage of total D_0
0.46 ppm Nat. U	60	52	112	10 %
1.71 ppm ^{232}Th	43	82	125	11 %
0.76 % K	535	185	720	63 %
Cosmic [b]		180	180	16 %
Totals	638	499	**1137**	
Percentage of total D_0	56 %	44 %		

[a] A beta attenuation factor of 0.9 is taken into account for beta dose rates for coarse grains (MEJDAHL 1979, AITKEN 1998).
[b] The cosmic dose contribution is calculated for a sampling depth of one metre.

Uranium contributes on average only 10 % of the total dose rate in the sediments analysed in this study. Therefore, any restrictions regarding the precision and accuracy of the uranium determination by NAA are less significant compared to, for example, erroneous K determinations. Potassium is the dominant contributor to the total dose rate with ~63% and thus any problems related to the K analysis would have a major impact on the accuracy of the dose rate result. But as shown in Fig. 9 K concentrations were determined by NAA with good reproducibility. From this comparison it is finally concluded, that NAA seems to provide reliable and reproducible results at least for the samples investigated in this study. In order to support this assumption gamma-spectrometry was carried out for a range of samples to provide cross-check values for the radionuclide concentrations.

3.3.4.2 Comparison of NAA and gamma-spectrometry results

All gamma-spectrometry results are listed in Appendix A Table A 1. Here, the main focus of interest is placed on the comparison with analytical results obtained by neutron activation analysis to check the reliability of the NAA results. Because NAA determines the mass concentration of uranium, thorium, and potassium in the sediment, it is not useful in terms of

the identification of radioactive disequilibria in the decay chains of U and, though less likely, of Th. A second disadvantage is that the NAA was carried out on only a small amount of material (several mg), and therefore does not allow for inhomogeneities in the sediment matrix. Gamma-ray spectrometry, in contrast, is carried out on larger samples (in Cologne for example 800 or 1600 g). Therefore, its results may be considered slightly more reliable as any heterogeneity of the sediment matrix should be averaged out to a greater degree.

In Fig. 10 the results of NAA and gamma-spectrometry are compared. With respect to the additional error which arises from comparing different analytical approaches the agreement of both data sets is still reasonably good with average ratios (γ-spec./NAA) of 1.06±0.33 for U (n=43), 0.96±0.17 for Th (n=48) and 0.99±0.10 for K (n=48).

HUNTLEY and PRESCOTT (2001), for example, also carried out duplicate analysis using NAA and in-situ γ-spectrometry and obtained data sets yielding average ratios (in-situ γ-spec./NAA) of 1.07±0.31 (U, n=8) and 1.04±0.21 (Th, n=8). VANDENBERGHE (2003) found very good agreement of NAA and laboratory gamma-spectrometry results for eight samples resulting in average ratios (γ-spec./NAA) of 0.96±0.08 for U and 0.98±0.08 for Th.

Similar to the observation in the duplicate NAA analysis the greatest discrepancies were found in the uranium data set. But no systematic trend could be found. The comparative data set of this study suggests that discrepancies are most likely due to analytical problems. Several NAA results for uranium concentrations were close to the detection limit and therefore show large uncertainties. In particular these samples show the largest differences in analytical results when compared to the gamma-spectrometry results (Fig. 10).

To summarise the results of the comparison there is no systematic trend such as a systematic underestimation of NAA compared to gamma spectrometry. The good agreement of the potassium contents is regarded as positive result of this comparative study. As mentioned above, K is the major contributor to the annual dose with ~63% on average coming from the decay of ^{40}K. Finally the NAA is considered to provide sufficient reliability at least for the samples investigated in this study which mostly were collected from homogeneous dune sands. Thus, the problem of small sample amounts analysed by NAA seems less important for the quality of the results.

Fig. 10: Comparison of the gamma-ray spectrometry results with those obtained by neutron activation analysis.

All data are also presented in Appendix A, Table A 1. The gamma-spectrometry measurements presented in these figures were carried out at the Nordic laboratory of luminescence dating in Roskilde, DK (Dr. A. Murray, NLLD at the risø national laboratory, data set 'R'), at the Department of Geography in Cologne (Dipl.-Geogr. N. Klasen, Dipl.-Geogr. J. Lomax, Dr. F. Preusser, data set 'C') and at the Forschungsstelle Archäometrie at the MPI in Heidelberg (Dr. A. Kadereit, data set 'HD'). Five values were excluded from the uranium data set, because the NAA results of the first analysis were below the detection limit. For clarity the 1:1 ratio is shown as dashed line in each graph.
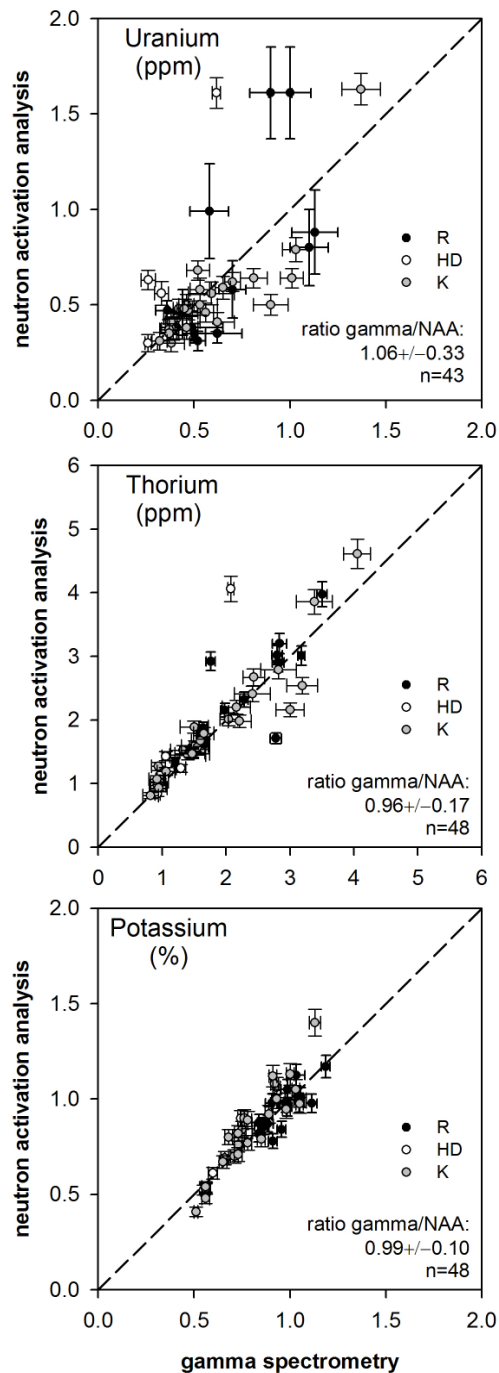
The impact of different approaches used for dose rate determination was evaluated by comparing the OSL ages calculated either with the NAA derived dose rate or with the γ-spectrometry based dose rate. With respect to the samples for which independent age control is provided, none of the methods yields in general the more accurate results. Only in eight out of the 48 comparisons the NAA based OSL ages differ significantly from γ-spectrometry based OSL ages with regard to the 2 σ significance level. This is considered to be the appropriate level for comparisons of analytical results from different techniques (GEYH 1980, 2005). Note, that systematic errors such as the uncertainty in beta-source calibration and water content assumption were not considered in the ages used for this comparison. In detail, all comparisons and related problems will be discussed in relation to the particular sites in chapter 1, including the probability of disequilibria being the reason for the discrepancy in the NAA and Gamma-spectrometry dose rates (see also the discussion in the following section). For all the samples with agreement of the NAA based and γ-spectrometry based age values the average dose rate was finally used for age calculation.

As no substantial and systematic discrepancy between γ-spectrometry and NAA dose rate based OSL data sets was found, it is concluded that the NAA results, which are the only ones available for all of the samples, are sufficiently reliable for those samples with no reference dose rate data set.

3.3.4.3 In-situ gamma-dose measurements

In-situ scintillometer measurements of the gamma dose rate were carried out at various sampling sites. Fig. 11 summarises the comparison of the in-situ measurements with the gamma dose rates (including the cosmic contribution) calculated from the U, Th, and K concentration determined by NAA and laboratory gamma-spectrometry, respectively. For those calculations the 'as found' water content was used and the actual sampling depth (see also Table A 3 in Appendix A).

Fig. 11: Comparison of the in-situ gamma-radiation measurement with the results of neutron activation analysis (NAA) and laboratory high-resolution gamma-spectrometry.
The dashed line represents the 1:1 ratio for clarity. The arrow indicates sample C7, which shows the most distinctive difference of both analytical results plus a significant deviation from the in-situ measurement (individual values are summarised in Appendix A, Table A 3).
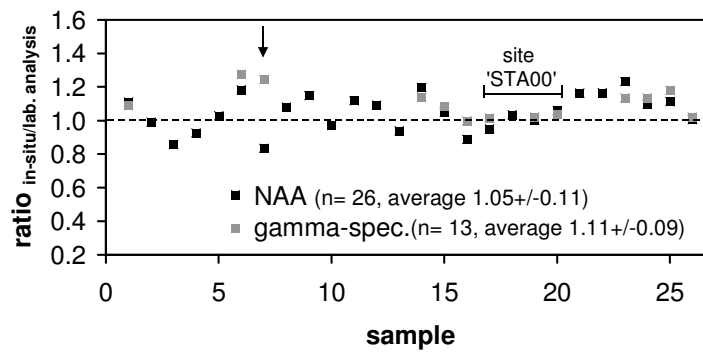
The scintillator probe used in this study for in-situ measurements of the gamma radiation was found to yield reliable results. This is concluded from the data set obtained for site STA00 (Schletau). Here an excellent agreement was found for NAA and laboratory γ-spectrometry results. Furthermore, both analytical approaches are in very good agreement with the in-situ measured gamma dose (±5%, see Fig. 11). The sediment sequence at site 'Schletau' appears homogeneous regarding the sediment structure; therefore this observation meets the expectations.

With an average ratio$_{in-situ/NAA}$ of 1.05±0.11 the NAA based gamma dose rate is in good agreement with the field measurements. The gamma dose values obtained from the laboratory gamma-spectrometry tend to overestimate the in-situ measured gamma radiation dose yielding an average ratio$_{in-situ/γ-spec.}$ of 1.11±0.09. But only 13 comparative data sets are available here. Except for sample C7 (indicated in Fig. 11 with an arrow) the γ-spectrometry results show a similar trend to the NAA results. The difference in C7 is most probably caused by a significant layer boundary close to the sampling position. The implication of this inhomogeneity on the age calculation will be discussed in detail chapter 1 (sampling site description 'Cottbus').

The good agreement observed between the laboratory data sets and the field measurements generally supports the assumption of a homogeneous gamma radiation field in the dune sands, which was expected from field observations.

From this comparative study it is concluded, that the NAA results, which are available for all samples investigated in this study, seem to provide a reliable data set in terms of being not less suitable than laboratory gamma-spectrometry. This is frequently supposed to be more reliable, as it is carried out on a substantially larger sample amount and therefore should better account for any inhomogeneities in radionuclide distribution. But, it is noted here, that this conclusion refers to the samples investigated in this study which mainly were collected from homogeneous dune sands. In case of inhomogeneous sediment sequences, this is not necessarily true; rather does the opposite apply.

3.3.4.4 Evidence for disequilibrium and its implication for age calculation

For accurate dose rate determination knowledge of the state of equilibrium in the decay series is required. The main disadvantage of dose rate estimation by neutron activation analysis is not to allow for investigation of the presence and the degree of equilibrium in the uranium and thorium decay series, as only the mass concentration of uranium, thorium, and potassium in the sediment is determined. Thus, the fundamental assumption in dose rate calculations based on NAA results is that the decay chains are, and have always been, in equilibrium. Gamma-ray spectrometry, in contrast, measures the activity of several daughter isotopes deriving from the U and Th decay chains. If only nuclides in the lower half of the decay chain are measured by γ-spectrometry, it is assumed that equilibrium at least has prevailed since deposition. Only if the activity ratio between different radioisotopes belonging to the decay series is one (state of equilibrium) the parent concentration can be determined from the activity of one or several daughter product activities measured by γ-ray spectrometry.

To allow an assessment of the existence and degree of disequilibrium in the samples investigated in this study gamma-ray spectrometry measurements were carried out for a range of samples in addition to the neutron activation analysis. If the decay series are in equilibrium both analytical approaches ought to yield the same concentration values for a sample within statistical uncertainties. In case significant differences are observed the decay chain is suspected to be in disequilibrium state, and, as the deviating daughter nuclide is to be identified by γ-spectrometry, the position of the opening in the decay chain can be determined as well. However, once a disequilibrium is found in the decay chain, an accurate dose rate determination would require both the U analyses and a knowledge of where the disequilibrium occurs in the uranium series and, of course, since when. READHEAD (1987) for

example presents a range of equations which are required when dose rates are modelled in case of decay series known to be in disequilibrium.

As indicated in Fig. 6, the first daughter isotope from the ^{238}U decay chain measured by the high-resolution γ-ray spectrometer used in the Cologne laboratory is ^{226}Ra. Therefore, the gamma-spectrometry results allow identification of disequilibria caused by gaseous diffusion of the radon isotope ^{222}Rn. No significant excess of ^{226}Ra compared to the next daughter isotope measured, here ^{214}Pb, was found. Therefore it can be concluded that the U decay chain is at least near equilibrium in the lower half.

Given a sufficient precision of the analytical approaches the comparison of the concentration of the mother isotope ^{238}U determined by NAA with the abundance of the daughter products further below in the decay series measured with γ-spectrometry allows detection of disequilibrium also in the upper half of the U decay chain:

> NAA > γ-spec. U content = daughter products deficient due to mobilisation from the system (leaching, diffusion)
>
> NAA < γ-spec. U content = daughter products show higher activity than ^{238}U, excess due to transport and deposition into the system

Fig. 12: Comparison of ^{238}U and ^{226}Ra contents from NAA and gamma-ray spectrometry, respectively, to check for radioactive disequilibria in the upper half of the uranium decay chain.
The solid line represents the 1:1 ratio (condition of secular equilibrium). The dashed lines mark the level of 20% of equilibrium.
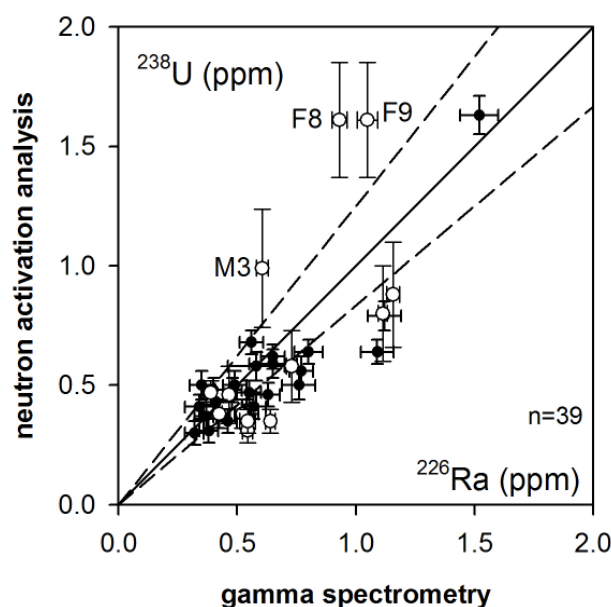
In Fig. 12 the ^{238}U concentration derived from NAA is compared with the ^{226}Ra content, which was the first daughter isotope measured by γ-spectrometry, to get an assessment of the existence and degree of disequilibria in the upper part of the ^{238}U decay chain. The mean average ratio (^{238}U/^{226}Ra) including all 39 samples is 0.94±0.29. However, in 17 of the samples the differences in concentration values are less than 20 % (U/Ra ratio between 0.80 and 1.20), but in 19 samples the difference exceeds 20 %. It is difficult to assess to what extent this discrepancy really indicates a disequilibrium or is just due to analytical uncertainties in the NAA, which were caused by low U contents close to the detection limit and the use of only small sample amounts. Taken the depositional context into account, no systematic trend is observed for the non-aeolian deposits from wet environments showing a higher discrepancy than those samples taken from dry dune sites. Therefore the inconsistency in the analytical results seems not be strictly indicative for the presence of disequilibrium, but is assumed to merely reflect analytical problems.

However, three samples were found to even exceed the ratio of 0.5 or 1.5, respectively (see samples F8, F9 and M3 in Fig. 12). In case of sample M3, a dune sand sample, the ratio between NAA and γ-spectrometry results of the Th content was also found to differ significantly (ratio 1.7). Therefore it is concluded that analytical problems rather that a disequilibrium cause the significant difference in the U concentration. Despite the large errors observed in the NAA results, for samples F8 and F9 the occurrence of a disequilibrium in the U decay chain can not be excluded. The ratios found in the comparison of the Th results are only 1.03 and 1.13 for F8 and F9 (K: 0.95 and 1.09). Both samples were taken from dune sand layers within the level of groundwater fluctuation and were saturated by water at the time of sample collection. Moreover, these sediments are overlying peat layers. This environment may enhance the establishment of disequilibrium in the U decay chain (see section 3.3.3.1). Therefore a likely disequilibrium has to be taken into account in dose rate and age calculation which will be further discussed in chapter 1.

For four samples also under suspicion of disequilibria in the U decay series because of their depositional history in wet environments low-level gamma-ray spectrometry measurements were carried out (see chapter 1 for further details on the samples). Because daughter isotopes of the upper half of the ^{238}U decay chain are measured, the existence of disequilibria can be tested by internal comparison of the daughter concentration. By that the additional error which arises from comparing different analytical approaches is eliminated.

The results for the U determination are shown in Fig. 13. No conclusive evidence for disequilibria in the uranium decay chain was found.

Fig. 13: High-resolution low-level gamma-ray spectrometry results for samples from wet environments being suspected of being not in equilibrium state.
All analyses were carried out by Dr. A. Kadereit, Forschungsstelle Archäometrie, MPI, Heidelberg, who also kindly provided the graph. Disequilibrium is indicated when the concentration values disagree in the 2σ-error range. The error bars shown in the graph represent the 1σ-errors. All values agree on the 2σ error level, therefore equilibrium is assumed for all the four samples. With reference to Fig. 6 a significant difference between the [234]Th and the [226]Ra content could indicate a disequilibrium caused by a loss of [234]U, for example when [234]U in its +6 oxidation state forms water soluble uranyl complexes, which are transported out of the system by percolating water. Significant excess of [226]Ra compared to the subsequent Pb and Bi daughter concentrations in the lower half of the decay series could provide evidence for disequilibrium due to migration of the noble gas radon, which follows in the [238]U decay chain as immediate daughter on [226]Ra (see Fig. 6).
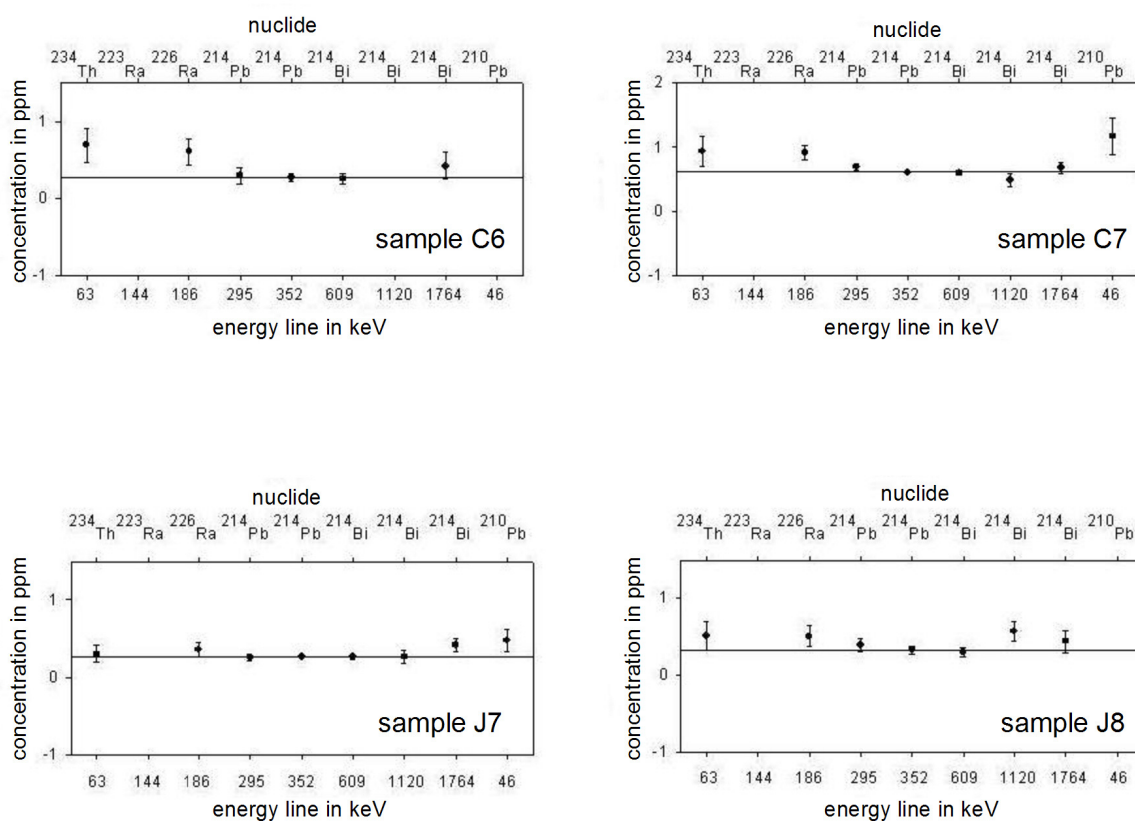
To evaluate the impact of unidentified disequilibria on the luminescence ages it has to be referred to the literature. Several studies have been carried out which present assessments for the uncertainty resulting from dose rate calculation erroneously assuming equilibrium. The implications of a radioactive disequilibrium for age calculation are discussed for example by OLLEY et al. (1996): for samples with average U, Th, and K activities showing significant (e.g. 50 %) disequilibrium in the U decay chain, dose rate estimations based on parent nuclide concentrations (e.g. NAA), thus erroneously assuming the decay chain is, and has always

been, in secular equilibrium, can result in an additional error in age calculation of 8 %. Regarding the samples investigated in this study this error should be smaller as the β- and γ-dose derived from the ^{238}U decay series contribute on average about 10 % to the total dry dose rate (see Table 4). This value is considerably lower than the 27 % contribution OLLEY et al. (1996) used for their calculations for sand deposits.

KRBETSCHEK et al. (1994) calculated a dose rate for sediments showing disequilibrium in the uranium decay chain indicated by a significant ^{234}U excess. The difference in the luminescence ages between the value based on the dose rate model taking the disequilibrium into account and the NAA based age value, which only considers the present day ^{238}U content, was only 8 % for a sediment deposited ~10 ka ago. With this sample derived from fine grained limnic sediments and a U content of more than 3 ppm the contribution of the uranium decay to the annual dose has to be considered to be much higher than in case of the dune sands investigated in this study with average U contents of less than 0.5 ppm. Furthermore the alpha dose contribution from U can be neglected in dose rate calculation for the etched quartz grains, whereas in the example of KRBETSCHEK et al. dealing with fine-grain dating it had to be taken into account.

Finally it is concluded, that even if a similar disequilibrium in the U series exists in the one or the other sample and is not identified and allowed for, the influence on the age calculation is assumed to be less than 8 %.

3.3.4.5 Assessment of the internal dose rate in quartz

The assumption that quartz contains no inherent radioactivity may not be generally valid. To get an estimation of internal dose contribution for the samples investigated in this study, 17 HF-etched quartz samples were analysed by neutron activation. The detection limit (DL) for K was 100 ppm, that for U 0.1 ppm. No measurable concentrations were found in the samples for U and K. But small amounts of Th were found in each sample (DL 0.05 ppm or 0.1 ppm), with a maximum value of 0.61 ppm and a minimum of 0.08 ppm with a mean value of 0.23±0.11 ppm for the 17 samples. Using the conversion factor given by MEJDAHL (1987) the beta dose rate of Th within the quartz grains would contribute on average only ~ 0.15 % to the total dry dose rate of the samples investigated here. The cosmic dose contribution is not considered here. If this would be added, the contribution of the internal dose would be even

lower. Finally it is concluded, that the internal radioactivity of quartz grains is negligible for the dose rate determination and subsequent age calculation in this study.

3.3.4.6 Water content estimation

The estimation of the uncertainty of the water content for dose rate calculation in this study was based on what is known about the history of the deposits and on the measured values of moisture contents (weight of water in % of the weight of dry sediment), which were determined from the loss of weight after drying (see Appendix A, Table A 4). Because present day moisture contents are not expected to be representative for longer time periods, all analysis for water content have been summarised to optimise the moisture content assumption. All samples taken from or from directly encompassing a palaeosol horizon were excluded from this analysis. These horizons contain a proportional higher content of fine grained material than the unweathered dune sand, thus resulting in generally higher moisture contents (higher also in the overlying sand and lower beneath because of poor drainage). Samples from other extraordinary sand layers such as influenced by varying ground water tables identified by soil properties etc. were also excluded.

The purpose of this data summary was to provide an improved overview of variations in moisture contents in dune sands as sections were included that had been sampled at different seasons throughout the year. Furthermore, to obtain a larger data set allowing for more variations, several sites were included from the western part of the European Sand Belt (The Netherlands, see FINK 2000, and western Germany, see WARREN 2002 and unpublished material) which at present are influenced by oceanic climate on contrary to the study area with a higher continentality of the climatic conditions. The incorporation of these water contents into the data summary is supposed to give a better estimation of the potential range of moisture content.

As shown in Fig. 14 most of the 182 samples have water contents between 2 to 6 weight-%. The mean and its standard deviation are 4.5 and 2.5 %. The average analytical error derived from the deviation of duplicate measurements of the 'as found' water contents for the samples of this study is about 10 %.

Fig. 14: Distribution of 'as found' water contents (expressed as water mass/dry mass) determined for 182 dune sand samples taken from dunes sites within the European Sand Belt.
The choice of samples is further explained in the text.
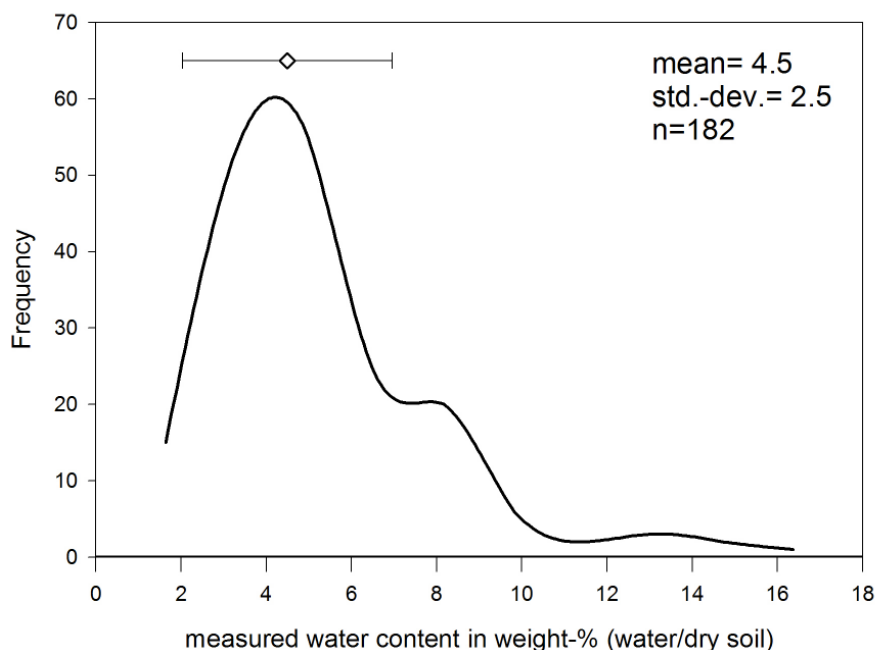
In this study for each sample dose rates were calculated assuming a minimum and a maximum water content depending on the measured moisture values, with 2.0±0.2 and 7.0±0.7 weight-% (equals the 1σ error range of the average water content) being the most frequently used values (see Appendix A, Table A 4). Higher values were used for samples with on average higher actual wetness, such as samples from soil horizons or with influence of fluctuating water tables.

Of course 7 % does not equal the maximum field capacity of sandy sediments. This varies with sorting and particle size distribution. In soil horizons with an increase of the proportion of fine grained material and organic matter content the field capacity is higher compared to the unaltered sediment. For a set of sand samples the saturation water content was measured by re-wetting of the sediment resulting in an average water content of 30 weight-% (mass water/mass dry sediment). This value would represent the maximum water content for the sands, which could be used to determine the absolute minimum dose rate. But this was not considered as it would introduce a large error in the dose rate estimates, for which no sound explanation could be given. In the well drained dune sands water saturation over longer periods can be excluded for sure. The upper and lower limits of moisture content as mentioned above mostly 7 and 2 % were established on the basis of the measured 'as found'

water content value range (see Fig. 14) combined with considerations regarding the pore volume of sandy soils.

Distribution of pore voids in terrestrial sandy soils (see SCHEFFER/SCHACHTSCHABEL 1992: 149) (note, that these values are related to soils, which contain higher amounts of fines and organic matter increasing on average the water capacity):

Coarse pore voidsfilled, if saturated, mostly water free, well drained		30±10 %
Medium pore voids	fluctuating water content	7±5 %
Fine pore voids	water filled in general	5±3 %

The study area was within the distribution of permafrost at least for a certain period of time at the end of the last glacial. Permafrost may have an effect on the dose rate calculation, because due to different densities of water, air, and ice filling in the pore voids different factors for radiation attenuation would apply. But here such differences in radiation attenuation were not considered in the water content assumption. The radiation attenuation factors for ice are not that different to those of water (see section 3.3.3.3) given a similar density of water and ice. Furthermore, permafrost was present in the study area according to RENSSEN and VANDENBERGHE (2003) during the Last Glacial Maximum (continuous permafrost) and during the Younger Dryas cold period (discontinuous permafrost, or at least seasonally deep frozen ground, HELBIG 1999). Only the latter has had an impact on the Late Glacial deposits investigated in this study. The Younger Dryas climate conditions prevailed for about 1000 years. This would result in a percentage of only ~7 % of the total burial time for a 15 ka old deposit during which the sediment might have been affected by frozen ground conditions. Furthermore, the well drained dune sands, which were predominantly sampled for luminescence dating, did not show prominent sediment structures being indicative for severe frost action. Therefore they are expected not to be affected considerably by permafrost.

The impact of an erroneous water content assumption on the error of luminescence ages is illustrated in Fig. 15 as the additional uncertainty in ages which arises from a 10 % over- or underestimation of the water content. For comparably dry sediments with water contents of less than 10 % the additional error introduced in the ages by erroneous water content estimates is small compared to the overall error in the OSL ages of ~ 8 % as found for the samples of this study. The impact of erroneous moisture assumptions is more significant for

samples from wet environments than for those from dry sites. But even for an absolute pore water content of 30 %, which equals the average saturation water content of the sediments investigated here, the additional error is still just 5 %.

Fig. 15: Impact of erroneous water content assumptions on the relative uncertainty of luminescence ages.
The extent to which the error in age increases in case of an erroneous water content estimate depends on the total water content of the sample. Here, the increase of the relative uncertainty is shown for an over- or underestimation of the relative actual soil moisture content by 10 % (from GEYH 2005: 111).

Increase of the relative error in ages (in %) with false water content estimation by 10%

absolute water content in %
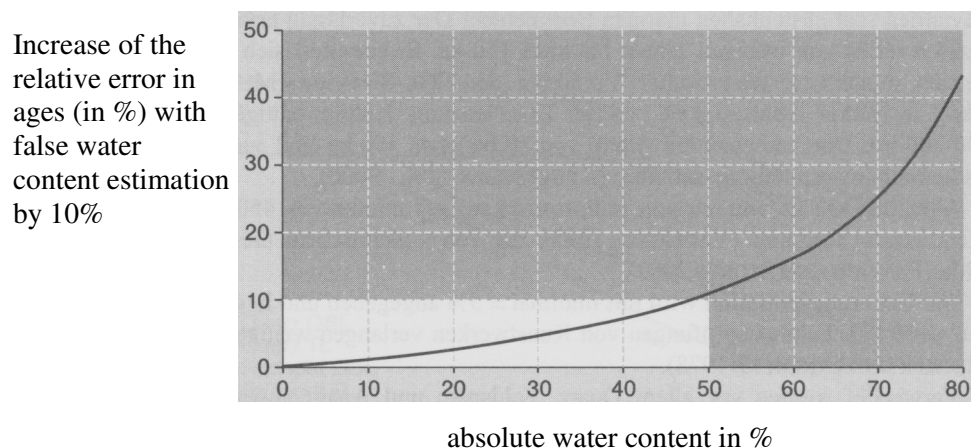
3.3.4.7 Impact of varying overburden thickness on the cosmic dose contribution

The software, which was used for dose rate calculation in this study (see section 3.3.5), calculates the cosmic ray dose contribution dependent on the sampling depth and considers the soft component in the range of 0 to 75 cm and radiation attenuation in sediments of a density of 2 g/cm³. All sites investigated in this study are located in lowland areas north of 40° N. For this reason the variations in cosmic radiation intensity dependent on geographic latitude and altitude have not been considered in detail. Variations in the magnetic field intensity of the earth are negligible for the relevant time span of only 20 ka in this study (PRESCOTT & HUTTON 1994).

The cosmic dose contribution to the total annual dose was found to range from 8 to 30 % of the annual dose, with on average the samples receiving 17±5 % of the total dose rate via the cosmic contribution. This average value is relatively high; therefore the cosmic dose contribution was investigated in more detail. First, the cosmic ray dose rates were calculated according to the present burial depths for all samples. For those sites being identified as composite profiles, whether based on these first age results and/or from field observation, the

cosmic dose contribution was calculated in detail including a variation of the sample's depth below surface due to the sedimentation history of the particular site. The procedure was adapted from that described by MUNYIKWA (2000). In Fig. 16 the modelling carried out for site 'Neuhaus' is presented in detail. Basically, for each period of deposition and burial an individual cosmic dose rate is calculated for the burial depth at that time. Finally, the individual dose rates are added to the total cosmic dose contribution which is than included in the calculation of the annual dose since deposition. A sufficient sampling resolution is necessary to allow such reconstruction.

From the model calculations carried out for the various dune sites it is concluded, that the modelling of the sedimentation history generally showed only minor changes in the total cosmic dose contribution. For most profiles the modelling had no significant influence on the finally resulting OSL ages. The relative difference between the ages that were calculated without taking variations in the overburden thickness into account to those ages based on the cosmic dose calculated for the contemporary sampling depth is only in the range of 1 to 8 %, on average only ~3 %.

Only at sites 'Neuhaus' and 'Jänschwalde' the modelling of the variation in cosmic dose contribution resulted in substantially, though still not significantly different age results showing a differences in ages of 7 and 8 %, respectively. At both sites a several thousand years old surface was covered by a several metres thick only a few hundreds of years old dune sand unit. At 'Jänschwalde' deposits of ~14.5 ka with dose rates < 1Gy/ka were buried with about 4 m of dune sand about 1800 years ago. At 'Neuhaus' ~12 ka old dune deposits with dose rates <1Gy/ka were covered by more than 4 m of dune deposits only 300 years ago.

It is concluded that the adaptation of the cosmic dose contribution to a model of the sedimentation history may improve the accuracy of OSL ages distinctly. But this holds true only if the sampling site meets several conditions, such as (i) a young (several hundred years) and (ii) thick (several metres of sediment) deposit on top of a considerably older sediment section. Furthermore, the detailed reconstruction of variations in the cosmic dose should be taken into consideration for sampling sites with extremely low terrestrial natural radioactivity as here the overall contribution of cosmic radiation to the annual dose might be even the main source of dose rate.

Fig. 16: The problem of modelling the cosmic dose contribution at sites with multiple phases of sedimentation.
a) Illustration of the reconstruction of the depositional history at site 'Neuhaus'. **b)** Illustration of the procedure applied to assess the best approximation to the 'true' cosmic dose contribution at site 'Neuhaus' following MUNYIKWA (2000).
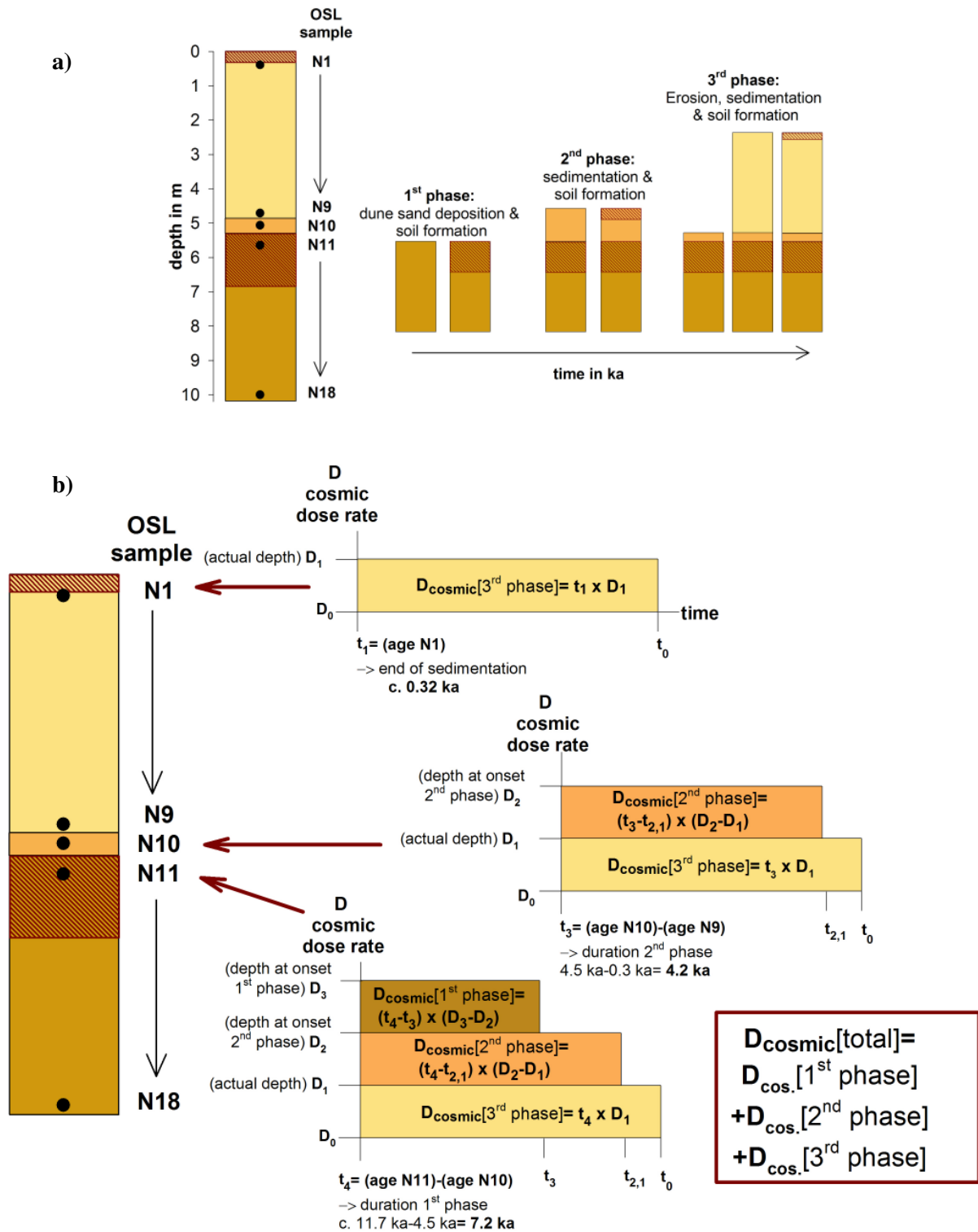
3.3.5 Dose rate calculation

Combining the various details described above kDthe total annual dose (D_0 in µGy/a or Gy/ka) for sand-sized quartz is finally calculated from:

$$D_0= (k\ D_{\alpha,\ dry}/1+HWF)+(b\ D_{\beta,\ dry}/1+HWF)+(D_{\gamma,\ dry}+D_{cosmic}/1+HWF)$$

where k is the relative measure of the poorer effectiveness of alpha particles compared to β and γ radiation (here a value of 0.035 was included according to BELL & ZIMMERMAN 1978, see section 3.2.1)

b takes into account the attenuation of the beta contribution dependent on the grain size used for dating (here values ±0.90 were taken into account according to MEJDAHL 1979, see also BRENNAN 2003, section 3.3.1)

the factors HWF correct for the effect of absorbed water in the sediment with H being the attenuation factor for α, β, and γ radiation with 1.5, 1.25, and 1.14 respectively and WF describing the water content (see section 3.3.3.3)

It is noted, that the alpha contribution from external radioactivity to the grains is negligible, because most of the outer alpha-irradiated shell is assumed to be removed by HF etching (assumption here 10±5 µm).

Dose rate calculation for all 183 samples of this study was carried out using the software program "*age calculation*" written by R. GRÜN, Canberra (revised version 1999), which is based on the dose conversion factors of ADAMIEC and AITKEN (1998).

In Appendix A, Table A 4 the results of the dose rate calculation are summarised together with various parameters necessary for dose rate determination. The average dose rate based on radionuclide concentrations measured by neutron activation analysis is 1.09±0.33 Gy/ka with values ranging from 0.68 to 2.18 Gy/ka. On average the relative 1 σ error of the of the D_0 values is ~6 %.

In case the dose rate calculated from the radionuclide contents determined by NAA agreed with the D_0 values based on the γ-ray spectrometry results at the 2σ level, the average of both values was generally used for age calculation. All dose rates finally included in the age calculation are summarised in Appendix E, Table E 1.

3.4 Using quartz as 'natural dosimeter' for palaeodose estimation by OSL

In section 3.2 the nature of ionising radiation and its interaction with quartz in particular was explained. In the following the processes will be described by which this environmental radiation is absorbed and stored in quartz crystals.

Charge interactions within an imperfect crystal lattice are the fundamental condition for luminescence production in minerals. For a better understanding of the processes giving rise to luminescence phenomena, a brief introduction will be given into some basic physical principles and the crystal structure of natural quartz and its lattice defects responsible for luminescence production.

3.4.1 Physical background for luminescence phenomena

Luminescence (from lat. *lumen*= 'cold light') is the emission of light produced for example by heating a solid to a temperature below that of incandescence (thermoluminescence, TL), by exposing it to light (photoluminescence), or ionising radiation (radioluminescence, RL, radiofluorescence, RF). While the term luminescence was first introduced by WIEDEMANN in 1888 (WIEDEMANN & SCHMIDT 1895 in KRBETSCHEK 1995), the luminescence phenomenon itself was described already much earlier by ROBERT BOYLE (1664, in AITKEN 1998). The occurrence of luminescence is explained as light emission due to charge transfer in substances with ordered structures, such as, for example, crystals of minerals. The mechanism in general is described on the basis of the so-called *energy band diagram* or *energy level model*, which is commonly used in solid state physics to explain energy transfer processes in conducting and semi-conducting materials, and insulators. The model consists of two energy levels or bands. The *valence band* represents the ground state of atoms with all energy states filled. The *conduction band* represents the unstable, excited states of freed electrons. In case of semi-conducting or insulating materials inbetween these two energy levels a 'forbidden energy gap' exists., The width of this gap is determined by the amount of energy which is necessary to transfer an electron from the valence band into the conduction band, or from the ground state to the excited state, respectively. Thus, semi-conducting materials show forbidden gaps of <3 eV and insulators even 'broader' gaps of 3 to 12 eV (STEFFEN 2000: 75). Quartz, the mineral used as natural dosimeter in this study, can be classified as insulator.

Excursus I illustrates, how to derive the abstract energy band model starting from the atom representing the smallest element of structure. For further explanations the reader is referred to basic literature of solid state physics (for example IBACH & LÜTH 1995).

3.4.1.1 Crystal structure, defects, centres and traps

An ideal crystal (represented by an energy band model such as shown in Excursus I) would exhibit no luminescence after exposure to sufficient energies to ionise electrons and transfer them across the forbidden energy gap into the conduction band. The electrons would remain in the excited state for a certain time, but then would return radiation-less to the valence band. The energy difference between the excited state and the ground state would be emitted as heat.

Luminescence production is coupled onto the existence of defects in the crystal lattice structure which serve as traps for the released electrons. Such charge traps are located within the forbidden gap. Imperfections are observed in nearly all naturally occurring minerals. They are already produced at the time of crystallisation. The range of defects varies with different thermodynamic conditions in a magmatic, metamorphic, or diagenetic context that have an impact on the processes of crystallisation. Furthermore, lattice defects can be created as radiation damage due to bombardment with alpha- or beta-particles, gamma-, X-rays, ultra-violet radiation, protons or neutrons. In case of the incorporation of radioactive elements such as uranium or thorium into the lattice, the crystal structure is considerably destroyed, if the radioactive decay and hence the ionising radiation considered to be effective on a geological time scale (for further details see KRBETSCHEK et al. 1997 and STEFFEN 2000). These statements given on the creation of crystal lattice defects underline the strong dependence of type and frequency of defects on specific conditions during formation, subsequent geological history and depositional context (e.g. strength of environmental radioactivity) of a crystal. As such, defects are a general precondition for luminescence phenomena; it is not surprising then that crystals, although of the same type of mineral, may show quite different luminescence properties according to the provenance and formation processes.

Excursus I: From the model of an atom to the energy level scheme

The ‚atomic level'

Motion of electrons in orbits on the inner atomic shells is characterised by wave functions with smaller amplitudes than for electrons in orbits on outer shells. Therefore orbits close to the nucleus more or less maintain their shell characteristics. The broader wave function of electrons in orbits on outer shells is a crucial requirement for the more distinct broadening, which in turn supports the possibility of an overlap with orbits of adjacent atoms to create molecule orbits.

Electron distribution in atomic structures:

Distance from the nucleus increases	Atomic shells	Number of electrons in s-, p-, d-, and f-orbits				Max. number of electrons	Max. number of orbits
		S	p	d	f		
	K	2	-	-	-	2	1
	L	2	6	-	-	8	4
	M	2	6	10	-	18	9
	N	2	6	10	14	32	16
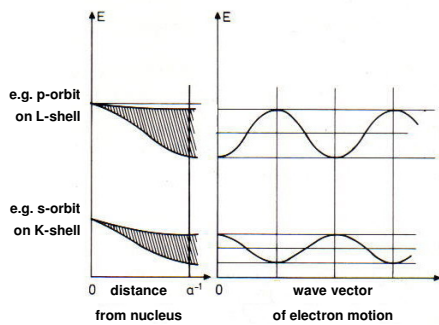
modified from Ibach & Lüth (1995): 140

The ‚molecule level'

The outermost orbits of adjacent atoms form molecule orbits, splitted up into the binding (filled with valence electrons responsible for chemical binding) and anti-binding orbit (free of electrons).

based on Ibach & Lüth (1995): 4 & 141
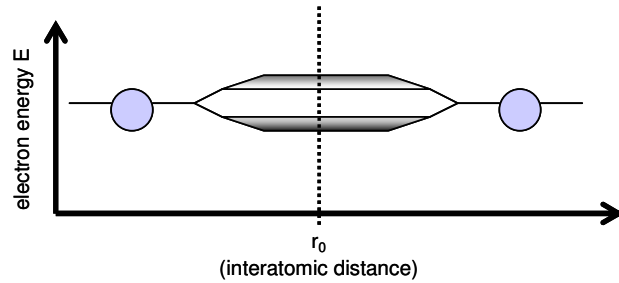
- anti-binding molecule orbit
- forbidden gap
- binding molecule orbit
- nucleus and atomic inner-shells

The ‚crystal level'

Because of the dense packing of atoms in solid matter such as crystals, molecule orbits form quasi-continuous bands.
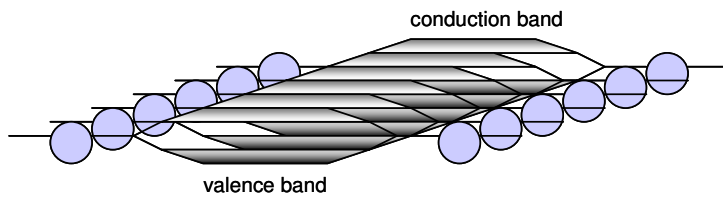
Model of the ‚crystal level'

The generalised *energy band* or *energy level model*
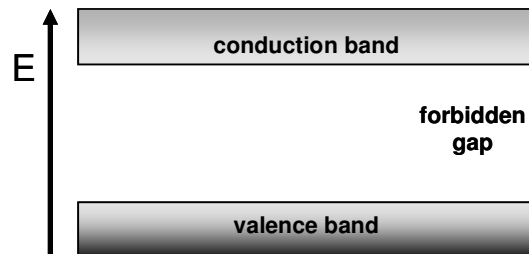
Knowledge of the defect characteristics is predominantly based on observations from electron paramagnetic resonance (EPR, or electron spin resonance - ESR), cathodoluminescence (CL) or radioluminescence (RL) measurements, combined with infrared spectroscopy, absorption measurements, and thermoluminescence studies (TL). Although there were already numerous comprehensive studies carried out on lattice defects, the correlation of radiation-induced phenomena with particular impurities is not fully understood (KRBETSCHEK et al. 1997, GÖTZE et al. 2001). According to their dimension in the lattice structure, defects are differentiated into point defects, and more extended line defects and face defects. Point defects occur in all, even very pure crystals, and are predominantly responsible for luminescence production in crystals. Three types of point defects are observed:

- vacancies: position in the lattice is not occupied
- interstitals: ion occupies an interlattice position and its position in the lattice structure is free, or a foreign ion is incorporated on an interlattice position for charge compensation
- substitution: foreign or impurity ions with similar ion radius substitute ions of the lattice

For a further description of defect types and circumstances of defect creation in various minerals the reader is referred to the literature, for example STEFFEN (2000) and KRBETSCHEK et al. (1997). In particular the latter study focuses on minerals suitable for dating (including detailed explanations of quartz). Here, only some typical defects in quartz are described which are predominantly involved in the creation of luminescence emissions.

Fig. 17: The crystal structure of alpha-quartz. Chemically quartz (SiO_2) is quite a simple structure. The most common form is the trigonal low-temperature alpha-quartz (in the following referred to as simply 'quartz'), which is thermally stable up to 573°C (ROTHE 1994, STEFFEN 2000). The basic component of the crystal lattice of quartz is the $[SiO_4]^{4-}$ tetrahedron, building angular connected hexagons with oxygen ions serving as junctions for two neighbouring tetrahedral.
a) three-dimensional network of linked $[SiO_4]^{4-}$ tetrahedra; here only the central Si ions are shown with different hatching indicating different horizontal levels (redrawn from KRBETSCHEK et al. 1997: 702)
b) model of a SiO4 tetrahedra with oxygen atoms placed on the corner positions and a silicon atom in the centre; for charge compensation of the resulting negative charge each O ion is linked to an other tetrahedron thus constructing the three-dimensional lattice structure (modified from ROTHE 1994: 19)
c) proportions of Si, O, and Al ions as a typical substitute for Si according to the ion radius (1 Å=10^{-8} cm) (values from ROTHE 1994: 19, KRBETSCHEK et al. 1997: 702)
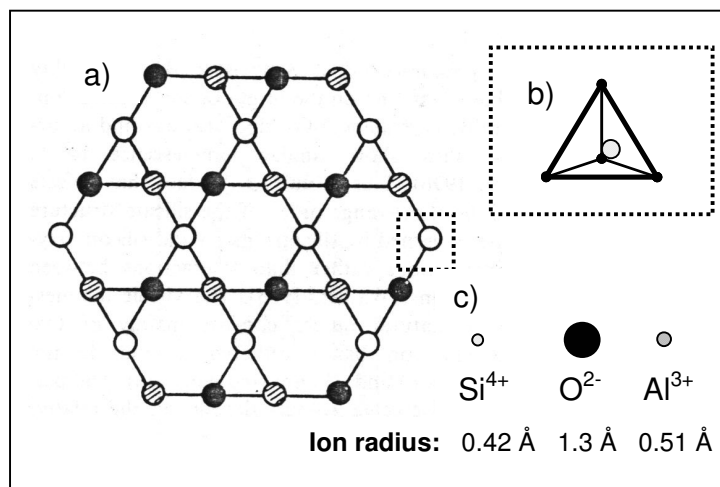
Starting from the idealistic scheme as presented in Fig. 17, the real quartz structure shows several point defects involved in luminescence mechanisms. Some of these defects are illustrated in Fig. 18. Aluminium is found to be a common trace element in quartz, where it substitutes the silicon atoms in the lattice. Besides the fact that Al is one of the eight most common elements in the Earth's crust, Al ions are typical substitutes for silicon. This is due to their likewise high valence and the similarity of the ionic radii of Al^{3+} (0.51 Å) and Si^{4+} (0.42 Å) (for comparison, the ion radius of oxygen is 1.3 Å with 1 Å=10^{-8} cm) (ROTHE 1994: 19, KRBETSCHEK et al. 1997: 702). Other substitutes are, for example, Ge^{4+} (0.53 Å), Ti^{4+} (0.64 Å), and Fe^{3+} (0.64 Å). From the schematic structure shown in Fig. 17 it becomes obvious that the three-dimensional crystal lattice of quartz contains sizeable hollow space in-between the linked $[SiO_4]^{4-}$ tetrahedra. In these structural channels interlattice positions are located, which play an important role in the creation of lattice defects. Additional cations, such as for example H^+, Na^+, K^+, or Li^+, can be incorporated on these interlattice positions for charge compensation (STEFFEN 2000, KRBETSCHEK et al. 1997, see Fig. 18 c).

Fig. 18: Some typical defects in the crystal structure of quartz.
(based on STEFFEN 2000 and Tab. 2 in KRBETSCHEK et al. 1997: 704).

Substitution
Al^{3+} substitutes a Si^{4+} position:
deficit of a positive charge

a)
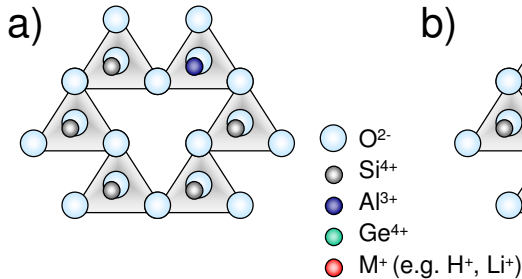
Vacancy
silicon vacancy :
excess of negative charge

b)

○ O^{2-}
○ Si^{4+}
● Al^{3+}
● Ge^{4+}
● M^+ (e.g. H^+, Li^+)
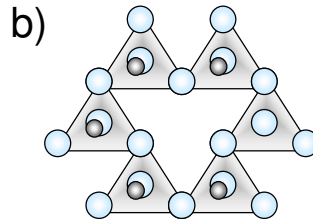
Defects resulting in deficit of positive charge or excess of negative charge → trapping centre for defect electrons = ‚**hole traps**'

Substitution and interstital
Ge^{4+} substitutes a Si^{4+} position,
cation on interstital position:
excess of a positive charge

c)
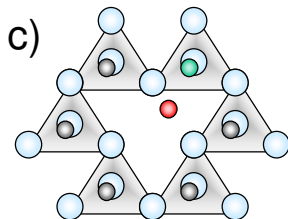
Vacancy
oxygen vacancy :
deficit of a negative charge

d)
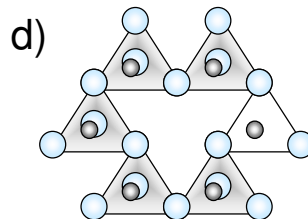
Defects resulting in excess of positive charge or deficit of negative charge → trapping centre for electrons = ‚**electron traps**'

These defects have in common that they are all characterised by either a charge excess or a charge deficit when compared to the charge equilibrium state of the perfect crystal lattice structure. Thus, two types of charge centres or charge 'traps' are differentiated and can be added to the model shown in Excursus I: the electron centres and the defect electron centres.

-Electron centres or electron traps (see Fig. 18, c and d): A defect which is characterised by an excess of positive charge or a deficit of negative charge tends to reach charge equilibrium with an electron. Consequently, excited electrons are attracted and trapped at such defects. Within the forbidden gap electron traps are found close beneath the conduction band.

-Defect electron centres or hole traps (see Fig. 18, a and b): In case an atom is ionised and an electron is knocked out the atomic structure, an unstable 'hole' is left behind. This defect electron represents an orbit not filled with the maximum number of electrons. Although this state does not exhibit charge equilibrium state it remains in the valence band, but concentrated in the energy level scheme at the upper level of the valence band, close to the forbidden gap. Regarding their dynamics, 'holes' or defect electrons behave like positively charged particles (IBACH & LÜTH 1995). Defects with a lack of positive charge or an excess of negative charge

are located in the forbidden energy gap near the upper level of the valence band and attract such positive 'holes', which are concentrated at the upper edge of the valence band. These trapping states play an important role in the production of luminescence emission. A filled hole trap represents a luminescence centre or recombination site that finally gives rise to the light emission known as luminescence after the recombination with an electron.

3.4.1.2 The luminescence phenomenon - a simple 'one-trap/one-centre' model

Nearly all conventional descriptions and explanations of the luminescence phenomenon start with the simple 'one-trap/one-centre' model introduced 60 years ago by RANDALL and WILKINS (1945, in MCKEEVER & CHEN 1997). Unfortunately, this simple model is far from reality in the sense that it is rare to find a real material for which it provides an accurate explanation for the wide variety of phenomena occurring in the creation of luminescence. As more and more perplexing luminescence behaviour is observed in experiments, more and more complex models have to be applied to explain those phenomena (see e.g. review given by MCKEEVER & CHEN 1997, MCKEEVER 2001, BØTTER-JENSEN et al. 2003). For the sake of simplicity the simple 'one-trap/one-centre' model is chosen here to describe the basic mechanism of luminescence.

The simplified energy level diagram illustrated in Fig. 19 (a) consists of one electron trap, formed by an oxygen vacancy defect, and one hole trap, formed by an Al^{3+}-substitution defect. This may be seen as the starting point. The next step is the phase of ionisation, the influence of ionising radiation which is ubiquitous in natural environments (see section 3.2 for detailed description on the source and nature of environmental radioactivity). The activation energy of this natural ionising radiation is sufficient to remove electrons from atoms and to provide them with energy to move around in the crystal, or, with regard to the energy level scheme, to transfer them to the conduction band. Because this excited state is unstable, after a certain time the freed electrons are trapped at defect positions in the lattice structure, for example an oxygen vacancy with one electron missing for charge equilibrium (Fig. 19 b). But it must be noted here, that the majority of electrons return radiation-less to the ground state, the valence band.

Fig. 19: Energy-level representation of the OSL process.
(modified and redrawn from AITKEN 1998: 14, WAGNER 1995:132).
a) Simplified scheme of defects in the crystal structure of quartz and translation of this defect structure into an energy level diagram representing a simple 'one-trap/one centre' model.
b) Exposure to ionising radiation (from natural sources like lithogenic radionuclides and cosmic radiation or from artificial irradiation in the laboratory) causes trapping of electrons and holes at defects.
c) Stimulation by light exposure (sunlight or light source of appropriate wavelength in the laboratory) releases the trapped electrons. The latter may recombine with a hole centre, subsequently giving rise to the emission of light.
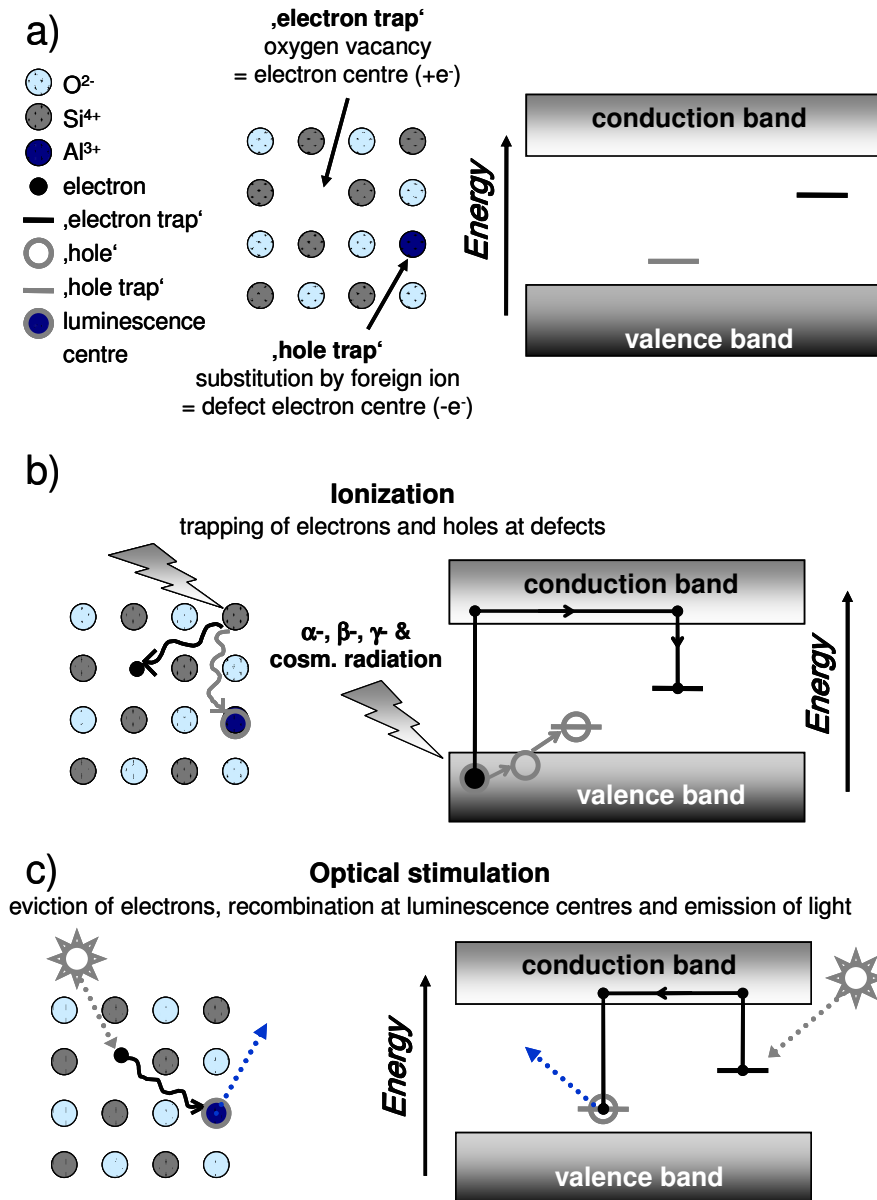
On the other hand, in the valence band a deficit of one negative charge remains unfilled, this hole is trapped by a hole trap, for example an AlO_4-centre on a silicon site in the lattice structure (Fig. 19 b). This hole trap together with the hole forms a 'recombination centre'.

This process of increasing charge absorption at defects maintains until the radiation flux is stopped and stimulation energy such as heat (thermally stimulated luminescence or thermoluminescence, TL) or light of appropriate wavelength (optically stimulated luminescence, OSL) is added to the system (Fig. 19 c). With the heat or light energy supply the trapped electrons are activated and transferred back onto the higher energy level of the conduction band. After short diffusion in the conduction band these electrons return to the valence band, a process being non-radiative (heat emission), or they are captured by electron traps again. Just a small percentage of electrons reach luminescence centres. If so, in the recombination process the energy difference between the conduction level and the energy level of these luminescence centres is emitted as light. This is what is measurable as luminescence signal. The luminescence emission stops as soon as all electron traps are empty.

3.4.2 Luminescence properties of quartz

To provide the basis for understanding the setting of measurement parameters (e.g. stimulation wavelength), possible sources of error and the various problems occurring during the dating procedure, the luminescence properties of quartz have to be explained in more detail. Although in this study OSL was used for dating, a discussion of luminescence properties of quartz necessarily must include references to the TL characteristics, not only because fundamental knowledge of OSL characteristics is based on TL studies. Furthermore, as will be shown, there is a direct relation between OSL and TL phenomena.

3.4.2.1 Characteristics of electron traps and TL peaks of quartz

The 'one-trap/one-centre-model' was used to describe the basic process of luminescence emission in crystals. A TL measurement in accordance with the 'one trap/one centre model' is expected to exhibit a glow curve with a gaussian shape and only one peak at a defined temperature. This highest luminescence intensity would be observed at the temperature, at

which most of the electrons are released from the traps. Subsequently light is emitted in the process of recombination of these electrons with the luminescence centres.

But if natural quartz is heated, for example up to 500°C, the TL glow curve clearly displays multiple peaks at various temperatures (see Fig. 20 a). The amplitude of a given TL maximum or the intensity of the luminescence emission at a given temperature, respectively, is indicative of the number of radiative recombinations taking place.Such a glow curve can no longer be explained with the 'one-trap-one centre model'. The variety of crystal defects in quartz, which was mentioned already (section 3.4.1.1), makes the appearance of various electron traps and recombination centres most likely.

Fig. 20: **a)** TL glow curves obtained for quartz which has been bleached (100 s green light stimulation at 25°C), irradiated (beta dose of 43 Gy) and preheated for 10 s at 110°C.
The dashed line represents the glow curve of one disc which was given an additional 2 s exposure to green light prior to the TL measurement (from WINTLE & MURRAY 1997: 613).
b) Energy level diagram introducing more electron traps to allow for the occurrence of multiple TL peaks as illustrated in graph a) (R= recombination centre, T_{1-8}= different electron traps giving rise to TL peaks at the given temperatures).
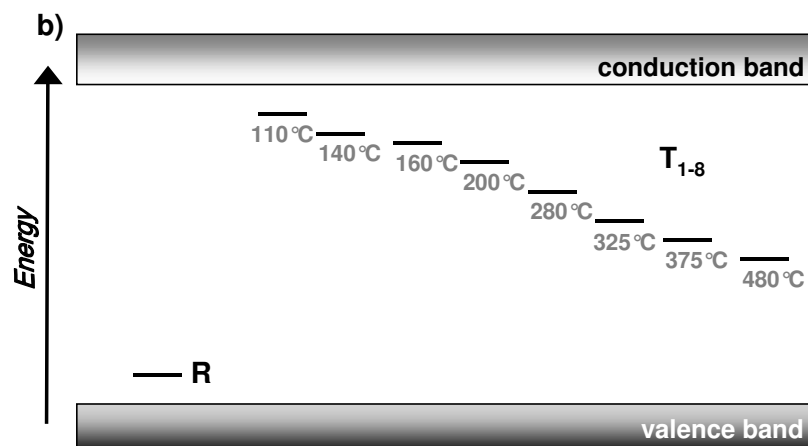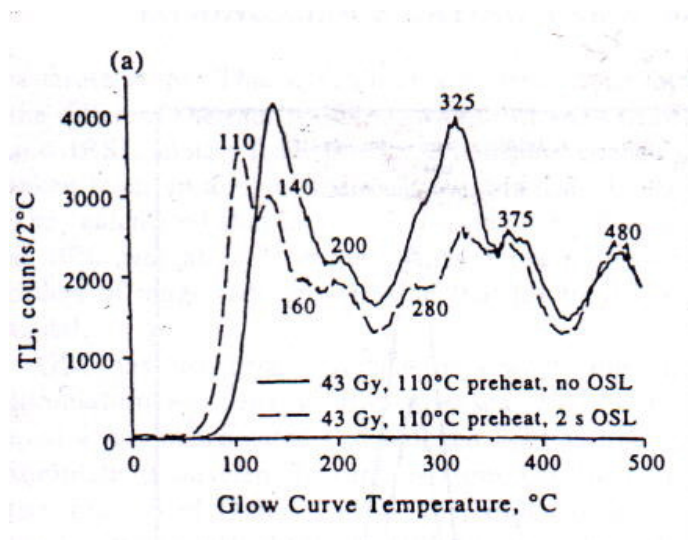
In Fig. 20 (b) a modified energy level diagram includes additional electron traps at various energy levels below the conduction band. TL traps are broadly divided into so-called 'shallow' traps close to the conduction band (in natural samples the initial charge population in these shallow traps is usually zero) and 'deep' traps which are thermally stable at ambient temperatures. The activation energy necessary to evict an electron from a particular trap corresponds with the distance of the trap to the conduction band and the temperature region in which they give rise to a TL peak: electrons in shallow traps require less activation energy for eviction and therefore give rise to TL peaks in the low temperature region. It is difficult to place the boundary between deep and shallow traps at a particular temperature, because peak temperatures are shifted with variations of the heating rate. SMITH and RHODES (1994), for example, relate deep traps to the temperature range from 280 to 400°C more generally spoken, the boundary temperature could be set around 300°C.

The so-called 'trap depth' below the conduction band (expressed in eV) is better suited to differentiate electron traps. This parameter describes the amount of energy which is necessary to transfer electrons in these traps into the excited state. The depth of traps relevant for dating purposes should be in the range of ~1.6 eV or more (AITKEN 1998: 14).

The variety of different electron traps involved in luminescence processes has been illustrated in Fig. 20, but not all these traps are suitable for dating. For dating purposes an electron trap has to meet several requirements:

1. thermal stability: The average residence time at a given temperature (commonly at ambient temperatures of 10-20°C) of an electron in the trap must be several orders of magnitude longer than the time span to be dated.

2. number of traps: The number of available traps must be constant throughout time, any increase or decrease would influence the trapping probability and hence the luminescence signal emission.

3. bleachability: An appropriate, naturally occurring and effective mechanism must exist to reset the geological clock at the event to be dated. In the case of sediment dating, this means that the traps must be light-sensitive allowing them to be emptied by sunlight exposure.

3.4.2.1.1   Thermal stability

Fig. 21 shows TL glow curves of quartz extracted from dune sands. One set of sub-samples represented by the black curves was heated to eliminate all luminescence signals prior to laboratory irradiation with a ^{60}Co-gamma source. The blue curves represent the natural TL emission of the c. 28 ka old sample, corresponding with an equivalent dose of 24.6 Gy. The most obvious difference is the missing of low temperature peaks < 300°C in the natural samples. On contrary, the artificially irradiated samples exhibit strong peaks in this temperature region similar to the glow curve obtained after laboratory irradiation shown in Fig. 20 (a). The shallow TL traps giving rise to peaks at about 160°C and 220°C (for a heating rate of 5°C/s) are unstable; three weeks after gamma-irradiation they are still filled. But in the 28 ka old sample they are already emptied. Only the deep traps above 300°C are still filled with electrons, thus showing sufficient thermal stability.

Fig. 21: TL glow curves obtained for six aliquots of sedimentary quartz.
The three blue curves represent glow curves of the natural signal intensity. The black curves were measured after resetting of the natural luminescence signal by heating to 500°C for 1 h, laboratory irradiation (8.9 Gy, ^{60}Co-gamma source) and storage at room temperature for three weeks. Both sets were measured using a heating rate of 5°C/s and a 10 s preheat at 160°C (thus explaining the sharp decline in the artificially irradiated sample set). By using the Hoya U340 filter the UV emission was detected only. The incandescent background was subtracted from the TL data for both sample sets. (Australian dune sand sample AU28, OSL age ~ 28 ka, further details on the sample given in LOMAX et al. 2003)
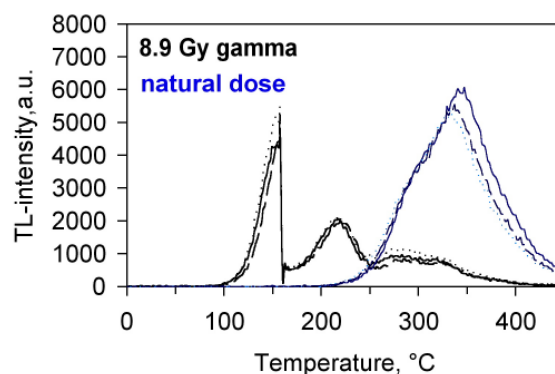
The thermal stability of a trap is characterised by the kinetic parameter τ, the lifetime. The mean lifetime τ of a trapped electron describes the average residence time in a trap, which is, among other parameters, dependent on the trap depth and temperature and can be calculated from:

$$\tau = s^{-1} \exp (E/k_B T)$$

where E is the energy needed for an electron to escape from the trap corresponding with the trap depth, s is the escape attempt frequency, k_B is the Boltzmann's constant and T the storage temperature.

Fig. 22 illustrates the relationship between lifetime and trap depth. The figure is based on trap depth values and lifetimes for various TL peaks in quartz measured by SPOONER and QUESTIAUX (2000) with a consistent methodological approach and therefore they can be compared directly. In the literature a large variety of trap depth and lifetime values are presented for the several TL traps. Those values are very difficult to compare (see for example values cited by AITKEN 1985: 272), because they are based on different methodological approaches or because experiments were carried out using different measurement parameters. For further details on techniques to obtain trap parameters needed for lifetime calculations and the relevant equations the reader is referred to CHEN and MCKEEVER (1997).

The figures illustrate the correlation of an increasing lifetime with an increasing trap depth. The shallow 110 °C TL peak lacks sufficient thermal stability and is only present in samples if less than a few hours are left in between irradiation and measurement (lifetime at 15°C ~7h, AITKEN 1985). For other shallow traps related to the TL peaks at 160°C and 220°C (for heating rate 5K/s) SPOONER and QUESTIAUX (2000) calculated lifetimes for storage at 20 °C of four weeks and c. 8,900 years for the latter. Those TL peaks may be useful for determining retrospective accident doses. These lifetime values explain the glow curves presented in Fig. 21, where the shallow 110°C trap is already emptied, but the TL traps at 160 and 220°C are still filled with electrons four weeks after irradiation. In the ~28 ka old natural samples all these shallow traps are emptied already.

Fig. 22: Illustration of the correlation of the TL peak temperature, trap depth, and lifetime.
Analyses were carried out on 90-125 μm quartz grains. TL peaks were measured using a heating rate
of 5 K/s, detection was through Hoya U340 filters in the UV emission band. The kinetic parameters of
the TL peaks were obtained by the 'variation of heating rate' method (based on data from SPOONER &
QUESTIAUX 2000: 662).
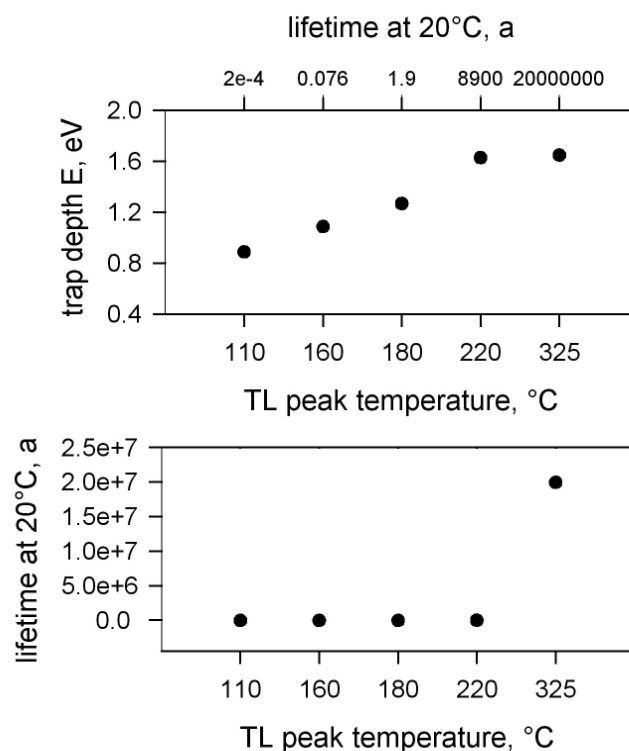
With a lifetime at 20°C of 160,000 years the 280°C TL peak has a thermal stability sufficient
only for dating Holocene or Late Glacial events (SPOONER & QUESTIAUX 2000). Electrons
giving rise to the TL peaks at about 325°C and 375°C have average lifetimes in excess of
several million years (e.g. 325°C peak ~20 Ma, see Fig. 22), depending on the storage
temperature even about 100 Ma or more (see AITKEN 1985: 272). Therefore, these deep traps
(> 1.6 eV) generally show sufficient thermal stability to be used for age determination of
sedimentary deposits being several hundreds of thousand years old. According to GRÜN
(1989) signals suitable for dating should provide a thermal stability of the related trap with
electron lifetimes of at least five to ten times higher than the age to be determined. Thus, for
example, to obtain reliable ages for sediments deposited 500 ka ago, the trap must have a
lifetime far beyond 2.5 Ma. The 325°C trap with a lifetime of ~20 Ma is considered to be
suitable for dating samples which have been deposited up to 1 million years ago (BØTTER-
JENSEN et al. 2003).

3.4.2.1.2   Number of traps

As already mentioned above, the upper dating limit is dependent on the thermal stability of the relevant traps. An other factor limiting the datable age range is the number of traps suitable for dating. In Fig. 23 the effect of saturation is illustrated: given a constant number of traps, the probability for electron trapping is reduced with an increasing density of filled traps. The dose response curve shows an exponential growth rather than a linear one when with an increasing radiation dose the trap population increasingly saturates with electrons. No further signal increase with dose is observed when all available traps are filled: the sample is saturated.

Fig. 23: Illustration of the problem of saturation of the electron trap population with increasing irradiation dose.
The quartz sample D15 (glaciofluvial sand from northern Germany, see HILGERS et al. 2001a for further details on the sample) has been irradiated with high laboratory beta-doses up to about 450 Gy. In the lower dose ranges up to 100 Gy a clear growth is visible, but the dose response curve is approaching the saturation level in the dose range of 150-200 Gy.
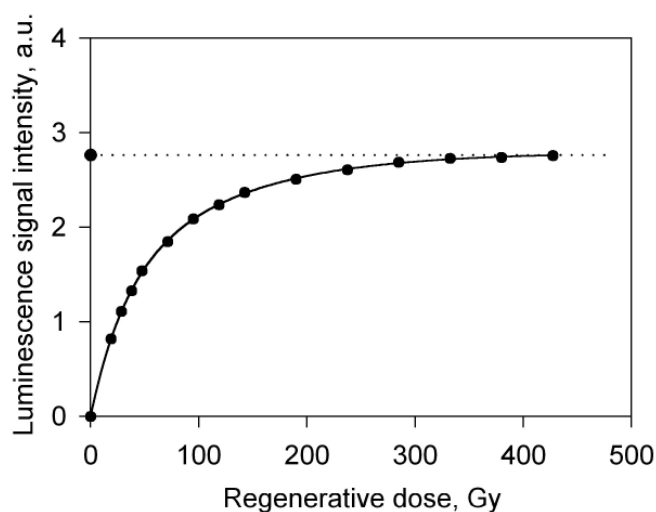
For a reliable age determination, the natural OSL signal intensities ought to be still in that part of the dose response curve which is characterised by a clear growth. The upper age limit is finally dependent on the total amount of available traps. WAGNER (1995: 131) quotes a number for defect concentration in quartz and feldspars of about 10^{-8} to 10^{-7}. Of course, this should be regarded as an order of magnitude only. The actual number is strongly dependent on the geological history of a crystal regarding its formation conditions etc. The annual dose rate is the second important factor. In environments with a high concentration of radionuclides and thus a strong ionising radiation flux, the available electron traps are

saturated in a shorter period of time, thereby shortening the datable age range for a given sample.

Another basic assumption which is made in the models describing the luminescence phenomenon is a constant number of traps throughout time. With an increase or decrease of the number of empty traps, electron as well as hole traps, the trapping probability would change. For instance new traps could be created during crystallisation processes or phase transitions due to annealing at high temperatures (> 573°C in the case of quartz). During irradiation with high laboratory dose rates additional, traps could be created, thus disturbing the expected exponential growth of the curve. The saturation level could be increased in case new traps are created. Conversely, the level can be lower if the trap number is reduced due to a destruction of the crystal lattice structure (WAGNER 1995, AITKEN 1985, STEFFEN 2000).

The samples investigated in this study are expected to be younger than 20 ka, and to have experienced doses rates of ~1 Gy/ka (see section 3.3.5) Therefore, saturation or creation of new traps is not likely to be a major problem to occur in the dating routine.

In contrast to the creation or destruction of lattice defects by strong heating or irradiation, sensitization of traps can be induced already by optical stimulation, irradiation with relatively low doses or moderate heating (e.g. below the phase transition temperature of quartz at 573°C). By that the probability for the recombination of freed electrons in luminescence centres and consequently the luminescence signal response is changed. In Fig. 24 this sensitivity change, the change in the luminescence recombination probability, is illustrated for quartz sand extracted from Holocene dune sand. Because luminescence measurements include repeated optical and thermal treatment as well as several cycles of artificial irradiation of the samples, the measurement protocol has to account for the occurrence of sensitivity changes and should include an appropriate correction procedure.

Fig. 24: Changes in sensitivity with repeated luminescence measurements.
The irradiation dose (here a test dose of ~1.5 Gy) was kept constant over the entire experiment. The sample (quartz extracted from ~ 300 years old dune sand, C-L0520_F2) was preheated at 260°C for 10 s prior to optical stimulation (100 s exposure to blue-light emitting diodes with the sample held constantly at 125°C). An increase of the signal intensity is observed, although the irradiation dose and all other measurement conditions were kept constant for each cycle. This increase is explained by a change in the luminescence recombination probability.
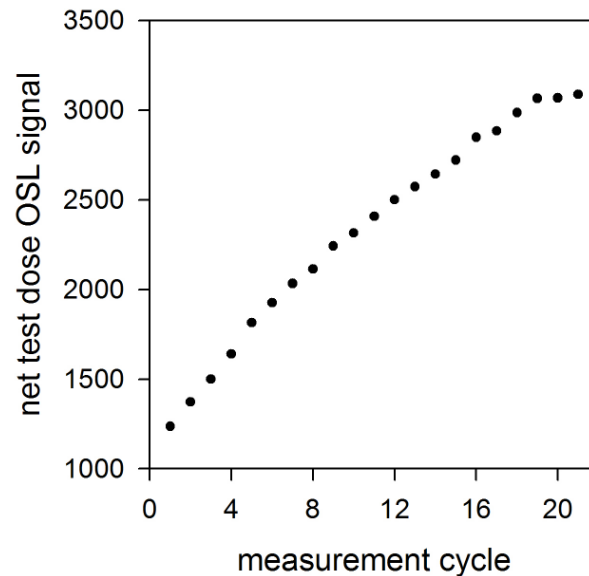
3.4.2.1.3   Bleachability

The key question in sediment dating is whether the mineral grains have been sufficiently exposed to sunlight in order to 'reset the luminescence clock' back to the zero level.

As already mentioned, the erasure of the trapped charge, thus the necessary resetting of the 'dating clock' at the point in time wanted to be dated, is by light exposure in case of luminescence dating of sediments. Therefore, to be suitable for dating, an electron trap must be light sensitive or 'bleachable'. For charge release, the activation energy of light is sufficient.

At this point, the reader is referred to Fig. 20 a). The dashed line represents the TL curve measured after a 2 s stimulation with green light. The most striking difference between both curves regarding the relevant temperature range for dating purposes above 300°C is the region of the 325°C peak, whose intensity is clearly reduced after light exposure. In contrast, the higher temperature peak at about 375°C remains unaffected.

According to the nomenclature of FRANKLIN and HORNYAK (1990) the TL peak measured at "325°C" is called the rapidly bleaching peak (RBP) and the one at "375°C" the slowly bleaching peak (SBP).[3]

As shown by SPOONER et al. (1988) the RBP is rapidly and apparently completely bleachable even with longer wavelengths from 400-700 nm. In contrast, bleaching of the SBP seems to be restricted to shorter wavelengths < 400 nm (the violet part of the visible spectrum and the near UV). But even with short wavelength the SBP intensity is reduced with a much slower depletion rate as found for the RBP.

The lower temperature peaks in quartz TL at 150-180°C and 200-220 °C also are easy and rapidly to bleach (FRANKLIN et al. 1995, in WINTLE 1997), but they lack the thermal stability to be used for most dating studies concerned with Late Quaternary sediments.

Correlation of RBP in TL and the OSL emission of quartz:

SMITH et al. (1986) first presumed from the easy bleachability of the 325°C TL peak, that the associated traps would also be the primary source of electrons responsible for the OSL signal of quartz. Numerous studies proved that the luminescence emission after optical stimulation could be correlated with the "325°C" TL traps (e.g. SPOONER et al. 1988, RHODES 1988, SCHOLEFIELD et al. 1994, WINTLE & MURRAY 1997, SPOONER & QUESTIAUX 2000). SPOONER and QUESTIAUX (2000) found similar trapping lifetimes and trap depth for the UV emissions of the 325°C TL peak and the OSL of quartz, respectively:

325°C TL peak, UV emission: trap depth 1.65 eV (heating rate 5K/s)
                                   lifetime 20,000,000 years (at 20°C)

OSL, UV emission: trap depth 1.59 eV
                                   lifetime 21,000,000 a (at 20°C)

The trap depth values are in good correspondence with other data reported for the main OSL trap (e.g. 1.66±0.03 eV, MURRAY & WINTLE 1999) and the "325°C" RBP of quartz (for

---

[3] The temperatures describing these peaks apply only to a ramp rate of 20°C/s (as described for example by FLEMING 1979 (in FRANKLIN & HORNYAK 1990). If lower heating rates are used a downward shift in TL peak temperatures is observed, e.g. the RPB is observed at 305°C with a rate of 5°C/s (PRESCOTT & FOX 1990), or the RBP at 275 °C and the SBP at 310-330°C for a ramp rate of only 1°C/s (FRANKLIN & HORNYAK 1990). Thus, for discussion of both peaks the peak temperatures should be shown in quotes, as recommended by FRANKLIN (1994), or just the terms RBP and SBP should be used rather than peak temperatures.

example 1.69 eV, WINTLE 1975, cit. in AITKEN 1992). This similarity supports the assumption that both luminescence emissions, the RBP in TL and the OSL signal, have a common origin with regard to the same trapped electron population.

Furthermore, the main OSL emission of quartz at 365 nm coincides well with the trend of the emission maximum of the RBP in TL spectral measurements at about 380 nm (FOX 1990, in PRESCOTT & FOX 1990, SCHOLEFIELD et al. 1994). This may indicate that both emissions are derived from electron recombination at the same luminescence centres.

WINTLE and MURRAY (1997) demonstrated by monitoring the quartz OSL as a function of preheat temperature, that there is a steep signal decrease at higher preheat temperatures, beginning just below 300°C. Heating to 330°C is sufficient to empty all traps contributing to the OSL signal. This further confirms that the temperature region around 325°C in the TL curve is the main contributor to the OSL signal.

3.4.2.2 Characteristics of luminescence centres and emissions of quartz

As described in section 3.4.1.1 not only a variety of electron traps exists in the quartz crystal structure, but even so various crystal defects, which serve as traps for holes thus creating different luminescence recombination centres. Quartz shows various luminescence emission bands that can be ascribed to several different intrinsic and extrinsic defects. GÖTZE et al. (2001) and KRBETSCHEK et al. (1997) present overviews of characteristic emission bands in the luminescence spectra of quartz and their proposed origin in different crystal lattice defects.

The effect of different luminescence centres is illustrated by spectral measurements. When the luminescence signal is not measured just as total light intensity (photons per °C or seconds regarding OSL) but as a wavelength resolved spectrum, luminescence emission is observed in different colours. In Fig. 25 radioluminescence spectra of two samples from this study are presented, which show the luminescence emission during beta irradiation. Beside the main emission in the near UV to violet wavelength range a second emission band is detected in orange to red wavelengths.

Fig. 25: Radioluminescence spectra of quartz.
The spectral measurements were carried out using the liquid nitrogen cooled CCD camera in the high-sensitivity luminescence spectrometer of the Freiberg Luminescence dating Laboratory (Dr. G. Erfurt). A 3.7 MBq 137Cs β-source is used for RL stimulation and the wavelength range effectively detected by the CCD chip ranges from 250 to ~970 nm (further details in ERFURT 2003). Natural samples extracted from dune sands were measured: sample STA 10 with a palaeodose of 2.13 Gy and sample JC3 with 10.8 Gy.
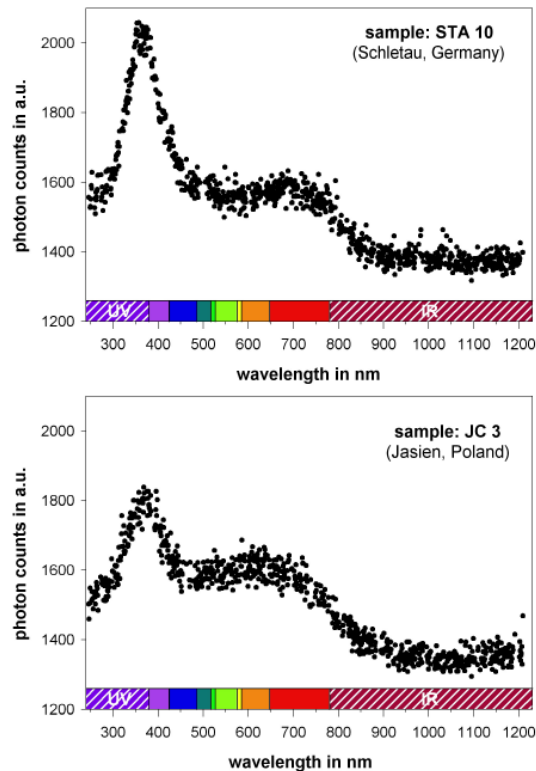
The colour or wavelength of the light emitted by a radiative recombination process is dependent on the energy difference between the conduction band and the energy level of the recombination centre in the forbidden gap. The relationship between energy and wavelength is expressed by the equation (AITKEN 1998: 16):

$$\text{Energy (eV)} = 1240 : \text{Wavelength (nm)}$$

With regard to the energy level diagram it can be summarised: the greater the distance between luminescence centre and conduction band, the more energy is released by the recombination of the electron and thus, the shorter is the wavelength of the emitted light.

With respect to Fig. 25 this would mean, that at least two different recombination centres are involved in the luminescence emission; those responsible for the orange-red emission being

located closer to the conduction band than those giving rise to the near UV to violet light signal.

Fig. 26 a) summarises the main TL emission bands of natural and laboratory irradiated quartz and correlates the various TL peaks with the wavelength at which the luminescence emission is observed. In terms of using a luminescence signal for dating on a geological timescale, of course, just the natural emissions corresponding with the thermally stable traps above 300°C, as discussed above, are relevant. These are the three main emission bands centred at 360-440 nm (near UV to violet), 460-500 nm (blue), and 600-650 nm (orange) (KRBETSCHEK et al. 1997).

Fig. 26 b) introduces the observation of a variety of luminescence centres to the energy level diagram. In the following the suitability of the different emission bands for dating will be discussed.

Fig. 26: **a)** Correlation of TL peak temperatures and main luminescence emission bands in quartz (from KRBETSCHEK et al. 1997: 707).
b) Energy level diagram including a variety of electron traps (T1-6) and three different recombination sites (R1-3) allowing emission of luminescence in three different wavelengths.
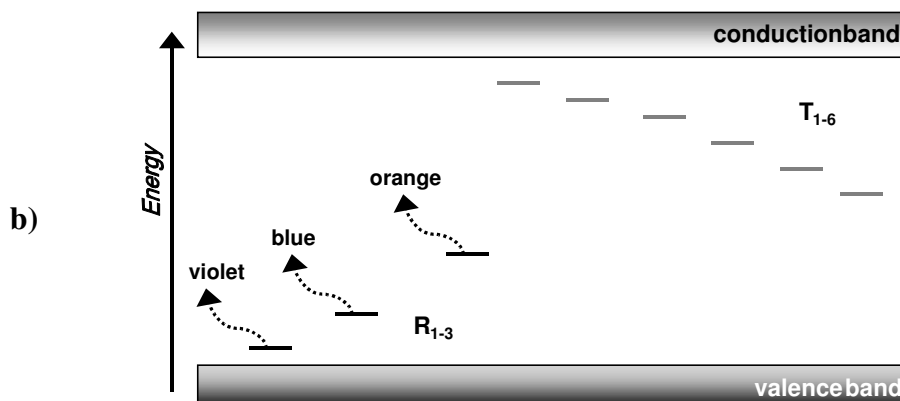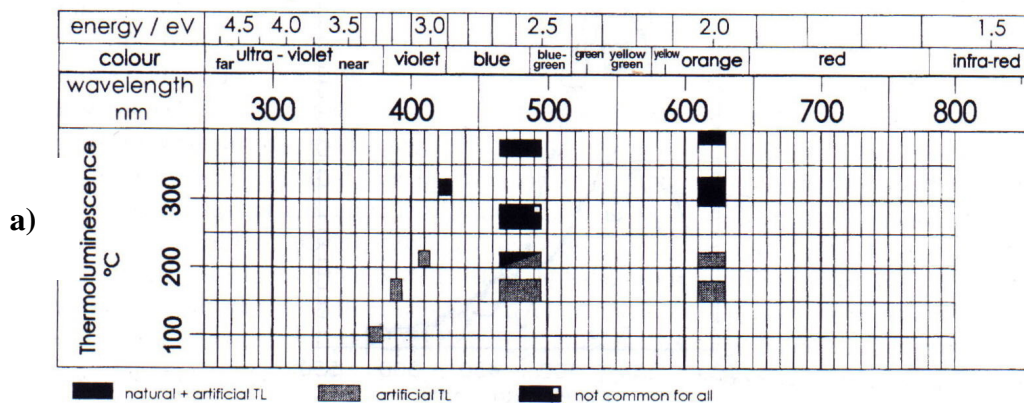
3.4.2.2.1   The 360-440 nm (near-UV-violet) emission band

The thermally unstable, but light sensitive "110°C" TL peak shows an emission band in the near-UV to violet as well as the RBP at "325°C" which is used for luminescence dating (e.g. SCHOLEFIELD et al. 1994, YANG & MCKEEVER 1990). The OSL emission of quartz, which is correlated to the RBP, is consequently also found in the near-UV centred at 365 nm as shown in Fig. 27 (HUNTLEY et al 1991).

Fig. 27: The OSL emission spectrum of Australian sedimentary quartz measured after stimulation with 647 nm laser light showing only a single emission band centred on 365 nm.
(from HUNTLEY et al. 1991, in KRBETSCHEK et al. 1997: 710)
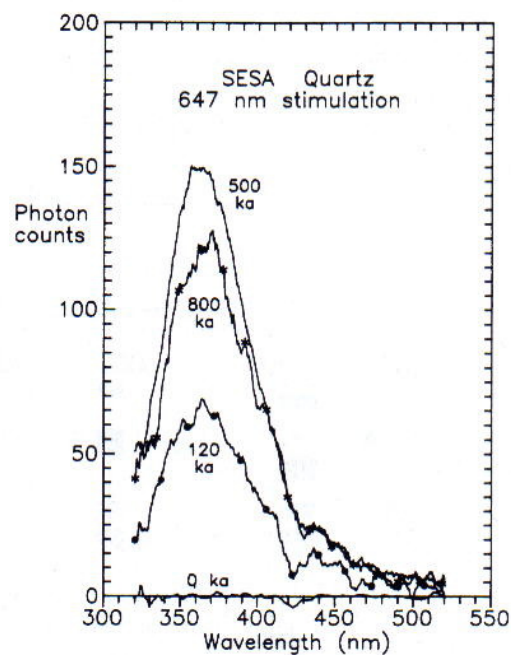
FRANKLIN et al. (1995, in WINTLE 1997) found further rapidly bleaching peaks at 150-180°C and 200-220 °C with emissions at 392 and 410 nm (see also artificial TL emission in Fig. 26 a). They concluded that the "110", "180", "220", and "325°C" TL peaks all use the same luminescence centre.

After artificial irradiation in the laboratory the light sensitive, rapidly bleaching but unstable electron traps as well as the main OSL trap are filled, whereas in the natural sample the shallow traps are mostly emptied as a result of their limited thermal stability. This causes the problem in OSL measurements, that all freed electrons compete at the same type of luminescence centre and contribute to the OSL emission in the near-UV. Consequently, to

make this OSL signal suitable for dating, the unstable component has to be eliminated. Appropriate experimental settings will be discussed in the next section.

3.4.2.2.2   *The 460-500 nm (blue) emission*

The blue emission band of quartz consists of overlapping components and therefore it is usually very broad. But the blue TL from natural quartz centred at ~485 nm (2.55 eV), for example, has been attributed to $[AlO_4]^0$ centres, which results from substitution by aluminium impurities at silicon sites in the crystal lattice (NASSAU & PRESCOTT 1975, in GÖTZE et al. 2001, 2005), but other defects are discussed as well.

The recombination of electrons which were released from hard-to-bleach traps seems to give rise to the blue emission of quartz. The emission centred at ~480-490 nm is linked to the recombination of electrons released from the SBP at about "375°C" (FRANKLIN & HORNYAK 1990, SCHOLEFIELD et al. 1994). Another peak observed to emit in the blue wavelength range is at 260-280°C, but as indicated in Fig. 26 a) this emission band is not common for all quartz TL spectra (e.g. FRANKLIN et al. 1995, in KRBETSCKEK et al. 1997).

3.4.2.2.3   *The 600-650 nm (orange) emission*

This orange emission band is often referred to as 'red TL', but according to DIN 5031 (see e.g. AITKEN 1998) red light is defined as emission at wavelengths ranging from 647-780 nm.

SIEGEL and MARRONE (1981, in GÖTZE et al. 2005) related the orange emission of quartz to the recombination of electrons in the non-bridging oxygen hole centre (NBOHC).

The saturation dose of this emission band is very high, usually beyond 10 kGy, therefore the orange or 'red' TL is considered to be suitable for long range dating up to a million years. But the applicability of this emission for sediment dating is limited by the poor light sensitivity. The 'red' TL of quartz resists sunlight bleaching much more firmly than the blue TL, and is bleached down only to high residual levels during prolonged sunlight exposure. LAI and MURRAY (2005), for example, report high signal residual levels of up to 40 % of the natural signal after sunlight bleaching of a sample with an expected age of 1.2 Ma. However, for samples zeroed by sufficient heating this emission seems suitable for dating (e.g. MIALLIER et al. 1994, FATTAHI & STOKES 2000). WESTAWAY and ROBERTS (2006) present a new

measurement technique based on the 'red TL' signal of quartz to date the last sunlight exposure of quartz from sedimentary environments. As their samples were from volcanic provenance, thus had been heated in the past, further research on a wider range of samples from sedimentary environments not involving volcanic activity will show the potential of this method.

To summarise the luminescence emissions with respect to their suitability for dating, the UV emission is characterised by a high optical sensitivity, which is essential to ensure bleaching during transport. But the signal saturates already at comparably low doses, thus the UV emission is not suitable for dating very old samples. The blue emission is optically sensitive, but for a complete resetting long exposure times to short wavelengths are required. The blue signal saturates at higher doses than the UV signal, therefore it is suitable to date further back in time. The orange emission shows only low optical sensitivity which can result in high residual doses. But this signal is characterised by a high saturation level. Therefore it should be suitable for very old, several hundreds of thousands years old deposits. In such old sediment the impact of residuals is reduced with increasing age, assuming that the residual level remains constant.

3.4.3 Extraction of the suitable OSL dating signal of quartz

Taking the various luminescence characteristics of quartz into account, the simple 'one-trap one-centre' model seems no longer appropriate to explain luminescence processes in quartz. Therefore a more detailed, though still simplified model of the crystal lattice defects involved in the luminescence process is introduced at this point which summarises the different characteristics of the defects in quartz as described above.

Fig. 28: Simplified energy level scheme illustrating electron traps (T$_{1-6}$) and luminescence centres (R$_{1-3}$) involved in luminescence processes in quartz.

Suitable for optical dating of sediments is only charge released from the rapidly bleachable, thermally stable "325°C" TL or main OSL trap, respectively, which subsequently recombines at (H$_3$O$_4$)^0 centres to give rise to light emission in the near UV. By adapting the appropriate measurement parameters any interference of other signals ought to be avoided. This will be further discussed in the text.
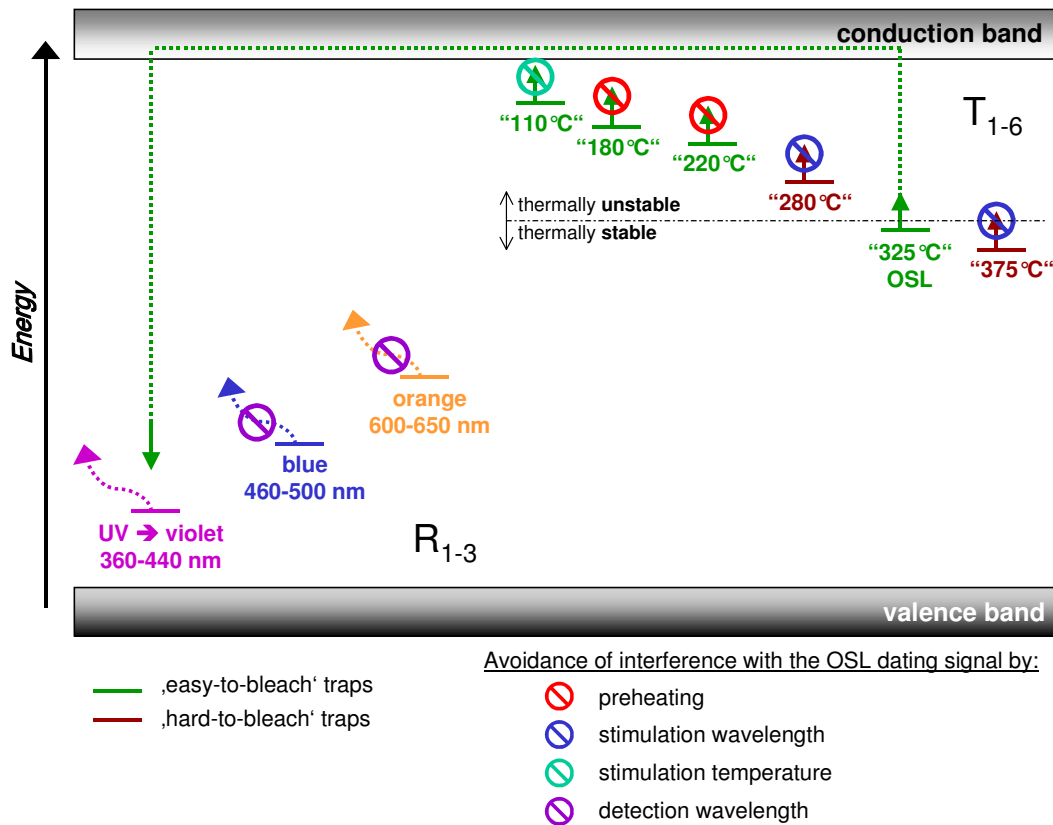
Table 5 summarises the characteristics of certain TL traps in the light of their suitability for dating purposes. In the following a brief summary will be presented of the various options and procedures, which are applied in luminescence measurements to avoid interference of unstable and unwanted components with the suitable dating signal.

More detailed energy band models that combine the numerous possibilities of charge transition to explain the various effects observed in the OSL of quartz are presented and discussed in detail by CHEN and MCKEEVER (1997), MCKEEVER and CHEN (1997), BAILEY (2001), and BØTTER-JENSEN et al. (2003).

Multiple traps and multiple recombination centres are involved in the creation of luminescence. A broad variety of charge transfer processes occurs, for example electrons can be transferred via the conduction band or not, or electrons can be retrapped after release. Some of these processes create effects which interfere with the suitable OSL signal and

therefore will be discussed in the following section to explain the choice of measurement parameters and the experimental setting of OSL measurements.

Table 5: Summary of trap characteristics and procedures for the extraction of main OSL signal suitable for quartz dating.

TL peak temperature @5°C/s	Trap depth	Thermal stability	Bleachability	Main emission band	Appropriate procedures to avoid interference with the OSL dating signal:			
					Preheat	stimulation wavelength	stimulation temperature	Detection filter
"110°C"	shallow	unstable	RPB	UV	✓		✓	
"180°C"			RPB	UV	✓			
"220°C"			RPB	UV	✓			
"280°C"			SPB	Blue		✓		✓
"325°C"=OSL	deep	stable	RBP	UV	OSL dating signal			
"375°C"			SBP	Blue		✓		✓

3.4.3.1 Appropriate preheat procedures

The shallow traps giving rise to the low temperature peaks up to ~220°C are unsuitable for dating studies on Quaternary sediments due to their lack of thermal stability. In natural samples these traps are generally empty, but they are filled after laboratory irradiation (see Fig. 21). Low temperature peaks in the range of 140 to 220°C involve the same luminescence centres and electron transport mechanism as the RBP. These shallow traps are light sensitive and easy to bleach by visible light as is the main OSL dating trap at "325°C" (FRANKLIN et al. 1995, in FRANKLIN et al. 2000). Thus, with optical stimulation electrons are released from the shallow traps and the OSL trap and subsequently compete for the same recombination site. Finally both electron populations, evicted from the stable and unstable traps, give rise to light emission of the same wavelength. The detected OSL signal from artificially irradiated samples would therefore contain an unstable component, which cannot be separated by using filter.

To avoid the influence of unwanted unstable signals interfering with the stable 'dating' signals two practical approaches are applicable: storage or a so-called 'preheating'. In general, the time necessary for the shallow traps to be emptied is much too long. Therefore samples are usually heated for a certain time after the laboratory irradiation prior to the luminescence measurement.

The impact of preheating on the equivalent dose determination is illustrated in Fig. 29. The unstable signal component is only present in the signals measured after laboratory irradiation but not in the natural signal, as shallow traps are already emptied given a sufficient long time of burial. Without thermal treatment prior to the OSL measurement, a steeper dose response curve can result which finally causes an underestimation of the equivalent dose and hence of the OSL age.

Fig. 29: Effect of thermal treatment after laboratory irradiation on the dose response curve.
If the contribution from unstable traps is not avoided by appropriate preheat procedures, the additional signal contribution present only in the artificially irradiated subsamples results in a steeper rise of the growth curve and finally in an underestimation of the equivalent dose.
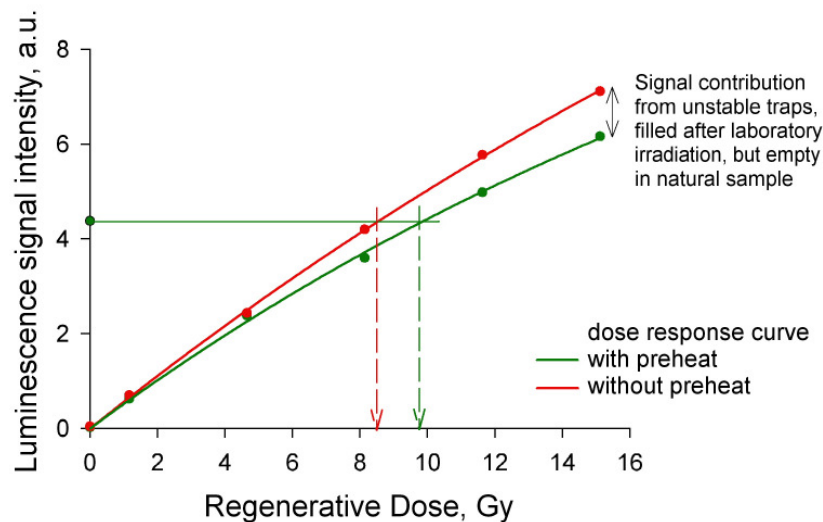
A second reason for pre-heating is to induce the process of charge transfer from shallow traps into deeper, thermally stable traps, the so-called thermal transfer. Such a transfer contributes to the natural signal through thermal decay of the unstable traps during millennia of burial and has to be imitated for the laboratory-irradiated samples prior to the measurement to equalise this indirect signal contribution in the natural and artificially dosed samples (RHODES 1988 in AITKEN 1992). This effect is also seen in Fig. 21. The natural TL response does not show any contribution from the low temperature traps, whereas three weeks after irradiation they are

still populated and the main trap at "325°C" shows only a minor luminescence intensity with only a low peak.

The 'preheat' temperature has to be well chosen, sufficiently high for the shallow traps to be emptied completely, and sufficiently low in order not to affect the electrons trapped in the stable traps (>280°C the OSL trap is already significantly thermally emptied, WINTLE & MURRAY 1998). This would result in a decrease of the luminescence intensity and finally in an age underestimation. In practice, the appropriate preheat temperature can be determined by the measurement of a so-called 'preheat plateau test' in which OSL measurements are carried out using different preheat temperatures. The equivalent dose values for each measurement are plotted against the preheat temperature. Only those preheat temperatures resulting in consistent equivalent dose values are considered to be adequate. Several examples of preheat plateau tests will be presented in the following sections.

Thermal effects:

Besides the wanted effects of preheating in the OSL measurement process there are also unwanted effects of thermal treatment which have an impact on the OSL signal. For a comprehensive description of these effects, their origin and impact, the reader is referred to CHEN and MCKEEVER (1997) and BØTTER-JENSEN et al. (2003) and cited references therein.

Impact of thermal quenching and thermal assistance on the measurement temperature

Thermal quenching describes the effect of decreasing luminescence efficiency (radiative transition probability/total transition probability) with increasing measurement temperature.

A decrease in the OSL intensity is observed when the temperature is raised during optical stimulation (illustrated e.g. in MURRAY and WINTLE 1998). Holes trapped at recombination centres show a thermal instability; at higher temperatures trapped holes are released from the hole centres (see Fig. 30 a). Because the number of luminescence centres available for radiative recombination of electrons from the conduction band is reduced at higher temperatures, the probability of radiative transitions and thus the luminescence efficiency decreases. Thermal quenching affects the main OSL signal derived from the "325°C" TL trap (e.g. SPOONER 1994) and gives rise to decreasing OSL signals observed for stimulation temperatures above 140°C. (see e.g. HUNTLEY et al. 1996 in BØTTER-JENSEN et al. 2003).

Fig. 30: Effects in the OSL process of quartz induced by thermal treatment of the sample.
Further explanations are given in the text (graph a) redrawn from BØTTER-JENSEN et al. 2003: 46, b)
redrawn from AITKEN 1998: 178, c) after AITKEN 1998).

a) Thermal quenching

c) Thermal transfer: Basic transfer

burial/irradiation

b) Thermal transfer: Recuperation

transport/bleaching

preheating

transport/bleaching

preheating

- ▬ OSL trap
- ▬ refuge trap

- ▬ ,easy-to-bleach' trap
- ▬ ,hard-to-bleach' trap
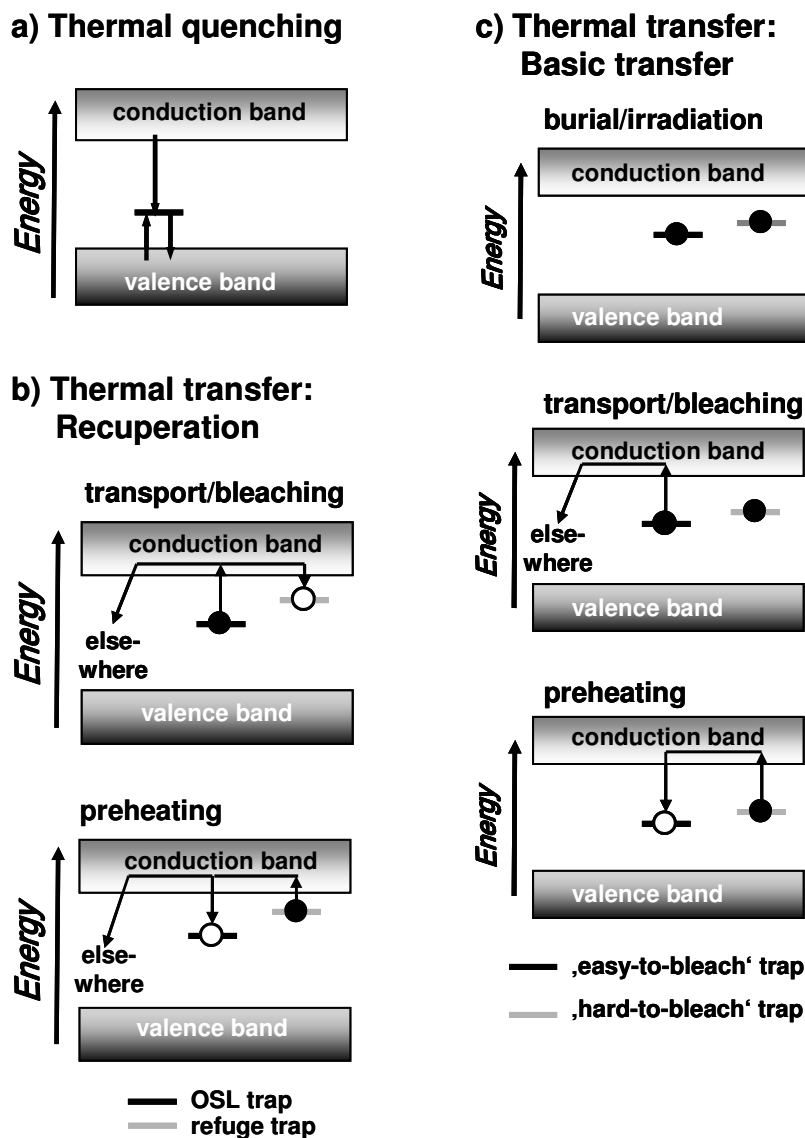
The initial decay of the OSL signal is more rapid at elevated temperatures, an effect known as thermal assistance. This effect is desirable in particular if weak signals are to be detected. A more rapid decay would give a better signal-to-noise ratio for the initial part of the OSL shine-down curve.

Finally, the appropriate temperature at which a sample is held during optical stimulation and OSL measurement is within the range of the wanted effect of thermal assistance and the unwanted effect of thermal quenching.

Impact of thermal transfer

Thermal transfer processes are distinguished into recuperation and basic transfer. Both result in a release of a trapped electron population that does not result from the post-depositional radiation exposure. The contribution of these electrons to the OSL signal is indistinguishable from that of the electrons trapped since deposition. Thus, thermal transfer increases the OSL intensity. In case the natural OSL is not affected in the same manner as the OSL resulting from laboratory irradiation an underestimation of the equivalent dose can result (more likely in case of strong recuperation effects). If the natural OSL intensity increased as well as the signal measured after artificial irradiation, the equivalent dose can be overestimated (more likely in case of substantial basic transfer).

Recuperation (Fig. 30 b):

With the onset of optical stimulation some of the electrons now released from the OSL trap are retrapped in refuge traps which are characterised by a poorer bleachability and a shorter retention lifetime than the OSL traps. After this phototransfer effect a thermal transfer effect follows during subsequent preheating or even during storage at ambient temperatures in case shallow traps serve as refuge traps. This thermal eviction of electrons from the refuge traps allows the retrapping of some of them in the OSL trap (AITKEN 1992, AITKEN & SMITH 1988). In subsequent OSL measurements electrons contribute to the total luminescence signal, which are not transferred to the OSL trap by radiation exposure but by bleaching and subsequent heating. Thus, the direct correlation of signal intensity to radiation dose is no longer possible. The recuperated signal can be monitored in OSL measurements if the signal response after preheating without previous irradiation is measured. So far, no correction procedure has been suggested. In general however, the percentage of the recuperation OSL is small, within a few percent of the natural OSL signal only.

AITKEN and SMITH (1988) showed that successive bleaching and heating/storage cycles reduce the level of recuperation. Thus, samples from sediments which experienced several erosion/sedimentation cycles prior to the final burial are expected to show much lower recuperation signals than sediment samples which have been deposited just after being weathered from the parent rock.

Basic transfer (Fig. 30 c):

Responsible for basic transfer are hard-to-bleach traps with at least an intermediate lifetime. In these light-insensitive traps electrons are stored without being affected by sunlight exposure during transport and deposition. Although these traps are not as deep or thermally stable, respectively, as the main OSL trap at "325°C" they show sufficient thermal stability or lifetime so that the traps remain populated during the period of burial until the OSL measurement process in the laboratory. Transfer of charge from shallow traps, whether easy- or difficult-to-bleach, to the stable OSL trap already is completed during burial given a sufficient length of the deposition period.

During preheating some electrons are released from the hard-to-bleach, thermally metastable traps and some of the electrons are retrapped in traps responsible for the OSL signal. During subsequent optical stimulation these electrons contribute to the overall OSL signal indistinguishable from electrons transferred to the OSL trap by post-depositional radiation (e.g. AITKEN 1998).

The strength of basic transfer processes is dependent on the retention lifetimes of the electrons in the hard-to-bleach traps involved in the transfer process, the thermal history of the sediment and the preheating used in the measurements. The latter is the only factor to be influenced in the measurement procedure. To avoid the impact of basic transfer on the main OSL signal the preheat temperature should be chosen to be below the temperature that affects such light-insensitive and thermally metastable traps.

Phototransfer

During optical stimulation some of the electrons released from the OSL traps can be captured by shallow, light-sensitive traps (Fig. 31). Then, in the course of further illumination, they are optically evicted from their temporary resting place and subsequently some of these electrons are retrapped in the OSL traps (e.g. AITKEN 1998). During further bleaching these recaptured electrons can finally be evicted from the OSL trap and contribute to the OSL signal.

Fig. 31: Simplified energy band model illustrating the phototransfer effect with the OSL trap and a competing shallow, light-sensitive trap.
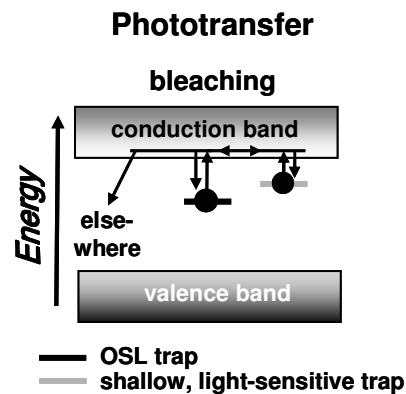
This so-called phototransfer of electrons from shallow, light-sensitive traps to the OSL trap and the subsequent release and radiative recombination of these electrons occurs during the optical stimulation. Therefore the contribution to the overall OSL signal is mainly situated in the later part of the OSL signal measurement, causing the depletion of the signal to be more slowly than would otherwise be the case. Because for equivalent dose determination the initial part of the shine-down curve is most relevant, the initial signal is lowered by the phototransfer effect and the total light-sum integrated over the initial part of the shine-down curve is not the same.

The "110°C "TL trap has been identified to be the shallow, light-sensitive trap serving as a temporarily resting trap for the electrons released from the OSL trap during shine down (SMITH & RHODES 1994, WINTLE & MURRAY 1997, BAILEY et al. 1997, BAILEY 1997). To prevent the "110°C" trap from being populated by electrons and to prevent competition of both light sensitive "110°C" and "325°C" traps during shine-down, optical stimulation is carried out at elevated temperature. WINTLE and MURRAY (1997) suggested carrying out OSL measurements at 125°C. This temperature is regarded to be sufficiently high to avoid phototransfer via the 110°C TL trap but low enough not to cause significant thermal quenching.

3.4.3.2 Appropriate optical stimulation and signal detection

Both high temperature peaks, at "325°C" and "375°C", show sufficient thermal stability for long-range dating. Nevertheless, the general applicability of the latter is limited by the difficulty of optical resetting of this signal, requiring high temperature, which is of course rare in the sediment's depositional history, or prolonged exposure to UV (SPOONER et al. 1988). The signal arising from an unbleachable residual component would finally result in an age overestimation. Therefore, as long as the degree of resetting of the SBP remains unsure, any contribution of this trap to the luminescence output should be avoided.

Obviously, preheating is not feasible, but by choosing an appropriate combination of stimulation wavelength and detection window, the interference of luminescence signals originated in the "375°C"-SBP is suppressed.

OSL stimulation spectra as presented by BøTTER-JENSEN et al. (1994, Fig. 33) or KUHN et al. (2000) generally show an increase in the OSL signal intensity of quartz with decreasing wavelength corresponding with an increasing stimulation energy. Whereas in TL measurements the increasing temperature results in emptying of deeper traps, in OSL measurements the main effect of increasing stimulation energy is to increase the detrapping probability and thus the OSL production rate rather than to access traps of increasing depth (WINTLE 1997).

Fig. 32: Exponential relationship between OSL intensity (In/I) of quartz and photon energy of the stimulation source.
(from BøTTER-JENSEN et al. 1994)
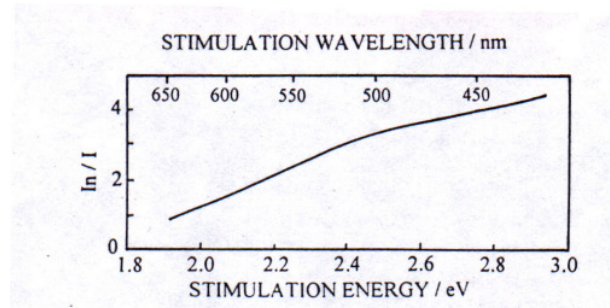
Because of the exponential relationship between the OSL emission intensity of quartz and the energy of the excitation light, it is desirable to use light sources for stimulation with short wavelengths to achieve the maximum signal output. Regarding the CW-OSL signal (see section 3.1), when the signal is measured during illumination, the detection window and the

stimulation wavelength must be strictly separated to avoid detection of light from the stimulation source. In case of quartz with the main OSL emission band centred at about 365 nm and a possible interference of a signal component arising from the "375°C"-SBP being sensitive to wavelength <400 nm, stimulation should be carried out using light sources emitting >400 nm. Because of the change in slope at about 2.5 eV (~500 nm) (see Fig. 32) KUHN et al. (2000) recommend to use only stimulation wavelengths that are far from the 500-520 nm region, otherwise an additional scatter in luminescence output from identical samples could result.

In OSL measurements now light emitting diodes (LEDs) emitting blue light with wavelengths of 470 ±30 nm are widely used for quartz stimulation (see Fig. 33 c). BØTTER-JENSEN et al. (1999 b) found that for similar power densities the high-energy light provided by blue LEDs gives order of magnitude greater quartz stimulation efficiency than that of the broad-band blue-green light (420-550 nm) filtered from a halogen lamp, which was previously used in quartz OSL measurements (see Fig. 33 b). Blue LEDs furthermore avoid the critical 500-520 nm region, which is well within the stimulation spectrum of the broad-band blue-green halogen light. Further advantages of the use of LEDs for stimulation instead of green (514 nm) laser or halogen lamps are discussed e.g. in BØTTER-JENSEN et al. (1999a, 1999 b).

It is interesting to note that the stimulation with blue LEDs at 470±30 nm is quite similar to the peak emission of the typical solar spectrum of natural sunlight that is shown in Fig. 33 a). This spectrum is representative of the sunlight spectrum of the northern middle latitudes in July and therefore reflects the natural bleaching conditions the samples investigated in this study were exposed to during aeolian transport. Thus the artificial bleaching during the luminescence measurements in the laboratory by blue LEDs refelects the resetting of luminescence signals resulting from the exposure to all solar wavelengths in the natural environment quite well.

Beside the wavelength of the stimulation source the power level is also important. The photon flux density at the sample (in mW/cm²) has an effect on the detrapping rate of charge. To obtain the maximum luminescence signal output, the power levels are usually selected to be as high as possible (WINTLE 1997). For comparison, the filtered light from the halogen lamp was measured to deliver a power of 16 mW/cm² to the sample, whereas an array of 49 blue LEDs deliver >60 mW/cm² to the sample at full power (BØTTER-JENSEN et al. 2003).

Fig. 33: Relation between optical stimulation, OSL emission of quartz and signal detection.
a) Typical solar spectrum of natural sunlight measured in northern middle latitudes in July (from www.hoenle.com, 01/2006).
b) Emission spectrum of the broad-band blue-green filtered halogen-lamp stimulation and transmission window of the detection filter Hoya U-340 used in quartz OSL measurements (from BØTTER-JENSEN & DULLER 1992).
c) Emission spectrum of the blue LED overlain with the transmission curves for the GG-420 long-pass filter and the detection filter Hoya U-340 used in quartz OSL measurements (from BØTTER-JENSEN et al. 1999b: 336).
d) RL emission spectrum of quartz (from Fig. 25) combined with the detection transmission window generated by the U-340 filter and the stimulation wavelength range from blue LEDs.
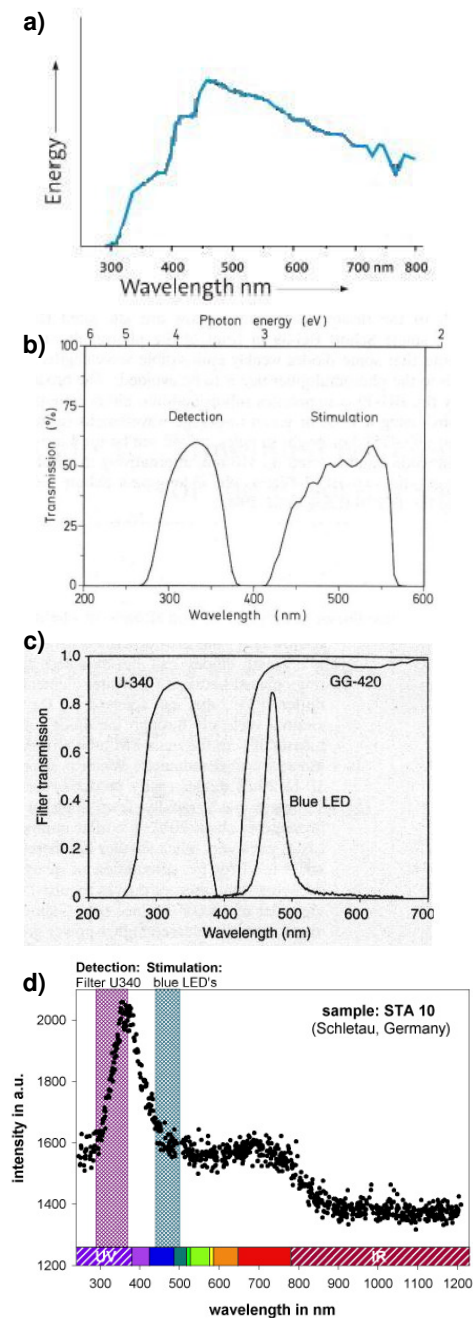
As aforementioned, while detecting the OSL signal it is necessary to prevent any scattered stimulation light reaching the photon counting system (photomultiplier tube) by using suitable filters (see Appendix C for a description of luminescence measurement equipment). The OSL emission of quartz has a maximum at ~ 360-380 nm (HUNTLEY et al. 1991). The best signal-to-noise ratio in the detection of the quartz emission was found for U-340 filter with the maximum transmission wavelength at 330 nm (limits for 50 % of the peak transmission 290-370 nm, AITKEN 1998: 209, see Fig. 33 b & c). In the luminescence measurement equipment used in this study signal detection is through a 7.5 mm Hoya U-340 filter. This filter is coated with metal oxide to attenuate the stray light from the transmission window which is observed in the red region of an uncoated U-340 filter (BØTTER-JENSEN 1997).

In Fig. 33 d) the quartz luminescence emission is plotted together with the transmission window for signal detection and the stimulation wavelength of the blue LEDs. It is clearly seen that the detection filter cuts off an appreciable part of the quartz emission spectrum. An extension of the detection range could be achieved by shifting the short-wavelength limit of the stimulation filters to longer wavelengths. But as discussed above, the signal intensity is reduced by stimulation with lower energy sources in higher wavelength ranges. It was found experimentally that the optimum signal-to-noise ratio as well as signal intensity is provided by the detection and stimulation filter combination as illustrated in Fig. 33 c) with the detection window defined by an U-340 filter and stimulation by blue LED. Blue long-pass GG-420 filter in front of the blue LEDs attenuate a significant part of the short-wavelength tail in the diode emission. By that the background luminescence count rate which includes scattered illumination light reaching the photomultiplier tube is reduced (e.g. BØTTER-JENSEN et al. 1999a).

3.5 Equivalent dose determination on sand-sized quartz grains

At the beginning of this study a comprehensive comparison of the various measurements procedures available for equivalent dose determination in luminescence dating studies was carried out. A summary of the results is presented in Appendix B (see also HILGERS et al. 2001 a, b; RADTKE et al. 2001). The conclusion drawn from this comparative study was that the best available way to measure the dose absorbed in the samples investigated here is the single aliquot regenerative (SAR) dose protocol for sand-sized quartz as proposed by MURRAY and WINTLE (2000). This protocol will be described in the following section as well as several tests which were carried out to test the robustness of the SAR protocol.

3.5.1 Sample preparation for equivalent dose measurements

Samples were taken from dune exposures (see chapter 1 for descriptions of the individual sections) by stainless steel tubes and unpacked into black photo bags under light proved conditions.

The sample preparation for luminescence dating was carried out under low-intensity red light. In general luminescence measurements were carried out on coarse quartz grains in the grain size range from 100 to 200 µm. This fraction was chosen because it is within grain size range most easily transported by aeolian processes and therefore supposed to be best bleached by sunlight during the aeolian transport. Further reasons for this choice concern the luminescence measurements, in particular the laboratory beta irradiation. All grains on a disc (see Appendix C for illustration) have to be evenly irradiated to ensure the same dose-signal response relation for each grain. ARMITAGE and BAILEY (2005) observed no dependence on the laboratory dose rate on grain sizes between ~50-250 µm using the same equipment and thus irradiation geometry as was used throughout this study. The grain size range should be as small as possible, so that effects such as radiation backscattering have the same impact on all grains. For numerous samples the grain size range after HF etching therefore was finally reduced to 100-150 µm or 90-150 µm.

After drying at temperatures <50°C (to prevent any luminescence signal loss due to thermal eviction), the dating fraction was extracted from the bulk samples by dry sieving. The samples were then subjected to hydrochloric acid, hydrogen peroxide, and sodium oxalate to remove carbonates, organic material, and clay, respectively. Heavy-liquid separation using sodium

polytungstate (2.62-2.68 g cm^{-3}) was used to concentrate quartz which was subsequently etched in HF (40 %) for 40 minutes to remove the outer volume influenced by alpha-particles, and to remove any feldspar contamination, in particular of Na-Ca-rich feldspars with densities in the range between 2.62 and 2.76 g/cm³.

After washing in HCl to dissolve fluorides, the purified quartz grains were mounted onto stainless steel discs 9 mm in diameter using silicon oil spray. From some samples only small amounts in the 100 to 200 µm fraction could be extracted, because they consisted of comparatively coarse material and, in addition, because of small amounts of the bulk sample. Some samples were re-sieved after HF-etching to the fraction 100 to 150 µm. All these variations have been taken into account with respect to the dose rate calculation.

In general, the discs used for luminescence measurements were covered with quartz grains in a mono-grain-layer (see Appendix C for illustration, central 8mm diameter covered with >1000 grains). The equipment used for the luminescence measurements, risø TL/OSL readers of the type TL DA 12 or 15, respectively, is described in Appendix C (for a summary on various measurement facilities used in luminescence studies see BØTTER-JENSEN et al. 2003).

3.5.1.1 Impact of feldspar contamination

As shown in Fig. B 7 b (Appendix B) feldspars are sensitive to blue light stimulation and therefore contribute to the OSL signal in a contaminated quartz sample. In Fig. 34 the shine-down curve of an etched and an unetched quartz sample is shown. The difference in the depletion rate and in the initial signal intensity is obvious. The additional signal in case of the unetched sample most likely is due to feldspar contamination.

From this contaminated, brighter OSL signal a higher equivalent dose is determined compared to that from pure quartz. Hence, if a dose rate for quartz would be assumed the dose rate calculation would be erroneous, thus leading to an age overestimation.

Because feldspar luminescence is sensitive to IR exposure, luminescence measurements using infrared-stimulation were carried out on the quartz samples to screen for feldspar contamination. The quartz signal is hardly affected by infrared stimulation (e.g. SHORT & HUNTLEY 1992, BULUR 1996, WALLINGA et al. 2002).

Fig. 34: Shine down curves for one aliquot with etched quartz and one with unetched quartz of the same sample.
The brighter signal and slower depletion rate in case of the unetched quartz is most likely due to a feldspar contamination.
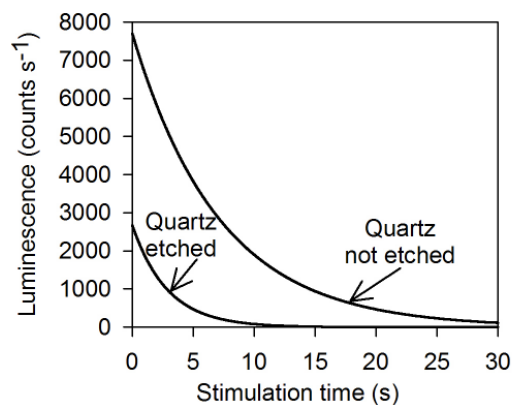
For a large number of discs from various samples test measurements using IR stimulation were carried out at the end of the routine measurement sequence to check for feldspar contamination. Test measurements using IRSL prior to the routine SAR measurements are not recommended as INOUE et al. (2005) observed an IRSL signal from quartz which they ascribe to a different trap in quartz rather than to feldspar contamination. But by application of conventional pre-heating treatments, as in the SAR measurements, this thermally unstable IRSL signal is annealed to a negligible intensity. Thus, INOUE et al. (2005) conclude, that IRSL measurements carried out in order to test quartz samples for feldspar contamination are valid after such thermal treatments.

The IRSL test measurements carried out in this study showed no luminescence signal at all. This observation indicates that any interference from feldspars was negligible in the tested samples. The shape of the OSL shine-down curves provides further evidence for feldspar contamination (see Fig. 34). From the rapid depletion rate of the OSL signals in the quartz samples investigated in this study it is concluded that a significant feldspar contamination is unlikely.

3.5.2 The single-aliquot regenerative-dose (SAR) protocol for coarse-grain quartz

When introducing the optically stimulated luminescence HUNTLEY et al. (1985) already suggested the possibility of using only a single aliquot for D_e determination. But not before the beginning of the 90ies single aliquot protocols were established for feldspars by DULLER (1991, 1995) and later GALLOWAY (1996), and for quartz by MURRAY et al. (1997), MURRAY and ROBERTS (1997, 1998), MURRAY and MEJDAHL (1999) and STRICKERTSSON and MURRAY (1999). The problem of changes in luminescence sensitivity was reported in various studies dealing with single aliquot regeneration protocols (e.g. DULLER 1991, MEJDAHL & BØTTER-JENSEN 1994). Luminescence sensitivity is the measure of the amount of luminescence emitted by a sample for a given radiation dose. This efficiency is sample dependent as it is related to the ability of the material to store energy from the radiation it is exposed to. Many of the processes involved in luminescence measurements, such as thermal treatment, repeated optical stimulation, and artificial irradiation with generally strong doses in short periods of time compared to the natural irradiation conditions, cause changes in the luminescence sensitivity. It is hardly possible to avoid these changes and as the amount of change varies from sample to sample and from measurement cycle to measurement cycle no constant factor can be used for correction. The major advantage of single aliquot regeneration protocols is that the change in sensitivity throughout the luminescence measurement is monitored and internally corrected for. In their single aliquot regenerative dose (SAR) protocol for quartz, MURRAY and ROBERTS (1998) correct for sensitivity changes in a repeated cycle of OSL and TL measurements and laboratory irradiation by using the correlation between the sensitivity changes in the 110°C TL signal and those in the previous OSL response. In later applications of the SAR protocol on heated quartz (MURRAY & MEJDAHL 1999) and sedimentary quartz (STRICKERTSSON & MURRAY 1999, MURRAY & WINTLE 2000) the OSL signal from a fixed test dose administered subsequent to the measurement of the natural and regenerated OSL is used as a surrogate for sensitivity changes in the natural and regenerated OSL signals. By dividing the natural and regenerated OSL signals by their subsequent test dose signals, sensitivity correction is achieved.

3.5.2.1 The routine SAR measurement procedure

The single aliquot regenerative dose protocol developed by MURRAY and WINTLE (2000) allows equivalent dose determination on a single aliquot of quartz. In the very first measurement step (prior to the OSL measurement of the natural signal intensity) the sub-sample is preheated in the same way as thermal treatment is carried out in all subsequent measurement cycles. Preheating after laboratory irradiation is necessary to redistribute charge trapped in the shallow, unstable traps (see section 3.4.3.1). To accurately estimate the equivalent dose, it is necessary to determine a heating treatment which ensures that the charge transferred during heating after laboratory irradiation is equal to that transferred in the natural sample during burial. Applying the same thermal treatment for the natural sample as the one used after artificial irradiation ensures equal conditions for all measurement cycles. Furthermore, any charge that might be trapped in shallow traps in very young samples is also transferred to the OSL traps. The appropriate preheat temperature is finally derived from preheat plateau tests (see section 3.5.2.3.2). Widely applied is a preheat procedure with the sample held at 260°C for 10 s (following MURRAY & WINTLE 2000).

After preheating, the sample is optically stimulated to measure the natural OSL signal, i.e. that resulting from the natural radiation exposure during burial. The illumination is always carried out at 125°C to avoid interference from the "110°C" traps (see section 3.4.3.1). A small test dose, usually 10 to 20 % of the expected D_e, is then administered. This irradiation is followed by heating of the sample to 160°C and immediate cooling as soon as the final temperature is reached. During the subsequent optical stimulation the OSL response to the test dose is measured. Then the next cycle starts with irradiation.

In Table 6 a generalised SAR sequence is described comprising six steps in each regeneration cycle.

Table 6: The single aliquot regenerative (SAR) dose protocol for quartz after MURRAY and WINTLE (2000).
A heating rate of 5° C/s was used in all measurements steps involving thermal treatment. Throughout this study the preheat temperature for most of the samples was reduced to 220°C to minimise thermal transfer effects. Furthermore, numerous samples were stimulated for only 50 s as the OSL signals of the samples investigated in this study proved to be reduced to the background level already after less than 10 s.

1. preheat for 10 s at 260° C
2. optical stimulation at 125° C for 100 s to measure and remove the OSL (L)
3. irradiation with test dose (Td)
4. heat to 160° C
5. optical stimulation shine-down at 125° C for 100 s to measure and remove the Td-OSL (T)
6. irradiation with the 1st regeneration dose (D_i)
7. repeat steps 1 to 6, using at least two other regeneration doses

In the routine application of the SAR protocol described in detail by MURRAY and WINTLE (2000) five regeneration cycles were suggested after the measurement of the natural signal. The first three cycles (R1-3) are used to obtain an apparent equivalent of the natural signal, and these three regeneration doses should be chosen so that they encompass the natural dose, with the second regeneration dose as close to the natural as possible. To monitor any signals due to recuperation effects, the fourth cycle of the routine measurement is applied without irradiation (R4). This zero-dose irradiation follows the highest regeneration dose (3rd regen. dose), so that any dose-dependent recuperation signals are most clearly seen. In the last regeneration cycle (R5) the first regeneration dose is repeated in order to check the reproducibility of the sensitivity corrected signal and hence the reliability of the correction. If the sensitivity corrected OSL signal of the fifth cycle (R5) equals that of the first cycle (R1) any sensitivity changes were corrected successfully.

In Fig. 35 the routine application of the SAR protocol is illustrated. The sensitivity, measured by the ratio of the last to the first test dose response (R5/R1), has increased by a factor of 1.18. After correction, this increase in sensitivity has no influence on the reproducibility of the measurements. This is indicated by the good agreement of the 5th regeneration point (R5, open triangle) with the 1st regeneration point (R1), which both were measured after administration of the same irradiation dose. The sensitivity corrected OSL signal measured in the 4th cycle (R4, without preceding irradiation) is represented by the open square. The recuperation value is calculated from this signal and expressed as percentage of the sensitivity corrected natural signal. With only 0.9 % only a small recuperation signal was detected in the example illustrated in Fig. 35.

Fig. 35: Determination of the D_e for one aliquot of sample F9 by using the routine application of the SAR protocol as summarised in Table 6.
After the measurement of the natural OSL response (horizontal dashed line), three regeneration cycles are applied (responses are shown as filled circles). The signal obtained after administering a zero dose in the fourth regeneration cycle is shown as an open square. In the last cycle the regeneration dose equals the first (open triangle).
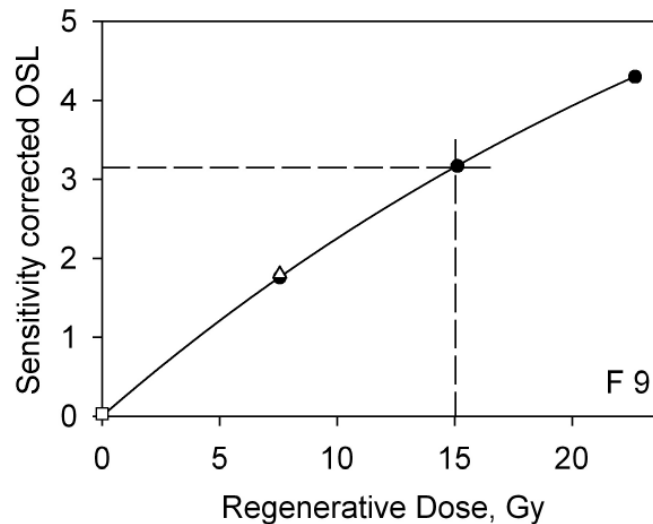
3.5.2.2 Basic principle of sensitivity correction in the SAR procedure

In Fig. 36 a high-resolution growth curve is presented in order to illustrate how sensitivity changes may prevent accurate estimates of the equivalent dose, D_e. Here, 22 regeneration cycles were measured using one aliquot of sample F5. A zero dose was given three times in order to monitor the recuperation effect. The smallest dose (0.5 Gy) was administered four times throughout the measurement procedure to check the recycling of the first dose point and by that robustness of the sensitivity correction procedure. The test dose response (test dose 1.3 Gy) is presented as filled squares with the values multiplied by factor 20 for clarity. There is a clear increase in sensitivity with increasing number of regeneration cycles. The uncorrected growth curve shows a more or less linear growth with increasing regeneration dose, but after sensitivity correction the growth curve is clearly sub-linear (compare Fig. 36 a and b). The underestimation of D_e in the absence of a correction is significant.

Fig. 36: High-resolution regenerated growth curve for one aliquot of sample F5.
The SAR protocol of is applied using a preheat of 260°C for 10 s. The only modification from the standard SAR procedure as proposed by MURRAY and WINTLE (2000) is the increased number of measurement cycles which include also repeated measurements of the recycling point and the recuperated signal. During the first cycle the natural OSL response (L_n, horizontal dashed line) and the signal from the subsequent test dose were measured. The test dose (1.3 Gy) was kept constant throughout the entire experiment. The regeneration doses (D_i) were (in order of administration): 0, 0.5, 1, 1.5, 2, 2.5, 0.5, 5, 10, 15, 20, 25, 0, 0.5, 30, 40, 45, 50, 0, 0.5 Gy.
a) The observed values of the regenerated OSL signal (L) are shown as filled circles, those measured after administering the test dose (T) as filled squares, multiplied by 20 for clarity. A zero dose was given three times (1st, 13th and 20th regeneration cycle) to monitor the OSL response due to recuperation effects. The smallest regeneration dose (0.5 Gy) was administered four times, in the 2nd (open circle), the 7th (open triangle), the 14th (open inverted triangle) and the last (open diamond) regeneration cycle to check the recycling. The results are shown in the inset illustrating only the lower dose range for clarity.
b) Corrected growth curve obtained by dividing all values of L from (a) by the corresponding values of T. The corrected regenerated OSL responses are shown as filled circles, the corrected natural signal as dashed line. The corrected OSL response to the recycling dose (0.5 Gy) is presented in the inset using the same symbols as in (a). The signals obtained after administering the zero dose are shown as squares.
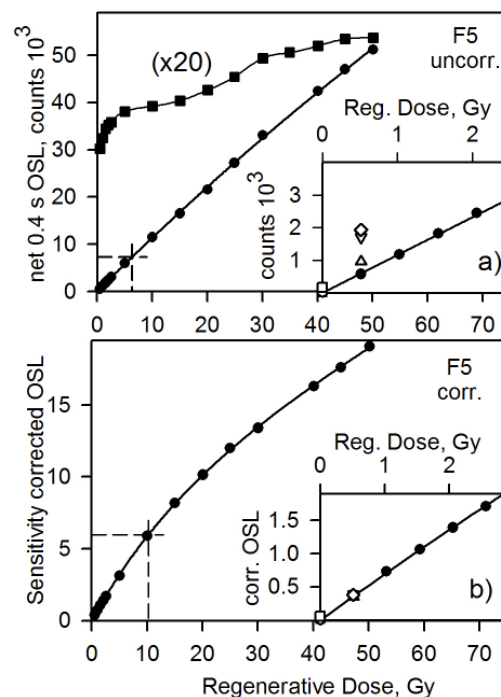
The basic assumption in using a test dose response to correct for any sensitivity changes is that a linear correlation exists between the natural and regenerated OSL signals and the OSL response on a test dose. To check this correlation two samples (F2 and F5) were measured using a constant regeneration dose (0.5 Gy) over 21 cycles; the test dose was also kept constant throughout the whole experiment (1.3 Gy). After measuring and removing the natural OSL signal during the first cycle, the regeneration cycle (irradiation, preheat, $OSL_{regen.\ dose}$, test dose, 160°C TL, $OSL_{test\ dose}$) was repeated 21 times on the same aliquot. In Fig. 37

the net signal (initial 0.4 s signal minus background) resulting from the repeated constant regenerative dose is plotted against the net signal measured after the test dose (open hexagons). The sensitivity increased by a factor of 2.96 over the 21 regeneration cycles for sample F2, and by a factor of 1.81 for sample F5. The data for both samples are consistent with straight lines passing through the origin. For both samples an excellent correlation was found between the regeneration and the test dose response with $r^2 = 0.996$. Therefore the fundamental requirement for using the OSL response to a constant test dose as surrogate for sensitivity changes in the OSL response to the regeneration dose is fulfilled.

Fig. 37: Relationship between the regeneration net OSL signal (background subtracted) and the subsequent net OSL signal after the test dose to monitor sensitivity changes over repeated measurement cycles (samples F2 and F5, site 'Finow').
21 cycles were measured after the natural signal was removed. Preheating was 260°C for 10 s. The regeneration (0.5 Gy) and test dose (1.3 Gy) were kept constant throughout this experiment (open hexagons). The solid lines represent the linear regression calculated for the results of the 21 cycles. The filled symbols show the response to the same regenerative dose (0.5 Gy) and test dose (1.3 Gy) as used for the open symbols. They represent measurements at different steps within a sequence of 21 regeneration cycles (2nd cycle: circle; 7th cycle: triangle; 14th cycle: inverted triangle; 21st cycle: diamond). During the other cycles, the test dose was kept constant but the regeneration doses which were administered increased successively from 0.5 up to 50 Gy to generate a growth curve (see Fig. 36).
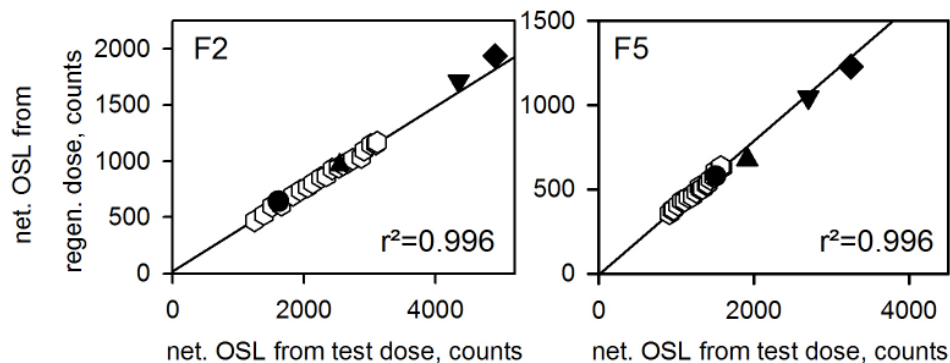
The filled symbols in Fig. 37 show the results of a second experiment using another aliquot of sample F2 and F5, respectively. Again the OSL response to the same doses as used for the open symbols is plotted (regenerative dose of 0.5 Gy and test dose of 1.3 Gy). This time the filled symbols represent measurements at different steps within a sequence of 21 regeneration cycles (2nd, 7th, 14th and 21st cycle). During the other cycles, the test dose was kept constant but the administered regeneration doses were increased successively from 0.5 up to 50 Gy to generate the growth curve presented in Fig. 36. Over the 21 cycles the sensitivity increased by a factor of 3.91 for sample F2 and 2.64 for sample F5.

A comparison of the results of both experiments clearly indicates that

(i) the sensitivity increases with repeated measurement cycles, and

(ii) the increase in sensitivity is dependent on the strength of the laboratory irradiation dose.

As both data sets show linearity between regenerated and test dose OSL, the principal condition for using the test dose signal to correct for sensitivity changes is met.

Apparently, the increase in sensitivity is very large for samples F2 and F5. Nevertheless, the correction procedure is successful as illustrated in the insets of Fig. 36 a) and b). Whereas the OSL signals originating from the constant regeneration dose of 0.5 Gy clearly deviate from each other without correction (inset graph a), there is no significant difference in the response to the regeneration dose after correction: the relevant symbols in graph b) lie on top of each other (open diamond is the repetition of the 0.5 Gy dose in the last regeneration cycle).

3.5.2.3 Testing the robustness of the SAR protocol

In the following section a range of experiments is described which were carried out in order to test the robustness of the SAR protocol. Variations of different parameters, such as the size of the test dose, the preheat temperature and the strength of the beta irradiation source were tested regarding their impact on the equivalent dose estimate. More in particular, these tests are important with respect to samples which received very low natural doses, i.e. very young deposits. For these samples, the laboratory treatment with irradiation doses being several times higher than those which they were exposed to in the natural environment may have a more significant impact than on older samples.

3.5.2.3.1   *Influence of test dose size*

In section 3.5.2.2 it was shown that sensitivity changes are not only dependent on the number of measurement cycles, but also dependent on the dose. Therefore it is preferable to keep the test dose as small as possible. For young samples the statistical limit on precision will be dictated by the size of the test dose signal if the test dose is kept at 10 to 20 % of D_e,. Therefore, it is important to know the acceptable range of doses that can be used as a test dose. In order to examine the effect of the test dose size on the D_e, recuperation and regeneration ratio, the sequence of Table 6 was measured using a range of test doses and a

fixed preheat of 240°C for 10 s. Sample F1, having the lowest luminescence signal intensity, was chosen for this test, because the test dose size is important with respect to the limit of applicability of the protocol to very young samples. The test doses used were 0.25, 0.5, 1, 1.5, 3, 6, 9 and 12 times the D_e, and the regeneration doses were 0.45, 0.76 and 1.07 Gy. The results are summarised in Fig. 38.

There is no systematic change in the equivalent dose (filled circles, Fig. 38 a) with changing relative test dose sizes. Even a test dose that is 12 times higher than the D_e does not cause a significant variation in D_e. This observation is similar to that of MURRAY and WINTLE (2000) and BANERJEE et al. (2000) who also could not find any dependence of the equivalent dose values on test dose size for values up to three times and 12 times of the D_e, respectively.

The ratio of the corrected fifth regeneration signal to the first signal shows no significant deviation from unity (see Fig. 38 b), open triangles), confirming good reproducibility. Therefore, any changes in luminescence sensitivity were successfully corrected.

The recuperation shows only a slight increase on average over the range of test doses (see Fig. 38 b), open squares). All these results suggest that test doses larger than the D_e will not significantly affect the equivalent dose estimation. This is encouraging for the application of the SAR protocol to young samples.

Fig. 38: Dependence of D_e, reproducibility and recuperation on the variation of the test dose (relative to D_e).

a) 48 aliquots of sample F1 were measured in groups of three with 8 different test doses: 0.25, 0.5, 1, 1.5, 3, 6, 9 and 12 times larger than the D_e (note that the x-axis has a logarithmic scale). The preheat was 240°C for 10 s and the five regeneration doses applied following the sequence of Table 6 were 0.5, 0.8, 1.1, 0, 0.5 Gy. Each data point (filled circles) represents the average of six D_e values with its associated standard error. The overall weighted average is shown as a dashed line.

b) Regeneration (or recycling) ratio as a function of test dose size obtained by dividing the corrected OSL response to the repeated first regeneration dose by the corrected OSL signal from the first regeneration dose (R5/R1) (open triangles). The ideal value of 1 is shown as dotted line. The recuperation as a function of test dose size observed after administering a zero dose (R4) is expressed as percentage of the corrected natural signal (open squares).
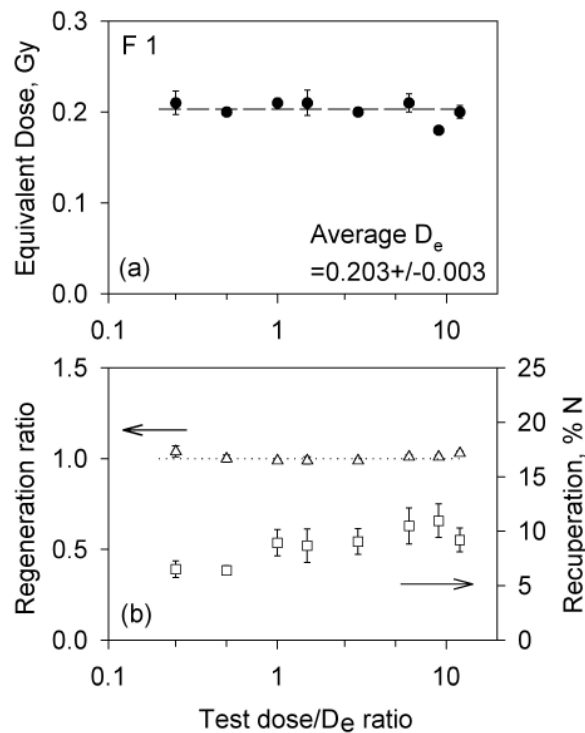
3.5.2.3.2   Influence of the pre-heat temperature and thermal transfer effects

After laboratory irradiation a preheat is employed to redistribute charge. MURRAY and WINTLE (2000) found no significant change in D_e or in recuperation signals over the preheat-temperature range of 160-300°C (with the sample held at the given temperature for 10 s). However, the electron population in traps as well as the trap characteristics may vary from one sample to the other. This could be due to the time of radiation exposure (i.e. depositional age) or to the geological history of the sample (see section 3.4.1.1). Therefore the effects of different preheat temperatures on the estimation of the equivalent dose for the samples investigated in this study were examined in more detail. Preheat plateaus were measured for

different samples. In Fig. 39 and Fig. 40 preheat plateaus are illustrated which were measured using three very young (F1, F2, STA11) and three older samples (F9, F20, R2). Usually 24 aliquots were measured in groups of three, using 8 different preheat temperatures in steps of 20° ranging from 160° to 300°C (each preheat was for 10 s). To obtain more reliable estimates for the two young samples (F1 and F2), 48 aliquots were used. The influence of the variation of the preheat temperature on the D_e, the amount of recuperation and the regeneration ratio was examined.

Fig. 39: Dependence of D_e, reproducibility and recuperation on the variation of preheat temperature.

a) Preheat plateau for sample F1 of the section 'Postdüne'. Aliquots were measured in groups of 3 using 8 different preheat temperatures from 160° up to 300° C (held for 10 s each). (The cycle was repeated and 48 aliquots were measured) Six regeneration cycles were measured as described in Table 6, the first to obtain the natural signal and then 5 with the following doses: 0.38, 0.63, 0.88, 0, 0.38 Gy (test dose: 0.25 Gy). Each data point (filled circles) shows the average and standard error of 6 aliquots, except for 240°C (30 aliquots) and 260°C (24 aliquots). The dashed line is the weighted average of the D_e values over the temperature range from 160 to 240°C.
b) The open triangles represent the ratio of the fifth to the first regenerated corrected OSL response as a function of preheat temperature. The ideal value of 1 is shown as dotted line. The open squares represent the corrected OSL signal due to recuperation observed after administering the zero dose in the fourth regeneration cycle and is expressed in % of the corrected natural signal.
c) Preheat plateau for sample F9 of the section 'Postdüne' obtained by using the same protocol as described in (a), but with different regeneration doses (7.56, 15.12, 22.68, 0, 7.56 Gy) and only three aliquots for each data point, except for 260°C (20 aliquots). The dashed line shows the average of 24 aliquots (three for each temperature).
d) Regeneration ratio and recuperation percentage for sample F9 with the data presentation as in (b).
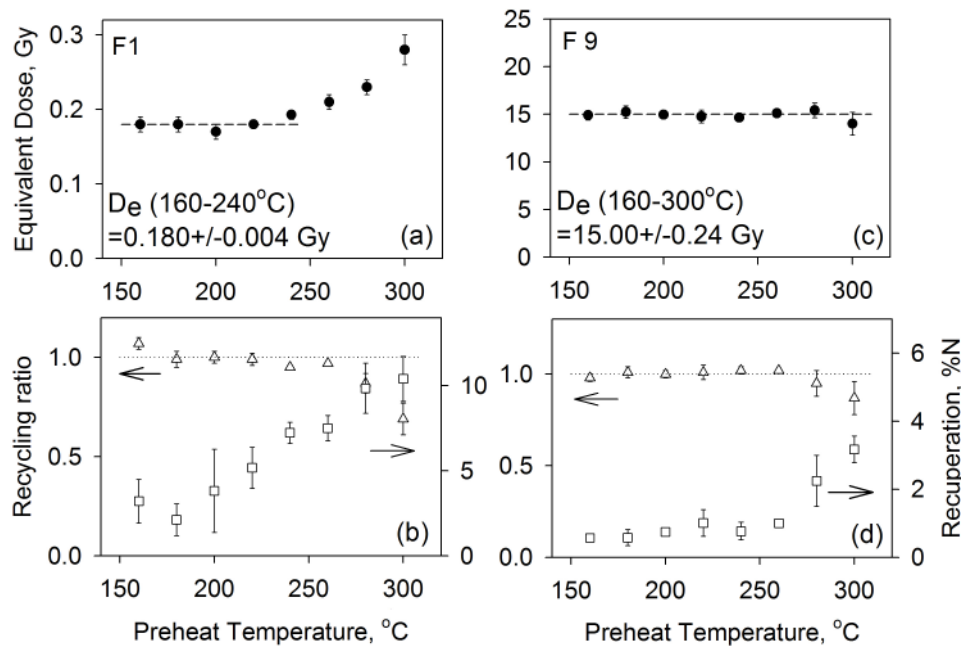
Fig. 40: Illustration of preheat protocols.

a) Dependence of the equivalent dose and the recuperation effect on varying preheat temperatures. Preheat plateaux for samples STA11, F2, F20, and R2 were measured on 24 aliquots per sample. Each data point represents the average of three aliquots, all measured using the same thermal treatment. The dashed lines indicate the range of the D_e plateau. The corrected OSL signal due to recuperation observed after administering the zero dose in the fourth regeneration cycle and expressed in % of the corrected natural signal is shown as open squares.
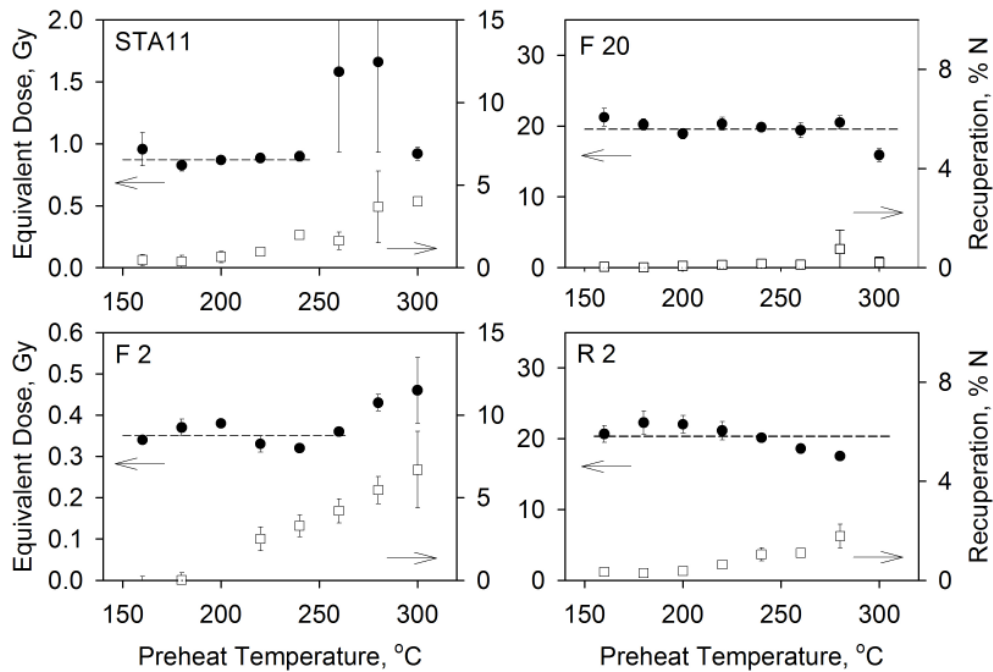
b) 'Dose recovery' preheat plateau test measured for sample AD4-5. All 24 aliquots were bleached prior to beta irradiation with the 'recovery dose' of 5.2 Gy (indicated by the dashed line for clarity). Subsequently, the aliquots were measured using the SAR protocol with different preheating treatments. Each data point represents the average of three aliquots.
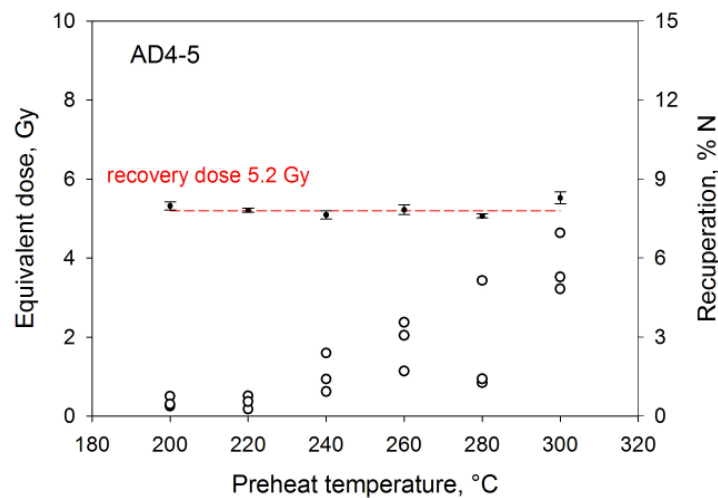
The results for the three older samples (F9, F20, and R2) are similar to those of MURRAY and WINTLE (2000), who found no systematic variation in D_e with preheat temperature in a sedimentary quartz sample with a D_e of 44.4 Gy. The preheat plateau of sample F9 covers the entire temperature range (see Fig. 39 c), as do those of R2 and F20, though with a larger scatter. By contrast, for the two youngest samples there is an increase in D_e (filled circles) with higher preheat temperatures. For sample STA11 this is difficult to state as a large scatter was observed for the three D_e values measured with preheat temperatures of 260°C and 280°C. For sample F1 (Fig. 39 a) the plateau covers the range from 160° up to 240°C, for sample F2 up to 260°C. This observation of an increase in D_e at higher temperature preheats could indicate thermal transfer, e.g. the release of charge trapped in thermally unstable, hard-to-bleach traps. This is considered in the experiment illustrated in Fig. 41.

In particular for samples F1 and F2 a substantial increase in the recuperation is observed with higher preheat temperatures (open squares in Fig. 39 and Fig. 40). Hence, it might be assumed, that recuperation can cause the increase in D_e with higher temperatures. This will be further investigated in the following.

The regeneration or recycling ratio, respectively, is shown as open triangles in Fig. 39 b) and d). Note, that because no significant deviation of the regeneration ratio from unity was found, it is not shown explicitly in Fig. 40.

BAILEY (2000) made a critical comment on the interpretation of preheat plateaux. If the D_e is shown to be a function of the preheating temperature, then it does not necessarily imply that the region of the preheat plateau will yield the correct equivalent dose. A flat region merely indicates that over a given temperature range there is no change in, for example, the thermal transfer of electrons or holes. A D_e that does not vary over a given preheat temperature range could be wrong, and vice versa the correct D_e obtained from a non-flat region. Thus, to support the overall assumption that D_e estimates from the flat region of the preheat plateau yield correct D_e values, a so-called 'dose recovery' preheat plateau test has to be conducted. For this experiment the natural OSL signal was removed from all aliquots by illumination (exposure to blue LEDs for 150 s at 125°C). Then a beta dose of 5.2 Gy was administered to all aliquots. This dose was treated as a surrogate of a 'natural' dose in the subsequent SAR measurements which were carried out using different preheat temperatures (preheating was always for 10 s, see Fig. 40 b). Over the temperature region of 180°C to 280°C the administered dose was recovered within 5 %, the best accuracy being observed between 220-

260°C. This experiment clearly supports the assumption that values from the preheat plateau region yield accurate D_e estimates. As shown in Fig. 40 b) recuperation signals are significantly lower using low-temperature preheats. The recuperation value for the preheat temperature of 220°C for example is only 0.53±0.25 %. By contrast a preheat temperature of 260°C, which is widely applied in SAR measurements on quartz, results in recuperation signals that measure 2.78±0.96 % of the natural signal. Thus, for the samples investigated in this study a relatively low preheat temperature of 220°C was chosen to keep any effect of recuperation as low as possible.

It was suggested earlier that a significant contribution of released charge from shallow, hard-to-bleach traps could cause the increase of the luminescence signals measured after high temperature preheats especially for younger samples (see preheat plateaus measured for samples F1 in Fig. 39 and F2 in Fig. 40). From the results presented in Fig. 38, charge inserted into these traps by the test dose can probably be excluded as a potential source of this transfer. This conclusion agrees with the observation of JAIN et al. (2002). They also found the dose contribution due to thermal transfer from the test dose to be insignificant, independent of the preheat temperature.

The experiment reported here was carried out to check the influence of natural hard-to-bleach components on the luminescence signal at different preheat temperatures. New preheat plateaus were measured for samples F1 and F9, but before measurement, all aliquots were bleached for 150 s with blue diodes at 125°C to remove the natural OSL signal. This experiment was carried out three times for each sample using three different test doses, 0.05 Gy (open squares), 0.31 Gy (open circles) and 3.1 Gy (open triangles) (see Fig. 40). For sample F1 this means test doses of around 25 %, 160 % and 1600 % of the expected D_e, and for sample F9 2 % (0.31 Gy) and 20 % (3.1 Gy). The 'standard preheat plateaux' (filled circles in Fig. 41 a) and b) are taken from Fig. 39 a) and c), respectively.

Fig. 41: Influence of preheat temperature and the magnitude of the test dose on thermal transfer.
a) Open symbols: Preheat plateaux for sample F1 were measured using different test doses. The data were obtained for 24 aliquots processed as described in the caption of Fig. 38 (a), but all aliquots were first stimulated for 150 s with blue diodes at 125°C to remove the natural OSL signal. The test doses applied were 25 % of the D_e (0.05 Gy, open square), 160 % (0.31 Gy, open circle) and 1600 % (3.1 Gy, open triangle). The preheat plateau using the standard procedure is taken from Fig. 39 (a) (filled circles).
b) Preheat plateaux for sample F9 measured after bleaching as described in (a) using the test doses of 0.31 Gy (2 % of the D_e, open circle) and 3.1 Gy (20 % of the D_e, open triangle). The standard preheat plateau is taken from Fig. 39 (c) (filled circles), the test dose used here was 3.8 Gy.

The experiment reported here was carried out to check the influence of natural hard-to-bleach components on the luminescence signal at different preheat temperatures. New preheat plateaus were measured for samples F1 and F9, but before measurement, all aliquots were bleached for 150 s with blue diodes at 125°C to remove the natural OSL signal. This experiment was carried out three times for each sample using three different test doses, 0.05 Gy (open squares), 0.31 Gy (open circles) and 3.1 Gy (open triangles) (see Fig. 40). For sample F1 this means test doses of around 25 %, 160 % and 1600 % of the expected D_e, and for sample F9 2 % (0.31 Gy) and 20 % (3.1 Gy). The 'standard preheat plateaux' (filled circles in Fig. 41 a) and b) are taken from Fig. 39 a) and c), respectively.

No dose was administered prior to the SAR measurements, therefore the resulting D_e should be near zero, as is the case for the preheat temperatures of 160-200°C. With increasing preheat temperatures the D_e clearly increases, i.e. significant OSL response in the first measurement cycle was observed after preheating, although the sample was completely bleached prior to heating. The behaviour of both the standard preheat plateau and the plateau from the previously bleached sample is similar in case of sample F1. Both datasets show an increase in D_e from about 220-240°C. There is no significant difference between the data sets from different test doses (compare different open signals in Fig. 41), confirming that the test dose charge is not the cause of the increased D_e.

It is assumed that natural charge was still trapped in light-insensitive traps, which were not (completely) emptied by the bleaching procedure applied (150 s blue light stimulation). This charge was thermally transferred into the main OSL trap during the preheat procedure when temperatures of more than 200/220°C were used. It seems likely that hard-to-bleach traps associated with the "280°C" TL peak are involved in the observed thermal transfer processes. These hard-to-bleached "280°C" TL traps are characterised by an electron-retention lifetime of about 200 ka. Pre-depositional electron filling is thus very likely (SPOONER priv. comm. in AITKEN 1998: 180). Besides this basic transfer being responsible for the OSL increase, recuperation may contribute significantly as well. The "280°C" TL traps could have served as refuge traps during bleaching for the photo-evicted electrons during prolonged bleaching. (Note that the "110°C" TL trap was eliminated as refuge trap, because bleaching was carried out at 125°C.)

Both the older sample (F9) and the younger sample (F1) show a similar increase in D_e with preheat temperature. This observation implies that the charge transfer takes place in both samples to the same extent. Nevertheless, the effect of this thermal transfer is much greater for the young sample. The D_e, which is calculated for the bleached data set (open symbols) at a preheat temperature of 280°C for example, amounts to roughly 50 % of the 'natural' D_e calculated for sample F1 (filled symbol in Fig. 41). By contrast, for the older sample F9 this percentage is only ~2 %. It is concluded that thermal transfer can have a significant impact on the equivalent dose estimation in case of very young samples with average D_e values of less than 0.5-1 Gy. Therefore it is probably necessary to reduce the preheat temperature for young samples to below 240°C for 10 s to avoid this transfer and thus an overestimation of the equivalent dose (and finally the age). From Fig. 39 and Fig. 40 it is concluded that such low temperatures are suitable for older samples as well, at least for the samples investigated in this

study. As a result from the described observations concerning the dependency of thermal transfer and recuperation on preheat temperatures, the standard preheat temperature used throughout this study was set to 220°C[4].

RHODES (2000) also concluded that, in some cases, thermally induced charge transfer can create significant problems in dating young materials with very small natural doses. In similar experiments as described here, JAIN et al. (2002) observed insignificant thermal transfer for preheat temperatures up to 240°C, but a subsequent increase to about 0.5 Gy at higher temperatures and therefore recommended low temperature preheats (in this case 200°C) to avoid this charge transfer.

3.5.2.3.3   *Influence of irradiation strength and the measurement equipment*

The strength of the beta source, the radiation dose in Gray per time unit (minutes or seconds), has to be determined for each individual beta source and irradiation geometry. This procedure is outlined and discussed in Appendix C. The beta dose rate that is delivered to the sample disc during irradiation is controlled by a mechanical shutter in front of the beta source. Thus, to increase the radiation dose, the shutter is simply held open for a longer time period. This process is computer controlled. In case a sample has to be irradiated with very low beta doses the time period needed to fully open and close the shutter can introduce an uncertainty in the true dose delivered to the sample. The sample is already exposed to radiation even when the shutter is not fully opened. Let's say the dose rate of the beta source is 0.11 Gy/s and a sample is irradiated for 1 second only. The dose which the sample receives in fact does not equal 0.11 Gy, because the radiation dose the sample is exposed to during the opening and closure of the shutter has to be added.

The impact of the uncertainty caused by the shutter time on the equivalent dose estimation increases with the decrease of the irradiation doses which are administered to the samples, as the percentage of the additional dose increases.

---

[4] At the beginning of this study a preheat of 260°C for 10 s was used for the samples F3-20, S2 & 3, M3 & 4, R2 & 3. But as all these samples are not as young as F1 and F2 no significant impact on the D_e is expected. Therefore, they were not remeasured with a lower preheat temperature.

To test the impact on very young samples, 13 quartz samples were selected which all have equivalent dose values of < 1Gy, mostly even <0.5 Gy. First, the D_e values were determined using a risø reader of type TL DA 15 equipped wit a 48-positions sample holder and a beta source delivering 0.11 Gy/s (reader "B"). A second set of subsamples from each of the samples was then measured on a risø reader of type TL DA 12 with a 24-positions sample holder (reader "A"). Furthermore the dose rate of the beta source included in this reader was about seven times lower than that of reader "B". The D_e values obtained for both measurements are plotted against each other in Fig. 42.

Fig. 42: Equivalent dose determination using irradiation sources of different strength.
The D_e values of 13 very young quartz samples (D_e <1 Gy) were measured on reader "A" equipped with a beta radiation source providing a dose rate of only ~0.016 Gy/s. A second set of the same samples was measured on reader "B" with a stronger beta source delivering ~0.11 Gy/s. For each sample set at least 18 aliquots were measured for D_e determination. The error bars represent the 1σ standard error of the mean and the solid line the linear regression line which is forced to pass through the origin.
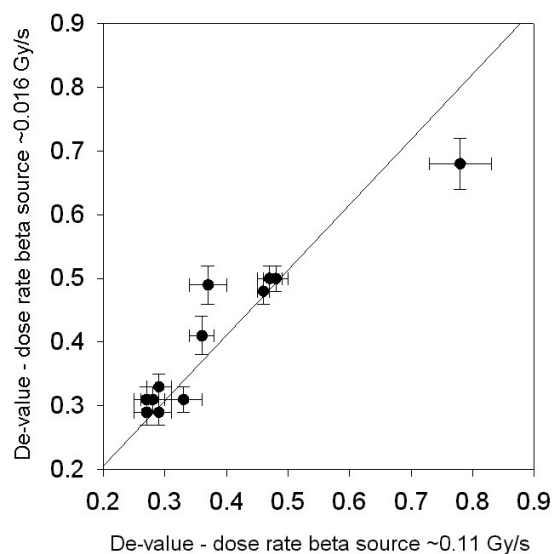
The agreement between both datasets is very good. Note, that the error bars shown in the graph represent the standard error only. The agreement would be even better if the standard deviation would be considered only.

From this comparison it is finally concluded that any uncertainty related to the exact determination of the 'true' administered beta dose during laboratory irradiation due to the design of the equipment is negligible. There is no significant effect even if very low doses are used as necessary in the dating process of very young samples.

The good agreement found between the two data sets obtained from different measurement devices (24- and 48-position sample holders) are encouraging also in terms of (i) the robustness of the applied measurement protocol to yield reliable and reproducible results and (ii) the quality of the measurement equipment by which comparable results are obtained from devices with slightly different technical design.

The latter argument refers to the discussion on an increased 'cross-talk' during illumination and irradiation in luminescence measurements using risø TL/OSL DA-15 readers (see BØTTER-JENSEN et al. 2000, 2003, BRAY et al. 2002). The sample holder of the new risø reader of the type TL/OSL DA-15 offers 48 disc positions. Compared to the old model TL DA-12 with only 24 positions the space in between two individual aliquots is narrowed. Thus, if one aliquot is placed directly beneath the beta source for irradiation, some scattered radiation can reach the neighbouring discs (cross-irradiation). This effect can further increase the uncertainty in the determination of the 'real' dose which in fact is administered to the sample compared to that which is expected according to the value entered in the software controlled system. This problem is reduced to some extent if the space between the sample positions is wider as is for the 24-position sample holder. The irradiation 'cross-talk', i.e. the percentage of dose given to an adjacent non-irradiated sample is, on average, 0.1735 ± 0.0004 % for a 4 mg mono-layer coarse-grain quartz sample using the 48-sample carousel; the 2nd nearest disc receives 0.004 ± 0.002 % of the primary beta dose (BØTTER-JENSEN et al. 2000). Finally, the additional dose caused by 'cross-talk' is considered to be very small and its effect on the equivalent dose estimates may be important only for ultra high precision D_e determinations such as required in radiation microdosimetry (see also discussion in BRAY et al. 2002).

Optical cross-talk results from scattered illumination light reaching the neighbouring discs and consequently causes a signal loss in adjacent discs. BØTTER-JENSEN et al. (2000) determined a reduction of the initial OSL intensities of the neighbouring discs by only 0.00599 ± 0.00007 % during stimulation with blue LEDs at full power using the 48 position carousel. By contrast, BRAY et al. (2002) observed a more effective cross-talk resulting in a signal loss of 0.014 % in the discs adjacent to the measurement position. From this value they simulated the expected depletion of OSL on an adjacent disc position that would result from a full SAR procedure measurement (including 14 OSL measurements with an illumination time of 50 s). The results show, that cross-illumination can have a severe effect on the D_e estimate with a signal reduction on the adjacent aliquot of ~9 % (up to 20 % if longer illumination

times are used). However, as BRAY et al. (2002) already mention, this is not a general figure, but tests on other TL/OSL readers ought to be conducted.

In this context the results presented in Fig. 42 indicate, that cross-irradiation and cross-illumination do not have a significant effect on the D_e estimates, at least in case of the equipment and the samples compared in this experiment.

3.6 Results of the equivalent dose (D_e) determination

The technique to release the absorbed dose and measure the luminescence emission of the quartz grains by using the single aliquot regenerative (SAR) dose protocol was explained in the previous section. In the following section, calculation procedures will be described that are used to translate the luminescence signal intensities into dose equivalents. Various problems and sources of errors related to the estimation of the equivalent dose values will be discussed as well.

3.6.1 Calculation procedure for equivalent dose estimates

3.6.1.1 Determination of the sensitivity corrected OSL signal

In this study only CW-OSL measurements were carried out, i.e. luminescence is monitored continuously while the light source is on. The luminescence measured takes the form of a decay curve. This so-called shine-down curve follows an exponential-like function from the beginning of excitation until all light-sensitive traps are emptied and luminescence ceases (CHEN & MCKEEVER 1997). The total luminescence signal, i.e. the amount of photons being detected, is proportional to the number of electrons that was trapped and hence to the absorbed dose. The total luminescence intensity can be calculated from the area beneath the shine-down curve.

In Fig. 43 a) several shine-down curves measured on the same aliquot are shown. In the first SAR cycle the OSL response to the natural dose the sample received during burial (natural luminescence = L_n) is measured. By this optical stimulation all the readily bleachable luminescence is removed which would be bleached by sunlight exposure during sediment transport. Thus, the sample is reset to a zero dose level prior to the following laboratory

irradiation. According to the SAR protocol the first irradiation dose is the fixed test dose; the corresponding test dose OSL (T_x) is measured as shine-down curve.

In the example presented in Fig. 43 a), seven regeneration cycles were applied incorporating a zero dose cycle for monitoring recuperation effects and a repeat of the first regeneration dose to check the reproducibility of the measurement protocol. The regeneration-doses used varied from sample to sample; these doses were based on screening measurements of the samples. It is clearly seen that the OSL intensity increases with increasing beta irradiation doses. In each SAR measurement cycle the OSL response of an aliquot to a known laboratory dose (L_x) and subsequently to the fixed test dose (T_x) is measured. The OSL response to a particular radiation dose is then determined from the integrated emission signal that is the area under the decay curve. Usually, only the first part of the decay curve is used. The selection of only a part of the luminescence signal instead of taking the light sum, e.g. the entire area beneath the shine-down curve, will be explained in the following.

In Fig. 43 a) the typical, non-exponential shape of OSL decay curves is shown. Although all measurements were carried out in order to prevent retrapping in the light-sensitive "110°C" TL trap, the decay remains slower than exponential with a long tail observed towards longer illumination times. This background level is not the same for each decay curve but obviously increases with increasing radiation dose. Therefore, it cannot be ascribed solely to an experimental background, for example to scattered illumination light. This would give rise to a constant noise. Already in their pioneer study on OSL, HUNTLEY et al. (1985) stated that the decrease in OSL emission does not follow a simple exponential function, as would be expected for a single trap system. In fact the quartz OSL decay curve was found to be rather complicated because of different components contributing to it. SMITH and RHODES (1994) described the OSL emission as the sum of three exponential decay curves, referred to as fast, medium, and slow component according to their relative optical depletion rates. These signal components show different thermal stabilities and dose responses and therefore are ascribed to be derived from different traps involved in the OSL process (BAILEY et al. 1997).

Fig. 43: Individual steps of equivalent dose determination using the single aliquot regenerative (SAR) protocol for quartz.

a) OSL shine-down curves measured as response to the natural radiation exposure and as response to laboratory beta irradiation using different radiation doses. The exponential decay is clearly seen as well as the background signal level which is derived from scattered illumination light and slowly-decreasing OSL. The first ten seconds of illumination are also shown in the inset for clarity.

b) Dose-response or growth curve plotted for one aliquot. Each net OSL signal (L_x) (background signal subtracted from the initial signal intensity) was divided by the net OSL signal (T_x) which was measured as response to the test dose in order to correct for the occurrence of sensitivity changes throughout the measurement procedures (bleaching, heating, irradiation). These sensitivity corrected OSL signals (L_x/T_x) are plotted against the corresponding regenerative dose, i.e. the laboratory beta dose that induced the signal L_x. The corrected natural OSL intensity as well as the signal monitoring the effect of recuperation (measured without previous irradiation) has a regenerative dose of zero. A curve is fitted through the data points (including the recycling and recuperation point), typically using a linear or exponential fit, to construct the dose response curve. Finally the equivalent dose, i.e. the regenerative dose that would yield an OSL intensity equivalent to the natural OSL intensity, is obtained by interpolation. By that one equivalent dose value is derived from only one aliquot.

c) In routine application not only one aliquot is measured. Here, dose response curves for 5 aliquots of the same sample are presented. The curves as well as the natural signals and the corresponding D_e values slightly deviate from each other. Reasons for this scatter are further explained in the text.

d) Equivalent dose distribution illustrated as a histogram. The dotted black line indicates the Gaussian normal distribution curve. The D_e value of a sample is finally derived from the mean of such distributions of individual D_e estimates. See the text for a discussion of the use of the arithmetic or weighted mean and further methods of D_e estimation in case of complex asymmetric equivalent dose distributions.
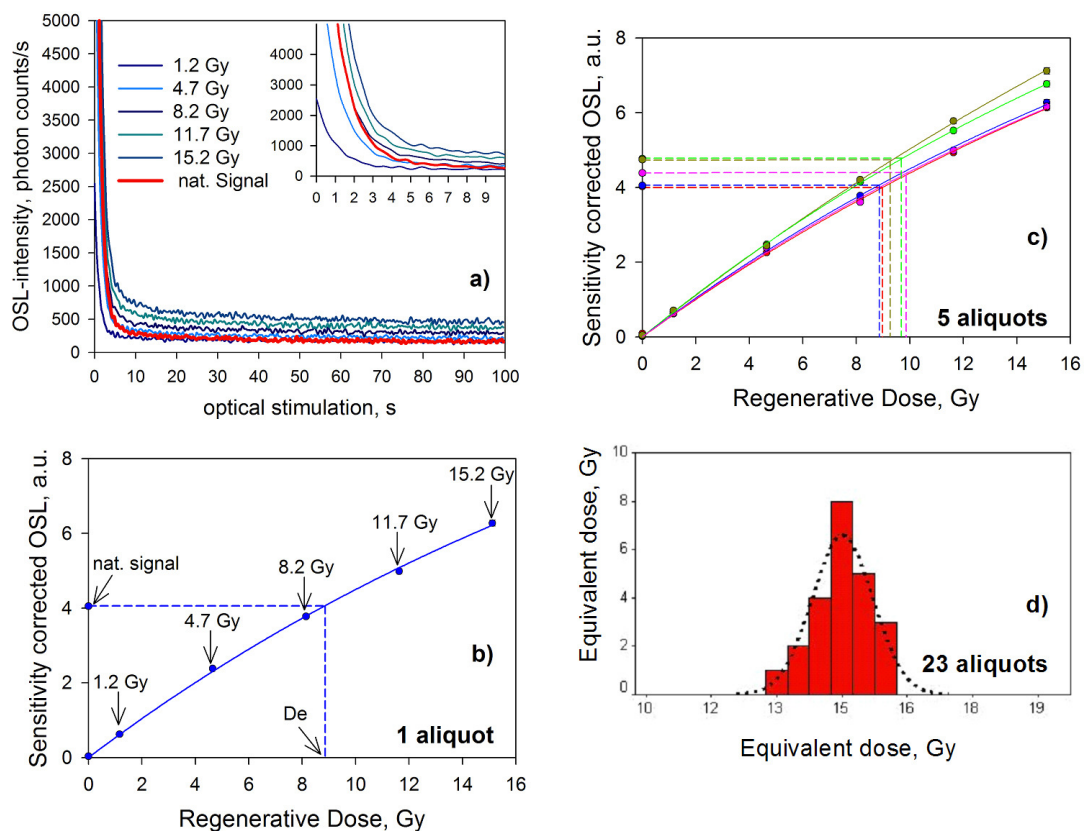
Subsequent studies identified even more than three components in quartz OSL decay curves. However, a universal behaviour for quartz was not observed (KUHNS et al. 2000, BULUR et al. 2000, JAIN et al. 2003, SINGARAYER & BAILEY 2003). Commonly, linear modulation (LM) OSL (BULUR 1996) is used in these studies for discrimination between the various OSL components and further investigation of their properties. With respect to the analysis of CW-OSL decay curves the different components and their characteristics are summarised as the following (according to e.g. BULUR et al. 2000, BAILEY et al. 1997):

- the fast and easy-to-bleach component, high detrapping rate, decays most rapidly with stimulation time and gives rise to the initial signal with steep decline, related to the "325°C" TL trap according to its dose response and thermal stability

- intermediate broad or medium component, related to shallow traps contributing to the "110°C" TL peak, component disappears when OSL is measured at 125°C

- slow broad and difficult-to-bleach component at longer illumination times is characterised by high saturation dose and thermal stability (deepest trap) but slow depletion rate (necessary exposure times to white light for bleaching the slow component down to negligible levels were found to be sample dependent and vary between 17 h and 1 week, SINGARAYER et al. 2000).

For calculation of the signal intensities only the initial luminescence signal (<1.2 s, BANERJEE et al. 2000) is used, although, as shown by MURRAY and WINTLE (1998), there is no significant influence on the result, if calculating the OSL response over the whole integral or if using only initial signal. But there are several advantages of using only the initial signal:

o minimizing the problems of interpreting complex multi-component decay curves. By using only the initial OSL response, it is assumed that this signal is dominated by the fast component (WINTLE & MURRAY 1998, BANERJEE et al. 2000).

o the better signal-to-noise-ratio, especially if measuring samples having only weak luminescence signal intensity. If the integral chosen for analysis is too large, the statistical uncertainty in the OSL signals after background subtraction increases (BANERJEE et al. 2000).

To obtain the net OSL signal, a background signal deriving from scattered illumination light and slowly-decreasing OSL must be subtracted (BØTTER-JENSEN et al. 1999b, MURRAY & WINTLE 1999). While the part of scattered light of the LEDs should contribute to the background signal to a similar extent throughout repeated measurement cycles, the

background signal which is ascribed to the medium and slow components of the OSL signal accumulates with the number of regeneration cycles (WINTLE & MURRAY 1997, see also Fig. 43 a). For the samples investigated in this study the OSL signal of the last 10 % of the stimulation time was subtracted as background as suggested by MURRAY and WINTLE (1999).

As was shown earlier (section 3.5.2), the luminescence sensitivity, i.e. the amount of luminescence emitted by a sample for a given radiation dose, varies not only from one sample to the other, but also from one measurement to the next measurement of the same sample. These changes affect the luminescence response to the regenerative doses (L_x) as well as the response to the fixed test dose (T_x). In section 3.5.2.2 it was shown that sensitivity changes monitored by the T_x signals show a linear relationship to those monitored by the L_x signals. Therefore, the sensitivity changes can be corrected by simply dividing the L_x signals by their corresponding T_x signals. For equivalent dose determination the ratio L_x/T_x is finally plotted as a function of laboratory dose (Fig. 43 b) with:

$$\text{Sensitivity corrected OSL signal for the laboratory dose x and the test dose x}$$

$$= \frac{\text{net } L_x}{\text{net } T_x} = \frac{L_x \text{ (initial integrated signal – integrated background signal)}}{T_x \text{ (initial integrated signal –integrated background signal)}}$$

3.6.1.2 Determination of the equivalent dose (D_e)

The software *Luminescence Analyst,* (version 3.07b, written by Dr. G.A:T. Duller, Aberystwyth, 2002) was used for analysis of the SAR measurements and calculation of the D_e values. Besides the calculation of the sensitivity corrected signal intensities, this program provides a variety of growth curve forms that can be fitted through the L_x/T_x ratios in order to construct a dose response curve such as shown in Fig. 43 b). Either linear, quadratic, linerar&exponential, or exponential functions can be fitted through the data points. For this purpose the uncertainties in each individual data point are required which are derived from photon counting statistics (BANERJEE et al. 2000). To calculate the error in the equivalent dose two sources of uncertainties are combined: (i) the deviation of the fitted growth curve from the measured data points, and (ii) the uncertainty in the ratio of L_n/T_n, i.e. the error derived from counting statistics of the sensitivity corrected natural signal (for further explanations the reader is referred to DULLER 2002).

In the routine application of the SAR protocol, multiple replicates of the equivalent dose are determined using about 12 to 24 subsamples (DULLER 2004). In this study ~18 aliquots of each sample were used for D_e estimation (see Appendix D, Table D.1). The aliquots were processed in several groups in order to take the influence of any variations in the measurement equipment (e.g. variations in the photomultiplier dark counts) into account.

Ideally, one would expect each sub-sample measured with the SAR protocol to yield the same equivalent dose value due to the same amount of trapped charge in the grains. Neither for natural samples nor for laboratory simulations is this observed to be the case. Various effects can cause a spread in the distribution of the equivalent dose values:

(a) incomplete resetting of the OSL signal at the time of deposition (poor bleaching) (e.g. MURRAY et al. 1995, CLARKE et al. 1999, FUCHS & LANG 2001);

(b) inhomogeneous dose rate distributions in particular on the grain-to-grain scale (microdosimetry effects) including external inhomogeneities in the beta dose radiation field but also differences in alpha dose contributions from inclusions within the grains (MURRAY & ROBERTS 1997, OLLEY et al. 1997, VANDENBERGHE 2003);

(c) contamination due to intrusion of grains with higher or lower absorbed doses from other layers (BATEMAN et al. 2003, LOMAX et al. 2006);

(d) random scatter due to OSL measurement imprecision resulting from photon-counting statistics (WALLINGA 2002, GALBRAITH et al. 2005);

(e) the variability of luminescence properties on a grain-to-grain scale which are presumably due to differences in the trace element geochemistry, the geological origin and history of the grains (e.g. type and number of charge traps), or the radiation history of the sample (including the number of cycles of deposition and erosion, i.e. the luminescence sensitization) (e.g. ADAMIEC 2000, DULLER et al. 2000, DULLER 2004);

(f) difficulties in precise D_e determination when the natural signal approaches the saturation level of the exponential growth curve (e.g. LOMAX et al. 2003, MURRAY & FUNDER 2003);

(g) a variable impact of thermal transfer effects which contribute an additional dose (significant, if at all, only for low dose samples, see section 3.5.2.3.2) (ROBERTS et al. 1999, 2000).

Investigations of thoroughly reset (well-bleached) sediments have refuted the idea that equivalent dose distributions are simple gaussian distributions arising solely from experimental errors (MURRAY et al. 1995, MURRAY & ROBERTS 1997). In Fig. 43 c and d the

scatter among the individual D_e estimates observed for a sample from a supposedly well-bleached homogeneous dune deposits is illustrated. The various sources of scatter in the equivalent dose distribution will be investigated and discussed in more detail later in this chapter. But obviously a certain dispersion of the individual D_e estimates has to be expected from natural materials such as sedimentary quartz.

The overall D_e value of a sample can be assessed from multiple, normally distributed replicates (Fig. 43 c) as the weighted mean where each D_e value is weighted by its precision resulting from the SAR measurement (see explanation of the error calculation for individual D_e measurements above). If the D_e estimates are determined with similar precision the arithmetic mean can also be used (e.g. GEYH 2000).

For 56 samples out of the 183 samples investigated in this study only three regeneration cycles were measured, for the 127 other five regeneration dose points were determined in order to construct a dose response curve. These 56 samples were the first to be measured of the entire study, therefore the analysing software *Luminescence Analyst, version 3.07b* (DULLER 2002) (described above) was not available yet.

The first 56 samples were measured following the suggestion of MURRAY and WINTLE (2000) to set three regenerative doses close to the expected equivalent dose in order to obtain a still linear relation of the dose response (see Fig. 44 a). Using this approach the error on the overall D_e is assessed by the spread in D_e estimates from a set of aliquots. The individual experimental error of each equivalent dose value derived from photon counting statistics and curve fitting parameters is not taken into account. Therefore for these samples no weighted mean could be calculated and the arithmetic mean served as basis for the equivalent dose estimation instead.

To finally summarise all 164 equivalent dose results in one data set for further statistical analysis it must be proved that there is no significant difference between the D_e values based on the arithmetic mean and those based on the error weighted mean. Therefore, for one sample the equivalent dose was determined using the SAR procedure with three regeneration dose point as well as with five dose points. The mean values agree within 1σ standard errors (see Fig. 44 a and b for representative dose response curves for each data set):

3 regen. doses	$\Rightarrow$ arithmetic mean =	12.75±0.29 Gy (n=13)
5 regen. doses	$\Rightarrow$ arithmetic mean =	12.70±0.17 Gy (n=15)
	$\Rightarrow$ weighted mean =	12.69±0.04 Gy (n=15)

Fig. 44: Comparison of SAR measurements using 3 different regenerative doses or five different irradiation doses, respectively.

a) Equivalent dose estimation for one aliquot of a Lateglacial dune sand sample by interpolation between three different dose points. These are chosen in such a way that they encompass the expected dose.

b) Equivalent dose estimation for one aliquot of the same sample as used for a). Here the relation between the individual dose points is not linear as in a), but rather exponential. Again, the D_e is determined by interpolation.

c) Comparison of the arithmetic and the weighted mean of 113 dune sand samples which were measured using the SAR protocol with five different regeneration doses. Note that all D_e values of the samples were used to calculate the final D_e estimate, i.e. including any outliers. The arithmetic mean is considered to be affected to a higher degree by the impact of only few outliers in the data set. Hence, any negative effect of using the arithmetic mean for D_e calculation should be more pronounced in this illustration than comparing the weighted and arithmetic mean calculated after exclusion of outliers.
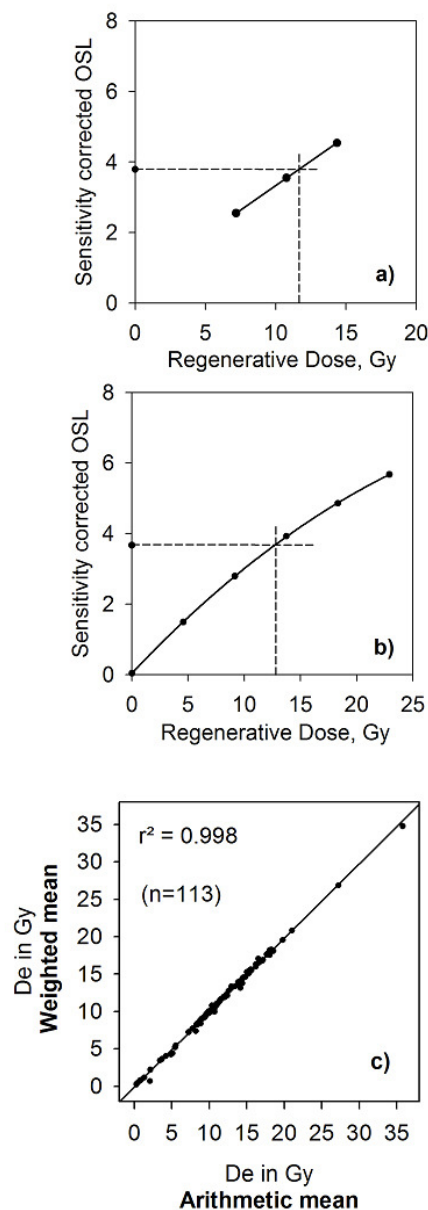
In Fig. 44 c) the weighted and arithmetic mean values, which were calculated for the 113 aeolian samples measured by using five different regenerative doses, are compared. An excellent agreement was found between the arithmetic and weighted mean values. This observation implies that the uncertainty in the estimate of the equivalent dose from each aliquot is nearly the same. If so, the individual D_e error can be set to 1, which would result in the weighted mean value to equal the arithmetic mean. The equality of the experimental errors from each aliquot was generally assumed in single aliquot studies which calculated the uncertainty in the overall equivalent dose by explicitly looking at the distribution of individual D_e results (DULLER et al. 2000). The aeolian samples investigated in this study, characterised by bright OSL signals, provide evidence to support this assumption.

With regard to both comparisons it is concluded that there is no major impact of the mode of measurement with three or five dose points allowing the interpretation of all D_e values obtained from aeolian samples as one data set.

3.6.1.3 Testing for normal distribution and impact of outlier exclusion

In a well-bleached sample from homogeneous sediments a narrowly defined D_e distribution with a low standard deviation and little asymmetry would be expected. However, numerous aeolian sand samples investigated in this study showed distributions with large standard deviations and significant asymmetry. In this study, appropriate statistical parameters are used to describe the shape of the D_e distributions (Fig. 45), rather than presenting histograms for each equivalent dose distribution.

The coefficient of variation ($v=$ standard deviation/mean) describes the spread of individual D_e estimates around the mean with high values indicating a broad scatter. The skewness describes the deviation of the distribution from a symmetric distribution, the zero value representing a normal distribution and positive values indicating a shift of the distribution peak to the lower edge of the scale and a tail towards high values. The excess describes the width of the peak. Again zero values represent a normal distribution. High values are indicative for broad distributions with a low peak height.

Fig. 45: Impact of the exclusion of outliers on the various statistical parameters describing the equivalent dose distributions.

Only the aeolian samples investigated in this study are included in the data comparison. For further discussion the reader is referred to the text. Note, that one coefficient of variation value is not shown in the left histogram, because it exceeds the value of 1. This value is included in the calculation of the mean, standard deviation, and median. It is also shown in the right graph (normally distributed values).
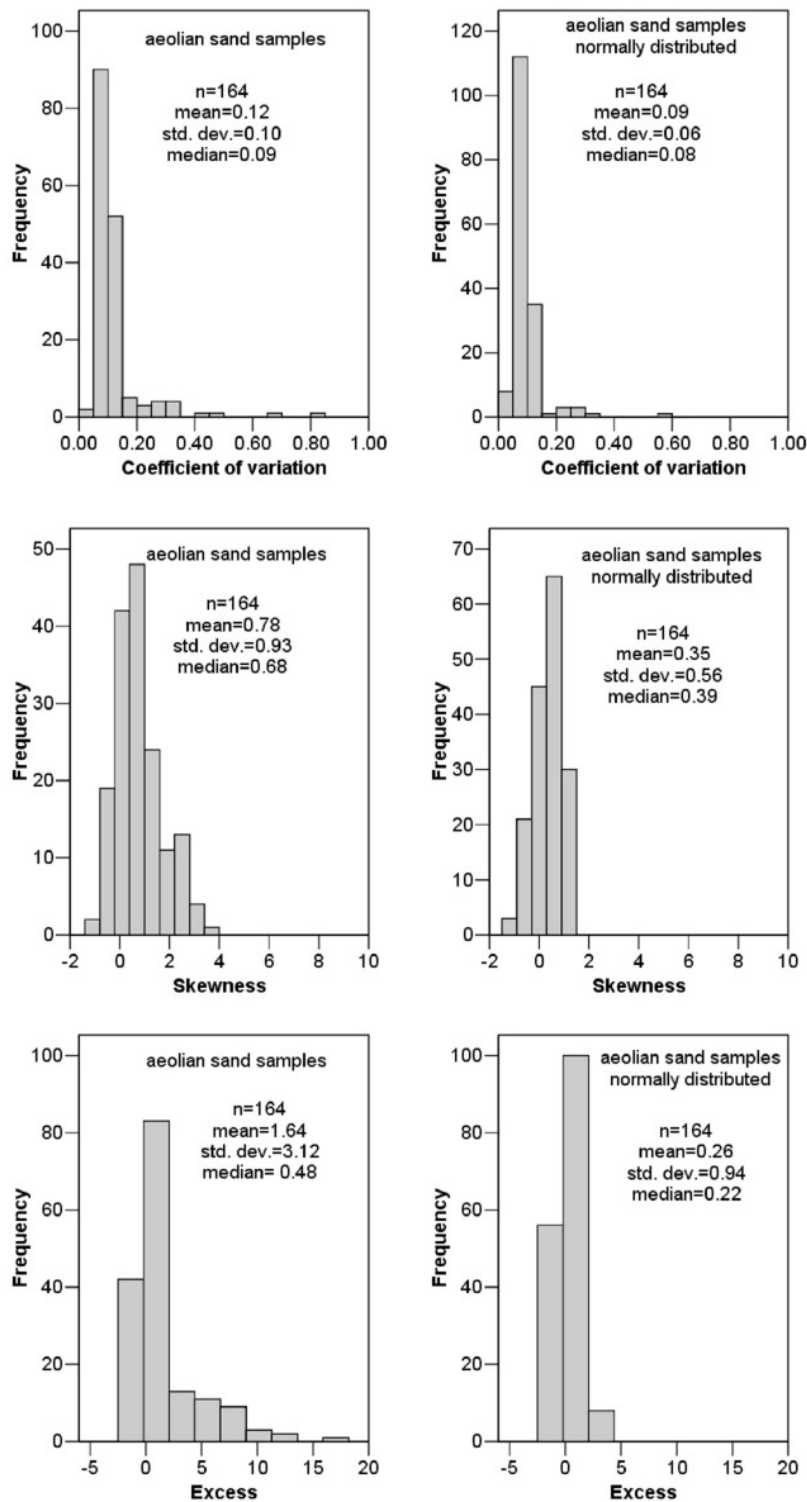
It is noted here, that out of the 183 samples investigated in this study, 18 were taken from non-aeolian sediments. One aeolian sample was identified to be of modern age (G17). This sample hardly showed any OSL signal at all and was excluded from further interpretation of the data set.

In fact all parameter plots (graphs on the left side) show a tail towards high values, or positive values in case of skewness and excess. Skewness and excess values which significantly deviate from zero indicate that at least the D_e values of some samples are not normally distributed. Therefore, each data set was tested for normal distribution using the *Kolomogorov-Smirnov* (KS) statistical test (with *Lilliefors'* significance) and also the *Shapiro-Wilk* normality test. The latter test represents a modification of the KS-test and is particularly suited for small populations of values with n<50. The basic principle of the *Kolmogorov-Smirnov* statistic is that from the classified values of a random sample a theoretical cumulative normal distribution is calculated whose mean and variance are estimated from the given random sample. The cumulative distribution of the random sample is then compared to the theoretical normal distribution. The significance with which the given distribution deviates from the theoretical normal distribution is determined by the maximum difference between the observed and theoretical cumulative distribution curve (e.g. SCHÖNWIESE 2000). In this study, the D_e values of the tested distributions were considered to be not normally distributed, if the significance level was found to be less than 0.05 (5 %). Using this criterium, the initial data sets of 112 out of the 164 aeolian sand samples were normally distributed. For the non-normally distributed samples, outliers from the normal distribution were excluded from the data set and the remaining distribution tested again.

This procedure was repeated until the significance level exceeded 0.05, indicating that at least 95 % of the D_e values could be considered to be normally distributed. These statistical tests were carried out using the statistical software package *SPSS version 11 or 12*, respectively.[5] The procedure is shown exemplarily in Fig. 46.

---

[5] The algorithms applied in this software for the tests used in this study can be found for example in www1.uni-hamburg.de/RRZ/Software/SPSS/Algorith.115/examine.pdf, 2006).

Fig. 46: Illustration of the procedure which was applied in order to identify and exclude outliers from the equivalent dose distributions.

The histograms present the D_e distributions of a Lateglacial dune sand sample (sample UM2, site' Ueckermünde-A') and the normal distribution curve fitted to the data. The initial data set consists of 20 individual D_e values that are not normally distributed according to the *Shapiro-Wilk (Kolmogorov-Smirnov)* test statistic. If the outlier towards the higher dose range is excluded (n=19) the data set still fails the test for normal distribution. If the outlier towards the lower dose range is excluded, finally all values are within the range of the normal distribution curve. This procedure was applied for each sample.
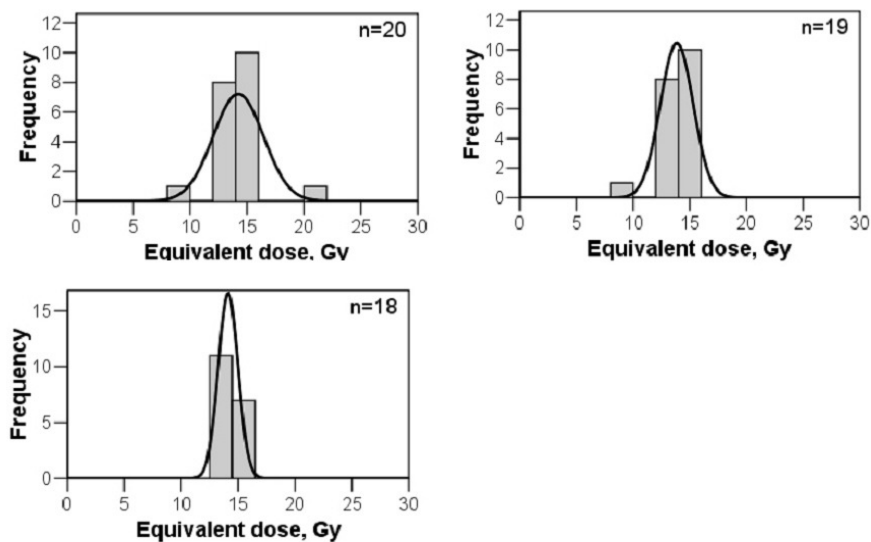
Fig. 47: Impact of the exclusion of outliers on the finally resulting D_e values of all aeolian sand samples.

The initial equivalent dose distribution was already normally distributed for 112 out of the 164 samples. For the remaining 52 samples the equivalent dose values calculated for the normally distributed data sets are compared to those obtained for all values including outliers (a). 41 of these 52 samples were measured using five regenerative doses; therefore also the impact on the weighted mean is shown in graph b). There is no significant impact of the outlier exclusion, and both data sets show strong correlation.
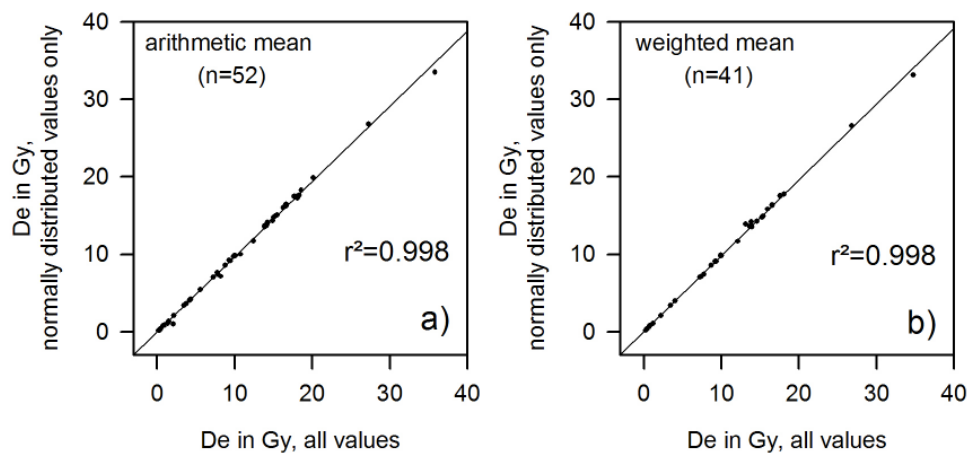
In Fig. 47 the impact of the exclusion of outliers on the resulting D_e mean is illustrated. The D_e values obtained from normally distributed data sets are in good agreement with those derived from data sets including the outliers. Thus, no significant impact of the outlier exclusion was observed, i.e. the presence of outliers had no significant impact regarding an over- or underestimation of the equivalent dose.

The statistical parameters for the normally distributed data sets are also summarised in Fig. 45 (graphs shown on the right side, see also Table D 1in Appendix D). In particular the tails towards high values of skewness and excess have been removed by this data processing including the test for normal distribution. The obtained mean or median values, respectively, for the different statistical parameters might be interpreted as threshold values at least for the sediments in the study area. Provided that the samples are well-bleached and the scatter in D_e estimates is only due to analytical errors and minor variations in the natural radiation environment, any D_e distribution found to exceed these threshold values could be influenced by other sources of scatter such as poor bleaching, significant microdosimetry effects, or post-sedimentary mixing. The application of such threshold values will be critically discussed in the next sections.

3.6.1.4 Discussion of the quality of the equivalent dose estimates

As was described earlier, the single aliquot regenerative dose protocol incorporates several internal tests for the quality of the D_e determination, such as the repetition of the first regeneration dose cycle and the inclusion of a zero dose cycle to monitor the recuperation effects.

The recuperation values (corrected zero dose OSL signal in percentage of the corrected natural luminescence intensity), which were obtained for the aeolian samples investigated in this study, range from 0.2 to 8.0 % with an average of 1.29±1.54 % (median 0.76 %).

As shown in Fig. 48 the highest values correspond with low equivalent dose values. Hence, if it at all, high recuperation signals have the greatest impact on the youngest samples with D_e values of about < 2 Gy. At this point it is noted again that the preheat temperature was reduced to 220°C in order to keep recuperation effects as low as possible (see section 3.5.2.3.2). From Fig. 48 it is now concluded, that this approach is in particular recommendable for samples with an equivalent dose expected to be less than 2 Gy.

Fig. 48: The effect of recuperation in relation to the equivalent dose shown for 164 quartz samples extracted from dune sands.
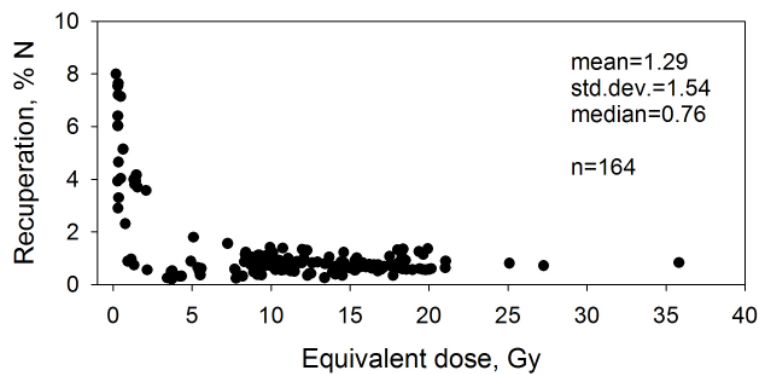
Average regeneration (or recycling) ratios were observed not to exceed a threshold of ± 10 % from unity, thus indicating that the protocol applied here was successful in correcting any sensitivity changes. The mean recycling ratio and corresponding standard deviation of the data set of 164 samples, which represents roughly about 3000 individual equivalent dose measurements estimates, is 1.02±0.02 (median 1.02).

However, as pointed out by MURRAY and WINTLE (2003), a good recycling ratio not necessarily implies a reliable performance of the SAR protocol. SAR measurements can result in inaccurate D_e estimates, which finally give rise to age over- or underestimation, although excellent recycling ratios were observed in the SAR measurements (see e.g. WALLINGA et al. 2000). Thus, the use of so-called 'dose recovery tests' is suggested to measure the accuracy with which a known dose can be determined using the SAR protocol (ROBERTS et al. 1999, WALLINGA et al. 2000, MURRAY & WINTLE 2003).

Several 'dose recovery tests' (DRT) were carried out in this study. For this purpose a set of sub-samples was optically bleached by exposing the aliquots to the blue LED light for 100 s while the aliquots were constantly held at 125°C during optical stimulation. Note that optical stimulation is carried out at 125°C in order to prevent any interference of the "110°C" TL trap. GALBRAITH et al. (2005) carried out artificial bleaching at room temperature and observed a residual dose of ~0.7 Gy after 100 s of stimulation, which they attributed to post-illumination transfer of charge cycled through the 110°C TL peak.

After optical resetting all sub-samples are irradiated with the same defined laboratory beta dose. This artificial dose is treated as an unknown dose in the subsequent SAR measurement. All measurement parameters are the same as used in the 'routine' SAR procedure for

determination of the 'natural' equivalent dose. The results of the 'dose recovery tests' are summarised in Table 7. The ratio of the administered laboratory dose to the dose value 'recovered' by the subsequent SAR measurement indicates the success of the 'dose recovery test'. In all test measurements the given dose was recovered with an uncertainty of ±1 %. Therefore, it is concluded that the SAR protocol with the measurement parameters used as described in the previous sections is able to measure an absorbed dose in the quartz samples investigated here with sufficient accuracy. Of course, this conclusion is generalised as DRT's ought to be carried out for each individual sample to take into account any sample dependent variability which is caused by different luminescence properties of the quartz samples. Furthermore, the artificial dose ought to be similar as the expected 'natural' equivalent dose in order to take the impact of growth curve construction (linear or exponential shape close to the saturation level) into account.

However, conducting 'dose recovery tests' for each of the 183 samples investigated in this study was not feasible, but at least, the samples chosen for DRT's are from different study areas (with exception of samples STA00-5 and -10 which are from the same section). The good recovery of the administered dose in 'dose recovery tests' supports the applicability of the SAR procedure to the measured samples. But the accuracy of the protocol can be ultimately validated only by comparison with independent age control. For a review of numerous comparative studies including SAR based OSL ages and independent age control the reader is referred to MURRAY and OLLEY (2002). They found a good reliability and accuracy of SAR quartz ages covering a wide age range (last century to at least 350 ka) and different depositional environments (aeolian, fluvial, lacustrine, marine, and glacio-fluvial/-lacustrine).

Table 7: Results of dose recovery tests for five quartz samples of this study.
All measurements were carried out on 8mm aliquots using the SAR protocol.

sample	dose recovery test		
	given dose (Gy)	ratio given/measured	n
UM 2	5.2	0.99	18 (18)
AD 4-5	5.2	1.01	18 (18)
JC-3	5.2	1.01	17 (18)
STA00-5	9.3	1.01	18 (18)
STA00-10	5.2	1.01	17 (18)

3.6.2 'Aeolian deposits are usually well-bleached' – a critical discussion

Optical ages of sediment samples represent the time elapsed since the mineral grains were last exposed to sunlight provided that the time and intensity of light exposure was sufficient to empty the OSL source traps. If this resetting of the OSL signal was incomplete, at least some grains may carry a residual OSL signal which causes an overestimation of the equivalent dose and hence of the OSL age. This is particularly relevant for fluvial and colluvial sediments since these materials may have been transported under conditions of short transport distances and reduced light intensities. The latter can be caused by sediment load in the water which results in filtering and attenuation of the solar spectrum. In such instances the resetting of the OSL signal was frequently observed to be incomplete (e.g. MURRAY et al. 1995, OLLEY et al. 1998, STOKES et al. 2001, JAIN et al. 2004, FUCHS et al. 2005, SINGARAYER et al. 2005). But "for aeolian materials, the degree of optical resetting at deposition is rarely a problem" (DULLER 2004: 191, see also SINGARAYER et al. 2005). This study presents a large OSL data set of aeolian deposits. Therefore in this section special emphasis is placed on the question whether insufficient bleaching indeed is unlikely to be a problem in wind-borne sediments as widely assumed.

Identification of poor bleaching in OSL dating studies can be achieved by various methods. The easiest way to identify overestimation of OSL ages is by comparison with independent age constraints and good chronostratigraphic control. If individual OSL ages differ significantly from the ages obtained for the over- and underlying sediment, the OSL age might be erroneous. If no independent chronology is available and a low sampling resolution does not allow the construction of a robust OSL chronology, then two options exist to test the equivalent dose estimates for incomplete resetting of the OSL signal. One set of techniques analyses the OSL signal in detail. The second approach concentrates on the examination and interpretation of the equivalent dose distribution. Both options will be discussed in the following sections in more detail.

3.6.2.1 Inconsistency with the chronostratigraphy

In this study a range of radiocarbon ages provide independent control for the OSL chronologies (see section 5.1 for a summary and chapter 1 for site dependent discussion). The comparison of OSL and ^{14}C ages showed two cases where the OSL ages significantly (2 σ range) overestimated the ^{14}C ages from related sediment layers. However, the overestimation of the true depositional age by OSL is not straightforward as the accuracy of the radiocarbon ages in these cases is doubtful (see chapter 1 and 1 for a detailed discussion).

With respect to the internal OSL chronostratigraphy, at site 'Neuhaus' two samples (N2 and N4) were identified to significantly overestimate the depositional age. Here, nine samples were taken from about 4.6 m of dune sand which were deposited 320 years ago according to seven OSL ages that are all in excellent agreement. Only two samples from the same sand unit showed significantly older ages of 480 and 700 years. It is most likely that these two samples give the wrong answer rather then the seven others. This age overestimation is explained by the significantly higher equivalent dose values. It is unlikely to be caused by erroneous dose rate estimations, as these were found to be quite homogeneous for this homogeneous sediment unit (see Appendix F for illustration). Higher equivalent dose values could be due, for example, to poor bleaching or intermixing of sand grains from older deposits. The latter hypothesis seems rather unlikely, because both older samples (N2 & N4) are from the top part of the section. They are encompassed by sediment layers dated consistently to 320 years. Significantly older deposits are found in the section at least 3 meters deeper than the sampling positions of samples N2 and N4. Furthermore, at the time of sampling no disturbance was observed in the cross-section. Thus, it is finally concluded that both samples most likely overestimate the depositional age because of incomplete resetting of the OSL signal. At this dune site more than 4.6 m of sand has been deposited in very short time 320 years ago. These Late Holocene aeolian remobilisations seem to be catastrophic, but locally restricted, events. Thus presumably at least some sediment was transported over very short distances, not only during bright daylight conditions, and rapidly buried after deposition. Under such circumstances restricted bleaching conditions seem less astonishing.

3.6.2.2 Detecting poor bleaching by OSL signal analysis

The overall advantage of using the signal analysis for identification of poor bleaching over any dose distribution method that concentrates on the inter-aliquot scatter is that by signal analysis other sources of scatter such as microdosimetry effects or post-depositional mixing can be excluded.

3.6.2.2.1   *The D_e versus illumination time plot*

When HUNTLEY et al. (1985) first described the application of optical dating they already mentioned the use of shine-plateau tests in order to detect partial bleaching. In order to construct a shine-plateau the equivalent dose is plotted against the OSL illumination time, i.e. for example for each second of illumination an individual D_e is calculated from the integrated sum light intensity. The sample is considered to be completely bleached, if the plot is flat. Hence, the D_e remains the same whether it is calculated from the first second of stimulation or from any other point in illumination time. For an insufficiently bleached sample the equivalent dose value is expected to increase with longer illumination time since the OSL signal at longer illumination time originates from traps which are more difficult to empty optically.

BAILEY (2003) suggested the suitability of such D_e (t) plots for the identification of partial bleaching in single aliquot studies based on the fact that the quartz OSL signal consists of several components with different light sensitivities (see section 3.6.1.1). The applicability of this approach is dependent on the pre-depositional dose, the spectrum and extent of bleaching in the past, and the signal intensity (SINGARAYER & BAILEY 2003, VANDENBERGHE et al. 2003).

VANDENBERGHE (2003) carried out numerous D_e (t) plots on aeolian and fluvial sediments. The relation of rising shine-plateaus to poor bleaching was not straightforward for none of the investigated aliquots, regardless of whether the sample was from aeolian, fluvio-aeolian or fluvial environments. He concluded a limited usefulness of shine-down plateaus for the identification of poor bleaching in quartz samples, contradictory to the findings of BAILEY et al. (2003). The interpretation of D_e (t) plots is complicated because any trend in the plateau, rising, falling or constant, can be attributed to a combination of causes, other than only partial bleaching. Furthermore, any successful identification of partial bleaching by the SAR D_e (t)

plot is related to the slow component only and hence does not provide any information on the degree of resetting of the fast component (VANDENBERGHE 2003). But it is this fast component, the initial OSL intensity, which is used for equivalent dose determination and for dating.

To conclude, even if the slow component is identified to be insufficiently bleached at the time of deposition, this does not necessarily imply that also the fast component is poorly bleached. Taking into account that the time required to reset the slow component is more than 100 times longer than that sufficient to bleach down the fast component (e.g. > 1000 s versus 10 s, AGERSNAP LARSEN et al. 2000) the D_e (t) plot seems inappropriate for identifying partial bleaching in particular for aeolian sediments (for further discussion see also VANDENBERGHE 2003, VANDENBERGHE et al. 2003, SINGARAYER & BAILEY 2003). Therefore this approach was not further considered for the aeolian samples investigated in this study. This decision was further supported by the results of a comprehensive study on the degree of optical resetting in modern-age aeolian and fluvial samples by SINGARAYER et al. (2005). They concluded from D_e (t) plots and component-resolved linearly modulated OSL measurements that in all the aeolian samples they investigated all quartz OSL components were fully reset by sunlight exposure. By contrary, the De (t) plots measured for modern-age fluvial samples showed that the incompletely bleached slow component could result in measurable residual signals up to 15 Gy.

3.6.2.2.2   *Correlation of OSL intensity versus equivalent dose*

LI (1994) first proposed the use of scatter in OSL intensities and equivalent doses for detection of poor bleaching in single aliquot analysis. This approach is not solely based on equivalent dose distributions but also takes into account the OSL signal. Therefore it is discussed in this section. LI suggested the identification of poorly bleached sub-samples by plotting the natural luminescence intensity versus the corresponding equivalent dose. This approach is based on the assumption that poorly bleached samples show a wide range of D_e values and an increasing trend of equivalent dose with the natural OSL intensity.

This basic principle of a correlation between high dose and high signal intensity was also the background for further developments, e.g. those proposed by COLLS (1999). But these approaches did not account for sensitivity changes in the quartz luminescence. These changes

can be induced for example by the first heating of the sample prior to the measurement of the natural OSL signal. Therefore the prerequisite of a direct correlation between light intensity and absorbed dose is lacking.

The limitations of the 'signal versus dose' method was demonstrated, for example, by FOLZ et al. (2001) showing no correlation between the natural OSL intensities and D_e values in poorly bleached fluvial samples which overestimated the known age by 40 %.

WALLINGA (2002) could demonstrate by numerical simulations that the number of grains contributing to the OSL signal and the proportion of poorly-bleached grains in the grain population are critical factors in this approach. He found statistically significant correlations of aliquot OSL intensity versus D_e only when large aliquots were used with a small percentage of grains (~10 %) which carried very high residual doses.

In Fig. 49 a few examples are illustrated which show dose versus OSL intensity plots for samples investigated in this study. These experiments were conducted following the refined version of the 'signal versus dose correlation' approach which was presented by LI (2001). This method is based on the sensitivity corrected OSL intensities of the natural signals. Two glaciofluvial-glaciolimnic sediment samples were chosen for this experiment, They are likely to be insufficiently bleached during transport, as the OSL ages clearly overestimate the depositional age deduced from the geological context. For comparison, two supposedly well-bleached aeolian samples were also measured.

On the contrary to the findings of FOLZ et al. (2001), the results presented in Fig. 49 are more encouraging. Although a strong correlation between light intensity and D_e values is absent, a larger data spread and a trend towards high signal intensities corresponding with high D_e values is observed for the non-aeolian samples UM9 and UM27. As expected for well-bleached deposits, the aeolian samples show only little data spread.

Fig. 49: Plot of equivalent dose values versus sensitivity corrected natural OSL intensities following Li (2001).
All equivalent dose values were determined using the SAR protocol. Here large aliquots consisting of more than >1000 quartz grains were used. The OSL ages based on the weighted average of the D_e values as shown here overestimate the expected depositional ages in case of samples UM27 and UM9, whereas those of samples UM20 and UM3 are in good agreement with the expected age deduced from an underlying palaeosol horizon. The overestimation of samples UM27 and UM9 is explained by incomplete resetting of the OSL signal at the time of deposition and burial.

Glaziofluvial-glaciolimnic sand   **Aeolian sand**
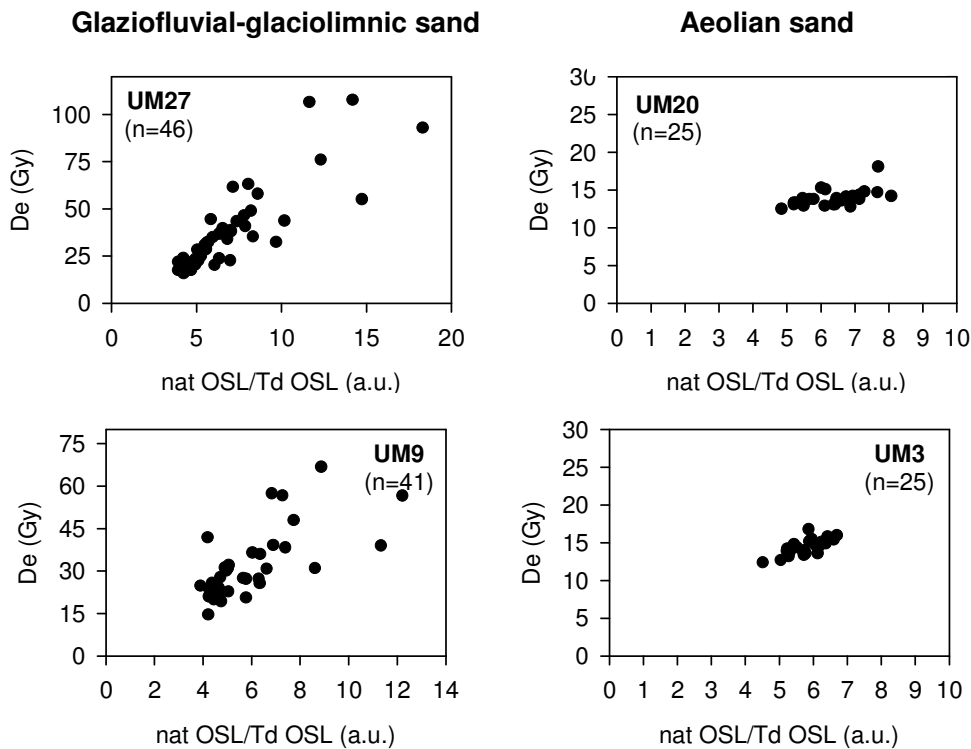
It is concluded, that at least in the examples illustrated in Fig. 49 poor bleaching is identified in the glaciofluvial-glaciolimnic sediments by the approach of Li (2001). This observation can be explained by the observation of Wallinga (2002) which was described before: with each aliquot large grain populations (>1000) were measured which contained only a small percentage of grains with a very high residual dose.

In such circumstances the 'signal versus dose' approach seems to be a powerful tool for identifying poor bleaching. But the major problem remains. Determination of the 'true' burial dose is difficult from these large aliquots containing poorly bleached grain populations. But reducing the number of grains per aliquot in a second cycle of SAR measurements would give a better resolution of the dose distribution and provide an improved basis for equivalent dose determination.

3.6.2.3 Identification of poor bleaching in D_e distributions

Incomplete resetting (partial bleaching) at deposition leaves some grains, or in the worst cases all grains of a sediment sample with an unknown residual signal. This residual leads to an apparent higher accumulated palaeodose during the burial period and this in turn results in an overestimation of the depositional age. The dose heterogeneity between fully and partially bleached grains in a sample causes an increased variability in equivalent dose values that is seen in D_e distributions as broad scatter amongst the individual dose values. Hence, identification of poor bleaching is widely based on the data spread observed in equivalent dose distributions.

3.6.2.3.1   *Asymmetry of D_e distributions*

The skewness characterises the degree of asymmetry of the D_e distribution around the mean. Positive skewness is interpreted as indication for poor-bleaching of a sample (MURRAY et al. 1995). Thresholds for identification of poor bleaching based on the skewness of equivalent dose distributions have not been suggested so far. Several implications for the interpretation of the scatter in D_e distributions are derived from the width (represented by v or S_N values) and the symmetry of the D_e distribution (represented by the skewness):

- for well-bleached samples a tight and symmetrical dose distribution is expected, that includes the normal spread due to experimental errors (WALLINGA 2002, see sample UM 22 in Fig. 50 for example);

- positively skewed distributions are supposed to indicate a small percentage of poorly bleached grains (e.g. WALLINGA 2002, OLLEY et al. 1998, see sample UM23 in Fig. 50 for example);

- wide but symmetrical distributions may be a hint on a large amount of poorly bleached grains or microdosimetry effects (WALLINGA 20002, OLLEY et al. 1999, MURRAY & ROBERTS 1997).

In Fig. 50 histograms are shown which illustrate the D_e distributions obtained for an aeolian and a glaciofluvial-glaciolimnic sample from study site 'Uckermünder-Heide-C' of this study (see chapter 4 and Appendix D for more details on the samples). Sample UM22 is in good agreement with independent age control provided by a palaeosol horizon, hence it is assumed to be well-bleached. This conclusion is supported by the tight equivalent dose distribution. On contrary, the D_e distribution sample UM23, in particular when measured with small aliquots, shows a clear asymmetry with a marked tail towards higher D_e values. This could indicate that grain populations are present which were not sufficiently bleached at the time of deposition and burial. In fact, the OSL ages derived from the two distributions presented in Fig. 50 for sample UM23 both clearly overestimate the expected depositional age.

Fig. 50: Dose distributions for samples UM22 and UM23. OSL measurements were carried out using either large aliquots (>1000 grains) or small aliquots (<100 grains).
The presented histograms were calculated from all aliquots with sufficient OSL response to create a dose response curve, i.e. outliers are still included in the data sets. For the well-bleached aeolian sample UM22 rather tight and symmetric distributions were obtained, whereas for the poorly-bleached non-aeolian sample UM23 broad distributions were observed. A significant tail towards high De values is particulary visible in the distribution derived from the small aliquots.
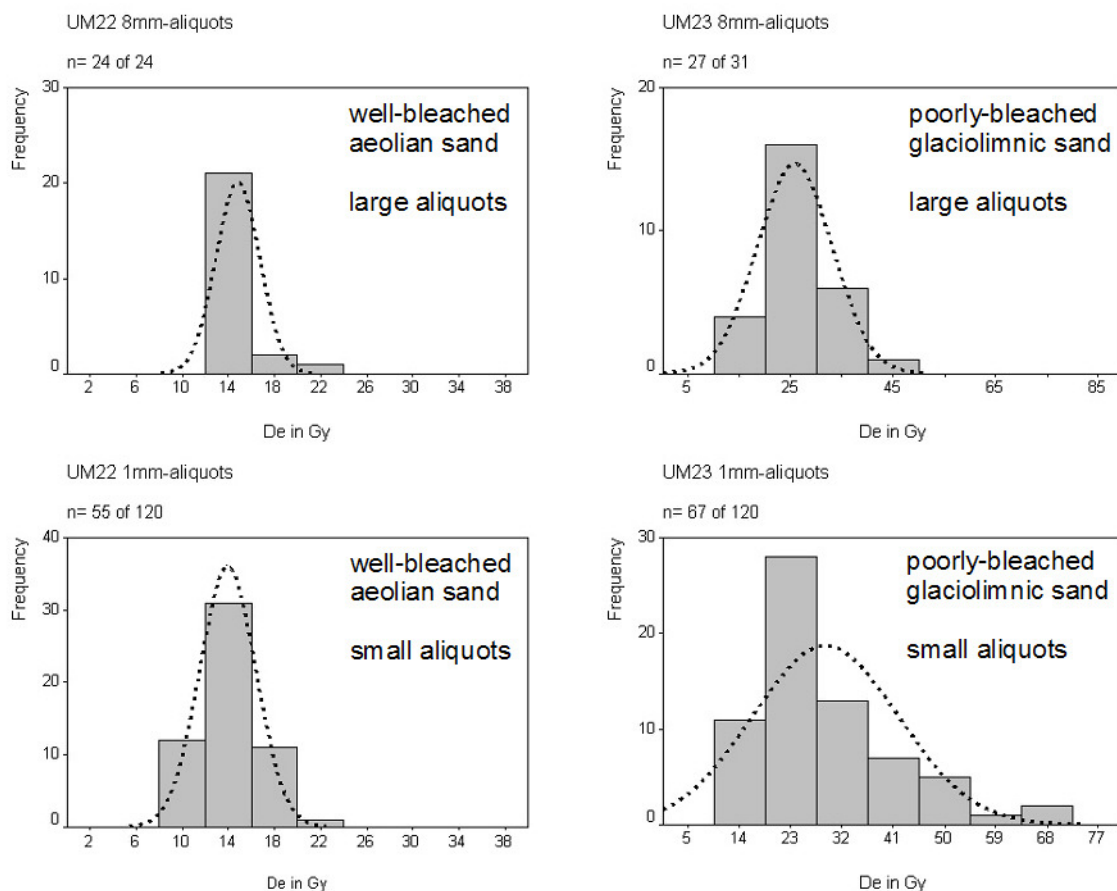
The comparison of the D_e distributions in Fig. 50 indicates that poorly-bleached samples can show a broad, but symmetric distribution (UM 23, large aliquots). This observation is in agreement with FUCHS et al. (2006) who conclude that poor bleaching not necessarily results in positively skewed distributions, because they obtained both, positively skewed as well as symmetric distributions in simulated insufficiently bleached samples (artificial mixture of bleached and partially bleached grains).

As numerous studies demonstrated, the success of identification of poor bleaching by the asymmetry of the D_e distribution is strongly dependent on the number of grains per aliquot.

A multi-grain aliquot of poorly bleached sediments may consist of grains that have received different light exposure energies, leaving grains with different residuals at the time of deposition. When a large number of grains are measured at a time, the sum of light from all grains is detected and by that the contribution of only a few grains carrying a higher dose can be averaged out (see distribution of UM23, large aliquots, Fig. 50). The probability to discriminate well-bleached grain populations from those containing poorly-bleached grains is consequently increased when the number of grains per sample is reduced. Hence, identification of poor bleaching in D_e distributions ought to be at its best when applied to small aliquots which consist of only a few grains or ultimately even of one grain (OLLEY et al. 1998, 1999, ROBERTS et al. 2000, WALLINGA 2002, FUCHS & WAGNER 2003).

In this context it is worth mentioning that most grains of a sub-sample show only dim light emission or no emission at all. From numerous single grain studies it is well-known that 80 to 95 % of the natural OSL emission comes from a small percentage (2-10 %) of grains (e.g. DULLER et al. 2000, THOMSEN et al. 2003, JACOBS et al. 2003). For a quartz sample with only ~20 % of grains yielding measurable OSL signals DULLER (2004) calculated 'effective' aliquot sizes which actually contribute to the OSL emission: for an aliquot containing approximately 1000 grains the effective size would comprise 200 grains, and ca. 200 grains would result in an 'effective' grain population of c. 40 grains.

To conclude, the asymmetry of D_e distributions is not an unambiguous criterion for identifying poor bleaching. Although positive skewness of D_e distributions indicates that the sample contains a small percentage of poorly bleached grains, symmetric distributions provide no assurance that problems with poor bleaching are generally absent (see for example

FUCHS et al. 2006). The strong dependence on the number of grains contributing to the OSL signal must always be considered in any interpretation of the skewness.

3.6.2.3.2   Thresholds for the relative scatter in equivalent dose distributions

The coefficient of variation (ν = standard deviation/mean equivalent dose, also described as fractional error S_N) has been used as an indicator for the extent of scatter in the equivalent dose distributions. CLARKE et al. (1999) suggested a threshold of $S_N > 0.10$ as indicator for poorly-bleached grain populations (see also FUCHS 2001, FUCHS & WAGNER 2003).

From simulation results obtained for poorly-bleached virtual samples WALLINGA (2002) concluded that this threshold is only successful for samples contaminated with a small number of poorly bleached grains. FUCHS and WAGNER (2003) demonstrated that the ν-value varies significantly with the number of grains measured per aliquot even if the material is well-bleached.

The variation of the ν-values is explained by the fact that other sources than only the degree of signal resetting contribute to the scatter in equivalent dose distributions. Such additional sources of scatter are for example the variability in intrinsic luminescence properties of the sample and in measurement conditions, heterogeneities in the beta dosimetry or post-depositional mixing of grains with different ages (for a summary of the various causes for D_e scatter see section 3.6.1.2). Threshold ν-values from the literature do not account for any variation in the part of the scatter which is related to sample inherent properties. Furthermore, general thresholds do not allow discrimination between the individual sources which contribute to the variation in D_e values. Hence, they are not suited to identify poor bleaching from the size of scatter in D_e distributions.

The use of threshold ν-values for identification of poorly bleached samples is improved, if the coefficients of variation are calculated for equivalent dose distributions derived from 'dose recovery tests' (DRT, see section 3.6.1.4). Because all sub-samples are completely bleached prior to irradiation, the data spread in the DRT distribution reflects the D_e variation of a well-bleached sample (FUCHS & LANG 2001, FUCHS & WAGNER 2003). Furthermore, threshold ν-values calculated from DRT distributions exclude other sources of scatter besides poor bleaching, notably the effects of variations in microdosimetry and post-depositional mixing. To obtain reliable thresholds for the D_e variability, it is crucial to use the same sample size for

the DRT measurements as for the measurement of the natural sub-samples, because the scatter due to measurement statistics increases with the reduction of the sample size (e.g. WALLINGA 2002, FUCHS & WAGNER 2003, LOMAX et al. 2003, BUBENZER et al. 2006).

The coefficients of variation calculated for DRT D_e distributions were used as criterion to discriminate poorly and well-bleached sediments in numerous studies (e.g. FUCHS & LANG 2001, FUCHS & WAGNER 2003, BUBENZER et al. 2006, FUCHS et al. 2006). But its application is restricted. 'Dose recovery tests' allow the examination of the random variability in D_e values which is induced only by instrumental errors, measurement statistics and the intrinsic luminescence properties of the sample. But these measurements do not take into account the scatter which is caused by any variation in the natural radiation field of the samples (see e.g. discussion in GALBRAITH et al. 2005).

More or less homogeneous beta sources are commonly used for irradiation of the sub-samples which are measured in 'dose recovery tests'. But in the natural environment the samples are exposed to a radiation field which represents the sum of alpha, beta, gamma, and cosmic radiation which all show different attenuation characteristics (see section 3.2.1). Microdosimetry effects, in particular concerning the beta radiation field, can cause an inhomogeneous irradiation on a grain-to-grain scale even in homogeneous dune deposits (see discussion in section 3.3.3.2 and 3.6.3.7). Some grains may incorporate a significant amount of radionuclides which than contribute an additional dose to these grains (internal microdosimetry effect, see e.g. discussion in VANDENBERGHE et al. 2003).

These variations in the natural irradiation of the samples are not taken into account in DRT measurements which use homogeneous and monoenergetic radiation sources for irradiation of the sub-samples. Thus, ν-values from DRT measurements underestimate the natural variation in D_e estimates even for well-bleached samples. Hence, they are not entirely suited to serve as threshold values for identification of poor bleaching.

3.6.2.3.3   Determination of the natural variation in D_e estimates from well-bleached deposits

As was discussed in the previous section, 'dose recovery tests' allow the examination of the random variability in D_e values. But as a measure for the precision of the data set in ideal conditions concerning bleaching and irradiation conditions, the coefficient of variation calculated from DRT distributions underestimates the natural variation in D_e estimates even for well-bleached samples.

A reliable estimate of the baseline variation, the 'true' data spread among natural sub-samples that all were well-bleached at the time of deposition and have absorbed the same natural radiation dose during burial, would provide a helpful tool in interpretation of any D_e distribution of samples from similar depositional environments (GALBRAITH et al. 2005). The crucial question in identifying poorly bleached samples is to which extent a scatter in D_e is acceptable as being due to natural variation only and when an additional source of scatter has to be taken into account.

The application of such a 'natural threshold variation' is restricted for various reasons; it is only valid for

- Samples from similar depositional environments (e.g. from homogenous sand deposits)
- the same size of the sub-samples (number and size of grains);
- material with similar luminescence properties, such as luminescence sensitivity (with regard to errors due to photon counting statistics);
- a certain dose range, as for samples close to the saturation level usually a higher scatter is expected than for lower dose samples in the linear or exponential part of the dose-response relation.

In the following section the estimation of such a real baseline variation in D_e for well-bleached samples based on the data set of this study will be discussed in detail.

3.6.3 The natural variation in equivalent dose estimates in the dose range 0-20 Gy from well-bleached aeolian deposits

The concept of using the average v-value of natural equivalent dose distributions of well-bleached samples as threshold for identification of poor bleaching requires a data set of well-bleached samples which are not affected by other sources of D_e scatter to an above-average amount. The present study compiles a large equivalent dose data set for samples taken from homogeneous aeolian sand deposits which are supposedly all well-bleached. Hence, this data pool would provide good premises to create a dimension for the baseline variation in natural samples from comparable depositional environments. The mean coefficient of variation of 0.09 ± 0.06 (see Fig. 45), which was determined from the set of 164 aeolian sand samples, therefore could serve as such a threshold value.

However, to support the reliability of this value, the necessary homogeneity of the data set has to be verified first. Any significant, non-uniform influence of a particular effect that causes an above-average dispersion of D_e values has to be ruled out (GALBRAITH et al. 2005, see section 3.6.1.2 for a summary of the various causes for scatter in D_e values). For example, it has to be ascertained that any D_e distributions are excluded from the data, which are derived from poorly bleached samples, or samples which were affected by bioturbation. In this section the impact of the various sources for scatter in equivalent dose distributions will be examined with regard to the present data set of 164 aeolian sand samples.

3.6.3.1 Measurement conditions

The additional data spread which might be introduced by variations of the measurement conditions (e.g. preheat procedure, test dose size) is regarded to be very small in the present data set. For all samples the single aliquot regenerative dose protocol was applied. The measurement parameters were kept constant as far as possible to obtain a methodically consistent data set.

However, parts of the scatter in dose distributions are attributed to the equipment which is used for luminescence measurements (e.g. instrument reproducibility, beta source spatial non-uniformity, THOMSEN et al. 2005). This source of scatter is included in the 'ideal' v-value which can be derived from 'dose recovery tests'.

Equivalent dose measurements which are carried out on quartz grains with substantial differences in grain diameters can show a larger spread in absorbed beta doses than D_e distributions determined for aliquots with grains from a narrow grain size range. This is explained by the dependence of beta radiation attenuation on the grain diameter (MEJDAHL 1979, BRENNAN 2003, see section 3.3.1). Thus, if the grains on a disc have variable diameters, they receive variable external beta doses. As this effect results in a variation of the absorbed beta doses on a grain-to-grain scale, it belongs to the microdosimetry effects. But as both, the natural and laboratory beta irradiation, are affected, 'dose recovery' measurements include the impact of this source of scatter. Therefore, this grain size dependent scatter in beta dosimetry is discussed at this stage already.

The impact of this microdosimetry effect can be minimised by choosing the grain size range for OSL measurements as small as possible. Therefore, most OSL measurements in this study were carried out using a comparatively narrow grain size range of 90-150 µm.

3.6.3.2 Photon counting statistics

The coefficient of variation calculated for D_e distributions includes the random scatter due to OSL measurement imprecision resulting from photon counting statistics (WALLINGA 2002, GALBRAITH 2003, GALBRAITH et al. 2005). A significant over-dispersion of the equivalent dose values due to variable measurement precision (GALBRAITH 2003) is not observed for the samples investigated in this study. The good agreement ($r^2 = 0.998$) between the D_e estimates based on the arithmetic and weighted mean, respectively (see Fig. 44 c), implies more or less equal individual errors of the D_e estimates or a similar precision of each SAR measurement, respectively.

Furthermore, an increase in D_e scatter induced by a variable impact of photon counting statistics is considered to have only minor importance for the samples investigated in this study. All measurements were carried out on large aliquots and all samples are characterised by good luminescence properties with intense OSL output. Bright signals cause less problems with photon counting. However, weaker OSL emissions are expected for low absorbed doses. Hence, dim signals might induce a larger data spread in equivalent dose distributions in the low dose range due to poor photon counting statistics and hence an increased uncertainty in

D_e determination. But from Fig. 51 it is concluded, that there is no strong correlation between low equivalent dose values (<1 Gy) and above-average coefficients of variation.

Fig. 51: Correlation between equivalent dose values and the corresponding coefficients of variation for all 164 aeolian samples.
No strong correlation is found between very low D_e values and high υ-values.
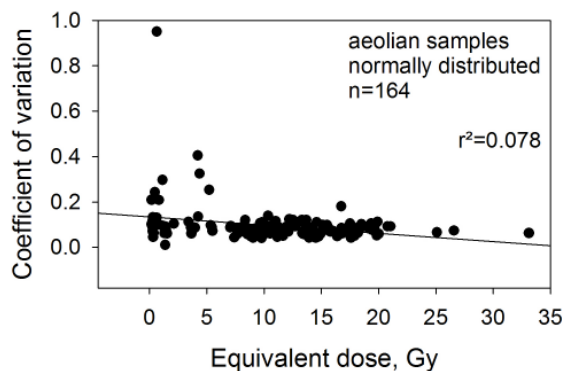
3.6.3.3 Dose range

Difficulties in precise D_e determination occur when the natural signal approaches the saturation level of the exponential growth curve (e.g. LOMAX et al. 2003, MURRAY & FUNDER 2003). This increased uncertainty can contribute an additional scatter to the D_e distribution. Almost all equivalent dose values determined in this study are within a range of only 0 to 20 Gy (see Fig. 51). Hence, interpolation of the natural OSL signals was always still in a region of the dose response curve with only very little curvature. Therefore the impact of non-linearity of the growth curves is considered to be negligible for the samples investigated in this study.

3.6.3.4 Intrinsic luminescence properties

Variability of the luminescence properties can occur on a grain-to-grain scale and contribute an additional scatter in D_e values between aliquots of the same sample. Such varieties in luminescence characteristics are presumably due to differences in the trace element geochemistry, the geological origin of the grains (e.g. type and number of charge traps), or the radiation history of the sample (including the number of cycles of deposition and erosion, i.e. the luminescence sensitization) (e.g. ADAMIEC 2000, DULLER et al. 2000, DULLER 2004). In this study OSL measurements were carried out on large, multi-grain aliquots in general, which

consist of more than 1000 grains. But even if taking in mind, that the 'effective' aliquot size, i.e. the number of grains yielding measurable OSL signals, is much smaller (e.g. 200 out of 1000, see DULLER 2004: 189, DULLER et al. 2000, JACOBS et al . 2003), variations in the luminescence properties ought to be averaged out to a major extent in such large sub-samples. However, the impact of variations of intrinsic luminescence properties on the dispersion of D_e values is reflected by 'dose recovery tests'.

In order to assess the baseline value for the coefficient of variation, which can be expected for the 'best case' scenario with 'ideal' conditions regarding bleaching and irradiation, 'dose recovery tests' were carried out. The results are summarised in Table 8.

Table 8: Summary of the υ-values obtained from 'dose recovery tests' carried out on 8mm and 1mm aliquots.
The number of aliquots used for D_e estimation is also shown with the number of aliquots measured in total put in parentheses.

aliquot size 8mm			
sample	given dose (Gy)	n	coefficient of variation
UM 2	5.2	18 (18)	0.04
AD 4-5	5.2	18 (18)	0.06
JC-3	5.2	17 (18)	0.05
STA00-5	9.3	18 (18)	0.03
STA00-10	5.2	17 (18)	0.02
		mean	0.04±0.02

aliquot size 1mm			
sample	given dose (Gy)	n	coefficient of variation
UM 6	17.4	30 (48)	0.13
UM 10	20.3	37 (65)	0.13
UM 26	10.3	29 (48)	0.14
STA00-5	9.3	57 (70)	0.12
		mean	0.13±0.01

The υ-values obtained from DRT distributions account for any D_e scatter introduced by (i) the measurement conditions, (ii) photon counting statistics, (iii) the shape of the dose response curve (if the recovery dose is within the expected natural dose range and not much lower), and (iv) intrinsic luminescence properties of the measured quartz sample. The average υ-value derived from the DRTs is 0.04±0.02. This value is smaller than the average υ-value of 0.09±0.06 which is calculated for the data set of 164 D_e distributions of natural samples.

Hence, the expected underestimation of the natural data spread by the coefficient of variation from dose recovery tests is actually observed (see section 3.6.2.3.2). The impact of incomplete bleaching, post-depositional mixing and microdosimetry variations in the natural environment on the equivalent dose dispersion is eliminated in dose recovery tests. Hence, it has to be investigated, whether the difference between the 'best case' υ-value of 0.04 and the 'natural' υ-value of 0.09 has to be attributed to the impact of the three aforementioned sources of scatter or whether this difference effectively the variability in absorbed doses due to the heterogeneity of the natural radiation. In this context, special focus is placed on the above-average coefficients of variation which create the tail in the υ-value histogram shown in Fig. 45.

3.6.3.5 Incomplete zeroing of the luminescence signal

A variable impact of thermal transfer can cause an over-dispersion of equivalent dose values. By thermal treatment during the measurement sequence, charge from hard-to-bleach traps can be transferred into the OSL trap and hence contribute an additional dose to the affected sub-samples (ROBERTS et al. 1999, 2000, THOMSEN et al. 2005). A significant impact of thermal transfer, if at all, is expected for low dose samples (see section 3.5.2.3.2). However, as shown in Fig. 51, no strong correlation is observed between the amount of scatter (coefficient of variation) and the size of the equivalent dose value. In this context it is pointed out, that in this study the preheat temperature was kept rather low at 220°C to minimise in particular any thermal transfer processes. Thus, the influence of variable thermal transfer effects on the spread in dose values is considered negligible.

By contrast, incomplete resetting of the OSL signal at the time of deposition is considered to be one of the major contributors to the scatter in equivalent dose values. The various options for identification of poorly-bleached samples have been discussed in the previous sections. The detection of insufficient bleaching by OSL signal analysis was concluded to be not particularly suited for aeolian deposits.

OSL measurements were carried out on large aliquots, i.e. the central 8 mm diameter of each disc was covered with a mono-layer of quartz grains (grain sizes between 100-200 µm). Thus, each aliquot consists of about 1000-2000 grains approximately (DULLER 2004 and direct

counting of grains on representative aliquots used in this study, see Appendix C for an illustration of a 'standard' aliquot). Detection of a small proportion of poorly bleached grains in such large grain populations is quite unlikely (e.g. WALLINGA 2002). Hence, it is concluded that an interpretation of the symmetry of the D_e distributions is not helpful for the discrimination of well- and poorly-bleached samples in case of the present data set.

OSL measurements of small grain populations or even single grains are assumed better to reflect any inhomogeneities in the dose distributions than those obtained for large, multi-grain aliquots. Thus, a comparison of both data sets ought to yield useful information on the presence of such irregularities.

Fig. 52: Equivalent dose determination using small (1 mm diameter covered with ~100-200 grains) or large (8 mm diameter covered with >1000 grains) aliquots of the quartz sand sample STA00-5 (site 'Schletau').

The 'natural dose' distributions reflect the natural scatter in the De distribution which can be caused by, for example, incomplete bleaching, post-sedimentary mixing, spatial variations in the radiation flux and changes in sample inherent luminescence properties (such as differences in the number and types of charge traps, or variations in the geochemistry among the individual grains). On the contrary, the scatter in the 'recovery dose' distribution is predominantly caused by measurement uncertainties and sample-inherent properties as the aliquots were completely bleached prior to homogeneous beta radiation in the laboratory (administered beta dose = 9.33 Gy). For both aliquot sizes, it is concluded that the sample has been sufficiently bleached at the time of deposition. Both 'natural' data sets show symmetric dose distributions, which are similar in shape to the 'dose recovery test' distributions.
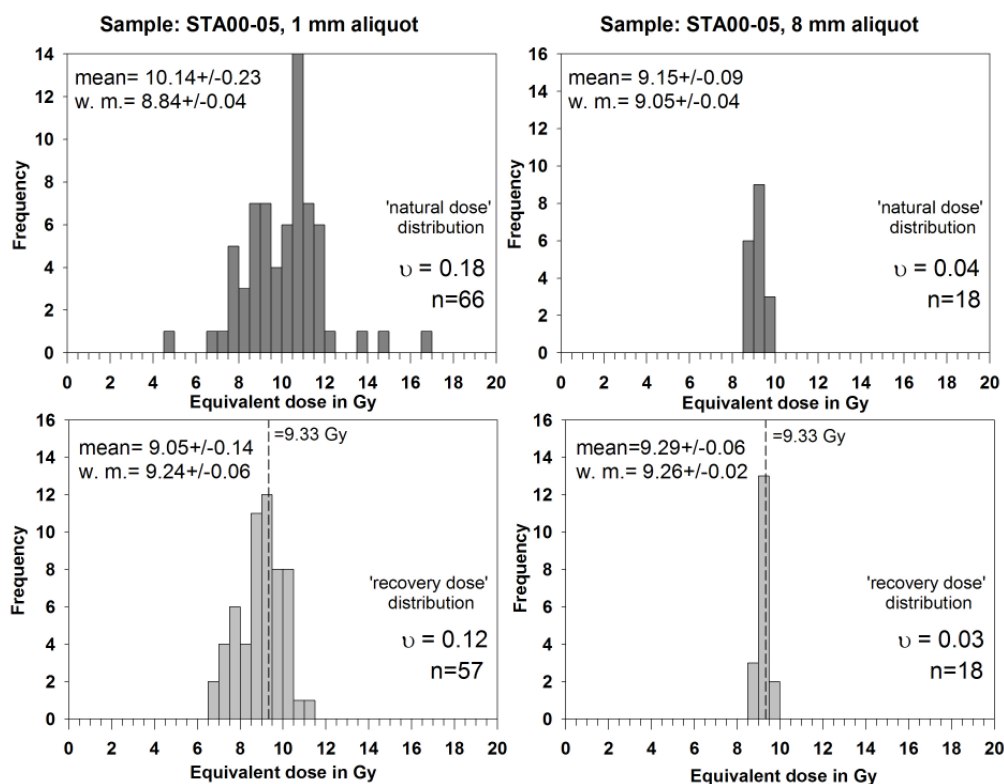
In Fig. 52 D_e histograms for sample STA-5 are presented which were obtained for small, 1mm sub-samples with less than 100 grains (1mm disc diameter covered with a monolayer of grains) and large, 8mm aliquots. This sample is considered to be well-bleached for various reasons. The distributions are rather symmetric for both aliquot sizes and the mean equivalent dose values show good agreement with a ratio of the D_e values (8mm/1mm) of 1.03. If poorly bleached, a higher mean D_e value would be expected to result from the 8mm aliquot measurements and a more asymmetric distribution for the 1mm aliquot data set. By contrast, both data sets show a similar spread in individual D_e estimates as observed in the 'dose recovery' distributions (see Fig. 52) for which the assumption of complete bleaching is valid.

For eight dune sand samples OSL measurements were carried out on 1mm aliquots in order to test, whether a true scatter in the D_e results is averaged out by using large aliquots. For each of the samples between 50 and 120 sub-samples were measured using small, 1mm aliquots. The luminescence signal intensities of a large proportion of aliquots were insufficient to use the dose response for growth curve construction. Furthermore, numerous SAR measurements showed very poor recycling (exceeding ±20 % from unity) indicating that the sensitivity correction did not work properly. Consequently a high percentage of aliquots had to be discharged from the data analysis. On average 58 % of the measured aliquots could be used for D_e estimation. Table 9 summarises the results of the 1mm aliquot measurements including the comparison to the D_e estimates from large aliquots.

Table 9: Summary of the equivalent dose measurements using 1mm aliquots for eight different aeolian samples.
The avarge υ-value calculated for the eight samples is 0.19±0.03.

Sample	Number of measured aliquots	Number of D_e estimates	Number of n.d. D_e estimates	Coefficient of variation of n.d. D_e estimates	Skewness of n.d. D_e estimates	Ratio mean D_e 8mm/1mm
F18	60	32	32	0.25	-0.20	1.05
JC3	60	30	28	0.20	0.22	1.01
AD4-4	75	44	44	0.17	-0.16	1.02
STA00-2	50	32	27	0.18	0.56	1.23
STA00-5	70	66	65	0.19	-0.17	1.03
UM6	70	32	30	0.15	-0.18	1.11
UM21	120	65	56	0.19	0.08	0.97
UM22	120	55	55	0.18	0.37	1.07

n.d.= normally distributed values

By reducing the number of grains per aliquot used for D_e determination, for seven out of eight samples no significant evidence is found for poor bleaching. The scatter in equivalent dose estimates with an average υ-value of 0.19±0.03 (n=8) is not much larger than the data spread observed in 'dose recovery tests' carried out on 1 mm aliquots (υ-value 0.13±0.01, n=4). The difference between both υ-values is similar to the difference between both values determined for 8mm aliquot data sets (natural υ-value=0.09 to DRT υ-value =0.04). With the exception of sample STA00-2, the good agreement between the equivalent dose values derived from 8mm and 1mm aliquots, respectively, supports the assumption that these aeolian samples were sufficiently bleached at the time of deposition.

In case of sample STA00-2 it is difficult to ascribe significant difference between large and small aliquot D_e values (ratio 8/1mm=1.23) unambiguously to poor bleaching as post-depositional mixing seems as likely. The OSL age based on the equivalent dose which is calculated from the 8mm data set is in good agreement with underlying deposits, whereas the '1mm age' agrees with the age of the overlying sediments. The 1mm aliquot data set is finally considered to provide the more reliable equivalent dose estimate. The υ-value of STA00-2 is in the range of the other values derived from small aliquot distributions of supposedly well-bleached samples. This agreement would argue for the absence of an additional scatter in D_e estimates caused by poor-bleaching in case of the 1mm data set if sample STA00-2.

With a coefficient of 0.25, sample F18 is characterised by an above-average scatter of the D_e estimates. But as indicated by the skewness of only -0.20 the distribution shows only little asymmetry. Moreover, the good agreement of the D_e values derived from 8mm and 1mm aliquots, respectively (ratio 8mm/1mm=1.05), argues against the contribution of a significant amount of poorly bleached grains to the OSL measurements. For a poorly bleached sample the 8mm aliquots very likely would give a higher mean D_e value. The increased data spread could be due to mixing of grain populations with different absorbed doses or ages, respectively. As both resulting OSL ages are still in agreement with the chronostratigraphy, supported by independent age control, the mean D_e values are concluded to yield reliable estimates for the true burial dose for sample F18.

Verification of the hypothesis that all samples investigated in this study are well-bleached by analysis of high-resolution D_e distributions obtained from small sub-samples or single grains is not feasible for a data set of 164 samples. As shown in Table 9 a large number of aliquots per sample has to be measured to obtain a sound data base for statistical analysis. This is

extremely time-consuming even for such young samples as those investigated in this study. Therefore, as an alternative, each OSL chronology was internally tested for its consistency (see also discussion in section 3.7 and detailed description of each dune site record in chapter 4). Furthermore, at numerous dune sites independent age control was provided for cross-checking of the OSL dates.

As was already mentioned in section 3.6.2.1 insufficiently bleached samples can be identified when they cause a clear inconsistency in the chronostratigraphic record. At site 'Neuhaus', two samples (N2 & N4) were identified to overestimate the depositional age most likely due to poor bleaching (see section 3.6.2.1) and hence excluded from the data set. The equivalent dose distributions of both samples showed very large scatter. Even for the normally distributed D_e values coefficients of variation of 0.60 (N2) and 0.25 (N4) were calculated. These high υ-values give rise to a part of the tail in the histogram of υ-values which is shown in Fig. 45.

Other samples, which also showed above-average dispersion of the equivalent dose estimates proved to be consistent with the chronostratigraphy. A reliable performance of the SAR protocol was indicated by recycling ratios close to unity and only very small recuperation effects. The dose rate estimates were found to be in good agreement with values obtained from samples of the same sediment unit. Hence, a likely cause for the large data spread could be post-depositional mixing of grain populations with different absorbed doses.

3.6.3.6 Post-depositional sediment mixing

Contamination of grain populations due to intrusion of grains with higher or lower absorbed doses from other sediment layers results in additional scatter (e.g. BATEMAN et al. 2003, LOMAX et al. 2006). This post-depositional mixing may be accomplished in aeolian deposits by the activity of burrowing organisms like rabbits or insects etc., and by the growth of plant roots (bioturbation). On dead the root may become entirely oxidised leaving behind a hollow root cast which may be subsequently filled by sediments from above (PYE 1983).

In general, the samples of the present study were taken away from obviously disturbed parts of the dune sections. But as the sampling tube was driven up to 15 or 20 cm deep into the sediment, it cannot be ruled out, that former root tubes or borrows have been sampled by accident.

In Fig. 45 the histogram of υ-values which were calculated for the normally distributed samples already, hence after exclusion of significant outliers, still shows a tail towards high values of >0.15. In total nine samples contribute to this tail. Samples N2 and N4 were already identified to be poorly bleached. The equivalent dose distributions of the remaining seven samples are illustrated in Fig. 52. Because the data sets are small regarding the number of individual D_e estimates and, because all measurements were carried out on large, multi-grain aliquots, the interpretation of the distributions in terms of their symmetry is restricted. Nevertheless, some conclusions can be drawn, for example at first, that all the histograms extent over a comparatively broad dose range.

Microdosimetry effects are rather unlikely to be the dominant cause for the observed broad D_e scatter, because all measurement were carried out on large aliquots containing >1000 grains. Thus, any variation in the radiation dose on a grain-to-grain scale can be expected to be averaged out. In case of samples with low doses (JA1, M1, STA00-11) increased analytical uncertainties may contribute to the data spread.

All samples were taken from sediments close to the surface (<0.5 m), or were taken from sediment layers which had been close to the surface at least for some time period during the past. Hence, post-sedimentary mixing of grain populations of different ages or different absorbed doses, respectively, seems to be a likely cause for the additional scatter in these equivalent dose distributions.

A complete homogenisation of the upper parts (0-50 cm depth) of sediment sequences by bioturbation has been postulated (see KÜHN 2003 and ref. therein). However, the present OSL data set yields no evidence for the hypothesis that samples taken from close to the surface are generally affected by bioturbation and hence yield erroneous depositional ages. Numerous examples in this study show, that OSL samples taken from only 20-30 cm below surface yield reliable age estimates which are consistent with the stratigraphy and, furthermore, with independent age control (see for example discussion in section 4.3.4).

With reference to the seven samples shown in Fig. 52 only sample UM17 yields an OSL age which underestimates the expected depositional age (see KÜHN 2003). With D_e values in the range of ~10 to ~22 Gy bright signals are expected. Thus, additional scatter introduced by photon counting statistics is negligible. This source of scatter may have a more significant

impact in case of samples JA1 M1, and STA00-1, which all show equivalent doses in the low dose range.

However, for none of the seven samples it can be excluded for sure, that bioturbation may have caused a mixture of grain populations that carry different absorbed doses. But despite the broad D_e distributions and the likely problem of post-depositional mixing, the finally derived OSL ages are in chronostratigraphic order within errors. Hence, they were included in the final interpretation of the age data set with the exception of UM17, which contradicts the expected age.

With respect to the data base, which is finally used for the assessment of the baseline variation in natural samples, these seven samples were excluded from the data set. For these samples an additional source of scatter, here induced by sediment mixing, cannot be ruled out for sure.

It has to be emphasized that further analysis of these seven samples ought to be carried out using single grains in order to investigate the impact of bioturbation on the dispersion of equivalent dose values. In particular contamination with grains from younger layers, which is very likely the case in layers close to the surface, is only detectable at the single grain level (BATEMAN et al. 2003).

Fig. 53: Equivalent dose distributions for aeolian sand samples which show a large spread in D_e values.

The normally distributed equivalent dose estimates show coefficients of variation >0.15 (JA1=0.20, JA2=0.28, UM17=0.18, G2=0.24, M1=0.30, N10=0.35, STA00-11=0.20). All OSL measurements were carried out using large (8mm) aliquots.
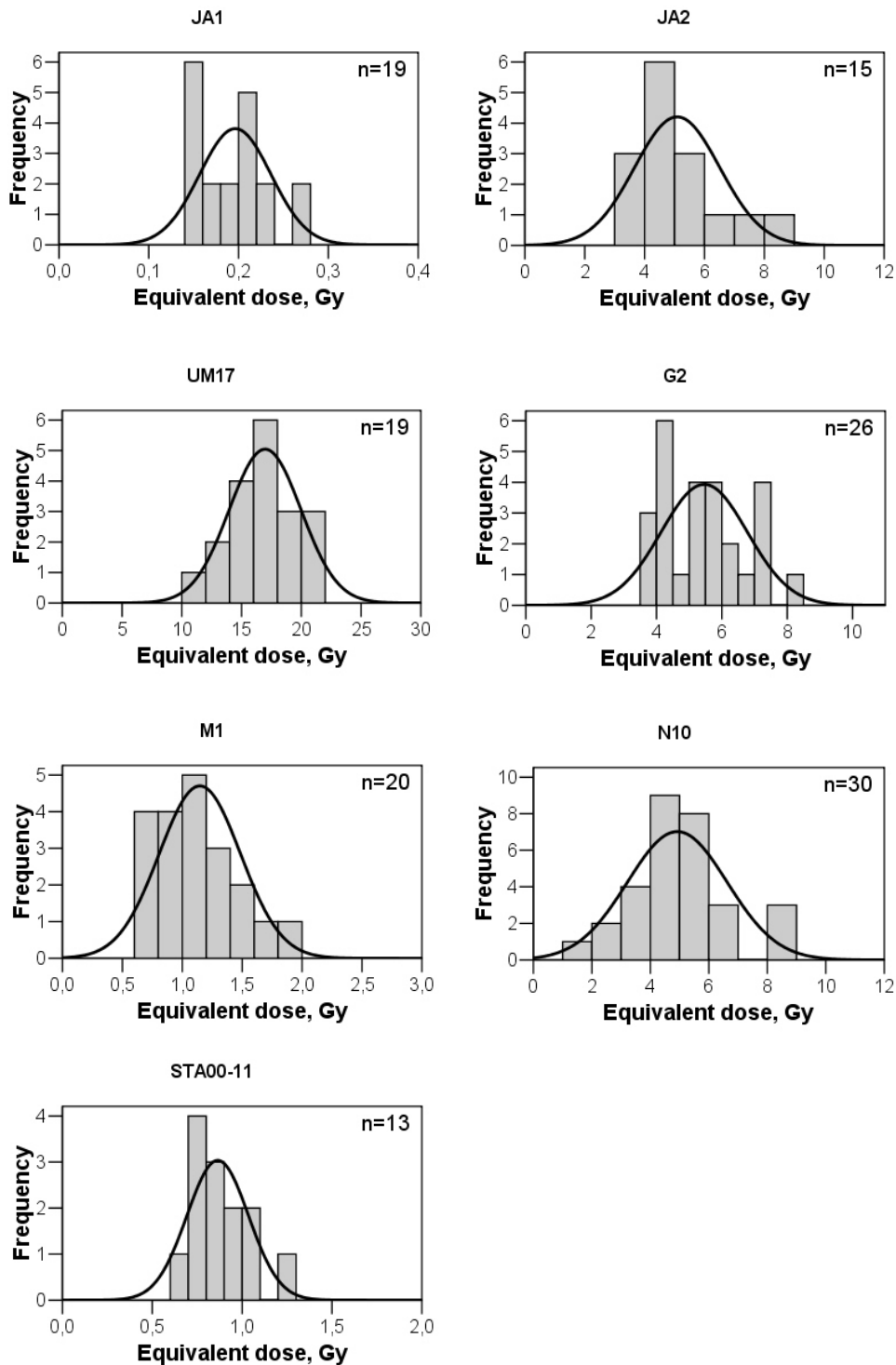
3.6.3.7 Heterogeneity in natural dosimetry

It is commonly assumed that in sediments sampled for luminescence dating the distribution of radionuclides or radiation sources, respectively, is homogeneous. But the radiochemical composition of the sediments can vary spatially. Hence, an inhomogeneous dose rate distribution results on the grain-to-grain scale (microdosimetry effects) (see section 3.3.3.2).

The data spread in equivalent dose values can be significantly increased even in a well-bleached sample, if the individual grains absorbed different radiation doses since burial. Inhomogeneities in the in the beta dose are a dominant contributor to these microdosimetry effects. MURRAY and ROBERTS (1997) for example observed a wide but symmetrical D_e distribution from supposedly well-bleached aeolian quartz grains and attribute the large spread of 23 % (of the mean) to microdosimetry effects supported by the results of OLLEY et al. (1997). NATHAN et al. (2003) demonstrated by Monte Carlo modelling, supported by experimental evidence from α-Al_2O_3:C measurements, that β-dose inhomogeneities indeed can cause a significant scatter in D_e values. KALCHGRUBER et al. (2003) concluded that 18 % of the relative data spread observed in the single grain dose distributions can be attributed to dose-rate inhomogeneities in the natural sediment. This value was derived from measurements of α-Al_2O_3:C grains which had been intermixed into a loess sediment for irradiation.

For the samples investigated in this study such inhomogeneities in the natural beta irradiation field most likely are also present in similar dimension. But the impact of these microdosimetry effects on the dispersion of D_e values is expected to be balanced in the large grain populations (>1000 grains) which were used for equivalent dose determination in this study.

Besides inhomogeneous contribution of the external beta dose, differences in the internal beta and in particular alpha dose from radiative inclusions within the grains cause a grain-to-grain scatter of the absorbed dose (e.g. VANDENBERGHE 2003, VANDENBERGHE et al. 2003). With respect to the samples investigated in this study the additional scatter in absorbed doses from variable internal radioactivity is considered to be insignificant. The internal radionuclide contents which were measured by NAA on 17 HF-etched quartz samples from different study areas were negligible (see section 3.3.4.5).

Further variation in microdosimetry can result from the presence and varying thickness of grain coatings which can be either higher (e.g. iron coatings due to enrichments in ^{226}Ra) or lower (e.g. carbonate coatings, OLLEY et al. 1997) in radioactivity when compared to the radiation dose of the sediment matrix. This variability of radiation dose on a grain-to-grain level cannot be excluded for sure for the samples of this study, because grain coatings, though not very thick, were present.

With regard to a larger scale than the grain-to grain variation in dosimetry, the results of comparative radionuclide analysis indicate that the spatial distribution of radionuclides and thus the natural radiation field in the investigated dune deposits is quite homogeneous. Neutron activation analysis was carried out on small sample amounts of only a few mg whereas for gamma-ray spectrometry either several hundred grams up to 1600 g of the bulk samples were used. The overall good agreement of the analytical results, at least for thorium and potassium, indicates a homogeneous distribution of the radionuclides. This result is further supported by the accordance with the results of in-situ gamma dose rate measurements (see discussion in sections 3.3.4.2 & 3.3.4.3). Hence considering a large scale, a rather homogeneous natural radiation environment can be assumed for the samples investigated in this study.

3.6.3.8 Determination of the threshold υ-value for natural samples

It was demonstrated that equivalent dose estimates always show a variation regardless whether they are obtained from single grains, aliquots containing only a few grains or multiple-grain aliquots. This scatter is due to systematic and random differences between the measured D_e values. At present, not all sources of scatter are fully understood, or quantified, some may even still be unknown (DULLER 2004, GALBRAITH et al. 2005).

The average coefficient of variation calculated from a range of 'dose recovery tests' represents the amount of scatter in equivalent dose estimates which can be expected only in the 'best case' scenario of complete bleaching and irradiation with a monoenergetic, homogeneous radiation source. The average υ-value obtained from DRTs in this study is 0.04 ± 0.02 (1σ standard deviation). This value accounts for the dispersion in D_e values that can be attributed to the experimental factors, measurement conditions and luminescence properties.

The mean data spread observed in natural equivalent dose distributions of all investigated samples was 0.09±0.06 (n=164). After exclusion of those samples, which were identified to be poorly-bleached or presumably affected by post-depositional mixing, the mean υ-value was re-calculated. For the data set of 155 well-bleached, aeolian sand samples the mean coefficient of variation is 0.08±0.02 (1σ standard deviation) and the median is also 0.08. It is concluded, that the difference between the 'ideal' (0.04) and 'true' (0.08) υ-values of 4 % (relative coefficient of variation) results from the differences between field and laboratory conditions, the latter being reflected by the DRT υ-value (see also discussion in GALBRAITH et al. 2005).

Bleaching conditions are different for both sample sets. In the laboratory the samples are not exposed to the full spectrum of sunlight, but to restricted wavelengths only (blue LEDs). But most likely the major contributor to the additional data spread observed in natural D_e distributions is the variability of the natural irradiation compared to the homogeneous laboratory irradiation.

In sediments the samples are exposed to gamma, beta, alpha and cosmic radiation, which all are characterised by different attenuation characteristics. Furthermore, it has to be taken in mind that in natural environment the irradiation geometry is different and more variable compared to the geometry in the measurement equipment.

An additional spread in absorbed dose values in natural samples can be induced by variations of the external alpha dose contribution due to uneven and incomplete removal of the outer alpha irradiated layer by HF etching of the quartz grains. As far as known the impact of this inhomogeneous external alpha contribution as source of D_e scatter has not been discussed in detail in the literature, but ought to be further investigated.

As aforementioned in section 3.6.2.3.3, the application of a 'natural variation threshold' for identification of additional sources of scatter in equivalent dose distributions, such as poor-bleaching, is restricted.

Therefore, the υ-value of 0.08±0.02 derived from the present, homogeneous data set can be considered as the baseline data spread for natural equivalent dose distributions which are obtained for:

- samples from similar depositional environments (homogenous, aeolian sand deposits);

- the similar size of the sub-samples (number of grains, grain size range);

- quartz samples with similar luminescence properties (overall the investigated samples showed a high luminescence sensitivity resulting in bright OSL signals even at low doses);

- samples with a similar absorbed doses in the range between 0-20 Gy (as for samples close to the saturation level a higher scatter has to be expected).

3.6.4 Equivalent dose calculation

In Table E 1 in Appendix E all equivalent dose values which were used for OSL age calculation are summarised. The equivalent dose estimates are derived from the weighted mean of the normally distributed D_e values. For a range of samples the D_e is based on the arithmetic mean (see sections 3.6.1.2 & 3.6.1.3). To assess the overall uncertainty of the mean equivalent dose values the standard deviation about the mean (1σ standard error) and a systematic error of 5 % associated with the beta source calibration are taken into account. The calibration uncertainty of 5 % is in accordance with the suggestion of AITKEN (1985: 248). However, this estimate seems to be conservative compared to values used in other studies, for example 2 % (VANDENBERGHE et al. 2004) or 3.5 % (MURRAY & FUNDER 2003). For calibration of the beta sources which are used in luminescence measurements quartz samples were irradiated with known doses from gamma sources. These gamma sources in turn have to be calibrated and the uncertainty resulting from this calibration is about 2.4 % already (ARMITAGE & BAILEY 2005, see also AITKEN 1985). The 5 % calibration error value is finally an estimated uncertainty that is based on the results of comparative calibration measurements carried out for the equipment used in this study (see Appendix C for discussion of the beta source calibration).

3.7 Age calculation and plausibility testing

All OSL ages, which were finally used for the chronostratigraphic interpretation of the individual dune sites, are presented in Appendix E, Table E 1 together with the dose rate and equivalent dose values.

The plausibility of the OSL chronologies was checked in detail for each dune site. To be considered as reliable depositional age, an OSL date had to:

> (i) yield an age which is consistent with the stratigraphic record (i.e. increasing age with increasing depth);
>
> (ii) agree with the OSL ages of the over-and underlying sediments from the same sediment unit in the 2σ confidence interval (see GEYH 1980, 2005);
>
> (iii) be in accordance with reliable independent age control (e.g. radiocarbon ages, marker horizons such as palaeosols and tephra layers).

For samples from the same, homogeneous dune sand unit similar dose rate and equivalent dose values are expected which finally result in consistent ages. By comparing the individual analytical results obtained for several samples from the same layer, in many instances, irregularities in the data set were revealed and, in most cases, could be eliminated by projected additional analysis. This is demonstrated for example in Fig. 54 (similar graphs are presented in Appendix F for each dune site to illustrate all analytical results). Due to the narrow spaced sampling of the sections, and hence the large number of samples, the identification of unreliable OSL dates or outliers, respectively, was improved.

Out of the data set of 164 aeolian samples 5 OSL ages were finally considered not to be reliable. The various reasons are discussed in detail in the description and interpretation of the individual sampling sites in chapter 4. But it can be summarised, that two ages (samples N2, N4) overestimated the depositional age most likely due to incomplete bleaching and three samples yielded younger ages than expected from the chronostratigraphy. For these latter three samples post-sedimentary mixing with younger sediments by bioturbation seems the likely cause for the age underestimation. At least the large D_e data spread observed in sample UM17, which gave a younger age than expected (see KÜHN 2003 and chapter 4, site 'Ueckermünder Heide-C'), indicates that bioturbation might be involved. Samples G12b and SHB-2, which were also excluded from the data set, are both inconsistent with the OSL based chronostratigraphy, which is supported by independent age control at both sites. However, to support the assumption that the age underestimation is caused by post-sedimentary mixing,

single grain analysis of these samples ought to be carried out, as the equivalent dose distributions obtained for large aliquots yielded no conclusive evidence on the presence of different grain populations. The five OSL ages, which were identified to be implausible, were excluded from the data set. Altogether, the accuracy of the luminescence chronology benefited from the exclusion of such outliers.

Furthermore, the high sampling resolution has enabled an improvement of the precision of OSL ages to a certain extent. If more than one sample was taken from a particular sediment unit, and the OSL ages of all samples from this layer were statistically concordant regarding the 5 % significance level, than the weighted mean was calculated from the individual age values (see 'mean age layer' in Table E 1, Appendix E). This mean OSL age and the corresponding standard deviation were finally included in the chronostratigraphic interpretation of the dating results (see chapter 4 for the discussion of the site specific chronologies and chapter 5 for the discussion of the data summary).

Fig. 54: Illustration of the quality check on the individual analytical results.
At site 'Glashütte', for example, for sample G3 (indicated in the graph by the circle) a higher OSL age was determined than for the underlying samples from the same dune sand unit. At first glance the higher age could be interpreted as due to incomplete bleaching. But as the equivalent dose is in good agreement with the D_e values of the underlying samples, the difference in ages is more likely caused by an erroneous dose rate determination. In fact, the dose rate value of sample G3 is lower than those from samples below. To test the reliability of the neutron activation analysis (NAA) results gamma-ray spectrometry (G.-spec.) was applied. A significant difference in analytical results is clearly seen in the potassium analyses. As shown, the OSL age for sample G3 based on the gamma-dose rate is in accordance with the ages obtained for samples from the same sediment unit. Here, the narrow spaced sampling clearly enhanced the possibility to identify erroneous analytical results.
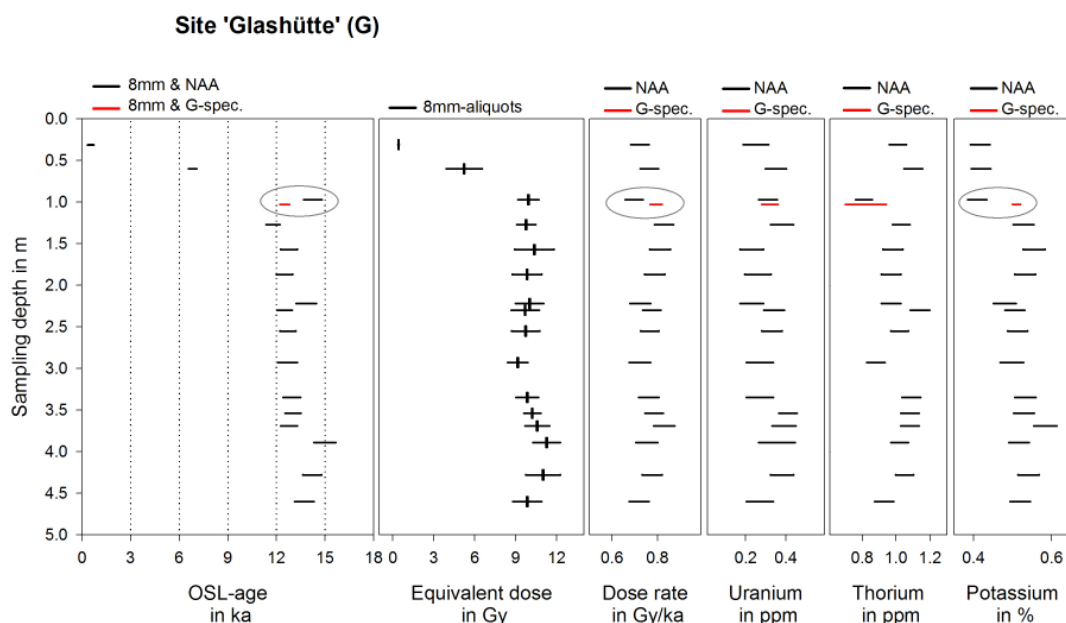
From the OSL data set presented in this study it is concluded that OSL dating of quartz is a reliable chronological tool for determination of depositional ages of aeolian sediments from the central part of the European Sand Belt.

The robustness of the single aliquot regenerative dose protocol for equivalent dose estimation of quartz was demonstrated. In comparison to other measurement protocols the SAR technique yielded more precise and, in many cases, more accurate results (see Appendix B). The quartz samples investigated in this study showed good intrinsic luminescence properties. The luminescence sensitivity, for example, proved to be invariably high which was expressed by bright signals even at low doses. This attribute improves the applicability of OSL dating for very young deposits (<100 yr).

The large data set of OSL ages of dune sand provides the possibility to test the common assumption that aeolian deposits are well-bleached (e.g. DULLER 2004, SINGARAYER et al. 2005). It was shown that incomplete resetting of OSL signals by sunlight exposure during transport and deposition cannot be ruled out in general for aeolian sand samples. In the present study only 1.2 % of the samples (2 out of 164) were unambiguously identified to be poorly bleached. Thus, poor bleaching truly seems to be the exception rather than a major problem in dune deposits.

4. The study sites

4.1 The position of the study area

4.1.1 The European Sand Belt

Extensive areas of cold-climate aeolian sand sheets and inland dunes occur throughout the northern European lowlands, along the margin of the Last Glacial inland ice sheets (e.g. KOSTER 1988), forming the so-called 'European Sand Belt' (ESB).

A large number of studies have been carried out on the description, dating and interpretation of these deposits in terms of palaeoenvironmental reconstruction. KOSTER (1988) reviews studies of major cold-climate dune fields and sand sheets in Europe (Table 1, p. 72 in KOSTER 1988) and North America (Table 2, pp. 73-74 in KOSTER 1988). In KOZARSKI (1991) numerous studies on cold-climate dunes and sand sheets in central and northern Europe are cited, and, more recently, SCHIRMER (1999a) summarised results of investigations from The Netherlands in the west, to Poland in the east. Recent research in the young morainic area in eastern Germany and western Poland has been reviewed (DE BOER 1993, 1995, SCHLAAK 1993, KAISER 2001).

KOSTER (2005) and SINGHVI et al. (2001) present the most recent summaries of luminescence dating studies concerning the age of the Late Pleistocene western European aeolian sediments and RADTKE (1998) has published numerous luminescence dating studies from northwestern Germany. KUHN (2000) and BARAY and ZÖLLER (1993, 1994) present multiple-aliquot TL and OSL ages for aeolian deposits from sites in NE Germany.

The European Sand Belt of aeolian sand deposits occurs only in patches in Great Britain (CATT 1977, BATEMAN 1995, 1998), but on the continent it extends from The Netherlands and northern Belgium in the west across northern Germany, southern Denmark, into Poland and the Baltic Region and into Belorussia, the northernmost Ukraine and as far as the north-western border of the Ural Mountain range in Russia (KOSTER 1988, ZEEBERG 1998, ASTAKHOV et al. 1999 and MANGERUD et al. 1999, the latter two both are cit. in HUBBERTEN et al. 2004, see Fig. 55). Within the ESB aeolian sand sheets are the dominant landform. They

cover much larger parts compared to the inland dune fields (CASTEL et al. 1989, KOSTER 1988, 2005).

Fig. 55: Extend of the European Sand Belt (ESB), maximum advances of Pleistocene inland ice sheets, and location of the study area.
(redrawn from ZEEBERG 1998)
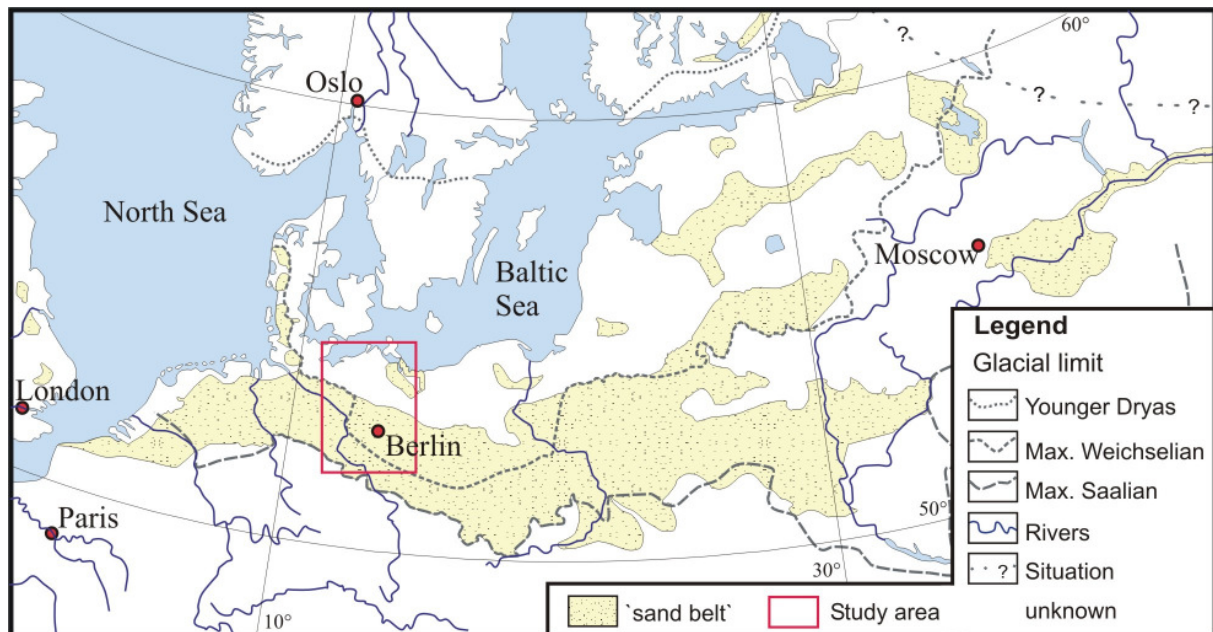
The northern margin of the sand belt in The Netherlands and western Germany is marked by marine deposits of the Holocene transgression of the North Sea. In Jutland, Denmark, and Schleswig-Holstein (N-Germany), the northern limit of the sand deposits coincides with the north-south trending maximum advance of the Late Weichselian inland ice. In eastern Germany and Poland, where the Weichselian ice advances are characterised by several sub-stages, aeolian sand deposits are widespread within the extent of the Last Glacial Maximum (LGM) Brandenburg ice advance (see Fig. 55). Here, the northern boundary of aeolian sand deposits is the Pomeranian stage, which marks the stationary terminus of an ice-sheet line north of the Last Glacial Maximum (LGM) (KOSTER 1978, in CASTEL et al. 1989).

The southern limit of the ESB coincides more-or-less with the northern loess boundary west of the River Rhine. East of the Rhine the southern border of the European Sand Belt is marked by the 200-metre contour-line north of the central German upland. Further east it is indicated by the maximum extent of Pleistocene ice sheets (e.g. CASTEL et al. 1989, see Fig. 55). At this southern margin the deposits of the ESB grade into fine-grained (loamy) sands or sandy loess and finally loess (KOSTER 2005). A typical sequence has been described along the

loess boundary in northern Germany as consisting of alternating layers of silty (loess derived) and sandy layers (GEHRT 1994, 1998, GEHRT & HAGEDORN 1996).

In the east the sand, later redistributed by the wind, originated in abandoned, unvegetated flood plains, fluvioglacial and fluviolacustrine terraces, proglacial outwash plains, till plains, lake shores, and abandoned spillway channels ('pradolinas', 'urstromtäler') (KOSTER 1988, 2005, KASSE 1997). In the western part of the sand belt the North Sea Basin with its fluvial sediments deposited by the Rhine, Meuse and north-German-Baltic river systems served as a source area.

The terminology applied to the cold-climate and more recent human-induced landforms of re-mobilised aeolian sand sheets is confused (CASTEL et al. 1989, DE BOER 1995, SCHIRMER 1999b, KASSE 2002, KOSTER 2005) with chronostratigraphical, geomorphological, sedimentological connotations used indiscriminately. In this study the definition and terms proposed by such reviewers as CASTEL et al. (1989), DE BOER (1995), ALISCH (1995), SCHIRMER (1999b), and KASSE (2002) are adopted.

All sandy aeolian deposits lacking a dune relief, for example not showing slip faces, are summarised as sand sheets which are spread over the bedrock or former landforms in a blanket-like form with a flat or undulating surface. Generally, cold-climate sand sheets *['dekzand' (Dutch), 'Flugdecksand' (German), 'aeldre flyvesand' or 'daeksand' (Danish)]* are distinguished from Holocene drift sands *['stuifzand' (Dutch), 'Wehsand' (German), 'yngre flyvesand' (Danish)]*. Periglacial structures are frequent and organic rich layers are generally missing in cold-climate deposits. In contrast, drift sands are defined as Holocene redistribution of Pleistocene deposits and are predominantly of anthropogenic origin.

According to an overview of cold-climate inland dune fields in northern America and Europe by (KOSTER 1988), the most widespread dune form is the parabolic dune which, however, varies considerably in shape and size. Transverse and longitudinal dune forms are also developed but are relatively rare.

4.1.2 Characterisics of the dunefields in the study area

The study area is located in northeast Germany and adjacent parts of Poland. It is characterised by a hummocky landscape of fresh glacial landforms left behind by the

Scandinavian ice sheet. Till plains, end moraines, ice-dammed lakes, and kettle holes are typical of this area. In proglacial areas outwash plains (sandurs) and fluvioglacial terraces were formed by meltwater drainage in ice-marginal valleys ('urstromtäler', pradolinas). Sand deposits provide an ample supply of sediments for the formation of inland dune fields and sand sheet areas (see Fig. 56).

Between the limits of the Brandenburg and the Pomeranian ice advances there are extensive dune fields with individual dunes up to 20 to 30 m high. The parabolic dunes form elongated fields up to 20-30 km length. Their steep leeward slopes face north or east (LOUIS 1929, LEMBKE 1939a, LEMBKE et al. 1970), suggesting that the sand-transporting wind was from west or southwest. Moreover, most parabolic dunes are open to the west and longitudinal dunes and sand ridges are west-east trending, indicating that the sand-transporting wind coming mainly from the west (e.g. LOUIS 1929, DE BOER 1995, SCHLAAK 1993, KAISER 2001). This finds support in simulation tests by ISARIN et al. (1997) for the Younger Dryas stadial.

Fig. 56: Orientation of parabolic dunes in relation to the direction of sand-transporting winds.
The horns of these crescentic dunes extend upwind because the higher central part has been blown forward while the basal zones have been stabilised by vegetation and moisture. Hence blowouts are typically found upwind or enclosed by the arms of the parabolic dunes (from GOUDIE 1995: 148).
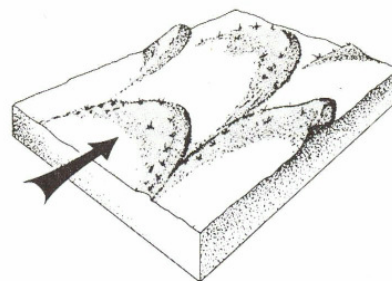
But it has to be noted that the dune form reflects the prevailing winds at the end of the period of dune formation. The dunes could conceivably have had a different shape in earlier times and only later were shaped or modified by westerly winds. SOLGER (1910 in LOUIS 1929), argued that katabatic winds from the east, caused by the inland ice-sheet, formed barchan dunes. But LOUIS (1929) outlined various morphological aspects that contradict SOLGER'S interpretation (see also KÁDÁR 1938 for discussion). Recently, however, MÖCKEL (2004) came to a similar conclusion to that offered by SOLGER. Using grain size analysis results derived from sands used in this study, he concluded that barchanoid dunes were transformed to parabolic dunes just before dune formation ceased.

Thus the orientation of the parabolic dunes (compare Fig. 56) and the location of the dune fields, as opposed to the form of the individual dunes, provide a further argument supporting the hypothesis of sand-transporting winds mainly from the west. KEILHACK (1917, in LOUIS 1929) first mapped the inland dune fields in northern Germany and mentioned their close association with large river valleys. This was further confirmed by PYRITZ (1972), who found that the majority of dune fields in Lower Saxony are located downwind or east of the various river courses (e.g. LEMBKE 1939a, KLIEWE & SCHULTZ 1970). This implies that westerly winds were responsible for the dune formation. KLIEWE and SCHULTZ (1970), for example, correlated all sand sheets and dune fields in their study area north of the Pomeranian ice advance with westerly-located source areas, such as meltwater streamways.

4.1.3 Chronology of the Weichselian glaciation

Three major Late Weichselian ice advances have been recognised in northeast Germany. The Brandenburg or Leszno Advance represents the maximum and oldest extent of the Late Weichselian glacier with the Głogów-Baruth 'urstromtal' serving as meltwater drainage. The next glacial limit, the Pomeranian Advance is associated with the Toruń-Eberswalde 'urstromtal'. The youngest, the Mecklenburg Advance, is represented by the distribution of the youngest Weichselian till north of the Rosenthal end moraine (HEERDT 1965, EIERMANN 1984, RÜHBERG 1987 all in EHLERS et al. 2004).

In the classic morphostratigraphic subdivision of the Weichselian glaciation in North Germany (WOLDSTEDT 1925, 1928 in EHLERS et al. 2004) the Frankfurt (or in Poland the Poznań) Advance associated with the Warsaw-Berlin 'urstromtal' was treated as an individual major stage between the Brandenburg and Pomeranian advances. According to more recent work the Frankfurt Advance is regarded only as a stage of the oscillating Brandenburg ice margin, because a till unit formed by the Frankfurt Advance is lacking (CEPEK 1965 in EHLERS et al. 2004). Several similar stages resulting from the oscillation of the ice margin during the Weichselian ice decay phase are recorded in northeast Germany. The youngest and northernmost ice-marginal valley, the Notec-Randow 'urstromtal' in Mecklenburg-Vorpommern, served as meltwater drainage for the retreating ice sheet which left behind the Velgast end moraine. With this northeastern Germany became ice-free.

The Elbe 'urstromtal' is not related to one particular glacial limit, for the lower reaches of the Elbe served as drainage for meltwater of the Brandenburg Advance, but was used also as a meltwater outlet for subsequent remelting stages. The Warsaw-Berlin (drainage of the Frankfurt sub-stage) and the Toruń-Eberswalde (drainage of the Pomeranian stage) ice-marginal valleys both converged in the Elbe (see Fig. 57).

Fig. 57: Location of the individual sampling sites in the study area and the position of Weichselian glacial limits, ice-marginal valleys, and the European Sand Belt.
Study area and sites: Elbe 'urstromtal': **1**-Neuhaus, **2**-Schletau, Głogów-Baruth 'urstromtal': **3**-Glashütte, **4**-Cottbus, **5**-Jänschwalde, **6**-Jasień (sites A-C), Toruń-Eberswalde 'urstromtal': **7**-Eberswalde (Rosenberg, Melchow, Finow, Spechthausen), **8**-Schorfheide (site A & B), Ueckermünder Heide: **9**- Ueckermünder Heide sites A-D, Altdarss: **1**0-Altdarss sites 1 & 4
(map based on LIEDTKE & MARCINEK 1995 and ZEEBERG 1998)
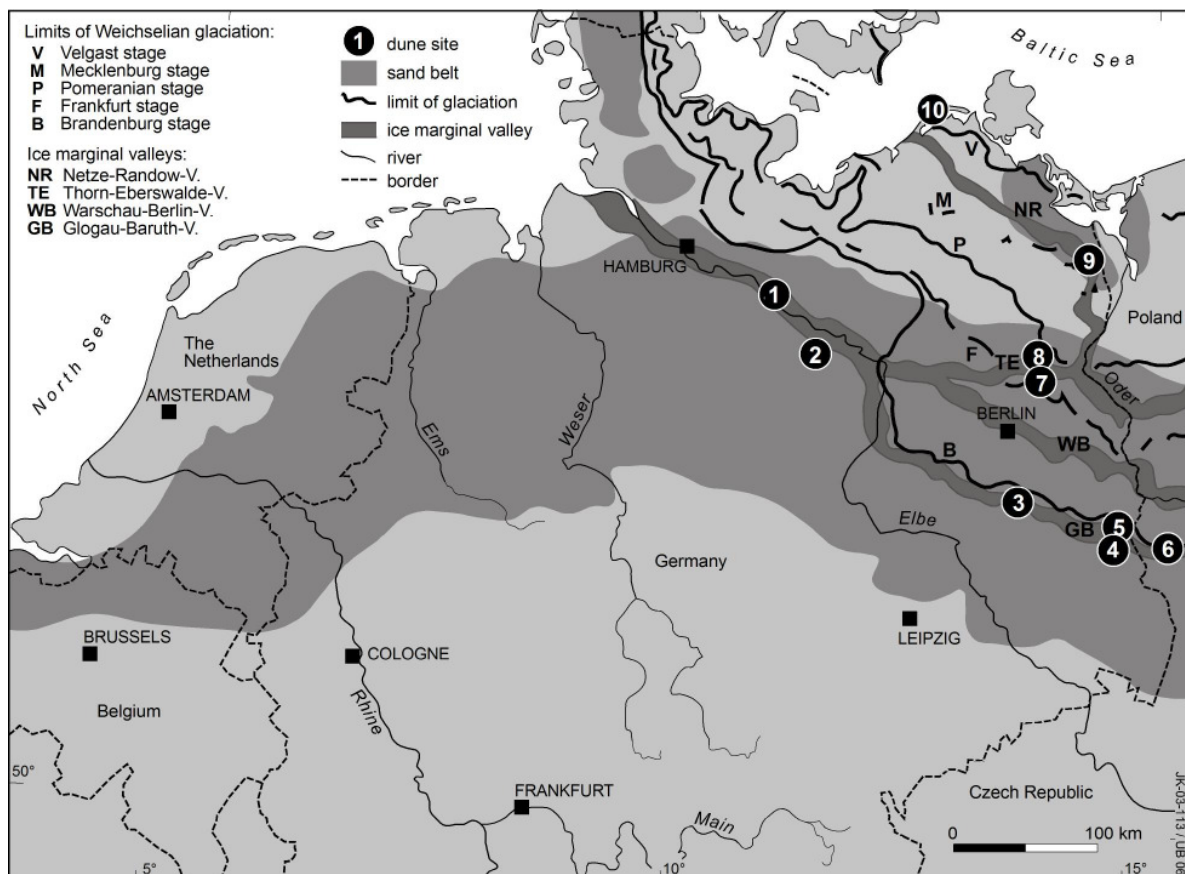
As shown in Fig. 57 most dune sites investigated in this study are located within ice-marginal valleys. Thus, a precise knowledge of the chronostratigraphy of the glaciation history in the study area is important for it provides a chronologic framework for inland dune development: the glacial chronology sets the upper time limit for the onset of aeolian activity following the retreat of the ice sheet and the exposure of sands that became the source areas for dune formation.

Although research on the glaciations in northeast Germany dates from the late 19th Century (for example TORELL 1875, BERENDT 1879, KEILHACK 1898, for summary see e.g. MARCINEK & SCHULZ 1995), the three major Late Weichselian ice advances are still relatively poorly dated (EHLERS et al. 2004, GÖRSDORF & KAISER 2001). The chronology is based on radiocarbon ages but as they are based on organic material the actual relation to the ice advance is frequently not clear. Furthermore calibration of these ages is difficult as they are well beyond the dendrochronological-based calibration curve (0-12.4 ka cal. BP, FRIEDRICH et al. 2004). It might be thought that glaciolacustrine banded silt and clay deposits in ice-dammed lakes at the ice margin would be useful in the determination of the chronology of the ice sheet retreat. But the application of varve chronologies to these sediments is limited by syn- and post-sedimentary deformation of sedimentary structures (SCHIRRMEISTER 1997).

Table 10 summarises available dates for the various ice advances including a generalised calibration of the ages in order to provide an approximate time frame for the interpretation of the OSL chronologies discussed in this chapter. In this context the dating of the last Weichselian deglaciation of Northeast Germany after the Mecklenburg Advance to around 14,000 ^{14}C yr BP seems to be the most reliable age assessment. It is based on an analysis of a large number (271) of radiocarbon dates from the Pomeranian Bay and Mecklenburg-Vorpommern (GÖRSDORF & KAISER 2001).

Table 10: Dating of the Late Weichselian glacial limits in northeast Germany and northwest Poland. Calibrated ages printed in bold letters were obtained by using the CALIB 4.1 ^{14}C calibration program (STUIVER et al. 1998).

Glacial limit	Uncalibrated ^{14}C ages with references	Calibrated ^{14}C ages including the 2σ error
Brandenburg-Leszno Advance	**21-22 ka BP** (EHLERS et al. 2004), **20 ka BP** (KOZARSKI 1988 in KOZARSKI 1993, LIEDTKE 1996)*	**>23 ka cal. BP**
Pomeranian Advance	**15.2 ka BP** (LIEDTKE 1996, KOZARSKI 1988 in KOZARSKI 1993)	15.2 ka BP= corr. age >17 cal. ka BP (EHLERS et al. 2004), **18.7-17.7 ka cal. BP**
Mecklenburg Advance	**>14.2 ka BP** (LAGERLUND & HOUMARK-NIELSEN 1993 in EHLERS et al. 2004), 14.1 BP (Rosenthal stage, LIEDTKE 1996), c**. 14.5 ka BP** (KAISER 2004)	14.2 ka BP= corr. age >16 cal. ka BP (EHLERS et al. 2004), **17.5-16.6 ka cal. BP** (14.5 ka BP =17.9-16.9 ka cal. BP)
Deglaciation after the Mecklenburg Advance	c. 14 ka BP (GÖRSDORF & KAISER 2001)	**17.3-16.3 ka cal. BP**

* JUSCHUS (2003: 84) reports a ^{14}C-age of 16,925±970 yr BP (18,875-21,410 yr cal. BP) for the maximum extent of the Brandenburg ice sheet, but explicitly mentions the possibility of underestimation due to contamination.

4.1.4 OSL sampling strategy

The impact of climate change can differ from one region to the other, both in intensity and in the geomorphic response. Therefore it is essential to investigate similar features over an extended area finally to identify and characterise the regional variability of aeolian activity triggered by climatic changes.

Five different study areas within the various ice-marginal valleys or large glacio-lacustrine basins, respectively were selected to obtain a south to north transect with respect to the timing of the exposure of sandy plains following the retreat of the Late Weichselian ice-sheet. Study areas were selected to test whether a shorter period of periglacial conditions towards the north is revealed in the aeolian record.

Several sites were sampled in each area so as to obtain a regional picture and avoid possibly anomalous site-specific observations and a selective view of the past. In this way the impacts of possible local catastrophic events are placed in perspective.

At site scale a complete record of deposition from the base up to the top of the dune improves the possibility of erosional gaps or equilibrium phases (erosion compensated by deposition) better to be identified. Thus sedimentation rates can be quantified. Furthermore, in luminescence dating a number of samples taken from the same sediment unit facilitates the detection of irregularities in the data set. To fulfil these requirements regularly spaced samples were taken from the top to the base of the exposed section.

4.2 The 'Finow soil' - a palaeosol as stratigraphic marker horizon

The so-called 'Finow soil' was exposed at several dune sites investigated in this study area. To provide the necessary background for the chronostratigraphic implications of this palaeosol a brief summary of its characteristics is presented here.

SCHLAAK (1993) first described a buried soil horizon at the base or within the lower parts of the dunes within the Eberswalde 'urstromtal'. The term 'Finowboden' or 'Finow soil' for this horizon is derived from its widespread occurrence in the area of the 'Obere Finow' within the Eberswalde valley.

Characteristic features of the 'Finow soil' are (SCHLAAK 1993, 1998, 1999):
-B horizon of a brown earth soil, dystric cambisol (fBv horizon)
-Average thickness of 10-20 cm
-Marked increase in the silt/clay to sand ratio compared with sediments above and below it
      resulting in enhanced water retention ability and a higher nutrient content and hence
      intensive root penetration
-Generally lacking a surface humus horizon, most likely it was intermixed into the lower B
      horizon by cryoturbate processes
-Diffuse boundaries to over- and underlying sediments are typical, often with finger-like
      protuberances of the 'Finow soil' into the adjacent deposits

Since the first description by SCHLAAK (1993) the 'Finow soil' has been reported from numerous dune sites throughout northeast Germany and western Poland (for example, SCHLAAK 1998, KAISER & KÜHN 1999, KOWALKOWSKI et al. 1999a, BOGEN et al. 2003, KÜHN 2003). A precise dating of this soil formation is crucial to its use as a chronostratigraphic marker that differentiates aeolian sand deposits. Radiocarbon dates of

small charcoal fragments derived from the soil horizon at various sites date the soil development to the Allerød and Early Younger Dryas. These ages form a cluster at about 10,300 yr ^{14}C BP (SCHLAAK 1998). However, the 'Finow soil' at the type locality 'Postdüne' near Eberswalde-Finow is particularly interesting because the fossil B horizon located in the lower part of the dune grades into a peat layer at its base. The peat layer was dated by ^{14}C to 11,400-10,130 yr BP and palynological results indicate Allerød up to Younger Dryas pollen assemblages. Further age control is provided by a thin layer of Late Allerød Laacher See tephra (LST) embedded within this peat layer (SCHLAAK 1993, 1998, see section 4.3.3.1, 'site Finow', for further discussion on the age of the LST). Luminescence dating has been carried out on the sediments over- and underlying the 'Finow soil' horizon at various sites in Brandenburg. But the multiple-aliquot ages published by BARAY and ZÖLLER (1993) and KUHN (2000) lack the precison which is necessary to unambiguously date the soil development to a particular Lateglacial chronozone.

4.3 Site descriptions and dating results

Because of the large data set all individual analytical results are summarised in Appendix A (dose rate data tables), Appendix D (equivalent dose data tables) and Appendix F (topographic maps showing the sampling sites, figures illustrating the individual analytical results and OSL ages at the sampling depth). All OSL ages used for the reconstruction of dune development at individual sites are summarised in Table E 1 (Appendix E). All exceptions from the general realised during data processing will be discussed in this chapter. All radiocarbon ages are presented in Appendix E, Table E 2 together with the appropriate reference.

Any correlation to Lateglacial climatic events and episodes in this chapter follows the chronology proposed by BJÖRK et al. (1998) based on the Greenland ice-core record. The choice of this record as a chronological framework for this study is discussed in detail in chapter 1.

4.3.1 Dune sites in the Elbe 'urstromtal'

Two dune sites, the sections 'Neuhaus' and 'Schletau', are located in the Elbe ice marginal valley. Within this 'urstromtal', aeolian deposits overlie fluvial deposits, notably the Late Weichselian 'Lower Terraces' of the River Elbe, but they also cover Holocene alluvium (CASPERS & SCHWARZ 1998, see Fig. 58).

Adjacent areas to the west and southwest are occupied by a mosaic of glaciofluvial sediments and tills correlated with the Warthe and Drenthe ice advances of the Saalian glaciation. Isolated Saalian till plateaus occur east of the Elbe and still further east are the proglacial outwash plains and end moraine ridges of the Weichselian ice advances. The fluvial and glaciofluvial deposits provide an abundant source for the dunes and sand sheets found along the river valley today (see Fig. 58).

Fig. 58: Morphological map of the study area 'Elbe ice marginal valley' with the location of the sampling sites 'Neuhaus' (N, dune site 1 in Fig. 57) and 'Schletau' (STA, dune site 2 in Fig. 57).
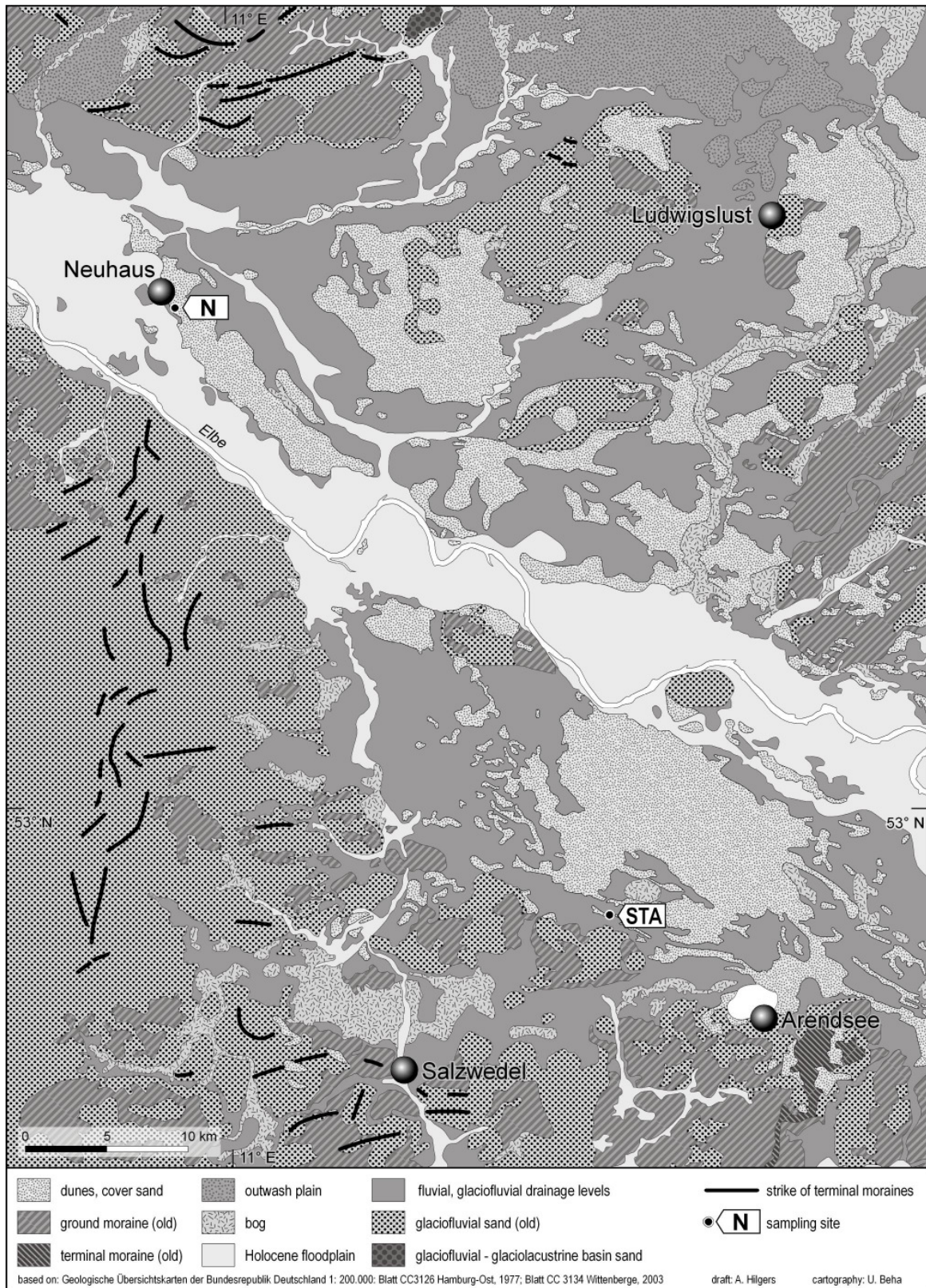
4.3.1.1 Site 'Neuhaus' (N)

The dune site 'Neuhaus' is situated on the Weichselian 'Lower Terrace' east of the River Elbe (see Fig. 58). The dune, which is about 8.3 m high, is located in the northernmost part of a NNW-SSE orientated dune field, the 'Carrenziener Heide', where the highest dunes attain heights of 20 m (CASPERS & SCHWARZ 1998). The sampling site is located in the central section of the main dune ridge south of Neuhaus. In the lower part of the section Fig. 59. are several thin, reddish-brown and discontinuous wavy bands or laminae that are a common feature of the dune sections investigated in this study. The sand is highly porous and the silt, clay and iron oxide-rich layers are caused by eluviation with rainwater flushing that transported weathering products (silt and clay and iron oxides resulting from weathering in overlying sediments) to lower levels in the (sand) profile (PYE 1983). The enriched laminae may reflect the lower limit of penetration of the wetting front after heavy rainfall. Once the first layer has been deposited permeability is reduced, favouring further deposition. Hence multiple bands can develop. Furthermore, the variability of the wetting front gives rise to the formation of these infiltration structures at various levels (see also PYE 1983).

Fig. 59: Schematic stratigraphic section of sampling site Neuhaus (N).
The OSL ages of samples N2 and N4 were excluded from the data set as they significantly overestimated the depositional age of the upper sediment unit (for further explanations it is referred to the text). OSL samples are numbered from the top to the bottom with N1 → N18.
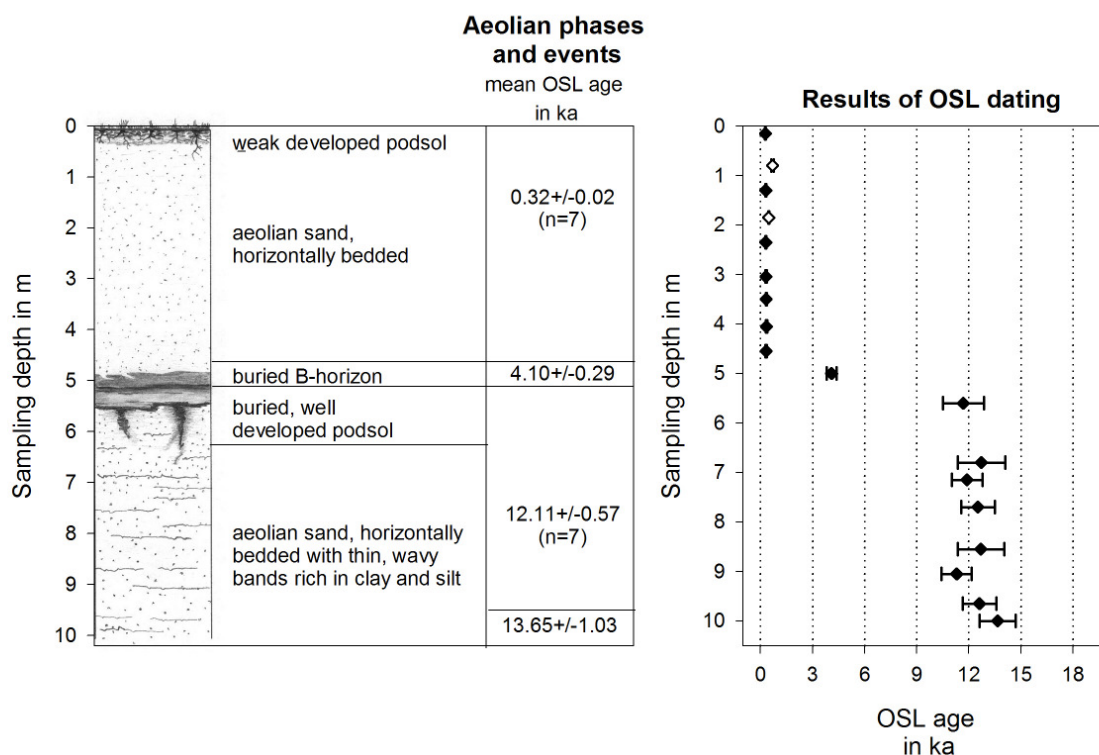
Eighteen samples were taken for OSL dating from the 'Neuhaus' section and the results suggest at least three phases of sedimentation (see Fig. 59). During the youngest phase about 4.6 m of dune sand were rapidly deposited some 320±20 years ago. This is the mean age from samples N1, 3, and 5 to 9. The weak development of the topsoil also indicates the short time that has elapsed since the deposition of the sand. Samples N2 and N4 were excluded from the data set of the upper part of the dune, because a significant deviation from the overlying and underlying depositional ages was detected. In both instances an erroneous palaeodose determination caused by insufficient bleaching of the OSL signals (see section 3.6.2.1) seems to be the most likely explanation for the age overestimation. With more than 4 m of dune sand being reworked in a very short time, it is possible that some material was not exposed to sufficient daylight during short distance transport. Age overestimation due to intermixing of older grains by bioturbation seems an unlikely explanation here, as old material for intermixing is not available near the two samples, N2 and N4: the underlying sediments to a depth of 4.6 m are of the same young depositional age.

A second phase of aeolian activity occurred c. 4.10±0.29 ka, based on the OSL age of sample N10. The sediment layer sampled as N10 differs from the overlying greyish dune sands and the underlying podsol. It is brownish and most likely represents parts of a B horizon of a soil, developed in a thicker sand unit that formerly covered the well-developed podsol soil below. The topsoil of this Mid-Holocene unit was presumably eroded during the latest aeolian event ~320 years ago. Thus, the soil which is now represented only by the eroded B horizon was developed about 4,000 years ago. Because of the large scatter observed in the equivalent dose distribution of sample N10, its OSL age ought to be interpreted with precaution. However, as it is consistent with the chronostratigraphy of the over-and underlying sediments it is not excluded from the data set (see section 3.6.3.6).

The well developed buried podsol represents a relatively prolonged phase of landscape stability during which intensive soil development took place. The samples taken from the substrate of this soil and the underlying dune sands all showed Lateglacial OSL ages ranging from 11.68±1.18 ka at the top to 13.65±1.03 ka at the bottom of the sampled section. The lowermost sediments could be correlated with aeolian activity in the Older Dryas (GI-1d 13.90-14.05 ka, sample N18 13.65±1.03 ka). Enhanced aeolian activity during the Younger Dryas (GS-1 11.50-12.65 ka) resulted in the formation of the old dune core represented in samples N17-11 (mean age of 12.11±0.57 ka). The reforestation and soil formation following

a climate amelioration at the beginning of the Holocene terminated this phase of major dune formation.

This model contradicts the observations of CASPERS and SCHWARZ (1998), who date the dune development in the 'Carrenziener Heide' as Holocene. This conclusion was based on the observation of the dunes and sand sheets overlying Holocene fluvial and alluvial deposits and extended peat-bogs discovered below the dune ridges. Palynological analysis dates the peat layers to the beginning of the Holocene into the Late Preboreal and up to early Boreal. This apparent anomaly in the Lateglacial age of the dune cores obtained by OSL can be explained by reactivation of the dune field in the Early Holocene. Dune site 'Neuhaus' stands in the western part of the forests developed on the Younger Dryas dunes. To the east, however, the land is low-lying and wetter with a high groundwater table, favouring peat-bog development at the beginning of the Holocene. Today, boggy areas are still found at the eastern edge of the dune field (see site map in Appendix F). The Boreal or younger coverage of the extended peat -bogs with dune sands resulted from the reactivation of aeolian processes, possibly by the disturbance of the protecting vegetation cover by forest fires. The proof of Lateglacial dune formation by luminescence dating at site 'Neuhaus' is supported by similar Lateglacial ages, which are presumed for dune cores standing on the Late Weichselian river terraces ('Lower Terrace') in a dune field west of the River Elbe near Bleckede, only 10 km west of the dune site 'Neuhaus' (CASPERS & SCHWARZ 1998).

The OSL results obtained for the upper part of the 'Neuhaus' dune are in agreement with the regional chronology of aeolian activity, which is predominantly correlated to human occupation of the area. Assuming the age of sample N10 to be reliable, the burial of the well-developed podsol at about 4.10±0.29 ka could be explained by an increased human impact in the course of the Late Neolithic and Bronze Age. According to CASPERS and SCHWARZ (1998) the forests which stabilised cover sand areas and dune fields, for example in the vicinity of Bleckede ('Bleckeder Staatsforst'), had been completely removed by forest clearing from about 4.5-5 ka BP until the Late Bronze Age.

The youngest phase of dune reactivation at site 'Neuhaus' about 320 years ago dates back to the medieval time, a period known for intensive forest clearings. CASPERS & SCHWARZ (1998) also found similar very young dune remobilisation at a dune site north of Stixe, about 8.5 km south of the site 'Neuhaus' and in the same dune field.

4.3.1.2 Site 'Schletau' (STA)

The dune site 'Schletau' is part of a large area of sand sheets and dunes that is located south of the recent course of the Elbe River. The dune is part of a 1.5 km long, SE to NW trending ridge, which is situated at the southern margin of the dune field (see Fig. 58, HEINEMANN in BREEST & VEIL 2001).

The dune at site 'Schletau' was sampled for luminescence dating in combination with the detailed archaeological investigation of a Mesolithic settlement site which was carried out by Dr. S. Veil and colleagues of the 'Landesmuseum Hannover-Urgeschichtsabteilung'. Samples STA001 to 11 were taken from a trench within an interdune depression and samples STA1 to 5 from two locations a few metres away, where the sediments were exposed along the face of a former sand pit[6].

This dune site was particularly interesting, because here OSL ages could be tested against independent age control provided by Early Mesolithic artefacts and radiocarbon ages (BREEST & VEIL 2001). In Fig. 60 is shown the 1.3 m deep trench at the top of the dune together with the OSL dating results obtained for the eleven samples and the ^{14}C ages of burned nutshells. The OSL ages indicate a gradual filling of the depression from the Lateglacial and into the Holocene. The detailed investigation of the equivalent dose distribution in sample STA00-5 taken to check the degree of bleaching in the dune sediments provided no evidence for insufficient bleaching (see section 3.6.2.3). It is concluded that the depression was filled by aeolian deposition rather than slopewash or mass movement of the sediment. The location of the sampling site may have favoured the preservation of this aeolian record as the depression could have served as a sediment trap.

---

[6] Samples STA1 to 5 were taken by Dr. Matthias Krbetschek, Freiberg, and kindly provided as well as gamma spectrometry results for samples STA1, 2, 3, and 5.

Fig. 60: Schematic stratigraphic section of sampling site Schletau (STA).
At a depth of ~0.60-0.70 m below surface a layer with Mesolithic artefacts was found. Several burned nutshells were sampled from the lower part of this artefact layer and dated by [14]C. OSL samples are numbered from the top to the bottom with STA00-11 → STA00-1.
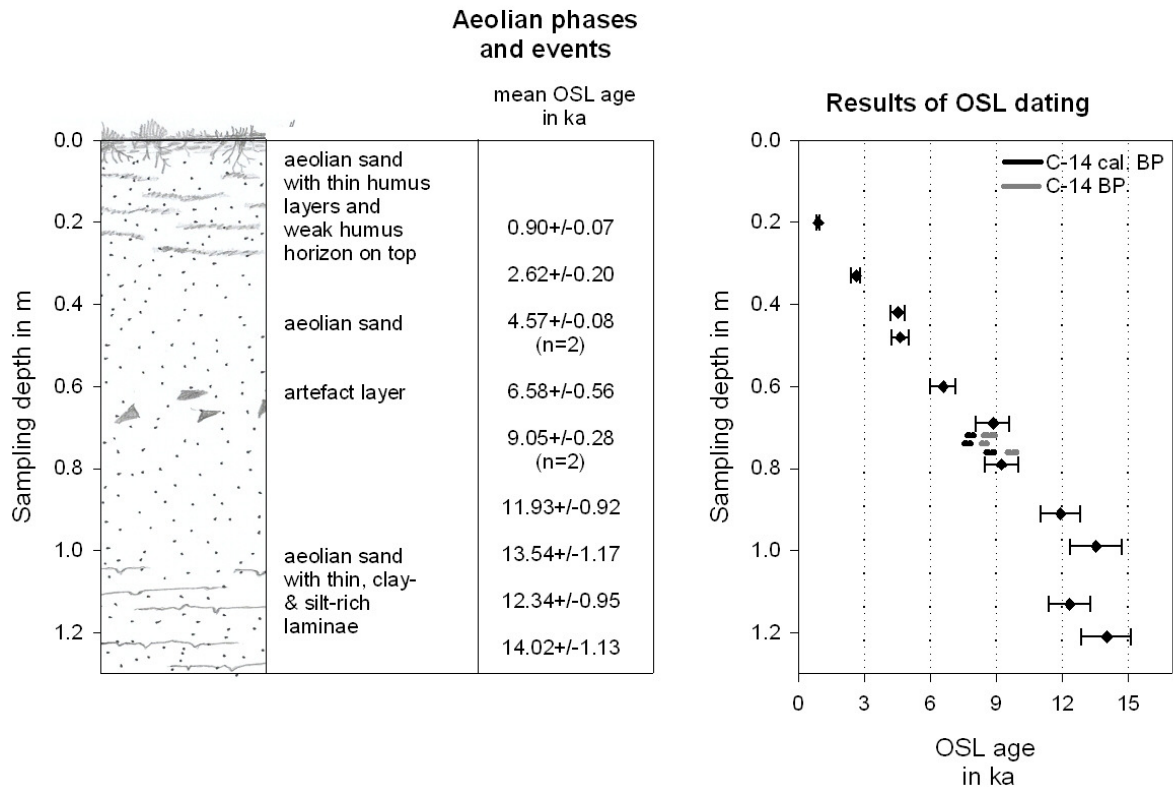
Three samples of burned nutshells were taken from the lower part of the sediment layer containing numerous Early Mesolithic artefacts and dated by ^{14}C to 8.84±0.17 ka cal. BP (weighted mean of the three ages, see BREEST & VEIL 2001: 242, Appendix E, Table E 2). This age further supports the Late Boreal age of the Mesolithic artefact assemblage. The OSL ages of 9.24±0.76 ka and 8.85±0.77 ka (samples STA00-5 and -6), which were obtained for the sediments correlated with the lower part of the artefact layer, show an excellent agreement with the independent chronological control (see Fig. 60). The OSL ages obtained for samples STA 2 and 3 from the section a few metres away also date aeolian deposition at 7.91±1.03 ka.

The burial of the Mesolithic settlement site is dated to about 6.58±0.56 ka by sample STA00-6, which was taken from the sediments overlying the layer with the maximum Mesolithic artefact concentration.

To derive an age assessment for the onset of the dune formation the additional samples were taken from the open trenches in the former sandpit about 5 and 10 m away from the main sampling sequence. The lowermost sample at position 1 was dated to 13.55±1.86 ka (sample

STA 1) and at position 2 to 15.48±1.17 ka (STA 4). The lowermost samples from the interdune depression, which represent the upper part of the dune body, yielded OSL ages of 14.02±1.13 ka, 12.34±0.95 ka and 13.54±1.17 ka (STA00-1 to -3). Thus, the major phase of dune formation most probably took place in pre-Allerød times, most likely during the Older Dryas (GI-1d 13.90-14.05 ka) and/or Oldest Dryas (GS-2a 14.70-16.90 ka). With respect to the individual analytical results shown in Appendix F it has to be noted that an age inversion was observed between samples STA001-3. For this reason sample STA00-2 was remeasured using small aliquots (1mm size) and yielded a significantly lower equivalent dose and age, respectively. The OSL age of STA00-2 based on the 1mm aliquot D_e value is in good agreement with sample STA00-4. Whether mixing of sediments of different age by bioturbation or incomplete bleaching is the reason for the observed difference in ages in the lower part of the section could not be explained, and because of the inconsistency in ages, no mean age was calculated for the sediment layers at the bottom.

The sediments below the artefact layer were deposited during the Younger Dryas period (sample STA00-4 11.93±0.92 ka). This is in good agreement with the expected pre-Boreal age, which is deduced from the Early Mesolithic artefact assemblage (BREEST & VEIL 2001). The sediments dated by sample STA 5 could be related to the same aeolian phase, for the date of 10.75±1.46 ka coincides, within errors, with the Younger Dryas/Preboreal transition at 11.5 ka.

With respect to the uppermost part of the sediment sequence shown in Fig. 60 the OSL ages indicate several phases of deposition. This result is in good agreement with HEINEMANN (in BREEST & VEIL 2001) who from investigation of the soil characteristics at the top of the dune also deduced several phases of sedimentation following Mesolithic settlement. Repeated reactivation of aeolian processes is in good agreement with the settlement history of the area (HEINEMANN in BREEST & VEIL 2001). Thus the OSL ages of 4.57±0.08 ka (mean age STA00-8 and -9), 2.62±0.20 ka (STA00-10), and ~900±70 years (STA00-11) most probably indicate dune activity related to forest clearing in the Late Neolithic, at the transition of the Bronze to the Iron Age, and in Medieval times.

4.3.2 Dune sites in the Głogów -Baruth 'urstromtal'

The Głogów-Baruth 'urstromtal' drained the Brandenburg or Leszno Advance, that represents the maximum Weichselian glacial limit in eastern Germany and western Poland (see e.g. EHLERS et al. 2004, MARKS 2004). It should be noted, however, that JUSCHUS (2003) found evidence for the maximum extent of the Weichselian ice sheet between Luckenwalde and Baruth reaching some 2 to 12 km further to the south than the Brandenburg end moraine. Because this maximum extent was just a short-term oscillation, no end moraines have been formed (JUSCHUS 2003, see Table 10 for information on the timing of this advance). In general, the Brandenburg Advance is still poorly dated to about c. 21-22 ka BP (>23 ka cal. BP, EHLERS et al. 2004: 142). Several dune sites within the Głogów-Baruth pradolina have been sampled for luminescence dating (see Fig. 57).

4.3.2.1 Site 'Glashütte' (G)

The location of the dune site 'Glashütte' within the Głogów-Baruth ice marginal valley is shown in Fig. 61. To the South the 'urstromtal' is bordered by Saalian till plains and to the north by pro-glacial outwash plains of the Brandenburg Advance (e.g. Baruth and Taubendorf sandur) and younger retreat stages (Reicherskreuz sandur). The adjacent young morainic area is a patchwork of elongated meltwater stream channels with numerous isolated till plateaus.

Within the Baruth ice-marginal valley several 'urstromtal' levels are distinguished in relation to different drainage phases of remelting of the Brandenburg ice-sheet. The 'Older Baruth urstromtal' (55-62 m a.s.l.) was formed by the discharge of the Brandenburg ice advance. The 'Younger Baruth urstromtal' terrace (50-55 m a.s.l.) represents the meltwater deposits of the first recessional moraine, the Reicherskreuz stage. At a lower level and further to the north, the so-called 'Youngest Baruth urstromtal' (<50 m a.s.l.) is attributed to the drainage of melting buried dead ice (MARCINEK 1961, in MARCINEK et al. 1970). JUSCHUS (2003) recognised a further drainage level, the 'Oldest Baruth urstomtal', correlated to the maximum extent of Weichselian ice sheet near Baruth. The fluvial and glaciofluvial deposits of the pro-glacial outwash plains and 'urstromtal' terraces provided ample supply of sand for the formation of dune fields and coversand areas.

Fig. 61: Morphological map of the study area 'Głogów-Baruth ice marginal valley' showing the location of the sampling site 'Glashütte' (G, dune site 3 in Fig. 57).
[sandur (a): Brandenburg Advance, sandur (b): Saarmund-Reichskreuz stage, 'urstromtal' discharge levels: (a): 'Older Baruth urstromtal' (55-62 m a.s.l., Brandenburg Advance,) (b): 'Younger Baruth urstromtal' (50-55 m a.s.l., Reicherskreuz stage), (c): Youngest Baruth urstromtal' <50 m a.s.l., drainage of remelting buried dead ice) (MARCINEK et al. 1970). (based on the maps by MARCINEK 1961 in MARCINEK et al. 1970, DE BOER 1995, JUSCHUS 2003).
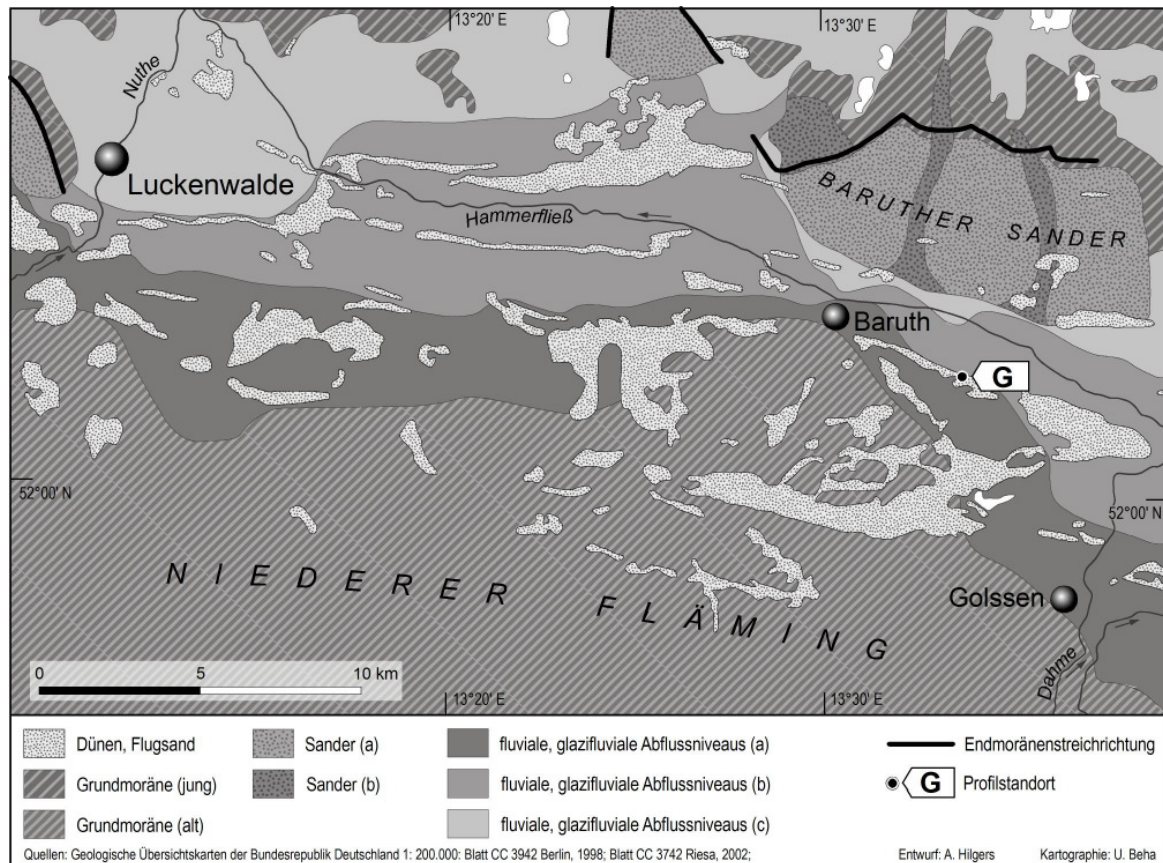
The 'Glashütte' dune is part of a NW-SE trending dune field that overlies the glaciofluvial deposits of the 'Older Baruth urstromtal' level at 55-62 m a.s.l.. DE BOER (1995) carried out a comprehensive study of the dunes in the vicinity of the study site which included the geomorphological mapping of the dune fields. Longitudinal dunes with individual dunes more than 300 m long and more than 100 m wide are widespread. Parabolic dunes are also present. The dunes reach maximum heights of ~25 m and their morphology indicates sand-transporting winds from the west and south (DE BOER 1995).

The dune, sampled for luminescence dating, is about 10 m high. A simplified sketch of the section exposed in the upper half of the dune is shown in Fig. 62. This sketch summarises three trenches, which were cut into the upper part of the dune at different positions but all within a span of 3.6 m. Regarding the linkage of the individual sections, samples G7 and G8 are considered to represent the same layer of dune sand bearing in mind stratigraphic position

and dune morphology. The intermediate and the lower trenches are linked by the presence of a buried soil horizon, which is the equivalent of the 'Finow soil'.

Fig. 62: Schematic stratigraphic section of sampling site Glashütte (G).
Note, that this section is a composite profile of three sections. Identification of the Finow soil horizon in the two lower sections allowed unambiguous combination of the sections. OSL samples are numbered from the top to the bottom with G1 → G15. Sample G12b was excluded from the data set, as most likely intermixing of younger material caused the underestimation of the expected age, which is deduced from the palaeosol horizon. Samples G16 and G17 were taken from distant parts of the dune and therefore not shown in the sketch.
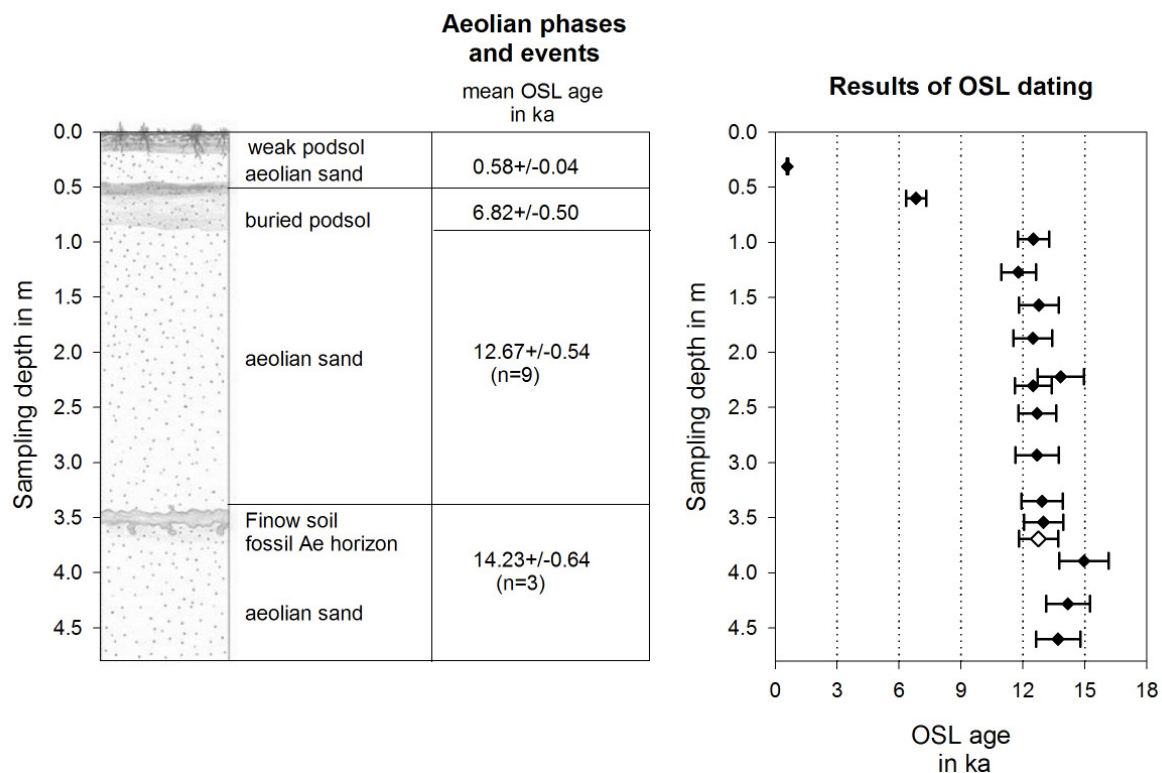
At site 'Glashütte' the Allerød 'Finow soil' palaeosol horizon, which was exposed about 3.5 m below the top of the dune, provided chronological control (Allerød, GI-1a-c: 12.65-13.90 ka). For the two samples taken from within and just below the fossil Bv horizon, G12 and G12b, a pre-Allerød age (>13.90 ka) was expected, but both samples yielded OSL results dating into the Late Allerød on average (G12: 13.00±0.94 ka and G12B: 12.76±0.95 ka). This could reflect ongoing aeolian deposition during soil formation, which has been described for other sites with Allerød soil developments (MANIKOWSKA 1991, SCHIRMER 1999a, SCHLAAK 1993). But this might only explain the Late Allerød age of sample G12. Sample G12B was taken from sediments interpreted as fossil Ae horizon below the fossil Bv horizon of the 'Finow soil'. Therefore an older age was expected as these sediments represent an older soil formation

than the 'Finow soil', and probably relating to the Bølling/Meiendorf period (GI-1e 14.04-14.69 ka) (pers. comm. Dr. N. Schlaak, 2000).

Because of its higher content of fines and therefore enhanced water retention the 'Finow soil' is usually a zone favoured by plant roots. Thus, bioturbation and intermixing of younger sediments into the fAe horizon cannot be ruled out as the cause for the lower than expected age. Further investigations of the palaeodose distribution using smaller sub-samples are necessary to prove this assumption. At this stage the age of sample G12B is considered not reliable and therefore is excluded from further interpretation.

The burial of the 'Finow soil' is dated to 12.67±0.54 ka considering the weighted mean of the OSL ages of samples G11 to G3, including sample G12 indicating the syn-sedimentary formation of the soil. This date would correlate with the onset of the climate amelioration at the beginning of the Younger Dryas (GS-1 11.5-12.65 ka).

It may be noted, that the dose rate of sample G3 was remeasured using gamma-spectrometry, because with an NAA based age of 14.23±1.07 ka it was identified as a distinct outlier (see Appendix F). With an equivalent dose value being in accord with those of the other samples of this sediment unit, the dose rate seemed to be the major cause for the presumed age overestimation. Indeed, the gamma spectrometry based OSL age fits into the whole data set much better and therefore was finally included in the age interpretation of site 'Glashütte'.

Above the Lateglacial dune sand deposit, represented by sample G3 to G12, sample G2 appears to represent a Mid Holocene phase of dune reactivation dated to 6.82±0.50 ka. As the sample was taken from the upper part of the exposed podsol soil, bioturbation might have caused an age underestimation here. In fact, the palaeodose distribution shows a large scatter of individual D_e (see section 3.6.3.6). Further investigations should be carried out using smaller sub-samples to clarify the cause of this scatter. Nevertheless, the age is chronostratigraphically consistent with the over- and underlying deposits, and is considered to be reliable. The podsol, from which sample G2 was taken, is buried by about 0.46 m of sand. Sample G1 dates this sand unit to 0.58±0.04 ka. This young age is supported by the presence of an only weakly developed top soil.

The reliability of the Mid to Late Holocene ages obtained for the topmost dune deposits finds supported in other dating studies carried out in the vicinity of site 'Glashütte'. BARAY and ZÖLLER (1993) have carried out thermoluminescence dating studies on two dune sites 'Klein

Ziescht' and 'Klasdorf' (see topographic map of site 'Glashütte', Appendix F). At 'Klein Ziescht' the Lateglacial dune formation most probably ended in the Younger Dryas according to a TL age of 12.4±2.6 ka obtained for a sample from the upper part of the dune sands (c. 2.6 m below surface, all TL ages reported here are measured on K-feldspar extracts). This age is in good agreement with the results obtained at site 'Glashütte' dating the last phase of Lateglacial dune formation to 12.67±0.54 ka. At the site 'Klasdorf' the Lateglacial dune formation also was terminated in the Younger Dryas (BARAY & ZÖLLER 1993). At site 'Klein Ziescht' dune sediments with embedded Meso- to Neolithic flint fragments were dated to 6.2±0.7 ka (ca. 2 m below surface). Thus, sample G2 dated to 6.82±0.50 ka might represent the same phase of dune reactivation most possibly caused by the impact of Neolithic groups. At least four subsequent aeolian phases are indicated at site 'Klein Ziescht' by three buried initial soil developments. BARAY and ZÖLLER (1993) recognise three different aeolian events occurring during the last 1000 years or so, based on the TL age from a sample directly below the lowermost buried soil of 1.1±0.5 ka. The youngest aeolian event dated at site 'Glashütte' therefore could very likely correlates with one of these three events recorded at site 'Klein Ziescht'.

Unfortunately no age constraint was obtained for the onset of dune formation at site 'Glashütte', because no sediments from the base of the dune could be sampled. However, two samples were taken from trenches which were expected to be close to or at the base of the dune. But whereas sample G16 probably dated a minor local aeolian event at about 10.01±0.83 ka leading to sand deposition in marginal parts of the dune, sample G17 taken from the base most probably derived from recent slope wash or slump deposits. Because this sample hardly gave any OSL signal it was not datable and excluded from the data set. The age of the onset of dune formation could not be assessed at site 'Glashütte', but the termination of the formation of the older dune core is dated by samples G13-15 taken from below the 'Finow soil'. These dune sands were dated to 14.23±0.64 ka. As all three OSL ages agree within 2 sigma errors they are considered to represent one phase of aeolian activity. It can be concluded, that the major period of dune formation at site 'Glashütte' ended with this pre-Allerød phase (> GI-1c 13.90 ka). The dune was stabilised by the formation of the 'Finow soil' during the subsequent interstadial of the Allerød.

Widespread formation of dunes and coversands started after the drying out of the meltwater stream channels when extensive sand sources became available on the 'urstromtal' terraces and on adjacent sandur plains (DE BOER 1995, JUSCHUS 2003). JUSCHUS (2003) found

evidence for a continuous deposition with no time between the different phases of discharge in the Głogów-Baruth 'urstromtal', which started with the drainage of the Brandenburg Advance at 21-22 ka (> 23 cal. BP, see Table 10). According to DE BOER (1995) aeolian processes commenced most likely in the Oldest Dryas (GS-2a 14.70-16.90 ka) with the deposition of sandy silty loess-like sediments, coversands and dunes were subsequently formed during the Older Dryas (GI-1d 13.90-14.05 ka). The sediments directly underlying the Allerød palaeosol, thus representing the top part of the older dune core, were dated by OSL to 14.23±0.64 ka. Taking into account that 6 m of dune sand were deposited before, this age would argue for an earlier onset of the dune formation at site 'Glashütte', most likely already at the end of the Oldest Dryas.

4.3.2.2 Site 'Cottbus' (C)

The dune sites 'Cottbus' and 'Jänschwalde' have been investigated in connection with archaeological excavations of the 'Brandenburgisches Landesmuseum für Ur- und Frühgeschichte' (Museum for Prehistory in Brandenburg) in the two brown-coal mines 'Cottbus-Nord' and 'Jänschwalde' in the Niederlausitz (see topographic map in Appendix F). These sites are located at the southern edge of the Głogów-Baruth 'urstromtal', where the River Spree coming from the south flows into the ice-marginal valley. Here, alluvial deposits of the River Spree ('Upper and Lower Spree alluvial fan') cover the glaciofluvial meltwater deposits of the 'Younger Baruth urstromtal' terrace. The alluvial sediments in turn are overlain by aeolian coversands and inland dune fields though at some sites they are intercalated with them (KÜHNER et al. 1999, see Fig. 63). A detailed reconstruction of the Late Pleniglacial and Lateglacial sedimentation history in the study area, including the chronology based on numerous radiocarbon ages, is presented for example by KÜHNER et al. (1999), BITTMANN and PASDA (1999), and PASDA (2002).

Fig. 63: Morphological map of the study area 'Głogów-Baruth ice marginal valley' showing the location of the sampling sites 'Cottbus' (C, dune site 4 in Fig. 57) and 'Jänschwalde' (J, dune site 5 in Fig. 57).
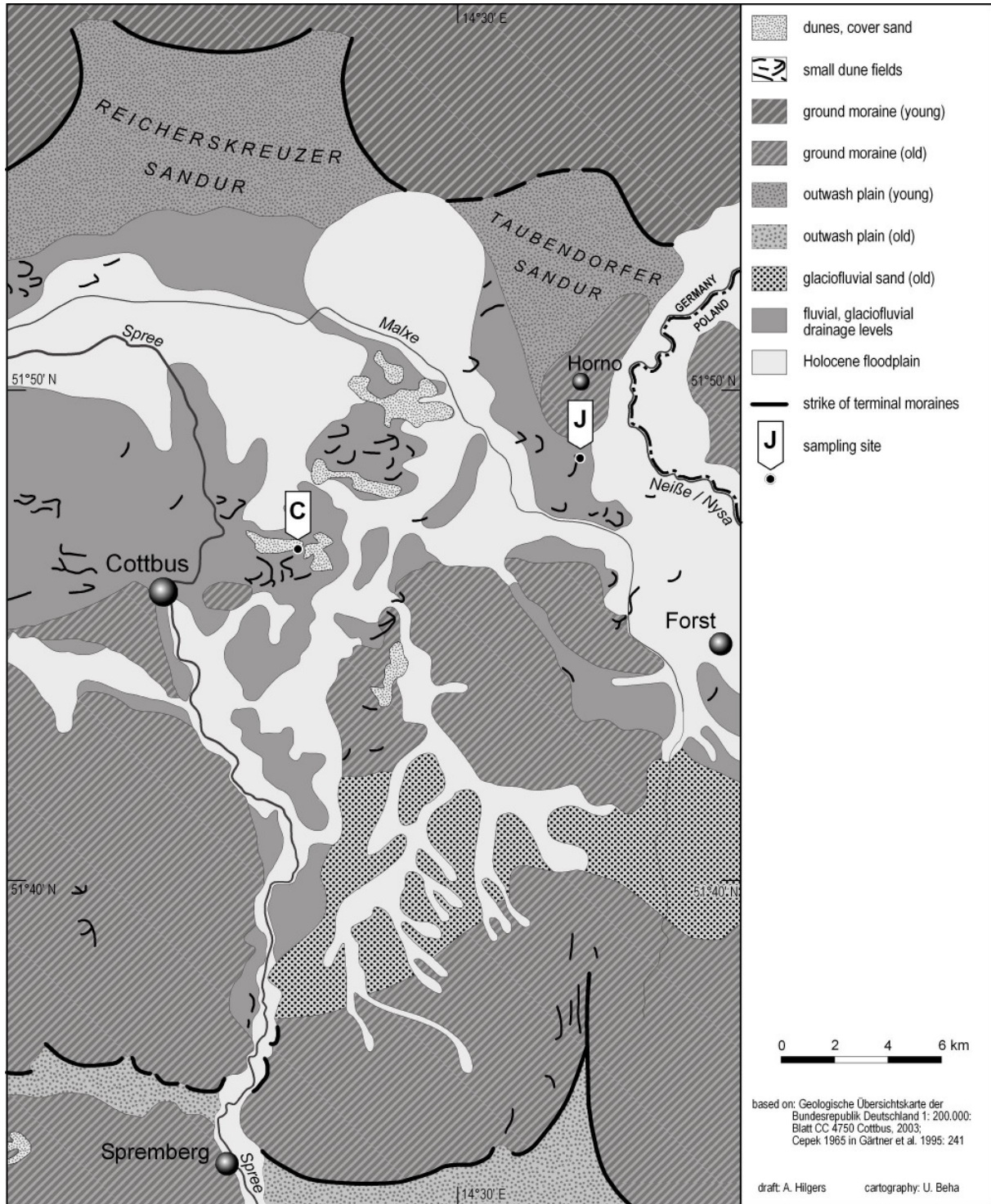
Site 'Cottbus' was chosen for luminescence dating, because this section provided excellent independent age control for crosschecking of OSL data with several radiocarbon ages and dendrochronological ages of fossil tree trunks. The exposed sediment sequence is illustrated in Fig. 64 together with the OSL and radiocarbon ages.

Fig. 64: Schematic stratigraphic section of sampling site Cottbus (C).
OSL samples are numbered from the top to the bottom with C1 → C7.
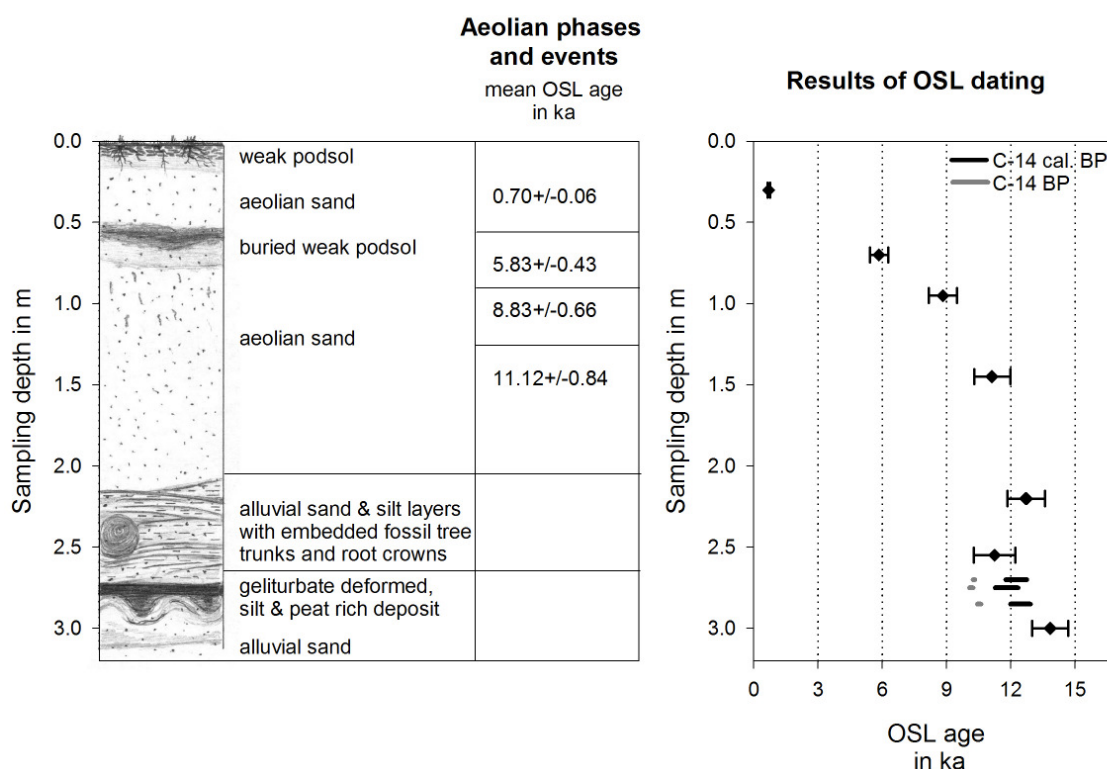
Fluvial or alluvial sands of the 'Upper Spree alluvial fan' are exposed in the lower part of the section. This sediment unit consists of sand-rich flood plain deposits alternating with silty, organic-rich mud deposits (so-called 'hanging mud'), which are related to paludal conditions at times of high groundwater table (PASDA 2002, KÜHNER et al. 1999). The sandy sediments at the bottom of the section were dated by OSL to 13.84±0.84 ka (sample C7). As was already discussed in section 3.3.4 the dose rate determination for sample C7 was problematic. The dose rate values, and hence the OSL ages, based on neutron activation analysis and gamma-ray spectrometry differ significantly (see also Appendix F for illustration of the individual analytical results). The analysis of low-level gamma-spectrometry yielded no evidence for radioactive disequilibrium in the uranium decay chain, which could be expected for water-laid deposits such as those sampled by C7 (see section 3.3.4.4). Furthermore, both dose rate values

deviate significantly from the in-situ measurement of the gamma-dose rate (see section 3.3.4.3). As shown in Fig. 64 sample C7 was taken just 10 cm below the silty peat layer. Thus, the gamma dose radiation field (30 cm distance) of sample C7 is also affected by the peat layer, which is supposed to have a much higher content of uranium, for example, than the sand unit sampled by C7 (see e.g. GEYH & TECHMER 1997, GEYH et al. 1997), see chapter 1). From the in-situ gamma dose rate measurement carried out for the sampling position of C7 a substantially higher gamma dose rate value was derived compared to the laboratory gamma-spectrometry results (ratio in situ/lab. 1.24). The in-situ measurement is considered to provide the more reliable gamma dose result as it takes the dose rate contribution from the mud layer into account. Finally, the OSL age was calculated using a combined dose rate of the in-situ gamma dose rate and the beta dose rate determined from the laboratory gamma spectrometry results. The resulting OSL age of 13.84±0.84 ka is in excellent agreement with the age expected for the sediments of the 'Upper Spree alluvial fan'. These alluvial sands are commonly correlated with the Older Dryas period (GI-1d 13.90-14.05 ka), which is deduced from the stratigraphic position between the 'foot mud' (not exposed at site 'Cottbus') and the 'hanging mud' horizons. These silt and peat rich layers date from the Bølling-Meiendorf and Allerød period, respectively, based on numerous ^{14}C ages (BITTMANN & PASDA 1999, KÜHNER et al. 1999).

At site 'Cottbus' the 'hanging mud' horizon is intensively deformed by geliturbation (see Fig. 64). As the formation of this peat layer is dated as Allerød, the deformation obviously was related to the Younger Dryas cold stadial conditions. Radiocarbon ages from the upper part of this mud layer indicate that the 'hanging mud' still formed the surface in the early Younger Dryas at site 'Cottbus' (10.52±0.09 ka BP, 12.45±0.48 ka cal. BP, KAYSER 1999, see Appendix E, Table E 2).

The 'hanging mud' layer is particularly interesting as over it and, in places, embedded in it, 5-10 m long trunks of pine and birch trees of an open pine forest are preserved (GAUTIER 1999). Radiocarbon dating of wood samples refers this forest to the second half of the Younger Dryas (10.28±0.03 & 10.15±0.08 ka BP, 12.25±0.48 & 11.80±0.54 ka cal. BP, SPURK et al. 1999, see Appendix E, Table E 2). According to GAUTIER (1997) the forest developed in low-lying positions with sufficient groundwater supply at the end of the Younger Dryas. But when at the transition to the Holocene the groundwater table rose (possibly due to periodic floods of the River Spree), the tree trunks were rotten above the roots, and eventually fell down.

Greyish clay-rich layers mark the end of this limnic-alluvial sedimentation. The clay was presumably responsible for the preservation of this buried fossil forest and is overlain by about 2.2 m of dune sand at site 'Cottbus'. The OSL samples C6 and C5 were taken from the alluvial deposits whereas samples C4 to C1 were taken from the dune sands on top.

Within errors the OSL results of C5 and C6 with 12.71±0.88 ka and 11.24±0.97 ka, respectively, are in good agreement with the ^{14}C ages of the wood and the 'hanging mud' and the dendrochronological results (SPURK et al. 1999, GAUTIER 1999, FRIEDRICH et al. 2004, see Fig. 64). To check for the occurrence of disequilibria in the U decay chain also for sample C6 low-level gamma-spectrometry measurements were carried out. But no evidence for disequilibrium was found (see section 3.3.4.4). It is interesting to note, that the multiple aliquot ages of 20.5±3.9 ka and 28.3±6.4 ka, which were obtained for the samples C5 and C6, respectively, significantly overestimate the expected age (see Appendix B). The most likely explanation for both the large errors and the overestimation is poor bleaching of this alluvial deposit. Here, the advantage of single aliquot dating becomes obvious. However, it cannot be excluded that the slight overestimation observed with the single aliquot derived OSL age of 12.71±0.88 ka for sample C5 must be ascribed to the impact of a few poorly bleached grains. Therefore, further measurements using small aliquot sizes should be carried out. But so far, the equivalent dose distribution of sample C5 with a relative standard deviation of only 5 % shows no evidence for heterogeneous bleaching. And as the OSL age still agrees within error with the radiocarbon ages any influence is regarded as negligible here (see Fig. 64).

The initial dune formation at site 'Cottbus' finally took place at the transition from the Younger Dryas to the Preboreal according to the OSL age of 11.12±0.84 ka obtained for sample C4 taken from the dune sands about 0.75 m above the alluvial sand and clay deposits. As the latter have been independently dated into the Late Younger Dryas the Early Preboreal age of sample C4 is in excellent agreement with the expected depositional age. Samples C3, 2, and 1 seem to represent separate aeolian events. This is obvious from the stratigraphy for sample C1 taken from above a buried soil, but unexpected for C3 and C2. However, the change in colour between the dunes sands sampled with C4 and C3 at about 1.35 m below surface points towards the presence of two different sediment units. C3 was dated to 8.83±0.66 ka and C2 to 5.85±0.43 ka. In an undisturbed section a soil horizon ought to occur between C3 and C2 according to the difference in ages, and the fact that such a horizon is missing can only be explained by erosion.

The Mid- and Late Holocene aeolian activity demonstrated by OSL dating is in good agreement with results of other studies carried out in the area. The formation of dunes some 15 m high on the alluvial fans of the River Spree northeast of Cottbus is commonly dated to the Atlantic period (c. 9.0-5.7 ka). Later phases of dune remobilisation are related to forest clearing during the Slavonic occupation of the Niederlausitz area at the beginning of the 6th century AD based on ^{14}C ages. Younger phases of remobilisation are reported for the 12th century AD (e.g. MAGALOWSKI & NOWEL 1982, NOWEL et al. 1972, BITTMANN & PASDA 1999).

4.3.2.3 Site 'Jänschwalde' (J)

The dune site 'Jänschwalde' is located about 11 km NE of site 'Cottbus' in the so-called Düringsheide at the northern edge of the Jänschwalde brown-coal mine (see Fig. 61, topographic map in Appendix F). Glaciofluvial sands of the 'Old Baruth urstromtal' level, which is related to the drainage of the Brandenburg Advance, and fluvial-alluvial sediments of the rivers flowing into the ice-marginal valley from the south are covered by undulating sand sheets and dunes (see Fig. 61). Individual longitudinal dunes up to 4 m in height trend WNW-ESE (SCHLAAK 1999c). Such a dune was exposed by mining activities at site 'Jänschwalde' next to the open face of the coal mine in 1998. As shown in Fig. 65 the sedimentary sequence was clearly separated into two by a well-developed, 50 cm thick, iron-humus podsol.

According to the mean OSL age of samples J1 to J6 the 3.5 m thick layer of dune sand was rapidly deposited on top of the soil 1.76±0.05 ka ago. This age is in good agreement with the assumed post-Bronze Age (< c. 3 ka) cover of the podsol as deduced from archaeological observations near the site 'Jänschwalde' (RÖSLER 1999). The ^{14}C age obtained for charcoal fragments sampled from the dune sands at site 'Jänschwalde' dates the dune sand deposition to 3.35±0.04 ka BP (3.58±0.11 ka cal. BP, see Appendix E, Table E 2 and Fig. 65). The significantly younger OSL ages are considered to be more reliable, first, because they are consistent in age, show no outliers and rapid sedimentation can be assumed for the homogeneous sand unit. Second, the charcoal fragments do not form a distinct layer, but are dispersed in the dune sand or are concentrated in small lenses. This suggests the charcoal has been reworked. Thus the event dated by ^{14}C does not necessarily represent the period of aeolian deposition.

Fig. 65: Schematic stratigraphic section of sampling site Jänschwalde (J).
OSL samples are numbered from the top to the bottom with J1 → J8.
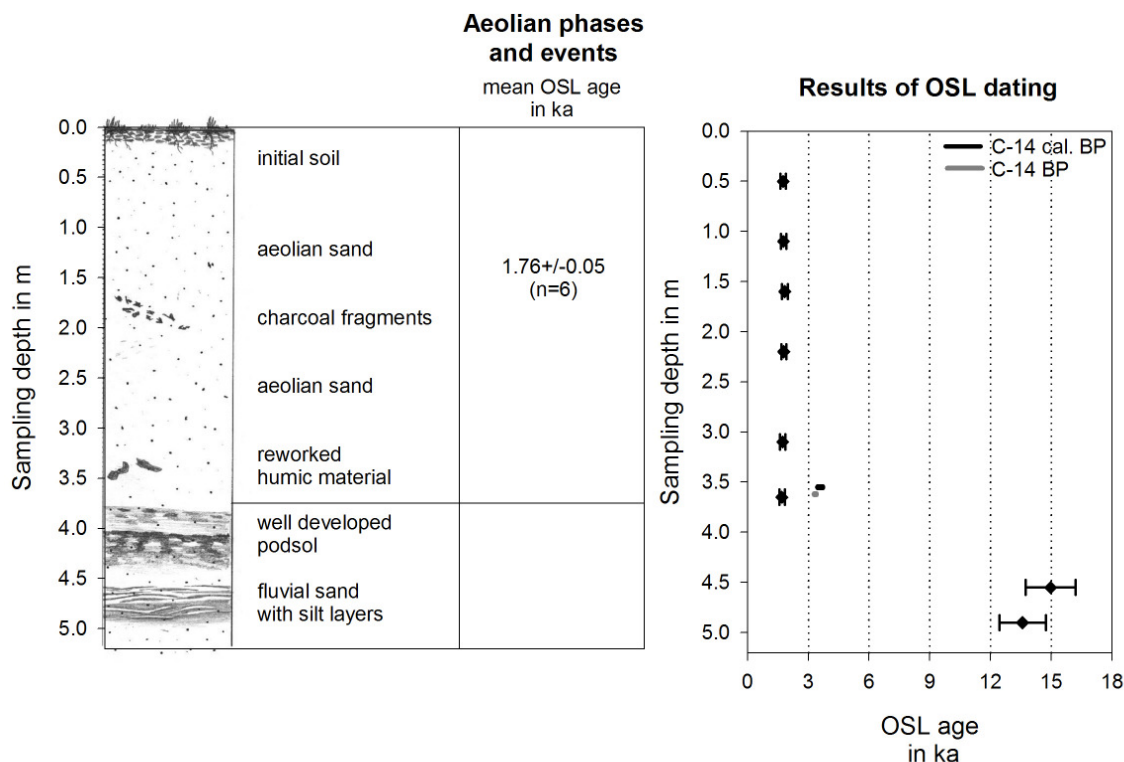
From the base of the section below the podsol horizon two samples, J7 and J8, were taken for OSL dating. SCHLAAK (1999c) concluded that this basal unit, consisting of grey-yellowish, medium to fine grained sand and silts, was laid down under periglacial conditions. He was led to this conclusion because he observed frost cracks, cryoturbations and ice-wedges as common features in this unit, although they were not present in the sediments exposed for OSL sampling. Because the sediments represented by J7 and J8 are thought to have been deposited under alluvial and fluvial conditions as well as by aeolian processes, disequilibria are not unlikely and low-level gamma-spectrometry tests have been carried out to check the equilibrium state of the U decay chain.

No evidence for disequilibria was found (see section 3.3.4.4). At the sampling position of sample J7 in-situ γdose rate measurements were taken to check the influence of the underlying silt-rich layers on the dose rate of the sandier sediments sampled with J7. Both data sets, the gamma spectrometry and NAA results, yielded similar gamma dose rates in comparison to the in-situ measurement of the gamma dose rate (ratios of 1.09 and 1.11 for in-situ to γ-spec. and NAA respectively, see section 3.3.4.3). Because the obtained ratios are well within the range of the average deviation of 1.05 (in-situ to NAA) and 1.11 (in-situ to γ-

spec.), it is concluded that sediment heterogeneities have only a minor influence on the overall dose rate. Finally, the average dose rate resulting from gamma ray spectrometry and NAA was used for age calculation of samples J7 and J8, as the individual dose rates as well as the OSL ages based on NAA or γ-spectrometry dose rate values, respectively, agree on the 2σ error level. The OSL ages obtained for samples J7 and J8 date the basal sediment unit as 14.23±0.98 ka on average. This age is in good agreement with the expected age derived from stratigraphic interpretations. For the silt-rich layers a correlation with the Lateglacial interstadial period, the Meiendorf, was postulated (GI-1e 14.05-14.70 ka), whereas the aeolian sand layers were correlated with the Older Dryas (GI-1d 13.90-14.05 ka) (SCHLAAK 1999c). OSL dating of such a fine stratigraphic resolution is impossible to achieve due to the broad errors in ages. But nevertheless, the postulated Lateglacial, pre-Allerød age could be reconstructed.

Multiple aliquot measurements carried out for the samples from site 'Jänschwalde' yielded substantially older ages of 19.6±4.0 ka (J7) and 23.5±8.3 ka (J8). As at the 'Cottbus' site the tendency towards age overestimation and the limited precision of the multiple aliquot dates is most likely caused by insufficient resetting during transport and deposition of the non-aeolian deposits. This interpretation is sustained by the age comparison for samples J1 to 6, which are of aeolian origin. Here the ratio of multiple to single aliquot derived ages is only 1.14 on average compared to the ratio obtained for samples J7 and 8 of 1.52.

4.3.2.4 Sites 'Jasień' (JA, JB, JC)

This study area near Jasień in Western Poland is also located close to the southern edge of the Głogów-Baruth 'urstromtal'. Here rivers from the south dissected the old Saalian till plains. These ground moraine patches now project from the expanded alluvial fans which the rivers, e.g. the Lubsza in Jasień, have deposited in proglacial valleys. These fluvial deposits provided ample source material for the formation of coversands and dune fields (see Fig. 66).

Three sites have been investigated, with Jasień-A being about 3 km east of Jasień-B and -C, which represent two different profiles at the same dune site (see also the topographic map in Appendix F). These sites were particularly interesting in the context of this study, as chronological control for crosschecking OSL chronologies was provided by numerous radiocarbon ages, palynological analysis, and the exposure of the 'Finow' palaeosol.

Fig. 66: Morphological map of the study area 'Głogów-Baruth ice marginal valley' showing the location of the sampling sites 'Jasień-A' (JA), 'Jasień-B' (JB), and 'Jasień-C' (JC) (summarised as dune sites 6 in Fig. 57).
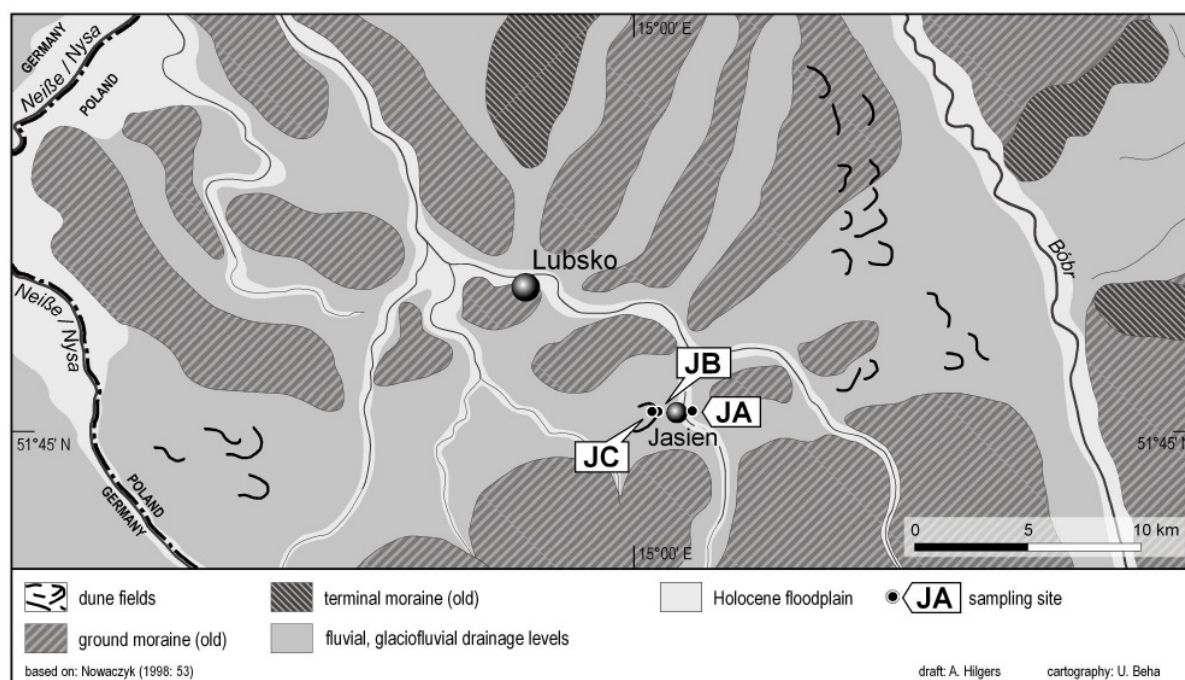
Site 'Jasień-A'

Site 'Jasień-A' represents a sequence of dune sands overlying the end moraine of the Warthe stage of the Saalian glaciation (see Fig. 67 & 68). A ventifact layer forms the boundary between the Saalian till and the c. 2.85 m thick dune sand deposit on top. Within these dune sands a buried soil horizon is exposed, which is correlated with the 'Finow soil' of Allerød age (see Fig. 68). With sample JA-7 the onset of dune formation could be placed at the transition from the Last Glacial Maximum to the Early Lateglacial at 16.30±1.20 ka. Thus, the ventifact layer most probably represents intensified aeolian processes during the maximum of the Last Glacial. Sample JA-6 taken from within the fossil Bv horizon gave an OSL age of 14.36±1.07 ka. This age is in good agreement with the expected pre-Allerød age (< 13.90 ka) of the substrate of the 'Finow soil' and also with the ^{14}C age of 13.2±0.5 ka cal. BP (11,130±120 yr BP, KOWALKOWSKI et al. 1999b, see Appendix E, Table E 2) obtained for this soil horizon. In agreement with this radiocarbon age the burial of the 'Finow soil' was assigned to the Younger Dryas period (GS-1 11.50-12.65 ka) by samples JA-5, -4, and -3 yielding an average age of 12.45±0.50 ka for the dune sand unit on top of the 'Finow soil'. A second ^{14}C age presented

by KOWALKOWSKI et al. (1999b) of 1,416±120 yr cal. BP (1,520±60 yr BP see Appendix E, Table E 2) derives from a similar stratigraphic position as OSL sample JA-3. With 12.22±0.82 ka the OSL age gives a much older result.

The most likely explanation at this stage is that the radiocarbon age is based on a date from burned root material. Unfortunately no further comment is made on the dated material in KOWALKOWSKI et al. (1999b). Sample JA-3 is in good agreement with the ages of the underlying sediments; no evidence for an erosional boundary is present between JA-3 and -4 and the equivalent dose distribution of sample JA-3 gave no hint on age overestimation due to poor bleaching. Accordingly the OSL date is considered to be reliable and is included in the final interpretation of the chronostratigraphy of the site.

At the top of the section samples JA-2 and -1 appear to represent two Late Holocene phases of aeolian deposition with OSL ages of 6.16±0.42 ka and 0.25±0.02 ka. As a well-developed Holocene soil is missing two phases of erosion must be assumed. Both were terminated when deposition of aeolian sediments, represented by the dated sediment layers, occurred. Both samples showed a broad scatter in equivalent dose values. Thus, the possibility of intermixing with younger material in these sediment layers close to the surface cannot be excluded. Further measurements ought to be carried out using a reduced number of grains per aliquot to test whether a mixing of different grain populations is really present in the samples. Thus, the ages should not be overrated in terms of their chronostratigraphic interpretation at this stage of the study. However, the stratigraphy of the section would support their reliability to a certain extent. On top of sample JA-2 a layer of reworked humic material is present. The very young age of sample JA-1 is considered to be reliable as the soil at the top of the section represents only an initial stage of soil development.

Fig. 67: Geomorphological mapping of the surrounding of the dune site 'Jasień-A'.
(from KOWALKOWSKI et al. 1999b: 4)
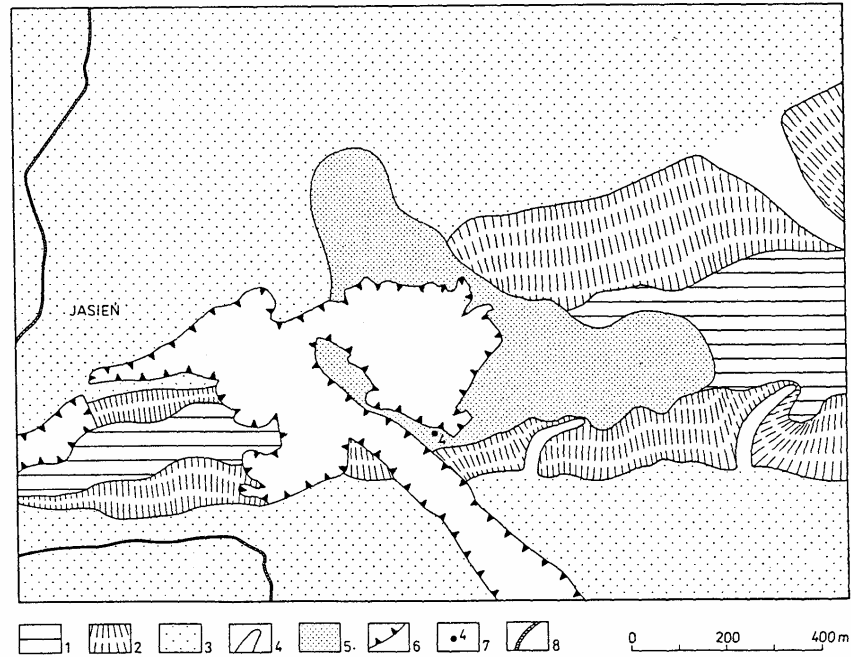
1-ground moraine plateau, 2-slopes, 3-alluvial cone, 4-valley bottom, 5-dunes and sand sheets, 6-exploration exposures, 7-research site 'Jasień-A', 8-railway

Fig. 68 Schematic stratigraphic section of sampling site 'Jasień-A' (JA).
OSL samples are numbered from the top to the bottom with JA1 → JA7.
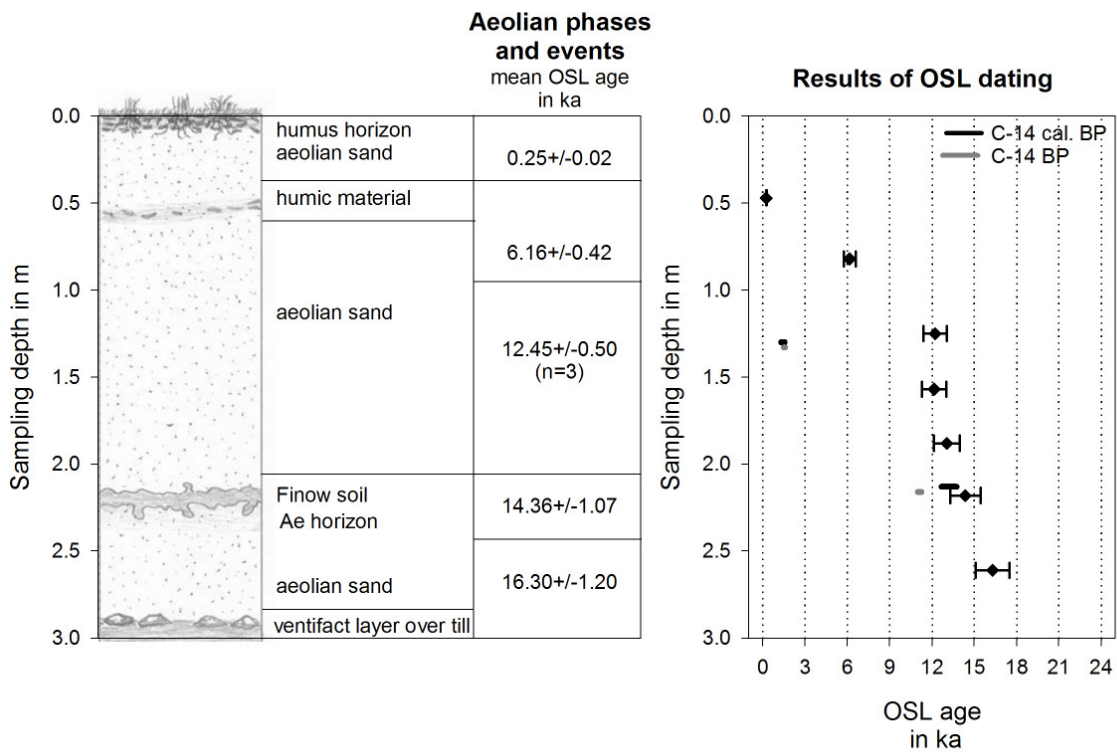
Site 'Jasień-B'

The sampling sections 'Jasień-B and -C' were exposed at a parabolic dune, open towards the west. The dune sands cover alluvial fan deposits of the River Lubsza (see Fig. 69). The dune site has been investigated and described in detail by KOWALKOWSKI et al. (1999a).

Fig. 69: Geomorphological mapping of the surrounding of the dune sites 'Jasień-B & -C'.
(from KOWALKOWSKI et al. 1999b: 4)
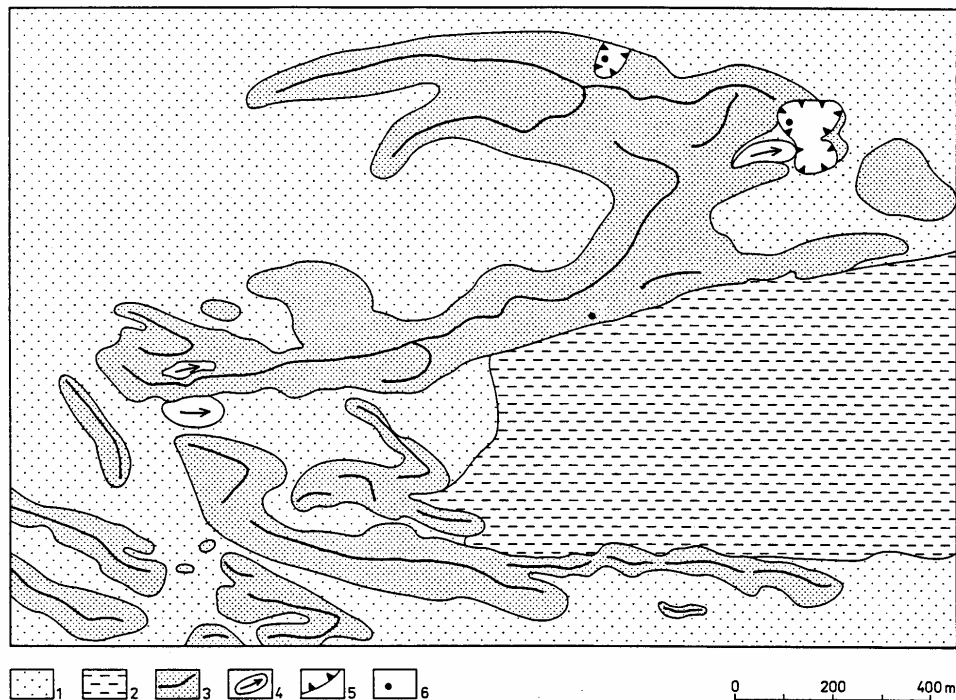
1-ground moraine plateau, 2-slopes, 1-alluvial cone, 2-biogenic accumulation plain, 3-dunes, 4-blowouts, 5-exploration exposures, 6-research sites (excavation exposure at the top: Jasień-C, eastern excavation exposure: Jasień-B

The exposures, revealed by the former use of the dune as a sandpit, are within the northern arm of the dune, perpendicular to the dune's morphological axis, exposing the sediment sequence in the distal part of the arm (KOWALKOWSKI et al. 1999a). Section 'Jasień-B' is a trench cut into the northern edge of the dune in a leeward position and 'Jasień-C' is located just a few tens of metres further northwest in the northern tail of the parabolic dune (see Fig. 69).

In a trench, cut into the floor of the former sand pit, the lower part of section 'Jasień-B' comprises alternating layers of biogenic and aeolian deposits. According to the pollen record and radiocarbon ages the formation of the multiple peat layers could be correlated with Allerød to Early Younger Dryas ages (KOWALKOWSKI et al. 1999a, see Appendix E, Table E

2). In the second half of the Younger Dryas aeolian processes finally dominated and a dune was formed on top of the organic layers. The OSL ages for the sand deposits underlying the Allerød peat (sample JB-1 12.96±0.95 ka) and overlying the early to mid Younger Dryas deposits (sample JB-2 11.34±0.86 ka) are - within errors - in good agreement with the independent age control (see Fig. 70). It should be noted that for cosmic dose calculation the burial depth was assumed to be much greater than the actual sampling depth for both samples, as a larger cover has to be deduced from the dune morphology before the just recent opening of the sandpit.

Fig. 70: Schematic stratigraphic section of sampling site Jasień-B (JB).
OSL samples are numbered from the bottom to the top with JB1 & 2 in the lower section and JB3 →
JB13 in the upper section.
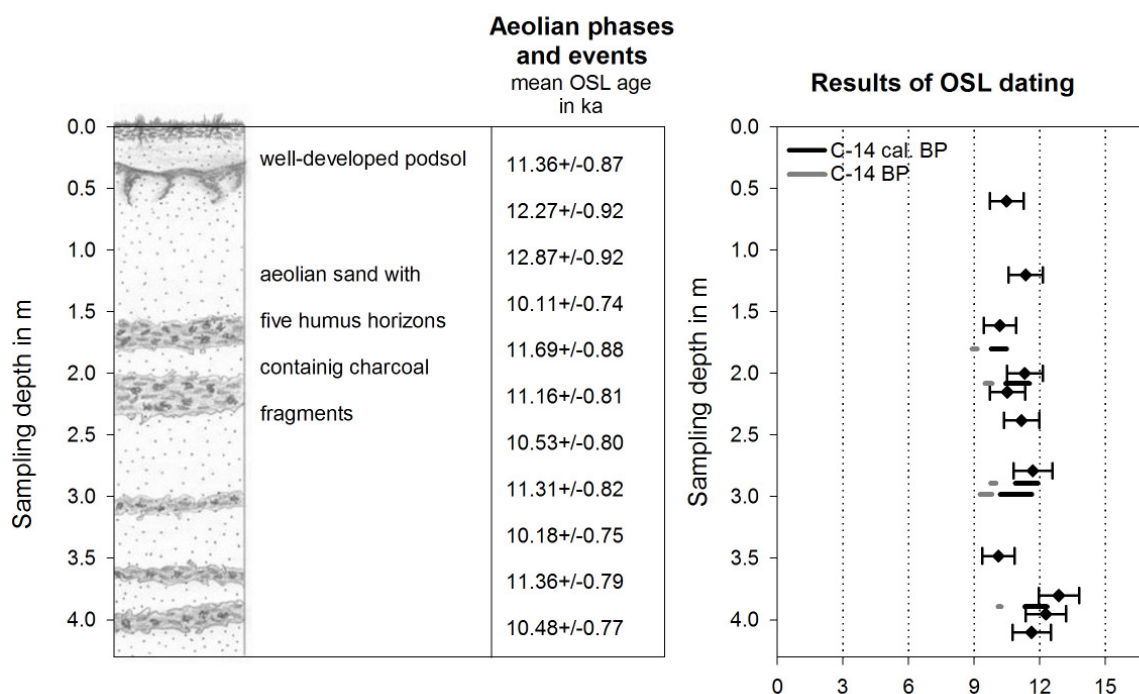
The upper part of section 'Jasień-B' is located at the northern edge of the dune in just a short distance of only a few metres from the lower section 'Jasień-B'. This sequence comprises about 4.3 m of dune sand and a series of five poorly developed arenosols with finger-like Ah horizons (see Fig. 70). The humus horizons contain charcoal and thus were dated by radiocarbon (see Appendix E, Table E 2 dates, KOWALKOWSKI et al. 1999a). The OSL data set is in reasonably good agreement with the calibrated radiocarbon data set (Fig. 70). The OSL ages date the deposition of more than 4 m of aeolian sand into the time span from the Younger Dryas up to the late Preboreal. This age range coincides with the time span given in

KOWALKOWSKI et al. (1999a) from the middle of the Younger Dryas until the beginning of the Boreal. The stratigraphic observation of several initial soil developments, which indicate at least a certain time of depositional quiescence, do not allow one to summarise all OSL ages by calculating a mean age for one major phase of dune formation although they agree within errors. The effect of this aeolian activity was not regional but local. The alternation of sand deposition and initial soil formation is most likely a result of fires, which repeatedly destroyed the vegetation cover (KOWALKOWSKI et al. (1999a). These fires are proved by the large amount of charcoal found in the humus horizons as well as in the sand layers in-between. As the plants had limited time to recover in-between the fires, the vegetation remained still poorly developed, whereas other dune areas in the vicinity by that time were stabilised by a closed vegetation cover. The uneven and commonly diffuse boundaries of the humus horizons indicate the possibility of a synsedimentary origin for these horizons (KOWALKOWSKI et al. 1999a). This is also explained by the less stabilised surfaces of the surrounding dune areas with poorly developed vegetation cover, and which could serve as a source of sand almost at all times.

Site 'Jasień-C'

Section 'Jasień-C' is located several hundreds of metres away from section B within the upper part of the c. 12 m high northern dune tail (see Fig. 69). Five OSL samples have been taken from the exposed upper 5 m (see Fig. 71). The 'Finow' palaeosol is exposed at 4.8 m below the surface (KOWALKOWSKI et al. 1999a). The OSL ages obtained for the overlying dune sand of 12.55±0.72 ka (mean age of JC-1 to 4) and the substrate of the soil with 14.32±1.07 ka (JC-5) are in good agreement with the Allerød age of the 'Finow soil' (GI-1a-c 12.65-13.90 ka). Furthermore, the OSL results agree with a radiocarbon age obtained for the fossil soil horizon of about 12,060±827 a cal. BP (10,290±200 a BP, pers. comm. Prof. Dr. A. Kowalkowski, 1999, see Appendix E, Table E 2).

Fig. 71: Schematic stratigraphic section of sampling site Jasień-C (JC).
OSL samples are numbered from the top to the bottom with JC1 → JC5.
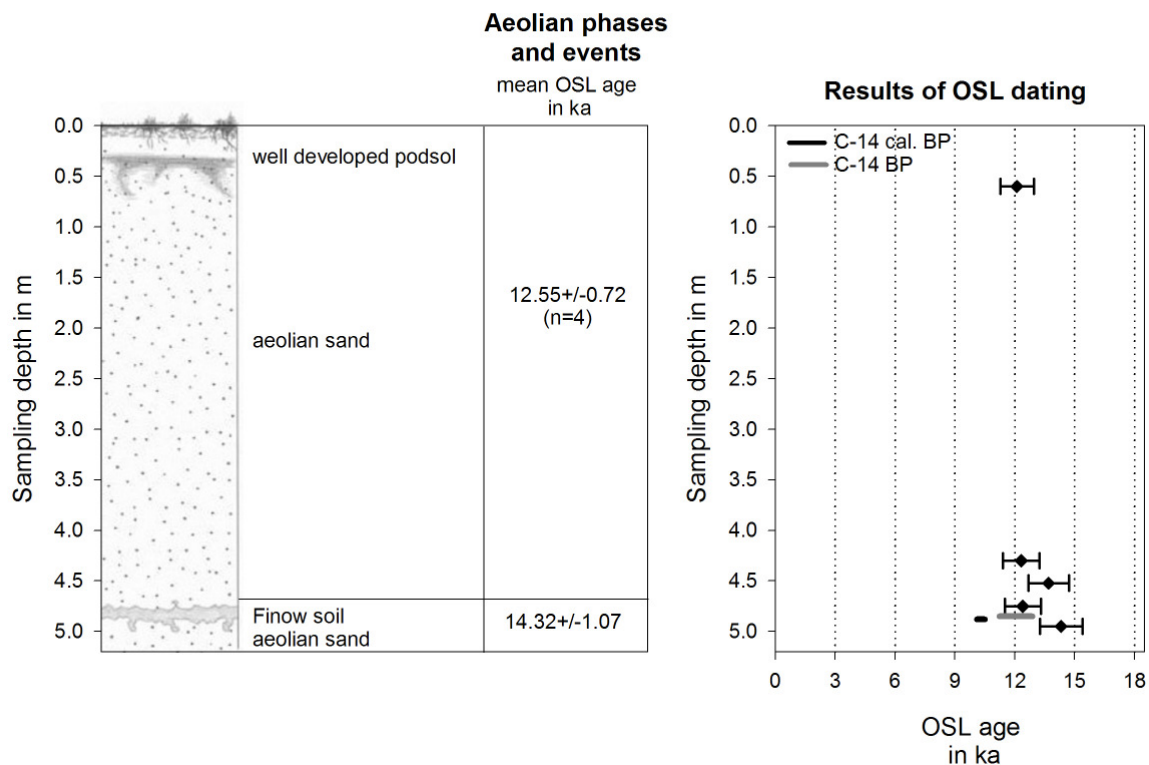
Although the age of sample JC3 agreed within the 2 sigma confidence level with the ages of the over- and underlying sediments (see Fig. 71 and Appendix F), it was remeasured using smaller aliquots containing less grains to check whether insufficient bleaching could be the reason for the slightly older age. But as both equivalent dose values agree within 1σ standard errors no conclusive evidence for poor bleaching was found (see Appendix F). The age based on the 1mm aliquot palaeodose was used for further interpretations of the chronological record (see also Fig. 71). If the slightly higher age can be ascribed to an erroneous dose rate estimate has to be clarified by further radionuclide analysis.

KOWALKOWSKI et al. (1999a) place the phase of major dune formation at Jasień in the Older Dryas (GI-1d 13.90-14.05 ka). Certainly, at the sampling site 'Jasień-C' the Allerød-age 'Finow soil' is found on top of an about 12 m high old dune core. But all these observations do not necessarily exclude an even older age for the dune. The OSL age of JC-5 dates the top of the pre-Allerød dune to 14.32±1.07 ka. Despite the broad error it nevertheless also allows a pre-Older Dryas age for dune formation. Further sampling, especially at the base of the dune is necessary to clarify the age of the onset of dune formation. Unfortunately, the base of the

dune was not exposed at the time of sampling, and it was not possible to obtain an age for the onset of dune formation at site Jasień-C. It would be interesting to see if the onset of Lateglacial aeolian deposition coincides with the onset at site 'Jasień-A', where the oldest dune deposits were dated at about 16.30±1.20 ka. The ages for the sediments directly underlying the 'Finow soil' exposed at both sites, however, showed an accordance of 14.36±1.07 ka (JA-6) and 14.32±1.07 ka (JC-5)!

A high sedimentation rate for the Younger Dryas period can be deduced from the dating results obtained for the upper part of section 'Jasień-C'. The well-developed podsol at the top indicates that Late Holocene phases of dune remobilisation, as observed at site 'Jasień-A', did not occur here. Even the intensive Preboreal sedimentation phase recorded at section 'Jasień-B' only a few hundreds of metres away is not recorded in section 'Jasień-C'. This illustrates in an impressive way the local restriction of aeolian events. While 4 m of sediment were deposited at site 'Jasień-B', no deposition at all is recorded at the nearby site 'Jasień-C'. The location of both sections with respect to the dune morphology readily accounts for this difference. 'Jasień-B' is situated at the leeward slope of the northern edge of the dune, where deposition is supposed to take place due to the prevalence of sand-transporting winds from the west, whereas site 'Jasień-C' is located at the northern tail of the dune. However, the possibility that this part of the dune was affected by deflation at the same time the sequence 'Jasień-B' accumulated, cannot be ruled out. The similar intensity of podsolisation of the topsoils exposed at sites 'Jasień-B and -C' might imply a similar length of time for both soils to develop.

4.3.3 Dune sites in the Toruń-Eberswalde 'urstromtal' and on the Schorfheide sandur

The east-west orientated Toruń-Eberswalde 'urstromtal' was first used as a meltwater-outlet during the remelting of Pomeranian inland-ice advance but remained as a meltwater drainage until the formation of the Rosenthal end moraine (EHLERS et al. 2004). The study area is located within the part of the Toruń-Eberswalde proglacial valley generally referred to as the Eberswalde 'urstromtal'. It extends from Niederfinow in the east to Liebenwalde in the west, varying in width between 3 and 8 km (SCHLAAK in GÄRTNER et al. 1995). The so-called Barnim, the ground moraine plateau deposited by the Brandenburg glacial advance, forms the southern margin of the valley. To the north the ice-marginal valley is bordered by proglacial outwash plains and the terminal moraine of the Pomeranian Advance as well as by patches of till plains of the Brandenburg Advance (Fig. 72).

Three different terrace levels related to the various phases of meltwater discharge are distinguished within the Eberswalde 'urstromtal'. Table 11 summarises the correlation of the terrace levels and also the sandur plain with stages of the Weichselian ice-sheet and links the individual sampling sites in this study area with the different morphological units. All terrace levels are characterised by numerous depressions caused by the delayed melting of covered dead ice. Today these channel like structures are water filled or boggy areas (LIEDTKE 1956/57). The expanded dune fields west and southwest of Eberswalde represent the most distinct morphological features in the landscape. In detail, the morphology of the predominantly parabolic dunes in the Eberswalde valley has been described (for example, LOUIS 1929, LIEDTKE 1957/58, SCHLAAK 1993).

Within the Eberswalde 'urstromtal' four dune sites have been sampled for OSL dating. All four sites can be linked by the occurrence of the 'Finow soil' palaeosol horizon. This includes also the two sections investigated in the dune field covering the Schorfheide sandur, which is located north of the Eberswalde valley (see Fig. 72).

Fig. 72: Morphological map of the study areas 'Toruń-Eberswalde ice marginal valley' and 'Schorfheide sandur' with the sampling sites 'Finow' (F), 'Spechthausen' (S), 'Melchow' (M), 'Rosenberg' (R) (summarised in Fig. 57 as dune sites 7), and 'Schorfheide-A' (SHA) and 'Schorfheide-B' (SHB) (summarised as dune sites 8 in Fig. 57).

Three different glaciofluvial discharge levels are distinguished: (a) 42.5-47 m a.s.l. (drainage of the Pomeranian Advance), (b) 37.5-42.5 m a.s.l. (drainage of the Parstein stage), (c) 35-37.5 m a.s.l. (drainage of the Angermünde stage) (heights according to SCHLAAK 2000)
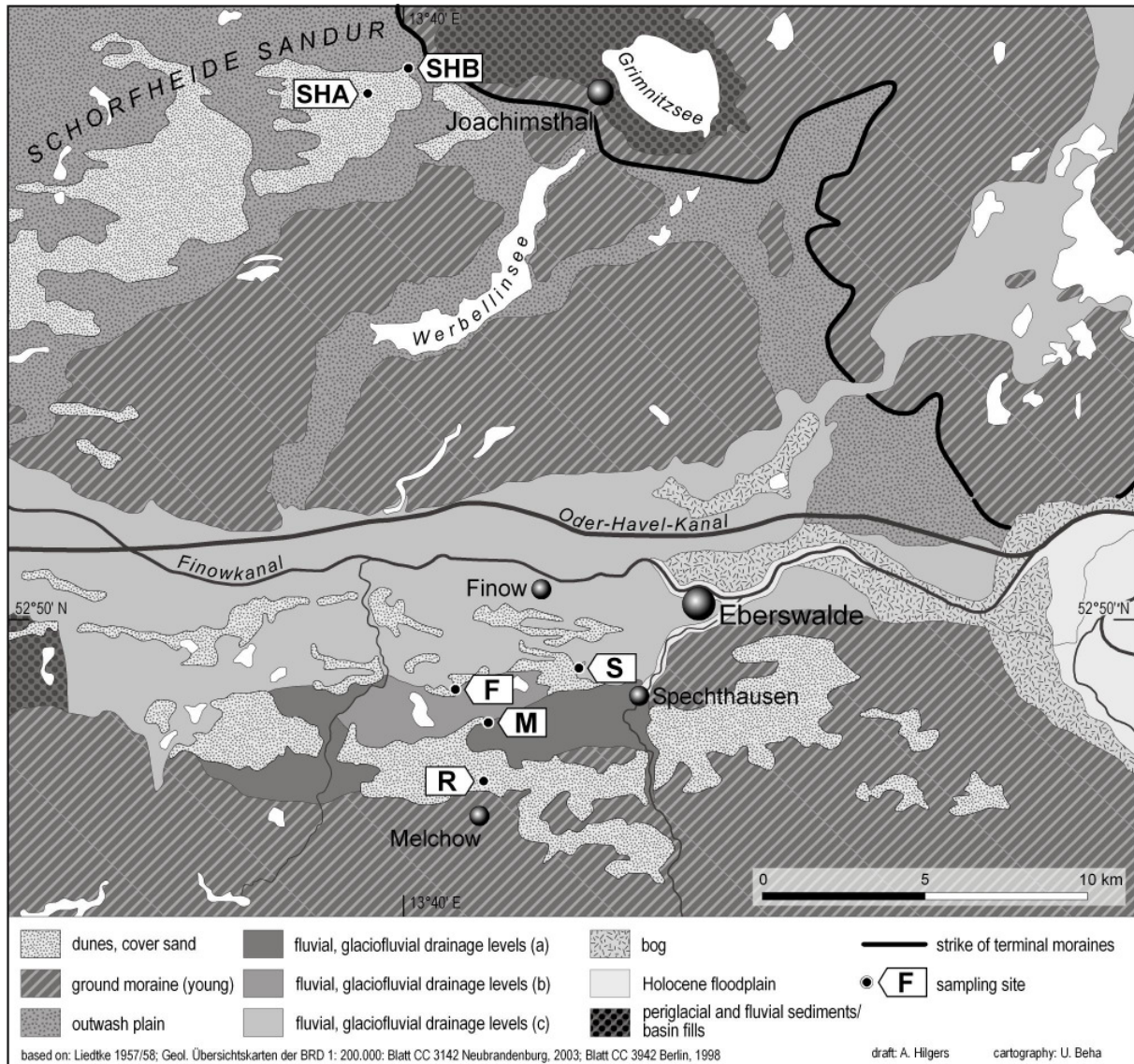
Table 11: The levels of fluvial-glaciofluvial discharge in the 'Eberswalde' ice-marginal valley and their correlation to the different stages of the inland-ice.

Terrace level (LEMBKE 1939b, LIEDTKE 1956/57)	Terrace level (SCHLAAK 2000)	Drainage of the stage of the ice-sheet	Age (4)	Location of the dune sites
45 m a.s.l. (1)	42.5-47 m a.s.l.	Pomeranian Advance (2)	c. 15.2 ka BP; **18.7-17.7 ka cal. BP**	Schorfheide A & B (Schorfheide sandur), Rosenberg & Melchow (highest terrace level)
40 m a.s.l. (2)	37.5-42.5 m a.s.l.	Parstein stage (3)		Finow & Spechthausen
36 m a.s.l. (1)	35-37.5 m a.s.l.	Angermünde stage (2)	c. 14.7 ka BP; **18.1-17.1 ka cal. BP**	

1: LEMBKE (1939b), 2: LIEDTKE (1956/57), 3: BROSE & PRÄGER (1977 in SCHLAAK 1993), 4: conventional ^{14}C ages after LIEDTKE (1996), calibrated using CALIB 4.1 (STUIVER et al. 1998)

4.3.3.1 Site 'Finow' - The 'Postdüne' (FA, FB, FC)

The study site 'Finow' is situated on the intermediate 'urstromtal' level of 37.5-42.5 m a.s.l. Here, the lakes Schwärze- and Samithsee indicate a former east-west trending channel structure preserved by dead ice. In between these two lakes the peat-bog area of the 'Grosses Postluch' is located, it is part of the same channel structure. At its southwestern edge a 6 m high parabolic dune is located. It was called 'Postdüne', because of the neighbouring 'Postluch', by SCHLAAK (1993), who investigated the feature in great detail. This is the type locality for the 'Finow soil' (SCHLAAK 1995), for it was here that chronological evidence (^{14}C ages, palynological studies and a layer of the Laacher See tephra) allowed dating of this fossil B horizon for the first time.

At the northern edge of the dune, the aeolian sand interdigitates with organic material derived from boggy areas in lower-lying sites (see Fig. 73). Within a peat horizon a layer of the Laacher See tephra (LST) is embedded. SCHLAAK (1993) was able to demonstrate the stratigraphic correlation of this LST layer with the fossil B horizon, the 'Finow soil'. This was the crucial observation for the dating of this palaeosol. As shown in Fig. 73) in the upper, drier parts of the dune the peat horizon, as such, disappears and becomes the 'Finow soil'.

The tephra derives from the explosive eruption of the Laacher See volcano about 40 km S of Bonn in the East Eifel volcanic region in western Germany. The LST layer is considered as the most important chronostratigraphic marker in central Europe for the Lateglacial time span because of its widespread distribution throughout Europe. Furthermore, this ash layer marks a distinct moment in time as the main phase of eruption only lasted for about ten hours and the ash is presumed to be deposited within the next few days throughout its affected area (SCHMINCKE et al. 1999).

In northeast Germany, for example, Laacher See tephra was found at about 150 sites (THEUERKAUF 2002). But to use the LST layer as a chronostratigraphic marker the precise dating is crucial. Numerous radiocarbon ages have been reported throughout the last decades dating the Laacher See eruption, for example, to 11,000±50 a BP (VAN DEN BOGAARD & SCHMINCKE 1985), 11,037±27 and 11,073±33 a BP (BAALES et al. 1999), 11,230±40 a BP (HAJDAS et al. 1995a), 11,210±95 a BP and 11,380±95 a BP (HAJDAS et al. 1995b), 11,018±120 a BP and 11,338±120 a BP (KLIEWE 1995 in DE KLERK et al. 2001). According to numerous varve chronologies obtained from lake sediments with embedded layers of the LST the eruption occurred about 200 varve years before the onset of the Younger Dryas cooling (e.g. KLEINMANN et al. 2002). As the beginning of the Younger Dryas period is dated to 12.68 ka BP by varve chronologies (LITT et al. 2001) the eruption of the Laacher See volcano took place during the Allerød 12,880 years ago. In the literature age values of 12,880 varve years BP (STEBICH 1999 in DE KLERK et al. 2001, BRAUER et al. 1999) up to 12,900 a cal. BP are also recorded (MERKT & MÜLLER 1999, SCHMINCKE et al. 1999). These data are in agreement with an ^{40}Ar/^{39}Ar date obtained for sanidine phenocrysts from the tephra itself of 12,900±560 yr (VAN DEN BOGAARD 1995).

The chronological constraints provided at site 'Finow' made this dune site particularly suitable for a comprehensive comparative study. Thus, at the beginning of this project, the different protocols used for OSL dating were first tested against the independent chronologies. The results have been reported by HILGERS et al. (2001b) and are also presented in Appendix B in detail. Here, only the single aliquot dating results of the quartz fraction will be discussed, as they were judged to yield the best age estimates compared to the expected depositional ages. Overall 20 luminescence samples were collected from three sections (Fig. 73).

Fig. 73: Description of the profile and location of the three sampling positions for luminescence dating (FA, FB, FC).
The horizontal distance from section A to section B is about 4 m. The positions of the ^{14}C samples are also shown (modified from SCHLAAK 1999, ^{14}C ages calibrated using CALIB-4.1, see Appendix E, Table.2). Note that only sample F10 and 11 are shown at section FC. OSL samples F12 to F18 were taken from above F10 and samples F19 and F20 from below sample F11 (from HILGERS et al. 2001b).
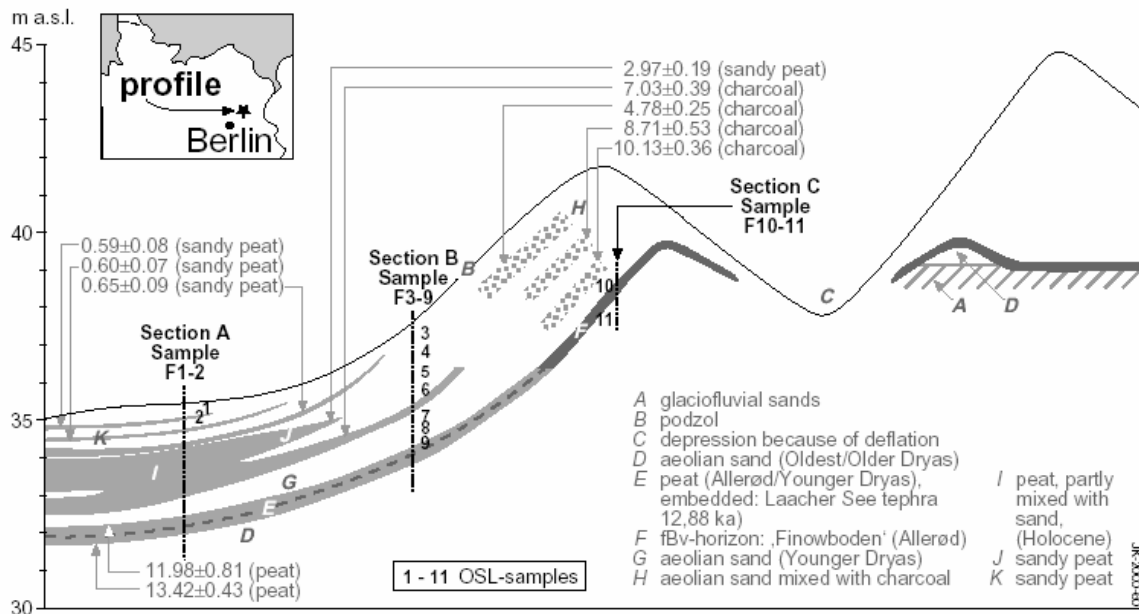
Site 'Finow-A'

In this onshore situation sandy peat layers are close to the surface. Samples F1 and F2 were taken from the aeolian sands above the peat (Fig. 73 and Fig. 74). The OSL ages obtained for F1 and F2 of 140±10 and 290±30 years are consistent with the ^{14}C age of 590±80 yr cal. BP which was obtained for the peat layer beneath them (595±70 yr BP, SCHLAAK 1999, see Appendix E, Table E 2). The interruption of peat growth by aeolian sand deposition has been explained as due to reactivation of aeolian processes following the extensive arable farming on sandy substrates in Medieval times, here most probably related to the Late Slavonic period at the end of the 13th century AD (SCHLAAK 1993, LUTZE 1995). Nevertheless it is difficult to place a limit on how young the samples F1 and 2 could be, as they might represent recent, but poorly bleached slope wash deposits. Several arguments support the conclusion that samples F1 and F2 in fact prove recent aeolian activity. First, the immature soil development on top of F1 argues for a limited time span since deposition of its substrate. Second, the dune is now stabilised by a forest cover. Third, historical records suggest that in the 14th and 15th century some farmland was abandoned as a result of war, plague and famine; thus the forest cover was re-established. After a short period of dune stabilisation the forests were exploited for fuel

during the 17th and 18th century to meet the needs of the expanding nearby capital city of Berlin with firewood and timber (LUTZE 1995). In addition, the OSL measurements themselves yield no evidence of poor bleaching or mixing of sediments with different ages with respect to the distribution of equivalent dose values. The results obtained for F1 and 2 are considered to be reliable and it seems very likely that the last sand mobilisation occurred just several decades ago.

Fig. 74: Schematic stratigraphic section of sampling site Finow-A (F).
OSL samples are numbered from the top to the bottom with F1 → F2.
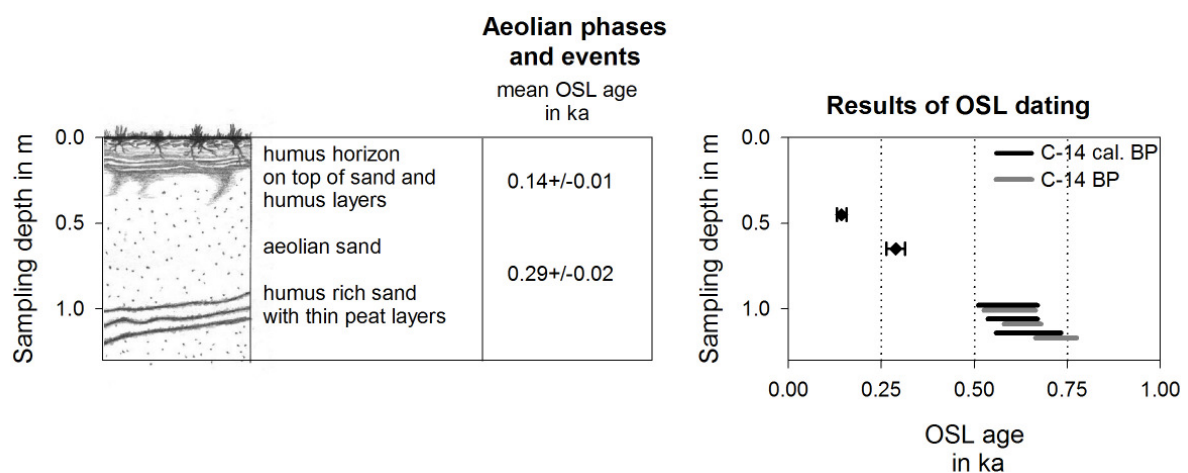
Site 'Finow-B'

The OSL samples F3 to F9 have been taken from the same trench as F1 and F2 but were about 4 m closer to the core of the dune (see Fig. 73 and Fig. 75). At the bottom of the sequence the peat layers with the embedded tephra layer were exposed. By palynological analysis the peat below the LST layer could be correlated with the Allerød interstadial and the peat on top of the Laacher See tephra with the Early Younger Dryas (SCHLAAK 1993). For all samples NAA and gamma spectrometry have been carried out to measure the radionuclide concentration. For all but sample F9, age calculation was based on the average dose rates, because both dose rate estimates showed good agreement within 2σ errors. Only sample F9 gave inconsistent radionuclide contents, with the most distinct difference observed for uranium (ratio NAA/γ-spectrometry 1.73). Disequilibrium in the U decay chain cannot be excluded, especially as the sediments are affected by fluctuations of the groundwater level. However, the OSL age based on the gamma spectrometry results is considered to be accurate

as it is in agreement with the palynological results and the ^{14}C ages obtained for the underlying peat and the age of the underlying LST layer (see Fig. 75).

With an average age of 11.37±0.56 ka the three lowermost samples (F7-9) date the deposition of the sand unit on top of the peat to the transition of the Younger Dryas to the Preboreal. This result is compatible with the results of pollen analysis which show that the upper parts of the peat developed during the earlier Younger Dryas. Thus aeolian accumulation had not begun before the later part of this cold period (SCHLAAK 1993). Furthermore, by ^{14}C the end of peat formation was dated to 11.98±0.81 ka cal. BP (Appendix E, Table E.2). This age is consistent with the OSL age of the directly overlying dune sands (11.93±0.91 ka, F9), and also with the average age of the whole sand unit of 11.37±0.56 ka (sample F9-F7). The rhythmic stratification of thin sand and peat layers in this sand unit indicates a delayed onset of aeolian activity in the Younger Dryas for there were several periods of stabilisation and peat formation. This observation fits well into the characterisation of the Younger Dryas climatic conditions with an early cooler and wetter phase and a later slightly warmer but drier climate (e.g. Renssen 1997, ISARIN et al. 1998). This would also argue for pronounced aeolian activity towards the end of the Younger Dryas rather than earlier.

The humic horizon exposed between samples F7 and 6 was dated as Preboreal (11.5-9.8 ka) based on palynology (SCHLAAK 1993). This observation is in accordance with the OSL ages of the substrate of 10.89±0.94 ka (F7) and of the overlying sediments of 9.65±0.83 ka (F6). In contrast, the radiocarbon age obtained for the humic horizon of 7.03±0.39 ka cal. BP (6.13±0.15 ka BP, see Appendix E, Tab. E.2) appears to be an underestimate of the presumably Preboreal age of the soil formation. Because of the good agreement of the OSL results with other ^{14}C ages throughout this section (see Fig. 75) and the contradiction of the radiocarbon age and the pollen data, the OSL ages are considered to yield the more reliable age estimate.

Fig. 75: Schematic stratigraphic section of sampling site Finow-B (F).
OSL samples are numbered from the top to the bottom with F3 → F9.
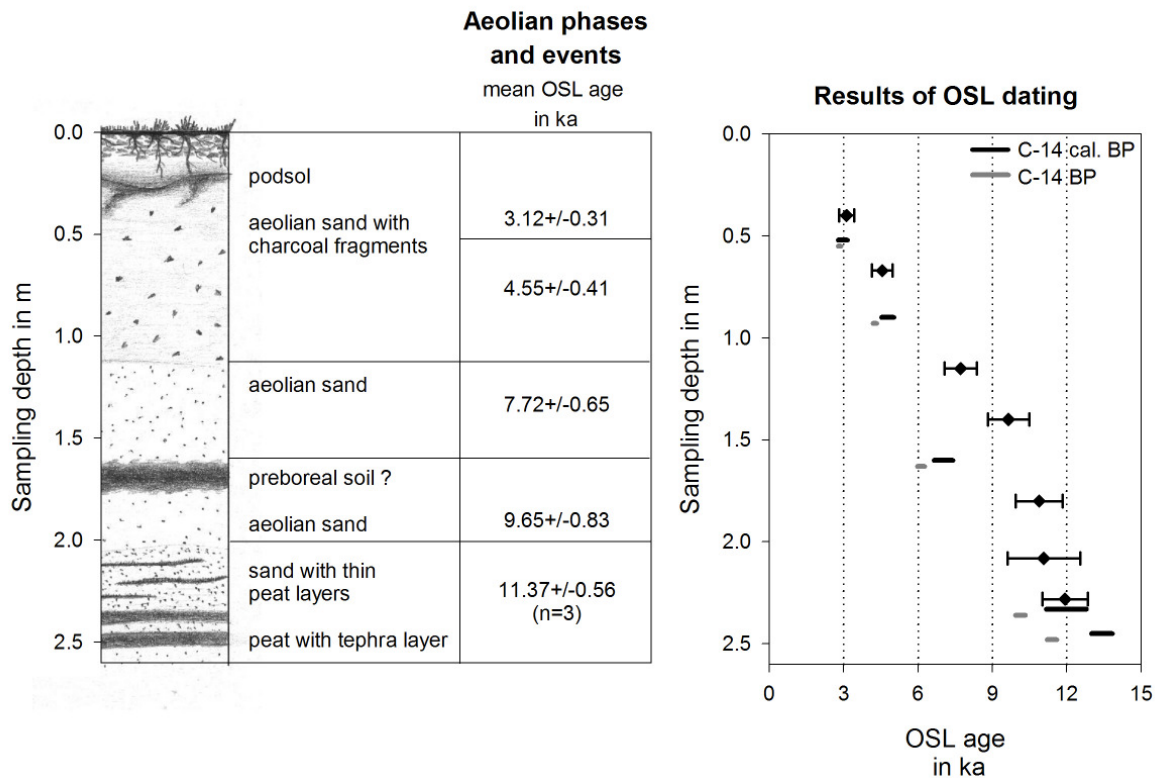
As shown in Fig. 75 several phases of dune remobilisation during the Holocene are recorded at site 'Finow-B' showing good agreement of OSL ages and calibrated ^{14}C ages. The question is to what extent human impact or natural causes were the reason. Disturbance of the vegetation cover by fires seems most likely, for charcoal fragments are abundant in the sediment sequence. It is difficult to judge whether wild or natural fires, e.g. those caused by lightning, or fires initiated by humans were responsible for forest clearing. Intensified occupation of the area by man accompanied by forest clearance for arable farming and pasture is reported by LUTZE (1995) for the period since 3.5 ka BC. This period seems to be represented by samples F3 and F4 from the top part of the section.

Site 'Finow-C'

Section 'Finow-C' is cut into the upper part of the dune slope (Fig. 73) where the 'Finow soil' is exposed about 2.2 m below surface. Samples F11, 19 and 20 date the substrate of this palaeosol as averaging 14.91±0.74 ka. This sand unit is at least 2.5 m thick (SCHLAAK 1993). The upper age limit for the dune formation is set by its situation on the intermediate 'urstromtal' terrace at the 40 m level, which is related to the drainage of the Parsteiner stage at around 18 ka (see Table 11). SCHLAAK (1993) explains the distinct bleaching of the sand deposits below the 'Finow soil' to high ground-water tables during the Older Dryas period, which most likely limited dune formation during this Lateglacial cold spell here. Combining both observations the formation of the older core of the 'Postdüne' most likely dates into the Oldest Dryas (GS-2a, 14.70-16.90 ka), after the formation of the glaciofluvial 'urstromtal' terrace around 18 ka and the post-depositional hydromorphic alternation during the Older Dryas (GI-1d, 13.90-14.05 ka). Thus, the OSL age of 14.91±0.74 ka obtained for the top part of the old dune core is in agreement with the expected ages from field observations.

Fig. 76: Schematic stratigraphic section of sampling site Finow-C (F).
OSL samples are numbered from the top to the bottom with F12 → F18, F10, F11, F19, F20.
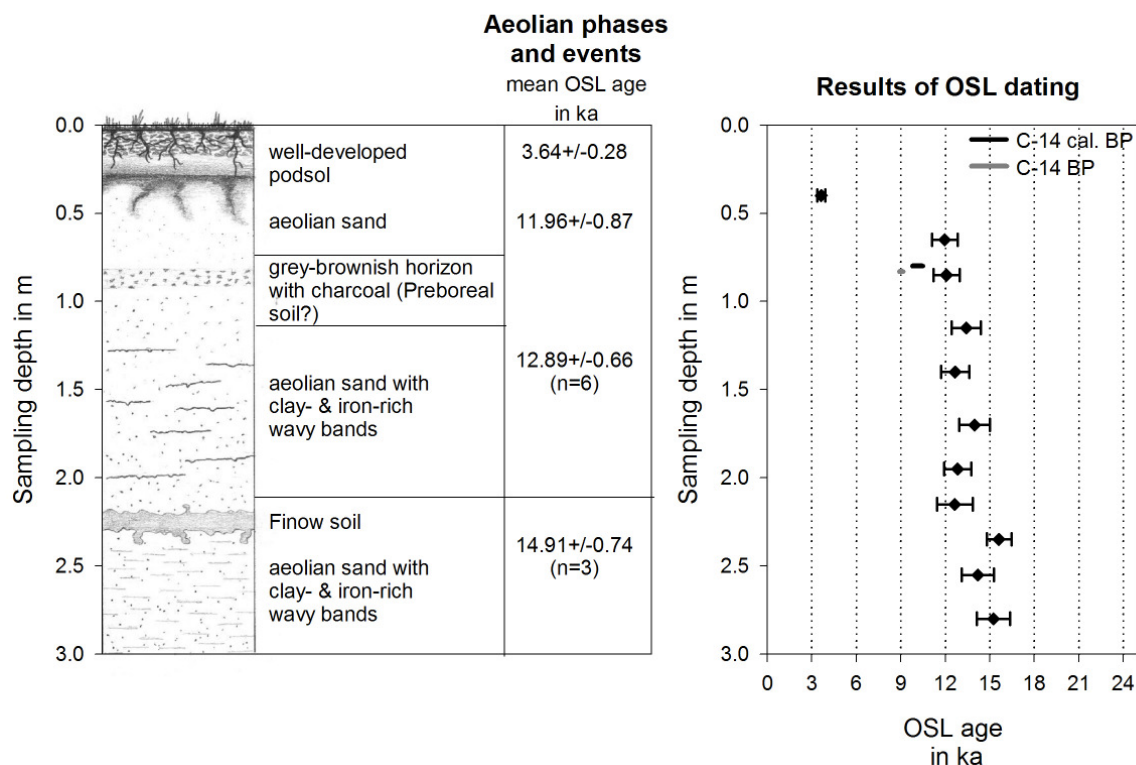
In these Oldest Dryas dune deposits the 'Finow soil' was formed during subsequent warmer periods in the Lateglacial. The soil was covered when dune formation resumed in the Younger Dryas. Sample F10 taken from dune sands directly above the palaeosol was dated to 12.64±1.21 ka. This date is based on the average dose rate calculated from NAA and gamma-spectrometry results and therefore considered to be more reliable than the other samples taken from the upper part of the section with dose rates based on NAA only. As shown in Fig. 76, the ages of samples F14-18 and F10 show a scatter, but still agree within errors. Thus an average age of 12.89±0.66 ka was calculated for this sand unit and would date the burial of the 'Finow soil' to the onset of the Younger Dryas (GS-1, 11.5-12.65 ka).

However, this observation is at odds with results from section 'Finow-B' a few metres away at the bottom of the dune, where aeolian deposition did not begin until the second half of the Younger Dryas. But again, within errors, both data sets agree. A re-measurement of sample F18 using small aliquots to test for incomplete bleaching of the OSL signals resulted in a slightly younger age than the large aliquots (1mm: 12.83±0.93 ka, 8mm: 13.43±0.98 ka). Therefore some of the samples may have been affected by minor poor bleaching causing a slight overestimation on average. On balance, however, the lowermost and the uppermost samples taken from this unit, F10 (12.64±1.21 ka) and F14 (12.08±0.88 ka), suggest that the burial of the 'Finow soil' most likely took place during the Younger Dryas.

Samples F14 and F13 encompass a charcoal bearing horizon which might represent a Preboreal soil development (SCHLAAK 1993). As shown in Fig. 76 the OSL age of sample F13 (11.96±0.87 ka) taken from above this horizon overestimates the calibrated ^{14}C age. But as both ages still agree within 2σ errors, the age of sample F13 can be accepted. With sample F12 the dune sands at the top of the section have been dated to 3.64±0.28 ka. This date coincides with the topmost sample of section 'Finow-B' F3 dated to 3.11±0.24 ka. It seems likely that the same aeolian accumulation event is represented; it was most likely induced by human activities. The similar state of soil development regarding the top soils at section both section supports this conclusion. On the other hand this would imply a substantial erosional gap, for there is no Mid-Holocene soil above the Preboreal horizon. That these 'missing' sediments are represented by the Mid-Holocene and Late Holocene deposits found at the bottom of the dune (Finow-B, samples F4-6) might be entertained.

4.3.3.2 Site 'Spechthausen' (S)

The dune site 'Spechthausen' is located some 3.6 km NE of site 'Finow' on the intermediate, 40 m 'urstromtal' level. The 'Finow soil' horizon is exposed within the 2.5 m section of aeolian sand (see Fig. 77). The palaeosol is covered by 1.2 m of aeolian sand in which a cambisol-podzol is developed. The ages of sample S4 (15.93±1.41 ka) and S3 (14.07±1.41 ka) agree within 2σ errors, thus a mean age of 15.00±1.32 ka was calculated for the lowermost part of the section. This age is in agreement with the expected pre-Allerød age (>GI-1a-c 13.90 ka) for the substrate of the 'Finow soil' and the expected maximum age of about 18 ka (see Table 11) for the underlying glaciofluvial sands of the 'urstromtal' terrace correlated to the Parstein stage. The aeolian sediments on top of the fossil soil horizon are dated to 12.88±0.37 ka representing the mean age of samples S2 and S1. Thus, burial is most likely coincident with the onset of the Younger Dryas (GS-1, 12.65-11.5 ka). This observation is compatible with the average OSL age of 12.89±0.66 ka for the dune sands on top of the 'Finow soil' at site 'Finow-C'.

Fig. 77: Schematic stratigraphic section of sampling site Spechthausen (S).
OSL samples are numbered from the top to the bottom with S1 → S4. Note, that sample S5 was taken from a dune sand unit a few metres away and is therefore not shown in the profile.
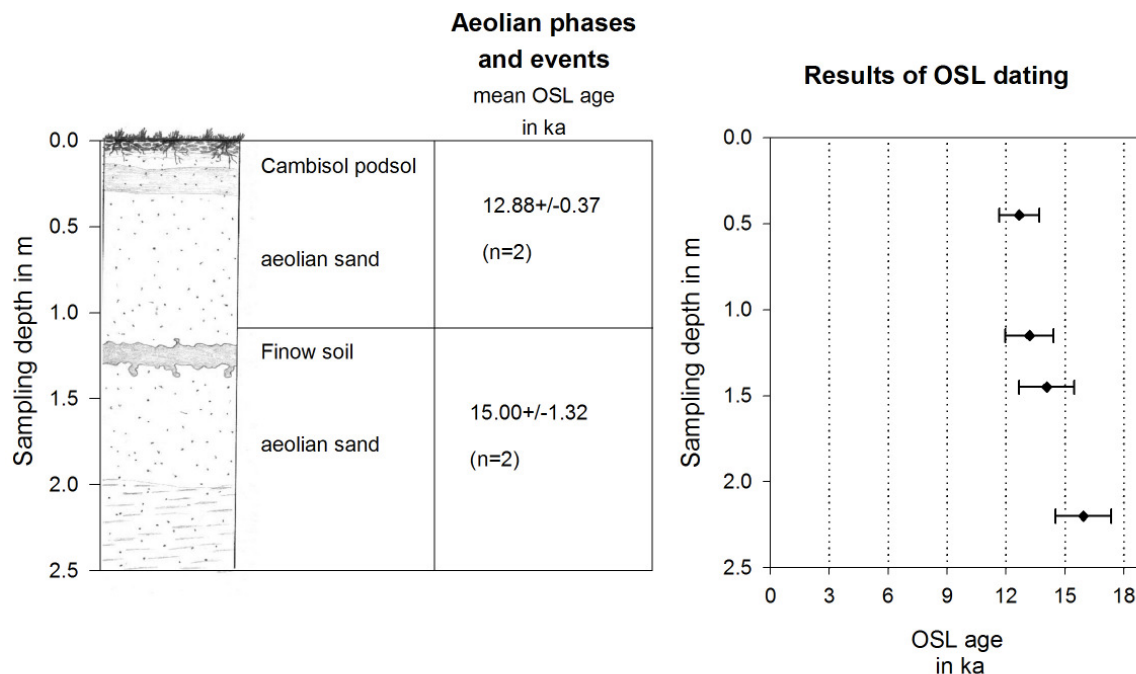
A fifth sample was taken just a few metres away from the trench 0.35 m below surface from the Ae horizon of a well-developed podsol, which was covered by a 10 to 15 cm thick aeolian sand layer. The OSL age of 3.36±0.30 ka indicates a Late Holocene remobilisation of aeolian processes. Whether bioturbation within the soil close to the surface may have caused this young age by intermixing of younger material from the surface into a layer of Lateglacial sands, might be resolved by a comparison of the single and multiple aliquot data sets. For mixed sediments a high scatter in the equivalent dose distribution would be likely to be observed in the SA data set, whereas the MA age would tend to yield an older age due to the dominance of the grain population of the originally deposited sediments. But here, the MAA and SAR ages obtained for sample S5 are in very good agreement with 3.84±0.35 and 3.36±0.18 ka (note, that only random errors are considered here). The multiple aliquot age has an extraordinarily small error of only 9 % compared to the error of other MA results obtained for samples from the same area exceeding in general 15 %, and the SAR palaeodose distribution shows little scatter with 6 % relative standard deviation. Both observations support the assumption that sample S5 represents an aeolian phase during the Late Holocene. Age underestimation caused by bioturbation seems unlikely. The Late Holocene dune reactivation recorded at site 'Spechthausen' at 3.36±0.30 ka coincides with the ages obtained for the uppermost samples at site 'Finow-B' and 'Finow-C' of 3.12±0.31 ka (F3) and 3.64±0.28 ka (F12). Rather than all three samples being affected by bioturbation and despite all giving similar results, it seems much more likely that they indeed represent one major phase of dune reactivation in the area. This is most probably related to increased human activities in the region during the Late Bronze Age and Iron Age.

4.3.3.3 Site 'Melchow' (M)

The dune site 'Melchow' is located on the highest 'urstromtal' level of about 45 m a.s.l.. The upper age limit for dune formation is provided by the terrace deposits correlated with the Pomeranian Advance at about 17.7-18.8 ka cal. BP (see Table 10). The sampling site was at the northern tail of an isolated parabolic dune. Only the upper two metres of dune sediments were exposed in the trench with the 'Finow' palaeosol located about 1.5 m below the surface (Fig. 78). The OSL age of 16.52±1.48 ka (sample M4) obtained for the substrate of the 'Finow soil' is in agreement with the expected age of >13.9 ka (pre-Allerød, GI-1a-c) and <17.7-18.7 cal. ka BP (younger than the underlying terrace deposits). The sediments represented by sample M4 presumably indicate a dune formed under cold, stadial conditions

during the Oldest Dryas (GS-2a, 14.7-16.9 ka). The 'Finow soil' was in turn buried during aeolian processes in the Younger Dryas period when the depletion of the vegetation cover with the onset of harsher climatic conditions, gave rise to dune reactivation. This is surmised from the mean OSL age of 12.65±0.85 ka obtained for samples M3 and 2 taken from the aeolian sand unit on top of this fossil horizon. The youngest reactivation of aeolian processes, which is indicated by the sand layer covering the humic horizon, was dated to the Medieval ages at about 1140 AD (0.86±0.09 ka sample M1). A correlation of this dune reactivation to the increased human impact during the Younger Slavonic period in the 11th to 13th century seems likely, as this phase was characterised by clearing of forested areas for the expansion of arable fields (LUTZE 1995).

Fig. 78: Schematic stratigraphic section of sampling site Melchow (M).
OSL samples are numbered from the top to the bottom with M1 → M4.
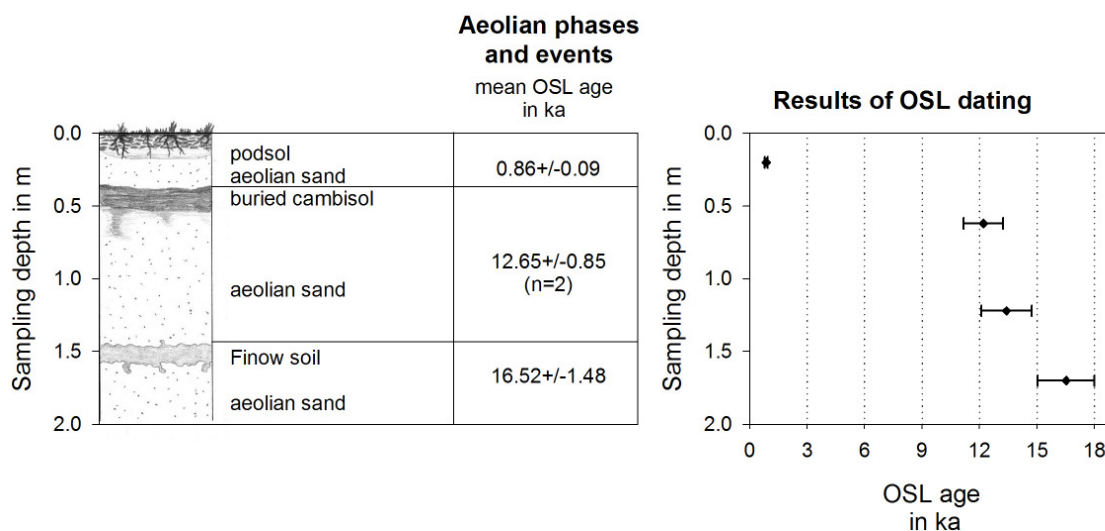
4.3.3.4 Site 'Rosenberg' (R)

The dune site 'Rosenberg' is located on the highest 'urstromtal' terrace within a parabolic dune field (see Fig. 72), which is characterised by a chaotic, active, hummocky relief. In contrast to the more gently rolling dunes on the next lower terrace level here steep dune slopes are dominant. The dunes attain heights of 22 m. Deflation depressions, some 10 m deep, are eroded into the terrace level (SCHLAAK 1998). The sediment sequence exposed at site 'Rosenberg' is illustrated in Fig. 79. Only the lower two metres of the section in which the 'Finow soil' is exposed have been sampled for OSL dating.

Fig. 79: Schematic stratigraphic section of sampling site Rosenberg (R).
OSL samples are numbered from the top to the bottom with R1 → R7.
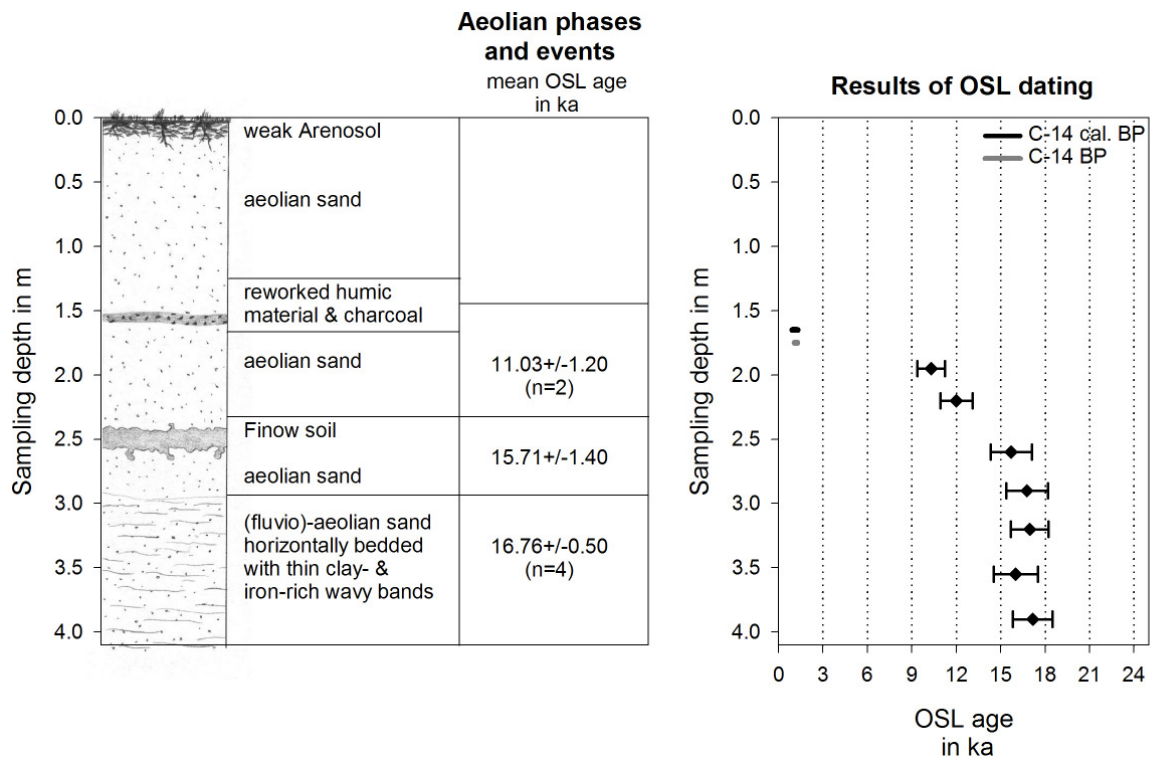
The base of section 'Rosenberg' is formed by a sand unit presumably of fluvio-aeolian origin, i.e. aeolian deposits that were reworked by fluvial processes (e.g. KASSE 1995). The observed significant overestimation of the multiple aliquot ages obtained for sample R5 of 50±10 ka could result from incorporation of older material during fluvial reworking (compared results in Appendix B).

On average the lowermost sand unit was dated to 16.76±0.50 ka (samples R4-7). This age is in good agreement with the upper age limit provided by the stratigraphic position of the site on the highest 'urstromtal' level. This terrace is correlated to the drainage of the Pomeranian Advance, which so far is dated to about 17.7-18.7 ka cal. BP (see Table 11).

The accordance of the OSL ages obtained for the lowermost aeolian deposits at sites 'Finow-C' (14.91±0.74 ka) and 'Spechthausen' (15.00±1.32 ka), on the one hand, and at 'Melchow' (16.52±1.48 ka) and 'Rosenberg' (16.76±0.50 ka), on the other, appears to sustain SCHLAAK's (1993) suggestion. From this observation it might be concluded that aeolian deposits were preserved already during the early Oldest Dryas (GS-2a 14.7-16.9 ka) on the highest 'urstromtal' level, while the preservation conditions on the lower level were restricted until the late Oldest Dryas. The highest dunes are found on the highest and oldest 'urstromtal' level

at the southern edge of the 'Eberswalde' ice marginal valley. On the lower level isolated dunes with much lower heights are dominant. SCHLAAK (1993) explains this with the variation in ground-water level throughout the Lateglacial period. High stands of ground-water restricted aeolian deflation on the lower levels whereas dune formation on the drier upper terrace already commenced.

The aeolian sand unit sample R3 yielded an OSL age of 15.71±1.40 ka. This aeolian sand served as substrate for the 'Finow soil' formation. The expected pre-Allerød age is confirmed by sample R3.

The 'Finow soil' is buried by 0.9 m of dune sand from which samples R1 and R2 were taken. Sample R1 dated to 10.30±0.94 ka yields a considerably younger age compared to R2 with 12.00±1.09 ka. But as both dates still agree within errors they have been averaged and date the burial of the 'Finow soil' at 11.03±1.20 ka, presumably marking the transition from the Younger Dryas to the Preboreal.

At section 'Rosenberg' the Younger Dryas dune sands have been partly eroded, most probably by the aeolian event that resulted in the deposition of the layer of reworked humic material and the top sand unit. The charcoal-bearing layer of dark brown sand above sample R1, which in turn is overlain by about 1.5 m of sand, was dated by radiocarbon to 1180±80 BP (770-960 cal. AD, SCHLAAK 1993, see Appendix E, Tab. E.2). The weak soil development at the surface supports the young age of its substrate. This massive remobilisation of dune sand in Medieval times is correlated to the early Slavonic colonisation, when new settlements in the region were established and forests were fired to establish arable land (SCHLAAK 1993, LUTZE 1995).

4.3.3.5 Site 'Schorfheide A' (SHA)

The 'Schorfheide' area is located at the northern edge of the 'Eberswalde urstromtal' and represents a proglacial outwash plain (sandur) related of the Pomeranian end moraine (see Fig. 72). Large areas of the outwash plain are covered with coversands and dune fields, where the parabolic dunes stand up to 18 m high (SCHLAAK 1998, GÄRTNER in GÄRTNER et al. 1995).

Two dune sites have been investigated here, 'Schorfheide A' (SHA) and 'Schorfheide B' (SHB) about 1.7 km further to the northeast.

Fig. 80: Schematic stratigraphic section of sampling site 'Schorfheide-A' (SHA).
OSL samples are numbered from the top to the bottom with SHA1 → SHA6.
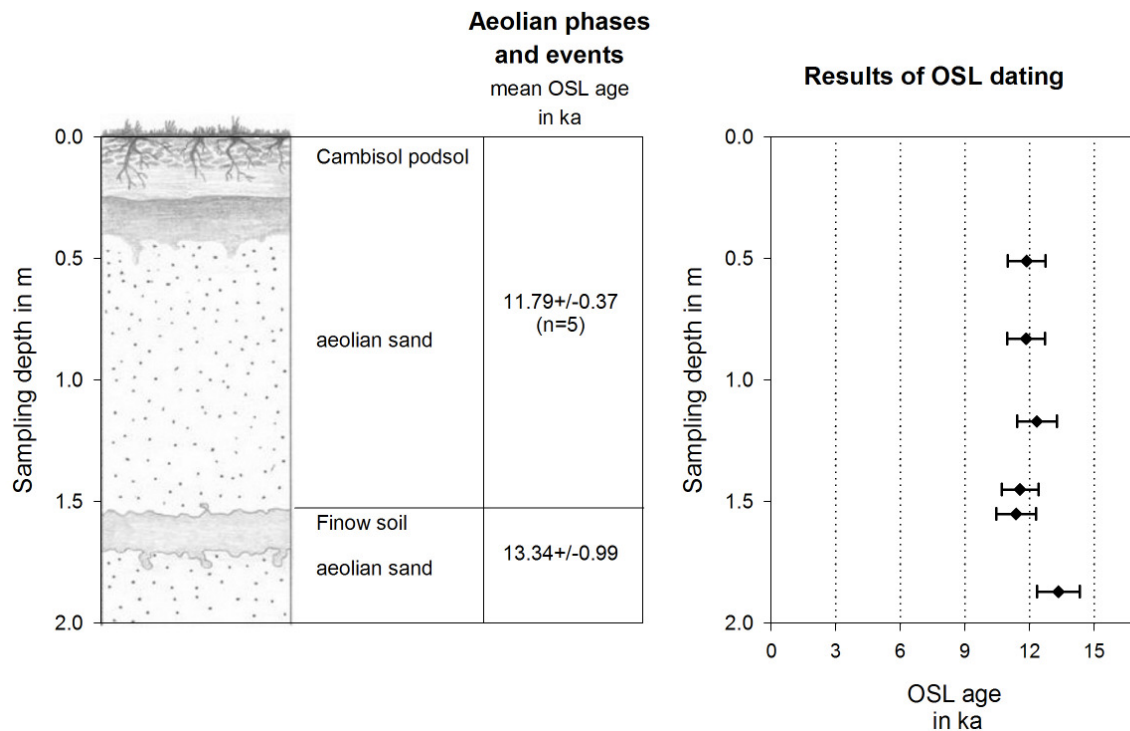
The sequence of 'Schorfheide-A' consists of about 2 m of aeolian sand with the 'Finow' palaeosol exposed between 1.55 to 1.65-1.70 m below surface. Six samples were taken from this trench. The upper age limit for the aeolian sediments exposed at site SHA is provided by the ages of the underlying glaciofluvial sandur deposits. These are correlated to the Pomeranian Advance, which is dated by ^{14}C to about 17.7-18.7 ka cal. BP (see Table 11).

In good agreement with this upper age limit the lowermost sample SHA 6 dates the aeolian sand deposits below the 'Finow soil' to 13.34±0.99 ka. Within errors, this OSL age indicates aeolian deposition at the transition from the Older Dryas (GI-1d, 13.90-14.05 ka) to the Allerød (GI-1a-c, 12.65-13.90 ka). A similar age was expected for sample SHA 5, which was taken from the upper part of the palaeosol horizon. The time span ascribed to the 'Finow soil' development comprises the Allerød with more favourable climatic conditions and the early Younger Dryas (SCHLAAK 1993, 1998, see section 4.2). But with only 11.04±0.81 ka the OSL age of sample SHA 5 seemed to underestimate the expected pre-Allerød age for the substrate of the soil development. As shown in Appendix F, the palaeodose value for sample SHA 5 agrees with that of the much older sample SHA 6 taken from below. In contrast, the dose rate value obtained for sample SHA 5 is the highest throughout the whole sample set. To check

whether an erroneous dose rate determination is the cause for the unexpected young age, the radionuclide analysis was repeated by using high-resolution gamma-ray spectrometry. The analytical results differ significantly (Appendix F). But the fact that all three radionuclide concentrations measured by NAA deviate from the γ-spectrometry results points towards analytical difficulties, rather than giving evidence for the occurrence of radionuclide disequilibria. However, as the final dose rates as well as the ages based on NAA or γ-spectrometry results agree within errors, the mean age of 11.37±0.93 ka was used for further interpretation of the aeolian record. Finally, the most likely explanation for the unexpected young age of sample SHA 5 is a syn-sedimentary development of the 'Finow soil'. The diffuse upper boundary of the palaeosol horizon as found at site SHA is a common feature of the 'Finow' horizon and generally described as being the result of syn-sedimentary soil formation (e.g. SCHLAAK 1993).

As shown in Fig. 80 the OSL ages of samples SHA 1 to 5 all agree within errors and are therefore considered to represent one phase of major aeolian activity with a mean age of about 11.79±0.37 ka. This age coincides with the second half of the Younger Dryas (GS-1, 11.50-12.65 ka) which is often described as the drier part characterised by an open vegetation cover (e.g. ISARIN et al. 1997, RENSSEN 1997, DE KLERK et al. 2001). From the well-developed topsoil it can be concluded that aeolian activity at this site ended in fact with the reafforestation at the beginning of the Holocene. Remobilisation of aeolian activity did not occur during the Holocene at this site.

4.3.3.6 Site 'Schorfheide B' (SHB)

At site 'Schorfheide B' a section of about 2 m was excavated. The basal parts of the sediment sequence consist of glaciofluvial sands of the 'Schorfheide' sandur which are overlain by aeolian sand in which the 'Finow' palaeosol is developed. The horizon is about 13 cm thick and buried by about 1.20 m of aeolian sand. At the bottom of the palaeosol horizon a layer of charcoal is exposed, which yielded a ^{14}C age of 10,390±315 ka BP (12,099±918 cal. BP, SCHLAAK 1998, see Appendix E).

Fig. 81: Schematic stratigraphic section of sampling site Schorfheide-B (SHB).
OSL samples are numbered from the top to the bottom with SHB1 → SHB5. Samples SHB 2 and 4
are considered to be unreliable (see discussion in the text).
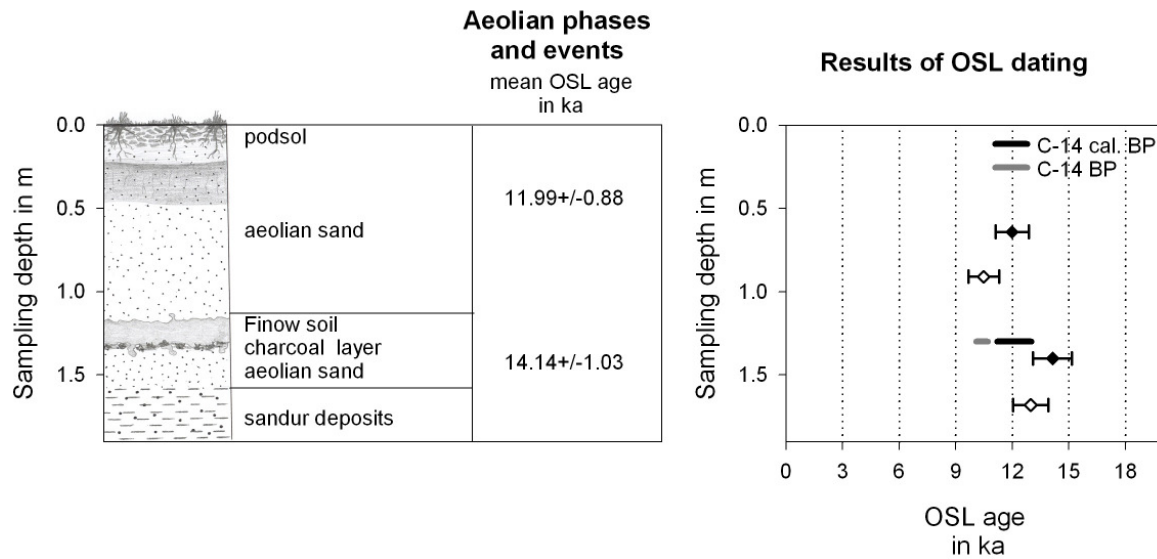
Four samples, two above and two below the palaeosol horizon, have been taken for OSL
dating. In the upper part of the section samples SHB 1 and 2 showed an inversion in ages with
SHB 2 being significantly younger than SHB 1 (12.00±0.46 vs. 10.49±0.43 ka for SHB 1 and
2, respectively). To check whether this discrepancy was caused by analytical problems related
to the neutron activation analysis, NAA measurements were repeated for sample SHB 2. The
radionuclide concentration for U, Th and K determined in the second analysis all agreed
within errors with the results of the first one. The dose rate values are therefore considered to
be reliable. The age inversion could be due to an erroneous D_e value as a marked difference is
observed between the values obtained for both of the samples. Because of the large number of
grains per aliquot (>1000) a detailed investigation of the equivalent dose distribution is
impossible. The original data sets of both samples showed outliers towards the high dose
region. But any grain population with D_e values below the average very likely remains
undetected because of the dominant luminescence output from older grains with higher
absorbed doses. Thus, post-sedimentary mixing of sediments of different ages is hardly
detectable by using the large, 8mm aliquot size consisting of >100 grains. To clarify the
reason of this age inversion, single grain measurements ought to be carried out so as to
identify possible younger grain populations. At present, the age of sample SHB 2 is
considered to be unreliable and is therefore excluded from further interpretations for three
listed reasons:

1. Deep root tubes were visible in particular next to the sampling position of sample SHB 2 reaching down to the palaeosol horizon. Material from close to the surface may have been mixed by bioturbation with older deposits sampled by SHB 2, causing an overall underestimation.

2. The age of sample SHB 1 as well as its palaeodose value is comparable with the results obtained at site SHA for the sediments in a similar stratigraphic position. The age of 11.99±0.88 ka of SHB 1 coincides well with the period of the Younger Dryas known to be a phase of enhanced aeolian activity, whereas the age of SHB 2 with 10.48±0.81 ka would date the aeolian deposition well into the Preboreal characterised by closed forests making aeolian activity less likely.

3. The age of sample SHB1 shows a better agreement with the ^{14}C age obtained for the charcoal layer below (12.10±0.92 ka cal. BP). The age of SHB2 does not contradict this ^{14}C age, but the discrepancy in age is difficult to explain.

The substrate for the development of this palaeosol is dated to about 14.14±1.03 ka. This age is in good agreement with the expected age of <17.7-18.7 ka cal BP (expected age of the underlying glaciofluvial deposits of the sandur, see Table 11) and >13.90 ka (onset of the Allerød chronozone assumed to be the period of aeolian quiescence and soil development). Furthermore, the OSL age of SHB3 is in good agreement with the ^{14}C age of the charcoal layer exposed in the overlying sediments (see Fig. 81).

With only 12.97±0.94 ka the expected age of the sandur deposits of about 17.7-18.7 ka cal. BP (see Table 11) was clearly underestimated by sample SHB 4. No explanation can be given so far and further analysis, e.g. a check for the occurrence of disequilibrium, ought to be carried out to clarify the reasons. A later reworking of the glaciofluvial deposits by aeolian processes cannot be excluded. Grain size analysis ought to be carried out further to investigate this possibility. At this stage of the study, the age of sample SHB 4 was considered to be unreliable and is excluded from further interpretations.

4.3.4 Dune sites in the 'Ueckermünder Heide' basin

In the Late Pleniglacial the 'Ueckermünder Heide' (study area 9 in Fig. 57) was part of the so-called 'Haffstausee', a large ice-dammed glacial lake (KEILHACK 1898, BRAMER 1964 in KÜHN 2003). Within this basin glaciofluvial and glaciolacustrine sands have been deposited. After desiccation they served as a sand source for the formation of aeolian sand sheets and dune fields (BRAMER 1964, Fig. 82). Unfortunately the exact timing and extent of the ice-dammed lake are not closely determined.

Fig. 82: Morphological map of the study area 'Ueckermünder Heide' showing the location of the sampling sites 'Ueckermünde A, B, C, and D' (UMA, UMB, UMC, UMD, summarised in Fig. 57 as dune sites 9).
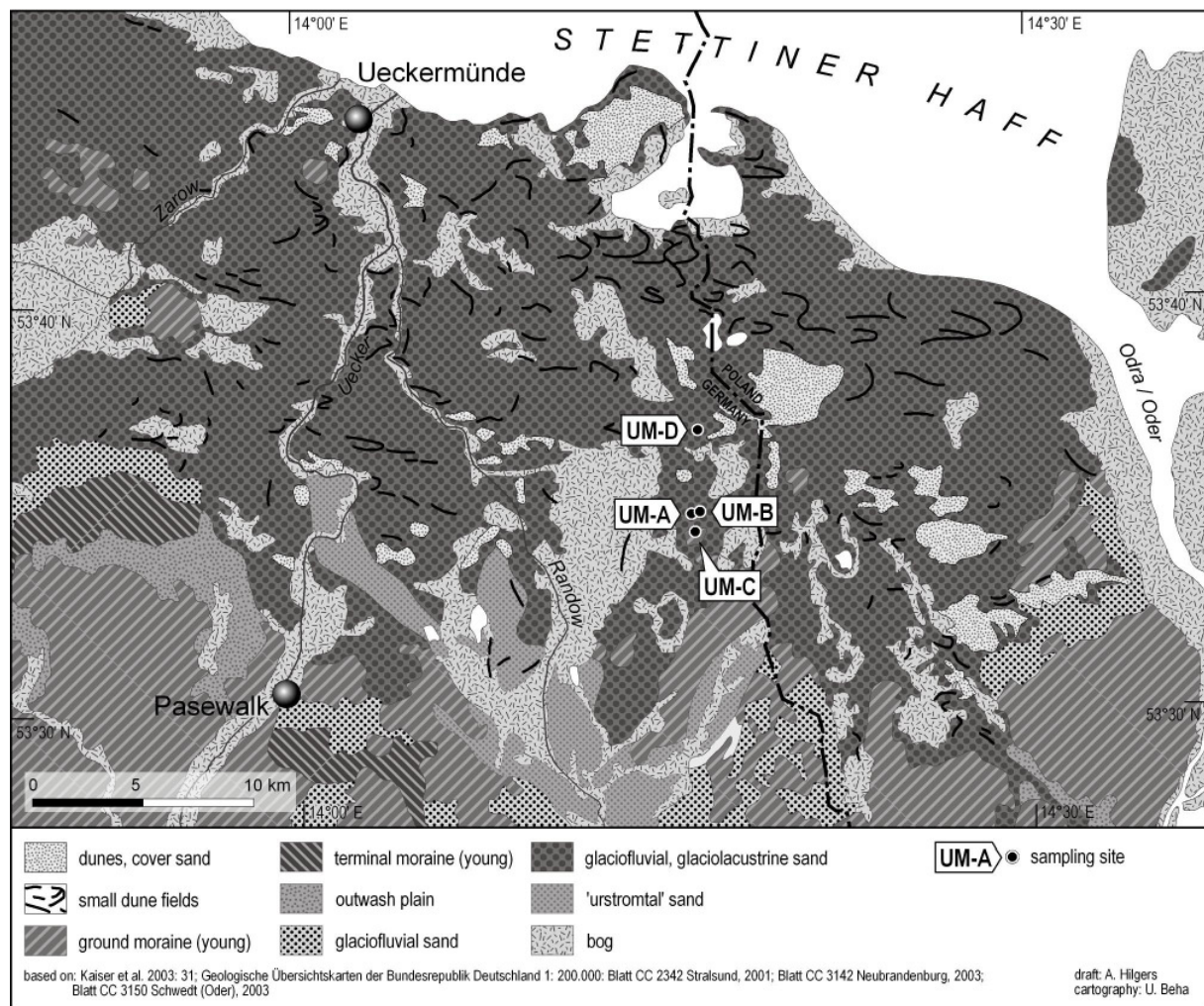
The presence of numerous Late Palaeolithic and Mesolithic sites in the area of the 'Ueckermünder Heide' demonstrate how attractive was this palaeolandscape of lakes, rivers, bogs and dunes for prehistoric man living from hunting, gathering and fishing (BOGEN et al. 2003, KAISER 2004, TERBERGER 2004). At dune sites UM-A and UM-D a geoarchaeological investigation was carried out after the discovery of Late Palaeolithic artefacts (see BOGEN et al. 2003 for a summary of the results). The OSL dates contribute further geochronological control for the burial of the artefact layers. But in the context of the present study these dune sites were particularly interesting as in both dune sections the 'Finow soil' was identified (KAISER and KÜHN 1999). This observation allows a correlation to other study areas further south and the exact timing of the soil development at this northernmost location of this palaeosol horizon and the subsequent onset of dune formation can be clarified by OSL dating.

BRAMER (1964, 1975) dated peat layers covered with fluvial sand into the Allerød chronozone by palynological studies, supported by radiocarbon ages of 11,397±120 and 11,839±200 ka BP (BRAMER 1975 in KAISER 2001). Based on these findings he identified a reactivation of the 'Haffstausee' in the transition period from the Late Allerød and in the Younger Dryas, and dated the major dune formation period to the Preboreal. But the evidence of a Lateglacial terrestrial palaeosol covered with aeolian sands (KAISER & KÜHN 1999) contradicts BRAMER's (1964) assumption of a reactivation of the ice-dammed lake ('Haffstausee') during the Younger Dryas. Therefore, the key question at sites 'Ueckermünde-A and D' was to date the aeolian burial of the terrestrial palaeosol. If a Younger Dryas age could be proved, as might be assumed from the underlying presumably Allerød 'Finow soil', terrestrial conditions at least in some areas must have prevailed during the Younger Dryas.

Sampling for OSL dating of the glaciofluvial-glaciolacustrine sediments at sites 'UM-A and -D' was carried out to test the applicability of luminescence dating to this kind of deposit. If successful, the dates could yield a valuable contribution to the Late Pleniglacial-Lateglacial chronostratigraphy of the study area, as the timing of the glacial lake phase is still poorly dated. Furthermore, with the dating of the termination of glaciolacustrine sedimentation the upper age limit for the onset of terrestrial conditions and thus for soil formation and aeolian processes is set.

A relative age estimate for the glacial lake phase so far is only inferred from its situation. The till plains and end moraine ridges (Rosenthal end moraine) forming the south-western and southern border of the 'Haffstausee' relate to the Mecklenburg Advance (see Fig. 82). The

absolute upper age limit, thus, would be the coverage with the inland ice glacier in the Late Pleniglacial and the beginning of the remelting phase of the Mecklenburg stage. The age of the Mecklenburg Advance is not very well-known. In Table 10 various age estimates are summarised and most probably the Mecklenburg Advance dates to between 16.6-17.9 ka cal. BP. According to GÖRSDORF and KAISER (2001) NE Germany was deglaciated after the retreat of the Mecklenburg ice-sheet around 14 ka ^{14}C BP based on a detailed analysis of radiocarbon data from the Pomeranian Bay. The data set shows that at about 14 ka ^{14}C BP the Pomeranian Bay was ice free again (calibrated to 16,793 BP, GÖRSDORF and KAISER 2001). Therefore, the age of about 16.8 ka cal. BP can be considered as a minimum age for the drainage of the glacial lake. To conclude, deposition of the glaciolacustrine sediments of the ice-dammed lake most probably occurred between 16.8 and 17.9 ka cal. BP.

4.3.4.1 Site 'Ueckermünde-A' (UMA)

Detailed descriptions of the pedological, sedimentological and archaeological investigations carried out at site UM-A are presented in BOGEN et al. (2003) and KÜHN (2003) including also some of the OSL dates discussed in the following (note that both studies refer to the site as 'Mützelburg Forst 9'). Six OSL samples were taken from the about 1.35 m of dune sand overlying the 10-15 cm thick 'Finow soil' horizon. From the glaciofluvial-glaciolacustrine sand serving as substrate for the soil formation a further five samples were taken (see Fig. 83).

Regarding the mean age calculated from samples UM1 to UM6 the burial of the palaeosol by dune sands is dated to 12.27±0.61 ka, that is, in the first part of the Younger Dryas (GS-1, 11.50-12.65 ka). Hence a correlation of the fossil B horizon with the 'Finow soil' can be supported (KAISER & KÜHN 1999, KÜHN 2003), as this soil formation is commonly assigned to the Allerød and Early Younger Dryas (SCHLAAK 1998). Archaeological findings in the upper part of the fossil soil horizon are interpreted as Ahrensburgian (BOGEN et al. 2003). The Ahrensburgian period in Central Europe and southern Scandinavia is predominantly correlated with the Younger Dryas, but the onset is recorded already during the Late Allerød and the period lasted some time into the Preboreal (TAUTE 1968, CLAUSEN 1995, KAISER & TERBERGER 1996, all cit. in BOGEN et al. 2003). It is concluded that, within errors, there is a good agreement of the OSL ages with the age estimates provided by the archaeological record and the palaeopedological interpretation. The onset of dune formation dates back to the Younger Dryas which contradicts the suggestion by BRAMER (1964) who dated the major

period of dune-building into the Preboreal. The postulated reactivation of the 'Haffstausee' during the Younger Dryas seems most unlikely.

Fig. 83: Schematic stratigraphic section of sampling site Ueckermünde-A (UMA).
OSL samples are numbered from the top to the bottom with UM1 → UM11. Because the equivalent dose measurements yielded evidence for poor bleaching of the glaciolacustrine deposits at the bottom of the section, the OSL ages of samples UM9-11 are regarded as maximum ages only.
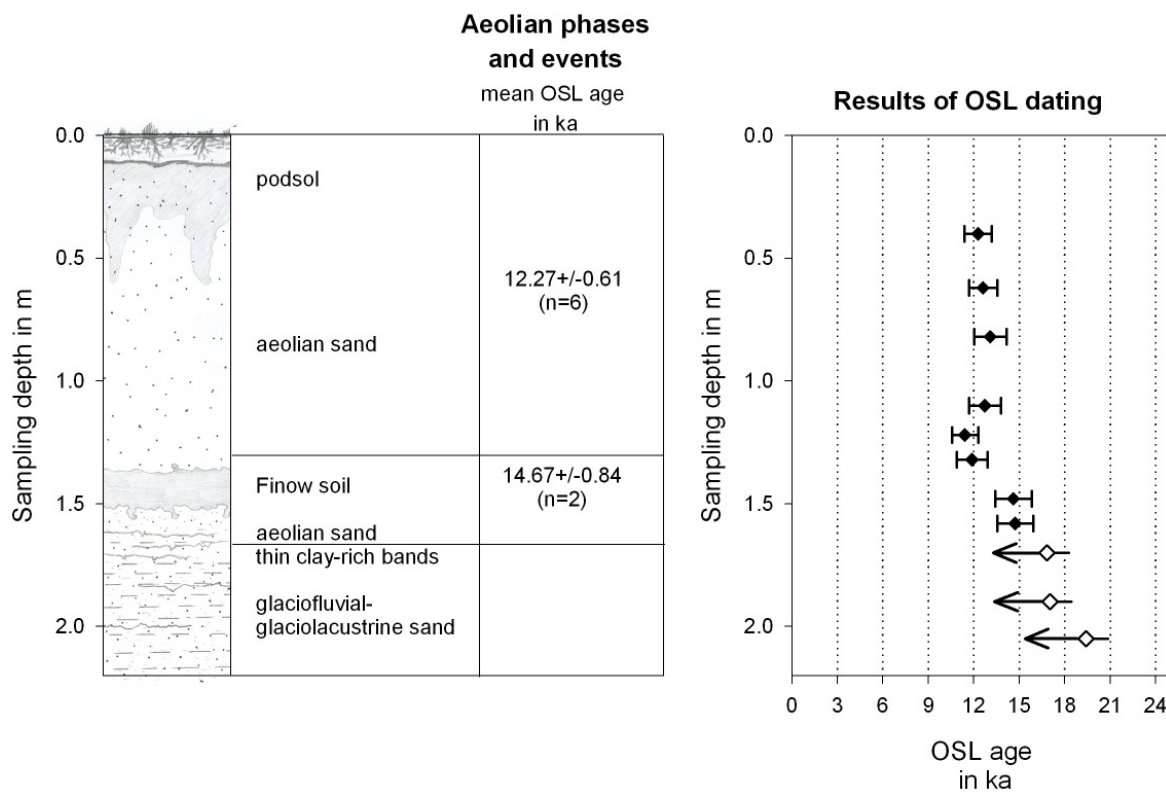
Samples UM7 and UM8 were taken from within and below the 'Finow soil' horizon. They yielded very similar ages of 14.61±1.22 ka and 14.72±1.17 ka. In contrast to the equivalent dose distributions obtained for the underlying samples UM9-11, samples UM7 and UM8 yielded much tighter distributions similar to the dune sands sampled with UM1-6. Some of the medium and coarse gravels that were found in the fossil soil horizon showed a ventifact shape (BOGEN et al. 2003). Both observations point towards aeolian processes being involved, which might also have caused aeolian reworking of the upper layers of glaciofluvial-glaciolacustrine sands resulting in the sediments represented by samples UM7 and UM8. The average age of 14.67±0.84 ka would date the deposition to the transition Oldest Dryas-Meiendorf/Bølling (GS-2a to GI-1e) at about 14.7 ka. This result is in good agreement with the dating of the 'Finow soil' formation during the Allerød starting at about 13.9 ka (GI-1a-c).

Dating of the glaciofluvial-glaciolacustrine sediments at the bottom of the section (samples UM9-11) proved to be difficult. As is discussed in more detail in Appendix D, the equivalent dose distributions of samples UM10 and 11 showed a broad scatter with a tail towards high dose values. Poor bleaching due to the mode of transport and deposition of these sediments is the most likely cause for the data spread. This assumption was further indicated by the results of D_e measurements on small aliquots containing only several tens of quartz grains. The resulting OSL ages of 16.85±1.42 ka (UM9), 17.02±1.39 ka (UM10) and 19.42±1.41 ka (UM11) therefore are considered as maximum ages only. However, at least the ages of samples UM9 and UM10 agree with the expected age range of 16.8-17.9 ka for the time of the glacial lake phase. Further investigations ought to be carried out, including equivalent dose measurements on single grains, to optimise the resolution in the low dose range of the equivalent dose distribution and to investigate the impact of poor bleaching. However, the results of UM9 and 10 are promising as they show the potential of OSL dating for getting an upper age limit of the glacial lake phase in the study area.

4.3.4.2 Site 'Ueckermünde-D' (UMD)

The sampling site 'Ueckermünde-D' is located about 3.4 km north of 'Ueckermünde-A', and lower within the 'Haffstausee' basin. This site has been investigated in detail since it was discovered to be a Late Palaeolithic flint knapping area (site 'Hintersee', see BOGEN 1999, KAISER & KÜHN 1999, KAISER et al. 2001, BOGEN et al. 2003 for summary of the observations regarding archaeology, sedimentology, and pedology).

The sediment sequence is similar to the one found at site UM-A with glaciofluvial/glaciolacustrine sands found in the lower part (OSL samples UM 27 to UM23) in which a B-horizon of about 10 cm thickness, the 'Finow soil', is developed and covered by dune sand (KAISER & KÜHN 1999). The topsoil has been disturbed and partly removed by ploughing (see Fig. 84), so that the upper 15-20 cm are missing.

Fig. 84: Schematic stratigraphic section of sampling site Ueckermünde-D (UMD).
OSL samples are numbered from the top to the bottom with UM20 → UM27. Because the equivalent dose measurements yielded evidence for poor bleaching of the glaciolacustrine deposits at the bottom of the section, the OSL ages of samples UM23-27 are regarded as maximum ages only.
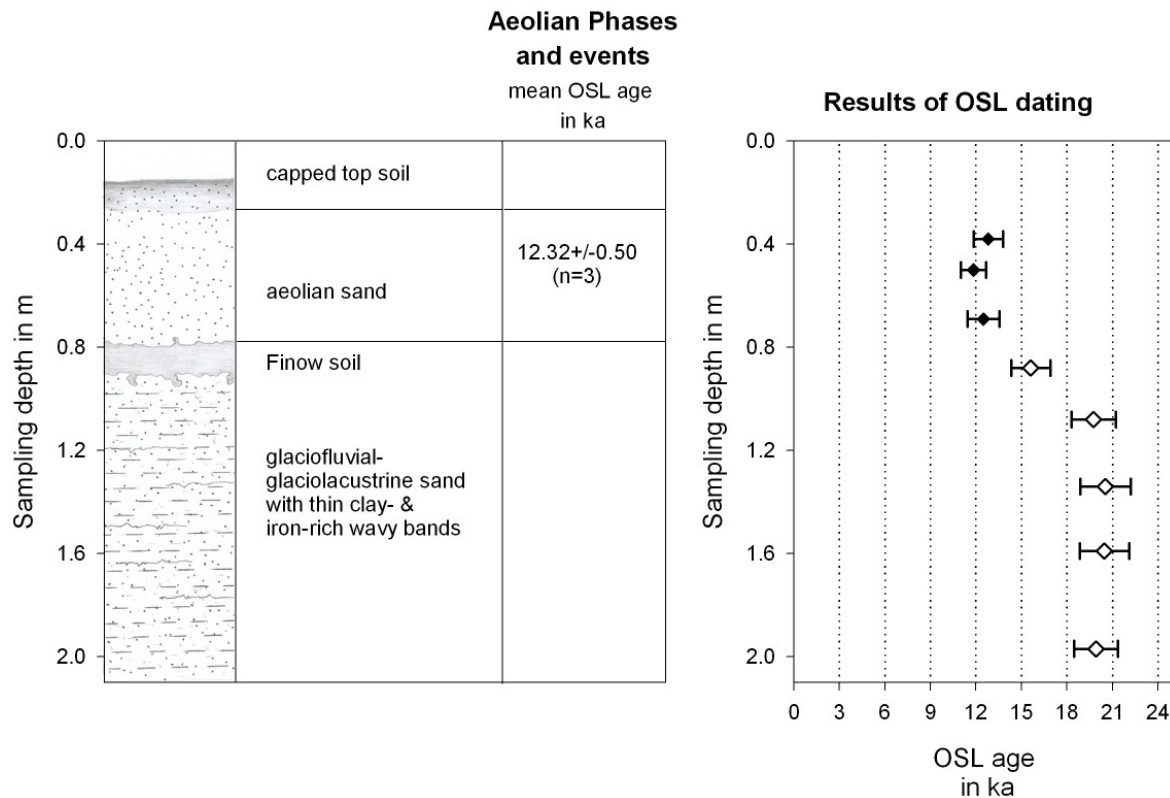
The artefacts were embedded in the fossil soil horizon. Based on the typology of the flint tools this site can be dated to the Ahrensburgian complex (see BOGEN et al. 2003 for discussion of the chronological uncertainty). The dune sands deposited above must be younger then the soil formation and the artefact deposition, with the latter dating from the period between the Allerød and the Preboreal, and most likely into the Younger Dryas. Hence, a Younger Dryas (GS-1, 11.5-12.65 ka) or even younger age can be deduced for the dune sand deposition based on the pedological and archaeological findings. The mean OSL age of 12.32±0.50 ka calculated from the aeolian sand samples UM20, 21, and 22 is in agreement with this anticipated age range (see Fig. 84). Furthermore, this age is consistent with the average OSL age of 12.27±0.61 ka that was obtained for the aeolian sand unit in the same stratigraphical situation at site UM-A. These results suggest a phase of increased aeolian activity and dune formation induced by the progressive deterioration of the climate during the Younger Dryas when the vegetation cover diminished and widespread sand deposits within the glaciolacustrine basin dried-out and were exposed to deflation processes.

Dating of the glaciofluvial-glaciolacustrine sands was as problematic as already explained for site UM-A. Poor bleaching is a major problem (see discussion in Appendix D). All ages are regarded as maximum ages, although with sample UM23 dated to 15.61±1.29 ka an age even younger than the expected age range of deposition of 16.8-17.9 ka was obtained. Moreover, the four lowermost samples UM24 to 27 all show maximum ages of about ±20 ka, which is similar to the lowermost sample at site UM-A (UM11 <19.42 ka). Based on the knowledge of the regional glacial chronostratigraphy at this time the 'Ueckermünder Heide' was still covered by the inland ice-sheet. Thus, these age estimates definitely overestimate the time of sedimentation of the glacial lake deposits. As at site UM-A, single grain studies are recommended to further improve the dating results for these poorly bleached deposits.

4.3.4.3 Site 'Ueckermünde-B' (UMB)

Site 'Ueckermünde-B' is located only about 250 m east of site UM-A. Three samples were taken for OSL dating from the 1.5 m deep trench. Within the sequence of aeolian sand a buried cambisol was exposed at about 0.5 m below surface. Samples UM13 and 14 taken from below the buried soil were dated to 9.24±0.64 ka and 15.44±1.15 ka, respectively. Sample UM12 dated the burial of the soil to 0.68±0.05 ka (see Fig. 85).

With an age of 15.44±1.15 ka, sample UM14 would indicate aeolian activity presumably already during the Oldest Dryas (GS-2a, 14.7-16.9 ka) and would agree within errors with OSL ages obtained for the substrate of the 'Finow soil' at site UMA of 14.67±0.84 ka and of <15.61 ka at UMD. The Early Boreal age of sample UM13 is difficult to explain, as a closed forest cover has to be assumed in the area based on palynological studies from archaeological sites in the vicinity (KAISER et al. 2001). On the other hand, the presence of Mesolithic people in the area, proved by several archaeological sites, might have resulted in some disturbance of the vegetation cover giving rise to minor, locally restricted, aeolian activity. No erosional gap could be identified between the sampling positions of UM13 and UM14 and the 'Finow soil' could be expected to be exposed, given the ages obtained for the samples from these sand layers. Nevertheless, until conclusive evidence is found to confirm the underestimation of sample UM13, it is considered to be reliable, though too much weight ought not be given it in any chronostratigraphic interpretation. The recent burial of the cambisol soil can be explained by reactivation of aeolian activity in Medieval times (OSL age UM12 0.68±0.05 ka) induced by extensive forest clearing. According to various studies GÄRTNER (1993) concludes that

150 to 600 years is the minimum time period sufficient for the development of podsolic soils. Thus, the OSL age seems reliable as the dating of the substrate deposition to about 700 years before present would result in sufficient time for the development of the podsol representing the topsoil at site UM-B.

Fig. 85: Schematic stratigraphic section of sampling site Ueckermünde-B (UMB).
OSL samples are numbered from the top to the bottom with UM12 → UM14.
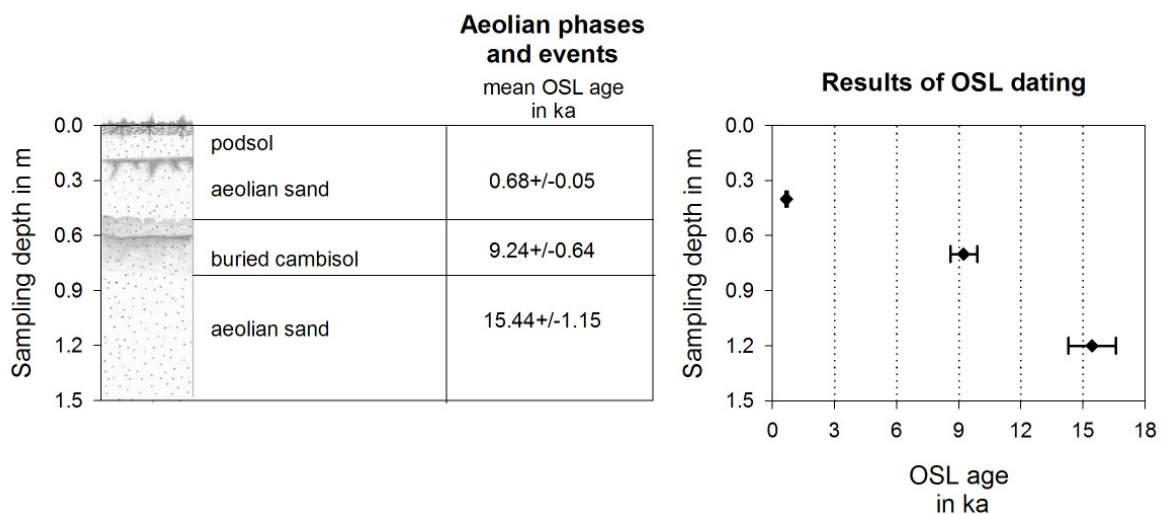
4.3.4.4 Site 'Ueckermünde-C' (UMC)

The site UM-C is situated about 1.7 km south of site UM-A where an island-like, hummocky till plateau forms a part of the ancient cliff of the former ice-dammed lake. This small patch of ground moraine could be correlated to the 'Mecklenburg Advance' (KÜHN 2003). The site sampled for OSL dating is located at the southeastern slope of the plateau, where the till is overlain by a sand sheet ('Decksand' according to the German typology, KÜHN 2003) which in turn is covered by aeolian sand (see Fig. 86). KÜHN (2003) has described this site in detail (therein referred to as site 'Len 4') with respect to the sedimentology and, in particular, pedology (including micromorphology). In summary, these results suggest that a soil ('Fahlerde') developed after deposition of the till by the Mecklenburg Advance and the formation of the 'Decksand'. The burial of this soil by aeolian sand dates into the Lateglacial. A cambisol finally developed and forms the topsoil. OSL dating of five samples, UM15-19, was carried out to provide chronological control for this hypothesis.

Fig. 86: Schematic stratigraphic section of sampling site Ueckermünde-C (UMC).
OSL samples are numbered from the top to the bottom with UM15 → UM19. The equivalent dose measurements of sample UM17 showed a substantial scatter in D_e values. Mixing of sediments of different ages cannot be excluded for sure; hence the age for UM17 was excluded from the data set.
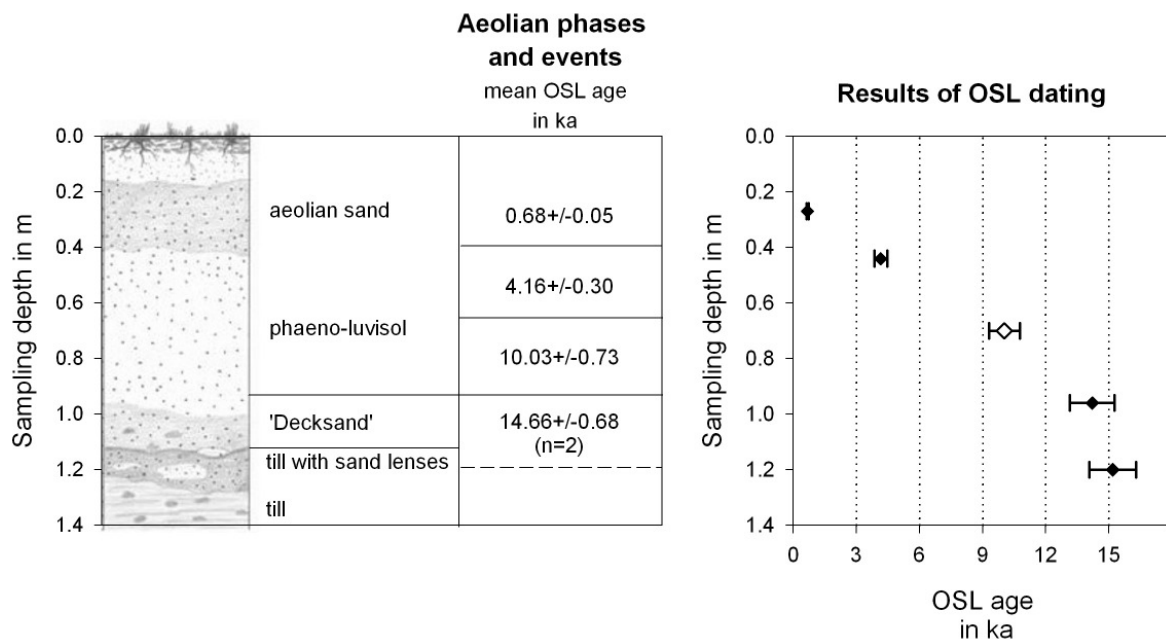
As shown in Fig. 86 all ages are in chronostratigraphic order, with the ages of the lowermost two samples giving the same age within errors. The samples were taken from different sedimentological units, the 'Decksand' (UM18) and the till (UM19). But it must be noted that UM19 was sampled from a large sand lens within the till matrix. Therefore, the OSL age of sample UM19 is not interpreted as age estimate for the till deposition, but is considered as being representative for the 'Decksand', thus should be equivalent to UM18. Periglacial conditions have to be assumed for the time after deposition and imply the presence of permafrost. Micromorphology (KÜHN 2003) suggests that the sandy deposits are intruded into the underlying loamy till deposits by geliturbate mixing. The difference in ages most probably results from a slightly underestimated dose rate for sample UM19. For dose rate determination the gamma dose rate resulting from the surrounding till has to be taken into account. This material is characterised by higher clay contents and, hence, higher radionuclide concentrations compared to the sandy material of the lenses sampled for neutron activation analysis only. But this uncertainty in dose rate estimation is regarded to have only minor influence on the finally resulting age of UM19, as it still agrees within errors with the age of UM18. On average the 'Decksand' layer is dated to 14.66±0.68 ka, the transition phase from the Oldest Dryas (GS-2a, 14.70-16.90 ka) to the Meiendorf/Bølling (GI-1e, 14.70-14.05 ka).

The development of 'Decksand' layers is still a matter of debate (see e.g. summary in KÜHN 2003, DE BOER 1995). Both samples, UM18 and 19, showed no clear evidence for poor bleaching. On the contrary, their equivalent dose distributions are similar to those obtained for aeolian deposits from the other sites in the area. This observation might support the assumption of a contribution of aeolian processes to the genesis of 'Decksand' layers as postulated for example by DÜCKER (1954) or FIEDLER et al. (1963) (both in DE BOER 1995).

Based on the presence of ventifacts in the 'Decksand' layer at a study site nearby KÜHN (2003) also concludes an aeolian influence for the formation of this layer. Finally, the coincidence of the average age obtained for UM18 and 19 of 14.66±0.68 ka with the mean age from UM7 and 8 at site UM-A of 14.67±0.84 ka might be just that and fortuitous, but nevertheless it is striking. At both sites aeolian processes somehow seem to be involved in the layer formation. Taking also the age into account that was obtained for the lowermost aeolian deposits at site UM-B of 15.44±1.15 ka (UM15), there might be evidence for widespread aeolian processes during the late Oldest Dryas (GS-2a, 14.70-16.90 ka). This phase of aeolian activity at the southern edge of the former glacial lake seems to be recorded at all three sites being located at slightly higher levels (UM-A, -B, and -C) when compared with site UM-D, which is located adjacent to low-lying peat bog areas. An earlier dry-out of the glaciofluvial-glaciolacustrine sediments at the higher position of sites UM-A and UM-B can be assumed in contrast to site UM-D, where aeolian deposition obviously did not commence before the Younger Dryas.

The interpretation of the three OSL ages obtained for the aeolian sand on top of the 'Decksand' at site 'UM-C' is problematic. The lowermost sample of this unit, UM17, was dated to 10.03±0.73 ka. A large data spread was observed in the equivalent dose distribution that has to be ascribed to bioturbation (see section 3.6.3.6 for discussion). However, further analysis of equivalent dose distributions providing a better resolution than the 8mm aliquots is necessary to clarify the source of scatter. This observation would further explain the underestimation of the expected Lateglacial age (KÜHN 2003).

Samples UM15 and 16 yielded much younger ages than the expected Lateglacial age with only 0.68±0.05 ka and 4.16±0.30 ka, respectively. As they were taken close to the surface from within the zone of recent root development, KÜHN (2003) attributes the underestimation to bioturbation. But some observations from the OSL data set contradict this conclusion. First, the original equivalent dose distributions for both samples showed a broad scatter. But none of the values lying outside the normally distributed data range would give an approximately

Lateglacial age. This would imply that the sediment would have had to be mixed up completely. With 1000 to 2000 grains per sub-sample used for palaeodose measurement, it is very likely to detect OSL signals from some grains that retain the original depositional palaeodose. A second argument against bioturbation causing such a substantial underestimation is based on the comparison to the uppermost samples from adjacent sites. The relative data spread observed in the initial equivalent dose distributions of samples UM1 (at 0.40 m depth) and UM20 (at 0.38 m depth) was similar to the relative spread found in UM15 (0.27 m) and UM16 (0.44 m). But both samples UM1 and UM20, although sampled from similar depth below surface, yield Younger Dryas ages in good accordance with the expected ages.

To conclude, bioturbation might have affected samples UM15 and UM16 to some extent. But it seems unlikely that this solely could explain the age underestimation compared to an expected Lateglacial age of >11.5 ka. Both ages are included in further interpretation of the aeolian record of the area. Aeolian activity at the nearby site UM-B was reliably dated to 0.68±0.05 ka. The OSL age obtained for the uppermost deposits at site UM-C yielded exactly the same age with 0.68±0.05 ka (UM15). This might be a coincidence, but nevertheless it could hint towards a more widespread reactivation of aeolian activity in the area during the Middle Ages.

4.3.5 Dune sites in the Altdarss area

The study area 'Altdarss' is located on the Fischland-Darss-Zingst barrier spit on the coast of the Baltic Sea north of the flat to slightly undulating till plains of the Weichselian Mecklenburg advance and end moraine ridges of the Velgast stage (see Fig. 87). Two sites 'Altdarss-1 and -4' have been investigated and sampled. A reconstruction of the Late Quaternary history of the study area has been summarised in a comprehensive study presented by KAISER (2001, see also KAISER et al. 2006).

In the Late Pleniglacial, the Altdarss area was part of a large glaciolacustrine basin (>700 km^2) which also included the Rostocker Heide and the Barther Heide, two basin-sand areas in the southwest and south. From the higher position of glaciolacustrine sediments compared to the surface level of the till plains, it can be deduced that the southern edge of the basin was

formed by unburied dead ice. Based on the knowledge of the regional landscape history, the deposition of the glaciolacustrine sediments up to 25 m thick in the huge ice-dammed lake is dated to about 14,000-13,000 yr BP (>15,200 cal. yr BP; KAISER 2001, GÖRSDORF & KAISER 2001). The duration of the lake phase is difficult to estimate and may span some hundreds of years at least, or a maximum of 1,000 to 2,000 years (KAISER 2001). Whatsoever, the lake phase was terminated and the terrestrial sedimentation commenced during the Oldest Dryas and Bølling according to palynological data (KAISER 2001). Under wet conditions caused by a high groundwater level, peat layers were formed in low-lying areas and soils in higher positions. The onset of widespread aeolian activity coincides with the falling groundwater table in the Younger Dryas (KAISER 2001, KAISER et al. 2006, LUDWIG 2002). At this time of the high-stand of the Baltic ice-dammed lake the study area was part of the mainland (LEMKE et al. 2002, Fig. 87).

Fig. 87: Morphological map of the study area 'Altdarss' with the sampling sites 'Altdarss-1' (AD1) and 'Altdarss-4' (AD4) (summarised in Fig. 57 as dune sites 10).
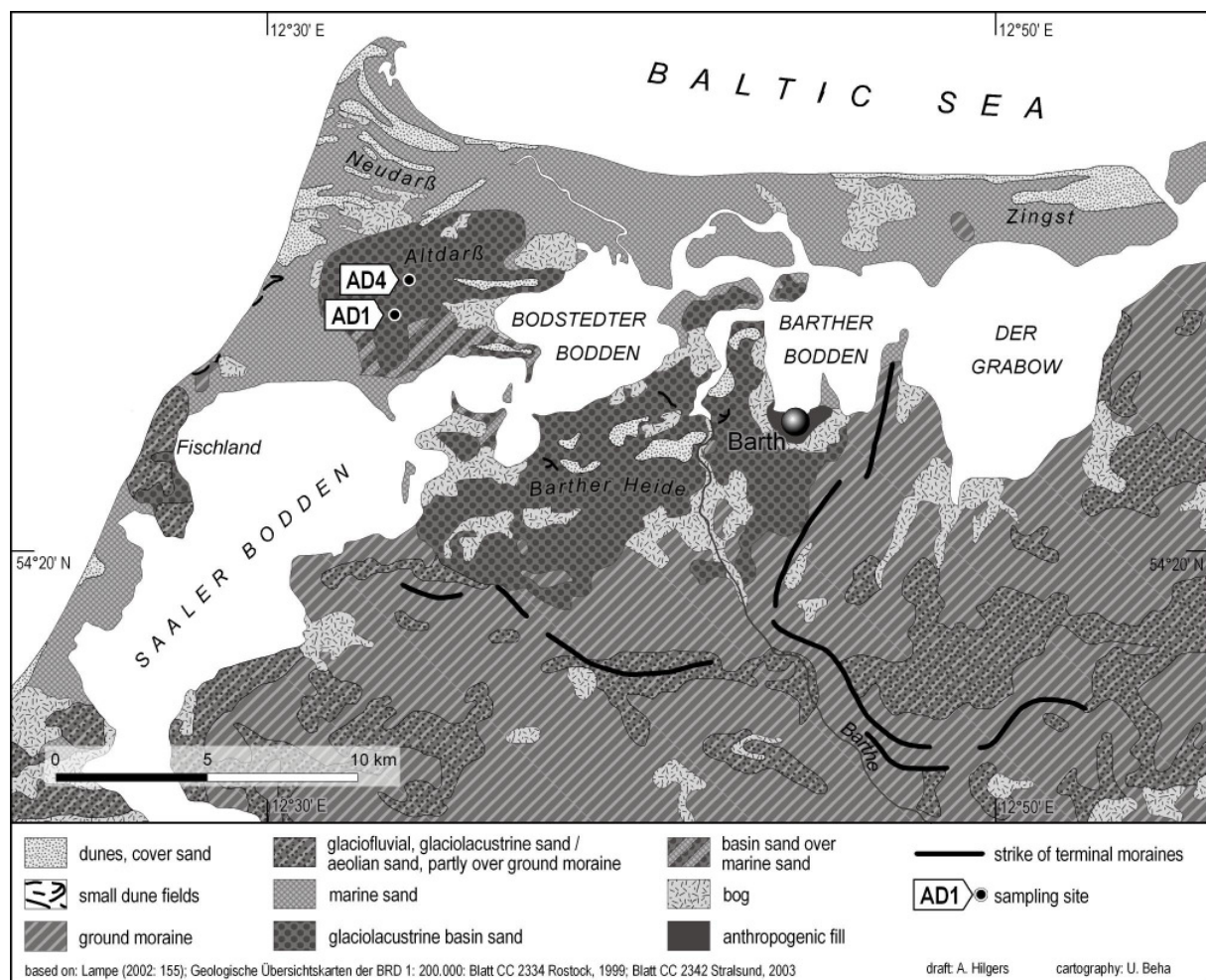
The fine- to medium-grained sands of the upper glaciolacustrine deposits provided the source material for the formation of 1-3 m thick aeolian sand sheets and low, (1-2 m high) parabolic and longitudinal dunes (KAISER et al. 2006, KAISER 2001). Aeolian processes continued until the surface was stabilised by reafforestation and soil formation following the amelioration of climatic conditions at the beginning of the Holocene. In the Subboreal and Subatlantic a significant rise in the ground-water level caused the formation of peat layers at low-lying sites. This ground-water rise was triggered by the Late Holocene transgression of the Baltic Sea (LAMPE 2005).

A detailed investigation of 42 profiles in the Altdarss area allowed KAISER et al. (2006) to reconstruct an extensive palaeosurface. All sections showed similar sediment sequences of a palaeosol developed on the glaciolacustrine sand and buried by aeolian sand layers of varying thickness. Two of the sites have been sampled for OSL dating. Note, that site AD-4 in this study represents study site ADO42 in KAISER et al. (2006) and site AD-1 correlates with their site ADO39.

4.3.5.1 Site 'Altdarss-4' (AD4)

Twelve samples were taken from the upper aeolian unit (Fig. 88). Sample AD4-1 from only 18 cm below the surface was dated to 3.35±0.23 ka. An age underestimation due to post-sedimentary mixing with surface material by bioturbation cannot be excluded completely. More detailed studies on the palaeodose distribution ought to be carried out further to investigate this possibility. So far these sediments also could be considered to represent a depositional event with only minor extent. That this reactivation is related to human impact is questionable, as for the onset of strong human impact on this landscape dates into the 13th-14th century (KAISER et al. 2006).

Fig. 88: Schematic stratigraphic section of sampling site Altdarss-4 (AD-4).
OSL samples are numbered from the top to the bottom with AD4-1 → AD4-14. Samples AD4-13 and
-14 most likely give minimum ages only due to problems in dose rate determination.
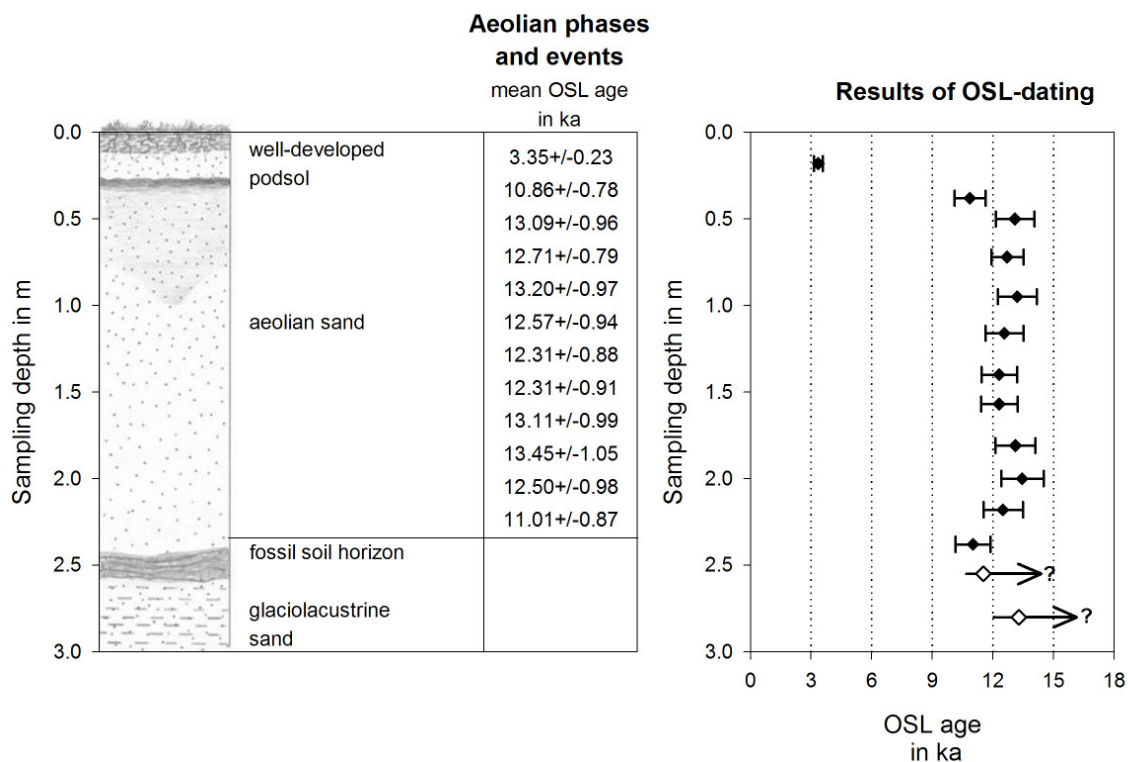
Ages of the underlying aeolian sand display a considerable scatter and do not increase consistently towards the base of the section (samples AD4-2 to -12, see Fig. 88). To check whether the scatter in age could be due to poor bleaching, further experiments have been carried out. The detailed investigation of the palaeodose distribution of the sample with the highest equivalent dose value (AD4-4) gave no evidence for a significant population of poorly bleached grains which could cause an overestimation of the palaeodose and hence the age (see Appendix F). Hence, the differences in age could arise from erroneous dose rate determination. To check the reliability of the NAA results, gamma spectrometry measurements have been carried out for several samples (see Appendix F). The dose rate values for AD4-4 differ significantly showing that dose rate determination is problematic here, and the OSL ages are to be treated with caution.

The aeolian sand was probably deposited within a very short period. The weighted mean of all OSL ages of the samples AD4-2 to -12 is 12.36±0.84 ka. Thus, the burial of the palaeosol horizon would be dated into the Younger Dryas period (GS-1, 11.50-12.65 ka BP). But because the ages of the whole sample set from AD4-12 up to -2 do not consistently agree within the 2σ error range, they were treated as individual age results rather than averaged.

Taking only samples AD4-12 and -2 from the base and the top of the aeolian sand unit into account, there is evidence to suggest that the palaeosol was buried during the Younger Dryas-Preboreal transition (AD4-12: 11.01±0.87 ka, AD4-2: 10.86±0.78 ka). At this stage of the study, no conclusive answer can be given to whether a Preboreal or a Younger Dryas burial of the palaeosurface is more likely. However, both results would agree with the dating of the palaeosurface into the Late Allerød to Younger Dryas (KAISER et al. 2006).

The interpretation of the OSL ages from the glaciolacustrine sands (samples AD4-13 and -14) below the buried soil is also problematic, predominantly caused by difficulties in dose rate estimation. Both samples underestimated the expected pre-Allerød age (>13.90 ka). The first problem concerns considerable changes in the sediment water content. The samples AD4-13 and -14 are taken from horizons, which are characterised by the influence of ground-water fluctuations. Higher water contents than the actual measured ones have to be assumed. This concerns in particular the time span after the Holocene sea-level rise of the Baltic Sea (LAMPE 2005) and before drainage improvements caused a drop of the ground-water level during the last century (starting in the early 20th century, KAISER et al. 2006). In order to account for these changes, the dose rate values and OSL ages have been calculated assuming water contents of up to 30 % (saturation) for at least 6,000 years.

Radioactive disequilibria in the uranium decay series could produce further difficulties in dose rate estimation. The occurrence of uranium disequilibrium, caused by the geochemical mobility of uranium and its daughter isotopes, is a well-known problem in waterlogged sediments. In contrast, it is rather unlikely in aeolian deposits. Disequilibria in the U decay chain occurring in connection with the sedimentation in lacustrine basins often result in uranium excess (KRBETSCHEK et al. 1994). As only the concentration of the parent nuclide of the ^{238}U decay chain is determined by NAA, the presence of disequilibrium could not be investigated. Uranium excess would cause an overestimation of the U content by NAA and yield 'too young' ages. The comparison of analytical results did not yield conclusive evidence for the presence of disequilibrium as the γ-ray spectrometer used does not measure the upper parts of the U decay chain. Therefore, as long as the glaciolacustrine sediments are not checked for radioactive disequilibria in detail, the OSL ages are considered as minimum ages only.

4.3.5.2 Site 'Altdarss-1' (AD1)

At site 'Altdarss-1' a fossil soil horizon was exposed, which was formed during the late Allerød according to palynological results (KAISER et al. 2006, see Fig. 87 & Fig. 89). Dating of this palaeosurface by radiocarbon did not yield straightforward results as the soil formation is either dated into the Late Allerød (12,809-12,700 cal. BP) or into the later part of the Younger Dryas (12,397-11,701 and 11,957-11,253 cal. BP, see Appendix E, Table E 2). KAISER et al. (2006) discuss the possibility of contamination with younger carbon by infiltration of humic acids and fungals and conclude that the buried soil surface most likely dates into the Late Allerød. However, the contamination, if present, seems not to have had such a drastic effect on the third radiocarbon age from the buried soil. Therefore, with respect to the given uncertainties, the age of the buried soil surface must be assumed to correlate with the Late Allerød to Younger Dryas time span.

Fig. 89: Schematic stratigraphic section of sampling site Altdarss-1 (AD1).
OSL samples are numbered from the top to the bottom with AD1-1 → AD1-4. Samples AD1-3 and -4 most likely give minimum ages only due to problems in dose rate determination.
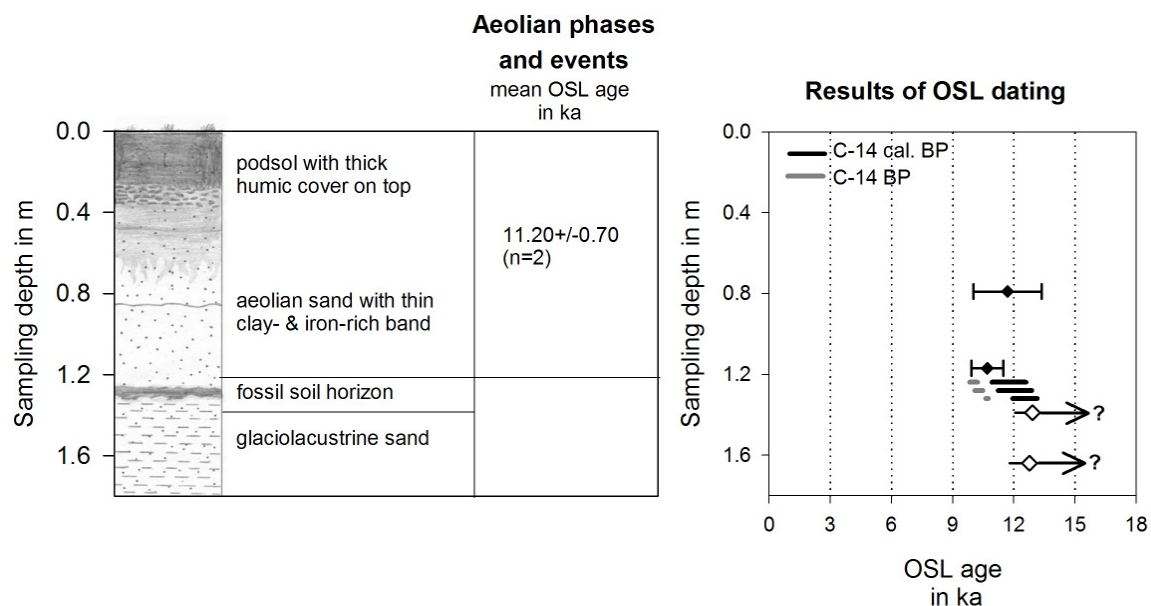
Luminescence dating was carried out on four samples from site 'Altdarss-1' further to support the chronology of the sediment record, but proved to be as problematic as at site 'Altdarss-4' (Fig. 89).

The OSL ages obtained for the glaciolacustrine sediments at the base of the section underestimate the expected pre-Allerød age. The variations in water content throughout the

time of burial were considered as described for site 'Altdarss-4'. In Appendix F the radionuclide contents determined for sample AD1-3 by neutron activation analysis are compared with the results of gamma-spectrometry. For all three radionuclides, U, Th and K, the individual values differ significantly. This might point towards analytical problems or inhomogeneous distribution of the radionuclides in the sediment rather than to disequilibrium in the U decay chain. No conclusive explanation can be given at this stage of the study. Because gamma spectrometry was carried out on a larger sample amount of 1600 g in contrast to the NAA, which uses only just a few mg, the γ-spectrometry derived dose rate and hence the age is considered to be more reliable. Furthermore, the gamma spectrometry results seem to be more accurate when compared to independent age control provided by ^{14}C results for three samples taken from the buried soil horizon directly overlying sample AD1-3. Taking the standard deviations into account the calibrated radiocarbon ages date the buried soil surface into the period Late Allerød to Early Preboreal. The substrate for this soil formation has to be older than the soil itself. Thus, the NAA based age of AD1-3 with 10.97±0.83 ka underestimates the expected age, whereas the gamma spectrometry derived age of 12.93±0.87 ka seems more reliable. However, both ages are still younger than the expected age of the glaciolacustrine deposition of presumably older 15.2 cal. ka BP (KAISER 2001). At this stage of the study the ages for samples AD1-3 and -4 are considered as minimum ages only due to the uncertainties in dose rate determination, notably in relation to water content fluctuations since deposition and the uncertainty about the presence of disequilibrium in the U decay chain.

The precise dating of the burial of the palaeosurface was also hampered by difficulties in dose rate determination. Nevertheless the results agree with the independent age control, which suggest a burial during the Younger Dryas possibly lasting into the Preboreal.

For sample AD1-1 the NAA and gamma spectrometry based dose rates differ significantly (see Appendix F). Consequently, also the resulting OSL ages deviate considerably dating the burial either into the Preboreal (10.87±0.85 ka with NAA) or early Younger Dryas (12.56±0.80 ka with γ-spectrometry). Within 2σ errors, both OSL ages agree with the radiocarbon ages obtained for the buried soil horizon, therefore it is difficult to state which dose rate estimate yields the more accurate result. To account for this uncertainty, the maximum age range of both age values, 11.69±1.67 ka, was considered for further interpretation of the chronostratigraphy. Sample AD1-2 also yielded an age dating the burial

of the palaeosurface into the Preboreal (10.70±0.79 ka) with the dose rate only derived from NAA. On average, the burial of the palaeosurface at site 'Altdarss-1' is dated to the Younger Dryas-Preboreal transition at 11.20±0.70 ka (mean of AD1-1 and -2, see Fig. 89). But as the dose rate comparison for sample AD1-1 already indicated, an early Younger Dryas age is also possible.

5. Discussion of the results

The aim of this study was to provide a chronology of the Lateglacial and Holocene aeolian record of the central European Sand Belt for landscape and climate reconstruction based on a consistent methodological approach. The fundamental question was, whether several phases of aeolian activity and periods of stabilisation and soil development could be defined and whether similarities or differences regarding their intensity, beginning and end, exist on a regional scale.

In a first step the luminescence dating protocol was evaluated, which was deemed to be best suited for dating aeolian, fluvial and glaciofluvial/glaciolacustrine sediments of depositional ages ranging from several hundreds of years up to about 20,000 years. In this context comparison of luminescence ages with independent age control played an important role. The comparative study of various luminescence dating protocols (in Appendix B), the internal checks of the protocol (in chapter 1), and the comparisons of OSL ages with radiocarbon chronologies (in chapter 1) demonstrated the robustness of the now widely applied single aliquot regenerative dose protocol for quartz.

Before the OSL data set is interpreted in terms of reconstruction of the aeolian record in northeast Germany, the results of the comparisons of ^{14}C and OSL ages which were carried out at various sites are summarised and discussed.

5.1 Comparison with radiocarbon ages

In checking the potential of luminescence dating methods it is necessary to date sediment sequences for which independent age control, for example by radiocarbon ages, is provided. The majority of radiocarbon ages used for the cross-checking are published as uncalibrated values. As luminescence ages are only comparable to calibrated ^{14}C data all cited uncalibrated radiocarbon ages used in terms of correlation have been calibrated into calendar years using the software *Calib 4.1* (STUIVER et al. 1998, see Table E 2 in Appendix E for a list of all ^{14}C ages including their reference). This program is not based on the latest calibration curve (FRIEDRICH et al. 2004, REIMER et al. 2004). The differences between the calibration file Intcal98 used in the *Calib 4.1* program and the revised version Intcal04 include only a few decades. Hence, the error which is introduced by using the former calibration file is

considered to be negligible with regard to comparisons of calibrated radiocarbon ages with luminescence data.

Several examples show a good consistency between the ^{14}C and the OSL chronostratigraphies. As the data comparisons have already been discussed in the context of the individual sites and are illustrated in the various site records in chapter 1, only a brief summary is presented.

In total 33 radiocarbon ages from the sites sampled for OSL dating were available for cross checking the OSL data set. In Fig. 90, 28 of these ages are compared with the OSL ages obtained for the sediment layers covering the ^{14}C dated material. The remaining five dates provide rough estimates for maximum or minimum age limits for the OSL ages as the luminescence samples were not taken from the sediments immediately burying the layers sampled for radiocarbon dating.

Fig. 90: Comparison of radiocarbon ages and optically stimulated luminescence ages of quartz extracted from dune sands.
In general, the OSL age of the dune sand directly overlying the layer dated by ^{14}C was included in the data set. Most of the radiocarbon ages were only available as uncalibrated ages. Therefore, calibration was carried out using the software CALIB 4.1 (STUIVER et al. 1998) (all ^{14}C ages are shown with the 2σ error, see Appendix E, Table E 2 for further details, references of the ^{14}C ages and the uncalibrated dates). All OSL ages were corrected to 'before 1950' to make them comparable to the calibrated ^{14}C data set. The solid line indicates equality and the dashed lines encompass the area with an uncertainty of ±20 %. Further explanations for the three outliers are given in the text.
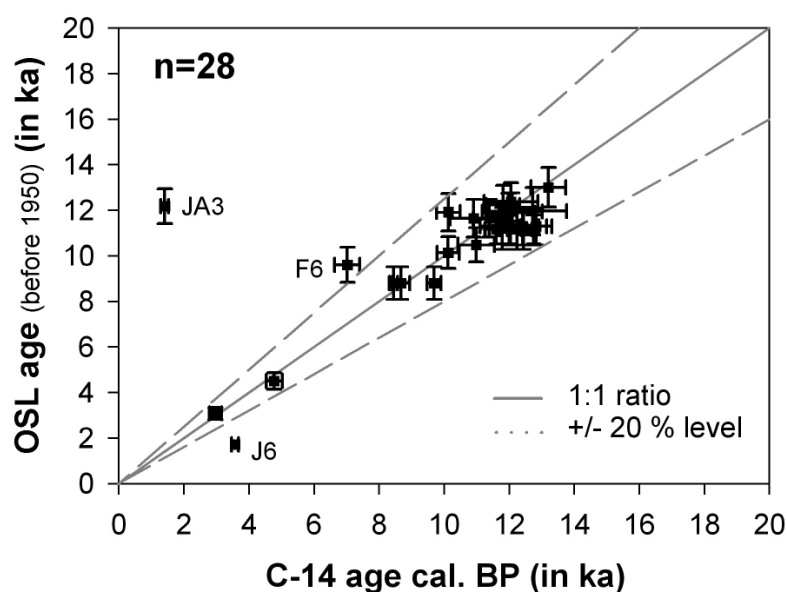
As illustrated in Fig. 90 both data sets show agreement within an uncertainty level of ±20 %, which though high is allowed for various reasons. First, the uncertainty introduced into the ^{14}C data set by the calibration of ^{14}C ages, which mostly were only available in an uncalibrated format, has to be borne in mind. As in almost all instances the samples for OSL and ^{14}C dating were not taken at the same time, there arises an additional uncertainty regarding the exact sampling position and relationship. Also the ages dated by the two methods do not involve the same events and therefore must differ from each other to a certain degree. Radiocarbon dating identifies the period of last dune stabilisation by vegetation, but luminescence dating determines the subsequent onset of aeolian activity.

However, three dates disagree by more than ±20 %. In two cases, samples F6 and JA3, the OSL ages yielded significantly higher ages. Regarding sample F6 the OSL age is assumed to provide the more accurate result, as it shows good agreement with palynological data from the relevant layer while the radiocarbon age underestimates the expected Preboreal age. The discrepancy in ages of sample JA3 is difficult to explain (see discussion in section 4.3.2.4). At site 'Jänschwalde' the explanation for the age deviation between ^{14}C and OSL ages is, that the charcoal was derived from an older charcoal horizon and was reworked by deflation (see discussion in section 4.3.2.3).

From the overall agreement with radiocarbon ages it is concluded that optically stimulated luminescence dating of quartz provides a powerful tool for dating of dune sand deposition, at least in the time span considered in this study, namely the last 15,000-20,000 years. This is promising in view of future studies dealing with dune sands that lack any carbon-bearing material suitable for ^{14}C dating, or sands deposited beyond the limit of ^{14}C.

While there are problems which rise from dating dune deposition with ^{14}C ages when reworked material is involved, radiocarbon chronologies are useful to establish age constraints for the deposits above the dune sands. But problems occur with precise dating of underlying substrates because there is no way of knowing the period of time that has elapsed between dune sand deposition and the termination of the formation of organic matter.

5.2 Reconstruction of dune development by OSL dating of quartz

The potential of OSL dating ages of dune sand deposits for the reconstruction of aeolian activity throughout the last c. 20,000 years has been demonstrated. But is OSL dating sufficiently precise and reliable to distinguish between phases of dune building that are indicative for changes in climatic conditions.

All the 159 OSL ages obtained for dune sands, which are considered to be reliable, are compiled in one summary graph (Fig. 91 a). At first glance the graph seems bimodal. The older part from the onset of aeolian activity at about 18 ka until about 10 ka seems to indicate a more or less continuous activity with a prominent peak at about 12.3 ka. The younger part is characterised by several periods with enhanced dune activity at about 6.3, 4.5, 3.5, and 1 ka that alternate with more or less clearly defined periods of aeolian quiescence. It is important to emphasize that the height of a peak is not related in any way to the intensity of a period, but merely reflects the existence of an age cluster.

For a better resolution of the youngest part of the OSL record the summary graph was recalculated using a class width of 100 years instead of 500 years (see Fig. 91 b and c). This better accounts for the fact that Late Holocene ages show uncertainties of just a few decades, whereas for the Lateglacial dates, errors are in the range of several centuries. Using a class width of 500 years for the young ages could mask individual periods of dune activity by summarising the ages in just one class (Fig. 91 b and c). In particular the last three millennia show a more diverse picture of aeolian activity using the class width of 100 years, whereas the record of the Mid-Holocene is similar in both graphs. The peak at about 1 ka is resolved in several peaks indicating dune sand deposition about 300, 700, 900 and 1800 years ago. Finally, for interpretation of the young aeolian record the summary curve in Fig. 91 c) is used.

Fig. 91: Compilation of all methodological rigorous OSL dates of dune sand deposits.
In case of multiple samples taken from the same lithological unit, a weighted mean of the ages was considered with the standard deviation taken as uncertainty. Otherwise just a few sites with deposition of thick sand units in just a short period of time and thus several samples yielding the same age would overwhelm the entire data-set. The graph was constructed following the probability density approach as described for example by SINGHVI et al. (2001). This approach permits the construction of a histogram such that the experimental errors are also included. The time span which is considered here, 25 ka, was subdivided into class intervals of 0.5 ka (or 0.1 ka in c). For each OSL age a Gaussian distribution is calculated with its mean representing the age value and the width of the distribution is determined by the individual error of the OSL age. The histogram value for each class interval is then calculated by summing the individual values of each age included in the compilation and dividing the sum by the total number of dates.
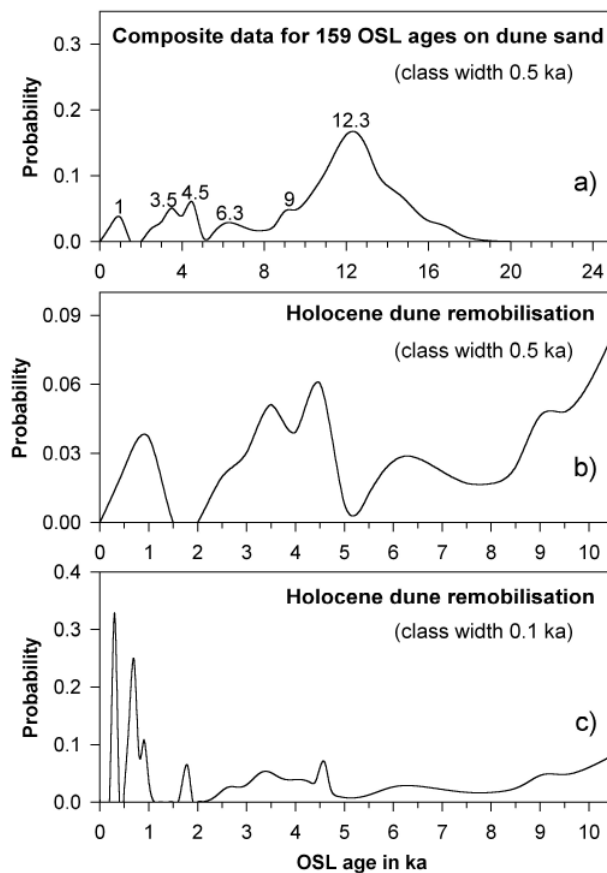
Any cluster of ages or peaks in the probability distribution curve can be interpreted either as caused by a sampling bias (such as a higher or accidental sampling density of sediments belonging to one particular interval) and/or as a reflection of an enhanced accumulation. As discussed in the text, it was not possible to sample sediments from the base of the dunes at all sites. Thus, the record might be slightly biased towards the later part of the Lateglacial. But because sampling was regularly spaced and multiple dates from the same stratigraphic unit were averaged any additional sampling bias ought to be excluded.

Fig. 92: Composite data as probability density curves for all regional subsets.
The figures at the peaks indicate the number of individual OSL samples which contribute to each particular age cluster (for further explanations see Fig. 91).
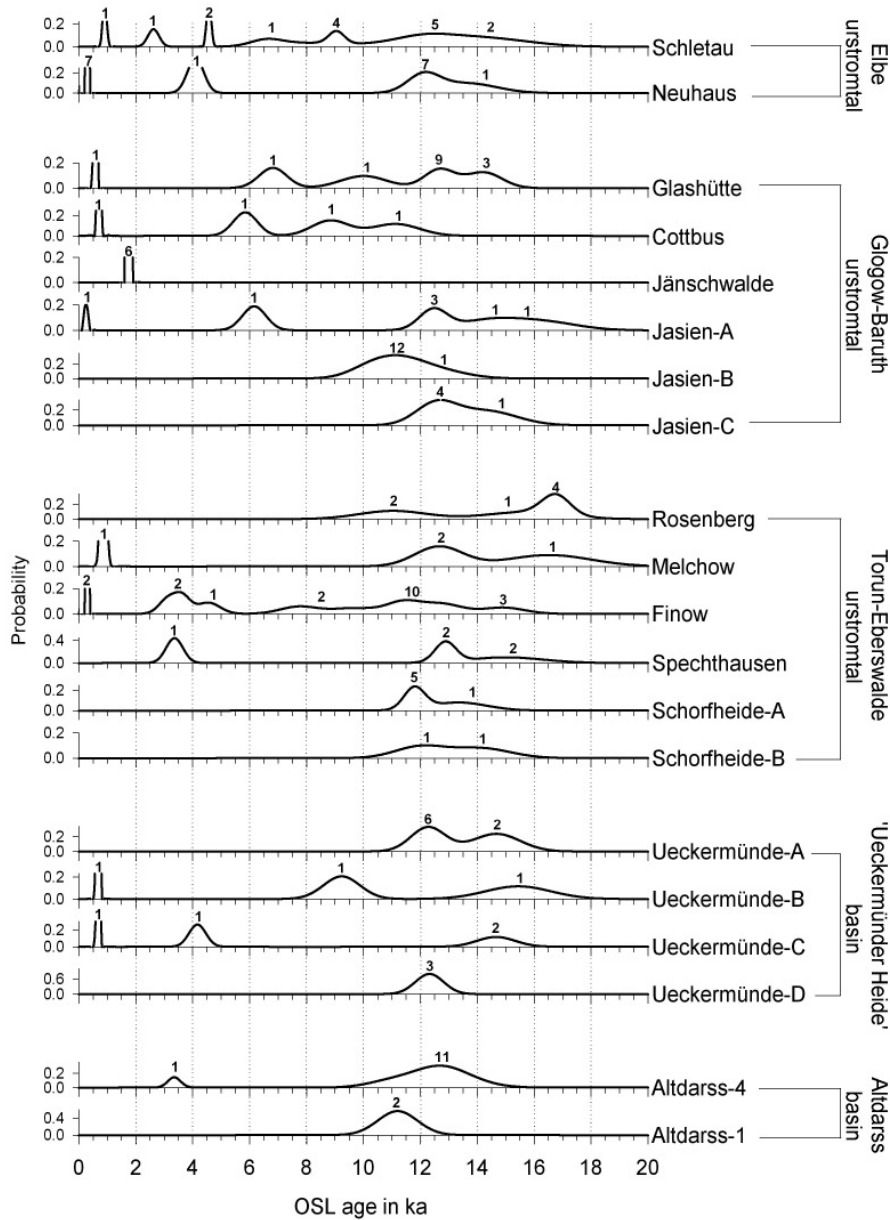
For a further characterisation of the different phases of aeolian activity the attention should be drawn to the individual site records as shown in Fig. 92 Again, two different periods of aeolian activity are indicated. During the older part of the record from about 18 to ~10.5 ka aeolian deposition is recorded in all of the five different study areas. Furthermore, towards the end of this phase, at about 12 ka, dune sand deposition took place at almost all of the twenty sites. A large number of samples (n= 85) were derived from this period. With reference to the

regularly spaced sampling of the dune sections this observation indicates that a substantial amount of sand was transported and deposited at the end of the Lateglacial.

The OSL record after ~10.5 ka shows a completely different picture. The comparison of the well-defined peaks from Fig. 91 a) or c) with the individual site records in Fig. 92 demonstrates that they are all represented at just a few or even at only a single site. All those peaks lack a regional distribution, yet they have a widespread occurrence in any one particular study area. Furthermore, in most cases the depositional event is evidenced by only one sample. It is deduced that the younger aeolian events resulted in deposition of only thin (maximum of a few dm) sand layers.

To conclude, the OSL record of dune sand deposition shows a sharp contrast between two time slices:

- an older period from about 18 to 10.5 ka with dune sand deposition occurring regionally throughout the study area characterised by substantial sand accumulation (old phase of dune formation and dune reactivation)
- a younger period since ~10.5 ka which is characterised by locally restricted and less pronounced aeolian events (young phase of dune reactivation)

Although the boundary at ~10.5 ka is not strictly congruent with the chronostratigraphic Lateglacial/Holocene boundary at 11,500 GRIP ice-core years ka (BJÖRCK et al. 1998), 11,590 varve years (LITT et al. 2003), or 11,590 dendro years (FRIEDRICH et al. 2004), both phases will be referred to as the old, Lateglacial, and the young, Holocene, period for ease of reference.

5.2.1 Lateglacial phase of dune formation and reactivation

The summary graph (Fig. 91) does not show a steady rise up to the maximum intensity at about 12.3 ka. Two shoulders can be observed. Fig. 92 allows a more detailed characterisation and timing of these two less pronounced phases of aeolian activity.

During the earlier part of the Lateglacial, aeolian sand deposition is not as widespread as during the later part around 12 ka ago. The oldest ages obtained in the study area are derived from three sites. They date the onset of aeolian accumulation to ~16.7 ka (weighted mean). Taking the error (1σ standard deviation) into account this earliest period lasted from about 16.9 to 16.5 ka. With respect to the reliability of the OSL ages site 'Jasień-A' is important. Here, the base of the dune was clearly defined by a ventifact layer with the OSL dated overlying sand representing in fact the onset of aeolian accumulation at this site.

From about 15.2 ka aeolian deposition occurred more widespread throughout the study area with OSL ages in this time-slice obtained from fourteen of the twenty sites. An interruption of dune formation is indicated around 13.7 ka by either a decrease of the individual distribution curves or a distinct increase after 13.7 ka (see Fig. 92). At some sites dune sand accumulation began about then. The small number of samples (n= 24) falling into this age range can be explained by the inability to identify and sample sediments from the base of the dunes at some sites. For instance at sites 'Glashütte' and 'Jasień-C' only the upper part of several meters of dune sand could be sampled successfully (see also chapter 1 for further details). Thus it may be that the age cluster dating the peak of the dune-building period to around 14.4 ka is shifted towards the termination of dune construction to some degree.

A differentiation of the dune formation period around 14.4 ka from the major peak in dune sand deposition around 12 ka is deduced from the individual site records as show in Fig. 92 The interruption of aeolian deposition observed in the graphs around 13.7 ka is further suggested by the stratigraphy of the sections. At eleven sampling sites a fossil soil horizon, identified as the 'Finow-palaeosol' (see chapter 4.2), supports the conclusion that this decrease in the OSL record is a period of aeolian quiescence and landscape stabilisation during which a soil was formed. This period is terminated with the onset of intensive dune

formation and reactivation. According to the weighted mean and the 1σ standard deviation of all OSL ages related to this phase dune activity lasted from about 12.87 ka to 11.05 ka with the maximum intensity at ~12 ka. This dune reactivation at the end of the Lateglacial is characterised by its occurrence throughout the five study areas with sand deposition dated at seventeen of the twenty sampling sites. None of the former or subsequent aeolian events recorded in the OSL data set showed a comparable regional impact.

To conclude, based on these observations the Lateglacial period of dune formation is divided in three phases:

- the **onset of aeolian deposition around 16.7 ka**, only occasionally recorded within the study area;
- a **early period of dune formation** lasting within errors from 15.2 until 13.7 ka with a peak of aeolian activity **around 14.4 ka**, recorded throughout the study area, although represented by only a limited number of samples at any one site;
- a **late period of dune formation and reactivation** from 12.9 to 11.1 ka within errors with the peak of activity **around 12.0 ka** which is characterised by its widespread occurrence and identification in a large number of samples indicative of the substantial amount of sand mobilised during this period.

The widespread occurrence of Lateglacial aeolian activity argues for a forcing factor with regional impact such as climatic conditions. Changes in the density of the vegetation cover for example could have an influence on the availability of the sand sources, and so trigger either the onset of dune formation or the stabilisation of dune surfaces.

In the following section the record of Lateglacial aeolian activity reconstructed by OSL is discussed in the light of what is known about climate and vegetation changes. Only if coincidences are found can the suitability of the OSL record of dune activity as a proxy record for climate-induced environmental changes be demonstrated.

5.2.1.1 Relation between dune formation and Lateglacial climate and vegetation changes

The climate of the Last Glacial Maximum until the Holocene was characterised by repeated, often short-lived alternations of warmer periods (interstadials) and much cooler periods (stadials). These Lateglacial climate changes are recorded in the high-resolution oxygen isotope records obtained from continuous cores from the polar ice sheets such as the GRIP (European Greenland Ice-core Project) ice-core (see Fig. 93, BJÖRCK et al. 1998).

Fig. 93: The oxygen isotope (δ^{18}O) record (‰ SMOW) from the GRIP deep ice-core of the Last Termination between 11.0 and 23.0 ka GRIP BP.
(modified from BJÖRCK et al. 1998: 288, based on data of JOHNSEN et al. 1992 and DANSGAARD et al. 1993)
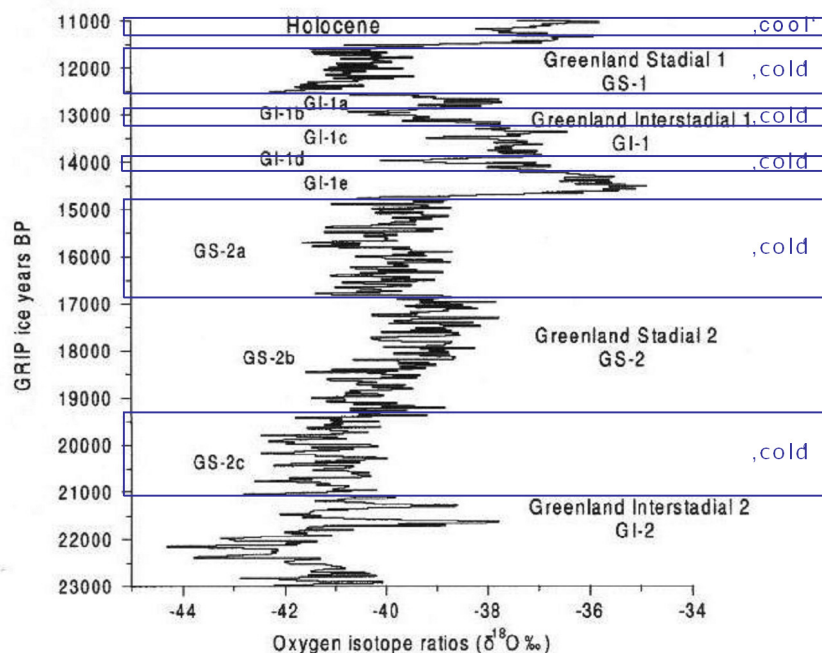
The GRIP core data indicate alternations of warmer and colder intervals of varied durations and character. Abrupt changes occurred within only a few decades. For example, there was a temperature decline of 11°C in 200 years during the rather short-lived event GI-1d and a drop of 7.5°C during the ~200-year-long cooling event GI-1b. A rapid and severe cooling of 15°C within only 150 years at the onset of the Greenland-Stadial 1 is evidenced, whereas the temperature during the Early Holocene Preboreal Oscillation (PBO) was lowered by only 4°C in 100 years (JOHNSEN et al. 1995, BJÖRCK et al. 1996). These rapid cooling episodes are seen as a reaction to the huge meltwater inputs on both sides of the North Atlantic resulting from the substantial re-melting of the Scandinavian-Laurentide-Barents Sea ice sheets and ice bergs

and from the drainage of glacial lakes such as Lake Agassiz and the Baltic Ice Lake during preceding warming intervals (e.g. GS-2b, GI-1e, GI-1a, see Fig. 93) (BJÖRCK 1995, BJÖRCK et al. 1996, BARD et al. 1996, BOND et al. 1997, BROECKER et al. 1989, EDWARDS et al. 1993).

In the marine record the so-called 'Heinrich event I' (H1) indicates a period of enhanced ice-rafted transport of detrital carbonate to the North Atlantic. These H events are known to result from major melting events with high freshwater discharges associated with the collapsed North Atlantic thermohaline circulation. H1 has been dated to 18.1-14.7 ka (BOND et al. 1997, 1999, SARNTHEIN et al. 2000) which appears to link it to the onset of Lateglacial warming at 19.5 ka (GS-2b dated to 16.9-19.5 ka, see Fig. 93). The switched-off thermohaline circulation finally caused a cooling of the Nordic Seas. Due to the strong coupling between sea-surface and atmospheric temperatures and the limited moisture transport from the cooled down sea-surface to the atmosphere climate in adjacent continental areas is influenced by a change towards cold and dry conditions. Therefore the repeated, often abrupt Lateglacial climate fluctuations affected also the continental part in the North Atlantic region (BJÖRCK et al. 1996, 1998).

Important general questions can be summarised thus: "*How much must climate change before we see an effect in our landscape*?". Furthermore the question of synchronicity arises. Whereas ice-core records, for example, preserve any information on climatic conditions immediately, terrestrial ecosystems may lag behind until a marked change is recorded: "*How long does it take until we see the effect of climate change in our landscape*?". The answer to both questions calls for a precise chronology of climate-triggered changes in the landscape in order to correlate the response of terrestrial ecosystems to particular climatic oscillations.

The OSL chronology of Lateglacial dune activity now has to be related to the chronology of climatic change in order to investigate whether aeolian activity occurred simultaneously with certain climatic conditions or occurred only after a delay. The challenge is to select a suitable chronological framework for climate change in the study area.

Traditionally the Lateglacial in north-west Europe is subdivided into the chronozones Bølling (including Oldest Dryas, 13-12 ^{14}C ka BP), Older Dryas (12-11.8 ^{14}C ka BP), Allerød (11.8-11 ^{14}C ka BP) and Younger Dryas (11-10 ^{14}C ka BP) according to the stratigraphic scheme proposed by MANGERUD et al. (1974). The Holocene is subdivided into the different climatostratigraphic periods Preboreal (10-9 ^{14}C ka BP), Boreal (9-8 ^{14}C ka BP), Atlantic (8-5

[14]C ka BP), Subboreal (5-2.5 ^{14}C ka BP), and Subatlantic (since 2.5 ^{14}C ka BP). This system dates back to BLYTT (1876), and was later modified by SERNANDER (1908), FIRBAS (1949) and many others (all cit. in LANG 1994).

One difficulty is that with ongoing research the climate characterisation of the individual units has changed since they were first described. The boundaries of these so-called chronozones in fact reflect boundaries of biozones (principally pollen zones and macrofossil assemblages). They are defined by radiocarbon data on evidence (e.g. macrofossils, peatlayers, charcoal fragments) derived from the biostratigraphic records representing changing climate conditions. But chronologies based on radiocarbon ages cannot directly be correlated to OSL records. Due to short- and long-term variations in the atmospheric $^{14}C/^{12}C$ ratio radiocarbon data show an age offset. Thus, for accurate dating and correlation to other proxies ^{14}C ages must be calibrated in order to establish their calendar-age equivalence, for example, by comparison to tree-ring records (0–12.4 cal. ka BP) or marine records (corals and foraminifera 12.4–26.0 cal. ka BP) (REIMER et al. 2004).

Further difficulties in radiocarbon dating of the Lateglacial-Holocene transition arise from a number of [14]C- age plateaux at that time, which have been found at ca. 12.7-12.6, 11.4-11.3, 11.0-10.9, 10.4-10.3, 10.0-9.9, and 9.6-9.5 ka ^{14}C BP (ref. summarised in BJÖRCK et al. 1997, 1998). Unfortunately, this period is of crucial importance for the investigation of the drastic climatic and environmental changes that took place during this transitional phase.

The last few decades have seen substantial progress in refining various calendar year based proxy records for palaeoenvironmental changes including ice-core records, varve chronologies and tree-ring records. But this progress is accompanied by an increasing confusion regarding the chronostratigraphic classification of the climate and environmental changes since the Last Glacial Maximum (see discussion e.g. in BJÖRCK et al. 1998, LITT et al. 2003, DE KLERK 2004, TERBERGER 2004, TERBERGER et al. 2004). For the purposes of this study, the event stratigraphy introduced by the INTIMATE group (INTegration of Ice-core, MArine and TErrestrial records, core programme of the International Quaternary Union) for the North Atlantic region based on the GRIP ice-core record (see Fig. 93) provides the soundest 'backbone chronology' for Lateglacial climatic changes.

Compared with the terrestrial evidence, much of which is highly fragmentary as a result of erosional processes causing gaps in the depositional record, oxygen isotope analysis of

drilling records from polar ice-sheets and glaciers provides relatively undisturbed and high resolution continuous records. Ice-core records are independently dated by the counting of annual ice layers down from the surface. Annually laminated lake sediment records from western and northern Germany, Poland, and Switzerland (LITT et al. 2001, 2003) and the tree-ring record of central Europe (FRIEDRICH et al. 2004) also provide calendar year records. In addition they give a direct geographical link to the study area in NE Germany and NW Poland. But the major disadvantage preventing their use as backbone chronology for this study is that they do not cover the entire time span incurred. The varve chronologies began at 14,450 varve yr BP (LITT et al. 2003) and the German oak-pine dendrochronology now extends back to 12,410 cal. yr BP (10,461 BC) (FRIEDRICH et al. 2004). A comparison of the GRIP record, varve chronologies from northwest Europe, and the German oak-pine dendrochronology suggests that synchronisation between GRIP ice years and treering years is within the stated uncertainty of ±30 yr for the GRIP record. This synchronisation indicates that the biotic response to changing climate conditions was not significantly delayed. This factor crucially supports the application of the GRIP record to the conditions in the study area.

But up to now the GRIP terminology has not been used in research dealing with Late Quaternary chronostratigraphies. Various terminologies still are used. For the sake of consistency and ease of correlation with other studies in this study the relation of the GRIP episodes to the the stratigraphic subdivision of the MANGERUD et al. scheme as presented by TERBERGER et al. (2004) is adopted: GS-1 Younger Dryas, GI-1a-c Allerød, GI-1d Older Dryas, GI-1e Bølling/Meiendorf, later part of GS-2a Oldest Dryas.

This correlation is based on the subdivision of different Lateglacial 'Vegetation phases of Vorpommern' proposed by DE KLERK (2002, DE KLERK et al. 2001). It has to be emphasized that the ^{14}C chronology (calibrated ages) of the different pollen zones deviates from the chronology of the Greenland ice-core events and furthermore has to be regarded as only tentative, for few reliable radiocarbon ages directly connected with the pollen diagrams are available (DE KLERK 2002, TERBERGER et al. 2004). By comparing pollen diagrams from northern Vorpommern with those of southern Mecklenburg, the northern part of Brandenburg, and the vicinity of Berlin DE KLERK and STOLZE (2002) could show that these 'Vegetation phases' are not easily transferable to the entire area investigated in this study. Differences exist for certain periods, but those relevant for the aeolian record will be discussed in the following. Because of the reasonably good correlation of the 'Vegetation phases' with the palaeoclimate record of the GRIP core and the geographic link to the study area this record of

Lateglacial changes in the vegetation cover has been included in the discussion of the aeolian record. Fig. 94 presents a comparison of these vegetation phases, the GRIP ice-core record and the OSL record of dune sand deposition.

Fig. 94: OSL record of Lateglacial phases of aeolian deposition.
Comparison of the Lateglacial climatic record derived from the GRIP deep ice-core (from BJÖRCK et al. 1998: 288), the chronology of vegetation phases in NE-Vorpommern (after DE KLERK 2002), and the aeolian record according to the OSL ages determined by this study. The OSL ages are shown as probability density function. Each OSL date determined for a dune sand unit is represented by a black symbol with the total number of OSL samples contributing to the individual age cluster also shown at the bottom of each column. (PBO = Pre-Boreal Oscillation).
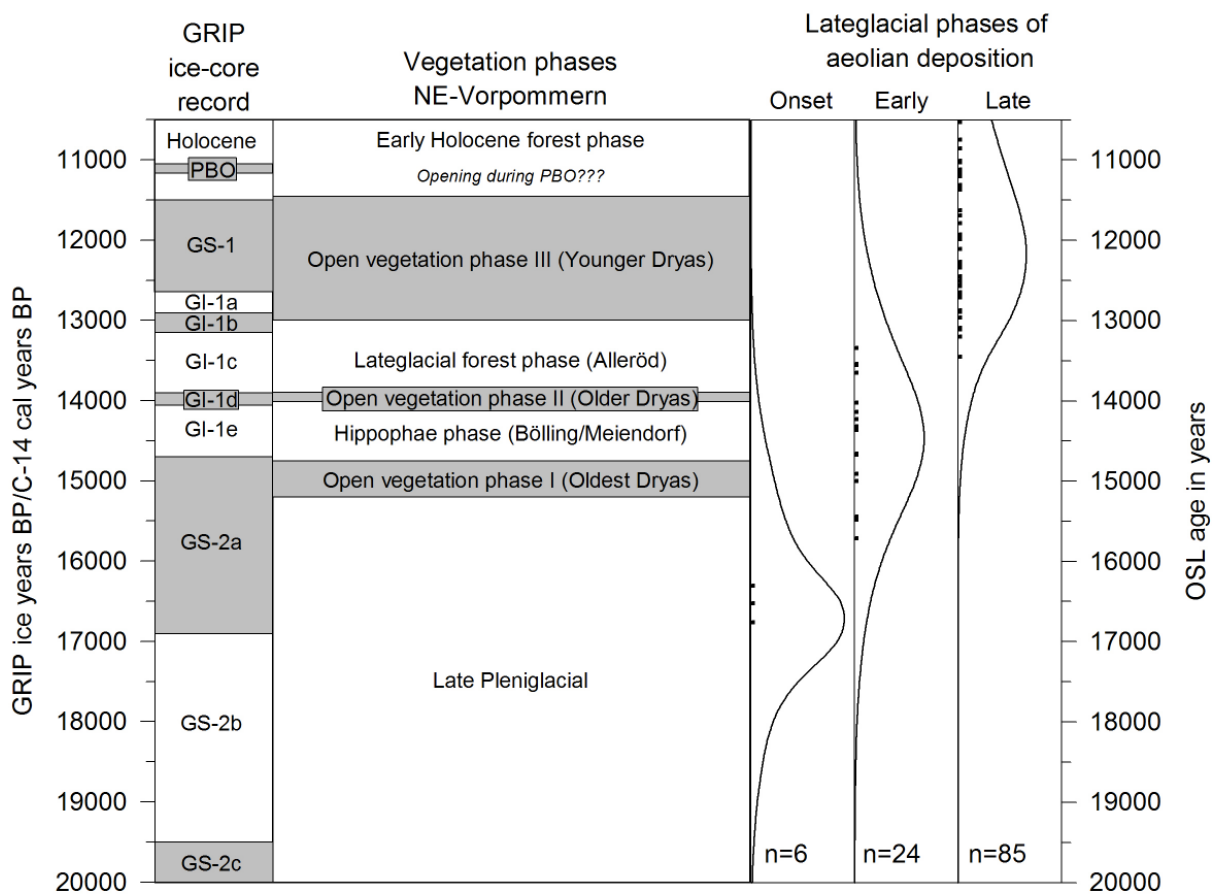
5.2.1.1.1   The onset of aeolian deposition

From Fig. 94 it is apparent that prior to –within the uncertainty of the OSL ages- 18 ka very little aeolian sand deposition occurred within the study area. The two northernmost study areas, 'Ueckermünder Heide' and 'Altdarss', were still covered by the Weichselian glacier by that time. Both areas became ice-free with the decay of the Mecklenburg Advance about 17.5-16.6 ka cal. BP (see Table 10, chapter 1 for discussion of the existing chronology). The onset of aeolian accumulation in the southernmost Głogów-Baruth urstromtal could be expected to commence after the drainage of the Brandenburg-Leszno Advance, presumably more than 23,000 years cal. BP ago (see Table 10, chapter 1). In the Toruń-Eberswalde urstromtal aeolian deposition probably was not possible before 18.7-17.7 ka cal. BP (Pomeranian Advance).

Aeolian deposition within the ice-marginal valleys was not possible before a source of sand became available, and thus not before the draining of the valley floors after the period of main discharge of meltwater. Deflation was restricted to areas where a lowered water table allowed the surface sediments to dry out but before significant vegetative colonisation. Also any aeolian deposits could persist where they were not washed by migrations of the braided river channels (VANDENBERGHE 1991).

From the observation that the oldest aeolian deposits in the Głogów-Baruth and in the Eberswalde urstromtal date from the same time at about 16.7 ka (see Fig. 92) it can be inferred that the major factor controlling the onset of aeolian deposition is not just the deglaciation and deactivation of the ice-marginal valleys as meltwater drainage.

The Late Weichselian Pleniglacial arid and cold polar desert conditions did not allow plant growth so that the bare sandy surfaces of the proglacial outwash plains and of the large braided-river floodplains provided ample supply for aeolian transport (VANDENBERGHE 1991, KASSE 2002). Stone pavements with ventifacts and sand wedges with primary infilling in the southernmost part of the study area provide evidence of an effective aeolian activity (BÖSE 1991, GOZDZIK 1991, DE BOER 1995). Despite this, aeolian deposits are rarely preserved in the period >17-18 ka. Their absence can be explained by the presence of permafrost. Because

infiltration of rain and snowmelt water was reduced by the frozen ground, overland flow was increased and caused a widespread reworking of aeolian deposits (e.g. MAARLEVELD 1976, RUEGG 1983, KOZARSKI 1990, MANIKOWSKA 1991a, KASSE 1997).

Aeolian sand transport occurred especially under dry permafrost conditions and in upland areas with a better drainage of the mollisol (BÖSE 1991). Any aeolian deposits on floodplains within the braided-river valleys were removed by rain and meltwater discharge in spring and summer. Fluvio-aeolian deposits are typical for this phase of high aeolian activity (SCHWAN 1987, KASSE 1997, 2002). The sediments lack organic matter. For this reason ^{14}C dating of the material is still not well established (KASSE 1997). Luminescence dating has been applied only sporadically up to now. MOL and RHODES (1997 in MOL 1997) dated fluvio-aeolian deposits from the Niederlausitz (Lower Lusatia) to 18 to 20 ka and BATEMAN and VAN HUISSTEDEN (1999) and VANDENBERGHE (2003) to between 17 and 24 ka in The Netherlands.

The limited preservation of aeolian deposits as a consequence of permafrost conditions implies that the onset of aeolian accumulation, dated by OSL, may have coincided with the dissipation of permafrost. In The Netherlands, for example, permafrost degradation and formation of large cryoturbations was dated by OSL for the time period from ~16 to 22 ka (BATEMAN & VAN HUISSTEDEN 1999, VAN HUISSTEDEN et al. 2000, 2001).

From what is known about the timing and distribution of periglacial features indicative for permafrost conditions, such as ice-wedge casts and sand wedges, it can be deduced that continuous permafrost limited the preservation of aeolian deposits in ice-free parts of the study area until about 18.7-17.7 ka cal. BP (Pomeranian Advance, 15.2 ka BP, LIEDTKE 1996). For the area north of the Pomeranian glacial limit a discontinuous permafrost is assumed with continuous permafrost restricted to a narrow zone along the margin of the retreating ice sheets between 15 and 17 ka (BÖSE 1991, KOZARSKI 1993, HELBIG 1999, RENSSEN & VANDENBERGHE 2003). In the till plains of the Mecklenburg Advance ice wedges filled with aeolian sand are also widespread. Because of their limited size and development they are not necessarily indicative for permafrost conditions, but could be developed as well under strong seasonally frozen ground conditions (or during a short period of permafrost conditions) (HELBIG 1999). Evidence indicates that permafrost conditions prevailed in the area until the Oldest Dryas and at least in some places permafrost survived even the warming following on the Oldest Dryas (KOZARSKI 1993, BÖSE 2000).

To summarise, the timing of the dissipation of permafrost in the study area is not very well established. But the degradation of continuous permafrost most likely dates back to around 18 ka, coincident with the less cold period GS-2b in the GRIP core dated to 19.5-16.9 ka BP (BJÖRCK et al. 1998).

With the permafrost degradation infiltration of rain and snow meltwater was increased. This resulted in drier surfaces enhancing the transportability of the dry, non-cohesive sand and prevented overland flow that previously destroyed aeolian deposits. This edaphic dryness was reinforced by an increased climatic aridity during the Greenland stadial GS-2a because of a limited moisture transfer to the atmosphere from the cool sea surface. These cold and dry polar desertic conditions characterised by a scarcity of vegetation favoured aeolian transport and sand sheet accumulation (KASSE 1997).

The oldest aeolian sediments dated in this study to about 16.7 ka indicate the environmental conditions favouring the accumulation and preservation of aeolian sand deposits. They postdate the permafrost degradation (presumably around 18 ka) and coincide with the onset of cold and dry climate of the GS-2a episode starting at 16.9 ka.

However, only a few samples were dated to this time slice and more dates are needed further to support this interpretation. But altogether the OSL ages obtained at the three sites are in good agreement with indirect dating indicated by the morphological position of the study sites. At site 'Jasień-A' these oldest aeolian sediments overlie a ventifact horizon with the formation of such stone pavements in the polar desert environment lasting until the ice-sheet retreated to the Pomeranian stage (KOZARSKI 1974, DYLIK 1967 in BÖSE 1991). The oldest deposits found in the Toruń-Eberswalde urstromtal must postdate the Pomeranian Advance as they were deposited on the highest urstromtal level that is correlated with the remelting of this stage. As this terrace level was already inactive during the meltwater drainage of the younger Angermünde stage at about 18.1-17.1 ka cal. BP (c. 14.7 ka ^{14}C BP, LIEDTKE 1996), conditions for the preservation of these deposits were favourable.

The onset of aeolian deposition was recognised in the Głogów-Baruth and in the Toruń-Eberswalde urstromtal more-or-less at the same time. This observation might be construed as suggesting that there was no major contrast in conditions from south to north, but such an interpretation is at present unwarranted.

5.2.1.1.2   The early-Lateglacial period of dune formation

Examination of Fig. 92 indicates widespread aeolian accumulation starting at about 15.5 ka (see also Fig. 94). In four of the five study areas dune sand deposition occurred during this early-Lateglacial period of dune formation between ~15.2 until ~13.7 ka. The onset of widespread dune formation apparently accompanied the development of the vegetation cover in the study area. According to the interpretation of numerous palynological studies from northeastern Vorpommern for the second half of the GS-2a (16.9-14.7 ka) an open vegetation cover can be deduced (DE KLERK et al. 2001). The 'open vegetation phase I' could be dated to 15,200-14,750 cal. yr BP based on radiocarbon data from northeastern Germany and northwestern Poland (see Fig. 94). This is not unexpected, as the formation of parabolic dunes, the dominant type of dune throughout the study area, is associated with partial stabilisation by vegetation. These observations are furthermore in agreement with other studies that relate the transition from sand-sheet to dune formation to enhanced plant growth in the Lateglacial (e.g. SCHWAN 1988, VANDENBERGHE 1991).

The pollen records from northeastern Vorpommern indicate a dry continental climate with little precipitation in accord with the cold conditions deduced from the ice-core records (Fig. 93). It is also compatible with the relative climatic dryness which can be assumed for this period at the end of 'Heinrich event I' (18.1-14.7 ka BP) when moisture transport from the cooled surface of the Nordic Seas was limited. The vegetation cover still was rather sparse and open and consisted mainly of herbs (DE KLERK et al. 2001, DE KLERK 2004). The vegetation cover was not dense enough completely to stabilise the dry, sandy surfaces, yet it was sufficient in places to stabilise the sand deposits and initiate the formation of dunes.

A further factor favouring dune formation and the preservation of aeolian deposits was the lack of fluvial and meltwater discharge in the proglacial valleys. Because the Lower Oder valley was ice-free by that time and drew water from further east, the widespread sandy deposits within the now inactive ice-marginal valleys provided the sediment sources for dune formation (BÖSE 1991).

At numerous sites aeolian activity ceased around 13.7 ka (see Fig. 92). In fact at eleven study sites a period of dune stabilisation is clearly documented by the palaeosol horizon, the 'Finow-soil', of Allerød age (see also Fig. 95 and section 4.2 & 4.3.3.1 for further details on the dating of the 'Finow-soil').

The widespread occurrence of this palaeosol horizon throughout the study area argues for a regional change in environmental conditions. The decline in aeolian activity at about 13.7 ka is in agreement with the climate amelioration at the onset of the Greenland Interstadial GI-1c at 13.9 ka (BJÖRCK et al. 1998). Based on the 'vegetation phases' proposed by DE KLERK et al. (2001) for northeastern Vorpommern a correlation of the period GI-1a-c with the Allerød chronozone seems likely (see also TERBERGER et al. 2004). The boundaries of this vegetation phase are ^{14}C dated to 13.9-13.0 ka cal. BP (DE KLERK et al. 2001) (see Fig. 94). This is compatible with the GRIP age of this period, 13.90-12.65 ka. The Allerød vegetation throughout the study area was characterised by a development of birch (predominantly on till plains) and pine forests (dominant on sandy soils) (TOBOLSKI & LITT 1994, DE KLERK et al. 2001, KAISER et al. 2003, THEUERKAUF 2003, TERBERGER et al. 2004), although the vegetation cover remained open for some time at the beginning of the Allerød at least according to evidence from Vorpommern (DE KLERK et al. 2001). This forest cover and the associated formation of the 'Finow-soil' provided an effective protection against deflation and explains the limited or absent aeolian activity which is indicated in the OSL record of aeolian deposition after about 13.7 ka.

Regarding the dating of the 'Finow-soil' itself, the OSL ages of the overlying and underlying sediments support the Allerød age of this soil development. At the individual sites the resolution of the luminescence ages often does not allow the unambiguous assignment of the under- and overlying sediments to the pre- and post-Allerød time, respectively (Fig. 95). But taking the OSL data-set as a whole, the dating of the soil development into the Allerød chronozone seems most likely.

Fig. 95: Summary of the OSL results obtained for the sediments over- and underlying the 'Finow-soil' at different sites throughout the study area.

The soil formation is dated to the Allerød interstadial based on radiocarbon ages, pollenanalytical studies, and the stratigraphic corrrelation to a layer of Laacher See tephra (SCHLAAK 1993, 1998). The OSL chronology presented here further supports this dating, although at numerous sites the dates would also allow soil formation to start already before the Allerød period. The OSL ages of the dune deposits overlying the 'Finow-soil' horizon indicate an onset of dune formation already at the beginning of the Younger Dryas. (chronology of the Lateglacial chronozones after BJÖRCK et al. 1998)
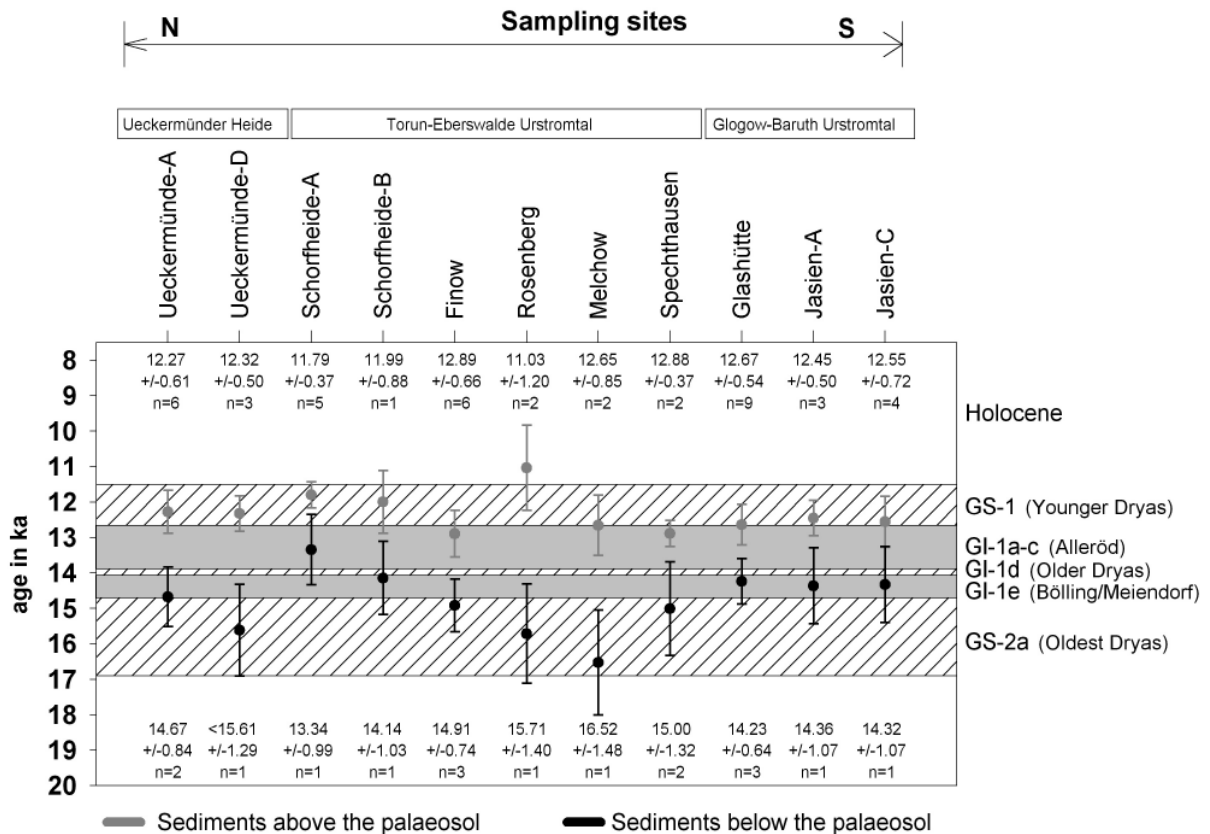
The dune sands directly overlying the fossil soil horizon are dated into or to the onset of the GS-1 or Younger Dryas stadial. The ages of the underlying sediments show greater variations at the different sites. In this context the higher precision of the OSL ages for the overlying sediments results from the calculation of the mean where several samples were taken from the same stratigraphic unit. With regard to the individual errors in ages of the sediments below the 'Finow-soil' it is difficult to ascribe the deposition of the sediments, representing the substrate for the soil development, to a particular Lateglacial event. Within errors, the whole time span including GS-2a until GI-1a-c, and thus from the Oldest Dryas until the Allerød inclusive, seems probable, although a concentration of the mean OSL ages in the Oldest Dryas and Bølling periods is noticeable in Fig. 95.

The ongoing aeolian activity in the first part of the Greenland interstadial 1 is remarkable, because according to the climatic conditions and the development of the vegetation a decrease in aeolian activity could be expected around 14.7 ka. At this point in time the GRIP ice-core record indicates a rapid climatic amelioration (see Fig. 93). From atmospheric general circulation model simulations, a substantial decrease in the storm activity over northwestern Europe is concluded for the transition from the GS-2a to the GI-1e at about 14.7 ka. This is explained by the northward shift of the Atlantic storm track. According to RENSSEN and BOGAART (2003) this could have caused a decrease in aeolian activity and might have contributed to a more stabilised landscape in the Greenland Interstadial GI-1e (14.05-14.70 ka). In the same period of time the so-called 'Hippophaë phase' is dated in northeastern Vorpommern (12,450-12,000 ¹⁴C yr BP, 14,750-14,000 cal. yr BP, DE KLERK et al. 2001). Compared with the open herbaceous vegetation cover in the preceding GS-2a cold episode, the *Hippophaë rhamnoides* shrubs that proliferated in the course of the climate amelioration formed large, dense stands. Although the vegetation remained open to some degree, erosion was reduced by a more effective stabilisation of the surface afforded by the extensive root system of *Hippophaë rhamnoides* shrubs. However, with respect to the continuation of aeolian deposition observed in the OSL record it appears that deflation did not cease but may have been restricted to still exposed parts of the land surface.

Ongoing dune formation in the first part of the Greenland Interstadial 1 in the study area is in good agreement with observations from other parts of the European Sand Belt. KASSE (1999) summarises evidence of continued aeolian sedimentation during the Bølling interstadial although with decreased intensity. Organic material or soils of Bølling age are rare throughout the European Sand Belt, in particular compared to the widespread occurrence of the Allerød soils (Usselo- or Finow-horizon). According to OSL results presented by VAN HUISSTEDEN et al. (2001) sand transport and accumulation still occurred in The Netherlands even when the climate ameliorated during the Bølling. The continuation of aeolian transport and deposition is attributed to the slow colonisation of the nutrient-poor sands by plants, so that stabilisation of the surfaces was delayed. Similar conditions are indicated in the study area.

The short-lived cooling event GI-1d (Older Dryas) was not recorded in the OSL-based account by a marked increase in dune sand deposition. Of course a precise correlation of the luminescence dates with a cooling event of only 100-150 years duration is beyond the resolution of OSL chronologies. But if aeolian activity was substantially enhanced again in the Older Dryas at least a noticeable cluster of OSL ages within this time span could be

expected. That such data are lacking is interpreted as evidence for only little sand accumulation in the Older Dryas.

This conclusion is in accord with the reconstruction of the vegetation cover throughout the study area. A substantial opening of the vegetation cover which is necessary to allow significant sand transport was only recognised in pollen profiles from northeastern Vorpommern where dwarf-shrubs (betula species), herbs and only incidental growth of trees dominated the vegetation cover (DE KLERK et al. 2001, 'Open vegetation phase II', 14,00-13,90 ka cal. BP, see Fig. 94). But DE KLERK and STOLZE (2002) pointed out that this 'Open vegetation phase II' is lacking or hardly detectable in pollen profiles investigated further south in S-Mecklenburg, N-Brandenburg and the vicinity of Berlin (see also BRANDE 1980, BRANDE & BÖSE 1990, both in BÖSE 1991). DE KLERK and STOLZE (2002) attribute this observation of a denser vegetation cover in the south to a lesser temperature decline.

The conclusion which is drawn from the OSL record, with major dune formation during the Oldest Dryas continuing into the Bølling warming and with only minor dune sand deposition in the Older Dryas, agrees with observations from the area in the vicinity of Berlin (BÖSE 1991).

By contrast, numerous studies from Poland describe the Older Dryas instead of the Oldest Dryas as the main period of dune formation (DYLIKOWA 1969, KOZARSKI et al. 1969, KOZARSKI 1978, 1990, NOWACZYK 1986, MANIKOWSKA 1991b, 1994). But as KASSE (1999, 2002) pointed out, this correlation lacks chronological constraints. In most instances dating of the dunes is based on the identification of the Allerød soil on top of the dunes. But this dates only the termination of dune formation by soil formation: the dune bodies could have been formed over a much longer time span than the Older Dryas (KASSE 2002). Correlations with organic layers dated into the Allerød for palynological reasons also seem to provide no conclusive evidence. TOBOLSKI and LITT (1994) discuss the confusion about the chronological position of the Lateglacial interstadials (Meiendorf, Bølling, Allerød) arising from the lack of reliable chronology which also concerns pollen profiles from Poland.

To conclude, a sound data base to provide reliable evidence for differences regarding the timing of the major period of dune formation in northeastern Germany and Poland is still missing. Thus any explanation of the differences by the presence of a climatic border along the River Oder (e.g. BÖSE 1991) must remain speculative. More luminescence studies which

focus on the event of dune formation independent of organic material could contribute valuable information further to clarify this controversy.

The OSL results obtained for northeastern Germany and northwestern Poland indicating an onset of aeolian deposition around 16.7 ka and a first period of dune formation lasting, within errors of the OSL ages, from 15.2 until 13.7 ka are in agreement with luminescence dating studies carried out in the UK and The Netherlands which suggest aeolian deposition between 14-18 ka (BATEMAN 1995, BATEMAN & VAN HUISSTEDEN 1999, BATEMAN et al. 2000, BATEMAN & DIEZ HERRERO 2001, VAN HUISSTEDEN et al. 2001, VANDENBERGHE et al. 2004, VANDENBERGHE 2003).

According to KASSE (2002) the period between 18 and 14.0/14.7 ka represents the major period of sand-sheet formation throughout northwest and central Europe with the formation of high parabolic dunes towards the end of this phase in Poland.

A further valuable contribution to the aeolian record of the study area is provided by OSL ages obtained for the 'Ueckermünder Heide` area. Within the errors of the OSL ages the onset of aeolian activity most likely dates back to the end of the Oldest Dryas at about 14.67±0.84 ka, 15.44±1.15 ka, and 14.66±0.68 ka (see sites UM-A, -B, and –C in Fig. 92). If reliable, these dates would represent the oldest, directly dated evidence for aeolian activity in Mecklenburg-Vorpommern. So far Lateglacial aeolian processes are documented by sand filled ice wedges. But the date of the sand filling remains unclear; attempts to date it by means of luminescence techniques have failed so far (HELBIG 1999). However, similar studies were successful in adjacent areas in northwestern Poland (BÖSE 2000) and further research should take up this topic again. According to TERBERGER et al. (2004) there are only indications for locally restricted aeolian activity during the Older Dryas. Chronological control to support the reliability of the OSL ages is only provided at site 'UM-A' were the oldest aeolian sediments underlie the 'Finow-soil' horizon. But altogether the onset of aeolian processes in the 'Ueckermünder Heide' is in reasonable agreement with the reconstruction of the landscape history which so far is predominantly based on the summary of radiocarbon data sets from the Pomeranian Bay and Mecklenburg-Vorpommern by GÖRSDORF and KAISER (2001). According to this study the area is assumed to be ice-free after the re-melting of the Mecklenburg Advance at c. 14 ka ^{14}C BP or 17.3-16.3 ka cal. BP. The phase of the ice-dammed lake in the basin ('Haffstausee') is assumed to last until 15.2 ka cal. BP (KAISER et al. 2003). The OSL ages of some 14.7 and 15.4 ka thus indicate the onset of aeolian

reworking of the widespread glaciofluvial-glaciolimnic deposits soon after the dessication. This observation seems to hold true for the sites at the outer margin of the lake basin, 'UM-A' and 'UM-B', but at site 'UM-D', which is located further towards the former centre of the lake, these early aeolian deposits were not found. Most likely in lower lying areas dessication was delayed; here the Allerød soil directly developed in the glaciofluvial/glaciolimnic deposits.

5.2.1.1.3 *The late-Lateglacial period of dune formation and reactivation*

The prominent peak in Fig. 91 about 12.3 ka represents the cluster of OSL ages dated to a period of aeolian activity and dune formation at the end of the Lateglacial. It is documented at most sites investigated in this study. Up to 5 m of sand was deposited at some sites. Considering the mean of all OSL dates belonging to this unit, and its standard deviation, the period of dune formation is dated to 11.05 to 12.87 ka. Therefore, a correlation of this marked increase of aeolian activity with changes in climate towards cold, stadial conditions during the GS-1 (11.50-12.65 ka) is apparent (see Fig. 93 and Fig. 94).

Both the onset and the termination of Greenland stadial 1 are characterised by the rapidity and amplitude of climatic change. A severe cooling of 15° C in only 150 years was reconstructed for the onset of the GS-1 event (JOHNSEN et al. 1995). The termination of this cooling event was characterised by a rapid warming of ~10° C within a decade (ALLEY et al. 1993). In varve chronologies, e.g. from northwestern Germany, the time of transition was also determined to last only 10 to 20 years (MERKT & MÜLLER 1999, see also LITT et al. 2003). This observation underlines the rapidity of this climate amelioration also in the continental parts of the North Atlantic region.

The reaction of the aeolian system on this last severe cooling event at the end of the Last Glacial is of special importance in view of the suitability of aeolian sediment records as proxy for palaeoclimate conditions. The drastic and rapid change had marked effect on the landscape, but in addition, the onset of Holocene warming led to the development of a denser vegetation cover and thus the preservation of the aeolian record.

In Fig. 94 it is clearly seen that the onset and termination of aeolian deposition do not strictly coincide with the chronological boundaries of the GS-1 event. According to the mean value and the standard deviation of all OSL ages identified as belonging to this late phase of

Lateglacial dune formation, this period lasted from 11.05 to 12.87 ka. The question arises whether the disagreement in timing is merely caused by the lack of precision of OSL dates or whether in fact aeolian activity had already commenced in the Late Allerød period and was still in train in Early Preboreal times.

Regarding the timing of the onset of dune formation after the Allerød period of dune stabilisation and soil formation, special focus is placed on those sites where the Allerød palaeosol horizon is preserved. Taking into account the uncertainties in luminescence dating a trend towards the burial of the soil horizon by dune sand already at the Allerød/Younger Dryas transition is indicated at numerous sites (Fig. 95).

It seems unlikely that an early onset of aeolian activity is linked to the GI-1b cooling event dated to 13.15-12.90 ka. A temperature decline of 7.5° C was deduced for this short-lived event, which is also recognised in European lake sediments and is widely known as so-called 'Gerzensee oscillation' (JOHNSEN et al. 1995, BJÖRCK et al. 1996, MERKT & MÜLLER 1999). But it had no major impact on the forest vegetation that was present at that time (KASSE 1999). Only a very slight decrease in vegetation cover is indicated by pollen profiles from northeastern Vorpommern. No evidence was found for increased erosion (DE KLERK et al. 2001).

As volcanic activity is considered to be an important cause of past climatic change, the effect of the explosive eruption of the Laacher See volcano, which occurred ~12,880 years ago about 40 km S of Bonn in the East Eifel volcanic region in western Germany, ought to be entertained. The dust thrown into the atmosphere from volcanic eruptions causes a back-scattering of incoming long-wave radiation that may cool the global temperature by 0.2-0.3° C for several years after the eruption (e.g. ZIELINSKI 2000, in NESJE & DAHL 2001). The effects of sulphuric acid aerosols can be significant following major eruptions. But it is certain that the Laacher See eruption did not induce the Younger Dryas. The mean residence time for the aerosols is calculated to vary between only one and five years (SCHÖNWIESE 1988, in LOWE & WALKER 1997) and the onset of the Younger Dryas cooling is dated to c. 200 varve years after the eruption (BRAUER et al. 1999, MERKT & MÜLLER 1999, LITT et al. 2001).

However, based on comparisons with recent eruptions, LITT et al. (2003) argue that the Laacher See eruption had a major impact on climate in central Europe. Increased precipitation, destruction of the vegetation cover for several years because of ash fall and acid

rain, and reduction of solar radiation causing a lowering of the temperature, are linked to it. Yet evidence for even a short-term effect on vegetation and landscape in the study area is lacking. Palynological studies from Mecklenburg-Vorpommern indicate scarcely any change in the terrestrial vegetation after the eruption. This suggests that the climatic impact of the eruption was too small to cause substantial changes in the vegetation cover in northeastern Germany (THEUERKAUF 2003). Thus the Laacher See eruption at 12.88 ka is not related to the early onset of aeolian processes at the Allerød/Younger Dryas transition.

To conclude, sound evidence for substantial opening of the Allerød forests, which allowed for aeolian processes to take place already during this interstadial period, is lacking. Therefore the inconsistency of the OSL record with the timing of the Allerød/Younger Dryas boundary is solely ascribed to the lack of precision of the OSL dates.

In the cold period of the Younger Dryas the presence of seasonally frozen ground or permafrost conditions, respectively (HELBIG 1999, RENSSEN & VANDENBERGHE 2003), changing river patterns and the diminution of the vegetation cover resulted in a period of renewed aeolian activity with the formation of dunes, sand sheets and substantial remodelling of already existing dunes.

Various proxy records show evidence of an increased aridity during the late Younger Dryas; these include palaeoglacier data, stable isotope records, pollen profiles with an increase in steppe plants, falling lake levels, and the change in the discharge system of rivers (LOWE & WALKER 1997 and ref. therein). The latter was also reconstructed, for example, in central Germany with multi-channel braided rivers typical in the first half of the Younger Dryas and meandering rivers in the later, drier part (ANDRES et al. 2001, LITT et al. 2003). Because of the incision of the rivers in the second half of the Younger Dryas the river banks dried out and so provided an ample supply for aeolian transport and dune formation towards the end of this cooler period. In consequence, enhanced aeolian activity and dune formation is usually related to the second, more arid half of the Younger Dryas (e.g. VANDENBERGHE 1991, KASSE 1999).

But, KASSE (2002) mentions the possibility that aeolian deposition occurred during the whole Younger Dryas and the overall dating of aeolian deposits to the second half of this cold period is an artefact of radiocarbon chronologies caused by ^{14}C plateaus present at the transition of the Younger Dryas to the Preboreal. Many luminescence dates from the UK date aeolian deposition between 13-11 ka and hence would indicate a longer period of dune formation

rather than the restriction to the Late Younger Dryas (BATEMAN 1995, 1998, BATEMAN et al. 2000).

No marked increase in aeolian activity, particularly in the Late Younger Dryas, is clearly documented in the OSL data set presented in this study. Indeed, the opposite seems to be indicated by the OSL ages (see Fig. 94). At the sites where the Allerød 'Finow soil' was exposed the OSL ages for the overlying dune sands suggest that dune formation had already commenced by the beginning of the Younger Dryas (Fig. 95). This observation corroborates the reconstruction of the vegetation cover during the Greenland stadial 1, for DE KLERK et al. (2001) found evidence for an abrupt decrease in the vegetation cover at the onset of the 'Open Vegetation Phase III of NE Vorpommern' (13.00-11.45 ka cal. BP).

In general the vegetation cover of the Younger Dryas in the northern part of the study area (sites Altdarss, Ueckermünder Heide, Elbe 'urstromtal') is described as park tundra, comparable to the recent forest tundra in which the vegetation is dominated by herbs, grasses, and shrubs as well as scattered trees or groups of trees at favourable sites (USINGER 2004, DE KLERK et al. 2001). In the southern parts of northeast Germany and adjacent parts in Poland (study sites in the Toruń-Eberswalde urstromtal, Głogów-Baruth urstromtal) the typical vegetation type was open pine forest (USINGER 2004, TOBOLOSKI & LITT 1994). This park-tundra-like vegetation was characterised by substantial stands of trees which dominate even the open vegetation areas. The estimation of the density of the tree stands remains difficult; therefore the term parkland rather than open forest might be preferable (USINGER 2004). An altogether denser vegetation cover has been reconstructed for southern parts of the study area (S-Mecklenburg, Berlin, Brandenburg) resulting in a more stable surface and less intense erosion (USINGER 2004, DE KLERK & STOLZE 2002). But the observation of massive, up to 5 m thick dune sand units deposited during the Younger Dryas, for example, at sites 'Glashütte' and 'Jasień-C' in the Głogów-Baruth urstromtal, provide evidence for enhanced aeolian activity at least at some locations in the southern part of the study area.

Using model simulations based on aeolian records from the Netherlands and central Poland ISARIN et al. (1997) suggested that during the Younger Dryas in north-western and central Europe sand-transporting winds were predominantly from the west. The OSL dating of the parabolic dunes in northeastern Germany from the Younger Dryas is in accord with this model for dunes are open to the west and located east of the source areas.

Similar to the controversy discussion on the onset of dune formation in the Younger Dryas, the termination of aeolian processes at the Lateglacial/Holocene transition remains a matter of debate. Several authors have suggested that aeolian activity most probably extended into the Preboreal throughout northwestern and central Europe (e.g. PYRITZ 1972, KOZARSKI 1978, 1990, KOSTER 1982, SCHWAN 1991, KASSE et al. 1995, KASSE 2002, MANIKOWSKA 1991, 1994, ALISCH 1995, SCHLAAK 1997, RADTKE et al. 1998, BATEMAN et al. 1999, KOWALKOWSKI et al. 1999a), and clearly Early Holocene aeolian activity is evidenced at a few of the sites investigated in this study (see Fig. 92).

The question is whether the environmental conditions allowed a widespread and long-continued aeolian activity or whether only locally restricted and more sporadic aeolian activity took place through the Early Holocene. Also, renewed aeolian activity might result from the deterioration of climatic conditions during the 'PBO event', the Preboreal oscillation.

The termination of the GS-1 cooling event was characterised by a rapid warming of ~10° C within a decade (ALLEY et al. 1993). In varve chronologies, e.g. from northwestern Germany, the time of transition was also determined to last only 10 to 20 years (MERKT & MÜLLER 1999, see also LITT et al. 2003). GOSLAR et al. (1998) reconstructed a temperature increase of more than 5°C in less than 80 years at the Younger Dryas-Preboreal transition. These observations emphasise the rapidity of this climate amelioration also in the continental parts of the North Atlantic region.

The response of the vegetation cover to this dramatic change in climatic conditions was comparatively quick. In general, the warming at the beginning of the Holocene resulted in the replacement of the steppe-tundra or parkland vegetation of the Younger Dryas by woodland communities, notably more or less closed birch forest with pines (USINGER 2004). Thus it appears that the vegetation reacted to the Early Holocene warming without major time-lag (HOEK 2001, in DE KLERK 2004, USINGER 2004). Even in the northern part of the study area, where the maximum openness of the park tundra vegetation is documented for the end of the Younger Dryas, the vegetation closed over with the formation of dense forests of birch and pine, rapidly developed from isolated stands of trees which were already present in favoured sites (DE KLERK 2004). Records from Poland indicate that the closure of the vegetation cover lasted no longer than 30-80 years (GOSLAR et al. 1993, in DE KLERK 2004). Thus, the vegetation record would argue against continuation of aeolian processes, as the surface was

stabilised by closed and dense vegetation covers already at the beginning of the Preboreal. However, BORK and DALCHOW (2003) mention that in dune fields stabilisation of the sandy surface by forests occurred with delay, because the substrate was less fertile and comparatively dry (see also KASSE 2002, VAN HUISTEDDEN et al. (2001) present the same argument for ongoing dune formation at the transition from the Oldest Dryas to the Bølling period). But whether this explains the dune formation into the Preboreal, remains speculative.

The Early Holocene warming appears to have been non-linear. An interruption of the general temperature rise by a minor climatic setback during the Preboreal was first discovered in pollen records from the Northern German lowlands (BEHRE 1966, in USINGER 2004). Evidence from various other palaeoclimate proxy records (lake deposits, marine records, oxygen isotope records from ice-cores, tree-rings) confirm the widespread impact of this short-lived cooling event, the 'Preboreal oscillation' (PBO), in Europe (e.g. Greenland, Switzerland, The Netherlands, Germany, Poland, Norway, Sweden) (BEHRE 1978, BECKER et al. 1991, GOSLAR et al. 1995, BJÖRCK et al. 1996, 1997, LITT et al. 2003). Unfortunately, pollen records of that time are contradictory regarding the effect of this climatic setback (e.g. JOHNSEN et al. 1995, USINGER 2004).

The contribution of the present study to this discussion is rather limited. As shown in Fig. 92, at several sites aeolian deposition was dated to the Early Holocene. The most pronounced Preboreal aeolian activity was found at site 'Jasień-B'. Here the stabilisation of the dune surface by vegetation was delayed after the termination of the Younger Dryas because repeated fires decreased the vegetation cover. This interpretation is demonstrated by the alternation of dune sand layers with five charcoal-bearing and ^{14}C dated initial soils (KOWALKOWSKI et al. 1999a). Radiocarbon ages also support Preboreal aeolian deposition at site 'Finow'. For all other sites the extension of the probability density curves do not necessarily indicate Preboreal aeolian activity, but could just as well be attributed to a lack of precision of the OSL ages. Because of the average uncertainty of the OSL ages presented in this study of ± 8% the resolution which is necessary reliably to distinguish between samples dating into the late Younger Dryas or to the early Preboreal is lacking.

5.2.1.2 Influence of human beings on Lateglacial landscapes

Any impact of human beings on the onset of dune formation or reactivation of dunes towards the end of the Lateglacial seems unlikely. Numerous archaeological findings prove that the northern German lowlands were inhabited in the Lateglacial and Early Holocene by people who lived by hunting, gathering and fishing. As far as is known settlement in the northern lowlands started with the technocomplex of the 'Hamburgian' at the temperature rise at c. 12,600 cal yr BC (onset of Bølling/Meiendorf interstadial, GI-1e) (TERBERGER 2004, TERBERGER et al. 2004). Although many sites document the distribution of these predominantly reindeer hunters in northwest Germany and also farther to the east in southern Poland, no 'Hamburgian' sites have so far been discovered in northeastern Germany (see e.g. BREEST & VEIL 1991: 95, TERBERGER et al. 2004: 158). During the Allerød the elk-hunting 'Federmesser' groups inhabited the study area (see TERBERGER et al. 2004: 159). The correlation of technocomplexes with Lateglacial chronozones is not high, as overlap with the following early 'Ahrensburgian' has been recorded for the transition period to the Younger Dryas from various sites throughout the lowland areas of the Netherlands, Germany and Poland (e.g. TERBERGER 2004, DEEBEN 1995). The 'Ahrensburgian' is typically connected to the reindeer hunters living in the open landscape of the cold and dry Younger Dryas (see site map in TERBERGER et al. 2004: 161). But for the very harsh and dry phases the hunter-gatherer people of the 'Ahrensburgian' presumably moved southward and the northern lowlands were more or less abandoned for periods of time (TERBERGER 2004).

Archaeological evidence of Late Palaeolithic occupation is frequently found on elevated well-drained sand sheet ridges and dunes in places near water such as river valleys, and the shores of lakes (DEEBEN 1995, see also for example BOGEN et al. 2003 for the dune sites in the Ueckermünder Heide, KAYSER 1999 for the area near site 'Cottbus'). These findings underline the attraction of a landscape consisting of lakes, rivers, bogs and dunes for prehistoric man living by hunting, gathering and fishing. Nevertheless, the impact of Late Palaeolithic groups on the landscape is negligible, presumably because of the small number of people and their way of life. Estimations of the population density in pre-historic times are difficult. Based on what is known from ethnological studies on hunter-gatherer populations of inland areas over the world GRAMSCH (2004, and references therein) presents an estimate of the absolute population number of about 1,500 to 15,000 individuals in the northern German lowlands with an area of about 150,000 km². Thus, with 0.01 to 0.1 person/km² just a very few migrating groups can be imagined to have inhabited the area until Neolithic times. The

widespread dune formation and reactivation of regional extent throughout the Lateglacial and the beginning of the Holocene cannot be ascribed to such a small population.

5.2.2 Multiple events of dune reactivation in the Holocene

With the rapid warming at the beginning of the Holocene a termination of aeolian activity could be expected due to the rapid re-colonisation of the study area by trees and the formation of a closed deciduous forest (e.g. LANG 1994). This led to intensified soil formation that generally protected sandy surfaces from deflation. But to the contrary the OSL record of dune sand deposition shows dune activity continuing throughout the Holocene as indicated by peaks in the OSL record at about 9 ka, 6.3 ka, 4.5 ka, 3.5 ka, 2.6 ka, 300 AD, 1100 AD, 1300 AD, and 1700 AD (see Fig. 91 c).

With the refining of the resolution of palaeoclimate proxy records (ice-core, marine cores, varve records) the former picture of a quite stable Holocene climate had to be re-drawn (Fig. 96). Several climate oscillations, millennial-scale or shorter cooling events are recorded during the Holocene. Although these climate fluctuations have not proved to have a global or even hemispherical synchronicity, they were highly significant at the regional scale (ZOLITSCHKA et al. 2003). Thus, the question arises whether Holocene dune reactivation can be linked to substantial disturbances of the dune-stabilising vegetation cover by climate oscillations.

5.2.2.1 Relevance of Holocene climate oscillations for dune remobilisation

The most pronounced climatic events throughout the Holocene are (see Fig. 96):
- the '8,200 cal. BP' cooling event (e.g. BARBER et al. 1999, KLITGAARD-KRISTENSEN et al. 1998)
- the 'Atlantic Climate Optimum' (e.g. 9,000-5,500 cal. BP, LITT 2003; 8,000-6,000 cal. BP, ZOLITSCHKA et al. 2003)
- the 'Subatlantic Breakdown' (1st millennium BC, e.g. ZOLITSCHKA et al. 2003)
- the 'Medieval Warm Epoch' (~1000-1300 AD, BRADLEY 2000; 700-1350 AD, HASS 1999)
- the 'Little Ice Age' (1350-1900 AD, with the most prolonged cooling from ~1550-1750 AD, BRADLEY & JONES 1993, BRADLEY 2000, HASS 1999, MANN et al. 1999).

The '8,200 cal. yr BP' cooling event is linked to the catastrophic drainage of the glacial lakes Agassiz and Ojibway at c. 8,470 cal. yr BP causing a huge freshwater influx from the Hudson Strait into the North Atlantic (BARBER et al. 1999, KLITGAARD-KRISTENSEN et al. 1998). Most subsequent climate fluctuations are assumed to result from a complex system of forcing factors, such as changes in the solar activity, ocean-atmosphere-interactions, and volcanic activity (for a summary see e.g. LOWE and WALKER 1997).

Centennial-scale intervals of low solar activity were identified to coincide with major cooling events which, in turn, are related to cold water reaching further south in the North Atlantic (KROMER et al. 2005). Such cooling events are recorded by ice rafted debris (IRD) on the North Atlantic sea floor left behind from southward drifting ice bergs for certain times. During the last six millennia such IRD events were recognised at 5,800, 4,200, 2,800, and 1,450 cal. BP (Bond cycles, BOND et al. 1997).

The combination of the OSL record of dune activity with the record of Holocene climatic oscillations in Fig. 96 shows no obvious coincidence of aeolian activity with any particular climate oscillations. Peaks in the OSL dune record seem to predate, for example, the cooling event at '8,200 cal. BP' and the IRD events. On the other hand an onset of dune remobilisation coincides with the onset of the 'Medieval warm epoch'.

Holocene climate oscillations are not the dominant trigger for dune reactivation, for two reasons. First, even throughout the 'Little Ice Age', one of the coldest periods in the Holocene with a temperature decline of 0.5 to 1.5°C (RIND & OVERPECK, 1993, in LOWE & WALKER 1997), the cooling was far from being as severe as during the Younger Dryas with a cooling of 15°C in 150 years (JOHNSEN et al. 1995). Thus, a substantial decrease in the vegetation cover allowing enhanced deflation of the bare dune surfaces, such as occurred in the Lateglacial stadial situation, cannot be expected in the Holocene.

Second, and the more convincing argument against climate as a major driving factor for dune reactivation is derived from Fig. 92. The sharp contrast between the character of Holocene aeolian activity compared to the Lateglacial phases of dune formation and remobilisation becomes obvious. While dune sand deposition, for example, during the Younger Dryas was recorded at nearly all study sites, each Holocene peak or 'aeolian event' is represented by a few sites, sometimes even by one site only. None of the Holocene events is documented in all five study areas. No event affects all sites of the same study area. This lack of synchronicity in

the temporal and spatial distribution of Holocene dune activity clearly argues against climate as the main trigger for dune reactivation, but points to localised human impacts such as vegetation clearance. Human beings developed mastery of their environment throughout the Holocene with an increasing pressure on the landscape resulting from a growing population.

Fig. 96: OSL record of Holocene dune reactivation.
Comparison of various Holocene climatic events (after various authors, see references in the text), periods of settlement with increased human impact or decrease (in particular indicated by grey boxes, timing of the periods as discussed in the text after various authors), and the aeolian record according to OSL ages of this study. Each black symbol represents an individual OSL age or the average age of several OSL dates from the same sand unit. The total number of samples contributing to this graph is 44. The ages are shown as probability density function.
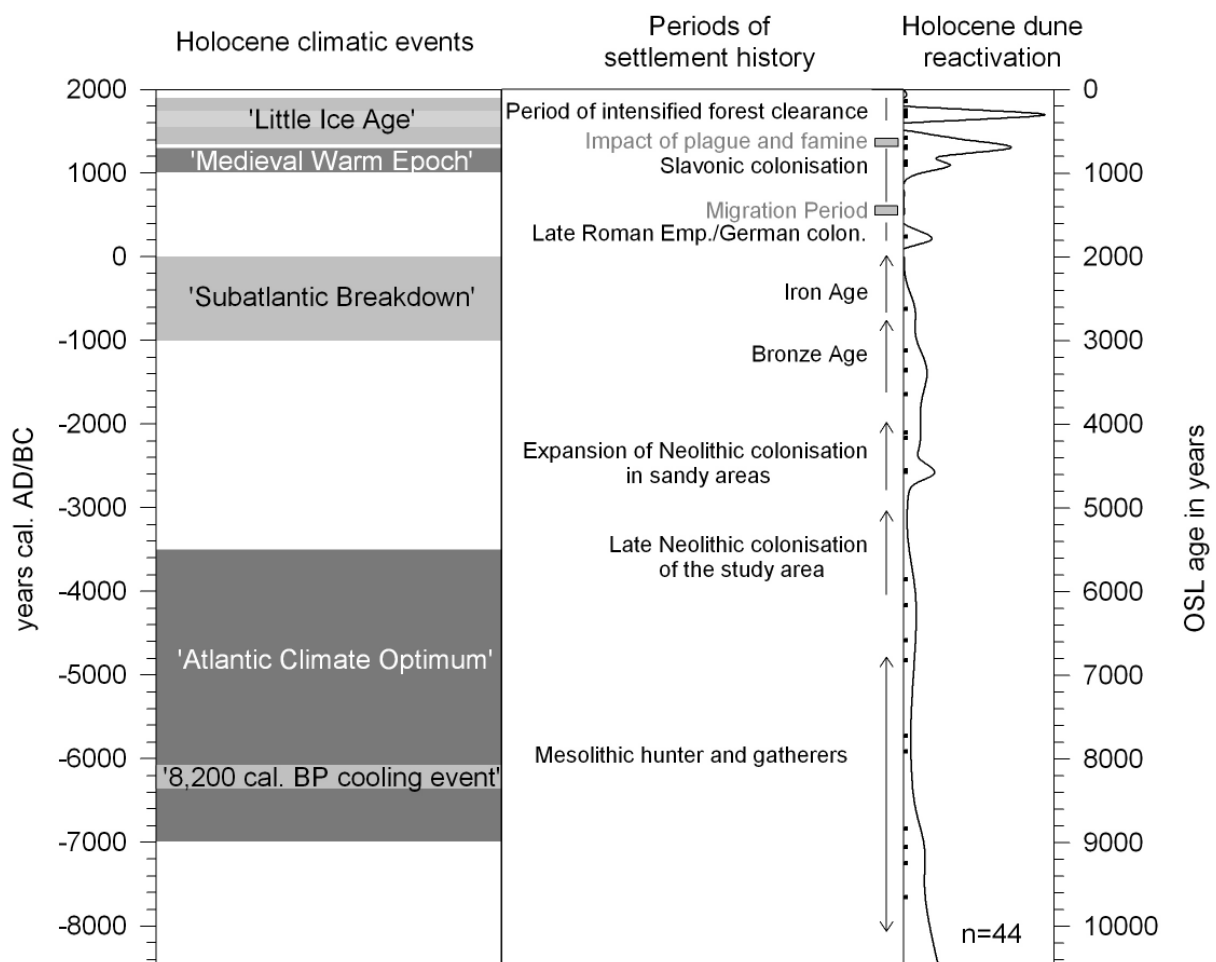
Yet climate fluctuations may indirectly have influenced the efficacy of Holocene aeolian processes. Changes in climatic conditions may have compelled people to intensify exploitation of their environment or to abandon a settlement area (concerning this relation see discussion in the next section).

Furthermore, certain climatic conditions may have favoured reactivation of aeolian processes. For example an increased risk of forest fires especially during prolonged periods of drought can be deduced from actual observations. With the disturbance of the vegetation cover aeolian processes would be enhanced after a fire.

FILION et al. (1991), for example, interpret peaks of Late Holocene dune activity in northern boreal forest areas in northern Québec, Canada, as a response to increased forest fire occurrence under cold and dry conditions which were disadvantageous for tree regeneration and conducive to sustained post-fire erosion.

5.2.2.2 Relation between human impact and dune reactivation in the Holocene

The scope of the following section is to investigate the occurrence of the various peaks in Holocene aeolian activity in the context of the settlement history of the study area. If obvious relations are found conclusions on the potential of the OSL record of dune remobilisation as a record of variations in human impact on the environment may be drawn.

5.2.2.2.1   9 ka peak

The summary graph in Fig. 91 indicates reactivation of aeolian deposition with a small peak at about 9 ka. But in contrast to the widespread aeolian activity during the stadial conditions in the Younger Dryas period, dune reactivation in the Early Holocene between about 10.5 and 7.5 ka is recorded at only five sites (see Fig. 92, sites STA, G, C, F, UM-B). Except for the 'Altdarss' study area dune sand deposition occurred in all study areas, although mostly only at one site. While at sites 'Glashütte', 'Cottbus' and 'Ueckermünde-B' the reactivation of aeolian activity is represented by only one unsupported OSL date, at site 'Schletau' the OSL results are in good agreement with independent chronological control provided by Mesolithic artefacts and radiocarbon ages (BREEST & VEIL 2001). The validity of the two OSL dates

from site 'Finow-B' finds support in palynological results. The sediments dated by OSL encompass a Preboreal soil horizon (SCHLAAK 1993).

During the Holocene the dominant vegetation association in the study area was of closed temperate deciduous mixed forests (LANG 1994). Thus, dune sand mobilisation in the time span between about 10.5 and 7.5 ka was possible only after substantial opening of the vegetation cover. From the local character of the dune remobilisation in this time-slice it is concluded that the short-lived '8,200 cal. yr BP cooling event' was not strong enough to result in a substantial opening of the forest cover. Archives such as lake sediments show constant environments with soils being stabilised due to an undisturbed vegetation cover during the time span concerned (e.g. KALIS et al. 2003, LITT 2003). Pollen records also yield no evidence for substantial opening (e.g. KAISER et al. 2001).

During the Mid-Holocene 'Atlantic Climate Optimum' from about 9,000 to 5,500 cal. BP (LITT 2003) temperatures were possibly slightly higher than at present (KALIS et al. 2003, ZOLITSCHKA et al. 2003). Low lake levels are interpreted as evidence for a decrease in precipitation until about 7,500 cal. BP when an increase in rainfall is indicated by higher lake levels. Whether fires could be generated more frequently in prolonged periods of drought remains speculative. However, opening of the forest cover by fires whether induced by lightning or other reasons would explain the locally restricted occurrence of dune remobilisation as observed in the study area.

Forest fires lit by human beings whether by chance or with intention (hunting) cannot be ruled out. But any of the impact of the hunter and gatherer communities of that time on the landscape is considered negligible. Mesolithic groups, who occupied the whole study area since the Preboreal (see e.g. GRAMSCH 2004), lived in harmony with their environment, their movements and exploitation of natural resources governed by seasonal rhythms. According to ethnological and archaeological data Mesolithic groups consisted of only 15 to 50 people. They migrated through a more-or-less well defined territory of 20 to 200 km diameter. Their resident time at a camp site was restricted to a few days or, at most, a few months (WENIGER 1991, GAMBLE 1996, ZALIZNYAK 1995, all cit. in STAPEL 1999). Based on these facts deleterious impact of Mesolithic people on their environment was negligible. But Mesolithic hunther and gatherer groups favoured dunes near rivers or lakes as campsites, where they were close to open waters but protected from floods. They tended to revisit former camps (KAYSER 1999, STAPEL 1999). These temporary periods of occupation could lead to

disturbance of the protecting vegetation cover at the dune surface and eventually result in a local reactivation of aeolian processes (see for example the incidence of dune sand deposition with Mesolithic artefacts at the top of the dune site 'Schletau'). ALISCH (1995) came to a similar conclusion for inland dune and coversand areas in Lower Saxony, where the onset of Holocene sand transport could be dated back to at least the Mid-Atlantic on the basis of Mesolithic artefacts and radiocarbon ages.

5.2.2.2.2   6.3 ka

The summary graph in Fig. 91 shows a peak centred around 6.3 ka. According to the regional subsets presented in Fig. 92 this cluster in OSL ages is caused by sand deposition at sites 'Schletau', 'Glashütte', 'Cottbus' and 'Jasień-A'. At site 'Schletau' independent age control supports the reliability of the OSL result. Here the age of 6.58±0.56 ka is in excellent agreement with ^{14}C results from burned nutshells embedded in the underlying sediments, together with a high concentration of Mesolithic artefacts. The ages at sites 'Glashütte' and 'Jasień-A' should not be overrated, as they might underestimate the true depositional age due to intermixed younger material. But both ages are still chronostratigraphically consistent with the over- and underlying deposits. Furthermore, the young age obtained at 'Glashütte' (6.82±0.50 ka) might be further supported by the results obtained by BARAY and ZÖLLER (1993) from the dune site 'Klein Ziescht' in the vicinity of site 'Glashütte'. There they dated dune sediments with embedded Meso- to Neolithic flint fragments (ca. 2 m below surface) to 6.2±0.7 ka. Within errors, the sample dated at site 'Glashütte' could perhaps represent the same phase of dune reactivation in Mid-Holocene possibly caused by human impact of Neolithic groups, as evidenced by Neolithic artefacts associated with the young dune deposits at site 'Klein Ziescht'.

Dune sand deposition at site 'Cottbus' dated to 5.85±0.43 ka seems likely to be linked to human occupation, for BITTMANN and PASDA (1999) present palynological data of human impact on the vegetation dating back to >4000 years cal. BP.

Summarising these observations, it might be concluded that the slight increase in aeolian activity with a peak at about 6.3 ka was the result of an opening of the vegetation cover due to the impact of the Neolithic settlers. But would this interpretation fit into the archaeological record of the study area?

The Neolithic colonisation represents the phase when humans increasingly established mastery of their environment. Forest clearance to create arable fields and settlements, and the use of forests for woodland pasture and as resource for building material and fuel are considered as a major impact on the environment (BARRETT 1999, KALIS et al. 2003). But the period of the Early and Middle Neolithic has to be distinguished from the period of the Late Neolithic with respect to human impact. Early Neolithic groups are described as inhabiting the landscape in small dispersed communities who practised a diverse and regionally varied suite of activities. Small scale cultivation was just one element in their subsistence base which included the collection of fruits and roots and husbandry of livestock (EDMONDS 1999). Thus, the life of Early and Middle Neolithic (7500-6300 cal. BP) people is still characterised by adaptation to the forest ecosystem. With a minimum of forest clearing it had only a minor influence on the landscape (KALIS et al. 2003, LANG 1994). For the Early Neolithic 'band pottery' settlements, for example, KACZANOWSKI and KOZŁOWSKI (1998, in ZYGMUNT 2004) assume a population of 20 to 100 people which would require forest clearance of ~10 to 50 hectares in order to feed the people.

Thus, dune reactivation due to an increased impact by Neolithic people could be expected in the Late Neolithic rather than Early Neolithic times. But the crucial question is, when did Neolithic settlers arrive in the study area? In general the Neolithic colonisation of the less fertile areas north of the loess belt in NW and Northern Europe was delayed (LANG 1994, KALIS et al. 2003). According to the archaeological record the so-called Early Neolithic 'band pottery' people from southeastern Europe occupied the German and Polish loess regions providing fertile soils for farming not before 7,500 cal. BP (LANG 1994, KACZANOWSKI & KOZŁOWSKI 1998 cit. in ZYGMUNT 2004, ZOLITSCHKA et al. 2003). Within the study area signs of Neolithic man are found only in more fertile Young morainic areas and even then the occupation comprised only isolated settlements (e.g in the Uckermark in northeastern Germany or in northwestern Poland in the 'Pyritzer Weizacker', e.g. KIRSCH 1994, WECHLER 1993).

In areas with less fertile, sandy soils such as represented by the study areas within ice-marginal valleys, the Mesolithic way of life, hunting and gathering continued. According to WECHLER (1993), in Brandenburg and Mecklenburg-Vorpommern Neolithic farmers and Mesolithic hunter and gatherer communities coexisted for about 1800 years (5600-3800 cal. BC). At the end of this period about 4000 cal. BC the Late Neolithic culture complex of the 'Funnel Necked Beaker Culture' evolved most probably by acculturation of Late Mesolithic

groups inhabiting the area before. So far no conclusive explanation has been given for this more or less abrupt cultural upheaval, but it resulted in a widespread expansion of the Neolithic economic area in Mecklenburg-Vorpommern, Brandenburg and Poland (WECHLER 1993, KIRSCH 1994). While areas providing more fertile, loamy soils were favoured for settlement (KIRSCH 1994), the less fertile sand-rich areas were occupied towards the end of the Neolithic period in northeastern Germany (e.g. GRINGMUTH-DALLMER 1999, HERKING 2004). The increase of human impact on the landscape recognised in pollen records is commonly associated with this colonisation of the Late Neolithic 'Funnel Beaker' people (LANG 1994).

Dated about 6.3 ka, or 4300 BC on average, the dune reactivation observed in the OSL record would predate the occupation of sandy plains by people of the 'Funnel Necked Beaker Culture' assumed to mark the End Neolithic time. In this context the distribution of the study sites showing this Mid-Holocene dune remobilisation is remarkable. The only sites affected are located closest to the loess regions in the south. At that time the loess belt had been occupied by 'band pottery' people for more than 1000 years. These Early Neolithic settlers are known to settle on fertile soils and in general would avoid the sandy plains in the ice-marginal valleys. But there are exceptions. Thus several settlement sites of the so-called 'Stichbandkeramik' period are found on the sand dunes of the upper Spree River, near Uhyst about 70 km south of the site 'Cottbus'. This has been explained as reflecting a northward migration of Neolithic people from the loess areas (KIRSCH 1994, ^{14}C age of charcoal from this site 4660-4460 cal. BC, Bln-3686, in WECHLER 1993). Even so, the reasons for dune reactivation about 6.3 ka at the dune sites investigated in this study remain a matter of speculation, although human impact appeals as a possible explanation.

5.2.2.2.3   4.5 ka

The OSL record of dune sand deposition shows a drop in activity around 5 ka and increases again up to the peak about 4.5 ka. Dune remobilisation at that time occurred according to the OSL dates at four sites, 'Schletau', 'Neuhaus', 'Finow-B', and' Ueckermünde-C', which are located in three different study areas (see Fig. 92). At site 'Finow-B' the agreement of the OSL age with independent age control provided by ^{14}C ages (charcoal) supports the reliability of the OSL chronology. At site 'Neuhaus' this young sand layer covers a well developed podzol indicating the onset of aeolian activity after a long period of dune stabilisation. At

'Schletau' the two ages of about 4.6 ka are in good agreement with the chronostratigraphy which is further supported by ^{14}C ages in lower parts of the section. For coversand areas and dune fields in adjacent areas of 'Neuhaus' and 'Schletau' the onset of deforestation by Late Neolithic people is dated to about 4.5-5 ka BP. It eventually resulted in an almost complete removal of the forest cover until the Late Bronze Age (CASPERS & SCHWARZ 1998).

Altogether this recent dune reactivation documented in the OSL record of dune deposits could be interpreted as result of intensified human impact. Indeed the occupation also of sandy areas such as dune fields close to rivers and lakes by Late and End Neolithic groups (2800 to 2200 BC) has been described for example for northeastern Germany by JACOBS (1991 in GRINGMUTH-DALLMER 1999). By the end of the Neolithic farming had reached all regions of central Europe. With the growth of the population the expansion in less fertile areas seems reasonable. The resulting increase of human impact in Late Neolithic times is much more clearly seen in pollen records and other archives, such as increased soil erosion, than man-made changes in the vegetation cover earlier (KALIS et al. 2003, LITT 2003).

5.2.2.2.4   3.5 ka

The increased aeolian activity continued during the 2nd millenium BC with a peak about 3500 years ago (Fig. 91 & Fig. 96). This dune reactivation is recorded at sites 'Finow-B', 'Finow-C', and 'Spechthausen' in the Toruń-Eberswalde ice-marginal valley and also at site 'Altdarss-4'. At site 'Finow-B' the OSL age is in agreement with the ^{14}C age of charcoal from sand layers below the OSL sampling position. At site 'Spechthausen' the sand layer dated to the Late Holocene directly covers a well-developed podzol, thus such a young age is in accordance with the expectation from field observations. Altogether the OSL ages obtained at site 'Spechthausen' (3.36±0.30 ka) and the sites 'Finow-B' (3.12±0.31 ka) and 'Finow-C' (3.64±0.28 ka) are in good agreement and may indeed represent one major phase of dune reactivation in the area. This is most probably related to increased human activities such as forest clearance by fires as indicated by an increased amount of charcoal fragments in the upper part of site 'Finow-B'. If the reactivation of aeolian processes at site 'Altdarss-4' might also be related to human impact is questionable, for the onset of strong human impact on this landscape dates into the 13th-14th century AD (KAISER et al. 2006).

The remobilisation of dunes about 3,500 years ago dates into the period of the Bronze Age (1.7-0.7 ka BC). From the archaeological record a growth of the population is reconstructed which resulted in increased human impact on the landscape. This growing pressure on the environment is documented by an increase of erosion (BORK & DALCHOW 2003) as a consequence of substantial opening of the forests as recorded in pollen records of that time (e.g. HERKING 2004, LANG 1994).

While the Neolithic colonisation started in regions with the most fertile soils, the growth of the population led to the expansion of human exploitation of areas with more fragile soils during the Bronze Age (BARRETT 1999). According to GRINGMUTH-DALLMER (1999) the Early Bronze Age may be characterised by settlements on isolated sand areas surrounded by areas with more fertile loamy soils such as till plains (1800-1100 BC), whereas the Late Bronze age increasingly shows sites located in areas with sandy soils, indicating an avoidance of loamy soils. The area of the Eberswalde ice-marginal valley with its numerous adjacent patches of till in the North and the Barnim till plain in the South thus would represent a preferable settlement area for the Early Bronze Age people.

The record of dune remobilisation in the Eberswalde area is in accord with the archaeological record concerning the impact of man on the environment. Yet it is remarkable that the Bronze Age expansion into sand-dominated areas is not widely evidenced at other sites in the study area. In particular, numerous archaeological sites discovered in the 'Niederlausitz' near sites 'Cottbus' and 'Jänschwalde' provide evidence for a significant impact of Bronze Age people on the landscape (the so-called 'Lusatian culture', 15th - 4th century BC, see e.g. BÖNISCH 1999). This observation underlines the problems related to the documentation of human-triggered dune reactivation. Because of its regional impact climate-induced dune activity is highly probable, though not necessarily recorded at numerous sites, whereas reactivation of dune activity caused by human impact is recorded more or less by chance, because this is strictly a local impact and not a regional parameter.

5.2.2.2.5   2.6 ka

The OSL record shown in Fig. 91 c) shows no steady decline after the peak at c. 3.5 ka, but a small shoulder is indicated at about 2.6 ka (see also Fig. 96). From Fig. 92 it becomes clear, that only a single OSL age was dated into this time-slice at site 'Schletau' in the Elbe

urstromtal. Here, a 2.62±0.20 ka dune sand remobilisation dates from the Early Iron Age which commenced about 700 BC (e.g. LANG 1994). By this time the formerly closed forests in the area had already been replaced by heath land in the course of intensive deforestation during the preceding Bronze Age (HEINEMANN in BREEST & VEIL 2001).

Overall the luminescence record does not indicate a widespread phase of dune reactivation during the Iron Age, although the comparably open landscape during the Early Iron Age with a forest cover of about 50 % (SCHMIDT & BORK 1999) might have favoured remobilisation of unprotected dune sand in deforested areas. Commonly the Iron Age in Europe was marked by an increase in population and human impact on the natural vegetation (LANG 1994) which is also indicated in the Fig. 97. According to LUTZE (1995), for example, the valley of the River Finow (Eberswalde urstromtal) is known to be a preferred settlement area in the pre-Roman Iron Age (700 BC-0 BC/AD). But obviously this human occupation did not cause any substantial dune remobilisation at the sites investigated in this study.

On the other hand, large areas are known to be abandoned by about 500 BC in the Early Iron Age. A regeneration of the formerly opened forest cover could be deduced from pollen analyses, for example from NW Poland. Re-occupation of these abandoned areas started not before 400-250 BC in the pre-Roman Iron Age (GRINGMUTH-DALLMER 1999, HERKING 2004, LEWCZUK 2002 in HERKING 2004).

The decrease in population density and the human impact reported for the Early Iron Age is in accordance with the so-called 'Subatlantic climatic breakdown'. This change in climatic conditions towards cooler and more humid conditions occurred throughout the northern European lowlands at the transition from the Subboreal to the Subatlantic. Obviously this climate deterioration correlates with the IRD event at 2,800 cal. BP (BOND et al 1997, for a summary of further evidence, see e.g. ZOLITSCHKA et al. 2003).

This temporary decline in human impact of only a few centuries and the subsequent increase during the pre-Roman Iron Age obviously has not left a clear imprint in the OSL record of dune activity at the study sites. This observation again underlines the high variability of man-made dune remobilisation with regard to the probability of recording such events in the limited number of investigated sites. This is in sharp contrast to the widespread recorded climate-triggered dune activity of the Lateglacial.

Fig. 97: Anthropogenic indices in a pollen diagram from Skrzetuszewo in central Poland near Poznań, about 150 km NE of site 'Jasień'.

In column A the various cultural phases are shown: N=Neolithic, B=Bronze Age, E=Iron Age, R=Roman Empire, M=Medieval Ages, N=Modern times. In column B six several settlement periods are indicated. The black area represents cereal as primary indicator of human impact and the hatched area secondary indicators (modified from LANG 1994: 242 presenting data from TOBOLSKI 1990).
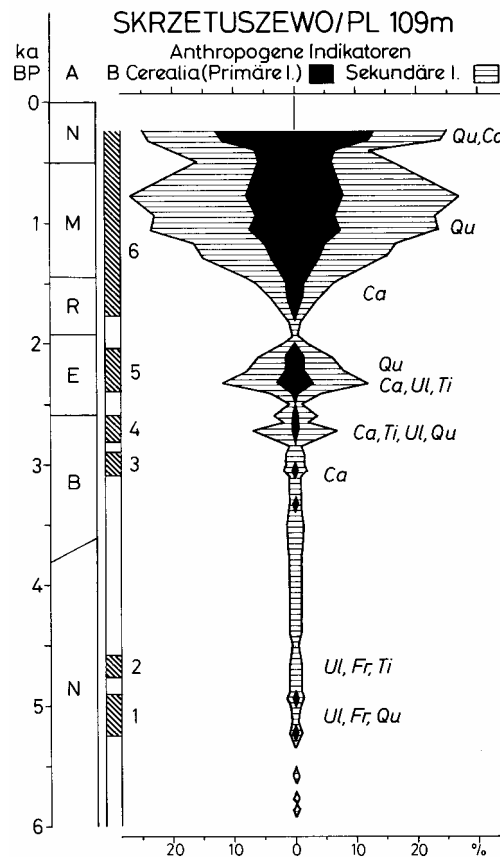
5.2.2.2.6   300 AD

The dune reactivation dated into the 3rd century AD is only recorded at site 'Jänschwalde' in the Głogów-Baruth urstromtal (see Fig. 92). Here a 4 m-high dune was formed in a short time at ~240 AD on top of a well-developed podzol soil, which formed the surface until the Bronze Age. This could be deduced from archaeological findings in the vicinity of site 'Jänschwalde'. Nearby, also in the 'Düringsheide', a large area with Bronze Age burials was discovered which was covered by dune sand several metres thick. With 1.76±0.05 ka the OSL age is in agreement with the assumed post-Bronze Age (< c. 3 ka) coverage of the podzol (RÖSLER 1999).

The massive sand accumulation at 'Jänschwalde' in the 3rd century AD thus is in accord with observations of dune activity from nearby dune sites in the Düringsheide, where the

accumulation of about 3 m of dune sand within a short period of time was dated to 260-425 cal. AD based on ^{14}C results (KRAUSKOPF & PASDA 1999). This dune reactivation is correlated with the German occupation of the area in the Late Roman Empire period between c. 250-400 AD. Intensive forest clearance is assumed for this period leaving behind large areas with sandy soil exposed to wind action. Deflation of the top soil was already a problem for the German settlers. This might be deduced from the discovery of a fence at one German settlement site in a dune area which is interpreted as protection against drift sand transport into the settlement (BRATHER 1999, KRAUSKOPF & PASDA 1999).

5.2.2.2.7   Break from 400-900 AD

A striking part of the aeolian record shown in Fig. 96 is the clear break in aeolian activity between 400 and 900 AD. This observation of landscape stabilisation is in good agreement with the pollen record, for example that shown in Fig. 97 also indicates a marked decline of anthropogenic influence on the vegetation in the first half of the 1st millenium AD. This accordance suggests a connection with the break-off in the settlement continuity because of movement of population between 400 and 600 AD known as the 'Migration period'. In abandoned areas villages deserted and open farmland reforested. SCHMIDT and BORK (1999) reconstructed a reforestation in northeastern Germany of 90 % during the Migration period. Numerous pollen records and pedological investigations (decrease in colluvial sedimentation, etc.) yield evidence for a stabilisation of the surfaces by a dense vegetation cover throughout northeastern Germany during the Migration Period and the early Medieval Ages (BORK et al. 1998). This widespread stabilisation explains the drop in the aeolian activity record.

Beside other reasons the deterioration of climate to colder and wetter conditions may have forced people to abandon the study area during the 'Migration Period' (LANG 1994, GRINGMUTH-DALLMER 1999, ZOLITSCHKA et al. 2003). This climatic deterioration is probably related to the cooling which is indicated by an IRD event in the North Atlantic at 1,450 cal. BP (500 AD, BOND et al. 1997).

5.2.2.2.8   1100 and 1300 AD

At about 1000 AD aeolian activity again becomes significant in the study area, showing peaks at about 1100 AD and in the first half of the 14th century before dunes stabilised again (see Fig. 96). During this period dune activity occurred in four of the five study areas at sites 'Schletau', 'Glashütte', 'Cottbus', 'Melchow' and at sites 'B' and 'C' in the 'Ueckermünder Heide' (Fig. 92). At all these sites the sand remobilisation is only documented by one OSL sample so that their reliability might be questionable. But all ages are in good agreement with the chronostratigraphy of the individual sites and they all passed the internal quality check for the OSL results. Furthermore, all the soils on top of the sediments sampled for OSL are at an early stage of development. Moreover, the observation of dune reactivation between 1100-1300 AD is in good agreement with a vast number of studies which also present evidence for widespread aeolian activity in the wider study area during the Medieval Ages (600/800-1500 AD) with a maximum observed during the 12th and 13th century (for example NOWEL et al. 1972, MAGALOWSKI & NOWEL 1982, BÖSE & BRANDE 1986, BARAY & ZÖLLER 1993, NOWACZYK 1993, SCHLAAK 1993, DE BOER 1995, PASDA 1999, KRAUSKOPF & PASDA 1999, BITTMANN & PASDA 1999, BÖSE et al. 2002). The Medieval reactivation of aeolian processes has also been reported from numerous other localities in northwestern Europe (e.g. CASTEL et al. 1989, KOSTER et al. 1993, ALISCH 1995, JANOTTA et al. 1997, RADTKE et al. 1998, FINK 2000).

This widespread recorded period of intensified dune remobilisation is explained by a period of deforestation which resulted from an explosion of the population in the study area. During the 6th-10th century AD the Early Slavonic settlers arrived and established new settlements. But forests still dominated the landscape during this early Medieval settlement period (LUTZE 1995, GRINGMUTH-DALLMER 1999). But the population increased rapidly; in the 10th century the number of people was already four times higher than in the 6th century (in HERKING 2004: 19). For the Young Slavonic period in the 11th to 13th century the archaeological record documents a considerable expansion of the settlements into areas previously not occupied. German colonisation since 1150 AD further intensified forest clearing because of the growing demand for new settlement areas, arable fields and wood for building and fuel (e.g. GRINGMUTH-DALLMER 1999). The enormous pressure on the landscape resulted in forest clearance in northeast Germany reducing the forest cover of 94 % at 650 AD to only 15 % 1310 AD (BORK et al. 1998). The extent of farming land which was made arable until the

early 14th century was not again attained until more recent times in Mecklenburg-Vorpommern and Brandenburg (SCHMIDT & BORK 1999).

The deforestation is also clearly shown in pollen records (for example HERKING 2004 for NW Poland) and by the increase of flood deposits related to the increased erosion from the cleared areas (e.g. SZMAŃDA et al. 2004).

Whether the climate amelioration during the 'Medieval Warm Epoch' (~1000-1300 AD, BRADLEY 2000; 700-1350 AD, HASS 1999) had a positive impact on the population growth is questionable. But it seems likely that prolonged drought episodes during this period (MANN et al. 1999, CROWLEY 2000) favoured deflation processes on the open areas of sandy soils. Occasional sand drift is still observed in the study area (e.g. LEMBKE 1939: drift sand accumulation of 1 m within one hour).

5.2.2.2.9   Break after 1350 AD

The termination of the period of medieval dune reactivation is indicated by the decline in the OSL record after the peak at about 1300-1350 AD as shown in Fig. 96. A stabilisation of the landscape might be deduced from this observation. This would correlate with a decrease in the human impact during the so-called 'Late medieval period of abandoned villages' lasting from second half of the 14th century and throughout the 15th century (BÖNISCH 1999).

In the 14th century the period of maximum medieval deforestation came to an abrupt end. In the first half of the 14th century several years with heavy rains, catastrophic floods and substantial erosion of the fertile soils resulted in famine. Together with the consequences of the outbreak of plague in 1348-1350 more than one third of the people living in northeastern Germany died. Vast areas were deserted. Villages were abandoned as well as the fields. Although they were still intensively used for grazing of livestock the forests could re-establish themselves (SCHMIDT & BORK 1999). The pollen record from Poland (Fig. 97) also shows a similar decrease in the human impact on vegetation.

The decline in population density and thus in human impact coincides with the deterioration of climatic conditions at the onset of the 'Little Ice Age' (LIA). Evidence not only from historical records, but also from tree-ring, marine and ice core data suggests that the initial onset of the LIA most likely dates back to around 1350 AD when climate deteriorated towards

the cool stormy first phase of the event. This first phase lasted until about 1550 AD and was characterised by longer and more severe winters compared with today and by an exceptionally high frequency of strong westerly winds (BRADLEY & JONES 1993, HASS 1999, MANN et al. 1999). This intensified storm activity does not find expression in increased dune remobilisation in the OSL age record of dune deposits. On the contrary, the lack of data suggests a period of dune stabilisation. This observation demonstrates the dominance of variations in the vegetation cover caused by human activities as the major controlling factor of dune activity in the Holocene compared to a direct impact of climatic fluctuations.

5.2.2.2.10 1600-1800 AD

The last reactivation of aeolian sand transport documented in the OSL record occurred between 1600 and 1800 AD. This activity is represented by dune deposits dated at sites 'Neuhaus', 'Jasień-A' and 'Finow'. The most pronounced dune remobilisation occurred at site 'Neuhaus' about 320 years ago (1680 AD) with c. 4.6 m of sand deposition in a short time. This result is in good agreement with observations from a dune site north of Stixe, located in the same dune field about 8.5 km south of the site 'Neuhaus', where CASPERS and SCHWARZ (1998) ascribe a similar very young dune remobilisation to the intensive forest clearings in the area.

The young OSL ages obtained at site 'Finow' are considered to be reliable, because both ages are entirely consistent with the ^{14}C age of the immediately underlying sandy peat layer. Furthermore, the initial state of the soil development on top of F1 argues a limited time span since deposition of its substrate. The same situation obtains at site 'Jasień-A'. The recent sand movement at site 'Finow' most probably results from intensified exploitation of the forests. Historical records prove that the forests were vastly exploited during the 17th and 18th century by forest pasturing and forest cropping to provide the expanding nearby capital city of Berlin with firewood and timber (LUTZE 1995).

This increase in human impact on the vegetation is recorded in various archives throughout the study area and adjacent regions. For example it is also seen in the pollen record from Poland shown in Fig. 97. In northwestern Germany deforestation resulted in drift sand deposition with a maximum between the 1610/1700 and 1850 (e.g. ALISCH 1995, CASTEL et al. 1989). A period of intensified soil erosion in the study area is observed for the late 17th

century and the 18th century following on the clearance of formerly abandoned fields from the 15th until the early 18th century (SCHMIDT & BORK 1999, BORK & DALCHOW 2003). The extensive devastation of the forests in the study area is responsible for the latest dune remobilisation also observed in the OSL record. It was terminated by planned afforestation: since the mid-19th century large areas were planted with pine forests to prevent sand drift as well as give an economic return (e.g. ALISCH 1995, RIEK & STROHBACH 2003).

Regarding the onset of this latest reactivation of dune activity a coincidence with the 'Little Ice Age' (LIA) with its most prolonged cooling from ~1550 to~1750 AD is noted. The last phase of the LIA from 1750 to 1900 AD was characterised by strong westerly winds in northern Europe with the maximum of storminess and coldness being recorded for the 1830s to 1860s (BRADLEY & JONES 1993, HASS 1999, MANN et al. 1999). These climatic conditions most probably reinforced the human impact on the landscape. For example, the enhanced storm activity in the mid-19th century in particular might have contributed to a further destruction of the remaining forests and an increased deflation of sandy soils from arable fields and open areas in general. The need for protection from the wind thus increased and finally resulted in the organised afforestation.

5.3 The chronostratigraphy of dune development in the European Sand Belt – New insights?

In spite of the large number of detailed studies on the chronostratigraphy of aeolian deposits in the European Sand Belt (ESB), "a firm chronology of phases of aeolian activity of supra-regional significance is still lacking" (KOSTER 2005: 132).

The last four decades have seen numerous studies on the chronology of the aeolian record throughout the sand belt. The stratigraphic record for most European countries is known in great detail. But many studies are localised, dealing with individual sites only, with no conclusions for wider areas (others present generalisations but lack a sound data base).

The contribution of the present study will be outlined regarding (i) the luminescence chronology of aeolian deposits in the ESB as published so far; (ii) the agreements or disagreements of the OSL record presented in this study with various models of periods of aeolian activity in the north Central European lowland.

5.3.1 Establishment of a chronology of dune construction by luminescence dating

By applying luminescence dating techniques the timing of aeolian activity resulting in sand deposition can be reconstructed. SINGHVI et al. (2001) summarised 303 luminescence dates on coversand and dune deposits in the European Sand Belt published at that time (see also KOSTER 2005). The results are shown in Fig. 98.

Fig. 98: Summary of multiple-aliquot luminescence ages on aeolian deposits from the European Sand Belt and comparison with the OSL record of this study.
a) Compilation of European coversand and inland dune ages, as probability density curves, for K-rich feldspar and quartz using TL, IRSL and GLSL analyses (after SINGHVI et al. 2001). The composite data curve combines quartz-based TL and GLSL ages (from KOSTER 2005: 139). This curve is compared to the summary data curve from this study in graph **b)**.
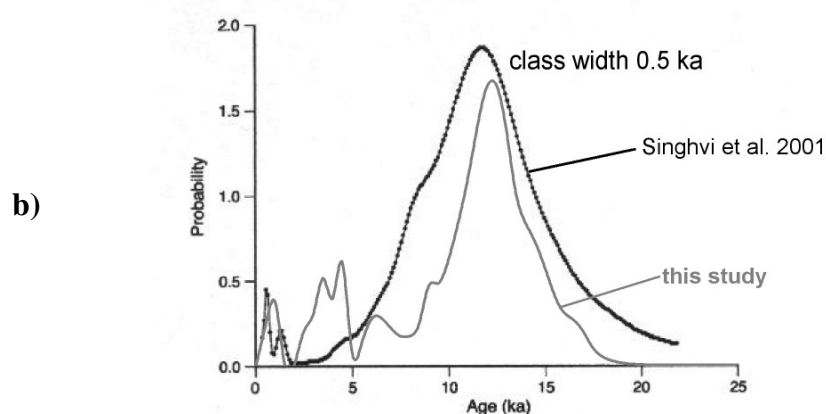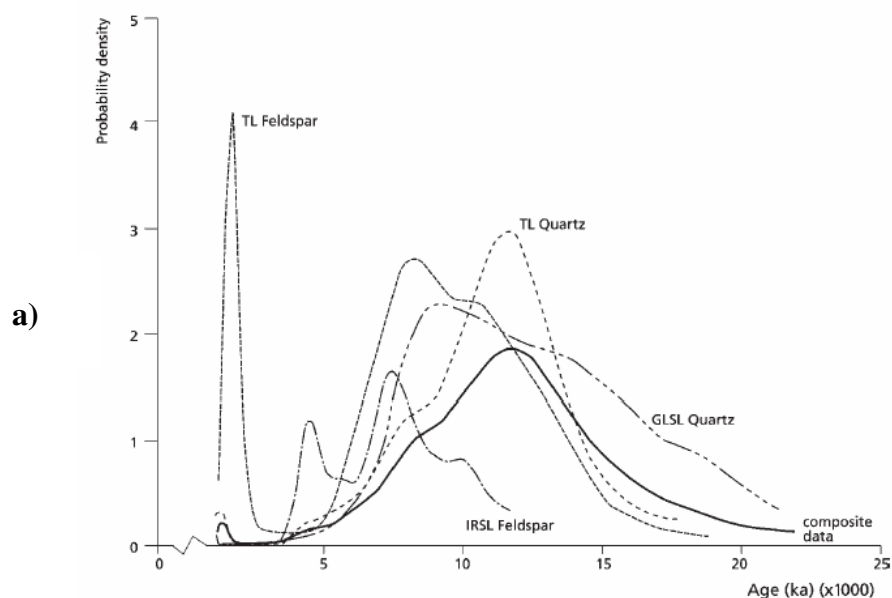
The majority of studies summarised by SINGHVI et al. (2001) have been carried out in the western part of the ESB, notably in the UK, Denmark, The Netherlands and western Germany. Only 11 ages were derived from dune sites within the study area in northeastern Germany (see Table 2 in SINGHVI et al. 2001, study of BARAY & ZÖLLER 1994). The multiple-aliquot TL and OSL ages published by KUHN (2000) are not included in the summary. He investigated 14 aeolian sand samples from 5 diffeent sites. The overall small number of luminescence dates available for aeolian deposits in the study area underlines the demand for such dating studies to be carried out in NE Germany further to complete the record.

The compilation of coversand and dune sand ages shown in Fig. 98 shows subsets of luminescence ages obtained by thermoluminescence on quartz and feldspars, and green light or infrared stimulated luminescence on quartz and feldspar, respectively. It is not further differentiated whether the additive or regenerative dose protocol was applied. All datasets show distinct differences in the number of age clusters (represented by peaks of the graph) and their timing. This summary illustrates the fundamental problem of luminescence studies on aeolian sand deposits carried out throughout the last two decades. The luminescence technique has seen several major steps of technical development and refinement with each study understandably focussing on the 'up-to-date' or 'state-of-the-art' approach of its time.

But comparative studies applying different luminescence techniques to the same samples show that substantial variations in ages obtained by different measurement techniques exist (e.g. RADTKE & JANOTTA 1998, RADTKE et al. 2001, HILGERS et al. 2001a, b). Thus it is difficult to conclude whether the high variability among the individual data sets presented in Fig. 98 reflects different episodes of deposition or whether it has to be ascribed to methodological problems of different technical approaches that were applied at different sites. In order to prevent any complication in comparing the chronologies of the individual dune sites a consistent methodological approach was followed throughout this study keeping the experimental settings constant for all samples. Based on the comparative studies carried out in this study (see Appendix B) and supported by the results of similar studies (e.g. RADTKE et al. 2001, VANDENBERGHE et al. 2004) the single aliquot regenerative dose protocol for sand sized quartz was applied (MURRAY & WINTLE 2000).

Numerous studies report on the problem of underestimation of feldspar luminescence ages, although such underestimation is neither systematic nor regionally specific (for example WALLINGA et al. 2001, RADTKE et al. 2001, MURRAY & OLLEY 2002, DULLER 2004,

PREUSSER 2003). Therefore, any further discussion on the comparison of the age records concentrates on the quartz luminescence data set (composite data curve in Fig. 98 a and b).

From the composite data set presented in Fig. 98 SINGHVI et al. (2001) and KOSTER (2005) conclude that aeolian sand deposits dating to the Last Glacial Maximum are rare and deposition strongly increased at about 15 ka. The cluster in ages at around 10-12 ka indicates intensified aeolian sand accumulation during the Younger Dryas cold episode. The comparably slow decrease of the summary graph during the first part of the Holocene might be interpreted as reflecting ongoing aeolian activity in the Holocene, probably until the Boreal. Peaks in (pre-)historic times reflect young aeolian reactivation of sand dunes resulting from human impact since the beginning of the Neolithic period.

The data curve summarising all OSL ages derived from this study shows a similar trend with a scarcity of dates from the LGM, the increase at ~15 ka and the peak at about 12 ka and also with the reactivation during the last two millennia. Only the peak between 2 and 5 ka is not as clearly seen in the composite data curve from SINGHVI et al. (2001).

These similarities have to be noted bearing in mind that both data sets represent different study areas, with this study predominantly carried out in northeastern Germany and the western part of the ESB represented by the summary graph of SINGVHI et al. (2001). Having this spatial discrepancy in mind it is difficult to ascribe any difference to methodological problems. The data summarised by SINGHVI et al. (2001) are predominantly based on the luminescence dates derived from multiple aliquot approaches. As could be demonstrated by the comparison of multiple and single aliquot techniques on the same samples of well-bleached dune sand, the single aliquot measurement protocol produces a substantial improvement regarding the precision of luminescence ages (VANDENBERGHE et al. 2004, RADTKE et al. 2001, HILGERS et al. 2001b). Based on these results the data curve representing the single aliquot results of this study likely shows a very similar record to that presented by SINGHVI et al. (2001), but with a much better resolution, resulting in much more clearly defined peaks.

Having the limitation of a direct comparison of both data sets in mind a tentative conclusion can be presented here:

- The OSL record of aeolian sand deposition in the central part of the ESB (northeastern Germany and adjacent parts in Poland) is comparable to the record from the western part of the ESB regarding the timing of the most prominent features which are (i) the onset, (ii) the dominant peak and (iii) the young Holocene reactivation.

- The data summary based on the single aliquot approach provides a higher resolution of the aeolian record due to the enhanced precision of the OSL dates.

The latter observation is crucial regarding the dating of events within the comparably narrow time frame of the Lateglacial with rather short-lived changes in climatic and environmental conditions. If phases of aeolian activity and dune formation are to be distinguished throughout the Lateglacial the single aliquot approach as used within this study is far better suited to assess useful chronologies.

Because of the difficulties with comparing data sets which are based on different methodological approaches one of the major advantages of the OSL record presented in this study is that the ages are internally consistent and thus all sites comparable each to the other. Of course it is not certain that, despite a careful consideration of the numerous sources of errors in luminescence dating, an undetected systematic uncertainty might shift the whole data set towards older or younger ages, respectively. This always has to be borne in mind.

It could be demonstrated that only the regional comparison of a certain number of sites with a narrow spaced sampling of each site is able to provide a data base in which phases of prominent aeolian activity in the Lateglacial can be distinguished (see Fig. 92 & Fig. 94). Neither an individual OSL record of one particular site nor the summary of all ages from numerous sites is able to provide the basis for establishing a chronology of phases of aeolian deposition. As illustrated in Fig. 92 each study site provides a different dune chronology as many local factors may interfere with the climate triggered dune formation. And the summary of all ages does not allow the identification of several aeolian phases in the Lateglacial because of the lack of precision. Instead a broad peak indicates aeolian activity throughout the entire Lateglacial (see Fig. 91).

5.3.2 Comparison of the OSL record with existing models of aeolian activity

The chronology of phases of aeolian activity which has been established previously is mainly based on radiocarbon dates of intercalated (peat) layers and palaeosols reflecting phases of non-deposition and dune stabilisation. From SCHIRMERs (1999a) summary shown in Fig. 99 it is clear that there is agreement on multiple phases of aeolian activity but disagreement regarding the number and exact timing of these episodes.

Fig. 99: Comparison of the periods of dune sand deposition and dune reactivation, which are derived from the OSL chronology of this study, with models on aeolian activity and dune formation in northern Central Europe.
The models were summarised by SCHIRMER (1999a) from various studies and arranged from west (The Netherlands) to east (Poland). The results of this study are included in the last column on the right. (redrawn and modified from SCHIRMER 1999a: 12-13)

The question is whether the OSL study presented here can contribute new information to these models and clarify some inconsistencies regarding the number and timing of prominent phases of dune formation.

With respect to Fig. 92 amongst the dune sites investigated in this study at least one site appears to support both 'extremes' of the presented models on aeolian activity, those comprising up to 12 aeolian phases (e.g. DE BOER 1995) and those only suggesting two phases (e.g. PYRITZ 1972) (see Fig. 99). This illustrates the importance of the size of the data base

from which a model is developed. The distinct variability of the dune records shown in Fig. 92 argues against multiple phase models as proposed by DE BOER (1995), for as they reflect the exception and not the average. A broad data base for these 'high resolution' models with regional validity is lacking. As was shown in the discussion on the relation of Holocene dune reactivation to the settlement history of the study area most of the young dune remobilisation seems to be related to human impact in some way. It is concluded that the suitability of multiple phase models is doubtful, because human impact always implies a locally restricted effect only. Thus, it is difficult to reconcile the generalising character of a model with the reality of a temporally and spatially highly variable impact on dune reactivation.

The other extreme is the two-fold model. Based on morphological, archaeological and pollenanalytical evidence already LEMBKE (1939) dated the dune formation to the Lateglacial and early Holocene (Preboreal) after the remelting of the inland ice, with later remobilisation being induced by human impact. This simple model was later supported by PYRITZ (1972). In section 5.2 of this discussion two major periods were distinguished based on the characterisation of dune building in time and space, hence by dating of dune sand deposition using OSL dating and by comparing the aeolian records on a local and regional scale. The following two time slices were distinguished within the uncertainty of the OSL chronology:

- an old, Lateglacial period of dune formation and dune reactivation from about 18 to 10.5 ka with dune sand deposition occurring regionally throughout the study area and with good agreement in timing of dune formation, the main trigger: climate and vegetation controlling the availability of the sediment sources.

- a young, Holocene period of locally restricted dune reactivation since ~10.5 ka which is characterised by a high variability regarding the intensity, temporal and spatial distribution of aeolian activity. The dominant forcing factor for dune reactivation after about 4.5 ka seems to be human impact with climate acting just as one secondary factor by influencing human reaction to climate oscillations.

The old, Lateglacial phase could be further differentiated in an Early-Lateglacial period starting with the onset of aeolian deposition around 16.7 ka and indicating, within errors of OSL chronologies, a first phase of dune formation from ~15.2 ka until 13.7 ka; thus, from the late Oldest Dryas (GS-2a) until the beginning of the Allerød (GI-1a-c), with a peak in aeolian activity around 14.4 ka. The second period of dune formation was dated by OSL to 12.9-11.1

ka, thus indicating dune formation throughout the entire Younger Dryas, and at some sites continuing into the Preboreal.

These phases of dune formation are at odds with numerous models which correlate the major period of dune formation with the short-lived Older Dryas (see, for example, models of SCHIRMER (1999a) and DYLIKOWA (1969) in Fig. 99). The OSL chronology clearly argues for only minor dune sand deposition during the Older Dryas with a more intense dune activity observed already earlier. This discrepancy most likely can be ascribed to shortcomings in the age assessment of the Older Dryas dune formation based only on radiocarbon dating of Allerød deposits, which of course only provides a minimum age for the underlying dune deposits (see discussion in section 5.2.1.1.2). Here, the OSL record can contribute valuable information on the timing of the first phase of dune formation, because by OSL the event of dune sand deposition is dated directly. Hence, the OSL based timing of the first period of dune building in the study area is considered to be more accurate, although not as precise as the ^{14}C chronology.

KASSE (2002) already based his model on Lateglacial aeolian sand deposition on a range of luminescence dates obtained for aeolian and fluvio-aeolian deposits from the UK and The Netherlands (see Table 12). The OSL data set presented in this study fits well into this model and, in turn, can further support its validity for a wider region, now that it is extended to the more central parts of the European sand belt in northeastern Germany. The change from sand sheet formation to dune formation in Phase II is explained by the development of sparse vegetation, which agrees with the observation and dating of the onset of dune deposition in this study to the late Oldest Dryas.

Table 12: Summary of the model on aeolian sand deposition proposed by KASSE (2002).
 (summarised from Figure 7 in KASSE 2002: 518)

Phases of aeolian sand deposition		Aeolian activity	Preservation potential	Aeolian accumulation	Dominant type of deposition
Phase I (c. 28-18 ka cal. BP)		high	low	low	fluvio-aeolian, fluvial
Phase II (c. 18-14.7/14.0 ka cal. BP)	a	high	high	high	sand sheets
	b	high	high	high	low dunes
Phase III (c. 13-10.2 ka cal. BP)		low	high	low	(low) dunes
		high	high	high	

Besides the comparability to the phases of aeolian sand deposition determined in western parts of the European Sand Belt (Tab 5.1, KASSE 2002), the OSL chronology of the NE German dune development is in agreement with the chronology of Late Wisconsinan dunefield formation in the northernmost part of the North American Great Plains. WOLFE (2006) summarised more than 150 optical and radiocarbon ages and concluded that dune activity in central Alberta, Canada, occurred in tundra settings between 15.7 and 13.4 ka and later again between 12.9 and 11.3 ka under parkland and grassland settings.

With regard to the discrimination of Holocene phases of enhanced aeolian deposition the following is concluded: Despite the disagreement with the model of SCHIRMER (1999a) concerning the timing of major periods of Lateglacial dune formation, the OSL data set of this study supports the differentiation of the Holocene into two phases; the period of little dune transformation and the human-triggered dune period in the Early and Late Holocene, respectively. From the summary record of OSL dates (see Fig. 91) the boundary between both periods could be roughly dated to 4.5 ka.

6. Conclusions

The overall aim of this study is to distinguish in the European Sand Belt (ESB) phases of dune sand deposition throughout the last 20,000 years and to investigate the relationship of aeolian phases to climatic and/or anthropogenically-induced landscape changes. The chronology of dune sand deposition at twenty different inland dune sites in northeastern Germany and adjacent areas in western Poland has been reconstructed by using optically stimulated luminescence (OSL) dating. The conclusions drawn from this large data set provide new information for both, the application of OSL dating and the interpretation of the aeolian record of the study area.

Aeolian record with regional validity

This study contributes to the chronology of the aeolian record of the ESB. It is the first comprehensive OSL-based study on the timing of dune development in northeastern Germany with regional validity.

The comparison of various models on phases of aeolian activity by SCHIRMER (1999a) (see Fig. 99) shows that there is general agreement that there have been multiple phases of aeolian activity. However, the number and exact timing of these periods remains a matter of debate. In this context, the OSL study presented here provides the following new information on Lateglacial and Holocene dune development in northeastern Germany and adjacent parts of western Poland (see Fig. 99 and Fig. 100):

- dune formation in GS2-a and GI-1e seems more significant than previously thought;
- dune formation most likely commenced at the beginning of GS-1 already, rather than in the second, drier part of this stadial period;
- since the Late Neolithic, after ~4,500 yr BP, human impact was the dominant factor for dune reactivation, although an indirect impact of Holocene climate fluctuation on aeolian processes is not to be underrated. For example, during prolonged periods of droughts people were compelled to exploit their environment and in so doing made possible the reactivation of aeolian processes.

The oldest ages obtained in this study date the onset of aeolian deposition to about 16.7 ka. Two major periods of enhanced aeolian activity and dune formation and stabilisation can be differentiated based on the comparison of individual dune site records. A first period lasted from about 15.2 to 13.7 ka with the peak of the age cluster at ~14.4 ka. After a period of extensive aeolian quiescence which allowed landscape stabilisation and soil formation, a second period of intensive aeolian activity began about 12.9 ka and terminated in the Preboreal at ~11.1 ka. A comparison of these results with the phases of aeolian sand deposition determined by KASSE (2002, 18-14.7/14.0 ka, 13-10.2 ka) for the western part of the European Sand Belt and WOLFE (2006, 15.7-13.4 ka, 12.9-11.3 ka) for the northernmost part of the North American Great Plains, underlines the similarity of the chronologies of cold-climate dune sand deposition throughout the northern American and European sand belts.

Fig. 100: Comparison of the OSL based record of Lateglacial dune sand deposition in northeastern Germany with periods of aeolian sand deposition in the western part of the ESB and in North America, which were determined from luminescence and radiocarbon chronologies.
The grey shaded areas indicated cold, stadial climate conditions or periods of enhanced aeolian sand deposition, respectively. (Timing of the aeolian periods after KASSE, 2002, and WOLFE, 2006, chronology of Lateglacial climatostratigraphic units after BJÖRCK et al. 1998)
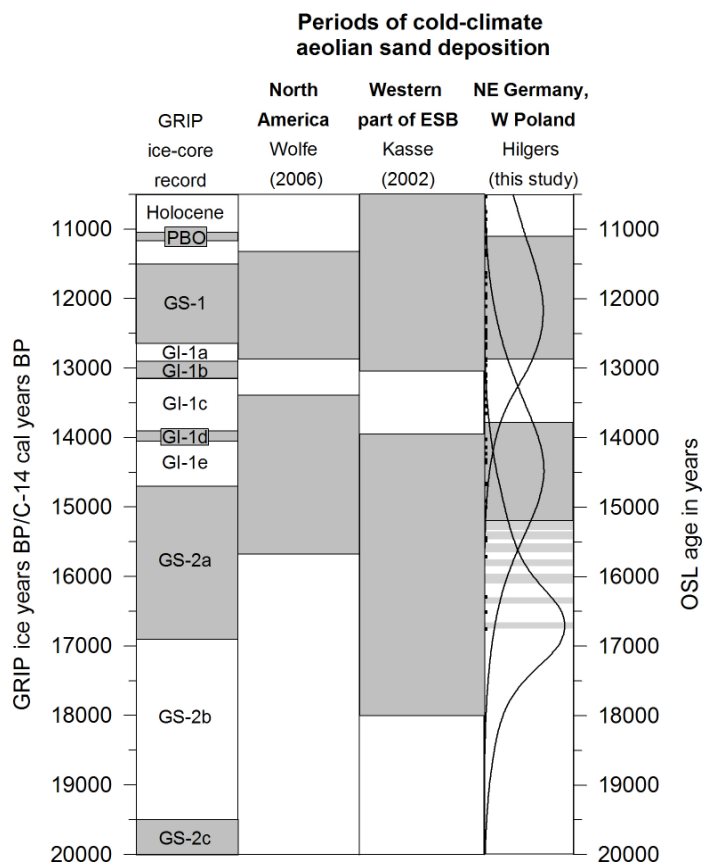
The correlation of these major periods of Lateglacial dune formation with the climatostratigraphy of this period, as reconstructed from the GRIP ice-core record (BJÖRCK et al. 1998), supports the observation that aeolian phases do not strictly coincide with glacial or stadial conditions (e.g. KASSE 2002). Widespread dune formation occurred midway through the Greenland Stadial 2a, or the Oldest Dryas, respectively, and continued into the following interstadial GI-1e. Ongoing dune formation beyond the Lateglacial/Holocene transition also seems likely.

Dune formation in the study area is mainly a reaction to the availability of source material, for it is controlled by factors such as the desiccation and exposure of sediment in valley floors, development of sparse vegetation, dissipation of permafrost, and so on. This response to climate-triggered environmental conditions limits the value of palaeodunes as direct climate proxies, at least for the resolution of the short-lived Lateglacial climate oscillations. When larger time scales are considered, the delayed response of dune activity on climatically-induced changes of environmental conditions become less important and the value of palaeodunes as a proxy record for palaeoclimate changes is enhanced.

Equivalent dose scatter in aeolian sediments

In addition to these chronological contributions several procedural problems concerning OSL dating have been considered and resolved, in part at least. The single aliquot regenerative (SAR) dose protocol for sand-sized quartz, which is now widely applied in OSL studies, was used for equivalent dose determination. Multiple replicates of equivalent dose (D_e) measurements of subsamples taken from the same sediment sample invariably show a certain variation among the individual estimates. The causes are neither fully understood, nor quantified at present. One major need in luminescence studies is to assess the extent of the scatter in D_e which is acceptable as being due to natural variation only and when an additional source of scatter such as incomplete bleaching has to be taken into account (GALBRAITH et al. 2005).

The present study provides a large data set which is derived from consistent measurement procedures applied to a set of samples from the same type of deposit and from the same geological provenance. It covers a comparatively narrow time span. From this data pool a reliable estimate of the baseline variation of ~8 % (relative standard deviation) has been derived. This data spread can be expected for subsamples that were all well-bleached at the

time of deposition and have absorbed the same – or at least very similar - natural radiation dose during burial. This figure for a 'natural threshold variation' provides a helpful tool in interpretation of any D_e distributions of samples of the following types:

- samples from depositional environments comparable to the dune sand deposits analysed in this study which – most likely - have undergone multiple sedimentation cycles in the geological past (with reference to similar luminescence properties, such as high luminescence sensitivity and hence small errors due to photon-counting statistics);

- D_e distributions obtained with a similar experimental setting (with reference to the size of aliquots containing >1000 grains, and the average number of 18 D_e replicates per sample);

- samples of a similar age range of several tens of years up to ~20,000 ka (with reference to the minimisation of an additional variation in D_e which is observed for samples close to the saturation level).

The central question in luminescence dating studies on sediments is the degree of bleaching of the sediment grains at the time of deposition and coverage. The results of this study support the general assumption that most dune sands can be assumed to be well bleached (e.g. DULLER 2004). Reasons for D_e scatter higher than the baseline variation are more likely to be found in extremely low equivalent dose values or post-sedimentary mixing of sediments close to the surface.

Implications for dose rate determination

The impact of multiple phases of deposition on the variation of the cosmic dose contribution was investigated in some detail, because the ratio of cosmic dose contribution to total annual dose ranged from 8 up to 30 % of the annual dose. The modelling of the sedimentation history showed only minor changes in the cosmic dose contribution. On average, the OSL ages calculated by taking the sedimentation history into account differ only by ~3 % on average from those ages which were determined using the contemporary depth cosmic dose equivalent. But the adaptation of the cosmic dose contribution to a model of the sedimentation history clearly improves the accuracy of OSL ages if, for example, the sampling site exhibits a young (several hundred years) and thick (several metres of sediment) deposit over a considerably older sediment section. Furthermore, the detailed reconstruction of variations in the cosmic dose should be taken into consideration for sampling sites with extremely low

terrestrial natural radioactivity, because cosmic radiation might be the major contributor to the annual dose rate.

Improvement of precision and accuracy of OSL chronologies

The potential of OSL chronologies of dune sands for the differentiation of phases of enhanced aeolian activity throughout the last ~20,000 years has been evaluated. Comparisons of multiple aliquot based results with those from SAR measurements clearly showed that the single aliquot procedure provides a much greater precision of luminescence dating then the previously used multiple aliquot based methods. By using a consistent methodical approach and keeping the SAR measurement parameters constant for all samples, uncertainties which arise from comparison of dates obtained by different luminescence measurement procedures and mineral fractions are minimised. However, although the ages determined in this study are internally comparable, they could conceivably all be systematically in error in one direction or the other. However, the good agreement of the OSL ages obtained with ^{14}C ages supports the accuracy of the OSL chronology.

The comparatively low precision of OSL ages, which show average relative 1σ errors of ~8 % in this study, limits their usefulness for the resolution of aeolian activity in relation to the short-lived Lateglacial climatic oscillations. But this lack of precision of OSL ages can to a certain degree be circumvented by an increase of the number of samples. In some instances, dating more than one sample from the same sediment unit revealed inconsistencies in the data set. However, most of these were eliminated by additional analyses.

Investigation of numerous sites and subsequent comparison of the results allowed a higher resolution of the aeolian record. This was necessitated by the number of short-lived climate oscillations which occurred throughout the Lateglacial. Although major phases of intensified dune sand deposition during the Lateglacial cannot be determined from the OSL data summary, comparison of records for individual sites on a local and regional scale enables the determination of such periods.

Closing statement

The sampling strategy adopted in this study of the European Sand Belt was appropriate to an intricate landscape with a complex chronology and parts of which had previously been investigated using techniques and procedures other than OSL. It is not implied that other techniques or simpler dating strategies are useless, for the strategy must be devised to fit the nature of the problem. However, dating a large number of samples from a spread of sites was considered essential for the investigation of a landscape with many physical and chronological complexities.

Though many theoretical difficulties and complications come to mind, in practice OSL dating has proved effective in unravelling the manifold problems associated with a major sector of the ESB. With the application of sensible checks in the field and in the laboratory, and bearing stratigraphic principles in mind at all times, the procedure appears to offer reasonable reliability.

The widespread distribution of materials suitable for OSL procedures and the relative ease of access to them, make it an indispensable tool for establishing chronologies for later Quaternary events, whether they be associated with glaciated or desert regions.

7. Summary

The study presented here is concerned with the reconstruction of dune formation and reactivation by means of optically stimulated luminescence (OSL) dating of dunes developed throughout the last 20,000 years in the central part of the so-called 'European Sand Belt' (ESB) in northeast Germany and adjacent areas in Poland (see Fig. 55 and Fig. 57 for the location of the study area).

In this area, proglacial outwash plains and abandoned unvegetated flood plains in the Weichselian ice-marginal valleys provided ample sand supply for the formation of cold-climate sand sheets and inland dunes at the end of the last glaciation.

Because dune formation is linked to specific climatic conditions, each layer of dune sand preserves information on the palaeoclimate prevalent at the time of deposition. In order to use this terrestrial archive for a chronology of climatic change, and for a regional correlation of the observations, precise dating of the depositional events is crucial.

The chronology of the Lateglacial and Holocene aeolian record in the European Sand Belt is fairly well known from the vast number of studies carried out in the last four decades. But whereas there is more or less an agreement on multiple phases of aeolian activity in the Lateglacial and Holocene, the existing models disagree regarding the number and the exact timing of these periods of dune formation (see for example compilation by SCHIRMER 1999a, illustrated in Fig. 99).

Almost all of the studies on the chronology of dune development in the study area are based on ^{14}C ages of carbon bearing layers intercalated in the dune sands, thus not dating the event of aeolian sedimentation directly. By contrast, optically stimulated luminescence (OSL) dating allows the direct dating of dune sand deposition and by that the timing of the environmental conditions which prevailed during formation of the dunes.

But although the advantages of OSL dating are obvious, the luminescence dates available so far have not been considered to a wider extent in summarising studies elsewhere. In particular because of the lack of precision they are often regarded as less helpful for resolving the dune chronologies and the climate history throughout the Lateglacial (see e.g. BARAY & ZÖLLER 1993 or KUHN 2000 for multiple-aliquot dating studies carried out in the study area).

Furthermore, the dating results of preceding luminescence chronologies are difficult to compare and to summarise as they were often based on different methical approaches used in luminescence dating studies (see compilation by SINGHVI et al. 2001). Thus, the compilation of luminescence dates of dune sand deposits from the UK, The Netherlands and NW Germany by SINGHVI et al. (2001, illustrated in Fig. 98 a) shows a confusing picture which results from the application of different methods, OSL and thermoluminescence, and different dating fractions, quartz and K-rich feldspars.

By contrast the present study provides the first comprehensive luminescence chronology of the Lateglacial and Holocene aeolian record that is based on a consistent methical approach and with regional validity for central parts of the European Sand Belt. The now widely applied single aliquot regenerative (SAR) dose protocol for coarse-grained quartz (MURRAY & WINTLE 2000) was used for equivalent dose determination. To prevent the inclusion of any systematic uncertainty associated to methical differences, the measurement parameters were kept constant as far as possible for all samples. Comparisons of multiple aliquot based OSL results with those from SAR measurements of the same samples clearly show that the application of the single aliquot procedure substantially improves the precision and the accuracy of the luminescence ages.

However, the comparatively 'poor' precision of the single aliquot based OSL ages, which show average 1σ errors of about ± 8 % in this study, still restricts their suitability for the resolution of aeolian activity in relation to the short-live Lateglacial climatic oscillations. But this study demonstrates that the lack of precision of OSL chronologies can be circumvented by an increase of the number of samples to certain extent. By dating more than only one sample from the same sediment unit some irregularities in the data set can be revealed and, in most cases, can be eliminated by additional analysis.

In order to create a data set with regional validity dune sites in five different study areas are investigated which are located in the Elbe-, the Głogów-Baruth-, and in the Toruń-Eberswalde-ice marginal valleys and in the glacio-lacustrine basins of the 'Ueckermünder Heide' and 'Altdarss' area (see Fig. 57). Within each of these study areas several dune sites are investigated in order to arrive at regional interpretations and not to stick to site-specific observations which may reflect only locally very restricted catastrophic events. In total 183 sediment samples from aeolian, fluvial, glacio-fluvial and glacio-lacustrine deposits were sampled at twenty different sites.

Outcomes of this study with relevance for the application of OSL dating

Multiple replicates of equivalent dose (D_e) measurements on sub-samples from the same sediment sample always show a certain variation among the individual estimates whose various causes are not all fully understood, or quantified at present. Incomplete bleaching of OSL signals, for example, can result in a large scatter of equivalent dose values and finally result in overestimation of OSL ages. Hence, one major demand in luminescence studies is to assess the extent of the scatter in D_e distributions which is acceptable as being due to natural variation. If such a baseline variation is known, additional sources of scatter between equivalent dose estimates can be identified and discriminated from this natural baseline variation (GALBRAITH et al. 2005).

The present study provides the large, homogeneous data set which is required for determination of average amount of D_e data spread that can be expected for sub-samples which all were well-bleached at the time of deposition and have absorbed the same natural radiation dose during burial. From the data pool of 155 aeolian sand samples a baseline variation of ~8 % (relative standard deviation) could be determined. This 'natural threshold variation' provides a helpful tool in interpretation of any D_e distributions obtained for samples which meet the following conditions:

- Samples from comparable depositional environments, i.e. aeolian sand deposits which underwent already multiple sedimentation cycles in the geological past (with reference to similar luminescence properties, such as high luminescence sensitivity and hence small errors due to photon counting statistics);

- Samples from sediments which are more or less homogeneous in terms of the environmental radiation field,

- Samples of a similar age range of several tens of years up to ~20,000 ka (with reference to the minimisation of an additional variation in D_e which is observed for samples close to the saturation level);

- D_e distributions obtained with a similar experimental setting (with reference to the size of aliquots containing >1000 grains, and the average number of 18 D_e replicates per sample).

The central question in luminescence dating studies on sediments is the degree of bleaching of the sediment grains at the time of deposition and coverage. This study supports the general assumption that overall dune sands can be assumed to be well-bleached (e.g. DULLER 2004). Only for two out of 164 dune sand samples incomplete resetting by sunlight is the most probable cause for the observed age overestimation.

This study clearly demonstrates that the investigation of numerous sites and subsequent comparison of the OSL chronologies allows a higher resolution of the aeolian record. This improvement is essential for the correlation of any period of enhanced aeolian deposition to the short-lived climate oscillations of the Lateglacial palaeoclimate record. While a distinction of major phases of intensified dune sand deposition during the Lateglacial is not possible from the OSL data summary, the comparison of the individual site records on a local and regional scale finally allows the determination of such periods (compare Fig. 91 and Fig. 92).

Outcomes of this study with relevance for the chronology of dune sand deposition in central parts of the European Sand Belt

The summary of 159 OSL ages obtained for Lateglacial and Holocene dune sands from northeastern Germany and adjacent areas in western Poland shows, that there is a lack of aeolian deposits dated to older than 18 ka (see Fig. 91). This agrees with other studies. Although aeolian activity was high under polar desert conditions the preservation conditions for aeolian deposits were poor. Because of the presence of permafrost, overland flow was increased and resulted in a widespread reworking of aeolian deposits of that time (e.g. BÖSE 1991, KASSE 1997, 2002).

A discrimination of different phases of enhanced aeolian activity is only possible on the basis of a comparison of the individual dune site records. This comparison shows that during the Lateglacial dune sand deposition occurred regionally widespread throughout the study area (Fig. 92). This widespread occurrence argues for a forcing factor with regional impact such as changes in climate conditions. However, the comparison of the OSL record to the climate record from the GRIP ice core shows that dune formation does not strictly coincide with climatostratigraphic units. This observation agrees with models on aeolian deposition for more western parts of the ESB (e.g. KASSE 2002). Widespread dune formation started in midstream the Greenland Stadial 2a, or the Oldest Dryas, respectively, and continued into the

following interstadial GI-1e. It seems to be more closely related to the onset of sparse vegetation growth in the study area (see e.g. DE KLERK et al. 2001, DE KLERK 2002, Fig. 94). Ongoing dune formation beyond the Lateglacial/Holocene transition seems also highly likely.

Dune formation in the study area is mainly a reaction on the availability of source material, thus is controlled by factors such as dissipation of permafrost, desiccation of valley floors, development of sparse vegetation. This response to climate triggered environmental conditions limits the value of palaeodunes as direct climate proxies, at least for the resolution of the short-lived Lateglacial climate oscillations. Nevertheless, with regard to larger time scales, the delayed reaction of dune activity to climate triggered changes of environmental conditions becomes less important and the value of palaeodunes as a proxy record for palaeoclimate changes increases.

Two major Lateglacial periods of enhanced aeolian activity and dune formation can be differentiated in the OSL record compiled by this study. Following on the onset of aeolian deposition at about 16.7 ka, the first major period of dune sand deposition lasted from about 15.2 to 13.7 ka with the peak of the age cluster at ~14.4 ka. After a period of extensive aeolian quiescence allowing landscape stabilisation and soil formation, a second period of intensive aeolian processes commenced about 12.9 ka and terminated in the Preboreal at ~11.1 ka. Further conclusions on Lateglacial dune development in NE Germany could be drawn from the OSL data set; (i) dune formation in GS2-a and GI-1e seems more significant than previously thought; (ii) dune formation commenced most likely already at the beginning of GS-1, rather than beginning in particular in the second, drier part of this stadial period (see Fig. 94).

A comparison of the results of this study with the phases of aeolian sand deposition determined by KASSE (2002, 18-14.7/14.0 ka, 13-10.2 ka) for more western parts of the European Sand Belt and WOLFE (2006, 15.7-13.4 ka, 12.9-11.3 ka) for the northernmost part of the North American Great Plains underlines the analogy in timing of cold-climate aeolian sand deposition throughout the Northern American and European sand belts. The correlation of these major periods of Lateglacial dune formation with the climatostratigraphy of this period, as reconstructed from the GRIP ice-core record (BJÖRCK et al. 1998), supports the observation that aeolian phases do not strictly coincide with glacial or stadial conditions (e.g. KASSE 2002) (see Fig. 100).

Aeolian activity did not cease with the reafforestation in the Holocene. Aeolian activity and dune reactivation was prevalent in the study area throughout the entire Holocene, although interrupted by periods of widespread aeolian quiescence (see Fig. 91). The comparison of this Holocene dune reactivation on a local and regional scale reveals a clear lack of synchronicity in the temporal and spatial distribution of the dune activity (see Fig. 92). This lack argues against climate as the main trigger for dune reactivation, because for oscillations in climate conditions at least a regionally widespread effect is expected. From the comparison of the aeolian events with Holocene climate fluctuations and the settlement history of the study area it is finally concluded that human impact seems to be the most likely cause for dune reactivation after ~ 4.5 ka. From this time on man developed mastery on the environment with a growing pressure on the landscape resulting from a growing population. Periods, when population density decreased, villages and fields were abandoned and forests could recover, are seen as breaks in the OSL record (see Fig. 96). However, an indirect impact of climate fluctuation on aeolian processes should not be underrated. Changes in the climate conditions had most likely an influence on the human behaviour in terms of forcing people to intensify exploitation of their environment or to abandon a settlement area. Certain climatic conditions may have favoured reactivation of locally restricted aeolian processes directly, for example increased the risk of forest fires during prolonged periods of droughts.

The present study demonstrates that by application of a consistent methical approach to a large data set, OSL dating has the potential to resolve the dune record of the last 20,000 years in northeastern Germany into individual phases of dune sand deposition. The conclusions drawn from this study provide new information for both, the application of OSL dating and the interpretation of the aeolian record of the study area.

8. Zusammenfassung

Das Ziel der vorliegenden Studie ist die Rekonstruktion der Genese und Reaktivierung von Binnendünen im Verlauf der letzten 20.000 Jahre über die Datierung mittels optisch stimulierter Lumineszenz (OSL). Das Arbeitsgebiet liegt in Nordostdeutschland und angrenzenden Gebieten Polens und damit in zentralen Teilen des so genannten ‚Europäischen Sandgürtels' (European Sand Belt, ESB) (siehe Fig. 55 und Fig. 57).

Hier im Gebiet der letzten, weichselzeitlichen Vereisung stellten beispielsweise ausgedehnte Sanderflächen oder auch die trocken gefallenen, vegetationslosen Urstromtalsande Sandliefergebiete für die Bildung von Flugsanddecken und Dünen unter kaltzeitlichen Bedingungen am Ende der letzten Eiszeit dar.

Das Auftreten äolischer Prozesse mit Dünenbildung ist an bestimmte Klima- und Vegetationsverhältnisse gebunden. Daher lassen sich umgekehrt aus dem Vorkommen von Dünen Rückschlüsse auf die Paläoumweltbedingungen ziehen, die zur Zeit der Dünengenese geherrscht haben müssen. Um Paläodünen jedoch als terrestrisches Archiv für die Rekonstruktion von Änderungen des Paläoklimas nutzen zu können, ist eine präzise Datierung der Dünensande erforderlich. Erst eine robuste Chronostratigraphie erlaubt schließlich die Ausweisung und den regionalen Vergleich von klimagesteuerten Phasen intensiver äolischer Morphodynamik und stellt darüber hinaus die Basis für eine Korrelation mit weiteren Paläoklimaproxies (z.B. Warvenchronologien, Eisbohrkernstratigraphien) dar.

In den vergangenen vier Jahrzehnten wurden zahlreiche Studien zur Chronologie der spätglazialen und holozänen Sandablagerungen im Bereich des Europäischen Sandgürtels durchgeführt. Die aus diesen Studien entwickelten Modelle zur äolischen Morphodynamik stimmen weitestgehend darin überein, dass im Verlauf der letzten ca. 20.000 Jahre mehrere Phasen der Dünenbildung und -umbildung mit morphologischen Ruhephasen wechselten. Deutliche Uneinigkeit herrscht jedoch im Hinblick auf die Frage nach der Anzahl und der zeitlichen Einordnung einzelner Akitivitätsphasen (für einen Vergleich verschiedener Modelle siehe Zusammenstellung von SCHIRMER 1999a in Fig. 99).

Nahezu alle Studien zur Chronologie der Dünengenese im Arbeitsgebiet in Nordostdeutschland basieren auf Radiokarbondatierungen kohlenstoffhaltiger Lagen (z.B.

Holzkohle, Torf, organische Substanz begrabener Bodenhorizonte), die in die Dünenkörper eingeschaltet sind. Mittels ^{14}C wird jedoch die eigentliche Dünenaktivitätsphase nur relativ datiert, also Minimal- oder Maximalalter für die Sandablagerung ermittelt. Im Gegensatz dazu wird mittels optisch stimulierter Lumineszenz (OSL) der Zeitpunkt der letzten Sonnenlichtexposition des Dünensandes und damit in der Regel das Ablagerungsdatum der Sande ermittelt. Die OSL-Datierung erlaubt somit den direkten zeitlichen Rückschluss auf die Paläoumweltbedingungen, die zur Zeit der Dünenbildung vorherrschten.

Trotz der offensichtlichen Vorteile der OSL-Altersbestimmungsmethode liegen nur wenige Lumineszenzdaten zur Rekonstruktion der spätglazialen und holozänen Dünengenese im Arbeitsgebiet vor (siehe BARAY & ZÖLLER 1993, KUHN 2000). Diese Datierungsstudien, wie auch die zusammenfassenden Darstellungen von SINGHVI et al. (2000) und RADTKE (1998), die sich jeweils räumlich auf den westlichen Teil des Europäischen Sandgürtels konzentrieren, basieren auf unterschiedlichen methodischen Ansätzen hinsichtlich der verwendeten Lumineszenzverfahren. Zwar wurden alle Datierungen mittels des so genannten 'Multiple-aliquot' Messverfahrens durchgeführt, jedoch wurden unterschiedliche Mineralfraktionen (Quarze oder Kalium-reiche Feldspäte) als Datierungsmaterial verwendet, und sowohl die Thermolumineszenz als auch die optisch stimulierte Lumineszenz zur Ermittlung der Paläodosis gemessen. Aus dieser methodischen Inkonsistenz resultiert ein sehr uneinheitliches Bild hinsichtlich der Ermittlung von Ablagerungsaltern äolischer Sedimente, wie es beispielsweise die Zusammenstellung von SINGHVI et al. (2001) für Daten aus Großbritannien, den Niederlanden und Nordwestdeutschland illustriert (siehe Fig. 98 a). Die zu beobachtenden Altersunterschiede lassen sich nicht zweifelsfrei unterschiedlichen Ablagerungsereignissen zuschreiben, sondern können gleichfalls – bis zu einem gewissen Grade- allein methodisch bedingt sein.

Die mangelnde Präzision früherer Lumineszenzdaten, die einerseits aus der Anwendung des ‚Multiple-aliquot' Verfahrens selbst resultierte, und andererseits auf die beschriebene eingeschränkte Vergleichbarkeit von TL- und OSL-Altern sowie Quarz- und Feldspataltern zurückzuführen ist, muss sicherlich verantwortlich gemacht werden für die bislang geringe Anwendung dieses Datierungsverfahrens für die Lösung chronologischer Fragestellungen im Arbeitsgebiet.

Die chronologische Auflösung von spätglazialen Dünenstratigraphien und ihre mögliche Verbindung zu den oft sehr kurzzeitigen Oszillationen des Klimas im Spätglazial erfordert aber indes ein Datierungsverfahren mit hoher Präzision.

Diese Arbeit legt nun die erste umfassende, auf dem Lumineszenzverfahren basierende Datierungsstudie zur Rekonstruktion der jungquartären Dünenentwicklung mit regionaler Bedeutung für den Raum der Jungmoränenlandschaft Nordostdeutschlands und angrenzender Gebiete in Polen vor. Aufgrund des methodisch konsistenten Ansatzes hinsichtlich des gewählten Lumineszenzverfahrens konnte die zeitliche Auflösung der Lumineszenzchronologien deutlich verbessert werden. Alle Sedimentationsalter wurden mit der so genannten 'Single-aliquot' Regenerierungstechnik nach MURRAY und WINTLE (2000) mittels optisch stimulierter Lumineszenz (OSL) an Quarzen ermittelt. Durch die Anwendung dieses Messverfahrens allein konnte schon eine substantielle Präzisierung der Einzeldaten erzielt werden gegenüber früheren, auf dem ‚Multiple-aliquot' Verfahren basierenden Quarzaltern, die oft eine relative Altersunsicherheit von mehr als 20 % aufweisen konnten.

Allerdings stehen die mit immer noch durchschnittlich ±8 % ermittelten Fehler (1σ Fehlerbereich) der 'Single-aliquot' Alter einer feinstratigraphischen Auflösung spätglazialer Dünenchronologien mittels OSL-Datierung entgegen. Die vorliegende Studie demonstriert aber deutlich, dass mit einer entsprechenden Beprobungsstrategie, die die Untersuchung mehrerer Dünenstandorte mit jeweils hoher Beprobungsdichte in verschiedenen Teilarbeitsgebieten umfasst, die eingeschränkte Präzision von OSL-Altern teils kompensiert werden kann.

Um eine Datenbasis zu schaffen, die Aussagen mit regionaler Relevanz erlaubt, wurden insgesamt 20 Dünenstandorte in fünf verschiedenen Teilarbeitsgebieten untersucht. Die Untersuchungsgebiete konzentrierten sich dabei auf Urstromtäler (Elbe-, Głogów-Baruther-, und Eberswalder-Urstromtal) sowie auf die spätpleistozänen Beckenlandschaften in der Ueckermünder Heide und auf dem Altdarss (siehe Fig. 57). Insgesamt wurden 183 Proben aus äolischen, fluvialen, glazifluvialen und glazilimnischen Sedimenten datiert, wobei die Mehrzahl der Proben (n=164) von Dünenstandorten stammt.

Ergebnisse dieser Arbeit mit Bedeutung für die Anwendung des OSL-Datierungsverfahrens für jungquartäre Sedimente

Die Anwendung des 'Single-aliquot' Verfahrens macht theoretisch die Bestimmung der Paläodosis (‚equivalent dose'=D_e) und damit auch des OSL-Alters an nur einer einzelnen Teilprobe (Aliquot) möglich. In der Routineanwendung wird jedoch stets eine Anzahl von mehreren Teilproben (in der vorliegenden Studie ±18 Aliquots) gemessen und die Paläodosis schließlich über den Mittelwert der Einzelergebnisse ermittelt. Messungen von mehreren Teilproben derselben Sedimentprobe zeigen immer eine Streuung der Einzelwerte. Bei Lumineszenzmessungen können Streubreiten auftreten, die die statistische Häufigkeitsverteilung von Mehrfachmessungen deutlich überschreiten. Die Ursachen für diese zusätzliche Datenvariation sind zahlreich, nicht alle sind bislang vollständig erklärt und einige sicherlich auch noch nicht bekannt. Zur Verbesserung der Präzision und Zuverlässigkeit von OSL-Altern von Sedimenten ist es allerdings notwendig zu unterscheiden, ob die Datenstreuung der natürlich zu erwartenden Varianz entspricht, oder aber beispielsweise auftritt, weil einige Teilproben aufgrund unzureichender Sonnenlichtexposition beim Sedimenttransport tatsächlich höhere Paläodosiswerte aufweisen. Diese schlecht gebleichten Teilproben könnten schließlich in einer Altersüberschätzung des Sedimentationszeitpunktes resultieren.

Für die erfolgreiche Anwendung der OSL-Datierung bei Proben mit hoher Datenstreuung wäre ein Grenzwert für die maximal zu erwartende natürliche Datenstreuung von Paläodosiswerten hilfreich (GALBRAITH et al. 2005). Die Anwendung eines generellen Grenzwerts von 10 % (relative Standardabweichung) zur Unterscheidung gut gebleichter Proben von schlecht gebleichten, wie ihn beispielsweise CLARKE et al. (1999) vorgeschlagen haben, hat sich in der Vergangenheit nicht bewährt. Zu viele Einflussfaktoren, die in den Materialeigenschaften des Quarzes einerseits, wie andererseits in den Messbedingungen begründet liegen, bleiben bei einem generellen Grenzwert unberücksichtigt.

Diese Studie legt nun einen großen, homogenen Lumineszenzdatensatz vor, der sich als Datenbasis zur Abschätzung einer 'Basisvariation' von Paläosdosiswerten eignet, da alle Daten mit einheitlichen Messbedingungen ermittelt wurden und damit untereinander vergleichbar sind. Darüber hinaus stammen alle berücksichtigten Proben aus gut-gebleichten Sanden, die einem homogenen, natürlichen Strahlungsfeld ausgesetzt waren und alle vergleichbare Lumineszenzeigenschaften aufwiesen.

Über die beobachtete Datenstreuung in 155 äolischen Sandproben wurde ein Mittelwert für die ‚natürliche Basisvariation' der Paläodosismesswerte von rund 8 % (relative Standardabweichung) ermittelt. Für andere Lumineszenzstudien kann dieser ‚natürliche Grenzwert' ein wichtiges Hilfsmittel sein bei der Interpretation von Datenstreuungen, die in Paläodosismessungen von Quarzproben auftreten. Wichtig ist gegenüber der Formulierung genereller Grenzwerte, das hier nun die Kriterien, die andere Proben für die erfolgreiche Anwendung der hier ermittelten ‚natürlichen Basisvariation' erfüllen sollten, formuliert werden können. Diese Proben sollten:

- ähnlich gute Lumineszenzeigenschaften, z.B. hinsichtlich ihrer Lumineszenzsensitivität, aufweisen;

- während des Ablagerungszeitraumes einem mehr oder weniger homogenen natürlichen Strahlungsfeld ausgesetzt gewesen sein,

- in etwa ein ähnliches Sedimentationsalter von sub-rezent bis ca. 20.000 Jahren aufweisen, da für deutlich ältere Proben (>100 ka) die natürliche Datenstreuung höher sein kann als der hier ermittelte Grenzwert;

- mit einer vergleichbaren Messanordnung gemessen worden sein (Teilproben bestehen aus >1000 Quarzkörnern, durchschnittlich wurden 18 Teilproben je Sedimentproben gemessen).

Ergebnisse dieser Arbeit im Hinblick auf neue Erkenntnisse zur Chronologie der Dünenentwicklung in zentralen Teilen des Europäischen Sandgürtels

Der in dieser Arbeit konsequent verfolgte methodische Ansatz erlaubt die Zusammenfassung aller 159 OSL-Altersdaten, die für Dünensandproben von zwanzig Einzelstandorten erhoben wurden, welche sich wiederum auf fünf Teilarbeitsgebiete zwischen Ostseeküste und Niederlausitz verteilen (siehe Fig. 91). Das Fehlen äolischer Ablagerungen, die älter sind als 18 ka, lässt sich aus den damaligen Permafrostbedingungen erklären. Zwar herrschte hohe äolische Aktivität, aber die Erhaltungsbedingungen für äolische Sedimente waren stark eingeschränkt. Der durch den gefrorenen Untergrund verstärkte Oberflächenabfluss führte zur weitgehenden Aufarbeitung äolischer Sedimente (siehe hierzu z.B. BÖSE 1991, KASSE 1997, 2002).

In der Gesamtzusammenfassung der OSL–Daten wird deutlich, dass die Altersungenauigkeit der einzelnen OSL-Alter keine feinstratigraphische Gliederung der Dünenentwicklung, insbesondere im Spätglazial, zulässt (siehe Fig. 91). Auch die Betrachtung der standortbezogenen Dünenchronologien zeigt deutlich, dass einzelne Zeitreihen wenig aussagekräftig sind für eine Ausweisung von Phasen erhöhter äolischer Morphodynamik mit regionaler Bedeutung. Erst über den Vergleich mit einheitlich bearbeiteten Dünenchronologien aus dem benachbarten Umfeld und, in einem zweiten Schritt, mit anderen Untersuchungsgebieten lassen sich modellhafte Phasen der Dünenbildung bzw. Reaktivierung herausarbeiten (s. Fig. 92 und Fig. 94).

Dem Einsetzen der Dünenbildung um rund 16,7 ka folgte demnach eine erste bedeutende spätglaziale Dünenbildungsphase zwischen rund 15,2 und 13,7 ka. Dieser Aktivitätsphase schloss sich eine Ruhephase mit Stabilisation der Dünen an, die –in Übereinstimmung mit den OSL-Daten (s. Fig. 95)- an elf der untersuchten Standorte durch den Allerød-zeitlichen ,Finow'-Bodenhorizont belegt wird. Diese Bodenbildung wird schließlich mit Einsetzen der nachfolgenden Aktivitätsphase mit teils mehreren Metern mächtigen Dünensanden überdeckt. Diese im Arbeitsgebiet am weitesten verbreitete Phase der Dünenbildung und –reaktivierung wird über die OSL-Alter auf 12,9 bis rund 11,1 ka datiert (vergl. Fig. 94 und Fig. 100).

Diese mittels OSL datierten Phasen verstärkter äolischer Dynamik mit Dünensandablagerung stimmen gut überein mit entsprechenden Phasen, die KASSE (2002) einerseits für den mehr westlichen Teil des Europäischen Sandgürtels ermittelt hat (18-14,7/14.0 ka, 13-10,2 ka), und WOLFE (2006) für den nördlichsten Teil der Nordamerikanischen Great Plains (15,7-13,4 ka, 12,9-11,3 ka). Beide Studien greifen zurück auf umfassende Altersdatensätze, kombiniert aus Lumineszenz- und Radiokohlenstoffaltern. Der Vergleich zeigt eine gute Übereinstimmung in der Chronologie äolischer Sandablagerungsphasen in den nordamerikanischen und europäischen Sandgürteln einerseits, unterstreicht aber andererseits, dass diese Phasen nicht synchron mit dem Verlauf des Paläoklimas im Spätglazial waren (vergl. Fig. 94 und Fig. 100).

Im Gegensatz zu zahlreichen anderen Modellen, die die Dünenentwicklung stärker an die kalt-trockenen Klimaverhältnisse der spätglazialen Stadiale binden (vergl. Fig. 99), zeigt sich jedoch in der vorliegenden Arbeit ein anderes Bild. So beginnt die Dünenbildung zwar in den Stadialen, z.B. im GS2-a und GS-1, aber dauerte doch deutlich über die Grenze Stadial-

Interstadial bis in das GI-1e und sehr wahrscheinlich auch über die Spätglazial-Holozän-Grenze in das Präboreal hinein an.

Stärker als direkt über das Klima ist die Dünenentwicklung im Spätglazial über die Verfügbarkeit von Sandquellen gesteuert worden, über die Auflösung des Permafrostes, das Trockenfallen der Sanderflächen und Urstromtalböden und das Aufkommen spärlicher Vegetation (vergl. KASSE 2002). Die verzögerte Reaktion auf die oft abrupte Erwärmung mindert die Eignung von Paläodünen als direkte Klimaproxies für die Zeit des Spätglazials mit seinen raschen Klimaumschwüngen. Auf längeren Zeitskalen betrachtet, verliert diese Verzögerung jedoch an Einfluss und, im Gegenzug, gewinnen Paläodünen als terrestrische Archive für das Paläoklima an Bedeutung.

Wie die Untersuchung der Dünenstandorte in Nordostdeutschland weiterhin zeigte, kam es im Verlauf des gesamten Holozäns bis in die jüngste Zeit hinein immer wieder zu Reaktivierungen der Dünen (siehe Fig. 91). Der regionale Vergleich der einzelnen Dünenchronologien innerhalb der fünf Arbeitsgebiete, wie auch der Teilgebiete untereinander, macht aber die hohe räumliche und zeitliche Variabilität dieser ‚äolischen Events' deutlich (siehe Fig. 92). Dieses uneinheitliche Auftreten von lokal eng begrenzten äolischen Aktivitätsereignissen macht Schwankungen der holozänen Klimaverhältnisse als direkten Auslöser für die Reaktivierung der Dünen unwahrscheinlich. Indes, ein sekundärer Effekt des Klimas lässt sich nicht gänzlich ausschließen. Beispielsweise kann nach längeren Trockenperioden die Gefahr der Waldbrände erhöht gewesen sein, die eine Auflichtung der schützenden Vegetationsdecke bewirken konnten.

Der Vergleich der mittels OSL datierten Dünenremobilisation mit der Besiedlungsgeschichte des Arbeitsgebietes unterstreicht schließlich die Bedeutung des Menschen, der in wachsendem Maße im Verlauf des Holozäns in die Landschaft eingegriffen hat. Die Gegenüberstellung der holozänen Dünenchronologien mit der Klimaentwicklung und Besiedlungsgeschichte im Arbeitsgebiet lässt den menschlichen Eingriff als dominanten Einflussfaktor für die Reaktivierung äolischer Prozesse erscheinen (Fig. 96). So scheinen sich beispielsweise Phasen des Bevölkerungsrückgangs durchaus als Unterbrechung in den Dünenchronologie abzuzeichnen. Ob dies nur eine zufällige Übereinstimmung ist, oder ob damit in der Tat ein Hinweis auf eine weitgehende Phase der Stabilisation der Landschaft und äolischer Ruhe gegeben ist, muss jedoch fraglich bleiben angesichts der vorgenannten hohen Variabilität holozäner äolischer Aktivität.

Aus dem vorliegenden OSL Datensatz kann geschlossen werden, dass im Arbeitsgebiet ab etwa 4500 Jahren vor heute der zunehmende menschliche Eingriff in die Naturlandschaft mit der Rodung der natürlichen Wälder und Ausweitung landwirtschaftlicher Flächen zum auslösenden und dominierenden Faktor für die Reaktivierung der spätweichselzeitlich angelegten Binnendünen wurde. Diese Einschätzung ist in guter Übereinstimmung mit dem von SCHIRMER (1999a) vorgestellten Modell zu Phasen erhöhter äolischer Dynamik im Spätglazial und Holozän. Die Ausweisung einzelner äolischer Phasen zur weiteren Untergliederung der holozänen Dünenaktivität, wie in einigen Modellen vorgeschlagen, wird angesichts der in dieser Arbeit dokumentierten großen raum-zeitlichen Variabilität des Auftretens solcher eher als ‚äolische Events' zu beschreibenden Ereignisse als wenig zielführend für die Anwendbarkeit der Modelle erachtet (Fig. 99).

Die hier vorliegende Studie macht deutlich, wie über eine hochauflösende Beprobungsstrategie und die konsistente Anwendung eines methodischen Ansatzes hinsichtlich der Lumineszenzmessungen das Potential der Sedimentdatierung mittels optisch stimulierter Lumineszenz (OSL) für den Zeitraum der letzten 20.000 Jahre verbessert werden kann. Diese Arbeit liefert damit einerseits neue Ergebnisse für die Anwendung der OSL-Datierung, und leistet andererseits einen wichtigen Beitrag zur Chronostratigraphie der Dünenentwicklung im zentralen Teil des ‚European Sand Belt'.

References

ADAMIEC, G. (2000): Variations in luminescence properties of single quartz grains and their consequences for equivalent dose estimation. - Radiation Measurements, **32**: 427-432.

ADAMIEC, G. & AITKEN, M.J. (1998): Dose-rate conversion factors: new data. - Ancient TL, **16**: 37-50.

AGERSNAP LARSEN, N., BULUR, E., BØTTER-JENSEN, L. & MCKEEVER, S.W.S. (2000): Use of the LM-OSL technique for the detection of partial bleaching in quartz. - Radiation Measurements, **32**: 419-425.

AITKEN, M.J. (1985): Thermoluminescence Dating. - London, 359 p.

AITKEN, M.J. (1992): Optical dating. - Quaternary Science Reviews, **11**: 127-131.

AITKEN, M.J. (1998): An Introduction to Optical Dating - The Dating of Quaternary Sediments by the Use of Photon-stimulated Luminescence. - Oxford, 267 p.

AITKEN, M.J. & SMITH, B.W. (1988): Optical dating: recuperation after bleaching. - Quaternary Science Reviews, **7**: 387-393.

ALISCH, M. (1995): Das äolische Relief der mittleren Oberen Allerniederung (Ost-Niedersachsen); spät- und postglaziale Morphogenese, Ausdehnung und Festlegung historischer Wehsande, Sandabgrabungen und Schutzaspekte. - Kölner Geographische Arbeiten, **62**, 180 p.

ALLEY, R.B., MEESE, D.A., SHUMAN, C.A., GOW, A.J., TAYLOR, K.C., GROOTES, P.M., WHITE, J.W.C., RAM, M., WADDINGTON, E.D., MAYEWSKI, P.A. & ZIELINSKI, G.A. (1993): Abrupt increase in Greenland snow accumulation at the end of the Younger Dryas event. - Nature, **362**: 527-529.

ALLKOFER, O. & SIMON, M. (1970): Strahlengefährdung im Höhenbereich des Überschallflugverkehrs. - Atompraxis, **16**: 186-195.

ANDRES, W. & LITT, T. (Guest Editors) (1999): Termination I in Central Europe (special issue). - Quaternary International, **61**, 72 p.

ANDRES, W., BOS, J.A.A., HOUBEN, P., KALIS, A.J., NOLTE, S., RITTWEGER, H. & WUNDERLICH, J. (2001): Environmental change and fluvial activity during the Younger Dryas in central Germany. - Quaternary International, **79**: 89-100.

ARMITAGE, S.J. & BAILEY, R.M. (2005): The measured dependence of laboratory beta dose rates on sample grain size. - Radiation Measurements, **39**: 123-127.

ARMITAGE S.J., DULLER G.A.T. & WINTLE A.G. (2000): Quartz from southern Africa: sensitivity changes as a result of thermal pre-treatment. - Radiation Measurements, **32:** 571-577.

ASTAKHOV, V.I., SVENDSEN, J.I., MATIOUCHKOV, A., MANGERUD, J., MASLENIKOVA, O. & TVERANGER, J. (1999): Marginal formations of the last Kara and Barents ice shelves in northern European Russia. - Boreas, **28**: 23-45.

AUCLAIR, M., LAMOTHE, M. & HUOT, S. (2003): Measurement of anomalous fading for feldspar IRSL using SAR. - Radiation Measurements, **37**: 487-492.

BAALES, M., BITTMAN, F. & KROMER, B. (1999): Verkohlte Bäume im Trass der Laacher See-Tephra bei Kruft (Neuwieder Becken): Ein Beitrag zur Datierung des Laacher See-Ereignisses und zur Vegetation der Alleröd-Zeit am Mittelrhein. - Archäologisches Korrespondenzblatt, **28**: 191-204.

BAILEY, R.M. (1997): Optical detrapping of charge from the 110°C quartz TL region. - Ancient TL, **15**: 7-10.

BAILEY, R.M. (2000): The interpretation of quartz optically stimulated luminescence equivalent dose versus time plots. - Radiation Measurements, **32**: 129-140.

BAILEY, R.M. (2001): Towards a general kinetic model for optically and thermally stimulated luminescence of quartz. - Radiation Measuremetns, **33**: 17-45.

BAILEY, R.M. (2003): Paper I: The use of measurement-time dependent single-aliquot equivalent-dose estimates from quartz in the identification of incomplete signal resetting. - Radiation Measurements, **37**: 673-683.

BAILEY, R.M. & ARNOLD, L.J. (2006): Statistical modelling of single grain quartz D_e distributions and an assessment of procedures for estimating burial dose. - Quaternary Science Reviews, **25**: 2475-2502.

BAILEY, R.M., SMITH, B.W. & RHODES, E.J. (1997): Partial bleaching and the decay form characteristics of quartz OSL. - Radiation Measurements, **27**: 123-136.

BAILEY, R.M., SINGARAYER, J.S., WARD, S. & STOKES, S. (2003): Identification of partial resetting using D_e as a function of illumination time. - Radiation Measurements, **37**: 511-518.

BALLARINI, M., WALLINGA, J., MURRAY, A.S., VAN HETEREN, S., OOST, A.P., BOS, A.J.J. & VAN EIJK, C.W.E. (2003): Optical dating of young coastal dunes on a decadal time scale. - Quaternary Science Reviews, **22**: 1011-1018.

BANERJEE, D., BØTTER-JENSEN, L. & MURRAY, A.S. (1999): Retrospective dosimetry: preliminary use of the single aliquot regeneration (SAR) protocol for the measurement of quartz dose in young house bricks. - Radiation Protection Dosimetry, **84**: 421-426.

BANERJEE, D., BØTTER-JENSEN, L. & MURRAY, A.S. (2000): Retrospective dosimetry: estimation of the dose to quartz using the single-aliquot regenerative-dose protocol. - Applied Radiation and Isotopes, **52**: 831-844.

BANERJEE, D., MURRAY, A.S., BØTTER-JENSEN, L. & LANG, A. (2001): Equivalent dose estimation using a single aliquot of polymineral fine grains. - Radiation Measurements, **33**: 73-94.

BARAY, M., & ZÖLLER, L. (1993): Aspekte der Thermolumineszenz-Datierung an Spätglazial-Holozänen Dünen im Oberrheingraben und in Brandenburg. - Berliner Geographische Arbeiten, **78**(1): 1-33.

BARAY, M. & ZÖLLER, L. (1994): Methodological Aspects of Thermoluminescence Dating of Late Glacial and Holocene Dune Sands from Brandenburg, Germany. - Quaternary Science Reviews, **13**: 477-480.

BARBER, D.C., DYKE, A., HILLAIRE-MARCEL, C., JENNINGS, A.E., ANDREWS, J.T., KERWIN, M.W., BILODEAU, G., MCNEELY, R., SOUTHON, J., MOREHEAD, M.D. & GAGNON, J.M. (1999): Forcing of the cold event of 8,200 years ago by catastrophic drainage of Laurentide lakes. - Nature, **400**: 344-348.

BARD, E., HAMELIN, B., ARNOLD, M., MONTAGGIONI, L., CABIOCH, G., FAURE, G. & ROUGERIE, F. (1996): Deglacial sea-level record from Tahiti corals and the timing of global meltwater discharge. - Nature**, 382:** 241-244.

BARRETT, J.C. (1999): Rethinking the Bronze Age Environment. - In: EDWARDS, K.J. & SADLER, J.P. (eds.): Holocene Environments of Prehistoric Britain. - Quaternary Proceedings, **7**: 493-500.

BATEMAN, M.D. (1995): Thermoluminescence dating of the British coversand deposits. - Quaternary Science Reviews, **14**: 791-798.

BATEMAN, M.D. (1998): The origin and age of coversand in North Lincolnshire, UK. - Permafrost and Periglacial Processes, **9**: 313-325.

BATEMAN, M.D. & DIEZ HERRERO, A. (2001): The timing and relation of aeolian sand deposition in central Spain to the aeolian sand record of northwest Europe. - Quaternary Science Reviews, **20**: 779–782.

BATEMAN, M.D. & GODBY, S.P. (2004): Late-Holocene inland dune activity in the UK, a case study from Breckland, East Anglia. - The Holocene, **14**(4): 579-588.

BATEMAN, M.D. & VAN HUISSTEDEN, J. (1999): The timing of last-glacial periglacial and aeolian events, Twente, eastern Netherlands. - Journal of Quaternary Science, **14**: 277–283.

BATEMAN, M.D., HANNAM, J. & LIVINGSTONE, I. (1999): Late Quaternary dunes at Twigmoor Woods, Lincolnshire, UK: a preliminary investigation. - Zeitschrift für Geomorphologie, **116**: 131-146.

BATEMAN, M.D., MURTON, J.B. & CROWE, W. (2000): Late Devensian and Holocene depositional environments associated with the coversand around Caistor, north Lincolnshire, UK. - Boreas, **29**: 1–15.

BATEMAN, M.D., FREDERICK, C.D., JAISWAL, M.K., & SINGHVI, A.K. (2003): Investigations into the potential effects of pedoturbation on luminescence dating. - Quaternary Science Reviews, **22**: 1169-1176.

BECKER, B., KROMER, B. & TRIMBORN, P. (1991): A stable-isotope tree-ring timescale of the Late Glacial/Holocene boundary. - Nature, **353**: 647-649.

BEHRE, K.-E. (1966): Untersuchungen zur spätglazialen und frühpostglazialen Vegetationsgeschichte Ostfrieslands. - Eiszeitalter und Gegenwart, **17**: 69-84.

BEHRE, K.-E. (1978): Die Klimaschwankungen im europäischen Präboreal.- Petermanns Geographische Mitteilungen, **122**: 97-104.

BEHRENDT, G. (1879): Gletschertheorie oder Drifttheorie in Norddeutschland. - Zeitschrift der Deutschen Geologischen Gesellschaft, **31**: 1-20.

BELL, W.T. & ZIMMERMAN, D.W. (1978): The effect of HF acid etching on the morphology of quartz inclusions for thermoluminescence dating. - Archaeometry, **20**: 63-65.

BELL, W.T. & MEJDAHL, V. (1981): Beta source calibration and its dependency on grain transparency. – Archaeometry, **23**(2): 231-240.

BITTMANN, F. & PASDA, C. (1999): Die Entwicklung einer Düne während der letzten 12.000 Jahre - Untersuchungsergebnisse von Groß Lieskow (Stadt Cottbus) in der Niederlausitz. - Quartär, **49/50**: 39-54.

BJÖRCK, S. (1995): A review of the history of the Baltic Sea, 13.0-8.0 ka BP. - Quaternary International, **27**: 19-40.

BJÖRCK, S., KROMER, B., JOHNSEN, S., BENNIKE, O., HAMMARLUND, D., LEMDAHL, G., POSSNERT, G., RASMUSSEN, T.L., WOHLFAHRT, B., HAMMER, C.U. & SPURK, M. (1996): Synchronized Terrestrial-Atmospheric Deglacial Records Around the North Atlantic. - Science, **274**: 1155-1160.

BJÖRCK, S., RUNDGREN, M., INGOLFSSON, O. & FUNDER, S. (1997): The Preboreal oscillation around the Nordic Seas: terrestrial and lacustrine responses. - Journal of Quaternary Science, **12**: 455-465.

BJÖRCK, S., WALKER, M.J.C., CWYNAR, L.C., JOHNSEN, S., KNUDSEN, K.-L., LOWE, J.J. & WOHLFARTH, B. (INTIMATE MEMBERS) (1998): An event stratigraphy for the Last Termination in the North Atlantic region based on the Greenland ice-core record: a proposal by the INTIMATE group. - Journal of Quaternary Science, **13**: 283-292.

BLYTT, A. (1876): Essay on the immigration of the Norwegian flora during alternating rainy and dry periods. - Kristiania, 89 p.

BOGEN, C. (1999): Ein neuer Stielspitzen-Fundplatz bei Hintersee/Kr. Uecker-Randow in Vorpommern - erste Ergebnisse einer Sondage. Festschrift für Bernhard Gramsch (Langenweißbach), 81-85.

BOGEN, C., HILGERS, A., KAISER, K., KÜHN, P. & LIDKE, G. (2003): Archäologie, Pedologie und Geochronologie spätpaläolithischer Fundplätze in der Ueckermünder Heide (Mecklenburg-Vorpommern). - Archäologisches Korrespondenzblatt, **33**: 1-20.

BOND, G., SHOWERS, W., CHESEBY, M., LOTTI, R., ALMASI, P., DEMENOCAL, P., PRIORE, P., CULLEN, H., HAJADAS, I. & BONANI, G. (1997): A pervasive millennial-scale cycle in North Atlantic Holocene and glacial climates. - Science, **278**: 1257-1266.

BOND, G., SHOWERS, W., ELLIOT, M., EVANS, M., LOTTI, R., HAJDAS, I., BONANI, G. & JOHNSEN, S. (1999): The North Atlantic's 1-2 kyr climate rhythm: relation to Heinrich events, Dansgaard/Oeschger cycles and the Little Ice Age. - In: CLARK, P.U., WEBB, R.S. & KEIGWIN, L.D. (ed.): Mechanisms of Global Climate Change at Millennial Time Scales. - Geophysical Monograph, **112**: 35-58.

BÖNISCH, E. (1999): Lausitzer Kulturen vor dem Braunkohlentagebau. Ausgrabungen des Jahres 1998. - Arbeitsberichte zur Bodendenkmalpflege in Brandenburg, **3**: 9-15.

BORK, H.-R. & DALCHOW, C. (2003): Landschaftsgeschichte. - In: FRIELINGHAUS, M., DALCHOW, C. & SCHÄFER, H. (ed.): Bodenlandschaften im Jung- und Altmoränengebiet - Exkursionsführer zur Jahrestagung der Deutschen Bodenkundlichen Gesellschaft. - Mitteilungen der Deutschen Bodenkundlichen Gesellschaft, **100**: 28-29.

BORK, H.-R., BORK, H., DALCHOW, C., FAUST, B., PIORR, H.-P. & SCHATZ, P. (1998): Landschaftsentwicklung in Mitteleuropa. - Gotha-Stuttgart, 328 p.

BÖSE, M. (1991): A palaeoclimate interpretation of frost wedge casts and aeolian sand deposits in the lowlands between Rhine and Vistula in the upper Pleniglacial and Late Glacial. - In: KOZARSKI, S. (ed.): Late Vistulian and Holocene aeolian phenomena in central and northern Europe. - Zeitschrift für Geomorphologie, NF **90**: 15-28.

BÖSE, M. (2000): Gravel Analyses of Weichselian Tills and OSL-Dates of sand wedges in western Poland. - Quaestiones Geographicae, **21**: 39-44.

BÖSE, M. & BRANDE, A. (1986): Zur Entwicklungsgeschichte des Moores "Alter Hof" am Havelufer (Berliner Forst Düppel). - Berlin-Forschungen, **I**: 11-42.

BÖSE, M., MÜLLER, M., BRANDE, A. & FACKLAM, M. (2002): Jungdünenentwicklung und Siedlungsgeschichte auf der Glindower Platte (Brandenburg). - Brandenburgische Geowissenschaftliche Beiträge, **9**(1/2): 45-57.

BØTTER-JENSEN, L. (1997): Luminescence techniques: Instrumentation and Methods. - Radiation Measurements, **27**(5/6): 749-768.

BØTTER-JENSEN, L. & DULLER, G.A.T. (1992): A new system for measuring optically stimulated luminescence from quartz samples. - Nuclear Tracks and Radiation Measurements, **20**: 549-553.

BØTTER-JENSEN, L., DULLER, G.A.T. & POOLTON, N.R.J. (1994): Exitation and emission spectrometry of stimulated luminescence from quartz and feldspars. - Radiation Measurements, **23**: 613-616.

BØTTER-JENSEN, L., DULLER, G.A.T., MURRAY, A.S. & BANERJEE, D. (1999a): Blue light emitting diodes for optical stimulation of quartz in retrospective dosimetry and dating. - Radiation Protection Dosimetry, **84**(1-4): 335-340.

BØTTER-JENSEN, L., MEJDAHL, V. & MURRAY, A.S. (1999b): New light on OSL. - Quaternary Science Reviews, **18**(2): 303-309.

Bøtter-Jensen, L., Bulur, E., Duller, G.A.T. & Murray, A.S. (2000): Advances in luminescence instrument systems. - Radiation Measurements, **32**: 523-528.

Bøtter-Jensen, L., McKeever, S.W.S. & Wintle, A.G. (2003): Optically Stimulated Luminescence Dosimetry. - Elsevier, 404 p.

Boyle, R. (1664): Experiments and considerations upon colours with observations on a diamond that shines in the dark. - London.

Bradley, R.S. (2000): Climate Paradigms for the Last Millennium. - PAGES Newsletter, **8**(1): 2-3.

Bradley, R.S. & Jones, P.D. (1993): 'Little Ice Age' summer temperature variations: their nature and relevance to recent global warming trends. - The Holocene, **3**(4): 367-376.

Bramer, H. (1964): Das Haffstausee-Gebiet: Untersuchungen zur Entwicklungsgeschichte im Spät- und Postglazial. - Habilitaion thesis (unpublished), University Greifswald.

Bramer, H. (1975): Über ein Vorkommen von Alleröd-Torf in Sedimenten der Ueckermünder Heide. - Wissenschaftliche Zeitschrift Universität Greifswald, Math.-Nat. Reihe **24**(3/4): 11-15.

Brande, A. (1980): Pollenanalytische Untersuchungen im Spätglazial und frühen Postglazial Berlins. - Verh. Bot. Ver. Prov. Brandenburg, **115**: 21-72.

Brande, A. & Böse, M. (1990): Environmental history of aeolian sand transport in the Berlin area. - Abstracts of Paper - International Symposium: Late Vistulian and Holocene aeolian phenomena in Central and Northern Europe (14-18 May 1990, Poland), Quaternary Research Institute, Adam Mickiewicz University Poznan: 5.

Brather, M.-J. (1999): Germanische Häuser und ein Backofen unter dem Teufelsberg bei Briesnig. - Arbeitsberichte zur Bodendenkmalpflege in Brandenburg, **3**: 83-92.

Brauer, A., Endres, C., Günter, C., Litt, T., Stebich, M. & Negendank, J.F.W. (1999): High resolution sediment and vegetation responses to Younger Dryas climate change in varved lake sediments from Meerfelder Maar, Germany. - Quaternary Science Reviews, **18**: 321-329.

Bray, H.E., Bailey, R.M. & Stokes, S. (2002): Quatification of cross-irradiation and cross-illumination using a Risø TL/OSL DA-15 reader. - Radiation Measurements, **35**: 275-280.

Breest, K. & Veil, S. (1991): The Late Upper Palaeolithic site of Schweskau, Ldkr Lüchow-Dannenberg (Germany), and some comments on the relationship between the Magdalenian and Hamburgian. - In: Barton, N., Roberts, A.J., Roe, D.A. (ed.): The Late Glacial in north-west Europe: Human adaptation and environmental change at the end of the Pleistocene. Council for British Archaeology Research Report, **77**:

Breest, K. & Veil, S. (with contributions by Heinemann, B., Hilgers, A., Willerding, U.) (2001): Die Ausgrabungen 2000 auf dem mesolithischen Dünenfundplatz Schletau, Ldkr. Lüchow Dannenberg. - Die Kunde, NF **52**: 239-254.

BRENNAN, B.J. (2003): Beta doses to spherical grains. - Radiation Measurements, **37**: 299-303.

BRENNAN, B.J., SCHWARCZ, H.P. & RINK, W.J. (1997): Simulation of the gamma radiation field in lumpy environments. - Radiation Measurements, **27**: 299-305.

BROECKER, W.S., KENNETT, J.P., FLOWER, B.P., TELLER, J.T., TRUMBOE, S., BONANI, G. & WÖLFLI, W. (1989): Routing of meltwater from the Laurentide Ice Sheet during the Younger Dryas cold episode. - Nature, **341**: 318-321.

BROSE, F. & PRÄGER, F. (1977): Beitrag zur Flußgeschichte von Neiße und Oder. - Zeitschrift für geologisches Wissen, **5**: 777-790.

BUBENZER, O., HILGERS, A. & H. RIEMER (2006): Luminescence dating and archaeology of Holocene fluvio-lacustrine sediments of Abu Tartur, Eastern Sahara. - Quaternary Geochronology (in press).

BULUR, E. (1996): An alternative technique for optically stimulated luminescence (OSL) experiment. - Radiation Measurements, **26**: 701-709.

BULUR, E., BØTTER-JENSEN, L. & MURRAY, A.S. (2000): Optically stimulated luminescence from quartz measured using the linear modulation technique. - Radiation Measurements, **32**: 407-411.

CASPERS, G. & SCHWARZ, C. (1998): Fluviatile und äolische Prozesse im Gebiet der unteren Elbe bei Neuhaus (Niedersachsen) seit dem Weichsel-Spätglazial. - Mitteilungen des Geologischen Institutes Universität Hannover, **38**: 49-64.

CASTEL, I., KOSTER, E. & SLOTBOOM, R. (1989): Morphogenetic aspects and age of Late Holocene eolian drift sands in Northwest Europe. - Zeitschrift für Geomorphologie NF, **33**(1): 1-26.

CATT, J.A. (1977): Loess and coversands. - In: SHOTTON, F.W. (ed.): British Quaternary studies - recent advances: 221-229.

CEPEK, A.G. (1965): Stratigraphie der quartären Ablagerungen des Norddeutschen Tieflandes. - In: GELLERT, J.F. (ed.): Die Weichsel-Eiszeit im Gebiet der Deutschen Demokratischen Republik: 45-65.

CHEN, R. & MCKEEVER, S.W.S. (1997): Theory of Thermoluminescence and Related Phenomena. World Scientific Singapore. - Singapore, 559 p.

CHITHAMBO, M.L. & GALLOWAY, R.B. (2000): On luminescence lifetimes in quartz. - Radiation Measurements, **32**: 621-626.

CLARK, R.J. & BAILIFF, I.K. (1998): Fast time-resolved luminescence emission spectroscopy in some feldspars. - Radiation Measurements, **29**: 553-560.

CLARK, R.J., BAILIFF, I.K. & TOOLEY, M.J. (1997): A preliminary study of time-resolved luminescence in some feldspars. - Radiation Measurements, **27**: 211-220.

CLARKE, M.L., RENDELL, H.M. & WINTLE, A.G. (1999): Quality assurance in luminescence dating. - Geomorphology, **29**: 173-185.

CLAUSEN, I. (1995): Alt Duvenstedt, Kreis Rendsburg-Eckernförde, LA 121. Ein Ahrensburger Kulturvorkommen in allerödzeitlichem Boden. - Archäologische Nachrichten aus Schleswig-Holstein, **6**: 103-126.

COLLS, A.E.L (1999): Optical dating of fluvial sediments from the Loire Valley, France. - Master of Science thesis (unpublished), University of Oxford.

CROWLEY, T. J. (2000): Causes of Climate Change Over the Past 1000 Years. - Science, **289**: 270-277.

DANIELS, F., BOYD, C.A. & SAUNDERS, D.F. (1953): Thermoluminescence as a Research Tool. - Science, **117**: 343-349.

DANSGAARD, W., JOHNSEN, S.J., CLAUSEN, H.B., DAHL-JENSEN, D., GUNDESTRUP, N.S., HAMMER, C.U., HVIDBERG, C.S., STEFFENSEN, J.P., SVEINBJÖRNSDOTTIR, A.E., JOUZEL, J. & BOND, G. (1993): Evidence for general instability of past climate from a 250-kyr ice-core record. - Nature, **364**, 218–220.

DE BOER, W.M. (1993): Late Vistulian and Holocene inland dunes in the central part of the former GDR - an overview of post-war research. - Quaestiones Geographicae **15/16**: 23-25.

DE BOER, W.M. (1995): Äolische Prozesse und Landschaftsformen im mittleren Baruther Urstromtal seit dem Hochglazial der Weichseleiszeit. - Berliner Geographische Arbeiten, **84,** 215 p.

DE KLERK, P. (2002): Changing vegetation patterns in the Endinger Bruch area (Vorpommern, NE Germany) during the Weichselian Lateglacial and Early Holocene. - Review of Palaeobotany and Palynology, **119**: 275-309.

DE KLERK, P. (2004): Changes in vegetation and environment at the Lateglacial - Holocene transition in Vorpommern (Northeast Germany). - In: TERBERGER, T. & ERIKSEN, B.V. (ed.): Hunters in a changing world. - Internationale Archäologie - Arbeitsgemeinschaft, Tagung, Symposium, Kongress, **5**: 27-42.

DE KLERK, P. & STOLZE, S. (2002): Unterschiede in Vegetation und Sedimentation zwischen N-Vorpommern und S-Mecklenburg: Ein spätglazialer Klimagradient? - Greifswalder Geographische Arbeiten, **26**: 161-165.

DE KLERK, P, HELBIG, H., HELMS, S., JANKE, W., KRÜGEL, K., KÜHN, P., MICHAELIS, D. & STOLZE, S. (2001): The Reinberg researches: palaeoecological and geomorphological studies of a kettle hole in Vorpommern (NE Germany), with special emphasis on a local vegetation during the Weichselian Pleniglacial/Lateglacial transition. - In: BILLWITZ, K. (ed.): Geoökologische und landschaftsgeschichtliche Studien in Mecklenburg-Vorpommern. - Greifswalder Geographische Arbeiten, **23**: 43-131.

DEEBEN, J. (1995): Human occupation of the southern Netherlands during the Younger Dryas (extended abstract). - Geologie en Mijnbouw, **74**: 265-269.

DÖRSCHEL, B., SCHURICHT, V. & STEUER, J. (1992): Praktische Strahlenschutzphysik. - Heidelberg-Berlin-New York, 499 p.

DÜCKER, A. (1954): Die Periglazialerscheinungen im holsteinschen Pleistozän. - Göttinger Geographische Abhandlungen, **16**: 5-54.

DULLER, G.A.T. (1991): Equivalent dose determination using single aliquots. - Nuclear Tracks and Radiation Measurements, **18**: 371-378.

DULLER, G.A.T. (1994): Luminescence dating using single aliquots: new procedures. - Quaternary Science Reviews, **13**: 149-156.

DULLER, G.A.T. (1995): Luminescence dating using single aliquots: methods and applications. - Radiation Measurements, **24**(3): 217-226.

DULLER, G.A.T. (2002): Luminescence Analyst, Version 3.07b (Manual).

DULLER, G.A.T. (2004): Luminescence dating of Quaternary sediments: recent advances. - Journal of Quaternary Science, **19**(2): 183-192.

DULLER, G.A.T., BØTTER-JENSEN L. & MURRAY, A.S. (2000): Optical dating of single sand-sized grains of quartz: sources of variability. - Radiation Measurements, **32**: 453-457.

DULLER, G.A.T., BØTTER-JENSEN, L. & MURRAY, A.S. (2003): Combining infrared- and green-laser stimulation sources in single-grain luminescence measurements of feldspar and quartz. - Radiation Measurements, **37**: 543-550.

DYLIK, J. (1967): The main elements of Upper Pleistocene palaeogeography in Central Poland. - Biul. Peryglac., **16**: 89-115.

DYLIKOWA, A. (1969): Problematyka wydm srodladowych w Polsce w swietle badan strukturalnych. (summary: Problematics of inland dunes in Poland in the light of structural examinations). - Prace Geograficzne IG PAN, **75**: 39-74.

EDMONDS, M. (1999): Inhabiting Neolithic Landscapes. - In: EDWARDS, K.J. & SADLER, J.P. (ed.): Holocene Environments of Prehistoric Britain. - Quaternary Proceedings, **7**: 485-492.

EDWARDS, R.L., BECK, J.W., BURR, G.S., DONAHUE, D.J., CHAPELL, J.M.A., BLOOM, A.L., DRUFFEL, E.R.M. & TAYLOR, F.W. (1993): A large drop in atmospheric $^{14}C/^{12}C$ and reduced melting in the Younger Dryas, documented with ^{230}Th ages of corals. - Science, **260**: 962-968.

EHLERS, J., EISSMANN, L., LIPPSTREU, L., STEPHAN, H.-J. & WANSA, S. (2004): Pleistocene glaciations of North Germany. - In: EHLERS, J. & GIBBARD, P.L.(ed): Quaternary Glaciations - Extent and Chronology, Part I: Europe, Developments in Quaternary Science, **2**: 135-146.

EIERMANN, J. (1984): Ein zeitliches, räumliches und genetisches Modell zur Erklärung der Sedimente und Reliefformen im Pleistozän gletscherbedeckter Tieflandsedimente - Ein Beitrag zur Methodik der mittelmaßstäbigen naturräumlichen Gliederung. - In: RICHTER, H. & AURADA, K. (ed.): Umweltforschung. Zur Analyse und Diagnose der Landschaft: 169-183.

ERFURT, G. (2003): Radiolumineszenzspektroskopie und -dosimetrie an Feldspäten und synthetischen Luminophoren für die geochronometrische Anwendung. - Ph.D. thesis, Bergakademie Freiberg, 129 p.

ERFURT, G. & KRBETSCHEK, M.R. (2003): Studies on the physics of the infrared radioluminescence of potassium feldspar and on the methodology of its application to sediment dating. - Radiation Measurements, **37**: 505-510.

ERFURT, G., KRBETSCHEK, M.R., BORTOLOT, V.J. & PREUSSER, F. (2003): A fully automated multi-spectral radioluminescence reading system for geochronometry and dosimetry. – Nuclear Instruments and Methods in Physics Research B, **207**: 487-499.

FATTAHI, M. & STOKES, S. (2000): Extending the time range of luminescence dating using red TL (RTL) from volcanic quartz. - Radiation Measurements, **32**: 479-485.

FAURE, G. (1986): Principles of Isotope Geology. - New York[2], 589 p.

FIEDLER, H.J., ALTERMANN, M. & NEBE, W. (1963): Bemerkungen zum Geschiebedecksand, Teil II. - Wissenschaftliche Zeitschrift der Technischen Universität Dresden, **12**(3): 13-14.

FILION, L., SAINT-LAURENT, D., DESPONTS, M. & PAYETTE, S. (1991): The late Holocene record of aeolian and fire activity in northern Québec, Canada. - The Holocene, **1**(3): 201-208.

FINK, T. (2000): Lumineszenzdatierung eines spätglazialen und holozänen Dünenprofils bei Ossendrecht (Niederlande) - Methodische Untersuchungen des Multiple und Single Aliquot Regenerierungsprotokolls für Quarze. - Diploma thesis, University of Cologne (unpublished), 112 p.

FIRBAS, F. (1949): Die spät- und nacheiszeitliche Waldgeschichte Mitteleuropas nördlich der Alpen. Erster Band: Allgemeine Waldgeschichte. - Jena, 480 p.

FOLZ, E., BODU, O., BONTE, P., JORON, J.L., MERCIER, N. & REYSS, J.L. (2001): OSL dating of fluvial quartz from Le Closeau, a Late Palaeolithic site near Paris - comparison with ^{14}C chronology. - Quaternary Science Reviews, **20**: 927-933.

FORMAN, S., WEBB, R.S., PIERSON, J., GOMEZ, J. & MARIN, L. (2003): Deciphering late Holocene eolian sand depositional records from western Nebraska; landscape response to extreme drought. - In: Geological Society of America, 2003 annual meeting, abstracts with programs, Geological Society of America, **35**: 6.

FORMAN, S.L., MARÍN, L., PIERSON, J., GÓMEZ, J., MILLER, G.H. & WEBB, R.S. (2005a): Aeolian sand depositional records from western Nebraska: landscape response to droughts in the past 1500 years. - The Holocene, **15**(7): 973-981.

FORMAN, S.L., PIERSON, J., GOMEZ, J. & MARIN, L. (2005b): Assesing the timing of late Holocene eolian deposition in the western U.S. by SAR dating: How young can we go? - Book of Abstracts, 11th International Conference on Luminescence and Electron Spin Resonance Dating - Cologne, Germany, July 24-29 2005: 65.

FORMAN, S.L:, SPAETH, M., MARÍN, L., PIERSON, J., GÓMEZ, J., BUNCH, F. & VALDEZ, A. (2006): Episodic Late Holocene dune movements on the sand-sheet area, Great Sand Dunes National Park and Preserve, San Luis Valley, Colorado, USA. - Quaternary Research, **66**: 97-108.

FRANKLIN, A.D. (1994): Lack of interaction between the rapidly and slowly bleaching TL peaks in an Australian quartz. - Ancient TL, **12**(1): 5-9.

FRANKLIN, A.D. & HORNYAK, W.F. (1990): Isolation of the rapidly bleaching peak in quartz TL glow curves. - Ancient TL, **8**(3): 29-31.

FRANKLIN, A.D., PRESCOTT, J.R. & SCHOLEFIELD, R.B. (1995): The mechanism of thermoluminescence in an Australian quartz. - Journal of Luminescence, **63**: 317-326.

FRIEDRICH, M., REMMELE, S., KROMER, B., HOFMANN, J., SPURK, M., KAISER, K.F., ORCEL, C. & KÜPPERS, M. (2004): The 12,460-year Hohenheim oak and pine tree-ring chronology from Central Europe - a unique record of radiocarbon calibration and paleoenvironment reconstructions. - Radiocarbon, **46**: 1111-1122.

FUCHS, M. (2001): Die OSL-Datierung von Archäosedimenten zur Rekonstruktion anthropogen bedingter Sedimentumlagerungen. Geoarchäologische Untersuchungen im Becken von Phlious, NE-Peloponnes, Griechenland. - Diss. Univ. Heidelberg, 197 p.

FUCHS, M. & LANG, A. (2001): OSL dating of coarse-grain fluvial quartz using single-aliquot protocols on sediments from the NE Peloponnese, Greece. - Quaternary Science Reviews, **20**: 783-787.

FUCHS, M. & WAGNER, G.A. (2003): Recognition of insufficient bleaching by small aliquots of quartz for reconstructing soil erosion in Greece. - Quaternary Science Reviews, **22**: 1161-1167.

FUCHS, M., STRAUB, J & ZÖLLER, L. (2005): Residual Luminescence signals of recent river flood sediments: A Comparison between quartz and feldspar of fine- and coarse-grain sediments. - Ancient TL, **23**(1): 25-30.

FUCHS, M., WODA, C. & BÜRKERT, A. (2006): Chronostratigraphy of a sediment record from the Hajar mountain range in north Oman: Implications for optical dating of insufficiently bleached sediments. - Quaternary Geochronology (in press).

GALBRAITH, R.F. (2003): A simple homogeneity test for estimates of dose obtained using OSL. - Ancient TL, **21**(2): 75-77.

GALBRAITH, R.F., ROBERTS, R.G., LASLETT, G.M., YOSHIDA, H. & OLLEY, J.M. (1999): Optical dating of single and multiple grains of quartz from Jinmium Rock Shelter, Northern Australia: Part 1, Experimental design and statistical models. - Archaeometry, **41**(2): 339-364.

GALBRAITH, R. F., ROBERTS, R.G. & YOSHIDA, H. (2005): Error variation in OSL palaeodose estimates from single aliquots of quartz: a factorial experiment. - Radiation Measurements, **39**: 289-307.

GALLOWAY, R.B. (1996): Equivalent dose determination using only one sample: alternative analysis of data obtained from infrared stimulation of feldspars. - Radiation Measurements, **26**: 103-106.

GAMBLE, C. (1996): Die Besiedlung Europas: 700 000 - 40 000 Jahre vor heute. - In: CUNLIFFE, B. (ed.): Illustrierte Vor- und Frühgeschichte Europas: 13-54.

GÄRTNER, P. (1993): Beiträge zur Landschaftsgeschichte des Westlichen Barnim. - Berliner Geographische Arbeiten, **77**.

GÄRTNER, P., BEHRENDT, L., BUSSEMER, S., MARCINEK, J., MARKUSE, G. & SCHLAAK, N. (1995): Quartärmorphologisches Nord-Südprofil durch Brandenburg. - Berichte zur deutschen Landeskunde, **69**(2): 229-262.

GAUTIER, Y. (1997): Späteiszeitlicher Kiefernwald - Archäologische und vegetationsgeschichtliche Untersuchungen im Tagebau Cottbus-Nord, Landkreis Spree-Neiße. - Archäologie Berlin und Brandenburg 1995-1996: 40-42.

GAUTIER, Y. (1999): Feuerstellen, Dünen, Wald: Bausteine einer spätglazialen Landschaft im Tagebau Cottbus-Nord. - Quartär, **49/50**: 29-33.

GEHRT, E. (1994): Die äolischen Sedimente im Bereich der nördlichen Lössgrenze zwischen Leine und Oker und deren Einflüsse auf die Bodenentwicklung. - PhD thesis, University of Göttingen (unpublished), 217 p.

GEHRT, E. (ed.) (1998): Äolische Sedimente und Bodenentwicklung im nördlichen Harzvorland. Exkursionsführer zur 17. Sitzung des Arbeitskreises Paläopedologie der Deutschen Bodenkundlichen Gesellschaft am 21. bis 23.5.1998 in Braunschweig. - Hannover, 132 p.

GEHRT, E. & HAGEDORN, J. (1996): Zur Entstehung der nördlichen Lössgrenze in Mitteleuropa. - In: Landesamt für Natur und Umwelt des Landes Schleswig-Holstein, Abt. Geologie/Boden (ed.): Böden als Zeugen der Landschaftsentwicklung - Beiträge aus dem Arbeitskreis „Paläopedologie" der Deutschen Bodenkundlichen Gesellschaft: 59-66.

GEYH, M.A. (1980): Einführung in die Methoden der physikalischen und chemischen Altersbestimmung. - Darmstadt, 276 p.

GEYH, M.A; (2000): Zum Umgang mit numerischen Altersangaben. - Regensburger Geographische Schriften, **33**: 1-17.

GEYH, M.A. (2005): Handbuch der physikalischen und chemischen Altersbestimmung. - Darmstadt, 211 p.

GEYH, M.A. & SCHLEICHER, H. (1990): Absolute Age Determination - Physical and Chemical Dating Methods and their Application. - Berlin-Heidelberg, 503 p.

GEYH, M.A. & TECHMER, A. (1997): ^{230}Th/^{234}U-Datierung der organogenen Sedimente der Bohrung Groß Todtshorn (Kr. Harburg; Niedersachsen). - In: FREUND, H. & CASPERS, G. (ed.) (1997): Vegetation und Paläoklima der Weichsel-Kaltzeit im nördlichen Mitteleuropa - Ergebnisse paläobotanischer, -faunistischer und geologischer Untersuchungen. - Schriftenreihe der Deutschen Geologischen Gesellschaft, **4**: 103-110.

GEYH, M.A., HENNIG, G, & OEZEN, D. (1997): U/Th-Datierung interglazialer und interstadialer Niedermoortorfe und Lignite - Stand und Zukunft. - In: FREUND, H., & CASPERS, G. (ed.) (1997): Vegetation und Paläoklima der Weichsel-Kaltzeit im nördlichen Mitteleuropa - Ergebnisse paläobotanischer, -faunistischer und geologischer Untersuchungen. - Schriftenreihe der Deutschen Geologischen Gesellschaft, **4**: 187-199.

GODFREY-SMITH, D., HUNTLEY, D. & CHEN, W.-H. (1988): Optical dating studies of quartz and feldspar sediments extracts. - Quaternary Science Reviews, **7**: 373-380.

GÖRSDORF, J. & KAISER, K. (2001): Radiokohlenstoffdaten aus dem Spätpleistozän und Frühholozän von Mecklenburg-Vorpommern. - Meyniana, **53**: 91-118.

GOSLAR, T., KUC, T., RALSKA-JASIEWICZOWA, M., RÓZÁNSKI, K., ARNOLD, M., BARD, E., VAN GEEL, B., PAZDUR, M., SZEROCZYNSKA, K., WICIK, B., WIECKOWSKI, K. & WALANUS, A. (1993): High-resolution lacustrine record of the Late Glacial/Holocene transition in central Europe. - Quaternary Science Reviews, **12**: 287-294.

GOSLAR, T., ARNOLD, M., BARD, E., KUC, T., PAZDUR, M.F., RALSKA-JASIEWICZOWA, M., RÓZÁNSKI, K., TISNERAT, N., WALANUS, A., WICIK, B. & WIECKOWSKI, K. (1995): High concentration of atmospheric ^{14}C during the Younger Dryas. - Nature, **377**: 414-417.

GOSLAR, T., RALSKA-JASIEWICZOWA, M., STARKEL, L., DEMSKE, D., KUC., T., LACKA, B., SZEROCZYNSKA, K., WICIK, B. & WIECKOWSKI, K. (1998): Discussion of the Late-Glacial recorded in the Lake Gosciaz sediments. - In: RALSKA-JASIEWICZOWA, M., GOSLAR, T., MADEYSKA, T. & STARKEL, L. (ed.): Lake Gosciaz, Central Poland. A monographic study: 171-175.

GÖTZE, J., PLÖTZE, M. & HABERMANN, D. (2001): Origin, spectral characteristics and practical applications of the cathodoluminescence (CL) of quartz - a review. - Mineralogy and Petrology, **71**: 225-250.

GÖTZE, J., PLÖTZE, M. & TRAUTMANN, T. (2005): Structure and luminescence characteristics of quartz from pegmatites. - American Mineralogist, **90**: 13-21.

GOUDIE, A. (1995): Physische Geographie. Eine Einführung. - Berlin-Oxford, 402 p.

GOZDZIK, J. (1991): Sedimentological record of aeolian processes from the Upper Plenivistulian and the turn of Pleni- and Late Vistulian in Central Poland. - Zeitschrift für Geomorphologie, NF **90**: 51–60.

GRAMSCH, B. (2004): From the Late Palaeolithic to the early Mesolithic in northeastern Germany. - In: TERBERGER, T. & ERIKSEN, B.V. (ed.): Hunters in a changing world. - Internationale Archäologie - Arbeitsgemeinschaft, Tagung, Symposium, Kongress, **5**: 183-201.

GRINGMUTH-DALLMER, E. (1999): Die ur-und frühgeschichtliche Besiedlung der Uckermark. - In: SCHMIDT, R., BORK, H.-R. & FISCHER-ZUJKOV, U. (ed.): Paläoböden und Kolluvien auf glazialen Sedimenten Nordostdeutschlands. - ZALF-Bericht, **37**: 22-25.

GRÜN, R. (1989): Die ESR-Altersbestimmungsmethode. Reihe: Hochschultext. - Berlin-Heidelberg, 132 p.

GUIBERT, P., BECHTEL, F., SCHVOERER, M., MÜLLER, P. & BALESCU, S. (1998): A new method for gamma-dose-rate estimation of heterogenous media in TL dating. - Radiation Measurements, **29**(5): 561-572.

HAJDAS, I., IVY-OCHS, S.D., BONANI, G., LOTTER, A.F., ZOLITSCHKA, B. & SCHLÜCHTER, C. (1995a): Radiocarbon age of the Laacher See Tephra: 11,230±40 BP. - Radiocarbon, **37**: 149-154.

HAJDAS, I., ZOLITSCHKA, B., IVY-OCHS, S.D., BEER, J., BONANI, G., LEROY, S.A.G., NEGENDANK, J.W., RAMRATH, M. & SUTER, M. (1995 b): AMS Radiocarbon dating of annually laminated sediments from Lake Holzmaar, Germany. - Quaternary Science Reviews, **14**: 137-143.

HARDER, D. (1996): Strahlenphysik und Strahlenbiologie. - In: SIEHL, A. (ed.): Umweltradioaktivität. Geologie und Ökologie im Kontext: 31-68.

HASS, H.C. (1999): Sedimentation Rates and Late Holocene Climate Change: A Case Study from the Skagerrak (NE North Sea). - GeoResearch Forum, **5**: 197-208.

HEERDT, S. (1965): Zur Stratigraphie des Jungpleistozäns im mittleren N-Mecklenburg. - Geologie, **14**: 589-609.

HELBIG, H. (1999): Die spätglaziale und holozäne Überprägung der Grundmoränenplatten in Vorpommern. - Greifswalder Geographische Arbeiten, **17**, 110 p.

HERKING, C.M. (2004): Pollenanalytische Untersuchungen zur holozänen Vegetationsgeschichte entlang des östlichen unteren Odertals und südlichen unteren Wartatals in Nordwestpolen. - Ph.D. thesis, University of Göttingen, 127 p.

HILGERS, A., GEHRT, E., JANOTTA, A. & RADTKE, U. (2001a): A Contribution to the Dating of the Northern Boundary of the Weichselian Loess Belt in Northern Germany by Luminescence Dating and Pedological Analysis. - Quaternary International, **76/77**: 191–200.

HILGERS, A., MURRAY, A. S., SCHLAAK, N. & RADTKE, U. (2001b): Comparison of Quartz OSL Protocols using Late Glacial and Holocene dune sands from Brandenburg, Germany. - Quaternary Science Reviews, **20**: 731-736.

HOEK, W.Z. (2001): Vegetation response to the ~ 14.7 and ~ 11.5 ka cal. BP climate transitions: is vegetation lagging climate? - Global and Planetary Change, **30**: 103-115.

HUBBERTEN, H. W., ANDREEV, A., ASTAKHOV, V.I., DEMIDOV, I., DOWDESWELL, J.A., HENRIKSEN, M., HJORT, CH., HOUMARK-NIELSEN, M., JAKOBSSON, M., KUZMINA, S. et al (2004): The periglacial climate and environment in northern Eurasia during the Last Glaciation. - Quaternary Science Reviews, **23**: 1333-1357.

HUIJZER, A.S. & ISARIN, R.F.B. (1997): The reconstruction of past climates using multi-proxy evidence: An example of the Weichselian Pleniglazial in northwest and central Europe. - Quarternary Science Reviews, **16**: 513-533.

HUNTLEY, D.J. & BARIL, M.R. (1997): The K content of K-feldspars being measured in optical and thermoluminescence dating. - Ancient TL, **15**: 11-13.

HUNTLEY, D.J. & HANCOCK, R.G.V. (2001): The Rb contents of the K-feldspar grains being measured in optical dating. - Ancient TL, **19**: 43-46.

HUNTLEY, D.J. & LAMOTHE, M. (2001): Ubiquity of anomalous fading in K-feldspars and the measurement and correction for it in optical dating. - Canadian Journal of Earth Sciences, **38**: 1093–1106.

HUNTLEY, D.J. & PRESCOTT, J. R. (2001): Improved methodology and new thermoluminescence ages for the dune sequence in south-east South Australia. - Quaternary Science Reviews, **20**: 687-699.

HUNTLEY, D.J., GODFREY-SMITH, D.I. & THEWALT, M.L.W (1985): Optical dating of sediments. - Nature, **313**: 105-107.

HUNTLEY, D.J., GODFREY-SMITH, D.I. & HASKELL, E.H. (1991): Light-induced emission spectra from some quartz and feldspars. - Nuclear Tracks and Radiation Measurements, **18**: 127-131.

HUNTLEY, D.J., HUTTON, J.T. & PRESCOTT, J.R. (1993): The stranded beach-dune sequence of south-east South Australia: a test of Thermoluminescence dating, 0-800 ka. - Quaternary Science Reviews, **12**: 1-20.

HUNTLEY, D.J., SHORT, M.A. & DUNPHY, K. (1996): Deep traps in quartz and their use for optical dating. - Canadian Journal of Physics, **74**: 81-91.

HÜTT, G., JAEK, I. & TCHONKA, J. (1988): Optical dating: K-feldspars optical response stimulation spectra. - Quaternary Science Reviews, **7**: 381-386.

IBACH, H. & LÜTH, H. (1995): Festkörperphysik - Einführung in die Grundlagen. - Berlin-Heidelberg-New York, 410 p.

ICRU (International Commission on Radiation Units and Measurements) (1998): Fundamental Quantities and Units for Ionizing Radiation. - ICRU Report **60**, 19 p.

INOUE, K., NAGATOMO, T. & IKEYA, M. (2005): Infrared stimulated luminescence in quartz. - Radiation Measurements, **39**: 191-196.

ISARIN, R.F.B., RENSSEN, H. & KOSTER, E.A. (1997): Surface wind climate during the Younger Dryas in Europe as inferred from aeolian records and model simulations. - Palaeogeography, Palaeclimatology, Palaeoecology, **134**: 127-148.

ISARIN, R.F.B., RENSSEN, H. & VANDENBERGHE, J. (1998): The impact of the North Atlantic Ocean on the Younger Dryas climate in northwestern and central Europe. - Journal of Quaternary Science, **13**: 447-453.

IVANOVICH, M. & HARMON, R.S. (ed.) (1982): Uranium series disequilibrium: Applications to environmental problems. Oxford, 571 p.

JACOBS, J. (1991): Die Einzelgrabkultur in Mecklenburg-Vorpommern. Schwerin.

JACOBS, J., DULLER, G.A.T. & WINTLE, A.G. (2003): Optical dating of dune sand from Blombos Cave, South Africa: II - single grain data. - Journal of Human Evolution, **44**: 613–625.

JAIN, M., BØTTER-JENSEN, L., MURRAY, A.S. & JUNGNER, H. (2002): Retrospective dosimetry: dose evaluation using unheated and heated quartz from a radioactive waste storage building. - Radiation Protection Dosimetry, **101**: 525-530.

JAIN, M., MURRAY, A.S. & BØTTER-JENSEN, L. (2003): Characterisation of blue-light stimulated luminescence components in different quartz samples: implications for dose measurements. - Radiation Measurements, **37**: 441-449.

JAIN, M., MURRAY, A.S. & BØTTER-JENSEN, L. (2004): Optically stimulated luminescence dating: How significant is incomplete light exposure in fluvial environments? - Quaternaire, **15**: 143-157.

JANOTTA, A., RADTKE, U., CZWIELUNG, K. & HEIDGER, M. (1997): Luminescence-Dating (IRSL/TL) of Lateglacial and Holocene Dune Sands and Sandy Loesses near Bonn, Gifhorn and Diepholz (Germany). - Quaternary Science Reviews, **16**: 349-355.

JOHNSEN, S.J., CLAUSEN, H.B., DANSGAARD, W., FUHRER, K., GUNDESTRUP, N., HAMMER, C.U., IVERSEN, P., JOUZEL, J., STAUFFER, B. & STEFFENSEN, J.P. (1992): Irregular interstadials recorded in a new Greenland ice core. - Nature, **359:** 311–313.

JOHNSEN, S.J., DAHL-JENSEN, D., DANSGAARD, W. & GUNDESTRUP, N. (1995): Greenland palaeotemperatures derived from GRIP borehole temperature and ice core profiles. - Tellus, **47B**: 624–629.

JUSCHUS, O. (2003): Das Jungmoränenland südlich von Berlin - Untersuchungen zur jungquartären Landschaftsentwicklung zwischen Unterspreewald und Nuthe. - Berliner Geographische Arbeiten, **95**, 152 p.

KACZANOWSKI, P. & KOZŁOWSKI, J.K. (1998): Wielka historia Polski (The Great History of Poland). FOGRA, Kraków, **1**: 382 p. (in Polish).

KÁDÁR, L. (1938): Die periglazialen Binnendünen des Norddeutschen und Polnischen Flachlandes. - Comptes-Rendus du Congr. Int. de Géographie, Section IIa Géographie Physique: 167-183.

KAISER, K. & KÜHN, P. (1999): Eine spätglaziale Braunerde aus der Ueckermünder Heide. Geoarchäologische Untersuchungen in einem Dünengebiet bei Hintersee, Kreis Uecker-Randow, Mecklenburg-Vorpommern. - Mitteilungen der Deutschen Bodenkundlichen Gesellschaft, **91**: 1037-1040.

KAISER, K. & TERBERGER, T. (1996): Archäologisch-geowissenschaftliche Untersuchungen am spätpaläolithischen Fundplatz Nienhagen, Lkr. Nordvorpommern. - Bodendenkmalpflege in Mecklenburg-Vorpommern, **43**: 7-48.

KAISER, K. (2001): Die spätpleistozäne bis frühholozäne Beckenentwicklung in Mecklenburg-Vorpommern - Untersuchungen zur Stratigraphie, Geomorphologie und Geoarchäologie. - Greifswalder Geographische Arbeiten, **24**, 208 p.

KAISER, K. (2004): Lake basin development in the Endinger Bruch area (Vorpommern, NE Germany) during the Late Pleistocene and Early Holocene. - Zeitschrift für Geomorphologie, NF **48**(4): 461-480.

KAISER, K., ENDTMANN, E., BOGEN, C., CZAKÓ PAP, S. & KÜHN, P. (2001): Geoarchäologie und Palynologie spätpaläolithischer und mesolithischer Fundplätze in der Ueckermünder Heide, Vorpommern. - Zeitschrift für geologische Wissenschaften, **29**: 233-244.

KAISER, K., BOGEN, C., CZAKÓ-PAP, S. & JANKE, W. (2003): Zur Geoarchäologie des mesolithisch-neolithischen Fundplatzes Rothenklempenow am Latzigsee in der Ueckermünder Heide. - Greifswalder Geographische Arbeiten, **29**: 27-68.

KAISER, K., BARTHELMES, A., CZAKÓ PAP, S., HILGERS, A., JANKE, W., KÜHN, P. & THEUERKAUF, M. (2006): A Lateglacial palaeosol cover in the Altdarss area, southern Baltic Sea coast (Northeast Germany): investigations on pedology, geochronology, and botany. - Netherlands Journal of Geosciences, **85**(3): 199-222.

KALCHGRUBER, R., FUCHS, M., MURRAY, A.S. & WAGNER, G.A. (2003): Evaluating dose-rate distributions in natural sediments using α-Al$_2$O$_3$:C grains. - Radiation Measurements, **37**(4-5): 293-297.

KALIS, A.J., MERKT, J. & WUNDERLICH, J. (2003): Environmental changes during the Holocene climatic optimum in central Europe - human impact and natural causes. - Quaternary Science Reviews, **22**(1): 33-79.

KASSE, C. (1995): Younger Dryas cooling and fluvial response (Maas River, The Netherlands) (extended abstract). - Geologie en Mijnbouw, **74**: 251–256.

KASSE, C. (1997): Cold-Climate Aeolian Sand-Sheet Formation in North-Western Europe (c. 14-12.4 ka); a Response to Permafrost Degradation and Increased Aridity. - Permafrost and Periglacial Processes, **8**: 295-311.

KASSE, C. (1999): Late Pleniglacial and Late Glacial aeolian phases in The Netherlands. - In: SCHIRMER, W. (ed.): Dunes and fossil soils. - GeoArchaeoRhein, **3**: 61-82.

KASSE, C. (2002). Sandy aeolian deposits and environments and their relation to climate during the Last Glacial Maximum and Lateglacial in northwest and central Europe. - Progress in Physical Geography, **26**(4): 507-532.

KASSE, C., VANDENBERGHE, J. & BOHNCKE, S. (1995): Climatic change and fluvial dynamics of the Maas during the late Weichselian and early Holocene. - In: FRENZEL, B. (ed.): European river activity and climatic change during the Lateglacial and early Holocene. ESF Project European Palaeoclimate and Man, Special Issue 9. - Paläoklimaforschung/Palaeoclimate Research, **14**: 123–150.

KAYSER, H. (1999): Spätglaziale Dünenlandschaften mit steinzeitlichen Rastplätzen im Tagebau Cottbus-Nord. - Arbeitsberichte zur Bodendenkmalpflege in Brandenburg, **3**: 17-22.

KEILHACK, K. (1898): Die Stillstandslagen des letzten Inlandeises und die hydrographische Entwicklung des Pommerschen Küstengebietes. - Jahrbuch der Preussischen Geologischen Landesanstalt, **19**: 90-152.

KEILHACK, K. (1917): Die grossen Dünengebiete Norddeutschlands. - Zeitschrift der Deutschen Geologischen Gesellschaft, **69**: 2-19.

KEMSKI, J., KLINGEL, R. & SIEHL, A. (1996): Die terrestrische Strahlung durch natürliche radioaktive Elemente in Gesteinen und Böden. - In: SIEHL, A. (ed.): Umweltradioaktivität. Geologie und Ökologie im Kontext: 69-96.

KIRSCH, E. (1994): Beiträge zur älteren Trichterbecherkultur in Brandenburg. Forschungen zur Archäologie im Land Brandenburg, **2**, 190 p.

KLEINMANN, A., MERKT, J. & MÜLLER, H. (2002): Sedimentologische und palynologische Untersuchungen an Ablagerungen des Siethener Sees und Blankensees (Brandenburg) - erste Ergebnisse. - Greifswalder Geographische Arbeiten, **26**: 59-62.

KLIEWE, H. (1995): Vulkanasche aus der Eifel in Nordrügen: Ein erdgeschichtlicher Rückblick. -Rugia Journal 1996: 52-55.

KLIEWE, H. & SCHULTZ, H.-J. (1970): Die periglaziäre Fazies im Jungmoränengebiete nördlich der Pommerschen Eisrandlage. - a contribution in: LEMBKE, H., ALTERMANN, M., MARKUSE, G. & NITZ, B.: Die periglaziäre Fazies im Alt- und Jungmoränengebiet nördlich des Lößgürtels. - In: RICHTER, H., HAASE, G., LIEBEROTH, I. & RUSKE, R. (ed.): Periglazial - Löß - Paläolithikum im Jungpleistozän der Deutschen Demokratischen Republik: 255-263.

KLITGAARD-KRISTENSEN, D., SEJRUP, H.P., HAFILDASON, H., JOHNSEN, S. & SPURK, M. (1998): A regional 8200 cal. yr BP cooling event in northwest Europe, induced by final stages of the Laurentide ice-sheet deglaciation? - Journal of Quaternary Science, **13**(2): 165-169.

KOSTER, E.A. (1978): De stuifzanden van de Veluwe; een fysisch-geografische studie. - PhD thesis, University of Amsterdam, 195 p.

KOSTER, E. A. (1982): Terminology and lithostratigraphic division of sandy eolian deposits in the Netherlands. An evaluation. - Geologie en Mijnbouw, **61**: 121-129.

KOSTER, E. A. (1988): Ancient and modern cold-climate aeolian sand deposition: a review. - Journal of Quaternary Science, **3**(1): 69-83.

KOSTER, E. A. (2005): Recent Advances in Luminescence Dating of Late Pleistocene (Cold-Climate) Aeolian Sand and Loess Deposits in Western Europe. - Permafrost and Periglacial Processes, **16**: 131-143.

KOSTER, E.A., CASTEL, I.I.Y. & NAP, R.L. (1993): Genesis and sedimentary structures of late Holocene aeolian drift sands in northwest Europe. - In: PYE, K. (ed.): The Dynamics and Environmental Context of Aeolian Sedimentary Systems. - Geological Society Special Publication, **72**: 247-267.

KOWALKOWSKI, A., NOWACZYK, B. & OKUNIEWSKA- NOWACZYK, I. (1999a): Chronosequence of biogenic deposits and fossil soils in the dune near Jasien, Western Poland. - GeoArchaeoRhein, **3**: 107-125.

KOWALKOWSKI, A., NOWACZYK, B. & OKUNIEWSKA- NOWACZYK, I. (1999b): Fossil soils chronosequence in the dune near Jasień, Głogów-Baruth pradolina. - Guidebook of Excursion, Jasień, 14.11.1999, Quaternary Research and Geoecology Insitute, Department of Geomorphology, Adam Mickiewicz University, Poznań, 12 p.

KOZARSKI, S. (1974): Evidences of Late-Würm permafrost occurrence in North-West Poland. -Quaestiones Geographicae, **1**: 65-86.

KOZARSKI, S. (1978): Das Alter der Binnendünen in Mittelwestpolen. - In: NAGL, H. (ed.): Beiträge zur Quartär- und Landschaftsforschung. Festschrift zum 60. Geburtstag J. Fink: 291-305.

KOZARSKI, S. (1988): Time and dynamics of the last Scandinavian ice-sheet retreat from northwestern Poland. - Geographia Polonica, **55**: 91-101.

KOZARSKI, S. (1990): Pleni and Late Vistulian aeolian phenomena in Poland: new occurrences, palaeoenvironmental and stratigraphic interpretations. - Acta Geographica Debrecina 1987–1988, Tomus XXVI–XXVII: 31–45.

KOZARSKI, S. (ed.) (1991): Late Vistulian (= Weichselian) and Holocene aeolian phenomena in Central and Northern Europe. - Zeitschrift für Geomorphologie, NF **90**: 206.

KOZARSKI, S. (1993): Late Plenivistulian deglaciation and the expansion of the periglacial zone in NW Poland. - Geologie en Mijnbouw, **72**: 143-157.

KOZARSKI, S., NOWACZYK, B., ROTNICKI, K. & TOBOLSKI, K. (1969): The eolian phenomena in west-central Poland with special reference to the chronology of phases of eolian activity. - Geographia Polonica, **17**: 231-248.

KRAUSKOPF, C. & PASDA, C. (1999): Aufwehung, Umbildung, Zerstörung - Zur Entwicklung der Dünen im Baruther Urstromtal zwischen Cottbus und Forst. - Archäologisches Korrespondenzblatt, **29**: 289-298.

KRBETSCHEK, M.R. (1995): Lumineszenz-Datierung quartärer Sedimente Mittel-, Ost- und Norddeutschlands. - PhD thesis, Bergakademie Freiberg, 122 p.

KRBETSCHEK, M.R. & TRAUTMANN, T. (2000): A spectral radioluminescence study for dating and dosimetry. - Radiation Measurements, **32**: 853-857.

KRBETSCHEK, M.R., RIESER, U., ZÖLLER, L. & HEINICKE, J. (1994): Radioactive disequilibria in palaeodosimetric dating of sediments. - Radiation Measurements, **23**: 485-489.

KRBETSCHEK, M.R., GÖTZE, J., DIETRICH, A. & TRAUTMANN, T. (1997): Spectral information from minerals relevant for luminescence dating. - Radiation Measurements, **27**(5/6): 695-748.

KRBETSCHEK, M.R., TRAUTMANN, T., Dietrich, A. & Stolz, W. (2000): Radioluminescence dating of sediments: methodological aspects. - Radiation Measurements, **32**: 493-498.

KROMER, B., CLAUSSEN, M., LATUSKE, N., REMMELE, S. & SCHLESER, G. (2005): Decadal variability of climate and solar forcing, reconstructd from ^{14}C and ^{10}Be, tree-ring climate proxies and stable isotopes - compared to results of the CLIMBER Climate System Model. - DEKLIM Report 2005: 50-53.

KÜHN, P. (2003): Spätglaziale und holozäne Lessivégenese auf jungweichselzeitlichen Sedimenten Deutschlands. - Greifswalder Geographische Arbeiten, **28**, 167 p.

KÜHNER, R., HILLER, A. & JUNGE, F.W. (1999): Die spätweichselzeitlichen Ablagerungen der Spree im Tagebau Cottbus-Nord und ihre zeitliche Einordnung unter besonderer Berücksichtigung von ersten ^{14}C-Daten an Hölzern. - Quartär, **49/50**: 8-20.

KUHN, R. (2000): Vergleichende Untersuchungen der Optisch (Grün) stimulierten Lumineszenz und der Thermolumineszenz von Quarz zum Zwecke der Altersbestimmung. - PhD thesis (unpublished), University of Heidelberg, 156 p.

KUHN, R., TRAUTMANN, T., SINGHVI, A.K., KRBETSCHEK, M.R., WAGNER, G.A. & STOLZ, W. (2000): A study of thermoluminescence emission spectra and optical stimulation spectra of quartz from different provenances. - Radiation Measurements, **32**: 653-657.

KUHNS, C.K., AGERSNAP LARSEN, N. & MCKEEVER S.W.S. (2000): Characteristics of LM-OSL from several different types of quartz. - Radiation Measurements, **32**: 413-418.

KUTZBACH, J.E., GALLIMORE, R., HARRISON, S., BEHLING, P., SELIN, R., LAARIF, F. (1998): Climate and biome simulations for the past 21,000 years. - Quarternary Science Reviews, **17**: 473-506.

LAGERLUND, E. & HOUMARK-NIELSEN, M. (1993): Timing and pattern of the last deglaciation in the Kattegat region. - Boreas, **22**: 337-347.

LAI, Z.-P. & MURRAY, A.S. (2005): Red TL of quartz extracted from Chinese loess: bleachability and saturation dose. - Book of Abstracts, 11th International Conference on Luminescence and Electron Spin Resonance Dating - Cologne, Germany, July 24-29 2005: 107.

LAMOTHE, M. & AUCLAIR, M. (1999): A solution to anomalous fading and age shortfalls in optical dating of feldspar minerals. - Earth and Planetary Science Letters, **171**: 319-323.

LAMOTHE, M. & AUCLAIR, M. (2000): The fadia method: a new approach in luminescence dating of single feldspar grains. - Radiation Measurements, **32**: 433-438.

LAMOTHE, M., AUCLAIR, M., HAMZAOUI, C. & HUOT, S. (2003): Towards a prediction of long-term anomalous fading of feldspar IRSL. - Radiation Measurements, **37**: 493-498.

LAMPE, R. (2002): Holocene evolution and coastal dynamics of the Fischland-Darss-Zingst peninsula. - Greifswalder Geographische Arbeiten, **27**: 155-163.

LAMPE, R. (2005): Late-glacial and Holocene water-level variations along the NE-German Baltic Sea coast - review and new results. - Quaternary International, **133-134**: 121-136.

LANG, G. (1994): Quartäre Vegetationsgeschichte Europas. - Jena, 462 p.

LEMBKE, H. (1939a): Morphologische Probleme in der Mark Brandenburg. - Zeitschrift für Erdkunde, **7**: 523-528.

LEMBKE, H. (1939b): Das Alter der norddeutschen Binnendünen. - Deutsche Geographische Blätter, **42** (1-4): 87-96.

LEMBKE, H., ALTERMANN, M., MARKUSE, G. & NITZ, B. (1970): Die periglaziäre Fazies im Alt- und Jungmoränengebiet nördlich des Lößgürtels. - In: RICHTER, H., HAASE, G., LIEBEROTH, I. & RUSKE, R. (ed.): Periglazial - Löß - Paläolithikum im Jungpleistozän der Deutschen Demokratischen Republik: 213-268.

LEMKE, W., JENSEN, J.B., BENNIKE, O., ENDLER, R., WITKOWSKI, A. & KUIJPERS, A. (2002): Spät- und postglaziale Flüsse und Seen in der heutigen westlichen Ostsee. - Greifswalder Geographische Arbeiten, **26**: 73-77.

LEPPER, K. & MCKEEVER, S.W.S. (2002): An objective methodology for dose distribution analysis. – Radiation Protection Dosimetry, **101**(1-4): 349-352.

LEWCZUK, J. (2002): Siedlungsdynamik in der vorrömischen Eisenzeit östlich der Oder. - In: GRINGMUTH-DALLMER, E. & LECIEJEWICZ, L. (ed.): Mensch und Umwelt im Odergebiet: 277-283.

LI, S.-H. (1994): Optical dating: insufficiently bleached sediments. - Radiation Measurements, **23**: 563-567.

LI, S.-H. (2001): Identification of well-bleached grains in the optival dating of quartz. - Quaternary Science Reviews, **20**: 1365-1370.

LIEDTKE, H. (1956/57): Beiträge zur geomorphologischen Entwicklung des Thorn-Eberswalder Urstromtales zwischen Oder und Havel. - Wissenschaftliche Zeitschrift der Humboldt-Universität Berlin, Math.-Nat.-Reihe, **VI**(1): 3-49.

LIEDTKE, H. (1957/58): Einige Beobachtungen an norddeutschen Dünen. - Wissenschaftliche Zeitschrift der Humboldt-Universität Berlin, Math.-Nat. Reihe, **VII**(4): 445-448.

LIEDTKE, H. (1996): Die eiszeitliche Gestaltung des Oderbruchs. - Heidelberger Geographische Arbeiten, **104**: 327-351.

LIEDTKE, H. & MARCINEK, J. (ed.) (1995): Physische Geographie Deutschlands. - Gotha, 559 p.

LITT, T. (2003): Environmental response to climate and human impact in central Europe during the last 15,000 years - a German contribution to PAGES-PEPIII. - Quaternary Science Reviews, **22**(1): 1-4.

LITT, T., BRAUER, A., GOSLAR, T., MERKT, J., BALAGA, K., MÜLLER, H., RALSKA-JASIEWICZOWA, M., STEBICH, M. & NEGENDANK, J.F.W. (2001): Correlation and synchronisation of Lateglacial continental sequences in northern central Europe based on annually laminated lacustrine sediments. - Quaternary Science Reviews, **20**: 1233-1249.

LITT, T., SCHMINCKE, H.-U. & KROMER, B. (2003): Environmental response to climatic and volcanic events in central Europe during the Weichselian Lateglacial. - Quaternary Science Reviews, **22**(1): 7-32.

LOMAX, J., HILGERS, A., WOPFNER, H., GRÜN, R., TWIDALE, C.R. & RADTKE, U. (2003): The onset of dune formation in the Strzelecki Desert, South Australia. - Quaternary Science Reviews, **22**: 1067-1076.

LOMAX, J., HILGERS, A., TWIDALE, C.R., BOURNE, J.A. & RADTKE, U. (2006): Treatment of broad palaeodose distributions in OSL dating of dune sands from the western Murray Basin, South Australia. - Quaternary Geochronology (in press).

LOUIS, H. (1929): Die Form der norddeutschen Bogendünen. - Zeitschrift für Geomorphologie, **4**(1928/29): 7-18.

LOWE, J.J. & WALKER, M.J.C. (1997): Reconstructing Quaternary Environments. - London, 446 p.

LUDWIG, A.O. (2002): Die spätglaziale Entwicklung im östlichen Küstengebiet Mecklenburgs (Rostocker Heide, Fischland). - Greifswalder Geographische Arbeiten, **26**: 83-86.

LUTZE, G. (1995): Die Geschichte der Landnutzung im Bereich der Agrarlandschaft Chorin. - In: GRIMME, H. & DALCHOW, C. (ed.): Die Jungmoränenlandschaft Nordostbrandenburgs. - Berliner Geographische Studien, **40**: 245-268.

MAARLEVELD, G.C. (1976): Periglacial phenomena and the mean annual temperature during the last glacial time in the Netherlands. - Biuletyn Peryglacjalny, **26**: 57-78.

MADSEN, A. T., MURRAY, A. S., ANDERSEN, T. J., PEJRUP, M. & BREUNING-MADSEN, H. (2005): Optically stimulated luminescence dating of young estuarine sediments; a comparison with ^{210}Pb and ^{137}Cs dating. - Marine Geology, **214**(1-3): 251-268.

MAGALOWSKI, G. & NOWEL, W. (1982): Untersuchungen an Binnendünen in der Umgebung von Cottbus und Beziehungen zur Besiedlungsgeschichte dieses Raumes. - Zeitschrift für geologische Wissenschaften, **10**(6): 829-843.

MANGERUD, J., ANDERSEN, S.T., BERGLUND, B.E. & DONNER, J.J. (1974): Quaternary Stratigraphy of Norden, a proposal for terminology and classification. - Boreas, **4**: 109-128.

MANGERUD, J., SVENDSEN, J.I. & ASTAKHOV, V.I. (1999): Age and extent of the Barents and Kara ice sheets in northern Russia. - Boreas, **28**: 46-80.

MANIKOWSKA, B. (1991a): Vistulian and Holocene aeolian activity, pedostratigraphy and relief evolution in Central Poland. - Zeitschrift für Geomorphologie, NF **90**: 131-141.

MANIKOWSKA, B. (1991b): Dune Processes, Age of Dune Terrace and Vistulian Decline in the Vistlulian Decline in the Vistlula Valley near Wyszogród, Central Poland. - Bulletin of the Polish Academy of Sciences, Earth Sciences, **39**(2): 137-148.

MANIKOWSKA, B. (1994): État des études des processus éoliens dans la région de Lódz (Pologne Centrale). - Biuletyn Peryglacjalny, **33:** 107-131.

MANN, M.E., BRADLEY, R.S. & HUGHES, M.K. (1999): Northern Hemispheric Temperatures During the Past Millenium: Inferences, Uncertainties, and Limitations. - Geophysical Research Letters, **26**(6): 759-762.

MARCINEK, J. (1961): Über die Entwicklung des Baruther Urstromtales zwischen Neiße und Fiener Bruch. - Wissenschaftliche Zeitschrift der Humboldt-Universität Berlin, Math.-Nat.-Reihe, **X**(1): 13-46.

MARCINEK, J., PRÄGER, F. & STEINMÜLLER, A. (1970): Periglaziäre Gestaltung der Täler. - In: RICHTER, H., HAASE, G., LIEBEROTH, I. & RUSKE, R. (ed.): Periglazial - Löß - Paläolithikum im Jungpleistozän der Deutschen Demokratischen Republik: 281-328.

MARCINEK, J. & SCHULZ, I. (1995): Im klassischen Gebiet der norddeutschen Eiszeitforschung im Raum der Pommerschen Eisrandlage um Chorin und der Finow. - Berliner Geographische Studien, **40**: 197-213.

MARKS, L. (2004): Pleistocene glacial limits in Poland. - In: EHLERS, J. & GIBBARD, P.L.: Quaternary Glaciations - Extent and Chronology, Part I: Europe, Developments in Quaternary Science, **2**: 295-300.

MCKEEVER, S. (2001): Optically stimulated luminescence dosimetry. - Nuclear Instruments and Methods in Physics Research B, **184**: 29-54.

MCKEEVER, S. & CHEN., R. (1997): Luminescence Models. - Radiation Measurements, **27**(5/6): 625-661.

MEAKINS, R.L., DICKSON, B.L. & KELLY, J.C. (1979): Gamma ray analysis of K, U and Th for dose-rate estimation in thermoluminescent dating. - Archaeomentry, **21**(1): 79-86.

MEJDAHL, V. (1979): Thermoluminescence dating: Beta-dose attenuation in quartz grains. - Archaeometry, **21**: 61-72.

MEJDAHL, V. (1987): Internal radioactivity in quartz and feldspar grains. - Ancient TL, **5**: 10-17.

MEJDAHL, V. & BØTTER-JENSEN, L. (1994): Luminescence dating of archaeological materials using a new technique based on single aliquot measurements. - Quaternary Science Reviews, **13**: 551-554.

MERKT, J. & MÜLLER, H. (1999): Varve chronology and palynology of the Lateglacial in Northwest Germany from lacustrine sediments of Hämelsee in Lower Saxony. - Quaternary International, **61**: 41-59.

MIALLIER, D. FAÏN, J., MONTRET, M., PILLEYRE, T., SANZELLE, S. & SOUMANA, S. (1994): Sun bleaching of the red TL of quartz: preliminary observations. - Ancient TL, **12**(1): 1-4.

MÖCKEL, A. (2004): Granulometrischer Vergleich mitteleuropäischer Binnendünen mit aktuellen Wüstendünen. - Diploma thesis (unpublished), Department of Geography, University of Cologne, 107 p.

MOL, J. (1997): Fluvial response to Weichselian climate changes in the Niederlausitz (Germany). - Journal of Quaternary Science, **12**: 43–60.

MOL, J. & RHODES, E.J. (1997): Optical dating of quartz from Weichselian fluvial deposits in eastern Germany. -In: MOL, J.: Fluvial response to climate variations: the Last Glaciation in eastern Germany. - PhD Thesis, Vrije Universiteit Amsterdam: 59–68.

MUNYIKWA, K. (2000): Cosmic ray contribution to environmental dose rates with varying overburden thickness. - Ancient TL, **18**: 27-34.

MURRAY, A.S. & FUNDER, S. (2003): Optically stimulated luminescence dating of a Danish Eemian coastal marine deposit: a test of accuracy. - Quaternary Science Reviews, **22**: 1177-1183.

MURRAY, A.S. & MEJDAHL, V. (1999) Comparison of regenerative-dose single-aliquot and multiple-aliquot (SARA) protocols using heated quartz from archaeological sites. - Quaternary Science Reviews, **18**(2): 223-229.

MURRAY, A.S. & OLLEY, J.M. (1999): Determining sedimentation rates using luminescence dating. - In: BRUNS, P. & HAAS, H.C. (ed.): Determination of Sediment Accumulation Rates. - GeoResearch Forum, **5**: 121-144.

MURRAY, A.S. & OLLEY, J.M. (2002): Precision and accuracy in the optically stimulated luminescence dating of sedimentary quartz: a status review. - Geochronometria **21**: 1-16.

MURRAY, A.S. & ROBERTS, R.G. (1997): Determining the burial time of single grains of quartz using optically stimulated luminescence. - Earth and Planetary Science Letters, **152**: 163-180.

MURRAY, A.S. & ROBERTS, R.G. (1998): Measurement of the equivalent dose in quartz using a regenerative-dose single-aliquot protocol. - Radiation Measurements, **29**: 503-515.

MURRAY, A.S. & WINTLE, A.G. (1979): Beta source calibration. – PACT, **3**: 418-427.

MURRAY, A.S. & WINTLE, A.G. (1998): Factors controlling the shape of the OSL decay curve in Quartz. - Radiation Measurements, **29**(1), 65-79.

MURRAY, A.S. & WINTLE, A.G. (1999): Isothermal decay of optically stimulated luminescence in quartz. - Radiation Measurements, **30**: 119-125.

MURRAY, A.S. & WINTLE, A.G. (2000): Luminescence dating of quartz using an improved single-aliquot regenerative-dose protocol. - Radiation Measurements, **32**: 57-73.

MURRAY, A.S. & WINTLE, A.G. (2003): The single aliquot regenerative dose protocol: potential for improvements in reliability. - Radiation Measurements, **37**: 377-381.

MURRAY, A.S., OLLEY, J.M. & CAITCHEON, G.C. (1995): Measurement of equivalent dose in quartz from contemporary water-lain sediments using optically stimulated luminescence. - Quaternary Science Reviews, **14**: 365-371.

MURRAY, A.S., ROBERTS, R.G. & WINTLE, A.G. (1997): Equivalent dose measurement using a single aliquot of quartz. - Radiation Measurements, **27**: 171-184.

NASSAU, K. & PRESCOTT, B.E. (1975): A reinterpretation of smokey quartz. - Physica Status Solidi, **29**: 659-663.

NESJE, A. & DAHL, S.O. (2001): The Greenland 8200 cal. yr BP event detected in loss-on-ignition profiles in Norwegian lacustrine sediment sequences. - Journal of Quaternary Science, **16**(2): 155-166.

NOWACZYK, B. (1986): The age of dunes, their textural and structural properties against atmospheric circulation pattern of Poland during the Late Vistulian and Holocene. - Adam Mickiewicz University Press, Seria Geografia, **28**, 245 p.

NOWACZYK, B. (1993): Aeolian events in structural landscape changes of the Brda outwash. - Quaestiones Geographicae, **15/16**: 65-75,

NOWACZYK, B. (1998): Dunes and aeolian cover sands in the vicinity of Jasień. - In: JÄGER, K.-D., KOWALKOWSKI, A., NOWACZYK, B. & SCHIRMER, W. (ed.): Dunes and fossil soils of Vistulian and Holocene age between Elbe and Wisła. - Guide-book of Excursion, INQUA Eurosiberian Subcommision for the study of the Holocene: 52-57.

NOWEL, W., ATANASOW, O. & ERD, K. (1972): Neue Ergebnisse zur Dünenbewegung im Baruther Urstromtal. Geologische Untersuchung einer Sandlagerstätte im Raume Cottbus. - Zeitschrift für angewandte Geologie, **18**(9): 410-418.

OLLEY, J.M., MURRAY, A.S. & ROBERTS, R.G. (1996): The effects of disequilibria in the uranium and thorium decay chains on burial dose rates in fluvial sediments. - Quaternary Science Reviews, **15**: 751-760.

OLLEY, J.M., ROBERTS, R.G. & MURRAY, A.S. (1997): Disequilibria in the uranium decay series in sedimentary deposits at Allen´s Cave, Nullarbor Plain, Australia: Implications for dose rate determinations. - Radiation Measurements, **27**(2): 433-443.

OLLEY, J.M., CAITCHEON, G.G. & MURRAY, A.S. (1998): The distribution of apparent dose as determined by optically stimulated luminescence in small aliquots of fluvial quartz: implications for dating young sediments. - Quaternary Science Reviews, **17**: 1033-1040.

OLLEY, J.M., CAITCHEON, G.G. & ROBERTS, R.G. (1999): The origin of dose distributions in fluvial sediments, and the prospect of dating single grains from fluvial deposits using optically stimulated luminescence. - Radiation Measurements, **30**: 207-217.

PASDA, C. (2002): Geoarchäologische Beiträge zur spätquartären Landschaftgeschichte des Baruther Urstromtals zwischen Cottbus und Forst (Brandenburg). - Greifswalder Geographische Arbeiten, **26**: 193-196.

PRESCOTT, J.R. & FOX, P.J. (1990): Dating quartz sediments using the 325°C TL peak: new spectral data. - Ancient TL, **8**(3): 32-34.

PRESCOTT, J.R. & HUTTON, J.T. (1988): Cosmic ray and gamma ray dosimetry for TL and ESR. - Nuclear Tracks and Radiation Measurements, **14**: 223-227.

PRESCOTT, J.R. & HUTTON, J.T. (1994): Cosmic ray contributions to dose rates for Luminescence and ESR Dating: large depths and long-term variations. - Radiation Measurements, **23**(2/3): 497-500.

PRESCOTT, J.R. & HUTTON, J.T. (1995): Environmental dose rates and radioactive disequilibrium from some Australian luminescence dating sites. - Quaternary Science Reviews, **14**: 439-448.

PRESCOTT, J.R. & STEPHAN, L.G. (1982): The contribution of cosmic radiation to the environmental dose for thermoluminescent dating. Latitude, altitude and depth dependences. - PACT, **6**: 17-25.

PRESCOTT, J.R. & ROBERTSON, G.B. (1997): Sediment dating by luminescence: a review. - Radiation Measurements, **27**(5/6): 893-922.

PREUSSER, F. (2003): IRSL dating of K-rich feldspars using the SAR protocol: comparison with independent age control. - Ancient TL, **21**(1): 17-23.

PREUSSER, F. & KASPER, H.U. (2001): Comparison of dose rate determination using high-resolution gamma spectrometry and inductively coupled plasma - mass spectrometry. - Ancient TL, **19**(1): 19-23.

PYE, K. (1983): Early post-depositional modification of aeolian dune sands. - In: BROOKFIELD, M.E. & AHLBRANDT, T.S. (ed.): Eolian Sediments and Processes: 197-221.

PYRITZ, E. (1972): Binnendünen und Flugsandebenen im Niedersächsischen Tiefland. - Göttinger Geographische Abhandlungen, **61**, 153 p.

RADTKE, U. (ed.)(1998): Lumineszenzdatierung äolischer Sedimente - Beiträge zur Genese und Altersstellung jungquartärer Dünen und Lösse in Deutschland. - Kölner Geographische Arbeiten, **70**, 124 p.

RADTKE, U. & JANOTTA, A. (1998): Ein Beitrag zur Beurteilung der Aussagekraft von Lumineszenzaltern für die Datierung von spätpleistozänen und holozänen Dünen anhand des Laacher See-Tuffes (12.900 J.v.h.): Der Testfall „Düne Mainz-Gonsenheim". - Kölner Geographische Arbeiten, **70**: 1-18.

RADTKE, U., CZWIELUNG, K., HEIDGER, M. & JANOTTA, A. (1998): Lumineszenz-Datierung spätglazialer und holozäner Dünensande in der Allerniederung bei Gifhorn (Niedersachsen) und bei Brockum, Kreis Diepholz (Niedersachsen). - Kölner Geographische Arbeiten, **70**: 19-45.

RADTKE, U., JANOTTA, A., HILGERS, A. & MURRAY, A.S. (2001): The Potential of OSL and TL for Dating Late Glacial and Holocene Dune Sands tested with independent Age Control of the Laacher See-Tephra (12,880 a) at the Section 'Mainz-Gonsenheim'. - Quaternary Science Reviews, **20**: 719-724.

RANDALL, J.T. & WILKINS, M.H.F. (1945): Phosphorescence and electron traps. - Proceedings of the Royal Society London A, **184**: 366-407.

READHEAD, M.L. (1987): Thermoluminescence dose rate data and dating equations for the case of disequilibrium in the decay series. - Nuclear Tracks and Radiation Measurements, **13**(4): 197-207.

REES-JONES, J. (1995): Optical Dating of young Sediments using Fine-Grain Quartz. - Ancient TL, **13**(2): 9-14.

REIMER, P. J., BAILLIE, M.G.L., BARD, E., BAYLISS, A., BECK, J. W., BERTRAND, C.J.H., BLACKWELL, P. G., BUCK, C. E., BURR, G. S., CUTLER, K. B., DAMON, P. E., EDWARDS, R. L., FAIRBANKS, R. G., FRIEDRICH, M., GUILDERSON, T. P., HOGG, A. G., HUGHEN, K. A., KROMER, B., MCCORMAC, G., MANNING, S., RAMSEY, C. B., REIMER, R. W., REMMELE, S., SOUTHON, J. R., STUIVER, M.; TALAMO, S., TAYLOR, F.W., VAN DER PLICHT, J. & WEYHENMEYER, C. E. (2004): IntCal04 - Terrestrial Radiocarbon Age Calibration, 0-26 Cal Kyr BP. - Radiocarbon, **46**: 1029-1058.

RENSSEN, H. & BOGAART, P. (2003): Atmospheric variability over the ~14.7 kyr BP stadial-interstadial transition in the North Atlantic region as simulated by an AGCM. - Climate Dynamics, **20**(2-3): 301-313.

RENSSEN, H. & VANDENBERGHE, J. (2003): Investigation of the relationship between permafrost distribution in NW-Europe and extensive winter sea-ice cover in the North Atlantic Ocean during the cold phases of the Last Glaciation. - Quaternary Science Reviews **22:** 209-233.

RENSSEN, H. (1997): The climate during the Younger Dryas stadial. Comparing global atmospheric simulation experiments with climate reconstructions based on geological evidence. - Netherlands Geographical Studies, **217**, 183 p.

RENSSEN, H. & ISARIN, R.F.B. (2001): The two major warming phases of the last deglaciation at ~ 14.7 and ~ 11.5 cal BP in Europe: climate reconstructions and AGCM experiments. - Global and Planetary Change, **30**: 117-153.

RENSSEN, H., ISARIN, R.F.B. & VANDENBERGHE, J. (2002): Thermal gradients in Europe during the last glacial-interglacial transition. - Geologie en Mijnbouw, **81**(1): 113-122.

RHODES, E.J. (1988): Methodological considerations in the optical dating of quartz. - Quaternary Science Reviews, **7**: 395-400.

RHODES, E.J. (2000): Observations of thermal transfer OSL signals in glacigenic quartz. - Radiation Measurements, **32**: 595-602.

RHODES, E.J., SINGARAYER, J.S., RAYNAL, J.-P., WESTAWAY, K.E. & SBIHI-ALAOUI (2006): New age estimates for the Palaeolithic assemblages and Pleistocene succession of Casablanca, Morocco. - Quaternary Science Reviews, **25**: 2569-2585.

RIEK, W. & STROHBACH, B. (2003): Forstwirtschaftliche Landnutzung. -In: FRIELINGHAUS, M., DALCHOW, C. & SCHÄFER, H. (ed.): Bodenlandschaften im Jung- und Altmoränengebiet - Exkursionsführer zur Jahrestagung der Deutschen Bodenkundlichen Gesellschaft. - Mitteilungen der Deutschen Bodenkundlichen Gesellschaft, **100**: 34-36.

RIND, D. & OVERPECK, J. (1993): Hypothesised causes of decade-to-century-scale climate variability: climate model results. - Quaternary Science Reviews, **12**: 357-374.

ROBERTS, R.G., GALBRAITH, R.F., OLLEY, J.M., YOSHIDA, H. & LASLETT, G.M. (1999): Optical dating of single and multiple grains of quartz from Jinmium rock shelter, northern Australia. Part II, results and implications. - Archaeometry, **41**: 365-395.

ROBERTS, R.G, GALBRAITH, R.F., YOSHIDA, H., LASLETT, G.M. & OLLEY, J.M. (2000): Distinguishing dose populations in sediment mixtures: a test of single-grain optical dating procedures using mixtures of laboratory-dose quartz. - Radiation Measurements, **32**: 459-465.

RÖSLER, H. (1999): Verweht und ausgegraben. Hügelgräber der Lausitzer Kultur in der Düringsheide. - Arbeitsberichte zur Bodendenkmalpflege in Brandenburg, **3**: 43-48.

ROTHE, P. (1994): Gesteine – Entstehung-Zerstörung-Umbildung. - Darmstadt, 162 p.

RUEGG, G. (1983): Periglacial eolian evenly laminated sandy deposits in the Late Pleistocene of North-West Europe, a facies unrecorded in modern sedimentological handbooks. - In: BROOKFIELD, M.E. & AHLBRANDT, T.S. (ed.): Eolian Sediments and Processes: 455-482.

RÜHBERG, N. (1987): Die Grundmoräne des jüngsten Weichselvorstoßes im Gebiet der DDR. - Zeitschrift für Geologische Wissenschaften, **15**: 759-767.

SARNTHEIN, M. et al. (2000): Fundamental modes and abrupt changes in North Atlantic circulation and climate over the last 60 kyr - concepts, reconstruction, and numerical modelling. - In: SCHÄFER, P., RITZRAU, W., SCHLÜTER, M. & THIEDE, J. (ed.): The Northern North Atlantic: A Changing Environment.

SCHEFFER/SCHACHTSCHABEL (SCHACHTSCHABEL, P., BLUME, H.-P., BRÜMMER, G., HARTGE, K.-H. & SCHWERTMANN, U.) (1992): Lehrbuch der Bodenkunde. - Stuttgart[13], 491 p.

SCHIRMER, W. (1999a): Dune phases and fossil soils in the European sand belt. - In: SCHIRMER, W. (ed.): Dunes and fossil soils. - GeoArchaeoRhein, **3**: 11-42.

SCHIRMER, W. (1999b): Definitions concerning coversand, fossil soil and paleosol. - In: SCHIRMER, W. (ed.): Dunes and fossil soils. - GeoArchaeoRhein, **3**: 187-190.

SCHIRRMEISTER, L. (1997): Sedimentstrukturen und Deformationen in Eisstauseeablagerungen NE-Brandenburgs und ihre fazielle Deutung. In: NITZ, B., NASS, A. (ed.): Beiträge zu ausgewählten Fragen des Quartärs in Ost- und Mitteleuropa. - Berliner Geographische Arbeiten, **84**: 113-146.

SCHLAAK, N. (1993): Studie zur Landschaftsgenese im Raum Nordbarnim und Eberswalder Urstromtal. - Berliner Geographische Arbeiten, **76**; 145 p.

SCHLAAK, N. (1995a): Eisrandsedimente und Dünen im Nordosten von Berlin. - In: SCHIRMER, W. (ed.): Quaternary field trips in Central Europe, INQUA, XIV International Congress, Berlin, Germany; Vol. 4, 1300.

SCHLAAK, N. (1995b): Äolische Formenkomplexe im Eberswalder Tal und die Pommersche Endmoräne auf der Neuenhagener Oderinsel. - Berliner Geographische Studien, **40**: 215-220.

SCHLAAK, N. (1997): Äolische Dynamik im brandenburgischen Tiefland seit dem Weichselspätglazial. - Arbeitsberichte Geographisches Institut der Humboldt-Universität Berlin, **24**: 58.

SCHLAAK, N. (1998a): Torun- Eberswalde ice marginal valley: Postdune (forest division 151/152).- In: JÄGER, K.-D., KOWALKOWSKI, A., NOWACZYK, B. & SCHIRMER, W. (ed.): Dunes and fossil soils of Vistulian and Holocene age between Elbe and Wisła.- Guide-book of Excursion, INQUA Eurosiberian Subcommision for the study of the Holocene: 27-28.

SCHLAAK, N. (1998b): Der Finowboden - Zeugnis einer begrabenen weichselspätglazialen Oberfläche in Dünengebieten Nordostbrandenburgs. - Münchener Geographische Abhandlungen A, **49**: 143-148.

SCHLAAK, N. (1999a): Postdüne (Eberswalder Urstromtal, Exkursionspunkt 3). In: SCHMIDT, R., BORK, H.-R. & FISCHER-ZUJKOV, U. (ed.): Paläoböden und Kolluvien auf glazialen Sedimenten Nordostdeutschlands. - ZALF-Bericht, **37**: 62-69.

SCHLAAK, N. (1999b): Typical aeolian sand profiles and palaeosols of the Glien till plain in the northwest of Berlin. - GeoArchaeoRhein, **3**: 97-105.

SCHLAAK, N. (1999c): Geomorphologisch-bodenkundliche Untersuchungen in den Vorfeldern des Tagebaus Jänschwalde. - Handout zur Exkursion des AK Paläopedologie der Dt. Bodenkundl. Ges., 13.11.1999, Tagebau Cottbus-Nord & Jänschwalde, 4 p.

SCHLAAK, N. (2000): Geomorphologische Karte des Gebietes um den Samith- und Schwärzesee - Eberswalder Urstromtal. (unpublished)

SCHMIDT, R. & BORK, H.-R. (1999): Paläoböden - Einführung in das Exkursionsgebiet, Physisch-geographische Rahmenbedingungen. - In: SCHMIDT, R., BORK, H.-R. & FISCHER-ZUJKOV, U. (ed.): Paläoböden und Kolluvien auf glazialen Sedimenten Nordostdeutschlands. - ZALF-Bericht, **37**: 5-20.

SCHMINCKE, H.-U., PARK, C. & HARMS, E. (1999): Evolution and environmental impacts of the eruption of Laacher See Volcano (Germany) 12,900 a BP. - Quaternary International, **61**: 61-72.

SCHOLEFIELD, R.B., PRESCOTT, J.R., FRANKLIN, A.D. & FOX, P.J. (1994): Observations on some thermoluminescence emission centres in geological quartz. - Radiation Mesurements, **23**(2/3): 409-412.

SCHÖNWIESE, C.-D. (1988): Volcanism and air temperature variations in recent centuries. - In: GREGORY, S. (ed.): Recent Climatic Change: 20-29.

SCHÖNWIESE, C.-D. (2000): Praktische Statistik für Meteorologen und Geowissenschaftler. - Stuttgart[3], 298 p.

SCHWAN, J. (1987): Sedimentologic characteristics of a fluvial to aeolian succession in Weichselian Talsand in the Emsland (F.R.G.). - Sedimentary Geology, **52**: 273–298.

SCHWAN, J. (1988): The structure and genesis of Weichselian to Early Holocene aeolian sand sheets in western Europe. - Sedimentary Geology, **55**: 197–232.

SCHWAN, J. (1991): Palaeowetness indicators in a Weichselian Late Glacial to Holocene aeolian succession in the southwestern Netherlands. - Zeitschrift für Geomorphologie, NF **90**: 155-169.

SELSING, L. & MEJDAHL, V. (1994): Aeolian stratigraphy and thermoluminescence dating of sediments of late Holocene age from Sola, southwest Norway. - Boreas, **23**: 92-104.

SERNANDER, R. (1908): On the evidences of Postglacial changes of climate furnished by the peat-mosses of Northern Europe - Geol. Fören., Stockholm, Förhandl., **30**: 465-473.

SHELKOPLYAS, V.N. & MOROZOV, G.V. (1965): Determination of the relative age of Quaternary deposits of the middle Dnieper by the thermoluminescence method. - Survey of Problems in the Study of the Quaternary Period. Nauka, Moscow (in Russian).

SHORT, M.A. & HUNTLEY, D.J. (1992): Infrared stimulation of quartz. - Ancient TL, **10**: 19-21.

SIEGEL, G.H. & MARRONE, M.J. (1981): Photoluminescence in as-drawn and irradiated silica optical fibers: An assessment of the role of nonbridging oxygen defect centers. - Journal of Non-Crystalline Solids, **45**: 235-247.

SIEHL, A. (1996): Grundlagen und geowissenschaftliche Aspekte der Umweltradioaktivität. - In: SIEHL, A. (ed.): Umweltradioaktivität. Geologie und Ökologie im Kontext: 1-30.

SINGARAYER, J.S. & BAILEY, R.M. (2003): Further investigations of the quartz optically stimulated luminescence components using linear modulation. - Radiation Measurements, **37**: 451-458.

SINGARAYER, J.S., BAILEY, R.M. & RHODES, E.J. (2000): Potential of the slow component of quartz OSL for age determination of sedimentary samples. - Radiation Measurements, **32:** 873-880.

SINGARAYER, J.S., BAILEY, R.M., WARD, S. & STOKES, S. (2005): Assessing the completeness of optical resetting of quartz OSL in the natural environment. - Radiation Measurements, **40**: 13-25.

SINGHVI, A. K., BLUSZCZ, A., BATEMAN, M. D. & SOMESHWAR RAO, M. (2001): Luminescence dating of loess-palaeosol sequences and coversands: methodological aspects and palaeoclimatic implications. - Earth-Science Reviews, **54**: 193-211.

SMITH, B.W. & RHODES, E.J. (1994): Charge movements in quartz and their relevance to optical dating. - Radiation Measurements, **23** (2/3), 329-333.

SMITH, B.W., AITKEN, M.J., RHODES, E.J., ROBINSON, P.D. & GELDARD, D.M. (1986): Optical dating: methodological aspects. - Radiation Protection Dosimetry, **17**: 229-233.

SOLGER, F. (1910): Studien über Nordostdeutsche Inlanddünen. - Forschungen zur deutschen Landes- und Volkskunde, **19**(1): 60-68.

SPOONER, N.A. (1994): On the optical dating signal from quartz. - Radiation Measurements, **23**: 593-600.

SPOONER, N.A. & QUESTIAUX, D.G. (2000): Kinetics of red, blue and UV thermoluminescence and optically-stimulated luminescence from quartz. - Radiation Measurements, **32**: 659-666.

SPOONER, N.A., PRESCOTT, J.R. & HUTTON, J.T. (1988): The effect of illumination wavelength on the bleaching of the thermoluminescence (TL) of quartz. - Quaternary Science Reviews, **7**: 325-329.

SPURK, M., KROMER, B. & PESCHKE, P. (1999): Dendrochronologische, palynologische und Radiokarbon-Untersuchungen eines Waldes aus der jüngeren Tundrenzeit. - Quartär, **49/50**: 34-38.

STAPEL, B. (1999): Mesolithische Besiedlungsspuren im Malxetal. - Arbeitsberichte zur Bodendenkmalpflege in Brandenburg, **3**: 23-30.

STEBICH, M. (1999): Palynologische Untersuchungen zur Vegetationsgeschichte des Weichsel-Spätglazial und Frühholozän an jährlich geschichteten Sedimenten des Meerfelder Maares (Eifel). - Dissertationes Botanicæ, 320.

STEFFEN, G. (2000): Farbe und Lumineszenz von Mineralien - Einführung in die kristallchemischen und kristallphysikalischen Ursachen. - Stuttgart-New York, 145 p.

STOKES, S. (1999): Luminescence dating applications in geomorphological research. - Geomorphology, **29**: 153-171.

STOKES, S., BRAY, H.E. & BLUM, M.D. (2001): Optical resetting in large drainage basins - tests of zeroing assumptions using single-aliquot procedures. - Quaternary Science Reviews, **20**: 879-885.

STRICKERTSSON, K. & MURRAY, A.S. (1999): Optically stimulated luminescence dates for Late Pleistocene and Holocene sediments from Nørre Lyngby, Northern Jutland, Denmark. - Quaternary Science Reviews, **18**: 169-178.

STUIVER, M., REIMER, P.J., BARD, E., BECK, J.W., BURR, G.S., HUGHEN, K.A., KROMER, B., MCCORMAC, F.G., PFLICHT, K. & SPURK, M. (1998): INTCAL98 Radiocarbon Age Calibration, 24,000-0 cal BP. - Radiocarbon, **40**: 1041-1083.

SUTTON, S.R. & ZIMMERMAN, D.W. (1978): Thermoluminescence dating: radioactivity in quartz. - Archaeometry, **20**: 67-69.

SZMAŃDA, J.B., OCZKOWSKI, H.L. & PRZEGIĘTKA, K.R. (2004): Age of the Vistula River overbank deposits in Toruń. - Geochronometria, **23**: 35-38.

TAUTE, B. (1968): Die Stielspitzengruppen im nördlichen Mitteleuropa. - Fundamenta A5, Köln-Graz.

TERBERGER, T. (2004): The Younger Dryas–Preboreal transition in northern Germany - facts and concepts in discussion. - In: TERBERGER, T. & ERIKSEN, B.V. (ed.): Hunters in a changing world. - Internationale Archäologie - Arbeitsgemeinschaft, Tagung, Symposium, Kongress, **5**: 203-222.

TERBERGER, T., DE KLERK, P., HELBIG, H., KAISER, K. & KÜHN, P. (2004): Late Weichselian landscape development and human settlement in Mecklenburg-Vorpommern (NE Germany). Eiszeitalter und Gegenwart, **54**: 138-175.

THEUERKAUF, M. (2002): Die Laacher See-Tephra in Nordostdeutschland: Paläoökologische Untersuchungen mit hoher zeitlicher und räumlicher Auflösung. - Greifswalder Geographische Arbeiten, **26**: 171-174.

THEUERKAUF, M. (2003): Die Vegetation NO-Deutschlands vor und nach dem Ausbruch des Laacher See-Vulkans (12880 cal. BP). - Greifswalder Geographische Arbeiten, **29**: 143-189.

THOMSEN, K.J., JAIN, M., BØTTER-JENSEN, L., MURRAY, A.S. & JUNGNER, H. (2003): Variation with depth of dose distributions in single grains of quartz extracted from an irradiated concrete block. - Radiation Measurements, **37**: 315-321.

THOMSEN, K.J., MURRAY, A.S. & BØTTER-JENSEN, L. (2005): Sources of variability in OSL dose measurements using single grains of quartz. - Radiation Measurements, **39**: 47-61.

TOBOLSKI, K. & LITT, T. (1994): Vorallerödzeitliche Seeablagerungen in Wielkopolska ("Grosspolen"). - In: LOTTER, A.F. & AMMANN, B. (ed.): Festschrift Gerhard Lang. - Dissertationes Botanicæ, **234**: 487-496.

TORELL, O. (1875): Über Schliffflächen und Schrammen auf der Oberfläche des anstehenden Muschelkalkes von Rüdersdorf (Bericht über den Vortrag und die anschließende Diskussion). - Zeitschrift der Deutschen Geologischen Gesellschaft, **27**: 961-962.

TRAUTMANN, T. (1999): Radiolumineszenzuntersuchungen an Feldspat. - Ph.D. thesis, Bergakademie Freiberg, 95 p.

TRAUTMANN, T. (2000): A study of radioluminescence kinetics of natural feldspar dosimeters: experiments and simulations. - Journal of Physics D: Applied Physics, **33**: 2304-2310.

TRAUTMANN, T., KRBETSCHEK, M.R., DIETRICH, A. & STOLZ, W. (1998): Investigations of feldspar radioluminescence: potential for a new dating technique. - Radiation Measurements, **29**(3/4): 421-425.

USINGER, H. (2004): Vegetation and climate of the lowlands of northern Central Europe and adjacent areas around the Younger Dryas - Preboreal transition - with special emphasis on the Preboreal oscillation. - In: TERBERGER, T. & ERIKSEN, B.V. (ed.): Hunters in a changing world. - Internationale Archäologie - Arbeitsgemeinschaft, Tagung, Symposium, Kongress, **5**: 1-26.

VAN DEN BOGAARD, P. (1995): ^{40}Ar/^{39}Ar ages of sanidine phenocrysts from Laacher See Tephra (12,900 yr BP): Chronostratigraphic and petrological significance. - Earth and Planetary Science Letters, **133**: 163-174.

VAN DEN BOGAARD, P. & SCHMINCKE H.-U. (1985): Laacher See Tephra: A widespread isochronous late Quaternary tephra layer in central and northern Europe. - Geological Society of America Bulletin, **96**: 1554-1571.

VAN HUISSTEDEN, J., VANDENBERGHE, J., VAN DER HAMMEN, T. & LAAN, W. (2000): Fluvial and aeolian interaction under permafrost conditions: Weichselian Late Pleniglacial, Twente, eastern Netherlands. - Catena, **40:** 307–321.

VAN HUISSTEDEN, J., SCHWAN, J.C.G. & BATEMAN, M.D. (2001): Environmental conditions and paleowind directions at the end of the Weichselian Late Pleniglacial recorded in aeolian sediments and geomorphology (Twente, Eastern Netherlands). - Geologie en Mijnbouw, **80**: 1–18.

VANDENBERGHE, D. (2003): Investigation of the optically stimulated luminescence dating method for application to young geological sediments. - PhD thesis, Department of Analytical Chemistry - Institute for Nuclear Sciences, University Gent, 298 p.

VANDENBERGHE, D., HOSSAIN, S.M., DE CORTE, F. & VAN DEN HAUTE, P. (2003): Investigation on the origin of the equivalent dose distribution in a Dutch coversand. - Radiation Measurements, **37**: 433-439.

VANDENBERGHE, D., KASSE, C., HOSSAIN, S.M., DE CORTE, F., VAN DEN HAUTE, P., FUCHS, M. & MURRAY, A.S. (2004): Exploring the method of optical dating and comparison of optical and ^{14}C ages of Late Weichselian coversands in the southern Netherlands. - Journal of Quaternary Science, **19**: 73–86.

VANDENBERGHE, J. (1991): Changing conditions of aeolian sand deposition during the last deglaciation period. - In: KOZARSKI, S. (ed.): Late Vistulian (=Weichselian) and Holocene Aeolian Phenomena in Central and Northern Europe. - Zeitschrift für Geomorphologie, NF **90**: 193-207.

VANDENBERGHE, J. (1995): The climate of the Younger Dryas in the Netherlands (extended abstract). - Geologie en Mijbbouw, **74**: 245-249.

VANDENBERGHE, J., ISARIN, R.F.B. & RENSSEN, H. (2001): Rapid climatic warming: palaeo-data analysis and modelling. - Global and Planetary Change, **30**: 1-5.

WAGNER, G.A. (1995): Altersbestimmung von jungen Gesteinen und Artefakten. - Stuttgart, 277 p.

WALLINGA, J. (2002): On the detection of OSL age overestimation using single aliquot techniques. - Geochronometria, **21**: 17-26.

WALLINGA, J., MURRAY, A.S. & BØTTER-JENSEN, L. (2002): Measurement of the dose in quartz in the presence of feldspar contamination. - Radiation Protection Dosimetry, **101**: 367-370.

WALLINGA, J., MURRAY, A.S. & DULLER, G.A.T. (2000): Underestimation of equivalent dose in single-aliquot optical dating of feldspars caused by preheating. - Radiation Measurements, **32**: 691-695.

WALLINGA, J., MURRAY, A.S., DULLER, G.A.T. & TORNQVIST, T.E. (2001): Testing optically stimulated luminescence dating of sand-sized quartz and feldspar from fluvial deposits. - Earth and Planetary Science Letters, **193**: 617-630.

WANG, X. & LU, Y. (2005): Extending luminescence dating back to 1 Ma in Chinese loess using the resuperated OSL signal of fine-grain quartz. - Book of Abstracts, 11th International Conference on Luminescence and Electron Spin Resonance Dating - Cologne, Germany, July 24-29 2005: 206.

WARREN, J. (2002): Binnendünen im Wandel der Zeit - Rekonstruktion der jungquartären Landschaftsentwicklung nördlich von Köln mittels Lumineszenzdatierung ausgewählter Dünen. - State examination thesis (unpublished), University of Cologne, 109 p.

WEBB, T. & KUTZBACH, J.E. (1998): An Introduction to „Late Quarternary climates: Data synthesis and model experiments". - Quaternary Science Reviews, **17**: 465-471.

WECHLER, K.-P. (1993): Mesolithikum - Bandkeramik - Trichterbecherkultur - Zur Neolithisierung Mittel- und Ostdeutschlands aufgrund vergleichender Untersuchungen zum Silexinventar. - Beiträge zur Ur- und Frühgeschichte Mecklenburg-Vorpommerns, 27, 174 p.

WENIGER, G.-CH. (1991): Überlegungen zur Mobilität jägerischer Gruppen im Jungpaläolithikum. - Saeculum, **42(**1): 82-103.

WESTAWAY, K.E. & ROBERTS, R.G. (2006): A dual-aliquot regenerative-protocol (DAP) for thermoluminescence (TL) dating of quartz sediments using the light-sensitive and isothermally stimulated red emissions. - Quaternary Science Reviews, **25**: 2513-2528.

WIEDEMANN, E. & SCHMIDT, G.C. (1895): Ueber Lumineszenz. - Annalen der Physik und Chemie, NF **54**: 604.

WINTLE, A.G. (1975): Thermal quenching of thermoluminescence in quartz. - Geophysical Journal of the Royal Astronomical Society, **41**: 107-113.

WINTLE, A.G. (1997): Luminescence dating: Laboratory procedures and protocols. - Radiation Measurements, **27**(5/6): 769-817.

WINTLE, A.G. (2005): Dose determination using luminescence and radiation source calibration. – oral presentation, 11th International Conference on Luminescence and Electron Spin Resonance Dating - Cologne, Germany, July 24-29 2005.

WINTLE, A.G. & HUNTLEY, D.J. (1979): Thermoluminescence dating of a deep-sea sediment core. - Nature, **279**: 710-712.

WINTLE, A.G. & HUNTLEY, D.J. (1980): Thermoluminescence dating of ocean sediments. - Canadian Journal of Earth Sciences, **17**: 348-360.

WINTLE, A.G. & MURRAY, A.S. (1997): The relationship between quartz thermoluminescence, photo-transferred thermoluminescence, and optically stimulated luminescence. - Radiation Measurements, **27**(4): 611-624.

WINTLE, A.G. & MURRAY, A.S. (1998): Towards the development of a preheat procedure for OSL dating of quartz. - Radiation Measurements, **29**(1): 81-94.

WOLDSTEDT, P. (1925): Die großen Endmoränenzüge Norddeutschlands. - Zeitschrift der Deutschen Geologischen Gesellschaft, **77**: 172-184.

WOLDSTEDT, P. (1928): Die Parallelisierung des nordeuropäischen Diluviums mit dem anderer Vereisungen. - Zeitschrift der Gletscherkunde, **16**: 230-241.

WOLFE, S. (2006): Late Wisconsinan and Holocene dunefield formation and evolution on the Northern Great Plains, Canada. - In: NICKLING, W.G., TURNER, S., GILLIES, J.A. & PUDDISTER, M.: Programm and Abstracts - Sixth International Conference on Aeolian Research, July 24-28 2006, University of Guelph, Ontario, Canada: 93.

YANG, X.H. & MCKEEVER, S.W.S. (1990): The pre-dose effect in crystalline quartz. - Journal Physics D: Applied Physics, **23**: 237-244.

ZALIZNYAK, L.L. (1995): The Swiderian Reindeer-Hunters of Eastern Europe. - Beiträge zur Ur- und Frühgeschichte Mitteleuropas, **5**.

ZEEBERG, J.J. (1998): The European sand belt in eastern Europe and comparison of Late Glacial dune orientation with GCM simulation results. - Boreas, **27**: 127-139.

ZIELINSKI, G.A. (2000): Use of palaeo-records in determining variability within the volcanic-climate system. - Quaternary Science Reviews, **19**: 417-438.

ZIMMERMAN, D.W. (1971): Thermoluminescence dating using fine grains from pottery. - Archaeometry, **13**: 29-52.

ZOLITSCHKA, B., BEHRE, K.-E. & SCHNEIDER, J. (2003): Human and climatic impact on the environment as derived from colluvial, fluvial and lacustrine archives - examples from the Bronze Age to the Migration period, Germany. - Quaternary Science Reviews, **22**(1): 81-100.

ZYGMUNT, E. (2004): Archaeological and Radiocarbon dating of alluvial fans as an indicator of prehistoric colonisation of the Głubczyce plateau (Southwestern Poland). - Geochronometria, **23**: 101-107.

Appendix A: Dose rate data tables

Table A 1: Radionuclide concentrations of all samples determined either by neutron activation analyis (NAA) or by gamma-ray spectrometry (γ-spec.).

Note that for samples with the U content below the detection limit (<DL) the U concentration which was determined by gamma-spectrometry was used for dose rate calculation. All NAA measurements were carried out by the Becquerel Lab., Lucas Heights, Sydney, Australia. The gamma-spectrometry measurements were carried out at: R= Roskilde (Dr. A.S. Murray, The Nordic Laboratory for Luminescence Dating, Department of Earth Sciences, Aarhus University, Risoe National Laboratories, Roskilde, Denmark). HD=Heidelberg (Dr. A. Kadereit, Forschungsstelle Archäometrie der Heidelberger Akademie der Wissenschaften am Max-Planck-Institut für Kernphysik, Heidelberg, Germany), C= Cologne (Department of Geography, University of Cologne, Cologne, Germany). F= Freiberg (Dr. M.R. Krbetschek, Sächsische Akademie der Wissenschaften, Abteilung Quartärgeologie, Bergakademie Freiberg, Germany). (--- = not determined)

Lab code	sample	U (ppm) NAA	Th (ppm) NAA	K (%) NAA	U (ppm) γ-spec.	Th (ppm) γ-spec.	K (%) γ-spec.	Lab.
C-L0501	N1	0.08 ±0.02	1.20 ±0.12	0.63 ±0.06	--- ---	--- ---	--- ---	
C-L0502	N2	0.40 ±0.06	1.00 ±0.10	0.61 ±0.06	--- ---	--- ---	--- ---	
C-L0503	N3	0.20 ±0.03	1.70 ±0.17	0.65 ±0.07	--- ---	--- ---	--- ---	
C-L0504	N4	0.45 ±0.05	1.78 ±0.09	0.63 ±0.03	--- ---	--- ---	--- ---	
C-L0505	N5	0.30 ±0.05	1.70 ±0.17	0.65 ±0.07	--- ---	--- ---	--- ---	
C-L0506	N6	0.50 ±0.08	1.20 ±0.12	0.66 ±0.07	--- ---	--- ---	--- ---	
C-L0507	N7	0.08 ±0.02	1.40 ±0.14	0.67 ±0.07	--- ---	--- ---	--- ---	
C-L0508	N8	0.20 ±0.03	1.60 ±0.16	0.66 ±0.07	--- ---	--- ---	--- ---	
C-L0509	N9	0.40 ±0.06	2.00 ±0.20	0.68 ±0.07	--- ---	--- ---	--- ---	
C-L0510	N10	0.33 ±0.05	1.35 ±0.07	0.73 ±0.04	--- ---	--- ---	--- ---	
C-L0511	N11	0.70 ±0.11	2.50 ±0.25	0.68 ±0.07	--- ---	--- ---	--- ---	
C-L0512	N12	0.30 ±0.05	1.60 ±0.16	0.65 ±0.07	--- ---	--- ---	--- ---	
C-L0513	N13	0.31 ±0.05	1.09 ±0.05	0.74 ±0.04	--- ---	--- ---	--- ---	
C-L0514	N14	0.28 ±0.07	1.15 ±0.06	0.73 ±0.04	--- ---	--- ---	--- ---	
C-L0515	N15	0.30 ±0.05	3.10 ±0.31	0.65 ±0.07	--- ---	--- ---	--- ---	
C-L0516	N16	0.24 ±0.06	1.32 ±0.07	0.77 ±0.04	--- ---	--- ---	--- ---	
C-L0517	N17	0.33 ±0.05	1.05 ±0.05	0.77 ±0.04	--- ---	--- ---	--- ---	
C-L0518	N18	0.35 ±0.05	1.26 ±0.06	0.77 ±0.04	--- ---	--- ---	--- ---	
C-L0519	F1	0.58 ±0.15	2.32 ±0.12	0.84 ±0.04	0.70 ±0.07	2.28 ±0.06	0.96 ±0.02	R
C-L0520	F2	0.35 ±0.05	2.16 ±0.11	0.86 ±0.04	0.62 ±0.13	1.98 ±0.06	0.87 ±0.02	
C-L0521	F3	0.38 ±0.06	1.52 ±0.08	0.88 ±0.04	0.49 ±0.16	1.48 ±0.08	0.84 ±0.04	
C-L0522	F4	0.46 ±0.12	1.54 ±0.08	0.78 ±0.04	0.44 ±0.08	1.48 ±0.06	0.91 ±0.02	
C-L0523	F5	0.38 ±0.06	1.24 ±0.06	0.91 ±0.05	0.41 ±0.08	1.25 ±0.03	0.89 ±0.02	
C-L0524	F6	0.47 ±0.05	1.34 ±0.07	0.87 ±0.04	0.36 ±0.06	1.21 ±0.05	0.88 ±0.03	
C-L0525	F7	0.31 ±0.05	1.88 ±0.09	0.96 ±0.05	0.52 ±0.04	1.64 ±0.06	0.99 ±0.02	
C-L0526	F8	1.61 ±0.24	2.91 ±0.15	1.01 ±0.05	0.90 ±0.11	2.82 ±0.09	1.06 ±0.03	
C-L0527	F9	1.61 ±0.24	3.20 ±0.16	1.13 ±0.06	1.00 ±0.11	2.84 ±0.11	1.03 ±0.04	
C-L0528	F12	0.30 ±0.05	1.75 ±0.09	0.84 ±0.04	--- ---	--- ---	--- ---	
C-L0529	F13	0.37 ±0.06	1.76 ±0.09	0.78 ±0.04	--- ---	--- ---	--- ---	
C-L0530	F14	0.38 ±0.10	1.44 ±0.07	0.85 ±0.04	--- ---	--- ---	--- ---	
C-L0531	F15	0.61 ±0.05	1.76 ±0.09	0.85 ±0.04	--- ---	--- ---	--- ---	
C-L0532	F16	0.26 ±0.07	1.63 ±0.08	0.97 ±0.05	--- ---	--- ---	--- ---	
C-L0533	F17	0.57 ±0.06	2.26 ±0.11	0.88 ±0.04	--- ---	--- ---	--- ---	
C-L0534	F18	0.70 ±0.08	2.81 ±0.14	0.98 ±0.05	--- ---	--- ---	--- ---	
C-L0535	F10	0.88 ±0.22	3.98 ±0.20	0.98 ±0.05	1.13 ±0.12	3.50 ±0.08	1.05 ±0.03	R
C-L0536	F11	0.35 ±0.05	1.78 ±0.09	0.86 ±0.04	0.50 ±0.06	1.62 ±0.09	0.85 ±0.04	

Lab code	sample	U (ppm) NAA		Th (ppm) NAA		K (%) NAA		U (ppm) γ-spec.		Th (ppm) γ-spec.		K (%) γ-spec.		Lab.
C-L0537	F19	0.53	±0.06	3.07	±0.15	1.09	±0.05	---	---	---	---	---	---	
C-L0538	F20	0.58	±0.06	3.15	±0.16	0.89	±0.04	---	---	---	---	---	---	
C-L0539	R1	0.35	±0.18	1.71	±0.09	0.90	±0.05	---	---	---	---	---	---	
C-L0540	R2	0.80	±0.20	3.01	±0.15	1.17	±0.06	1.10	±0.10	3.18	±0.06	1.19	±0.02	R
C-L0541	R3	<DL	---	1.62	±0.08	0.82	±0.04	0.54	±0.08	1.67	±0.07	0.83	±0.03	
C-L0542	R4	0.59	±0.15	1.88	±0.09	0.80	±0.04	---	---	---	---	---	---	
C-L0543	R5	0.49	±0.05	1.80	±0.09	0.79	±0.04	---	---	---	---	---	---	
C-L0544	R6	0.35	±0.18	1.78	±0.09	0.81	±0.04	---	---	---	---	---	---	
C-L0545	R7	0.32	±0.05	1.43	±0.07	0.72	±0.04	---	---	---	---	---	---	
C-L0546	M1	0.64	±0.16	1.96	±0.10	0.92	±0.05	---	---	---	---	---	---	
C-L0547	M2	0.35	±0.18	3.09	±0.15	0.95	±0.05	---	---	---	---	---	---	
C-L0548	M3	0.99	±0.25	2.92	±0.15	0.98	±0.05	0.58	±0.10	1.76	±0.07	1.11	±0.03	R
C-L0549	M4	<DL	---	3.02	±0.15	1.05	±0.05	0.92	±0.13	2.80	±0.08	0.99	±0.03	
C-L0550	S1	0.57	±0.14	2.10	±0.11	0.98	±0.05	---	---	---	---	---	---	
C-L0551	S2	<DL	---	1.81	±0.09	0.98	±0.05	0.56	±0.13	1.64	±0.07	0.98	±0.03	R
C-L0552	S3	<DL	---	1.71	±0.09	0.98	±0.05	0.80	±0.16	2.78	±0.09	0.91	±0.03	
C-L0553	S4	0.35	±0.18	1.42	±0.07	0.99	±0.05	---	---	---	---	---	---	
C-L0554	S5	0.35	±0.18	1.25	±0.06	0.78	±0.04	---	---	---	---	---	---	
C-L0555	C1	0.53	±0.06	1.16	±0.06	0.54	±0.03	---	---	---	---	---	---	
C-L0556	C2	0.37	±0.06	0.87	±0.04	0.62	±0.03	---	---	---	---	---	---	
C-L0557	C3	0.34	±0.05	0.99	±0.05	0.57	±0.03	---	---	---	---	---	---	
C-L0558	C4	0.30	±0.05	0.97	±0.05	0.54	±0.03	---	---	---	---	---	---	
C-L0559	C5	0.31	±0.05	1.12	±0.06	0.46	±0.02	---	---	---	---	---	---	
C-L0560	C6	0.63	±0.05	1.24	±0.06	0.53	±0.03	0.26	±0.04	1.29	±0.08	0.56	±0.02	HD
C-L0561	C7	1.61	±0.08	4.06	±0.20	0.90	±0.04	0.62	±0.02	2.07	±0.05	0.74	±0.02	
C-L0562	J1	0.46	±0.05	1.06	±0.05	0.55	±0.03	---	---	---	---	---	---	
C-L0563	J2	0.27	±0.07	1.04	±0.05	0.52	±0.03	---	---	---	---	---	---	
C-L0564	J3	0.27	±0.07	1.05	±0.05	0.52	±0.03	---	---	---	---	---	---	
C-L0565	J4	0.41	±0.05	1.06	±0.05	0.48	±0.02	---	---	---	---	---	---	
C-L0566	J5	0.29	±0.07	0.86	±0.04	0.53	±0.03	---	---	---	---	---	---	
C-L0567	J6	0.48	±0.05	1.35	±0.07	0.54	±0.03	---	---	---	---	---	---	
C-L0568	J7	0.30	±0.05	0.84	±0.04	0.52	±0.03	0.26	±0.02	0.93	±0.04	0.55	±0.01	HD
C-L0569	J8	0.56	±0.06	1.43	±0.07	0.61	±0.03	0.33	±0.04	1.06	±0.06	0.60	±0.02	
C-L0603	JA1	0.22	±0.06	1.00	±0.05	0.48	±0.02	---	---	---	---	---	---	
C-L0604	JA2	0.15	±0.04	0.93	±0.05	0.44	±0.02	---	---	---	---	---	---	
C-L0605	JA3	0.40	±0.04	1.09	±0.05	0.35	±0.02	---	---	---	---	---	---	
C-L0606	JA4	0.39	±0.06	1.24	±0.06	0.37	±0.02	---	---	---	---	---	---	
C-L0607	JA5	0.32	±0.05	1.21	±0.06	0.47	±0.02	---	---	---	---	---	---	
C-L0608	JA6	0.26	±0.07	1.11	±0.06	0.52	±0.03	---	---	---	---	---	---	
C-L0609	JA7	0.16	±0.04	1.08	±0.05	0.50	±0.03	---	---	---	---	---	---	
C-L0610	JB1	0.78	±0.06	1.65	±0.08	0.57	±0.03	---	---	---	---	---	---	
C-L0611	JB2	0.37	±0.06	1.16	±0.06	0.52	±0.03	---	---	---	---	---	---	
C-L0612	JB3	0.19	±0.05	1.05	±0.05	0.54	±0.03	---	---	---	---	---	---	
C-L0615	JB4	0.20	±0.05	1.12	±0.06	0.53	±0.03	---	---	---	---	---	---	
C-L0613	JB5	0.36	±0.05	1.03	±0.05	0.47	±0.02	---	---	---	---	---	---	
C-L0614	JB6	0.46	±0.05	1.37	±0.07	0.59	±0.03	---	---	---	---	---	---	
C-L0616	JB7	0.27	±0.07	1.18	±0.06	0.55	±0.03	---	---	---	---	---	---	
C-L0617	JB8	0.33	±0.05	1.09	±0.05	0.56	±0.03	---	---	---	---	---	---	
C-L0618	JB9	0.26	±0.07	0.97	±0.05	0.58	±0.03	---	---	---	---	---	---	
C-L0619	JB10	0.31	±0.05	0.98	±0.05	0.55	±0.03	---	---	---	---	---	---	

Lab code	sample	U (ppm) NAA	Th (ppm) NAA	K (%) NAA	U (ppm) γ-spec.	Th (ppm) γ-spec.	K (%) γ-spec.	Lab.
C-L0620	JB11	0.19 ±0.05	1.07 ±0.05	0.59 ±0.03	--- ---	--- ---	--- ---	
C-L0621	JB12	0.45 ±0.05	1.26 ±0.06	0.51 ±0.03	--- ---	--- ---	--- ---	
C-L0622	JB13	0.27 ±0.07	0.92 ±0.05	0.51 ±0.03	--- ---	--- ---	--- ---	
C-L0623	JC1	0.32 ±0.05	1.18 ±0.06	0.50 ±0.03	--- ---	--- ---	--- ---	
C-L0624	JC2	0.32 ±0.05	1.09 ±0.05	0.54 ±0.03	--- ---	--- ---	--- ---	
C-L0625	JC3	0.34 ±0.05	1.27 ±0.06	0.54 ±0.03	--- ---	--- ---	--- ---	
C-L0626	JC4	0.44 ±0.05	1.87 ±0.09	0.61 ±0.03	--- ---	--- ---	--- ---	
C-L0627	JC5	0.32 ±0.05	1.14 ±0.06	0.54 ±0.03	--- ---	--- ---	--- ---	
C-L0628	STA00-1	0.50 ±0.06	1.27 ±0.06	0.80 ±0.04	0.46 ±0.04	0.94 ±0.11	0.75 ±0.02	C
C-L0629	STA00-2	0.43 ±0.05	1.28 ±0.06	0.71 ±0.04	--- ---	--- ---	--- ---	
C-L0630	STA00-3	0.43 ±0.05	1.19 ±0.06	0.70 ±0.04	0.41 ±0.07	1.06 ±0.14	0.71 ±0.02	
C-L0631	STA00-4	0.38 0.06	1.07 ±0.05	0.69 ±0.03	0.39 ±0.03	0.97 ±0.07	0.66 ±0.02	
C-L0632	STA00-5	0.37 ±0.06	1.03 ±0.05	0.67 ±0.03	0.39 ±0.07	0.96 ±0.14	0.65 ±0.02	
C-L0633	STA00-6	0.30 ±0.05	0.97 ±0.06	0.53 ±0.03	0.38 ±0.07	0.93 ±0.13	0.56 ±0.02	
C-L0634	STA00-7	0.41 ±0.05	0.93 ±0.06	0.48 ±0.03	0.38 ±0.03	0.95 ±0.13	0.56 0.02	
C-L0635	STA00-8	0.37 ±0.06	1.07 ±0.05	0.54 ±0.03	0.37 ±0.05	0.92 ±0.13	0.56 ±0.02	
C-L0636	STA00-9	0.31 ±0.05	1.00 ±0.05	0.50 ±0.03	--- ---	--- ---	--- ---	
C-L0637	STA00-10	0.37 ±0.06	1.10 ±0.06	0.48 ±0.03	--- ---	--- ---	--- ---	
C-L0638	STA00-11	0.36 ±0.05	1.10 ±0.06	0.57 ±0.03	--- ---	--- ---	--- ---	
C-L0684	STA1	--- ---	--- ---	--- ---	0.70 ±0.07	1.60 ±0.15	0.79 ±0.11	F
C-L0685	STA2	--- ---	--- ---	--- ---	0.57 ±0.04	1.23 ±0.10	0.66 ±0.09	
C-L0686	STA3	--- ---	--- ---	--- ---	0.61 ±0.05	1.28 ±0.15	0.68 ±0.08	
C-L0687	STA4	0.31 ±0.05	1.28 ±0.06	0.78 ±0.04	--- ---	--- ---	--- ---	
C-L0688	STA5	--- ---	--- ---	--- ---	0.63 ±0.07	1.48 ±0.10	0.69 ±0.10	
C-L0639	UM1	0.39 ±0.06	1.41 ±0.07	0.81 ±0.04	--- ---	--- ---	--- ---	
C-L0640	UM2	0.22 ±0.06	1.43 ±0.07	0.81 ±0.04	--- ---	--- ---	--- ---	
C-L0641	UM3	0.48 ±0.05	1.52 ±0.08	0.76 ±0.04	0.42 ±0.03	1.33 ±0.20	0.73 ±0.02	C
C-L0642	UM4	0.38 ±0.06	1.59 ±0.08	0.84 ±0.04	0.46 ±0.06	1.51 ±0.21	0.75 ±0.02	
C-L0643	UM5	0.68 ±0.05	1.57 ±0.08	0.90 ±0.05	0.52 ±0.06	1.55 ±0.12	0.76 ±0.02	
C-L0644	UM6	0.41 ±0.05	1.67 ±0.08	0.77 ±0.04	0.62 ±0.09	1.6 ±0.14	0.78 ±0.02	
C-L0645	UM7	0.56 ±0.06	2.67 ±0.13	0.89 ±0.04	0.59 ±0.12	2.43 ±0.17	0.78 ±0.02	
C-L0646	UM8	0.58 ±0.06	2.01 ±0.10	0.79 ±0.04	0.53 ±0.05	2.04 ±0.14	0.85 ±0.02	
C-L0647	UM9	0.35 ±0.05	1.45 ±0.07	1.06 ±0.05	0.37 ±0.05	1.40 ±0.28	0.93 ±0.02	
C-L0648	UM10	0.62 ±0.05	2.41 ±0.12	1.00 ±0.05	0.70 ±0.04	2.41 ±0.28	0.93 ±0.02	
C-L0649	UM11	0.54 ±0.06	1.66 ±0.08	0.86 ±0.04	--- ---	--- ---	--- ---	
C-L0650	UM12	0.29 ±0.07	1.32 ±0.07	0.83 ±0.04	--- ---	--- ---	--- ---	
C-L0651	UM13	0.53 ±0.06	2.59 ±0.13	0.88 ±0.04	--- ---	--- ---	--- ---	
C-L0652	UM14	0.71 ±0.06	2.46 ±0.12	0.92 ±0.05	--- ---	--- ---	--- ---	
C-L0653	UM15	0.69 ±0.06	2.51 ±0.13	1.21 ±0.06	--- ---	--- ---	--- ---	
C-L0654	UM16	0.82 ±0.05	2.28 ±0.11	1.27 ±0.06	--- ---	--- ---	--- ---	
C-L0655	UM17	0.79 ±0.06	2.27 ±0.11	1.26 ±0.06	--- ---	--- ---	--- ---	
C-L0656	UM18	1.14 ±0.06	4.16 ±0.21	1.31 ±0.07	--- ---	--- ---	--- ---	
C-L0657	UM19	1.32 ±0.07	5.47 ±0.27	1.53 ±0.08	--- ---	--- ---	--- ---	
C-L0658	UM20	0.33 ±0.05	1.98 ±0.10	0.70 ±0.04	--- ---	--- ---	--- ---	
C-L0659	UM21	0.47 ±0.05	1.89 ±0.09	0.82 ±0.04	0.47 ±0.05	1.50 ±0.22	0.73 ±0.02	C
C-L0660	UM22	0.48 ±0.05	1.49 ±0.07	0.71 ±0.04	0.45 ±0.04	1.47 ±0.20	0.73 ±0.02	
C-L0661	UM23	0.46 ±0.05	2.20 ±0.11	0.92 ±0.05	0.56 ±0.04	2.16 ±0.22	0.89 ±0.02	
C-L0662	UM24	<DL ---	1.47 ±0.07	1.08 ±0.05	0.44 ±0.05	1.47 ±0.27	0.92 ±0.02	
C-L0663	UM25	0.59 ±0.06	2.16 ±0.11	0.80 ±0.04	0.65 ±0.04	3.00 ±0.22	0.68 ±0.02	
C-L0664	UM26	0.29 ±0.07	1.38 ±0.07	0.93 ±0.05	--- ---	--- ---	--- ---	

Lab code	sample	U (ppm) NAA	Th (ppm) NAA	K (%) NAA	U (ppm) γ-spec.	Th (ppm) γ-spec.	K (%) γ-spec.	Lab.
C-L0665	UM27	0.43 ±0.05	1.43 ±0.07	0.84 ±0.04	--- ---	--- ---	--- ---	
C-L0666	AD4-1	0.63 ±0.05	1.88 ±0.09	0.56 ±0.03	--- ---	--- ---	--- ---	
C-L0667	AD4-2	0.64 ±0.05	2.63 ±0.13	0.97 ±0.05	--- ---	--- ---	--- ---	
C-L0668	AD4-3	0.45 ±0.05	2.18 ±0.11	0.98 ±0.05	--- ---	--- ---	--- ---	
C-L0669	AD4-4	0.50 ±0.06	2.54 ±0.13	0.95 ±0.05	0.90 ±0.09	3.19 ±0.24	0.98 ±0.02	∩
C-L0670	AD4-5	0.53 ±0.06	1.98 ±0.10	1.00 ±0.05	--- ---	--- ---	--- ---	
C-L0671	AD4-6	0.56 ±0.06	2.25 ±0.11	0.95 ±0.05	--- ---	--- ---	--- ---	
C-L0672	AD4-7	0.79 ±0.06	2.72 ±0.14	1.02 ±0.05	--- ---	--- ---	--- ---	
C-L0673	AD4-8	0.46 ±0.05	1.67 ±0.08	1.01 ±0.05	--- ---	--- ---	--- ---	
C-L0674	AD4-9	0.40 ±0.04	1.68 ±0.08	0.95 ±0.05	--- ---	--- ---	--- ---	
C-L0675	AD4-10	0.38 ±0.06	1.71 ±0.09	0.92 ±0.05	--- ---	--- ---	--- ---	
C-L0676	AD4-11	0.37 ±0.06	1.29 ±0.06	0.94 ±0.05	--- ---	--- ---	--- ---	
C-L0677	AD4-12	0.64 ±0.05	2.79 ±0.14	1.05 ±0.05	1.01 ±0.06	2.82 ±0.28	1.03 ±0.02	
C-L0678	AD4-13	1.63 ±0.08	5.87 ±0.29	1.06 ±0.05	--- ---	--- ---	--- ---	∩
C-L0679	AD4-14	0.64 ±0.05	1.98 ±0.10	0.98 ±0.05	0.81 ±0.07	2.21 ±0.18	1.05 ±0.02	
C-L0680	AD1-1	0.50 ±0.06	1.79 ±0.09	1.12 ±0.06	0.53 ±0.09	1.65 ±0.16	0.91 ±0.02	
C-L0681	AD1-2	0.74 ±0.06	3.00 ±0.15	1.21 ±0.06	--- ---	--- ---	--- ---	∩
C-L0682	AD1-3	1.63 ±0.08	4.61 ±0.23	1.40 ±0.07	1.37 ±0.10	4.05 ±0.21	1.13 ±0.03	
C-L0683	AD1-4	0.88 ±0.05	2.65 ±0.13	1.28 ±0.06	--- ---	--- ---	--- ---	
C-L0689	SHA-1	0.47 ±0.05	1.74 ±0.09	0.87 ±0.04	--- ---	--- ---	--- ---	
C-L0690	SHA-2	0.37 ±0.06	1.77 ±0.09	0.84 ±0.04	--- ---	--- ---	--- ---	
C-L0691	SHA-3	0.42 ±0.05	1.67 ±0.08	0.95 ±0.05	--- ---	--- ---	--- ---	
C-L0692	SHA-4	0.76 ±0.06	2.38 ±0.12	1.04 ±0.05	--- ---	--- ---	--- ---	
C-L0693	SHA-5	0.79 ±0.06	3.86 ±0.19	1.13 ±0.06	1.03 ±0.07	3.38 ±0.28	1.000 ±0.02	∩
C-L0694	SHA-6	0.55 ±0.06	2.32 ±0.12	1.00 ±0.05	--- ---	--- ---	--- ---	
C-L0695	SHB-1	0.35 ±0.05	1.47 ±0.07	0.82 ±0.04	--- ---	--- ---	--- ---	
C-L0696	SHB-2	0.32 ±0.08	1.32 ±0.07	0.83 ±0.04	--- ---	--- ---	--- ---	
C-L0697	SHB-3	0.42 ±0.05	2.46 ±0.12	0.84 ±0.04	--- ---	--- ---	--- ---	
C-L0698	SHB-4	0.62 ±0.05	2.28 ±0.11	0.87 ±0.04	--- ---	--- ---	--- ---	
C-L0699	G1	0.25 ±0.06	1.01 ±0.05	0.42 ±0.03	--- ---	--- ---	--- ---	
C-L0700	G2	0.35 ±0.05	1.10 ±0.06	0.42 ±0.03	--- ---	--- ---	--- ---	
C-L0701	G3	0.31 ±0.05	0.81 ±0.05	0.41 ±0.02	0.32 ±0.04	0.82 ±0.12	0.51 ±0.01	∩
C-L0702	G4	0.38 ±0.06	1.03 ±0.05	0.53 ±0.03	--- ---	--- ---	--- ---	
C-L0703	G5	0.23 ±0.06	0.98 ±0.06	0.56 ±0.03	--- ---	--- ---	--- ---	
C-L0704	G6	0.26 ±0.07	0.97 ±0.06	0.53 ±0.03	--- ---	--- ---	--- ---	
C-L0705	G7	0.23 ±0.06	0.97 ±0.06	0.48 ±0.03	--- ---	--- ---	--- ---	
C-L0706	G8	0.34 ±0.05	1.14 ±0.06	0.51 ±0.03	--- ---	--- ---	--- ---	
C-L0707	G9	0.33 ±0.05	1.02 ±0.05	0.51 ±0.03	--- ---	--- ---	--- ---	
C-L0708	G10	0.27 ±0.07	0.88 ±0.05	0.50 ±0.03	--- ---	--- ---	--- ---	
C-L0709	G11	0.27 ±0.07	1.09 ±0.05	0.53 ±0.03	--- ---	--- ---	--- ---	
C-L0710	G12	0.41 ±0.05	1.08 ±0.05	0.53 ±0.03	--- ---	--- ---	--- ---	
C-L0711	G12B	0.39 ±0.06	1.08 ±0.05	0.58 ±0.03	--- ---	--- ---	--- ---	
C-L0712	G13	0.36 ±0.09	1.02 ±0.05	0.52 ±0.03	--- ---	--- ---	--- ---	
C-L0713	G14	0.38 ±0.06	1.05 ±0.05	0.54 ±0.03	--- ---	--- ---	--- ---	
C-L0714	G15	0.27 ±0.07	0.93 ±0.06	0.52 ±0.03	--- ---	--- ---	--- ---	
C-L0715	G16	0.27 ±0.07	0.86 ±0.05	0.45 ±0.03	--- ---	--- ---	--- ---	
C-L0716	G17	0.26 ±0.07	0.91 ±0.05	0.46 ±0.03	--- ---	--- ---	--- ---	

Table A 2: Results of the duplicate neutron activation analysis.
(mean=arithmetic mean of both analytical results and 1σ standard deviation, <DL= below detection limit, DL as indicated, n.r.= not reliable)

sample	U in ppm		Mean U in ppm		Th in ppm		Mean Th in ppm		K in %		Mean K in ppm	
F1	0.47	±0.05	**0.58**	±0.16	2.24	±0.11	**2.32**	±0.11	0.92	±0.05	**0.84**	±0.11
	0.69	±0.17			2.40	±0.12			0.76	±0.04		
F2	0.35	±0.05	**0.35**	±0.05	2.00	±0.10	**2.16**	±0.22	0.82	±0.04	**0.86**	±0.05
	<DL	0.50			2.31	±0.12			0.89	±0.04		
F3	0.38	±0.06	**0.38**	±0.06	1.54	±0.08	**1.52**	±0.04	0.85	±0.04	**0.88**	±0.03
	<DL	0.50			1.49	±0.07			0.90	±0.04		
F4	0.29	±0.07	**0.46**	±0.23	1.55	±0.08	**1.54**	±0.02	0.80	±0.04	**0.78**	±0.03
	0.62	±0.16			1.52	±0.08			0.76	±0.04		
F5	0.38	±0.06	**0.38**	±0.06	1.20	±0.06	**1.24**	±0.06	0.87	±0.04	**0.91**	±0.07
	<DL	0.50			1.28	±0.06			0.96	±0.05		
F6	0.47	±0.05	**0.47**	±0.05	1.21	±0.06	**1.34**	±0.18	0.85	±0.04	**0.87**	±0.03
	<DL	0.50			1.47	±0.07			0.89	±0.04		
F7	0.31	±0.05	**0.31**	±0.05	1.82	±0.09	**1.88**	±0.08	1.00	±0.05	**0.96**	±0.06
	<DL	0.50			1.93	±0.10			0.92	±0.05		
F8	1.50	±0.08	**1.61**	±0.16	2.81	±0.14	**2.91**	±0.13	1.03	±0.05	**1.01**	±0.03
	1.72	±0.26			3.00	±0.15			0.99	±0.05		
F9	1.52	±0.08	**1.61**	±0.12	3.08	±0.15	**3.20**	±0.17	1.07	±0.05	**1.13**	±0.08
	1.69	±0.25			3.32	±0.17			1.18	±0.06		
F10	0.72	±0.06	**0.88**	±0.22	3.90	±0.20	**3.98**	±0.11	0.97	±0.05	**0.98**	±0.01
	1.03	±0.26			4.05	±0.20			0.99	±0.05		
F11	0.35	±0.05	**0.35**	±0.05	1.75	±0.09	**1.78**	±0.04	0.87	±0.04	**0.86**	±0.02
	<DL	0.50			1.80	±0.09			0.85	±0.04		
F14	0.53	±0.06	**0.38**	±0.21	1.49	±0.07	**1.44**	±0.08	0.86	±0.04	**0.85**	±0.01
	0.23	±0.06			1.38	±0.07			0.84	±0.04		
F16	0.23	±0.06	**0.26**	±0.04	1.58	±0.08	**1.63**	±0.07	1.01	±0.05	**0.97**	±0.06
	0.28	±0.07			1.68	±0.08			0.92	±0.05		
F18	0.47	±0.05	**0.70**	±0.32	2.81	±0.14	**2.81**	±0.01	1.07	±0.05	**0.98**	±0.13
	0.92	±0.06			2.80	±0.14			0.88	±0.04		
SHB2	0.29	±0.07	**0.32**	±0.04	1.34	±0.07	**1.32**	±0.03	0.83	±0.04	**0.83**	±0.002
	0.34	±0.05			1.30	±0.07			0.83	±0.04		
JA6	0.20	±0.05	**0.26**	±0.08	1.08	±0.05	**1.11**	±0.04	0.52	±0.03	**0.52**	±0.004
	0.31	±0.05			1.14	±0.06			0.53	±0.03		
J5	0.28	±0.07	**0.29**	±0.01	0.90	±0.05	**0.86**	±0.06	0.53	±0.03	**0.53**	±0.004
	0.3	±0.05			0.81	±0.04			0.54	±0.03		
G13	0.28	±0.07	**0.36**	±0.11	1.03	±0.05	**1.02**	±0.01	0.52	±0.03	**0.52**	±0.03
	0.43	±0.05			1.01	±0.05			n.r.			
UM2	0.22	±0.06	**0.22**	±0.06	1.56	±0.08	**1.43**	±0.19	0.78	±0.04	**0.81**	±0.04
	<DL	0.10			1.29	±0.06			0.84	±0.04		
R5	0.49	±0.05	**0.49**	±0.05	1.82	±0.09	**1.80**	±0.04	0.79	±0.04	**0.79**	±0.01
	<DL	0.50			1.77	±0.09			0.78	±0.04		
R7	0.32	±0.05	**0.32**	±0.05	1.44	±0.07	**1.43**	±0.02	0.72	±0.04	**0.72**	±0.004
	<DL	0.50			1.41	±0.07			0.72	±0.04		

Table A 3: Results of in-situ gamma dose rate measurements.
Comparison of in-situ measurements of the total gamma radiation dose using a scintillator probe with the calculated gamma dose rates based on the radionuclide concentrations determined by NAA or high-resolution γ-ray spectrometry in the laboratory, the cosmic dose contribution according to the actual sampling depth and radiation attenuation dependent on the actual water content (as determined by water content analysis in the laboratory).

sample	in-situ γ-dose rate (µGy/a)	calculated γ- & cosmic dose based on NAA (µGy/a)	ratio in-situ/NAA
J2	324	379	0.86
J5	333	336	0.99
J7	342	308	1.11
C1	421	454	0.93
C4	386	375	1.03
C6	447	378	1.18
C7	579	693	0.83
F4	587	491	1.20
F6	508	484	1.05
F8-9	526	593	0.89
F12	561	519	1.08
F13	570	496	1.15
F15	508	524	0.97
F17	596	533	1.12
F18	640	586	1.09
F19	561	598	0.94
STA00-1	456	480	0.95
STA00-	447	446	1.00
STA00-	430	406	1.06
ST00-11	465	449	1.03
AD4-5	657	565	1.16
AD4-9	587	504	1.17
AD4-14	666	541	1.23
UM4	543	495	1.10
UM9	579	520	1.11
UM10	579	575	1.01

Mean ratio & standard deviation= **1.05±0.11 (n=26)**

sample	in-situ γ-dose rate (µGy/a)	calculated γ- & cosmic dose based on lab. γ-spectrometry (µGy/a)	ratio in-situ/ gamma-spec.
F4	587	516	1.14
F 6	508	469	1.08
F8-9	526	527	1.00
STA00-1	456	449	1.02
STA00-	447	438	1.02
STA00-	430	414	1.04
J7	342	314	1.09
C6	447	350	1.28
C7	579	465	1.24
AD4-14	666	587	1.13
UM4	543	479	1.13
UM9	579	490	1.18
UM10	579	567	1.02

Mean ratio & standard deviation= **1.11±0.09 (n=13)**

Table A 4: Summary of parameters for dose rate calculation and finally resulting dose rates.
The subscripts in the grain size column indicate the grain size fraction which was obtained by re-sieving after the HF-etching. Note that "n.a." (not available) in the water content column marks those samples for which no water content was measured for various reasons. The column "H₂O-content range assumed" shows the values used for dose rate calculation for the individual samples with min/average/max values in weight-%. The dose rates used for age calculation take the range between the assumed minimum and maximum water content into account. The dose rate values were either based on the radionuclide concentrations determined neutron activation analysis (NAA) or gamma-ray spectrometry (γ-spec.).

Lab. code	sample	grain size (mm)	H_2O-content (weight-%).		H_2O-c. range assumed	depth (m)	dose rate NAA (Gy/ka)		dose rate γ-spec. (Gy/ka)	
C-L0501	N1	0.1-0.2 $_{0.09-0.15}$	n.a.	n.a.	2/4.5/7	0.15	0.92	±0.09	---	---
C-L0502	N2	0.1-0.2 $_{0.09-0.15}$	n.a.	n.a.	2/4.5/7	0.80	0.91	±0.08	---	---
C-L0503	N3	0.1-0.2 $_{0.09-0.15}$	n.a.	n.a.	2/4.5/7	1.30	0.94	±0.09	---	---
C-L0504	N4	0.1-0.2 $_{0.09-0.15}$	n.a.	n.a.	2/4.5/7	1.85	0.97	±0.05	---	---
C-L0505	N5	0.1-0.2 $_{0.09-0.15}$	n.a.	n.a.	2/4.5/7	2.35	0.94	±0.09	---	---
C-L0506	N6	0.1-0.2 $_{0.09-0.15}$	n.a.	n.a.	2/4.5/7	3.04	0.94	±0.09	---	---
C-L0507	N7	0.1-0.2 $_{0.09-0.15}$	n.a.	n.a.	2/4.5/7	3.50	0.86	±0.09	---	---
C-L0508	N8	0.1-0.2 $_{0.09-0.15}$	n.a.	n.a.	2/4.5/7	4.05	0.89	±0.09	---	---
C-L0509	N9	0.1-0.2 $_{0.09-0.15}$	n.a.	n.a.	2/4.5/7	4.55	0.97	±0.09	---	---
C-L0510	N10	0.1-0.2 $_{0.09-0.15}$	n.a.	n.a.	2/4.5/7	5.00	1.03	±0.05	---	---
C-L0511	N11	0.1-0.2 $_{0.09-0.15}$	n.a.	n.a.	2/4.5/7	5.60	1.14	±0.10	---	---
C-L0512	N12	0.1-0.2 $_{0.09-0.15}$	n.a.	n.a.	2/4.5/7	6.80	0.94	±0.09	---	---
C-L0513	N13	0.1-0.2 $_{0.09-0.15}$	n.a.	n.a.	2/4.5/7	7.15	0.98	±0.05	---	---
C-L0514	N14	0.1-0.2 $_{0.09-0.15}$	n.a.	n.a.	2/4.5/7	7.70	0.95	±0.06	---	---
C-L0515	N15	0.1-0.2 $_{0.09-0.15}$	n.a.	n.a.	2/4.5/7	8.55	1.00	±0.09	---	---
C-L0516	N16	0.1-0.2 $_{0.09-0.15}$	n.a.	n.a.	2/4.5/7	9.05	0.97	±0.06	---	---
C-L0517	N17	0.1-0.2 $_{0.09-0.15}$	n.a.	n.a.	2/4.5/7	9.65	0.97	±0.06	---	---
C-L0518	N18	0.1-0.2 $_{0.09-0.15}$	n.a.	n.a.	2/4.5/7	10.0	0.98	±0.06	---	---
C-L0519	F1	0.1-0.2 $_{0.09-0.15}$	6.51	n.a.	3//6//9	0.45	1.25	±0.08	1.38	±0.05
C-L0520	F2	0.1-0.2 $_{0.09-0.15}$	6.24	n.a.	3//6//9	0.65	1.19	±0.06	1.25	±0.06
C-L0521	F3	0.1-0.2 $_{0.09-0.15}$	3.17	n.a.	2/4.5/7	0.40	1.20	±0.06	1.19	±0.07
C-L0522	F4	0.1-0.2 $_{0.09-0.15}$	4.88	n.a.	2/4.5/7	0.67	1.12	±0.07	1.23	±0.05
C-L0523	F5	0.1-0.2 $_{0.09-0.15}$	3.84	n.a.	2/4.5/7	1.15	1.19	±0.07	1.18	±0.04
C-L0524	F6	0.1-0.2 $_{0.09-0.15}$	5.23	n.a.	3//6//9	1.40	1.16	±0.06	1.14	±0.05
C-L0525	F7	0.1-0.2 $_{0.09-0.15}$	6.03	n.a.	3//6//9	1.80	1.23	±0.07	1.29	±0.04
C-L0526	F8	0.1-0.2 $_{0.09-0.15}$	29.18	n.a.	17//25.5//34	2.08	1.37	±0.10	1.27	±0.06
C-L0527	F9	0.1-0.2 $_{0.09-0.15}$	31.45	n.a.	17//25.5//34	2.28	1.47	±0.10	1.27	±0.07
C-L0528	F12	0.1-0.2 $_{0.09-0.15}$	2.17	n.a.	2/4.5/7	0.40	1.17	±0.06	---	---
C-L0529	F13	0.1-0.2 $_{0.09-0.15}$	3.96	n.a.	2/4.5/7	0.65	1.12	±0.06	---	---
C-L0530	F14	0.1-0.2 $_{0.09-0.15}$	4.42	n.a.	2/4.5/7	0.85	1.20	±0.06	---	---
C-L0531	F15	0.1-0.2 $_{0.09-0.15}$	3.87	n.a.	2/4.5/7	1.15	1.22	±0.06	---	---
C-L0532	F16	0.1-0.2 $_{0.09-0.15}$	4.07	n.a.	2/4.5/7	1.40	1.27	±0.07	---	---
C-L0533	F17	0.1-0.2 $_{0.09-0.15}$	4.79	n.a.	2/4.5/7	1.70	1.26	±0.07	---	---
C-L0534	F18	0.1-0.2 $_{0.09-0.15}$	5.32	n.a.	2/4.5/7	1.95	1.45	±0.07	---	---
C-L0535	F10	0.1-0.2 $_{0.09-0.15}$	11.67	±0.82	6//12/18	2.15	1.42	±0.10	1.50	±0.06

Lab. code	sample	grain size (mm)	H₂O-content (weight-%).		H₂O-c. range assumed	depth (m)	dose rate NAA (Gy/ka)		dose rate γ-spec. (Gy/ka)	
C-L0536	F11	0.1-0.2 $_{0.09-0.15}$	4.11	±0.14	2/4.5/7	2.35	1.15	±0.06	1.16	±0.06
C-L0537	F19	0.1-0.2 $_{0.09-0.15}$	4.55	n.a.	2/4.5/7	2.55	1.48	±0.08	---	---
C-L0538	F20	0.1-0.2 $_{0.09-0.15}$	4.11	n.a.	2/4.5/7	2.80	1.31	±0.07	---	---
C-L0539	R1	0.1-0.2 $_{0.09-0.15}$	5.85	n.a.	2/4.5/7	1.95	1.22	±0.09	---	---
C-L0540	R2	0.1-0.2 $_{0.09-0.15}$	8.53	±0.32	4//8//12	2.20	1.59	±0.10	1.68	±0.06
C-L0541	R3	0.1-0.2 $_{0.09-0.15}$	4.25	±0.01	2/4.5/7	2.60	1.16	±0.06	1.18	±0.05
C-L0542	R4	0.1-0.2 $_{0.09-0.15}$	5.38	±0.40	2/4.5/7	2.90	1.17	±0.07	---	---
C-L0543	R5	0.1-0.2 $_{0.09-0.15}$	4.13	±0.29	2/4.5/7	3.20	1.12	±0.06	---	---
C-L0544	R6	0.1-0.2 $_{0.09-0.15}$	5.34	±0.15	2/4.5/7	3.55	1.10	±0.08	---	---
C-L0545	R7	0.1-0.2 $_{0.09-0.15}$	4.90	±0.34	2/4.5/7	3.90	0.98	±0.06	---	---
C-L0546	M1	0.1-0.2 $_{0.09-0.15}$	7.67	±0.38	3//6//9	0.20	1.34	±0.08	---	---
C-L0547	M2	0.1-0.2 $_{0.09-0.15}$	3.29	±0.23	2/4.5/7	0.62	1.37	±0.09	---	---
C-L0548	M3	0.1-0.2 $_{0.09-0.15}$	4.78	±0.06	2/4.5/7	1.22	1.51	±0.11	1.46	±0.06
C-L0549	M4	0.1-0.2 $_{0.09-0.15}$	5.05	±0.03	2/4.5/7	1.70	1.56	±0.09	1.48	±0.07
C-L0550	S1	0.1-0.2 $_{0.09-0.15}$	3.34	±0.01	2/4.5/7	0.45	1.38	±0.08	---	---
C-L0551	S2	0.1-0.2 $_{0.09-0.15}$	4.41	±0.10	2/4.5/7	1.15	1.33	±0.08	1.32	±0.06
C-L0552	S3	0.1-0.2 $_{0.09-0.15}$	4.02	±0.05	2/4.5/7	1.45	1.37	±0.09	1.38	±0.07
C-L0553	S4	0.1-0.2 $_{0.09-0.15}$	5.34	±0.08	2/4.5/7	2.20	1.25	±0.09	---	---
C-L0554	S5	0.1-0.2 $_{0.09-0.15}$	1.33	±0.05	2/4.5/7	0.35	1.09	±0.08	---	---
C-L0555	C1	0.1-0.2 $_{0.09-0.15}$	1.97	n.a.	2/4.5/7	0.30	0.91	±0.05	---	---
C-L0556	C2	0.1-0.2 $_{0.09-0.15}$	3.37	n.a.	2/4.5/7	0.70	0.94	±0.05	---	---
C-L0557	C3	0.1-0.2 $_{0.09-0.15}$	3.68	n.a.	2/4.5/7	0.95	0.87	±0.05	---	---
C-L0558	C4	0.1-0.2 $_{0.09-0.15}$	4.06	n.a.	2/4.5/7	1.45	0.82	±0.04	---	---
C-L0559	C5	0.1-0.2 $_{0.09-0.15}$	9.65	n.a.	5//10//15	2.20	0.70	±0.03	---	---
C-L0560	C6	0.1-0.2 $_{0.09-0.15}$	11.77	n.a.	5//10//15	2.55	0.83	±0.04	0.79	±0.04
C-L0561	C7	0.1-0.2 $_{0.09-0.15}$	6.76	n.a.	6//9//12	3.00	1.59	±0.07	1.10	±0.03
C-L0562	J1	0.1-0.2 $_{0.09-0.15}$	3.15	n.a.	2/4.5/7	0.50	0.88	±0.05	---	---
C-L0563	J2	0.1-0.2 $_{0.09-0.15}$	3.13	n.a.	2/4.5/7	1.10	0.79	±0.05	---	---
C-L0564	J3	0.1-0.2 $_{0.09-0.15}$	3.94	n.a.	2/4.5/7	1.60	0.78	±0.05	---	---
C-L0565	J4	0.1-0.2 $_{0.09-0.15}$	3.02	n.a.	2/4.5/7	2.20	0.76	±0.03	---	---
C-L0566	J5	0.1-0.2 $_{0.09-0.15}$	2.62	n.a.	2/4.5/7	3.10	0.76	±0.05	---	---
C-L0567	J6	0.1-0.2 $_{0.09-0.15}$	6.21	n.a.	3//6//9	3.65	0.81	±0.05	---	---
C-L0568	J7	0.1-0.2 $_{0.09-0.15}$	3.88	n.a.	2/4.5/7	4.55	0.79	±0.04	0.81	±0.02
C-L0569	J8	0.1-0.2 $_{0.09-0.15}$	5.89	n.a.	3//6//9	4.90	0.94	±0.05	0.86	±0.04
C-L0603	JA1	0.1-0.25 $_{0.09-0.2}$	0.00	n.a.	2/4.5/7	0.47	0.76	±0.04	---	---
C-L0604	JA2	0.1-0.25 $_{0.09-0.2}$	0.47	n.a.	2/4.5/7	0.82	0.71	±0.03	---	---
C-L0605	JA3	0.1-0.25 $_{0.09-0.2}$	0.70	n.a.	2/4.5/7	1.25	0.68	±0.03	---	---
C-L0606	JA4	0.15-0.3 $_{0.15-0.25}$	1.26	n.a.	2/4.5/7	1.57	0.69	±0.03	---	---
C-L0607	JA5	0.1-0.2 $_{0.09-0.15}$	3.53	n.a.	2/4.5/7	1.88	0.76	±0.04	---	---
C-L0608	JA6	0.1-0.2 $_{0.09-0.15}$	1.82	n.a.	2/4.5/7	2.18	0.79	±0.04	---	---
C-L0609	JA7	0.1-0.25 $_{0.09-0.2}$	3.81	n.a.	2/4.5/7	2.61	0.73	±0.04	---	---
C-L0610	JB1	0.1-0.2 $_{0.09-0.15}$	18.57	n.a.	9//18//27	5.20	0.81	±0.04	---	---
C-L0611	JB2	0.1-0.2 $_{0.09-0.15}$	8.59	n.a.	4//8//12	5.03	0.73	±0.04	---	---

Lab. code	sample	grain size (mm)	H$_2$O-content (weight-%).		H$_2$O-c. range assumed	depth (m)	dose rate NAA (Gy/ka)		dose rate γ-spec. (Gy/ka)	
C-L0612	JB3	0.1-0.2 $_{0.09-0.15}$	2.67	n.a.	2/4.5/7	4.10	0.74	±0.041	---	---
C-L0615	JB4	0.1-0.2 $_{0.09-0.15}$	3.26	n.a.	2/4.5/7	3.95	0.74	±0.041	---	---
C-L0613	JB5	0.1-0.2 $_{0.09-0.15}$	3.17	n.a.	2/4.5/7	3.80	0.71	±0.036	---	---
C-L0614	JB6	0.1-0.2 $_{0.09-0.15}$	2.88	n.a.	2/4.5/7	3.48	0.87	±0.046	---	---
C-L0616	JB7	0.1-0.2 $_{0.09-0.15}$	3.85	n.a.	2/4.5/7	2.79	0.79	±0.045	---	---
C-L0617	JB8	0.1-0.2 $_{0.09-0.15}$	3.90	n.a.	2/4.5/7	2.38	0.81	±0.042	---	---
C-L0618	JB9	0.1-0.2 $_{0.09-0.15}$	4.06	n.a.	2/4.5/7	2.15	0.82	±0.047	---	---
C-L0619	JB10	0.1-0.2 $_{0.09-0.15}$	4.36	n.a.	2/4.5/7	2.00	0.80	±0.042	---	---
C-L0620	JB11	0.1-0.2 $_{0.09-0.15}$	2.96	n.a.	2/4.5/7	1.61	0.83	±0.045	---	---
C-L0621	JB12	0.1-0.2 $_{0.09-0.15}$	3.33	n.a.	2/4.5/7	1.20	0.83	±0.040	---	---
C-L0622	JB13	0.1-0.2 $_{0.09-0.15}$	n.a.	n.a.	2/4.5/7	0.60	0.79	±0.042	---	---
C-L0623	JC1	0.1-0.2 $_{0.09-0.15}$	0.98	n.a.	2/4.5/7	0.60	0.81	±0.039	---	---
C-L0624	JC2	0.1-0.2 $_{0.09-0.15}$	2.21	n.a.	2/4.5/7	4.30	0.77	±0.042	---	---
C-L0625	JC3	0.1-0.2 $_{0.09-0.15}$	2.96	n.a.	2/4.5/7	4.52	0.78	±0.042	---	---
C-L0626	JC4	0.1-0.2 $_{0.09-0.15}$	4.82	n.a.	2/4.5/7	4.75	0.90	±0.047	---	---
C-L0627	JC5	0.1-0.2 $_{0.09-0.15}$	3.21	n.a.	2/4.5/7	4.95	0.76	±0.042	---	---
C-L0628	STA00-1	0.1-0.2 $_{0.09-0.15}$	2.75	±0.22	2/4.5/7	1.21	1.12	±0.06	1.04	±0.04
C-L0629	STA00-2	0.1-0.2 $_{0.09-0.15}$	3.73	±0.57	2/4.5/7	1.13	1.02	±0.06	---	---
C-L0630	STA00-3	0.1-0.2 $_{0.09-0.15}$	2.43	±0.15	2/4.5/7	0.99	1.01	±0.06	1.00	±0.04
C-L0631	STA00-4	0.1-0.2 $_{0.09-0.15}$	2.54	±0.12	2/4.5/7	0.91	0.98	±0.05	0.95	±0.03
C-L0632	STA00-5	0.1-0.2 $_{0.09-0.15}$	1.75	±0.11	2/4.5/7	0.79	0.96	±0.05	0.94	±0.04
C-L0633	STA00-6	0.1-0.2 $_{0.09-0.15}$	2.76	±0.01	2/4.5/7	0.69	0.82	±0.04	0.86	±0.04
C-L0634	STA00-7	0.1-0.2 $_{0.09-0.15}$	2.39	±0.03	2/4.5/7	0.60	0.79	±0.04	0.86	±0.03
C-L0635	STA00-8	0.1-0.2 $_{0.09-0.15}$	3.90	±0.15	2/4.5/7	0.48	0.86	±0.05	0.86	±0.04
C-L0636	STA00-9	0.1-0.2 $_{0.09-0.15}$	3.30	±0.00	2/4.5/7	0.42	0.80	±0.04	---	---
C-L0637	STA00-10	0.1-0.2 $_{0.09-0.15}$	4.94	±0.29	2/4.5/7	0.33	0.81	±0.05	---	---
C-L0638	STA00-11	0.1-0.2 $_{0.09-0.15}$	4.44	±0.15	2/4.5/7	0.20	0.91	±0.05	---	---
C-L0684	STA1	0.1-0.2 $_{0.09-0.15}$	7.30	n.a.	2/4.5/7	1.59	---	---	1.17	±0.15
C-L0685	STA2	0.1-0.2 $_{0.09-0.15}$	2.10	n.a.	2/4.5/7	0.90	---	---	1.01	±0.12
C-L0686	STA3	0.1-0.2 $_{0.09-0.15}$	2.20	n.a.	2/4.5/7	0.90	---	---	1.04	±0.11
C-L0687	STA4	0.1-0.2 $_{0.09-0.15}$	3.00	n.a.	2/4.5/7	1.25	1.05	±0.06	---	---
C-L0688	STA5	0.1-0.2 $_{0.09-0.15}$	1.00	n.a.	2/4.5/7	0.58	---	---	1.08	±0.13
C-L0639	UM1	0.1-0.2 $_{0.09-0.15}$	3.01	n.a.	2/4.5/7	0.40	1.14	0.06	---	---
C-L0640	UM2	0.1-0.2 $_{0.09-0.15}$	4.39	n.a.	2/4.5/7	0.62	1.13	±0.06	---	---
C-L0641	UM3	0.1-0.2 $_{0.09-0.15}$	3.96	n.a.	2/4.5/7	0.82	1.10	±0.06	1.05	±0.04
C-L0642	UM4	0.1-0.2 $_{0.09-0.15}$	4.48	n.a.	2/4.5/7	1.10	1.15	±0.06	1.08	±0.04
C-L0643	UM5	0.1-0.2 $_{0.09-0.15}$	4.82	n.a.	2/4.5/7	1.22	1.27	±0.07	1.10	±0.04
C-L0644	UM6	0.1-0.2 $_{0.09-0.15}$	4.28	n.a.	2/4.5/7	1.32	1.09	±0.06	1.15	±0.05
C-L0645	UM7	0.1-0.2 $_{0.09-0.15}$	8.33	n.a.	4//8//12	1.48	1.26	±0.06	1.15	±0.05
C-L0646	UM8	0.1-0.2 $_{0.09-0.15}$	5.25	n.a.	2/4.5/7	1.58	1.17	±0.06	1.21	±0.04
C-L0647	UM9	0.1-0.2 $_{0.09-0.15}$	3.78	n.a.	2/4.5/7	1.70	1.32	±0.07	1.21	±0.05
C-L0648	UM10	0.1-0.2 $_{0.09-0.15}$	4.88	n.a.	2/4.5/7	1.90	1.39	±0.07	1.34	±0.05
C-L0649	UM11	0.1-0.2 $_{0.09-0.15}$	4.20	n.a.	2/4.5/7	2.05	1.19	±0.06	---	---

Lab. code	sample	grain size (mm)	H₂O-content (weight-%).		H₂O-c. range assumed	depth (m)	dose rate NAA (Gy/ka)		dose rate γ-spec. (Gy/ka)	
C-L0650	UM12	0.1-0.2	6.63	±2.32	3//6//9	0.40	1.11	±0.06	---	---
C-L0651	UM13	0.1-0.2	6.60	±2.80	3//6//9	0.70	1.31	±0.06	---	---
C-L0652	UM14	0.1-0.2	7.36	±2.96	3//6//9	1.20	1.35	±0.07	---	---
C-L0653	UM15	0.1-0.2	7.71	±0.25	3//6//9	0.27	1.64	±0.09	---	---
C-L0654	UM16	0.1-0.2	7.07	±0.17	3//6//9	0.44	1.70	±0.09	---	---
C-L0655	UM17	0.1-0.2	6.75	±0.22	3//6//9	0.70	1.67	±0.09	---	---
C-L0656	UM18	0.1-0.2	7.32	±0.18	4//8//16	0.96	1.87	±0.10	---	---
C-L0657	UM19	0.1-0.2	5.99	±0.83	4//8//16	1.20	2.18	±0.12	---	---
C-L0658	UM20	0.1-0.2 ₀.₀₉₋₀.₁₅	3.11	n.a.	2/4.5/7	0.38	1.06	±0.06	---	---
C-L0659	UM21	0.1-0.2 ₀.₀₉₋₀.₁₅	3.60	n.a.	2/4.5/7	0.50	1.19	±0.06	1.08	±0.04
C-L0660	UM22	0.1-0.2 ₀.₀₉₋₀.₁₅	4.15	n.a.	2/4.5/7	0.69	1.06	±0.06	1.07	±0.04
C-L0661	UM23	0.1-0.2 ₀.₀₉₋₀.₁₅	5.49	n.a.	3//6//9	0.88	1.27	±0.07	1.26	±0.04
C-L0662	UM24	0.1-0.2 ₀.₀₉₋₀.₁₅	5.26	n.a.	3//6//9	1.08	1.36	±0.07	1.21	±0.04
C-L0663	UM25	0.1-0.2 ₀.₀₉₋₀.₁₅	6.29	n.a.	3//6//9	1.34	1.18	±0.06	1.14	±0.04
C-L0664	UM26	0.1-0.2 ₀.₀₉₋₀.₁₅	8.17	n.a.	3//6//9	1.59	1.17	±0.07	---	---
C-L0665	UM27	0.1-0.2 ₀.₀₉₋₀.₁₅	6.79	n.a.	3//6//9	1.97	1.11	±0.06	---	---
C-L0666	AD4-1	0.1-0.2 ₀.₀₉₋₀.₁₅	5.15	±1.28	2/4.5/7	0.18	1.02	±0.05	---	---
C-L0667	AD4-2	0.1-0.2 ₀.₀₉₋₀.₁₅	4.83	±1.34	2/4.5/7	0.38	1.43	±0.07	---	---
C-L0668	AD4-3	0.1-0.2 ₀.₀₉₋₀.₁₅	2.75	±0.30	2/4.5/7	0.50	1.36	±0.07	---	---
C-L0669	AD4-4	0.1-0.2 ₀.₀₉₋₀.₁₅	3.66	±0.22	2/4.5/7	0.72	1.35	±0.07	1.52	±0.05
C-L0670	AD4-5	0.1-0.2 ₀.₀₉₋₀.₁₅	3.79	±0.11	2/4.5/7	0.95	1.36	±0.07	---	---
C-L0671	AD4-6	0.1-0.2 ₀.₀₉₋₀.₁₅	3.92	±0.08	2/4.5/7	1.16	1.34	±0.07	---	---
C-L0672	AD4-7	0.1-0.2 ₀.₀₉₋₀.₁₅	4.94	±0.07	2/4.5/7	1.40	1.48	±0.07	---	---
C-L0673	AD4-8	0.1-0.2 ₀.₀₉₋₀.₁₅	3.83	±0.22	2/4.5/7	1.57	1.32	±0.07	---	---
C-L0674	AD4-9	0.1-0.2 ₀.₀₉₋₀.₁₅	4.33	±0.19	2/4.5/7	1.81	1.24	±0.07	---	---
C-L0675	AD4-10	0.1-0.2 ₀.₀₉₋₀.₁₅	3.46	±0.18	2/4.5/7	2.00	1.21	±0.07	---	---
C-L0676	AD4-11	0.1-0.2 ₀.₀₉₋₀.₁₅	3.44	±0.21	2/4.5/7	2.18	1.20	±0.07	---	---
C-L0677	AD4-12	0.1-0.2 ₀.₀₉₋₀.₁₅	4.13	±0.24	2/4.5/7	2.38	1.46	±0.07	1.52	±0.05
C-L0678	AD4-13	0.1-0.2 ₀.₀₉₋₀.₁₅	11.93	±1.35	5/10/15	2.55	1.79	±0.09	---	---
C-L0679	AD4-14	0.1-0.2 ₀.₀₉₋₀.₁₅	1.87	±0.27	2/4.5/7	2.80	1.32	±0.07	1.45	±0.05
C-L0680	AD1-1	0.1-0.2	4.75	n.a.	2/4.5/7	0.79	1.46	±0.09	1.26	±0.05
C-L0681	AD1-2	0.1-0.2	7.30	±0.13	3/6/9	1.17	1.64	±0.09	---	---
C-L0682	AD1-3	0.1-0.2	12.81	±3.70	5/10/15	1.39	2.03	±0.11	1.71	±0.07
C-L0683	AD1-4	0.1-0.2	6.18	±0.05	3/6/9	1.64	1.70	±0.09	---	---
C-L0689	SHA-1	0.1-0.2	2.92	±0.48	2/4.5/7	0.51	1.23	±0.07	---	---
C-L0690	SHA-2	0.1-0.2	2.96	±0.42	2/4.5/7	0.83	1.16	±0.06	---	---
C-L0691	SHA-3	0.1-0.2	3.39	±0.74	2/4.5/7	1.17	1.27	±0.07	---	---
C-L0692	SHA-4	0.1-0.2	4.38	±0.70	2/4.5/7	1.49	1.46	±0.08	---	---
C-L0693	SHA-5	0.1-0.2	7.38	±0.39	3//6//9	1.60	1.62	±0.09	1.53	±0.06
C-L0694	SHA-6	0.1-0.2	4.48	±0.26	2/4.5/7	1.87	1.37	±0.07	---	---
C-L0695	SHB-1	0.1-0.2	2.67	±0.18	2/4.5/7	0.64	1.13	±0.06	---	---
C-L0696	SHB-2	0.1-0.2	2.84	±0.01	2/4.5/7	0.91	1.11	±0.07	---	---
C-L0697	SHB-3	0.1-0.2	3.38	±0.04	2/4.5/7	1.40	1.21	±0.06	---	---

Lab. code	sample	grain size (mm)	H₂O-content (weight-%).		H₂O-c. range assumed	depth (m)	dose rate NAA (Gy/ka)		dose rate γ-spec. (Gy/ka)	
C-L0698	SHB-4	0.1-0.2	2.91	±0.19	2/4.5/7	1.68	1.27	±0.07	---	---
C-L0699	G1	0.1-0.2	0.43	±0.08	2/4.5/7	0.31	0.72	±0.04	---	---
C-L0700	G2	0.1-0.2	2.44	±0.60	2/4.5/7	0.60	0.76	±0.04	---	---
C-L0701	G3	0.1-0.2	2.11	±0.97	2/4.5/7	0.97	0.70	±0.04	0.79	±0.03
C-L0702	G4	0.1-0.2	3.12	±1.27	2/4.5/7	1.27	0.83	±0.04	---	---
C-L0703	G5	0.1-0.2	3.83	±1.57	2/4.5/7	1.57	0.81	±0.05	---	---
C-L0704	G6	0.1-0.2	4.14	±1.87	2/4.5/7	1.87	0.79	±0.04	---	---
C-L0705	G7	0.1-0.2	2.41	±2.22	2/4.5/7	2.22	0.72	±0.05	---	---
C-L0706	G8	0.1-0.2	4.06	±0.15	2/4.5/7	2.30	0.77	±0.04	---	---
C-L0707	G9	0.1-0.2	3.33	±0.56	2/4.5/7	2.55	0.77	±0.04	---	---
C-L0708	G10	0.1-0.2	2.39	±0.66	2/4.5/7	2.93	0.72	±0.05	---	---
C-L0709	G11	0.1-0.2	0.69	±0.18	2/4.5/7	3.35	0.76	±0.04	---	---
C-L0710	G12	0.1-0.2	3.55	±0.02	2/4.5/7	3.54	0.79	±0.04	---	---
C-L0711	G12B	0.1-0.2	2.55	±0.24	2/4.5/7	3.69	0.83	±0.05	---	---
C-L0712	G13	0.1-0.2	2.30	±0.30	2/4.5/7	3.89	0.75	±0.05	---	---
C-L0713	G14	0.1-0.2	2.28	±0.68	2/4.5/7	4.28	0.78	±0.04	---	---
C-L0714	G15	0.1-0.2	2.32	±0.01	2/4.5/7	4.60	0.72	±0.04	---	---
C-L0715	G16	0.1-0.3	1.22	±0.32	2/4.5/7	1.40	0.70	±0.05	---	---
C-L0716	G17	0.1-0.3	1.12	±0.52	2/4.5/7	0.80	0.72	±0.05	---	---

Appendix B: Choice of measurement protocol and mineral fraction for dating

At the beginning of this study the most suitable measurement technique had to be chosen from the variety of measurement protocols which were applied in luminescence dating studies at that time (reviewed e.g. by WINTLE 1997, AITKEN 1998). At the start of this study the single aliquot regenerative dose protocol (SAR) for optical dating of sand sized quartz, that is now widely applied in luminescence dating studies, had just been introduced by MURRAY and ROBERTS (1998) and MURRAY and WINTLE (2000). By that time only a few studies had been carried out using this SAR technique. Therefore, its potential for dating of the sediments investigated in this study was tested against other luminescence protocols and, furthermore, against independent age control. Furthermore, the mineral fraction had to be selected as quartz and K-rich feldspars both show different properties which are either advantageous or disadvantageous with special regard to luminescence dating studies. In the following the selection process will be summarised. The aim was to identify the dating protocol and mineral fraction that would give the most precise and most accurate results in terms of reconstructing dune formation within the last 20,000 years.

The luminescence stimulation: *IR-RF vs. OSL*

The suitability of IR-RF (infrared-radiofluorescence) for dating feldspars of Holocene and Late Glacial age was tested by ERFURT (2003), who among others also dated two samples investigated in this study, sample F1 and F4 from the site 'Postdüne' in Brandenburg. A substantial age overestimation and large errors were observed in comparison to the OSL data obtained on quartz which were in excellent agreement with the independent age control. The IR-RF ages of 3.3±1.8 ka for sample F1 and 9.5±4.4 ka for F4 (ERFURT 2003: 92-93) were considerably higher than the quartz OSL ages with only 0.143±0.013 ka (F1) and 4.6±0.4 ka (F4). Sandy peat layers or charcoal fragments from underlying sediments were dated by radiocarbon to 510-670 cal. BP (below F1) and 2,660-3,030 cal. BC (below F4) (see chapter 1 for more details on these samples). The conclusion drawn from this and other comparative studies was a lower dating limit of IR-RF of potassium-rich feldspars of c. 15 ka, because the IR-RF sensibility of younger samples is not sufficient to be used for dating (TRAUTMANN 1999, ERFURT 2003). KRBETSCHEK and TRAUTMANN (2000) tested, among other materials and minerals, the suitability of quartz for radiofluorescence dating. They found the RL-dose-

characteristics to be too complex and highly variable among various samples and concluded that extensive further research on the RF of quartz is necessary to use it in dating studies.

The luminescence stimulation: *TL vs. OSL*

The key assumption of luminescence dating is the effective and complete resetting of the luminescence signal by sunlight exposure of sufficient duration. GODFREY-SMITH et al. (1988) demonstrated that to bleach the optically stimulated luminescence intensity down to 1 % of the initial value exposure to bright sunlight for just a few seconds for quartz and a few minutes for feldspars are sufficient. In contrast, the TL signals of quartz and feldspar decreased only to 17 % of its unbleached intensity after 20 h of sunlight exposure (see Fig. B 1). Optical bleaching of the quartz OSL response proceeds at a proportionately slower rate, when the same experiment is carried out with the light intensity being reduced by a factor of 10 (daylight of an overcast day compared to bright sunlight on a clear day). The signal resetting is 10 times more slowly (GODFREY-SMITH et al. 1988).

Fig. B 1: The effect of exposure to bright sunlight on the OSL and TL intensities of quartz and feldspar.
Each point represents the average of 4 samples measured. OSL stimulation was carried out with a 514 nm laser; the heating rate for TL measurements was 5°C/s. The TL intensities were calculated from the TL peaks at 320-330 °C (quartz) and 310-320 °C (feldspar) (from GODFREY-SMITH et al. 1988: 375).
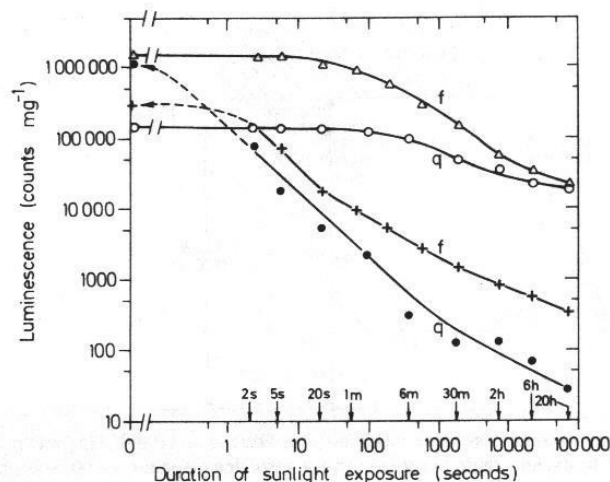
From Fig. B 1 it becomes clear that TL signals, whether of quartz or feldpars, are not effectively resetted, a residual signal remains even after prolonged bleaching of 20 h. These TL residuals are also present in well-bleached aeolian sediments, but do not necessarily cause age overestimations. HUNTLEY et al. (1993), for example, dated an Australian fossil dune

system to ~800 ka by TL of quartz in good agreement with oxygen isotope data. SELSING and MEJDAHL (1994) compared ^{14}C ages with feldspar TL ages of Norwegian late Holocene dune sand and concluded that it is possible to obtain reliable ages for well-bleached sediments as young as 1.6 ka. In case of even younger deposits the precise determination of the residual signal and a successful correction seems more difficult as illustrated in Fig. B 2 using IRSL and TL ages obtained for K-feldspars extracted from dune deposits (data summarised from RADTKE et al. 1998 and FINK 2000).

Fig. B 2: The problem of TL residuals for the age determination of very young aeolian deposits.
The ratio of TL to IRSL ages are plotted for samples yielding IRSL ages of less than 1 ka (left graph) and ages ranging from 1 to 17 ka (right graph). All data were obtained by using the 'multiple-aliquot regenerative-dose' protocol on coarse grains of potassium rich feldspars. All the samples were taken from dune sites within the European Sand Belt; the sites Brockum and Lilienberg are located in NW Germany and Ossendrecht in the Netherlands. Further details on the sites and the experimental details are given in RADTKE et al. (1998) and FINK (2000). While the IRSL and TL ages of samples older than 1 ka are in reasonably good agreement, the TL residual cause a substantial age overestimation in case of deposits younger than < 1ka. Problems with the determination and appropriate correction of this TL residual are most likely the reason for the sever overestimation of TL compared to IRSL.
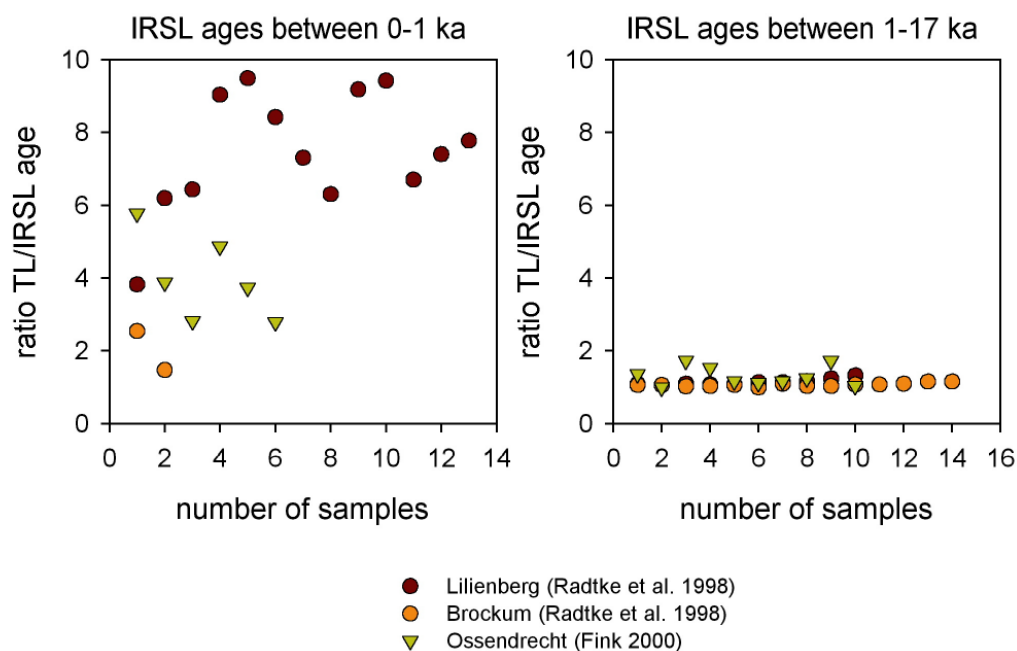
While for sediments with depositional IRSL ages older than 1 ka the ratio of TL to IRSL ages is closer to unity (Lilienberg 1.14±0.08, Brockum 1.07±0.05, Ossendrecht, 1.30±0.26), for younger deposits <1 ka the ratio is much higher (Lilienberg 7.51±1.64, Brockum 2.02±0.75, Ossendrecht 3.98±1.17). This overestimation by TL could be due to insufficient bleaching

taking the possibility into account that in case of locally restricted Late Holocene dune reactivation sunlight exposure times during only short distance transport were not long enough. But as the ratios obtained for older sediments >1 ka do not indicate severe problems with poor bleaching (ratios close to unity), it seems more likely that the main problem is caused by problems related to correct determination and subtraction of the residual signal in case of the very young deposits. The smaller the absorbed dose accumulated since deposition, thus the younger a sample, the higher the proportion of the residual compared to the total absorbed dose. Thus, the negative effect of TL residuals has a higher impact on young samples than on old samples. As this study is concerned with young aeolian deposits difficulties with TL residuals argue against the application of TL protocols for equivalent dose determination. Finally, if bleaching conditions were indeed restricted during transport and deposition in any case OSL protocols yield the more accurate results, although they might also overestimate the true depositional age.

To conclude, optical dating is the preferred technique for dating Quaternary sediments, in particular if very young deposits are to be dated. In optical dating the luminescence signals are used for dating which are most sensitive to light. Thus, resetting of the 'OSL clock' by sunlight exposure is far more rapidly and completely than is the 'TL clock' (see Fig. B 1). Therefore, the uncertainty in the degree of bleaching is smaller in OSL than in TL studies. And if indeed under restricted bleaching conditions the resetting of the luminescence signals is incomplete, the TL residuals will be higher than those of OSL and hence cause a more severe age overestimation.

The measurement technique: *single aliquot vs. multiple aliquot protocols*

The decision to concentrate on optical dating was explained above. The next question was which OSL technique and which mineral fraction would yield the most accurate and precise results. In the following the single-aliquot and multiple-aliquot-protocols used for OSL dating of quartz will be compared. Finally, the decision of using quartz instead of K-rich feldspars is discussed. For further description of the various methods and protocols used in luminescence dating it is referred to, for example, in AITKEN (1998), WINTLE (1997), STOKES (1999), MURRAY and OLLEY (1999), CLARKE et al. (1999), and DULLER (2004).

Multiple aliquot protocols:

Two basic approaches are used in luminescence dating studies for the estimation of equivalent doses (D_e), the additive and regenerative dose method. Furthermore, depended on the number of subsamples (aliquots) used for the D_e determination, multiple aliquot protocols are distinguished from single aliquot protocols. Examples for the measurement results obtained by the multiple aliquot additive dose (MAA), multiple aliquot regenerative dose (MAR) and the single aliquot regenerative dose protocol (SAR) are shown in Fig. B 3.

In multiple-aliquot approaches luminescence measurements are made on many different aliquots which were divided into several groups of subsamples with all members of each group been exposed to same laboratory radiation dose. For one group the laboratory dose is zero, this set is used to determine the natural OSL intensity.

The luminescence response to optical stimulation is measured for each aliquot and is plotted against the strength of the laboratory irradiation dose. In order to construct a growth curve or dose response curve a line is then fitted to the average luminescence intensities (see Fig. B 3, a and b). In case of the additive dose method the equivalent dose value is obtained by extrapolation of the line to zero intensity, and the dose intercept is taken to be the D_e. The problem related to the additive dose protocol, especially when larger doses are involved, as with older samples, is the sublinearity – the rate of increase of growth falls off as the applied dose increases. This complicates the extrapolation of the growth curve onto the dose-axis, and increases the uncertainty in the D_e estimation.

To obtain equivalent doses by applying the regeneration protocol the natural OSL is compared with the OSL resulting from aliquots which have been artificially bleached down to a low level and then exposed to laboratory irradiation with increasing doses. The natural OSL intensity then is directly compared with the OSL resulting from laboratory irradiation and the equivalent dose value finally determined by interpolation. The advantage of interpolation instead of extrapolation is that uncertainties due to a non linear, e.g. exponential shape of the dose response curve are reduced, if not eliminated. The critical disadvantage of the regenerative approach is the possibility of sensitivity changes: a change in luminescence intensity per unit dose between the measurement of the natural OSL and the measurement of the regenerated OSL induced by the bleaching, pre-heating or irradiation procedures, for

example. Such sensitivity changes may prevent accurate estimates of the equivalent dose and

finally can result in an over- or underestimation of the luminescence age (AITKEN 1998).

Fig. B 3: Multiple aliquot additive dose (MAA, a), multiple aliquot regenerative dose (MAR, b), and single aliquot regenerative dose (SAR, c) growth curves for quartz extracted from dune sand (sample F5, site 'Finow').
For the multiple aliquot data sets 48 aliquots were measured. The SAR growth curve represents the results obtained on one aliquot. In both multiple aliquot data sets the inter-aliquot scatter is evident despite the application of a 'short-shine' normalisation procedure. In contrast, the SAR data shows very little scatter from the fitted growth curve. (redrawn from HILGERS et al. 2001b)
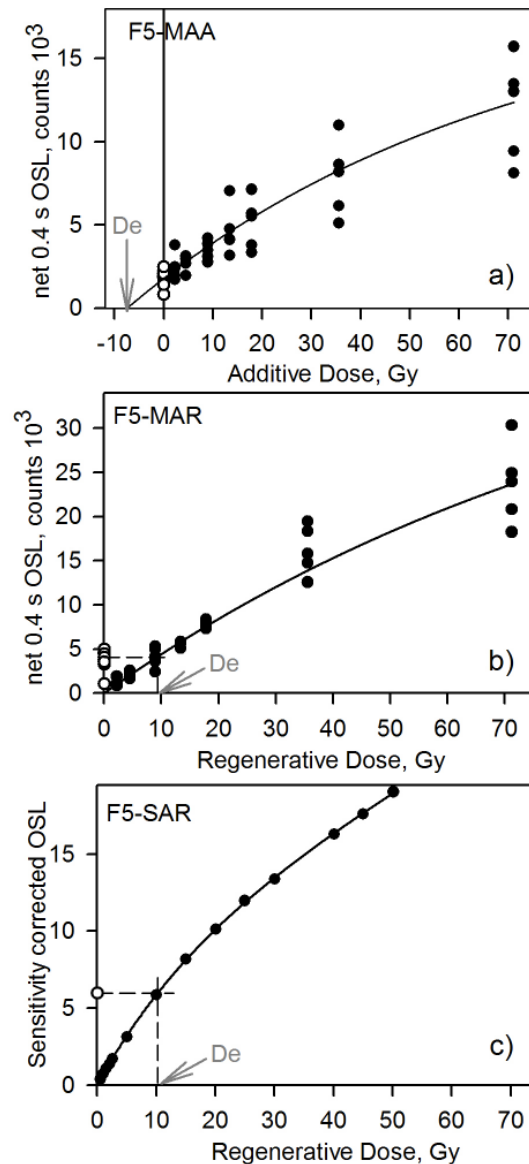
Measurements following the multiple aliquot approaches were typically made on about 24-48 subsamples (aliquots) of a sample with each disc consisting of about 1000 grains (DULLER 2004). But the aliquots prepared from a sample are not identical. Each aliquot may contain grains with different luminescence brightness and most of the measured luminescence is known to arise from a small fraction of grains only. This is due to differences in luminescence characteristics between the grains with a high percentage showing no luminescence signal at all (DULLER et al. 2000, ADAMIEC 2000). The luminescence response therefore can vary considerably among several aliquots, although all sub-samples received the same radiation dose. This scatter of the individual aliquots of the different dose groups is clearly seen in Fig. B-3 a) and b). A method that is in common use for alleviating this problem is to initially make a brief OSL measurement of each aliquot and to subsequently use this initial luminescence response to normalise the data among each other. This so-called 'short shine normalisation' was applied in this study as well in order to minimise the inter-aliquot scatter and, thus, to increase the precision of the equivalent dose determination. These normalisation measurements are carried out prior to irradiation. Aliquots, which were further processed following the regeneration method, were bleached for several hours by sunlight exposure also prior to irradiation. But as seen in Fig. B 3 despite the normalisation procedure carried out for all subsamples still a considerable scatter of the individual values away from the fitted growth curve was observed.

Single aliquot protocol:

For a detailed description of the single aliquot measurement protocol it is referred to section 3.5.2. Here, just the major advantages compared to multiple aliquot protocols are discussed. The single aliquot regenerative (SAR) dose protocol as proposed by MURRAY and WINTLE (2000) enables the correction of sensitivity changes which can be induced by the different OSL measurement procedures, such as optical stimulation, heating, irradiation. Furthermore, internal checks are included in the routine measurement cycle to test the robustness of the protocol for the particular sample to be dated. But there are several further advantages of single aliquot protocols regarding sediment dating (see e.g. discussion in BANERJEE et al. 1999, 2001; MEJDAHL & BØTTER-JENSEN 1994, BØTTER-JENSEN et al. 2003):

1. High disc-to–disc scatter in multiple aliquot measurements result in large uncertainties in multiple aliquot based D_e values. Problems of choosing an adequate procedure for normalisation of the signals of different aliquots are circumvented by using the single

aliquot approach. Because all measurements are carried out on only one aliquot, the analytical precision is greatly increased. The uncertainty of the equivalent dose is finally calculated from the reproducibility of the measurements. There is only a minor impact of the mathematical uncertainty with which the growth curve is fitted to the dose points in single aliquot data sets, whereas in multiple aliquot data sets this is a major problem (see Fig. B 3). By multiple aliquot techniques only one equivalent dose value can be obtained for each set of aliquots. An improvement of the precision by making multiple measurements of one sample generally it is not feasible because of the large amount of effort involved in making already only one multiple aliquot measurements.

2. Because single aliquot measurements are automated and computer controlled to a large extent, the measurement of multiple subsamples in routine dating is feasible. Furthermore, systematic investigations of the effect on D_e by varying measurement parameters, such as preheat temperature, are more practicable.

3. The determination of multiple D_e values for numerous aliquots of one sample allows a more detailed investigation of the dose distribution within the sample. This can yield valuable information for the identification of poorly bleached material.

To test whether the single aliquot approach is able to provide more precise equivalent dose estimates and thus, more precise OSL ages, for the material investigated in this study a range of samples from different sites was dated using the SAR procedure and either the MAR or the MAA protocol. About 48 aliquots were measured in total in the multiple aliquot measurements of which thirteen aliquots were used to determine the natural OSL signals. All aliquots were normalised using the initial luminescence signal induced by a brief 0.1 s stimulation with blue-green light. All subsamples used in the MAR measurements were bleached by exposing them to sunlight for several hours prior to irradiation. The single aliquots ages are based on the average equivalent dose value obtained from ~18 subsamples. Further details on the relevant measurement parameters of this comparative study are summarised in Table B 1. The results are compared in Fig. B 4.

Table B 1: Technical parameters used for comparative luminescence measurements.

Method	K-feldspar MAA & MAR (Multiple-Aliquot Additive & Regenerative Dose Protocol)	Quartz MAA & MAR (Multiple-Aliquot Additive & Regenerative Dose Protocol)	Quartz SAR (Single-Aliquot Regenerative Dose Protocol)
Normalisation		0.1 s short shine stimulation	---
Bleaching	for MAR: several hours with sunlight	for MAR: several hours with sunlight	100 s with blue diodes
Irradiation	^{60}Co-γ-source	^{60}Co-γ-source	^{90}Sr/^{90}Y-β-source
Filterset for detection	HA3-BG39-2xBG3-GG400	HA3 & U340	U340
Preheating	220 °C/120 s or 160°C/5 h	220 °C/300 s	220-260 °C/10 s *
Stimulation	50 or 100 s IR-diodes (880±80 nm)	100 s blue/green broad-band filtered halogen lamp (485±65 nm)	100 s blue diodes (470±30 nm)
Aliquot temp. during stimulation	50°C	125 °C	125 °C
Integral used for D_e calculation	0-10 s	0-0.4 s	0-0.4 s
Background subtraction	(late light in case of MAA)	90-100 s	90-100 s

*preheat temperatures were in the range of 220, 240 or 260°C

Fig. B 4: Comparison of age estimates from multiple aliquot additive (a) and regenerative dose (b) protocols with those derived from the single aliquot regenerative dose protocol for quartz samples from various sites within the study area.
The solid lines have a slope of one.
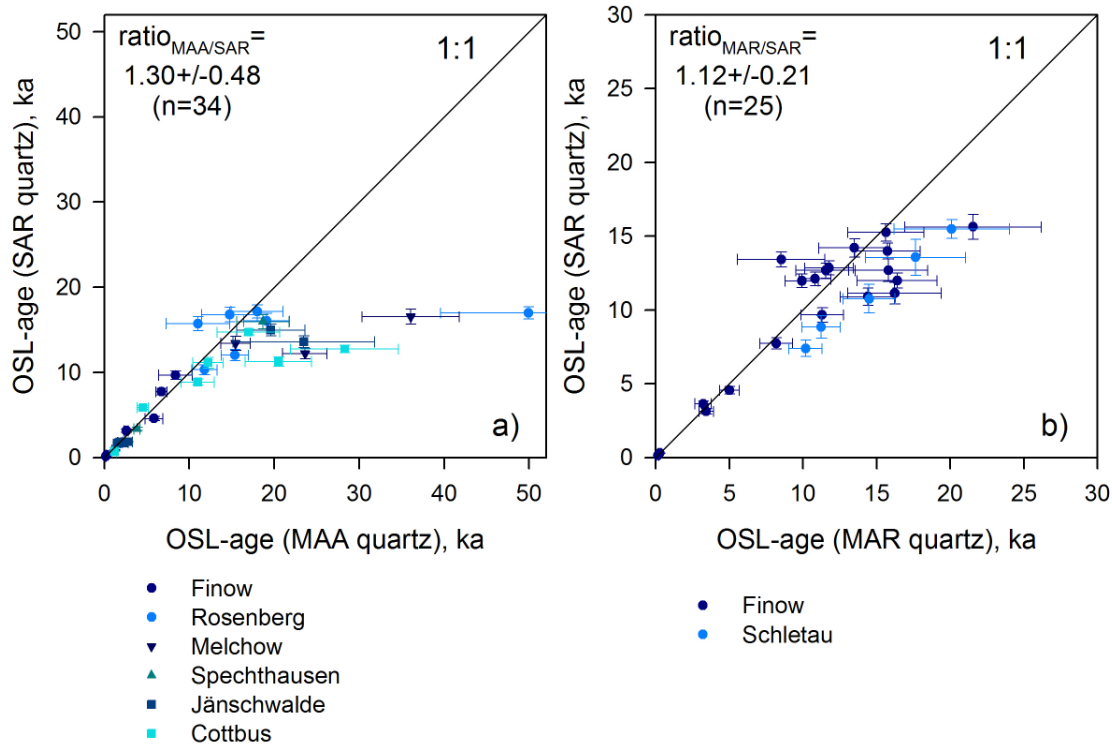
The larger uncertainties on the multiple aliquot data make it impossible to state categorically that the age estimates of the multiple aliquot protocols differ from the SAR protocol in most cases. Nevertheless systematic trends can be examined taking only the mean ages into account and disregarding the uncertainties in ages. In both plots it is interesting to note, that a reasonably good agreement in ages was found at low doses or for young ages up to c. 10 ka, respectively. The ratio of MAA to SAR values is 1.13±0.26 (n=17) for data < 10ka and for higher ages >10 ka this ratio increases to 1.47±0.58 (n=17). For the comparison of MAR to SAR ages the trend is similar as with the comparison of the MAA data set: for young deposits (<10 ka) the MAR to SAR ratio is 1.00±0.21 (n=9) and for ages >10 ka 1.19±0.19 (n=16). Such a distinct systematic discrepancy between a protocol which makes no correction for sensitivity changes (MAR) and one which explicitly measures these changes and corrects for them (SAR) is not surprising. The sensitivity change observed between the SAR natural and the first regeneration cycle was by a factor of 1.08±0.01 given for example the average of samples F1-11. Such an increase in sensitivity must have been present in the corresponding MAR data set as well, but was not detected in the MA measurement routine and was not

corrected for. FINK (2000) tested the applicability of the correction procedure for sensitivity changes in multiple aliquot measurement of quartz using the OSL response to a test dose. The experimental setting was the same as in this study. But this approach was not very successful regarding the improvement of the precision of multiple aliquot results. Most likely the use of an external irradiation source implying transport of the samples and by that a possible loss of material from the discs complicated this sensitivity correction. For the same reason the normalisation procedure was not very successful in reducing the disc-to-disc scatter. This variation in the luminescence response to the same radiation dose was a problem in all multiple aliquot measurements on quartz carried out in this comparative study. Most likely the main reason for the large errors in multiple aliquot ages has to be ascribed to this disc-to-disc variation. This prevents precise equivalent dose estimation, because a large mathematical error results from the curve fitting through these scattered data points.

Inhomogeneous bleaching could be as a source of scatter as well, in particular as the multiple aliquot dates seem to overestimate the single aliquot ages in several cases (see Fig. B 4). If the OSL signal of a sample was no completely set to zero during transport and deposition, some grains carry residual signals. Because in multiple aliquot measurements 48 discs were analysed and by that a substantial larger number of grains, the probability to detect these residual signals is greatly increased compared to SAR measurements. But an increased inter-aliquot scatter caused by inhomogeneous bleaching seems unlikely, because no evidence for poor bleaching was found in the single aliquot data sets.

Different stimulation sources were used for multiple and single aliquot measurements (see Table B 1). The multiple aliquot data set was measured with the broad blue/green (420-550 nm) band filtered from a quartz-halogen lamp and blue (440-500 nm) light emitting diodes (LED) were used for stimulation in the single aliquot measurements. This difference in the stimulation wavelength is unlikely to be the reason for any disagreement in the age results found in this data set. BØTTER-JENSEN et al. (1999b) could demonstrate by comparison of LED stimulated data with that obtained by broad-band halogen lamp stimulation, that excitation with 470 nm LED light stimulates the same set of OSL traps in quartz than those stimulated by broad-band source. They found no evidence for the assumption that by illumination with shorter wavelengths charge from deep traps are more efficiently stimulated than by the broad-band source. The comparison of 34 equivalent dose values showed no significant difference between the results obtained by the different stimulation sources with an

average of the D_e ratios $_{blue/green}$ of 0.98±0.02. But the use of the broad-band halogen lamp as stimulation source for might have caused an additional scatter into the multiple aliquot data sets. KUHN et al. (2000) found a change in the OSL response of quartz to stimulation wavelength in the range of 500–520 nm which they make responsible for an additional scatter in the quartz data sets.

From the comparison of multiple aliquot and single aliquot age results it is concluded that, because of the large age uncertainties, both multiple aliquot approaches, MAA and MAR, lack the precision which is necessary to achieve a meaningful luminescence chronology for the Late Glacial and Holocene dune deposits investigated in this study. The higher precision of the single aliquot ages is striking. But as some SA and MA ages were found to disagree significantly (see Fig. B 4) this comparison does not allow a conclusion on the potential of both approaches regarding the accuracy of the ages. A very precise SAR age can yield an inaccurate result with the imprecise MA age better matching the 'true' age.

Finally, for testing the accuracy of various luminescence methods and to support the refinement of dating protocols for sequences with unknown ages validation against independent ages is necessary. A suitable test site should provide chronological control not only by one other dating method but by several sources of age information at best. The dune site 'Postdüne' near Finow in Brandenburg, north-eastern Germany meets these requirements (for a detailed site description it is referred to chapter 1). This site provides excellent age control for cross-checking the OSL chronologies: a ^{14}C-dataset, the 'Finow palaeosol' horizon assumed to be developed during the Allerød interstadial period, palynological information and a layer of Laacher See tephra as a well-known chronomarker in Central Europe for the Late Glacial time. The ^{14}C ages for the 'Finow palaeosol' are taken from literature and the youngest and oldest age value of four values is shown in Fig. B 5 (SCHLAAK 1997, further details in Appendix E).

The eruption of the Laacher See volcano is dated to 12,880 up to 12,900 a BP (for example BRAUER et al. 1999, MERKT & MÜLLER 1999, SCHMINCKE et al. 1999, KLEINMANN et al. 2002, LITT et al. 2001, VAN DEN BOGAARD 1995).

The OSL results obtained from multiple and single aliquot measurements of quartz are compared to further chronological data in Fig. B 5. Again the higher precision of single aliquot data compared to those obtained by multiple aliquot approaches is evident.

It should be emphasised here that the ^{14}C samples and the luminescence samples were taken at different times. This comparison thus includes any additional uncertainty in the field extrapolation of stratigraphic relationships. Despite the additional uncertainty induced by the sampling at different times, with the exception of the age for sample F6 and F13, the stratigraphy/age relationship between the luminescence ages based on the SAR quartz ages and the independent chronological controls is excellent. Note that there is no stratigraphic uncertainty in the case of the 'Finow' palaeosol or the Laacher See tephra, which were unambiguously identified at the time the luminescence samples were taken.

Fig. B 5: Comparison of the quartz luminescence and ^{14}C ages with sampling depth for the dune site 'Postdüne'.
The assumed Allerød-age of the 'Finow' palaeosol and the Laacher See tephra age are also shown.
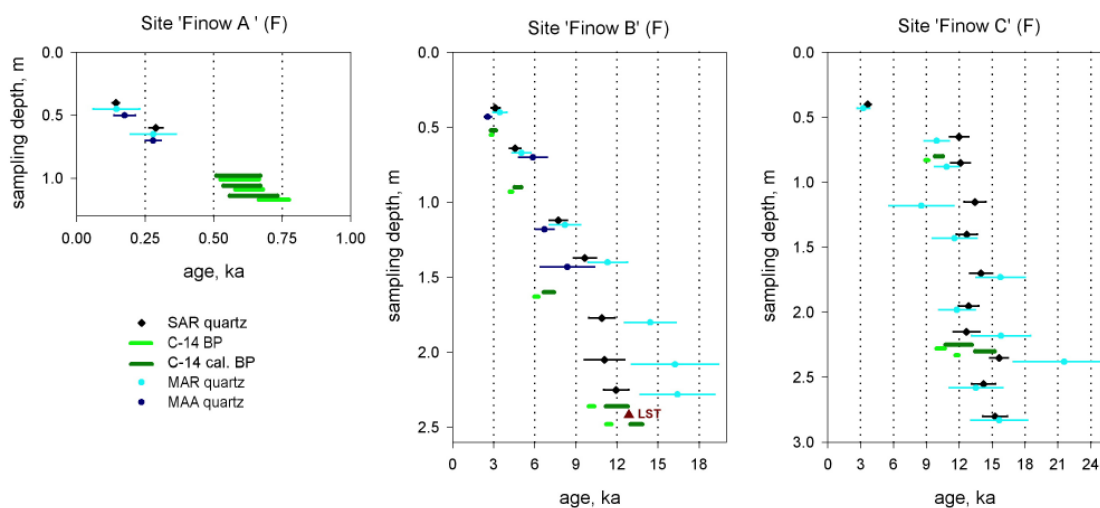
The radiocarbon age of 6.13±0.15 BP (7.03±0.39 cal. BP) causes the outlier F6 in the OSL data set, regardless which kind of OSL protocol was used. Although, taking the very broad errors of the MAA into account, this age still agrees with the calibrated radiocarbon age within the errors. But, this ^{14}C age is not consistent with the palynological results which date the deposits into the Preboreal, correlated with the time span from c. 10.6 to 11.5 cal. BP. Thus, the single-aliquot OSL ages of 9.7±0.8 ka (F6) and 10.9±0.9 ka (F7) would fit even better in this case. The disagreement in case of sample F13 may be attributed to the problem of sampling, but cannot be finally explained. But on the 2σ level both ages, ^{14}C and SAR OSL still agree.

With regard to the multiple aliquot based ages the much larger errors are obvious with relative age uncertainties of about 18 % found in the MA data sets and only ~5 % for SAR ages (note, that systematic errors such as the water content uncertainty and the error of source calibration are not regarded in these values). Nevertheless, because of these large uncertainties for a range of samples there is still a good agreement with the radiocarbon data set and the SAR ages. Whereas at sites 'Finow A and B' the multiple aliquot ages are consistent with the chronostratigraphy, in particular at site 'Finow-C' the MAR ages show a large scatter which is not present in the SAR data set. Finally the MAR ages clearly fail the comparison especially for those samples derived from stratigraphic positions for which the best cross-check data base is available, thus the lower parts of site 'Finow B' and 'Finow C' with palynological data proving Younger Dryas vegetation assemblages, the Laacher See tephra layer, the Allerød palaeosol. On average the multiple aliquot results clearly overestimate the depositional ages. Poor bleaching seems unlikely to be the reason for this overestimation, as no such evidence was found in the SA data sets. Probably uncorrected sensitivity changes in the MA data set caused the difference in equivalent doses and consequently in the luminescence ages.

From this comparative study it can be finally concluded, that the OSL ages obtained using the SAR protocol for quartz show both, a higher precision and accuracy in comparison to multiple aliquot based ages of the same samples. RADTKE et al. 2001 came to the same conclusion in their comparative dating study on Late Glacial dune deposits. In particular the improved precision achieved by application of the single aliquot approach is necessary for optimising the chronostratigraphic resolution of young aeolian deposits of Late Glacial and Holocene ages as those dealt with in this study. Therefore the SAR protocol is considered to be the most appropriate luminescence technique for quartz dating.

The mineral fraction: *quartz vs. K-rich feldspars*

Besides the question of the appropriate measurement protocol the question had to be answered whether quartz or feldspar is better suited to date Late Glacial and Holocene dune deposits. It is noted here, that commonly potassium rich orthoclase are used in luminescence dating studies. The disadvantages of the use of Na-rich feldspars for dating are discussed for example in KRBETSCHEK et al. (1997).

Quartz and K-rich feldspars differ in their luminescence properties. Therefore they have to weigh regarding their suitability for the particular question investigated in the dating study. In

the following several luminescence characteristics will be compared for both mineral fractions in order to decide whether quartz or feldspars are better suited for the samples analysed in this study.

Bleachability: GODFREY-SMITH et al. (1988) demonstrated that the OSL intensity of quartz is bleached to 1% of the initial value after 10 seconds sunlight exposure whereas 9 min exposure was necessary for K-feldspars. After 30 min bleaching by bright sunlight the quartz signal was reduced to 0.01%, a negligibly low level in the range of the experimental background. In contrast, feldspar signals showed no sign of having finally reached a residual level; after 20 h bleaching a residual of 0.1% was still present (see Fig. B 1). The more rapid and complete resetting of the quartz luminescence may be advantageous in dating application particularly on non-aeolian sediments, which are supposed to received just a brief sunlight exposure prior to deposition. With respect to only short sunlight exposure in short distance transport during very recent dune reactivation processes, the more light sensitive quartz luminescence seems to be advantageous as well.

Saturation level and upper age limit: One of the great advantages of working with feldspars compared to quartz is that feldspar reaches its saturation limit generally at higher doses. Thus enables to date further back in time than by using quartz as a dosimeter. In Fig. B 6 this difference in dose response behaviour is expressed by the more linear growth curve in case of the feldspar sample compared to the exponential dose response curve obtained for quartz. The higher saturation level and by that the option of dating samples by feldspar which are already saturated regarding their quartz OSL signal is not a decisive criterion in this study as only sediments of Late Glacial and Holocene age are considered. This time period is well within the application range of quartz.

Fig. B 6: Multiple aliquot growth curves for K-feldspars and quartz obtained by using the multiple-aliquot regenerative dose protocol.
The sample D8 was taken from from Late Glacial coarse silty loess deposits at the northern loess boundary in Northern Germany (see HILGERS et al. 2001a for more details). A considerable higher scatter of the quartz subsamples in the group of natural aliquots as well as in the highest dose groups is clearly seen as well as the exponential growth of the dose response curve in comparison to the more linear growth in case of the potassium-rich feldspars.
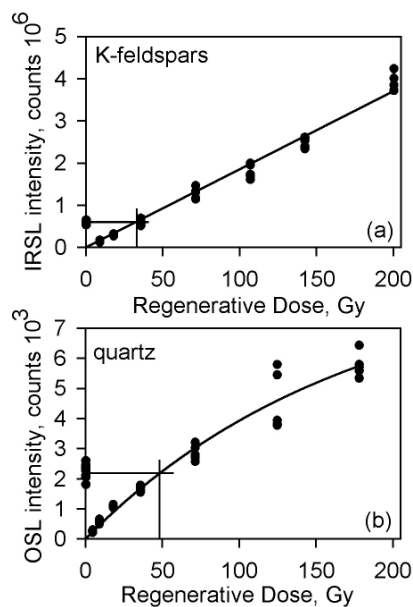
Brightness and lower age limit: Typically, quartz is orders of magnitudes less radiation-luminescence sensitive compared to feldspar (e.g. KRBETSCHEK et al. 1997). GODFREY-SMITH et al. (1988) found feldspar signal intensities to be 50 times or even 240 times brighter compared to those of quartz. Because of the ^{40}K incorporated in the crystal lattice of feldspars they receive a higher dose compared to a quartz crystal of the same depositional age. Thus, a stronger irradiation dose can induce a higher luminescence signal.

Therefore K-rich feldspars may be favoured over quartz when small absorbed doses of very young samples are to be measured, especially in such circumstances where the environmental dose rates are low. In this study the average annual dose was found to be only ~ 1 Gy/ka (see section 3.3.5).

A comparison of quartz and feldspar luminescence signal intensities of a dune sand sample from this study (sample STA 1) is presented in Fig. B 7. Here the difference between the intensity of the signals used for feldspar (in graph a) and quartz dating (in graph b), respectively, is not as significant as reported by GODFREY-SMITH et al. (1988). The feldspar

signal is brighter only by a factor of ~4 compared to the quartz signal of the same sample obtained for the same irradiation dose. The faster resetting of the quartz luminescence signal by optical stimulation compared to the feldspar shine-down also becomes clear in Fig. B 7 b.

Fig. B 7: Comparison of the luminescence signal intensities of K-rich feldspar and quartz extracts from the same dune sand sample (sample STA 1, site 'Schletau').
a) luminescence response measured, after artificial β-irradiation and preheating (10 s at 220°C), with infra-red stimulation and detection in the blue wavelength range. This experimental setting more or less is used in feldspar dating. Typically quartz does not show any response on IR stimulation. **b)** luminescence response measured, after artificial β-irradiation and preheating (10 s at 220°C), with blue light stimulation and detection in the UV wavelength range. This experimental setting more or less is used in quartz dating. During all luminescence measurements the sample was held at 40°C. The stronger intensity of the feldspar dating signal compared to the quartz signal is seen, but also the slower depletion rate of the feldspar signal.

a)   **b)**
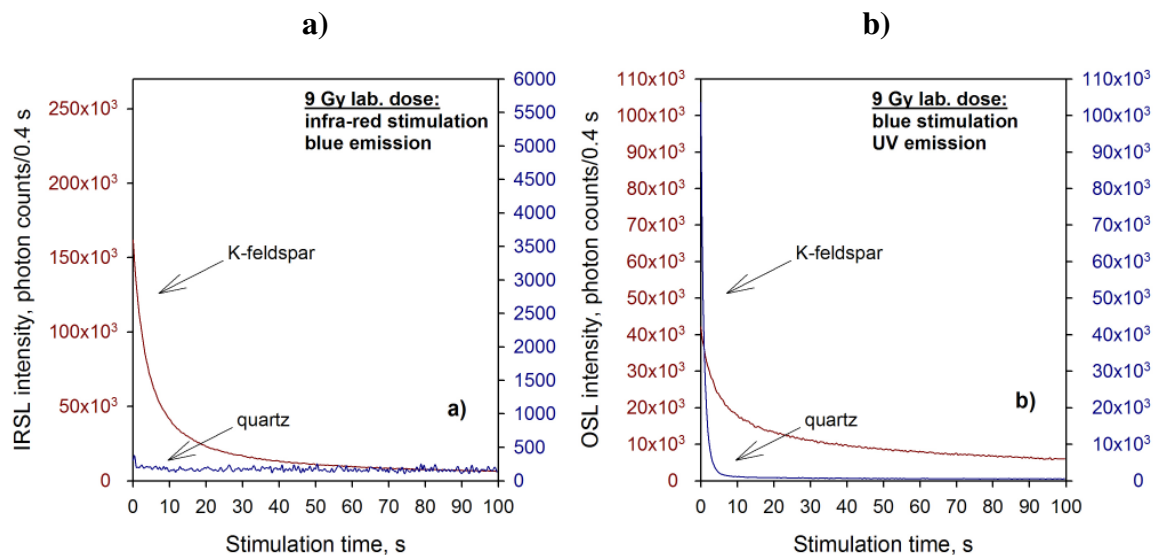
For the quartz samples investigated in this study it can be generally concluded, that the brightness of the quartz OSL was not a limiting factor even for dating of very young deposits and also taking the low average annual dose into account. Representative for the typical sample behaviour of the quartz extracts in Fig. B 8 the luminescence response after a laboratory dose of only 0.16 Gy is shown. The OSL signal is still clearly distinguishable from the experimental background noise. It is concluded that the sufficient brightness of the OSL signals of quartz does allow dating of sediments as young as only about 100 years. Thus quartz seems as appropriate as feldspar.

Fig. B 8: Shine down curve obtained for quartz of the dune sand sample N6, which had been irradiated with a β-dose of only 0.16 Gy.
An aliquot containing about 1000-2000 grains was measured, the same aliquot size typically used throughout the whole study. A sufficient brightness was observed, still clearly distinguishable from the background noise.
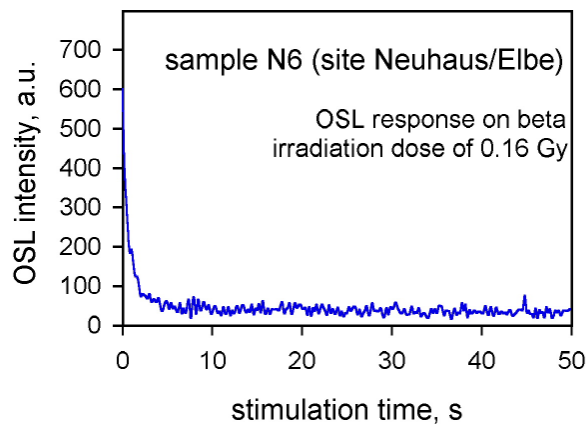
Internal dose rate: The amount of the radioactive isotope ^{40}K incorporated into potassium rich feldspars can contribute a large percentage to the total dose rate delivered to the sample. This internal dose rate component is independent on uncertainties related to the estimation of sediment water content and the cosmic dose rate for composite sections with multiple phases of deposition. By that the uncertainty in dose rate calculation is reduced and consequently the error in age. Furthermore, feldspar subsamples of well-bleached sediments usually show less inter-aliquot scatter than the quartz fraction. This is also seen for example in Fig. B-6. Therefore multiple aliquot equivalent dose estimates obtained from potassium-rich feldspars often yield a higher precision when compared with the multiple aliquot ages of the quartz fraction of the same sample (e.g. RADTKE et al. 2001, RADTKE & JANOTTA 1998, HILGERS et al. 2001a). This higher precision in D_e estimates together with the reduced uncertainty in dose rate determination results in a higher precision of feldspar ages and make feldspar the preferable dating fraction over quartz.

Fading: An increasing number of comparative studies on independently dated sediments showed, at least in some circumstances, the tendency of feldspar ages to underestimate the expected ages significantly (e.g. WALLINGA et al. 2001, RADTKE et al. 2001). One likely explanation for this observation is a luminescence signal instability, a phenomenon known as 'anomalous fading'. Hereby trapped charge which is predicted to be stable over the time

period of hundreds of thousands of years is lost during laboratory experiments commonly not lasting longer than a few weeks. This loss of trapped charge affects many, though not all feldspars, but is not known to affect quartz samples (e.g. DULLER 2004). However, testing of feldspar samples for the occurrence of fading is necessary. But in general the results of such experiments are more qualitative than quantitative. With that it is difficult to correct for fading unless independent age control is available. Nevertheless, several procedures have been suggested that provide a test for the occurrence of fading and, if present, to correct for the signal loss (see for example AUCLAIR et al. 2003, HUNTLEY & LAMOTHE 2001, LAMOTHE et al. 2003, LAMOTHE & AUCLAIR 1999, 2000).

Fig. B 9: Comparison of multiple aliquot (MAA or MAR) feldspar ages and single aliquot (SAR) quartz ages for dune sand samples from various sites investigated in this study.
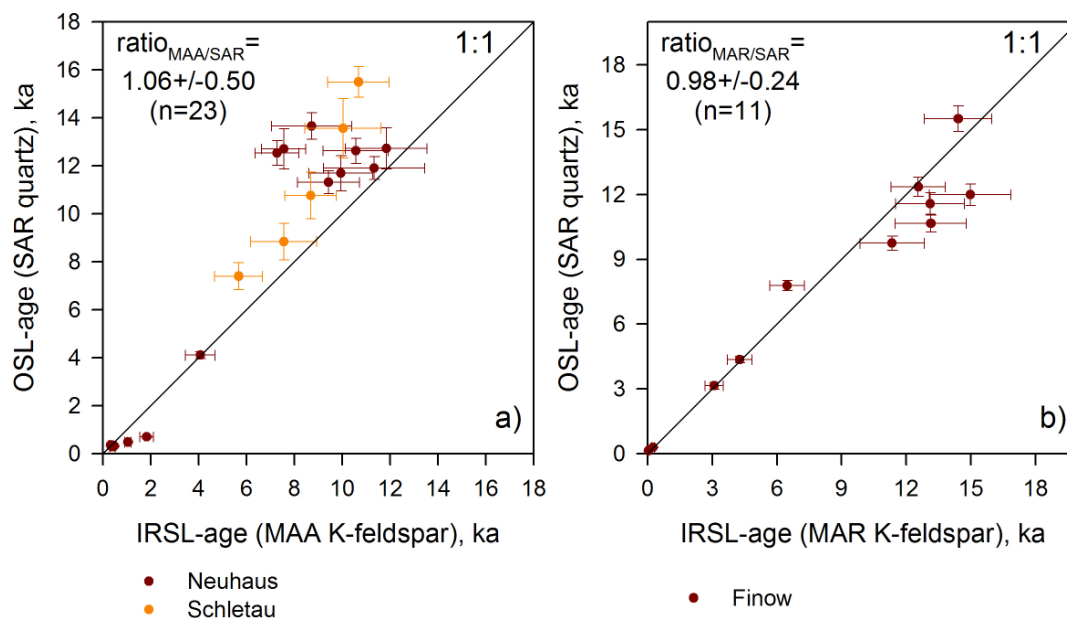
In Fig. B 9 feldspar ages of some dune sand samples investigated in this study are plotted against the single aliquot ages obtained on the quartz fraction of the same samples. In particular the multiple aliquot additive dose data shown in graph a) tend to underestimate the ages obtained by the quartz fraction. Taking only ages >1 ka into account the feldspar /quartz ratio is only 0.79. This could be interpreted as evidence for fading of the feldspar signals. But detailed fading tests should be carried out to support this assumption, in particular as a severe underestimation of feldspar ages is not seen in the MAR feldspar data set.

The feldspar ages obtained at the test study site 'Finow' are presented in Fig. B 10 together with the SAR quartz results and further chronological control. Regarding the precision the K-

feldspar ages are competitive with the SAR quartz ages. With respect to the agreement with the independent age control the feldspar ages more or less show a similar trend as the quartz results and agree within errors with the ^{14}C ages (see discussion of the outlier at site 'Finow–B' above). Only the lowermost sample at site 'Finow-B' seems to slightly overestimate the expected age. Altogether the precision and accuracy of multiple aliquot feldspar ages is comparable to that of the SAR quartz ages. But as it can not be excluded for sure that some feldspar samples might be affected by 'anomalous fading' all D_e measurements in this study were finally carried out on the quartz fraction.

Fig. B 10: Comparison of quartz and feldspar luminescence ages and ^{14}C ages with sampling depth for the dune site ‚Postdüne'.
Radiocarbon ages indicating the Allerød-age of the 'Finow' palaeosol (site 'Finow-C') and the Laacher See tephra age are also shown. In case of quartz, the ages based on the SAR equivalent dose value are shown. For potassium-rich feldspars the MAR protocol was used for palaeodose estimation.
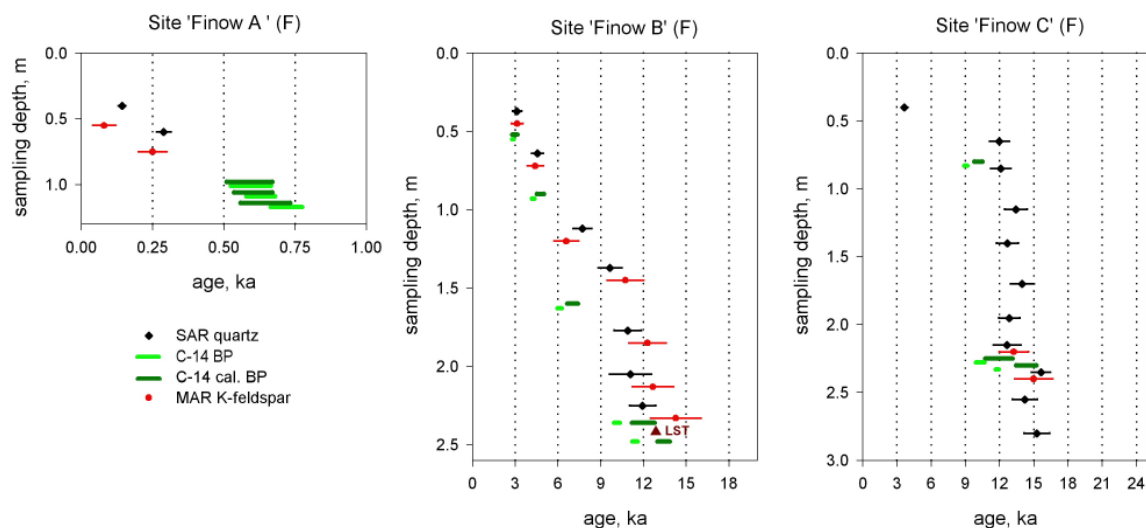
Conclusion

From the detailed comparative studies it is concluded, that the optically stimulated luminescence dating of quartz using the single aliquot regenerative dose protocol (MURRAY & WINTLE 2000) provides the most precise and most accurate luminescence chronologies compared to the independent age control. Therefore this protocol was applied to all samples of this study, keeping all measurement parameters as far as possible constant throughout the entire study to compile a comparable and uniform data set which forms the basis for any statistical analysis and interpretation.

Appendix C: Luminescence measurement equipment and beta source calibration

Preparation of the sub-samples for OSL measurements

In Fig. C 1 a sub-sample or aliquot, respectively, is illustrated which is representative for the '8mm' aliquots typically used for OSL measurements in this study. The central 8mm diameter of a stainless steel disc is covered with approximately 1000 to 2000 quartz grains (for a grain size range of c. 100-200µm). Therefore it is referred to these sub-samples as 'large, multi-grain' or '8mm' aliquots. The discs are prepared by, first, giving the discs a short spray with silicone oil, than sprinkling the loose quartz grains on the thin oil film, and finally knocking off the surplus. This should leave a mono-layer of grains stuck to the surface of the disc with adhesion achieved by the silicone oil film. It is crucial that the grains are mounted on the disc in a mono-layer in order to provide homogeneous irradiation conditions for each grain (MURRAY & WINTLE 1979).

Fig. C 1: Photograph of a 'standard' aliquot used for OSL measurements in this study.
(Visible black spots are artefacts of the microscope photograph. Picture by courtesy of B. Schwabe).

2 mm
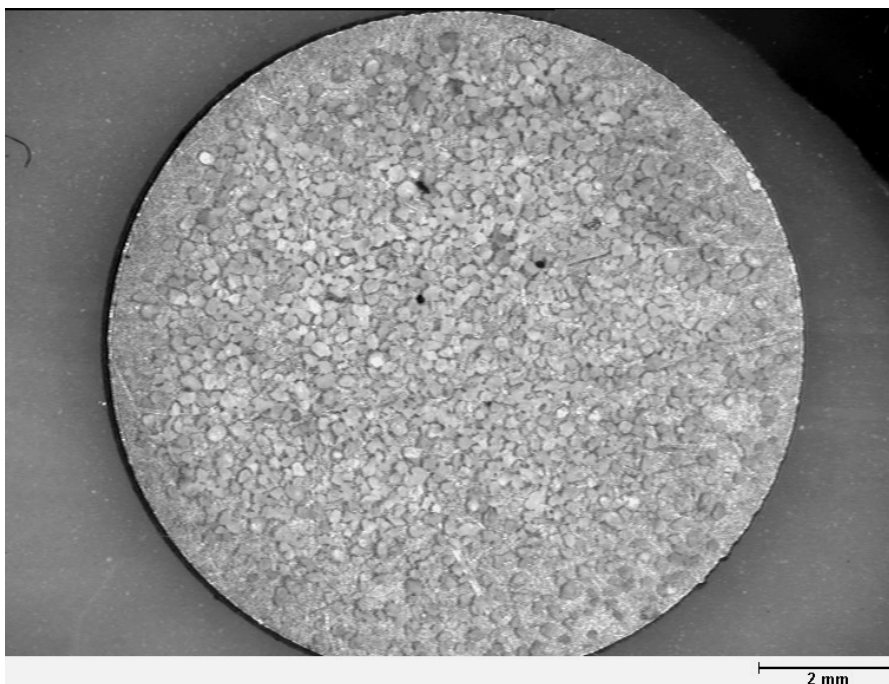
The Risø luminescence reader

All luminescence measurements were carried out on Risø luminescence readers, either of type TL/OSL-DA-12 or type TL/OSL-DA-15. These readers are controlled by slave computers ('minisys') and fully automated measurement sequences are programmed using a sequence editor on a host computer. For a recent summary of the developments in the OSL measurement technology and more detailed descriptions of the individual components of the equipment the reader is referred to, for example, BØTTER-JENSEN et al. (2003). The basic features of a luminescence reader are illustrated in Fig. C 2.

Fig. C 2: Basic features of the equipment used for luminescence measurements ('luminescence reader').
(sketch by courtesy of R. Grün).
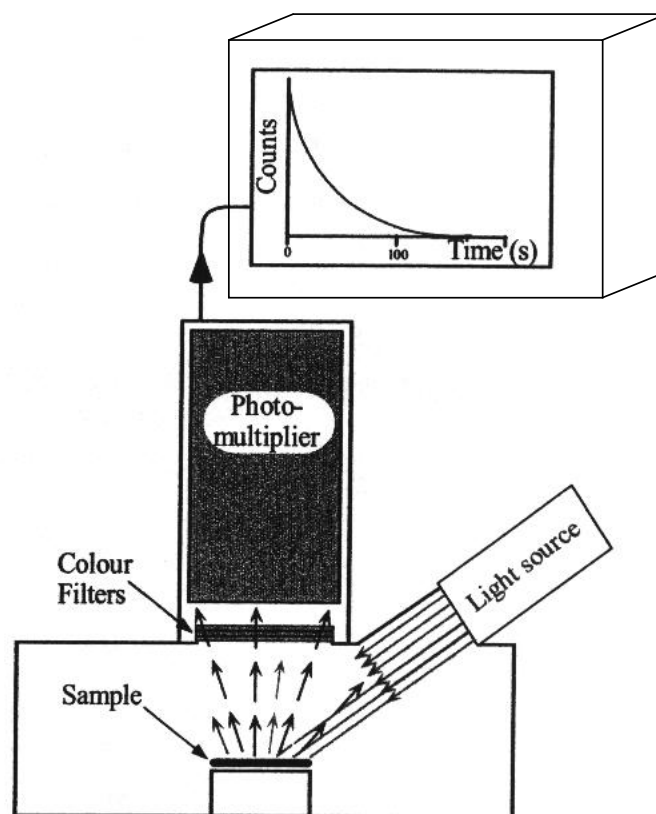
The individual discs (see e.g. Fig. C 1) are placed on a sample changer, a turntable that offers positions for the automated measurements of either 48 (reader type TL-DA-15) or 24 (TL-DA-12) sub-samples. This sample carousel is placed in a light tight sample chamber. By rotation of the turntable the aliquots are moved sequentially above a lift mechanism that raises

the samples into the measurement position directly beneath the luminescence detector, here the photomultiplier (PM) tube (e.g. type EMI 9235). A heater strip is mounted on the surface of the sample-lift. This heating element allows reproducible, electronically controlled heating of the samples, either for preheating, stimulation at elevated temperatures, or thermoluminescence measurements. The luminescence emission of the sample is monitored continuously while the light source is on (continuous wave =CW-OSL). The optical stimulation units in all Risø readers used in this study are built up of up to seven clusters each of seven blue (470±30 nm) light-emitting diodes (LEDs) arranged in a ring between the sample heater plate and the PM tube (see Fig. C 2). At total power the array of seven LED clusters deliver 35 mW/cm^2 to the sample. An optical feedback servo-system stabilises the light emission of the blue LEDs. Narrow band filters discriminate between the stimulation light and the emission light of the samples and to prevent scattered excitation light from entering the PM tube. A green long-pass GG-420 filter is fitted in front of each blue LED cluster to minimise the directly scattered blue light able to reaching the PM cathode (cut-off filter in Fig. C 3). Detection of the luminescence emission of quartz samples by the photomultiplier is through 7.5 mm Hoya U-340 filters (BØTTER-JENSEN et al. 1999a, b, 2000).

The luminescence measured takes the form of a decay curve (so-called 'shine-down' curve), that follows an exponential-like function from the beginning of excitation until all traps are emptied and luminescence ceases (see Fig. C 1).

Fig. C 3: Schematic of the blue LED (light-emitting diodes) cluster unit used as optical stimulation unit in the automated Risø TL/OSL reader.
Seven clusters making a total of 42 LEDs illuminate the sample at a distance of 35 mm. Note the GG-420 cut-off filter in front of each cluster of diodes. The heating element is used for any thermal treatment of the sample with the heating rate and maximum temperature being computer controlled (PM tube=photomultiplier tube). (from BØTTER-JENSEN et al. 1999b: 336)
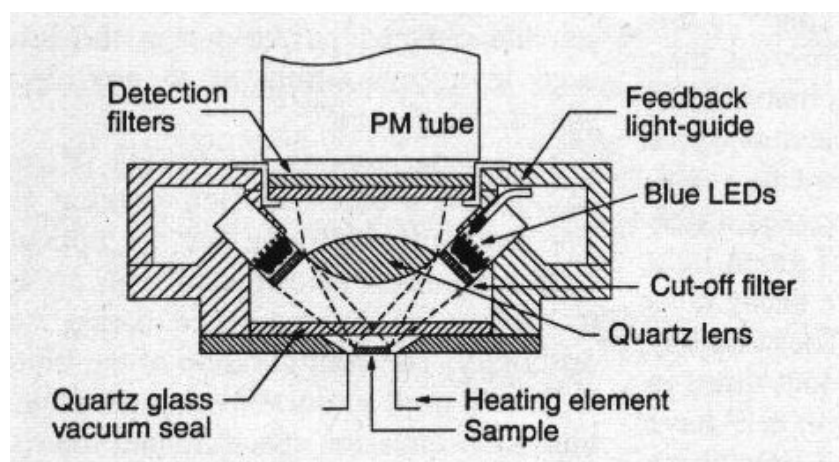
For in-situ irradiation of the samples a beta irradiator is attached to the reader (not shown in Fig. C 2). This beta source is based on the radionuclide ^{90}Sr/^{90}Y with an activity of 1.5 GBq (40 mCi) typically providing a dose rate at the sample position of about 0.1 Gy s^{-1} (BØTTER-JENSEN et al. 2003). The dose rate of each beta source has been determined by calibration against known gamma doses. The dose rate varied for the different sources in the different readers used in this study between ~0.01 (with increased, >5 mm source-to-sample distance) and ~0.18 Gy/s.

Beta source calibration

In OSL measurements laboratory irradiations of the samples are usually performed by means of a beta source which has been calibrated against a gamma source whose strength is accurately known (uncertainty of gamma source calibration ~2.4 % cited in ARMITAGE & BAILEY 2005). Various materials have been employed for such calibrations, for example, CaF$_2$, Al$_2$O$_3$:C, or quartz (MURRAY & WINTLE 1979, BELL & MEJDAHL 1981, ERFURT et al. 2003, ARMITAGE & BAILEY 2005). In this study calibration of beta sources were all carried out on natural quartz samples as is in numerous studies, although it should be mentioned that the applicability is still a matter of debate (see e.g. ERFURT et al. 2003).

To be suited as calibration material, reference samples should have the same elemental composition and thus the same stopping power and the same grain size as the material which is used in measurements carried out in the dating process. Furthermore, calibration samples should be characterised by excellent luminescence behaviour with respect to the precision and reproducibility of luminescence measurements (WINTLE 2005). In this study two different quartz samples are used as calibration reference material: sample DK (grain size 190-250 µm) and sample AU (grain size 100-200 µm) from Australian dune sands. The purified quartz grains were annealed at least at 500°C for 1 h before gamma irradiation to remove any trapped charge from the traps and to fully sensitise them (BELL & MEJDAHL 1981).

Gamma irradiation with known doses was carried out either with a ^{137}Cs γ-source (Risø National Laboratory, Roskilde, Denmark) or a ^{60}Co γ-source. (Department of Nuclear Medicine at the University of Düsseldorf, Germany). Calibration of the beta sources of the luminescence readers is then accomplished by OSL measurements of the γ-irradiated quartz samples using the same experimental setting as is used in the routine measurements for

equivalent dose determination. Thus, aliquots are prepared as aforementioned and the single aliquot regenerative dose protocol after MURRAY and WINTLE (2000) is applied for the calibration measurement. Because backscattering of electrons depends on the atomic number of the backing material, it is crucial to use the same material, e.g. stainless steel discs, for the calibration measurements as is used in routine measurements (MURRAY & WINTLE 1979). By comparing the OSL observed from the gamma irradiated grains with that induced on re-irradiation by the beta source, the strength of the beta source, the dose rate, can be determined.

For each reader used in this study calibration measurements were carried out routinely several times a year. In Fig. C 4 the results of a comparison of calibration measurements are shown to illustrate the reliability of the calibration procedure used in this study. Furthermore, this comparison provides the basis for the assessment of the overall uncertainty related to the beta source calibration which has to be accounted for in the equivalent dose error calculation.

The calibration values A, B, and C agree within errors. However, the mean value of B deviates from value A by 1.1 %, and value C deviates from value A by 4.1 %.

The difference in calibration values obtained for the two samples could be partly due to the difference in grain sizes. However, ARMITAGE and BAILEY (2005) observed no dependence on the laboratory dose rate on grain sizes between ~50-250 µm using the same equipment and thus irradiation geometry as was used throughout this study.

To conclude, the uncertainty in beta source calibration, which is finally included in the error propagation for the assessment of the overall error in equivalent dose determination, is estimated to 5 %. This value is a conservative estimate, but it fully allows for the variability in beta source calibration using different gamma sources for reference irradiation and different reference materials.

Fig. C 4: Comparison of calibration values obtained for the same beta source.
Two different sedimentary quartz samples served as reference material: one sampled from Danish sediments (sample DK, 190-250 µm) and one from Australian dune sands (sample AU, 100-200 µm). Two different gamma sources were used for irradiation of the calibration quartz: a [137]Cs γ-source (Risø National Laboratory, Roskilde, Denmark) and a [60]Co γ-source (Department of Nuclear Medicine at the University of Düsseldorf, Germany). The laboratory gamma doses (4.59 or 8.9 Gy, respectively) were recovered using the single-aliquot regenerative dose protocol (MURRAY & WINTLE 2000). The error bars represent the 1σ standard deviation around the mean.

Appendix D: Equivalent dose determination

Table D 1: Results of the equivalent dose calculation.
All results are presented as calculated for all aliquots, which were measured. If the values were not normally distributed, the D$_e$ values were re-calculated after exclusion of the outliers for the normally distributed data sets. The corresponding values are presented as well (column normally distributed values).

Sample	All values								Normally distributed values							
	Arithmetic mean				Weighted mean				Arithmetic mean				Weighted mean			
	Mean De (Gy)	Standard deviation	Standard error	Coefficient of variation	Mean De (Gy)	Standard deviation	Standard error	n	Mean De (Gy)	Standard deviation	Standard error	Coefficient of variation	Mean De (Gy)	Standard deviation	Standard error	n
N1	0.32	0.08	0.02	0.26	0.31	0.08	0.01	16	0.27	0.02	0.01	0.07	0.26	0.02	0.01	10
N2	2.11	1.79	0.46	0.85	0.68	1.79	0.01	15	1.00	0.60	0.19	0.60	0.63	0.60	0.01	10
N3	0.32	0.07	0.02	0.23	0.31	0.07	0.01	14	0.29	0.02	0.01	0.09	0.29	0.02	0.01	11
N4	0.49	0.21	0.05	0.42	0.49	0.21	0.01	16	0.45	0.11	0.03	0.25	0.47	0.11	0.01	15
N5	0.30	0.03	0.01	0.11	0.29	0.03	0.01	16	---	---	---	---	---	---	---	---
N6	0.31	0.04	0.01	0.13	0.31	0.04	0.01	16	---	---	---	---	---	---	---	---
N7	0.29	0.03	0.01	0.11	0.29	0.03	0.01	16	---	---	---	---	---	---	---	---
N8	0.32	0.05	0.01	0.14	0.31	0.05	0.01	16	0.31	0.03	0.01	0.09	0.31	0.03	0.01	15
N9	0.34	0.05	0.01	0.13	0.33	0.05	0.01	16	0.32	0.01	0.00	0.04	0.32	0.01	0.01	10
N10	4.92	1.70	0.31	0.35	4.21	1.70	0.02	30	---	---	---	---	---	---	---	---
N11	13.42	0.83	0.22	0.06	13.35	0.83	0.08	15	---	---	---	---	---	---	---	---
N12	12.08	0.97	0.25	0.08	11.91	0.97	0.08	15	---	---	---	---	---	---	---	---
N13	11.64	0.58	0.15	0.05	11.67	0.58	0.08	15	---	---	---	---	---	---	---	---
N14	11.95	1.06	0.27	0.09	11.93	1.06	0.07	15	---	---	---	---	---	---	---	---
N15	12.60	1.17	0.30	0.09	12.74	1.17	0.07	15	---	---	---	---	---	---	---	---
N16	11.10	0.77	0.20	0.07	11.00	0.77	0.08	15	---	---	---	---	---	---	---	---
N17	12.27	1.50	0.39	0.12	12.21	1.50	0.08	15	---	---	---	---	---	---	---	---
N18	12.95	1.61	0.41	0.12	13.31	1.61	0.08	15	---	---	---	---	---	---	---	---
F1	0.19	0.03	0.01	0.16	---	---	---	24	0.19	0.02	0.004	0.10	---	---	---	23
F2	0.35	0.02	0.00	0.06	---	---	---	24	---	---	---	---	---	---	---	---
F3	3.74	0.33	0.08	0.09	---	---	---	18	---	---	---	---	---	---	---	---
F4	5.36	0.52	0.12	0.10	---	---	---	18	---	---	---	---	---	---	---	---
F5	9.40	1.22	0.29	0.13	---	---	---	18	9.16	0.68	0.16	0.07	---	---	---	17
F6	11.07	0.80	0.19	0.07	---	---	---	18	---	---	---	---	---	---	---	---
F7	13.68	1.66	0.39	0.12	---	---	---	18	---	---	---	---	---	---	---	---
F8	14.60	1.62	0.38	0.11	---	---	---	18	---	---	---	---	---	---	---	---
F9	15.43	1.87	0.41	0.12	---	---	---	21	15.10	1.07	0.24	0.07	---	---	---	20
F12	4.33	0.67	0.15	0.15	---	---	---	21	4.25	0.57	0.13	0.14	---	---	---	20
F13	13.40	0.80	0.17	0.06	---	---	---	21	---	---	---	---	---	---	---	---
F14	14.51	0.60	0.13	0.04	---	---	---	21	---	---	---	---	---	---	---	---
F15	16.39	0.81	0.18	0.05	---	---	---	21	---	---	---	---	---	---	---	---
F16	16.02	1.15	0.25	0.07	---	---	---	21	---	---	---	---	---	---	---	---
F17	18.33	1.65	0.37	0.09	---	---	---	20	17.60	0.73	0.18	0.04	---	---	---	16
F18	19.41	1.49	0.33	0.08	---	---	---	21	---	---	---	---	---	---	---	---
F10	18.51	1.88	0.41	0.10	---	---	---	21	---	---	---	---	---	---	---	---
F11	18.02	1.22	0.27	0.07	---	---	---	21	---	---	---	---	---	---	---	---
F19	21.03	1.93	0.43	0.09	---	---	---	20	---	---	---	---	---	---	---	---
F20	20.01	1.18	0.26	0.06	---	---	---	21	---	---	---	---	---	---	---	---

| Sample | All values | | | | | | | | Normally distributed values | | | | | | | |
| | Arithmetic mean | | | | Weighted mean | | | | Arithmetic mean | | | | Weighted mean | | | |
	Mean De (Gy)	Standard deviation	Standard error	Coefficient of variation	Mean De (Gy)	Standard deviation	Standard error	n	Mean De (Gy)	Standard deviation	Standard error	Coefficient of variation	Mean De (Gy)	Standard deviation	Standard error	n
R1	12.53	1.52	0.37	0.12	---	---	---	17	---	---	---	---	---	---	---	---
R2	19.64	1.76	0.41	0.09	---	---	---	18	---	---	---	---	---	---	---	---
R3	18.36	1.51	0.35	0.08	---	---	---	18	---	---	---	---	---	---	---	---
R4	19.60	1.97	0.46	0.10	---	---	---	18	---	---	---	---	---	---	---	---
R5	18.95	1.71	0.40	0.09	---	---	---	18	---	---	---	---	---	---	---	---
R6	17.56	1.73	0.41	0.10	---	---	---	18	---	---	---	---	---	---	---	---
R7	16.78	1.01	0.24	0.06	---	---	---	18	---	---	---	---	---	---	---	---
M1	1.15	0.34	0.08	0.30	---	---	---	20	---	---	---	---	---	---	---	---
M2	16.77	1.42	0.34	0.08	---	---	---	18	---	---	---	---	---	---	---	---
M3	19.92	2.24	0.53	0.11	---	---	---	18	---	---	---	---	---	---	---	---
M4	25.10	1.64	0.39	0.07	---	---	---	18	---	---	---	---	---	---	---	---
S1	17.87	1.72	0.46	0.10	---	---	---	14	17.50	1.09	0.30	0.06	---	---	---	13
S2	17.50	1.24	0.29	0.07	---	---	---	18	---	---	---	---	---	---	---	---
S3	19.36	2.02	0.48	0.10	---	---	---	18	---	---	---	---	---	---	---	---
S4	20.16	1.65	0.39	0.08	---	---	---	18	19.85	1.03	0.25	0.05	---	---	---	17
S5	3.72	0.33	0.08	0.09	---	---	---	18	3.66	0.22	0.05	0.06	---	---	---	17
C1	0.64	0.08	0.02	0.13	---	---	---	18	---	---	---	---	---	---	---	---
C2	5.60	0.58	0.14	0.10	---	---	---	18	5.49	0.39	0.09	0.07	---	---	---	17
C3	7.70	0.64	0.15	0.08	---	---	---	18	---	---	---	---	---	---	---	---
C4	9.08	0.60	0.15	0.07	---	---	---	17	---	---	---	---	---	---	---	---
C5	9.05	0.75	0.16	0.08	---	---	---	21	8.92	0.48	0.11	0.05	---	---	---	20
C6	9.10	0.42	0.09	0.05	---	---	---	21	---	---	---	---	---	---	---	---
C7	16.37	1.34	0.29	0.08	---	---	---	21	16.16	0.95	0.21	0.06	---	---	---	20
J1	1.55	0.09	0.02	0.06	---	---	---	18	---	---	---	---	---	---	---	---
J2	1.40	0.09	0.02	0.06	---	---	---	18	---	---	---	---	---	---	---	---
J3	1.43	0.11	0.03	0.08	---	---	---	18	---	---	---	---	---	---	---	---
J4	1.47	0.11	0.03	0.08	---	---	---	18	1.37	0.01	0.005	0.01	---	---	---	8
J5	1.31	0.08	0.02	0.06	---	---	---	18	---	---	---	---	---	---	---	---
J6	1.38	0.13	0.03	0.09	---	---	---	17	---	---	---	---	---	---	---	---
J7	11.93	0.80	0.17	0.07	---	---	---	21	---	---	---	---	---	---	---	---
J8	12.22	1.17	0.26	0.10	---	---	---	20	---	---	---	---	---	---	---	---
JA1	0.30	0.20	0.04	0.66	0.22	0.20	0.00	29	0.20	0.04	0.01	0.20	0.19	0.04	0.004	19
JA2	5.10	1.42	0.37	0.28	4.38	1.42	0.04	15	---	---	---	---	---	---	---	---
JA3	8.36	0.76	0.19	0.09	8.30	0.76	0.06	15	---	---	---	---	---	---	---	---
JA4	8.85	1.00	0.26	0.11	8.35	1.00	0.06	15	---	---	---	---	---	---	---	---
JA5	10.17	1.07	0.28	0.11	9.93	1.07	0.07	15	---	---	---	---	---	---	---	---
JA6	11.30	0.59	0.15	0.05	11.30	0.59	0.06	15	---	---	---	---	---	---	---	---
JA7	11.98	0.97	0.25	0.08	11.84	0.97	0.07	15	---	---	---	---	---	---	---	---
JB1	10.68	0.63	0.16	0.06	10.56	0.63	0.06	15	---	---	---	---	---	---	---	---
JB2	8.39	0.78	0.20	0.09	8.22	0.78	0.05	15	---	---	---	---	---	---	---	---
JB3	8.79	0.88	0.23	0.10	8.70	0.88	0.05	15	8.59	0.48	0.13	0.06	8.58	0.48	0.06	14
JB4	9.04	0.53	0.14	0.06	9.03	0.53	0.05	15	---	---	---	---	---	---	---	---
JB5	9.27	0.66	0.17	0.07	9.18	0.66	0.05	15	9.21	0.65	0.17	0.07	9.12	0.65	0.05	14
JB6	8.80	0.44	0.11	0.05	8.84	0.44	0.05	15	---	---	---	---	---	---	---	---
JB7	9.43	0.69	0.18	0.07	9.23	0.69	0.05	15	---	---	---	---	---	---	---	---
JB8	9.43	1.31	0.34	0.14	9.35	1.31	0.05	15	9.13	0.68	0.18	0.07	9.08	0.68	0.05	14

| Sample | All values | | | | | | | | Normally distributed values | | | | | | | |
| | Arithmetic mean | | | | Weighted mean | | | | Arithmetic mean | | | | Weighted mean | | | |
	Mean De (Gy)	Standard deviation	Standard error	Coefficient of variation	Mean De (Gy)	Standard deviation	Standard error	n	Mean De (Gy)	Standard deviation	Standard error	Coefficient of variation	Mean De (Gy)	Standard deviation	Standard error	n
JB9	8.70	0.71	0.18	0.08	8.57	0.71	0.05	15	---	---	---	---	---	---	---	---
JB10	9.15	0.47	0.12	0.05	9.09	0.47	0.05	15	---	---	---	---	---	---	---	---
JB11	8.51	0.71	0.18	0.08	8.47	0.71	0.05	15	---	---	---	---	---	---	---	---
JB12	9.54	0.60	0.16	0.06	9.44	0.60	0.05	15	---	---	---	---	---	---	---	---
JB13	8.31	0.56	0.15	0.07	8.25	0.56	0.04	15	---	---	---	---	---	---	---	---
JC1	9.95	0.54	0.14	0.05	9.96	0.54	0.05	15	9.85	0.40	0.11	0.04	9.80	0.40	0.06	14
JC2	9.50	0.75	0.19	0.08	9.46	0.75	0.05	15	---	---	---	---	---	---	---	---
JC3	10.37	1.07	0.28	0.10	10.76	1.07	0.05	15	---	---	---	---	---	---	---	---
JC4	11.23	0.51	0.14	0.05	11.17	0.51	0.06	14	---	---	---	---	---	---	---	---
JC5	10.96	1.04	0.27	0.10	10.82	1.04	0.05	15	---	---	---	---	---	---	---	---
STA00-1	15.30	1.49	0.35	0.10	15.11	1.49	0.07	18	---	---	---	---	---	---	---	---
STA00-2	15.34	1.46	0.34	0.09	15.45	1.46	0.07	18	---	---	---	---	---	---	---	---
STA00-3	14.07	1.87	0.44	0.13	13.89	1.87	0.08	18	13.68	0.89	0.22	0.07	13.62	0.89	0.08	17
STA00-4	11.48	0.91	0.21	0.08	11.51	0.91	0.05	18	---	---	---	---	---	---	---	---
STA00-5	9.15	0.38	0.09	0.04	9.05	0.38	0.04	18	---	---	---	---	---	---	---	---
STA00-6	7.79	0.99	0.23	0.13	7.73	0.99	0.03	18	7.41	0.32	0.08	0.04	7.41	0.32	0.04	15
STA00-7	5.52	0.48	0.11	0.09	5.45	0.48	0.03	18	---	---	---	---	---	---	---	---
STA00-8	4.20	0.55	0.13	0.13	4.04	0.55	0.02	18	4.09	0.34	0.08	0.08	3.99	0.34	0.02	17
STA00-9	3.68	0.32	0.07	0.09	3.63	0.32	0.02	18	---	---	---	---	---	---	---	---
STA00-10	2.16	0.27	0.07	0.13	2.20	0.27	0.01	15	2.12	0.22	0.06	0.10	2.13	0.22	0.01	14
STA00-11	0.94	0.24	0.06	0.26	0.83	0.24	0.01	15	0.86	0.17	0.05	0.20	0.82	0.17	0.01	13
STA1	15.79	1.09	0.24	0.07	---	---	---	20	---	---	---	---	---	---	---	---
STA2	8.90	0.71	0.16	0.08	---	---	---	20	---	---	---	---	---	---	---	---
STA3	7.75	0.57	0.13	0.07	---	---	---	20	7.67	0.45	0.10	0.06	---	---	---	19
STA4	16.32	0.95	0.21	0.06	---	---	---	20	---	---	---	---	---	---	---	---
STA5	11.57	0.93	0.21	0.08	---	---	---	20	---	---	---	---	---	---	---	---
UM1	14.15	1.62	0.31	0.11	13.13	1.62	0.05	27	13.84	0.59	0.13	0.04	13.95	0.59	0.07	20
UM2	14.23	2.21	0.49	0.16	13.90	2.21	0.06	20	14.13	0.86	0.20	0.06	14.19	0.86	0.06	18
UM3	14.16	1.08	0.22	0.08	14.05	1.08	0.07	24	---	---	---	---	---	---	---	---
UM4	14.39	0.96	0.20	0.07	14.18	0.96	0.07	24	---	---	---	---	---	---	---	---
UM5	14.50	0.95	0.19	0.07	14.49	0.95	0.07	24	---	---	---	---	---	---	---	---
UM6	15.01	1.38	0.28	0.09	15.23	1.38	0.07	24	14.77	0.70	0.15	0.05	14.77	0.70	0.07	23
UM7	17.73	1.40	0.31	0.08	17.60	1.40	0.09	20	---	---	---	---	---	---	---	---
UM8	18.09	3.66	0.68	0.20	17.54	3.66	0.11	29	17.24	1.83	0.35	0.11	17.52	1.83	0.11	27
UM9	29.40	8.30	1.66	0.28	21.30	8.30	0.30	25	---	---	---	---	---	---	---	---
UM10	33.77	9.67	1.97	0.29	27.57	9.67	0.35	24	---	---	---	---	---	---	---	---
UM11	29.88	7.62	1.35	0.25	24.77	7.62	0.27	32	24.23	2.66	0.61	0.11	23.09	2.66	0.29	19
UM12	0.77	0.10	0.02	0.12	0.77	0.10	0.01	20	0.76	0.08	0.02	0.10	0.76	0.08	0.01	19
UM13	12.31	0.82	0.18	0.07	12.12	0.82	0.05	20	---	---	---	---	---	---	---	---
UM14	21.06	1.90	0.43	0.09	20.79	1.90	0.14	20	---	---	---	---	---	---	---	---
UM15	1.33	0.62	0.14	0.47	1.17	0.62	0.01	20	1.12	0.11	0.03	0.09	1.11	0.11	0.01	17
UM16	8.22	2.66	0.60	0.32	7.36	2.66	0.03	20	7.16	0.66	0.17	0.09	7.10	0.66	0.03	16
UM17	16.97	3.01	0.69	0.18	16.74	3.01	0.07	19	---	---	---	---	---	---	---	---
UM18	27.25	2.67	0.61	0.10	26.85	2.67	0.13	19	26.82	1.94	0.46	0.07	26.59	1.94	0.14	18
UM19	35.83	6.47	1.45	0.18	34.75	6.47	0.20	20	33.50	2.06	0.50	0.06	33.13	2.06	0.21	17
UM20	13.88	1.13	0.23	0.08	13.63	1.13	0.07	24	13.71	0.76	0.16	0.06	13.60	0.76	0.07	23

| Sample | All values | | | | | | | | Normally distributed values | | | | | | | |
| | Arithmetic mean | | | | Weighted mean | | | | Arithmetic mean | | | | Weighted mean | | | |
	Mean De (Gy)	Standard deviation	Standard error	Coefficient of variation	Mean De (Gy)	Standard deviation	Standard error	n	Mean De (Gy)	Standard deviation	Standard error	Coefficient of variation	Mean De (Gy)	Standard deviation	Standard error	n
UM21	14.24	1.19	0.24	0.08	14.09	1.19	0.07	24	---	---	---	---	---	---	---	---
UM22	14.84	1.91	0.39	0.13	14.62	1.91	0.07	24	14.36	0.91	0.19	0.06	14.25	0.91	0.07	22
UM23	25.80	7.34	1.41	0.28	21.36	7.34	0.26	27	---	---	---	---	---	---	---	---
UM24	32.17	9.36	1.87	0.29	26.93	9.36	0.38	25	31.22	8.23	1.68	0.26	26.83	8.23	0.38	24
UM25	29.30	9.77	1.88	0.33	24.10	9.77	0.30	27	28.46	8.91	1.75	0.31	23.72	8.91	0.30	26
UM26	28.59	9.48	1.76	0.33	24.54	9.48	0.25	29	25.71	6.36	1.27	0.25	23.94	6.36	0.25	25
UM27	29.77	9.52	1.77	0.32	24.80	9.52	0.27	29	28.36	8.20	1.58	0.29	24.74	8.20	0.27	27
AD4-1	3.43	0.44	0.09	0.13	3.45	0.44	0.01	25	3.38	0.38	0.08	0.11	3.41	0.38	0.01	24
AD4-2	15.65	1.51	0.34	0.10	15.51	1.51	0.06	20	---	---	---	---	---	---	---	---
AD4-3	18.57	2.00	0.45	0.11	18.08	2.00	0.07	20	18.28	1.57	0.36	0.09	17.77	1.57	0.07	19
AD4-4	19.80	1.45	0.32	0.07	19.55	1.45	0.08	20	---	---	---	---	---	---	---	---
AD4-5	18.06	1.11	0.25	0.06	17.93	1.11	0.06	20	---	---	---	---	---	---	---	---
AD4-6	17.12	1.09	0.24	0.06	16.80	1.09	0.07	20	---	---	---	---	---	---	---	---
AD4-7	18.09	1.15	0.26	0.06	18.20	1.15	0.07	20	---	---	---	---	---	---	---	---
AD4-8	16.31	1.03	0.23	0.06	16.24	1.03	0.06	20	---	---	---	---	---	---	---	---
AD4-9	16.24	1.01	0.22	0.06	16.32	1.01	0.06	20	---	---	---	---	---	---	---	---
AD4-10	16.66	2.15	0.48	0.13	16.57	2.15	0.06	20	16.23	1.02	0.23	0.06	16.32	1.02	0.06	19
AD4-11	15.32	1.63	0.36	0.11	15.40	1.63	0.06	20	15.01	0.88	0.20	0.06	14.94	0.88	0.06	19
AD4-12	16.64	1.21	0.27	0.07	16.53	1.21	0.06	20	16.49	1.04	0.24	0.06	16.41	1.04	0.06	19
AD4-13	19.42	0.93	0.21	0.05	19.50	0.93	0.07	20	---	---	---	---	---	---	---	---
AD4-14	17.02	0.95	0.21	0.06	17.16	0.95	0.07	20	---	---	---	---	---	---	---	---
AD1-1	16.23	1.49	0.33	0.09	15.97	1.49	0.06	20	16.00	1.11	0.25	0.07	15.83	1.11	0.06	19
AD1-2	17.68	1.19	0.27	0.07	17.64	1.19	0.08	20	17.49	0.86	0.20	0.05	17.55	0.86	0.08	19
AD1-3	21.33	2.64	0.59	0.12	20.98	2.64	0.09	20	---	---	---	---	---	---	---	---
AD1-4	20.44	1.48	0.33	0.07	20.32	1.48	0.09	20	---	---	---	---	---	---	---	---
SHA1	14.62	0.82	0.19	0.06	14.55	0.82	0.06	18	---	---	---	---	---	---	---	---
SHA2	14.44	1.32	0.31	0.09	13.77	1.32	0.06	18	---	---	---	---	---	---	---	---
SHA3	15.56	1.36	0.32	0.09	15.61	1.36	0.08	18	---	---	---	---	---	---	---	---
SHA4	17.15	1.06	0.25	0.06	16.90	1.06	0.07	18	---	---	---	---	---	---	---	---
SHA5	18.01	0.91	0.21	0.05	17.92	0.91	0.07	18	---	---	---	---	---	---	---	---
SHA6	18.29	1.28	0.30	0.07	18.23	1.28	0.08	18	---	---	---	---	---	---	---	---
SHB1	13.89	1.97	0.47	0.14	13.91	1.97	0.05	18	13.55	1.38	0.33	0.10	13.57	1.38	0.06	17
SHB2	12.42	2.34	0.55	0.19	12.10	2.34	0.04	18	11.73	0.67	0.17	0.06	11.69	0.67	0.04	16
SHB3	16.53	1.40	0.33	0.08	17.03	1.40	0.06	18	---	---	---	---	---	---	---	---
SHB4	16.62	1.33	0.34	0.08	16.43	1.33	0.08	15	---	---	---	---	---	---	---	---
G1	0.48	0.17	0.04	0.35	0.47	0.17	0.01	20	0.42	0.04	0.01	0.09	0.42	0.04	0.01	16
G2	5.46	1.32	0.26	0.24	5.21	1.32	0.02	26	---	---	---	---	---	---	---	---
G3	9.87	0.99	0.23	0.10	9.97	0.99	0.04	19	9.72	0.77	0.18	0.08	9.92	0.77	0.04	18
G4	9.95	0.70	0.16	0.07	9.76	0.70	0.05	19	---	---	---	---	---	---	---	---
G5	10.74	1.43	0.33	0.13	10.36	1.43	0.05	19	---	---	---	---	---	---	---	---
G6	9.94	1.07	0.25	0.11	9.82	1.07	0.04	19	---	---	---	---	---	---	---	---
G7	10.11	1.02	0.23	0.10	10.01	1.02	0.04	19	---	---	---	---	---	---	---	---
G8	9.65	1.03	0.24	0.11	9.68	1.03	0.04	19	---	---	---	---	---	---	---	---
G9	9.81	1.02	0.23	0.10	9.72	1.02	0.03	19	---	---	---	---	---	---	---	---
G10	9.18	0.74	0.16	0.08	9.15	0.74	0.04	21	---	---	---	---	---	---	---	---
G11	10.06	1.06	0.23	0.11	10.03	1.06	0.04	21	9.84	0.84	0.19	0.09	9.84	0.84	0.04	19

| Sample | All values | | | | | | | | Normally distributed values | | | | | | | |
| | Arithmetic mean | | | | Weighted mean | | | | Arithmetic mean | | | | Weighted mean | | | |
	Mean De (Gy)	Standard deviation	Standard error	Coefficient of variation	Mean De (Gy)	Standard deviation	Standard error	n	Mean De (Gy)	Standard deviation	Standard error	Coefficient of variation	Mean De (Gy)	Standard deviation	Standard error	n
G12	10.28	0.63	0.14	0.06	10.21	0.63	0.04	21	---	---	---	---	---	---	---	---
G12b	10.51	0.89	0.19	0.08	10.58	0.89	0.04	21	---	---	---	---	---	---	---	---
G13	11.34	1.00	0.22	0.09	11.27	1.00	0.05	21	---	---	---	---	---	---	---	---
G14	10.95	1.27	0.28	0.12	11.01	1.27	0.05	21	---	---	---	---	---	---	---	---
G15	10.70	3.33	0.73	0.31	9.96	3.33	0.04	21	10.01	1.05	0.24	0.11	9.84	1.05	0.05	20
G16	7.26	0.89	0.19	0.12	7.23	0.89	0.04	21	7.05	0.61	0.14	0.09	7.05	0.61	0.04	19
G17	0.05	0.04	0.01	0.73	0.04	0.04	0.00	20	---	---	---	---	---	---	---	---

The problem of incomplete bleaching in equivalent dose determination of glaciofluvial-glaciolimnic deposits

Dating of the glaciofluvial-glaciolimnic sediments at the sites 'Ueckermünde-A' and 'Ueckermünde-D' was problematic (see section 4.3.4 for a detailed description of the sites). At first, all samples were dated using 8mm aliquots. But the ages calculated from these D_e estimates clearly overestimated the expected ages for these deposits. By the time indicated by the OSL ages, up to ~20 ka (see Table D 2 for OSL ages), the area was still covered by the inland ice-sheet (GÖRSDORF & KAISER 2001). This age overestimation most probably is caused by poor bleaching of these glaciofluvial-glaciolimnic deposits due to the sedimentation context with transport in muddy water. This was already indicated in some D_e distributions by outliers towards very high equivalent doses (illustrated in the following histograms, see e.g. sample UM10).

To prove this assumption and finally to improve the dating results, some of the samples were re-measured using smaller aliquots each consisting of less than 100 grains. In case of samples which contain only a small proportion of poorly bleached grains the reduction of the number of grains per aliquot even up to single grains is advisable. The use of such small aliquots enhances the probability to detect the grain population at the lower end of a dose distribution which is assumed to be most sufficiently bleached (e.g. OLLEY et al. 1998, WALLINGA 2002, FUCHS & WAGNER 2003). In fact, using small aliquots the D_e distributions are clearly skewed towards high values, mostly likely caused by a few grains containing high residual doses due to poor bleaching.

Several statistical models are available which can be applied to obtain the 'best' D_e estimate from complex distributions which will finally give the 'true' burial age ('minimum age model', 'central age model', 'leading edge', lowest 5 % of D_e values etc., see for example FUCHS & LANG 2001, GALBRAITH et al. 1999, LEPPER & McKeever 2002, OLLEY et al. 1998). For a discussion of the applicability of the various models the reader is referred to GALBRAITH et al. 2005, BAILEY and ARNOLD 2006, and FUCHS et al. 2006. At this stage of the study, all ages obtained for the 1mm aliquot measurements of the glaciofluvial-glaciolimnic samples are interpreted as maximum ages only. Equivalent dose calculation was carried out in the same way as for the large aliquots used throughout this study (see section 3.6.1.3) with exclusion of values which disagree with a normal distribution at a 0.05 significance level. It cannot ruled

out that the D_e values, based on the weighted mean of the normal distributed 1 mm aliquot D_e values, still overestimates the 'true' burial dose, and, hence, yield ages which overestimate the time of deposition. Application of more sophisticated statistical models, as those aforementioned, would be advisable. But for the successful application of any of the statistical models, much larger data sets are required than available for the samples yet. To optimize the results, single grain measurements ought to be carried out as well. Furthermore, BAILEY and ARNOLD (2006) pointed out that no single age-model is appropriate for all problematic dating studies in general and the best suited statistical model has to be evaluated first.

However, as this study is considered with the reconstruction of dune formation the precise and accurate dating of the underlying substrates of course is desirable, but beyond the major scope of this study. Further research will concentrate on this topic.

The following histograms illustrate the comparison of equivalent dose distributions obtained for large (8mm) and small (1mm) aliquots of quartz extracted from aeolian and glaciolacustrine sand samples from the sampling sites 'Ueckermünder Heide-A and –D'.

The initial D_e distributions are always shown. If these were not normally distributed the histogram for the normally distributed data is also presented below. For samples UM 6 and UM10 'dose recovery' tests were carried out to illustrate the equivalent dose distributions which are obtained for 'ideal' bleaching and homogeneous irradiation conditions.

For a comparison of the impact of poor bleaching on the resulting ages and the improvement of the age results by using smaller aliquots for equivalent dose determination it is referred to Table D 2.

Table D 2: Comparison of the equivalent dose values and OSL ages obtained for 8mm and 1mm aliquots.

	De (Gy)	De error (Gy)	arithmetic mean				weigthed mean				n	aliquot size	OSL age (ka) [using NAA based dose rates]	sample
			De a. mean	std. dev.	std. err.	ν-value	De w. mean	std.dev.w.m.	std.err. w.m.	ν-value				
all	15.23	0.76	15.01	1.38	0.28	0.09	15.23	1.38	0.07	0.09	24			
ND	14.77	0.74	14.77	0.70	0.15	0.05	14.77	0.70	0.07	0.05	23	8mm	13.52 ±0.99	UM6
all	13.31	0.68	14.37	2.68	0.47	0.19	13.31	2.68	0.15	0.2	32			
ND	13.29	0.68	13.90	2.01	0.37	0.14	13.29	2.01	0.15	0.15	30	1mm	12.16 ±0.90	UM6
all	27.57	1.42	33.77	9.67	1.97	0.29	27.57	9.67	0.35	0.35	24			
ND	27.57	1.42	33.77	9.67	1.97	0.29	27.57	9.67	0.35	0.35	24	8mm	19.84 ±1.47	UM10
all	24.16	1.24	29.16	10.35	1.35	0.35	24.16	10.35	0.27	0.43	59			
ND	23.25	1.20	25.55	6.27	0.90	0.25	23.25	6.27	0.28	0.27	49	1mm	16.73 ±1.24	UM10
all	24.77	1.27	29.88	7.62	1.35	0.25	24.77	7.62	0.27	0.31	32			
ND	23.09	1.19	24.23	2.66	0.61	0.11	23.09	2.66	0.29	0.12	19	8mm	19.42 ±1.41	UM11
all	26.09	1.31	31.27	13.81	1.53	0.44	26.09	13.81	0.13	0.53	81			
ND	25.43	1.28	26.43	6.66	0.81	0.25	25.43	6.66	0.13	0.26	68	1mm	21.40 ±1.54	UM11
all	14.09	0.71	14.24	1.19	0.24	0.08	14.09	1.19	0.07	0.08	24			
ND	14.09	0.71	14.24	1.19	0.24	0.08	14.09	1.19	0.07	0.08	24	8mm	11.83 ±0.84	UM21
all	12.04	0.61	16.70	5.44	0.68	0.33	12.04	5.44	0.09	0.45	65			
ND	14.54	0.73	15.13	2.70	0.36	0.18	14.54	2.70	0.11	0.19	56	1mm	12.21 ±0.86	UM21
all	14.62	0.73	14.84	1.91	0.39	0.13	14.62	1.91	0.07	0.13	24			
ND	14.25	0.72	14.36	0.91	0.19	0.06	14.25	0.91	0.07	0.06	22	8mm	13.48 ±1.00	UM22
all	13.27	0.67	13.97	2.43	0.33	0.17	13.27	2.43	0.09	0.18	55			
ND	13.27	0.67	13.97	2.43	0.33	0.17	13.27	2.43	0.09	0.18	55	1mm	12.55 ±0.94	UM22
all	21.36	1.10	25.80	7.34	1.41	0.28	21.36	7.34	0.26	0.34	27			
ND	21.36	1.10	25.80	7.34	1.41	0.28	21.36	7.34	0.26	0.34	27	8mm	16.81 ±1.28	UM23
all	20.25	1.02	28.62	12.85	1.57	0.45	20.25	12.85	0.13	0.63	67			
ND	19.78	1.00	24.05	7.07	0.94	0.29	19.78	7.07	0.14	0.36	56	1mm	15.57 ±1.18	UM23
all	24.80	1.27	29.77	9.52	1.77	0.32	24.80	9.52	0.27	0.38	29			
ND	24.74	1.27	28.36	8.20	1.58	0.29	24.74	8.20	0.27	0.33	27	8mm	22.20 ±1.62	UM27
all	25.33	1.27	34.83	16.36	1.81	0.47	25.33	16.36	0.14	0.65	82			
ND	22.18	1.12	24.18	5.33	0.75	0.22	22.18	5.33	0.14	0.24	50	1mm	19.90 ±1.44	UM27

Aeolian sand: UM6 8mm & 1mm

UM6 8mm-aliquots

n= 24 of 24

UM6 1mm-aliquots

n= 32 of 70

UM6 8mm-aliquots

n= 23 of 24

UM6 1mm-aliquots

n= 30 of 70
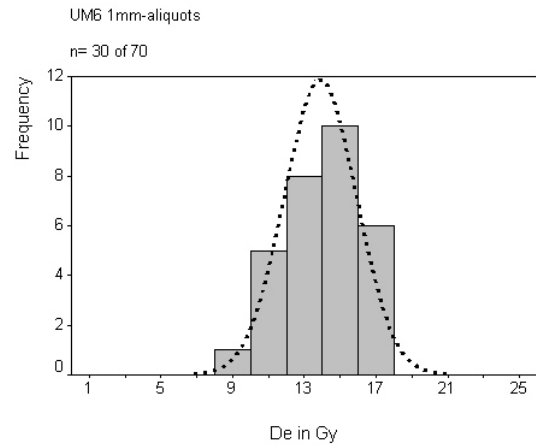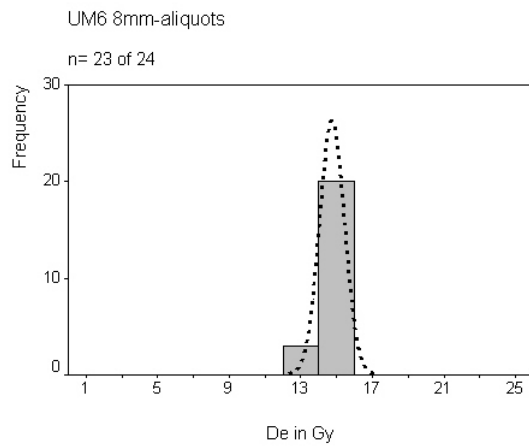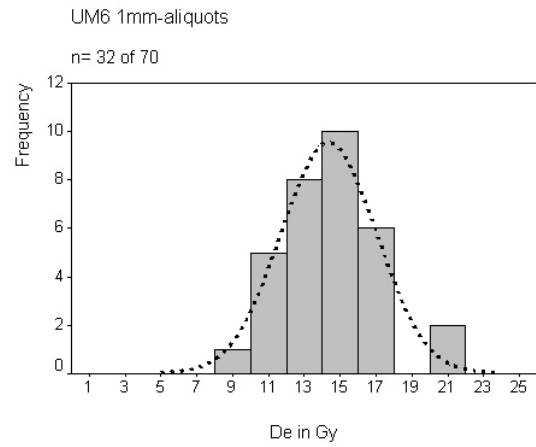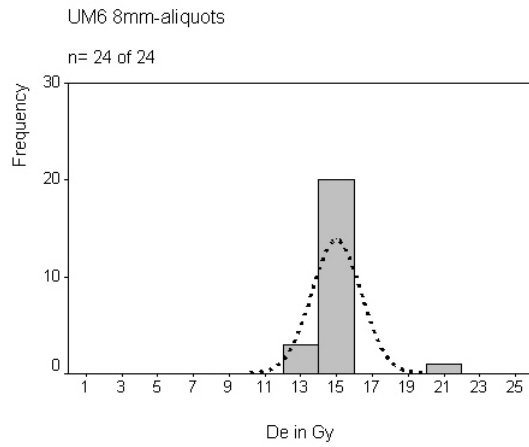
UM6 1mm-aliquots

n= 20 of 48, dose recovery test
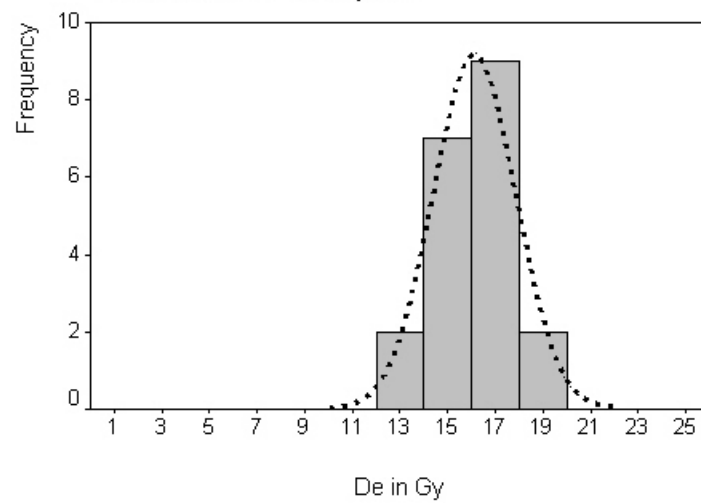
# Glaciolacustrine sand: UM10 8mm & 1mm

UM10 8mm-aliquots

n= 24 of 34

n= 7 > 58 Gy

UM10 1mm-aliquots

n= 59 of 120

UM10 1mm-aliquots

n= 49 of 120

UM10 1mm-aliquots

n= 37 of 65, dose recovery test
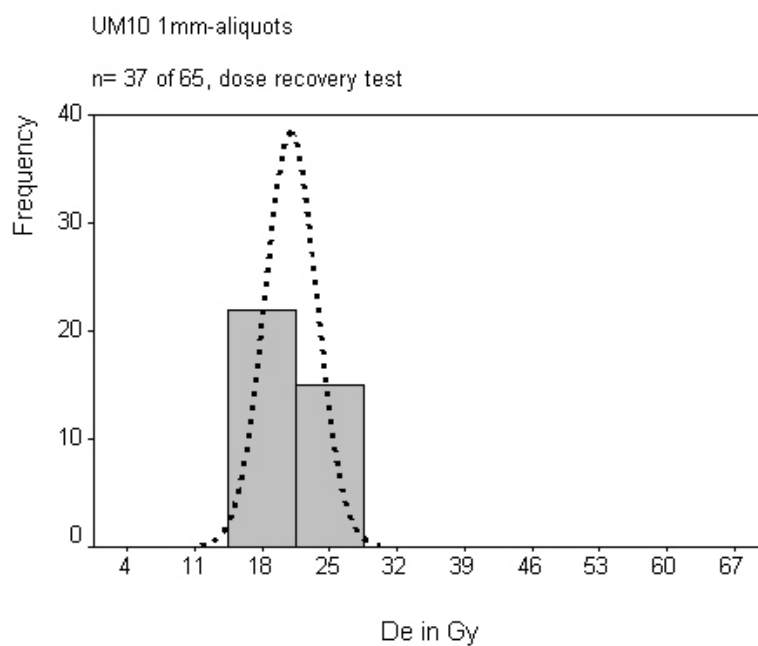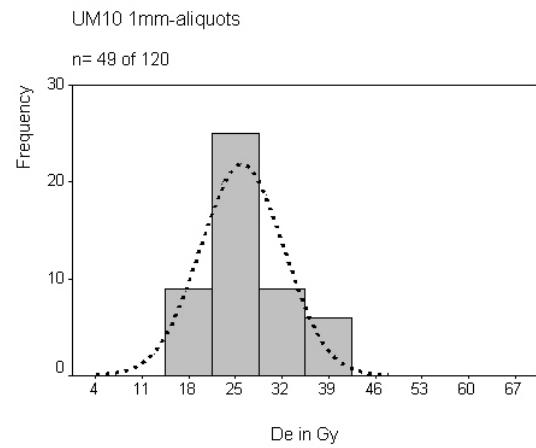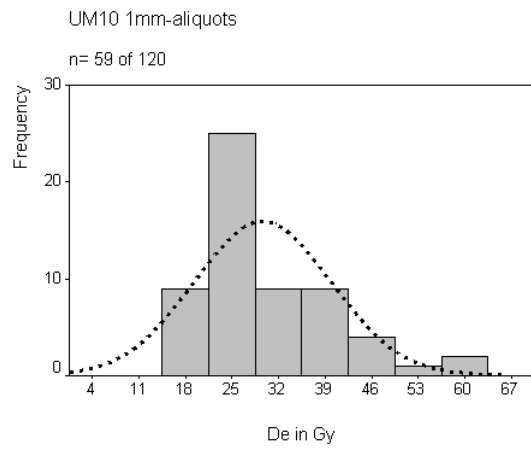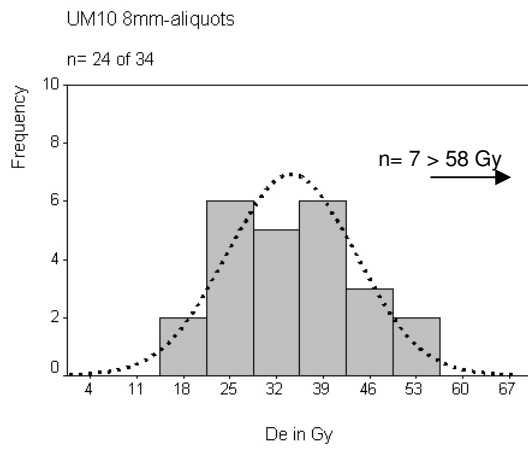
Glaciolacustrine sand: UM11 8mm & 1mm

UM11 8mm-aliquots

n= 32 of 34

n=2 > 58 Gy

UM11 1mm-aliquots

n= 81 of 120

n=5 > 82 Gy

UM11 8mm-aliquots

n= 19 of 34

UM11 1mm-aliquots

n= 68 of 120
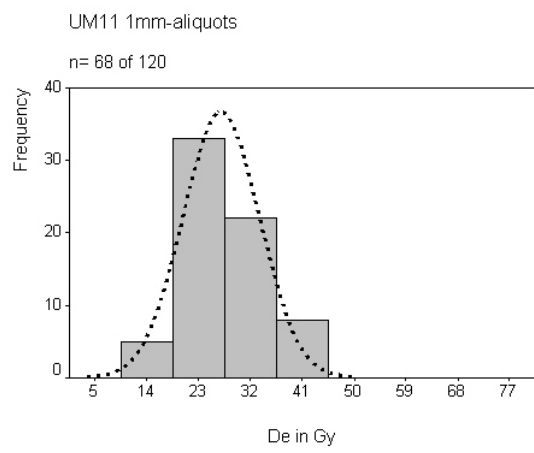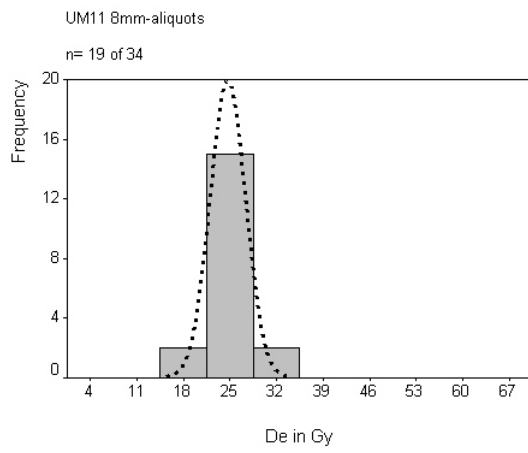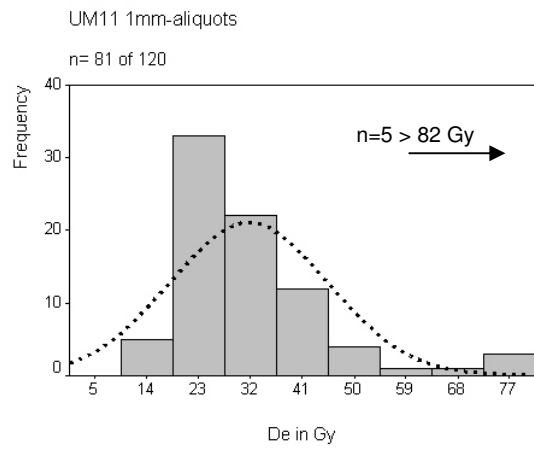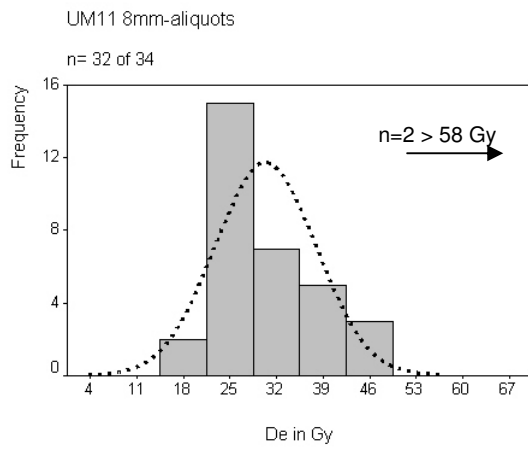
Aeolian sand: UM22 8mm & 1mm

UM22 8mm-aliquots

n= 24 of 24

UM22 1mm-aliquots

n= 55 of 120

UM22 8mm-aliquots

n= 22 of 24
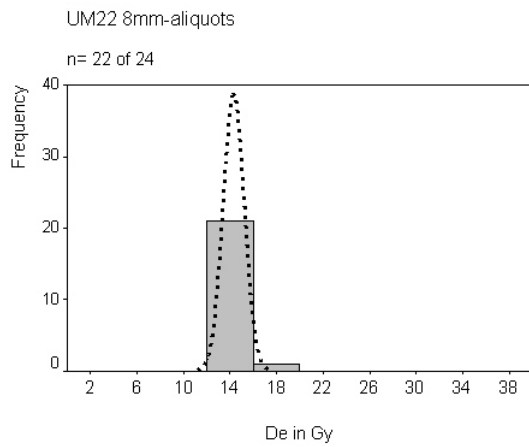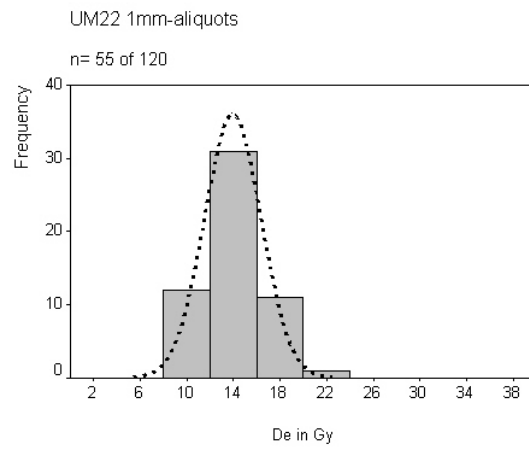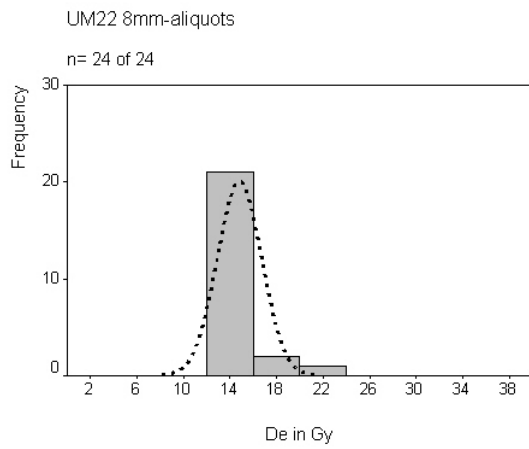
Glaciolacustrine sand: UM23 8mm & 1mm

UM23 8mm-aliquots

n= 27 of 31

UM23 1mm-aliquots

n= 67 of 120

UM23 1mm-aliquots

n= 56 of 120
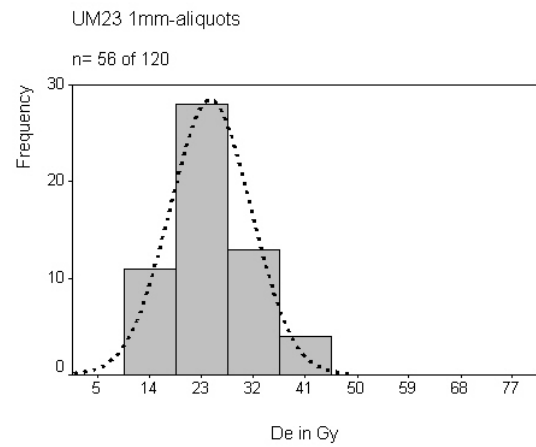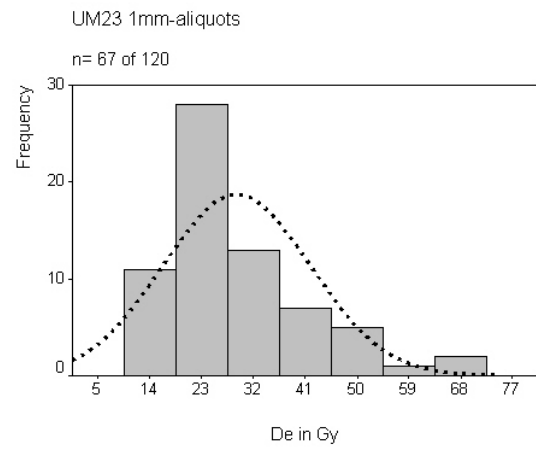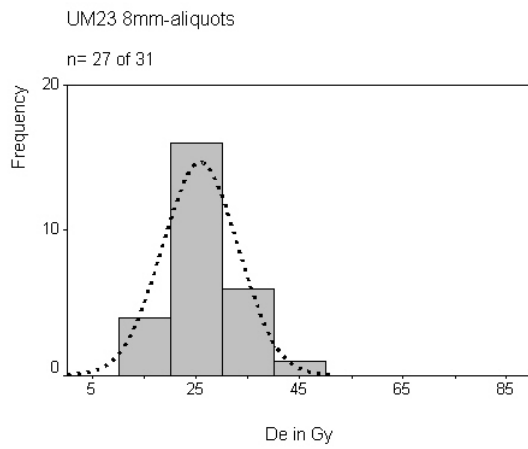
Glaciolacustrine sand: UM27 8mm & 1mm

UM27 8mm-aliquots

n= 29 of 35

UM27 1mm-aliquots

n= 82 of 120

UM27 8mm-aliquots

n= 27 of 35

UM27 1mm-aliquot

n= 50 of 120
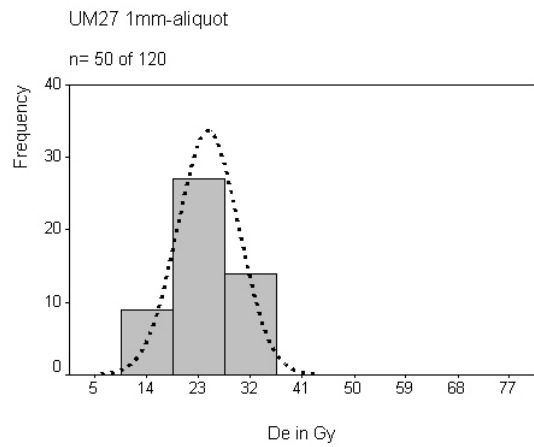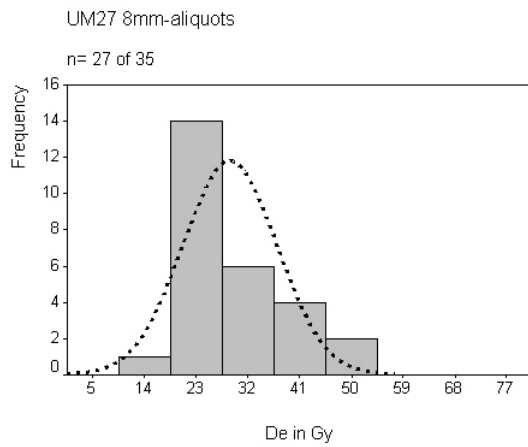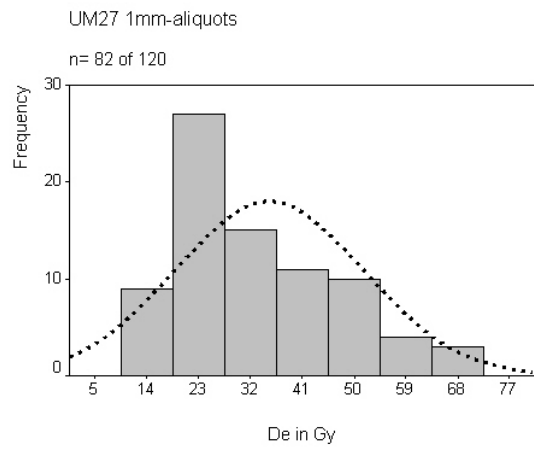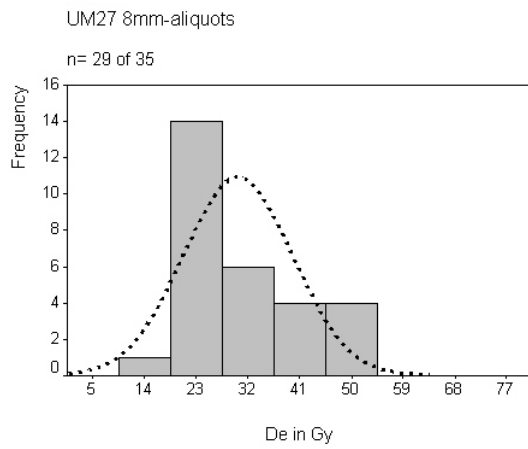
Appendix E: Results of OSL dating and list of ^{14}C ages

Table E 1: List of OSL dating results.

Summary of the dose rates (D_0) and equivalent dose values (D_e, including the uncertainty associated with the beta source calibration of 5 %) which were used to calculate the ages. If not other stated (see column 'comment'), than the dose rate is based on neutron activation analysis and equivalent dose measurements which were carried out on 8mm aliquots. Shaded rows indicate non-aeolian deposits. Ages which were considered to be implausible are shown in italics; they were excluded from the data set.

Site location	Lab code	Sample	Depth (m)	Dose rate (Gy/ka)		Equivalent dose (Gy)		OSL age (ka)		Comment	Aeolian phases mean age of sand units (ka)
Neuhaus 10°56'38'' E. 53°16'35'' N	C-L0501	N1	0.15	0.92	±0.09	0.26	±0.01	0.29	±0.03	---	0.32±0.02 (n=7)
	C-L0502	N2	0.80	0.91	±0.08	0.63	±0.03	*0.70*	*±0.07*	*not plausible (poor bleaching ?)*	
	C-L0503	N3	1.30	0.94	±0.09	0.29	±0.02	0.31	±0.03	---	
	C-L0504	N4	1.85	0.97	±0.05	0.47	±0.02	*0.48*	*±0.03*	*not plausible (poor bleaching ?)*	
	C-L0505	N5	2.35	0.94	±0.09	0.29	±0.02	0.31	±0.03	---	
	C-L0506	N6	3.04	0.94	±0.09	0.31	±0.02	0.32	±0.04	---	
	C-L0507	N7	3.50	0.86	±0.09	0.29	±0.01	0.33	±0.04	---	
	C-L0508	N8	4.05	0.89	±0.09	0.31	±0.02	0.35	±0.04	---	
	C-L0509	N9	4.55	0.97	±0.09	0.32	±0.02	0.33	±0.04	---	
	C-L0510	N10	5.00	1.03	±0.05	4.21	±0.21	4.10	±0.29	---	4.10±0.29
	C-L0511	N11	5.60	1.14	±0.10	13.35	±0.67	11.68	±1.18	---	12.11±0.57 (n=7)
	C-L0512	N12	6.80	0.94	±0.09	11.91	±0.60	12.72	±1.37	---	
	C-L0513	N13	7.15	0.98	±0.05	11.67	±0.59	11.89	±0.89	---	
	C-L0514	N14	7.70	0.95	±0.06	11.93	±0.60	12.52	±0.96	---	
	C-L0515	N15	8.55	1.00	±0.09	12.74	±0.64	12.69	±1.34	---	
	C-L0516	N16	9.05	0.97	±0.06	11.00	±0.56	11.30	±0.87	---	
	C-L0517	N17	9.65	0.97	±0.06	12.21	±0.62	12.62	±0.96	---	
	C-L0518	N18	10.00	0.98	±0.06	13.31	±0.67	13.65	±1.03	---	13.65±1.03

Site location	Lab code	Sample	Depth (m)	Dose rate (Gy/ka)		Equivalent dose (Gy)		OSL age (ka)		Comment	Aeolian phases mean age of sand units (ka)
Finow 13°41'43" E. 52°48'35" N	C-L0519	F1	0.45	1.31	±0.09	0.19	±0.01	0.14	±0.01	DR av. NAA & gamma	0.14±0.01
	C-L0520	F2	0.65	1.22	±0.08	0.35	±0.02	0.29	±0.02	DR av. NAA & gamma	0.29±0.02
	C-L0521	F3	0.40	1.20	±0.10	3.74	±0.20	3.12	±0.31	DR av. NAA & gamma	3.12±0.31
	C-L0522	F4	0.67	1.18	±0.08	5.36	±0.29	4.55	±0.41	DR av. NAA & gamma	4.55±0.41
	C-L0523	F5	1.15	1.19	±0.08	9.16	±0.49	7.72	±0.65	DR av. NAA & gamma	7.72±0.65
	C-L0524	F6	1.40	1.15	±0.08	11.07	±0.59	9.65	±0.83	DR av. NAA & gamma	9.65±0.83
	C-L0525	F7	1.80	1.26	±0.08	13.68	±0.79	10.89	±0.94	DR av. NAA & gamma	11.37±0.56 (n=3)
	C-L0526	F8	2.08	1.32	±0.16	14.60	±0.82	11.07	±1.47	DR av. NAA & gamma	
	C-L0527	F9	2.28	1.27	±0.07	15.10	±0.79	11.93	±0.91	DR gamma	
	C-L0528	F12	0.40	1.17	±0.06	4.25	±0.25	3.64	±0.28	---	3.64±0.28
	C-L0529	F13	0.65	1.12	±0.06	13.40	±0.69	11.96	±0.87	---	11.96±0.87
	C-L0530	F14	0.85	1.20	±0.06	14.51	±0.74	12.08	±0.88	---	12.89±0.66 (n=6)
	C-L0531	F15	1.15	1.22	±0.06	16.39	±0.84	13.41	±0.98	---	
	C-L0532	F16	1.40	1.27	±0.07	16.02	±0.84	12.66	±0.94	---	
	C-L0533	F17	1.70	1.26	±0.07	17.60	±0.90	13.97	±1.03	---	
	C-L0534	F18	1.95	1.45	±0.07	18.54	±0.95	12.83	±0.93	De 1mm aliquots	
	C-L0535	F10	2.15	1.46	±0.12	18.51	±1.01	12.64	±1.21	DR av. NAA & gamma	
	C-L0536	F11	2.35	1.15	±0.09	18.02	±0.94	15.61	±1.41	DR av. NAA & gamma	14.91±0.74 (n=3)
	C-L0537	F19	2.55	1.48	±0.08	21.03	±1.14	14.19	±1.09	---	
	C-L0538	F20	2.80	1.31	±0.07	20.01	±1.03	15.24	±1.12	---	
Rosenberg 13°42'06" E. 52°47'08" N	C-L0539	R1	1.95	1.22	±0.09	12.53	±0.73	10.30	±0.94	---	11.03±1.20 (n=2)
	C-L0540	R2	2.20	1.64	±0.12	19.64	±1.07	12.00	±1.09	DR av. NAA & gamma	
	C-L0541	R3	2.60	1.17	±0.08	18.36	±0.98	15.71	±1.40	DR av. NAA & gamma	15.71±1.40
	C-L0542	R4	2.90	1.17	±0.07	19.60	±1.08	16.77	±1.42	---	16.76±0.50 (n=4)
	C-L0543	R5	3.20	1.12	±0.06	18.95	±1.03	16.96	±1.27	---	
	C-L0544	R6	3.55	1.10	±0.08	17.56	±0.97	16.01	±1.48	---	
	C-L0545	R7	3.90	0.98	±0.06	16.78	±0.87	17.16	±1.35	---	
Melchow 13°42'24" E. 52°48'05" N	C-L0546	M1	0.20	1.34	±0.08	1.15	±0.10	0.86	±0.09	---	0.86±0.09
	C-L0547	M2	0.62	1.37	±0.09	16.77	±0.90	12.20	±1.03	---	12.65±0.85 (n=2)
	C-L0548	M3	1.22	1.49	±0.12	19.92	±1.13	13.40	±1.32	DR av. NAA & gamma	
	C-L0549	M4	1.70	1.52	±0.11	25.10	±1.31	16.52	±1.48	DR av. NAA & gamma	16.52±1.48
Spechthausen 13°44'54" E. 52°48'54" N	C-L0550	S1	0.45	1.38	±0.08	17.50	±0.93	12.67	±1.01		12.88±0.37 (n=2)
	C-L0551	S2	1.15	1.33	±0.10	17.50	±0.92	13.19	±1.22	DR av. NAA & gamma	
	C-L0552	S3	1.45	1.38	±0.11	19.36	±1.08	14.07	±1.41	DR av. NAA & gamma	15.00±1.32 (n=2)
	C-L0553	S4	2.20	1.25	±0.09	19.85	±1.02	15.93	±1.41	---	
	C-L0554	S5	0.35	1.09	±0.08	3.66	±0.19	3.36	±0.30	---	3.36±0.30

Site location	Lab code	Sample	Depth (m)	Dose rate (Gy/ka)		Equivalent dose (Gy)		OSL age (ka)		Comment	Aeolian phases mean age of sand units (ka)
Cottbus 14°24'48" E. 51°46'18" N	C-L0555	C1	0.30	0.91	±0.05	0.64	±0.04	0.70	±0.06	---	0.70±0.06
	C-L0556	C2	0.70	0.94	±0.05	5.49	±0.29	5.85	±0.43	---	5.85±0.43
	C-L0557	C3	0.95	0.87	±0.05	7.70	±0.41	8.83	±0.66	---	8.83±0.66
	C-L0558	C4	1.45	0.82	±0.04	9.08	±0.48	11.12	±0.84	---	11.12±0.84
	C-L0559	C5	2.20	0.70	±0.03	8.92	±0.46	12.71	±0.88	---	---
	C-L0560	C6	2.55	0.83	±0.04	9.10	±0.46	11.24	±0.97	DR av. NAA & gamma	
	C-L0561	C7	3.00	1.17	±0.04	16.16	±0.84	13.84	±0.84	DR gamma & in-situ gamma	
Jänschwalde 14°33'51" E. 51°48'33" N	C-L0562	J1	0.50	0.88	±0.05	1.55	±0.08	1.76	±0.13	---	1.76±0.05 (n=6)
	C-L0563	J2	1.10	0.79	±0.05	1.40	±0.07	1.77	±0.14	---	
	C-L0564	J3	1.60	0.78	±0.05	1.43	±0.08	1.84	±0.15	---	
	C-L0565	J4	2.20	0.76	±0.03	1.37	±0.07	1.79	±0.12	---	
	C-L0566	J5	3.10	0.76	±0.05	1.31	±0.07	1.73	±0.14	---	
	C-L0567	J6	3.65	0.81	±0.05	1.38	±0.08	1.69	±0.13	---	
	C-L0568	J7	4.55	0.79	±0.04	11.93	±0.62	14.96	±1.23	DR av. NAA & gamma	---
	C-L0569	J8	4.90	0.94	±0.05	12.22	±0.66	13.58	±1.16	DR av. NAA & gamma	
Jasien-A 15°01'38" E. 51°45'18" N	C-L0603	JA1	0.47	0.76	±0.04	0.19	±0.01	0.25	±0.02	---	0.25±0.02
	C-L0604	JA2	0.82	0.71	±0.03	4.38	±0.22	6.16	±0.42	---	6.16±0.42
	C-L0605	JA3	1.25	0.68	±0.03	8.30	±0.42	12.22	±0.82	---	12.45±0.50 (n=3)
	C-L0606	JA4	1.57	0.69	±0.03	8.35	±0.42	12.15	±0.87	---	
	C-L0607	JA5	1.88	0.76	±0.04	9.93	±0.50	13.05	±0.91	---	
	C-L0608	JA6	2.18	0.79	±0.04	11.30	±0.57	14.36	±1.07	---	14.36±1.07
	C-L0609	JA7	2.61	0.73	±0.04	11.84	±0.60	16.30	±1.20	---	16.30±1.20
Jasien-B 14°59'42" E. 51°45'08" N	C-L0610	JB1	0.90	0.81	±0.04	10.56	±0.53	12.96	±0.95	---	12.96±0.95
	C-L0611	JB2	0.73	0.73	±0.04	8.22	±0.41	11.34	±0.86	---	11.34±0.86
	C-L0612	JB3	4.10	0.74	±0.04	8.58	±0.43	11.63	±0.87	---	11.63±0.87
	C-L0615	JB4	3.95	0.74	±0.04	9.03	±0.45	12.27	±0.92	---	12.27±0.92
	C-L0613	JB5	3.80	0.71	±0.04	9.12	±0.46	12.87	±0.92	---	12.87±0.92
	C-L0614	JB6	3.48	0.87	±0.05	8.84	±0.44	10.11	±0.74	---	10.11±0.74
	C-L0616	JB7	2.79	0.79	±0.04	9.23	±0.46	11.69	±0.88	---	11.69±0.88
	C-L0617	JB8	2.38	0.81	±0.04	9.08	±0.46	11.16	±0.81	---	11.16±0.81
	C-L0618	JB9	2.15	0.81	±0.05	8.57	±0.43	10.53	±0.80	---	10.53±0.80
	C-L0619	JB10	2.00	0.80	±0.04	9.09	±0.46	11.31	±0.82	---	11.31±0.82
	C-L0620	JB11	1.61	0.83	±0.04	8.47	±0.43	10.18	±0.75	---	10.18±0.75
	C-L0621	JB12	1.20	0.83	±0.04	9.44	±0.47	11.36	±0.79	---	11.36±0.79
	C-L0622	JB13	0.60	0.79	±0.04	8.25	±0.41	10.48	±0.77	---	10.48±0.77
J-C 14°59'42" E. 51°45'08" N	C-L0623	JC1	0.60	0.81	±0.04	9.80	±0.49	12.11	±0.84	---	12.55±0.72 (n=4)
	C-L0624	JC2	4.30	0.77	±0.04	9.46	±0.48	12.32	±0.91	---	
	C-L0625	JC3	4.52	0.78	±0.04	10.69	±0.55	13.70	±1.02	De 1mm aliquots	
	C-L0626	JC4	4.75	0.90	±0.05	11.17	±0.56	12.40	±0.90	---	
	C-L0627	JC5	4.95	0.76	±0.04	10.82	±0.54	14.32	±1.07	---	14.32±1.07

Site location	Lab code	Sample	Depth (m)	Dose rate (Gy/ka)		Equivalent dose (Gy)		OSL age (ka)		Comment	Aeolian phases mean age of sand units (ka)
Schletau 11°21'14''E. 52°56'23'' N	C-L0628	STA00-1	1.21	1.12	±0.06	15.11	±0.76	14.02	±1.13	DR av. NAA & gamma	14.02±1.13
	C-L0629	STA00-2	1.13	1.02	±0.06	12.59	±0.65	12.34	±0.95	De 1mm aliquots	12.34±0.95
	C-L0630	STA00-3	0.99	1.01	±0.06	13.62	±0.69	13.54	±1.17	DR av. NAA & gamma	13.54±1.17
	C-L0631	STA00-4	0.91	0.98	±0.05	11.51	±0.58	11.93	±0.92	DR av. NAA & gamma	11.93±0.92
	C-L0632	STA00-5	0.79	0.96	±0.05	8.79	±0.44	9.24	±0.76	DR av. NAA & gamma. De 1mm aliquots	9.05±0.28 (n=2)
	C-L0633	STA00-6	0.69	0.82	±0.04	7.41	±0.37	8.85	±0.77	DR av. NAA & gamma	
	C-L0634	STA00-7	0.60	0.79	±0.04	5.45	±0.27	6.58	±0.56	DR av. NAA & gamma	6.58±0.56
	C-L0635	STA00-8	0.48	0.86	±0.05	3.99	±0.20	4.64	±0.39	DR av. NAA & gamma	4.57±0.08 (n=2)
	C-L0636	STA00-9	0.42	0.80	±0.04	3.63	±0.18	4.52	±0.34	---	
	C-L0637	STA00-10	0.33	0.81	±0.05	2.13	±0.11	2.62	±0.20	---	2.62±0.20
	C-L0638	STA00-11	0.20	0.91	±0.05	0.82	±0.04	0.90	±0.07	---	0.90±0.07
	C-L0684	STA1	1.59	1.17	±0.15	15.79	±0.83	13.55	±1.86	---	13.55±1.86
	C-L0685	STA2	0.90	1.01	±0.12	8.90	±0.47	8.84	±1.15	---	7.91±1.03 (n=2)
	C-L0686	STA3	0.90	1.04	±0.11	7.67	±0.40	7.39	±0.86	---	
	C-L0687	STA4	1.25	1.05	±0.06	16.32	±0.84	15.48	±1.17	---	15.48±1.17
	C-L0688	STA5	0.58	1.08	±0.13	11.57	±0.61	10.75	±1.46	---	10.75±1.46
Ueckermünde-A 14°16'41'' E. 53°35'01'' N	C-L0639	UM1	0.40	1.14	±0.06	13.95	±0.70	12.27	±0.89	---	12.27±0.61 (n=6)
	C-L0640	UM2	0.62	1.13	±0.06	14.19	±0.71	12.61	±0.92	---	
	C-L0641	UM3	0.82	1.07	±0.07	14.05	±0.71	13.08	±1.06	DR av. NAA & gamma	
	C-L0642	UM4	1.10	1.12	±0.07	14.18	±0.71	12.72	±1.05	DR av. NAA & gamma	
	C-L0643	UM5	1.22	1.27	±0.07	14.49	±0.73	11.41	±0.86	---	
	C-L0644	UM6	1.32	1.12	±0.07	13.29	±0.68	11.88	±1.00	DR av. NAA & gamma. De 1mm aliquots	
	C-L0645	UM7	1.48	1.20	±0.08	17.60	±0.88	14.61	±1.22	DR av. NAA & gamma	14.67±0.84 (n=2)
	C-L0646	UM8	1.58	1.19	±0.07	17.52	±0.88	14.72	±1.17	DR av. NAA & gamma	
	C-L0647	UM9	1.70	1.26	±0.08	21.30	±1.11	*16.85*	*±1.42*	DR av. NAA & gamma. *(maximum age (poor bleaching)*	---
	C-L0648	UM10	1.90	1.37	±0.09	23.25	±1.20	*17.02*	*±1.39*	DR av. NAA & gamma. De 1mm aliquots. *(maximum age (poor bleaching)*	
	C-L0649	UM11	2.05	1.19	±0.06	23.09	±1.19	*19.42*	*±1.41*	*(maximum age (poor bleaching)*	
UM-B 14°16'54'' E. 53°35'04'' N	C-L0650	UM12	0.40	1.11	±0.06	0.76	±0.04	0.68	±0.05	---	0.68±0.05
	C-L0651	UM13	0.70	1.31	±0.06	12.12	±0.61	9.24	±0.64	---	9.24±0.64
	C-L0652	UM14	1.20	1.35	±0.07	20.79	±1.05	15.44	±1.15	---	15.44±1.15

Site location	Lab code	Sample	Depth (m)	Dose rate (Gy/ka)		Equivalent dose (Gy)		OSL age (ka)		Comment	Aeolian phases / mean age of sand units (ka)
Ueckermünde-C 14°1640" E. 53°3407" N	C-L0653	UM15	0.27	1.64	±0.09	1.11	±0.06	0.68	±0.05	---	0.68±0.05
	C-L0654	UM16	0.44	1.70	±0.09	7.10	±0.36	4.16	±0.30	---	4.16±0.30
	C-L0655	UM17	0.70	1.67	±0.09	16.74	±0.84	*10.03*	*±0.73*	*not plausible (bioturbation?)*	---
	C-L0656	UM18	0.96	1.87	±0.10	26.59	±1.34	14.21	±1.06	---	14.66±0.68 (n=2)
	C-L0657	UM19	1.20	2.18	±0.12	33.13	±1.67	15.17	±1.12	---	
Ueckermünde-D 14°1643" E. 53°3652" N	C-L0658	UM20	0.38	1.06	±0.06	13.60	±0.68	12.81	±0.96	---	12.32±0.50 (n=3)
	C-L0659	UM21	0.50	1.19	±0.06	14.09	±0.71	11.83	±0.84	---	
	C-L0660	UM22	0.69	1.06	±0.07	13.27	±0.67	12.49	±1.04	DR av. NAA & gamma. De 1mm aliquots	
	C-L0661	UM23	0.88	1.27	±0.08	19.78	±1.00	*15.61*	*±1.29*	DR av. NAA & gamma. De 1mm aliquots. *(maximum age, poor bleaching)*	---
	C-L0662	UM24	1.08	1.21	±0.04	26.83	±1.39	*22.12*	*±1.41*	DR gamma. *(maximum age, poor bleaching)*	
	C-L0663	UM25	1.34	1.16	±0.07	23.72	±1.22	*20.52*	*±1.67*	DR av. NAA & gamma. *(maximum age, poor bleaching)*	
	C-L0664	UM26	1.59	1.17	±0.07	23.94	±1.22	*20.46*	*±1.63*	*(maximum age, poor bleaching)*	
	C-L0665	UM27	1.97	1.11	±0.06	22.18	±1.12	*19.90*	*±1.44*	De 1mm aliquots. *(maximum age, poor bleaching)*	
Altdarss-4 12°3205" E. 54°2456" N	C-L0666	AD4-1	0.18	1.02	±0.05	3.41	±0.17	3.35	±0.23	---	3.35±0.23
	C-L0667	AD4-2	0.38	1.43	±0.07	15.51	±0.78	10.86	±0.78	---	10.86±0.78
	C-L0668	AD4-3	0.50	1.36	±0.07	17.77	±0.89	13.09	±0.96	---	13.09±0.96
	C-L0669	AD4-4	0.72	1.52	±0.05	19.26	±0.98	12.71	±0.79	DR gamma. De 1mm aliquots	12.71±0.79
	C-L0670	AD4-5	0.95	1.36	±0.07	17.93	±0.90	13.20	±0.97	---	13.20±0.97
	C-L0671	AD4-6	1.16	1.34	±0.07	16.80	±0.84	12.57	±0.94	---	12.57±0.94
	C-L0672	AD4-7	1.40	1.48	±0.07	18.20	±0.91	12.31	±0.88	---	12.31±0.88
	C-L0673	AD4-8	1.57	1.32	±0.07	16.24	±0.81	12.31	±0.91	---	12.31±0.91
	C-L0674	AD4-9	1.81	1.24	±0.07	16.32	±0.82	13.11	±0.99	---	13.11±0.99
	C-L0675	AD4-10	2.00	1.21	±0.07	16.32	±0.82	13.45	±1.05	---	13.45±1.05
	C-L0676	AD4-11	2.18	1.20	±0.07	14.94	±0.75	12.50	±0.98	---	12.50±0.98
	C-L0677	AD4-12	2.38	1.49	±0.09	16.41	±0.82	11.01	±0.87	DR av. NAA & gamma	11.01±0.87
	C-L0678	AD4-13	2.55	1.69	±0.10	19.50	±0.98	*11.52*	*±0.83*	*minimum age, dose rate. water content and/or disequilibrium?*	---
	C-L0679	AD4-14	2.80	1.29	±0.10	17.16	±0.86	*13.28*	*±1.23*	DR av. NAA & gamma. *(minimum age, dose rate. water content and/or disequilibrium?)*	

Site location	Lab code	Sample	Depth (m)	Dose rate (Gy/ka)		Equivalent dose (Gy)	OSL age (ka)	Comment	Aeolian phases mean age of sand units (ka)
Altdarss-1 12°31'41" E. 54°24'07" N	C-L0680	AD1-1	0.79	1.46 ±0.09 / 1.26 ±0.05		15.83 ±0.79	11.69 ±1.67	min-max age range for DR NAA & gamma	11.20±0.70 (n=2)
	C-L0681	AD1-2	1.17	1.64 ±0.09		17.55 ±0.88	10.70 ±0.79	---	
	C-L0682	AD1-3	1.39	1.62 ±0.08		20.98 ±1.05	*12.93 ±0.87*	DR gamma. *(minimum age, (dose rate. water content and/or disequilibrium?)*	---
	C-L0683	AD1-4	1.64	1.59 ±0.10		20.32 ±1.02	*12.77 ±0.97*	*minimum age, dose rate. water content and/or disequilibrium?*	
Schorfheide A 13°38'53" E. 52°58'25" N	C-L0689	SHA-1	0.51	1.23 ±0.07		14.55 ±0.73	11.86 ±0.87	---	11.79±0.37 (n=5)
	C-L0690	SHA-2	0.83	1.16 ±0.06		13.77 ±0.69	11.84 ±0.88	---	
	C-L0691	SHA-3	1.17	1.27 ±0.07		15.61 ±0.78	12.34 ±0.93	---	
	C-L0692	SHA-4	1.49	1.46 ±0.08		16.90 ±0.85	11.55 ±0.85	---	
	C-L0693	SHA-5	1.60	1.58 ±0.10		17.92 ±0.90	11.37 ±0.93	DR av. NAA & gamma	
	C-L0694	SHA-6	1.87	1.37 ±0.07		18.23 ±0.91	13.34 ±0.99	---	13.34±0.99
Schorfheide B 13°40'06" E. 52°58'58" N	C-L0695	SHB-1	0.64	1.13 ±0.06		13.57 ±0.68	11.99 ±0.88	---	11.99±0.88
	C-L0696	SHB-2	0.91	1.11 ±0.07		11.69 ±0.59	*10.48 ±0.81*	*not plausible (bioturbation?)*	---
	C-L0697	SHB-3	1.40	1.21 ±0.06		17.03 ±0.85	14.14 ±1.03	---	14.14±1.03
	C-L0698	SHB-4	1.68	1.27 ±0.07		16.43 ±0.83	*12.97 ±0.94*	*not plausible (disequilibrium?)*	---
Glashütte 13°33'38" E. 52°02'02" N	C-L0699	G1	0.31	0.72 ±0.04		0.42 ±0.02	0.58 ±0.04	---	0.58±0.04
	C-L0700	G2	0.60	0.76 ±0.04		5.21 ±0.26	6.82 ±0.50	---	6.82±0.50
	C-L0701	G3	0.97	0.70 ±0.04		9.92 ±0.50	12.51 ±0.75	DR gamma	12.67±0.54 (n=9)
	C-L0702	G4	1.27	0.83 ±0.04		9.76 ±0.49	11.78 ±0.84	---	
	C-L0703	G5	1.57	0.81 ±0.05		10.36 ±0.52	12.77 ±0.96	---	
	C-L0704	G6	1.87	0.79 ±0.04		9.82 ±0.49	12.48 ±0.94	---	
	C-L0705	G7	2.22	0.72 ±0.05		10.01 ±0.50	13.83 ±1.11	---	
	C-L0706	G8	2.30	0.77 ±0.04		9.68 ±0.49	12.50 ±0.90	---	
	C-L0707	G9	2.55	0.77 ±0.04		9.72 ±0.49	12.69 ±0.92	---	
	C-L0708	G10	2.93	0.72 ±0.05		9.15 ±0.46	12.68 ±1.05	---	
	C-L0709	G11	3.35	0.76 ±0.04		9.84 ±0.49	12.92 ±1.00	---	
	C-L0710	G12	3.54	0.79 ±0.04		10.21 ±0.51	13.00 ±0.94	---	
	C-L0711	G12B	3.69	0.83 ±0.05		10.58 ±0.53	*12.76 ±0.95*	*not plausible (bioturbation?)*	---
	C-L0712	G13	3.89	0.75 ±0.05		11.27 ±0.57	14.96 ±1.20	---	14.23±0.64 (n=3)
	C-L0713	G14	4.28	0.78 ±0.04		11.01 ±0.55	14.18 ±1.07	---	
	C-L0714	G15	4.60	0.72 ±0.04		9.84 ±0.49	13.70 ±1.08	---	
	C-L0715	G16	1.40	0.70 ±0.05		7.05 ±0.36	10.01 ±0.83	---	10.01±0.83
	C-L0716	G17	0.80	0.72 ±0.05		0.04 ±0.00	*0.06 ±0.01*	*not plausible (recently reworked)*	---

Table E 2: Summary of radiocarbon ages and the calibration results.

(*calibration was carried out using the software calib 4.1, see STUIVER et al. 1998, the uncertainties of the calibrated ages are based on the 2σ errors)

Site	Stratigraphic position	C-14 Lab.-Nr.	C-14 age uncal. BP		C-14 age cal. BP max	min	material	reference	calibration resul*t age cal. BP max	min	age cal. BP	
F	below F9, below LST	Bln 4407	11400	±200			peat	Schlaak (1999)	13843	12988	13416	±428
F	below F9, above LST	Bln 4304	10130	±200	c. 8800 (BC)		peat	Schlaak (1993)	12796	11172	11984	±812
F	between F6 and F7	Hv 22367	6125	±150			charcoal	Schlaak (1999)	7413	6643	7028	±385
F	between F4 and F5	Bln 4317	4250	±80	3030	2660 (BC)	charcoal	Schlaak (1993)	5028	4534	4781	±247
F	between F3 and F4	Hv 22369	2835	±60			sandy peat	Schlaak (1999)	3159	2782	2971	±189
F	below F2	Hv 22372	595	±70			sandy peat	Schlaak (1999)	670	510	590	±80
F	below F2	Hv 22371	630	±50			sandy peat	Schlaak (1999)	669	536	603	±67
F	below F2	Hv 22370	720	±55			sandy peat	Schlaak (1999)	733	559	646	±87
F	between F13 and F14	Hv 22373	9030	±125			charcoal	Schlaak (1999)	10492	9776	10134	±358
R	above R1	Bln 4283	1180	±80	770	960 (AD)	charcoal	Schlaak (1993)	1285	931	1108	±177
R	between R2 and R3		10840	±355			charcoal	Schlaak (1998 a)	13769	11695	12732	±1037
C	between C6 and C7		10282	±26			treerings of fossil pine trunks	Spurk et al. (1999)	12728	11769	12249	±480
C	between C6 and C7		10148	±84			treerings of fossil pine trunks	Spurk et al. (1999)	12334	11264	11799	±535
C	~C6-C7		10520	±85			organic material (???)	Kayser (1999)	12924	11966	12445	±479
J	J6		3350	±40			charcoal	Schlaak (1999, pers. comm.)	3689	3470	3580	±110
STA	~STA00-5 - STA00-6	Hv 24135	8720	±185	7965	7535	burnt nut-shell	Breest & Veil (2001)	9915	9485	9700	±215
STA	~STA00-5 - STA00-6	Hv 24136	7700	±165	6620	6375	burnt nut-shell	Breest & Veil (2001)	8570	8325	8448	±123
STA	~STA00-5 - STA00-6	Hv 24137	7825	±170	7000	6455	burnt nut-shell	Breest & Veil (2001)	8950	8405	8678	±273
STA					7050	6720	weighted mean	Breest & Veil (2001)	9000	8670	8835	±165
JA	JA3		1520	±60			???	Kowalkowski (1999, pers. comm.)	1535	1296	1416	±120
JA	between JA6 & JA5		11130	±120			???	Kowalkowski (1999, pers. comm.)	13748	12676	13212	±536
JB	between JB1 & JB2	Gd-12090	10870	±210			wood	Kowalkowski et al. (1999)	13316	12343	12830	±487
JB	between JB1 & JB2	Gd-10803	10640	±250			peat	Kowalkowski et al. (1999)	13152	11698	12425	±727
JB	between JB1 & JB2	Gd-10807	10200	±280			peat	Kowalkowski et al. (1999)	12908	11110	12009	±899
JB	JB4	Gd-12085	10150	±80			charcoal	Kowalkowski et al. (1999)	12332	11303	11818	±515
JB	~JB7	Gd-11399	9870	±120			charcoal	Kowalkowski et al. (1999)	11902	10894	11398	±504
JB	JB9	Gd-12088	9650	±180			charcoal	Kowalkowski et al. (1999)	11548	10431	10990	±559
JB	below JB7	Gd-10801	9540	±270			charcoal	Kowalkowski et al. (1999)	11635	10190	10913	±723
JB	between JB10 & 11		9020	±110			charcoal	Kowalkowski et al. (1999)	10471	9785	10128	±343
JC	between JC4 & 5		10290	±200			???	Kowalkowski (1999, pers. comm.)	12886	11233	12060	±827
AD-1	between AD1-2 & -3	Hv-24639	10680	±60	12809	12700	wood	Kaiser et al. (2006), calib 5.0.1 (2005)			12755	±55
AD-1	between AD1-2 & -3	Poz-3207	10280	±200	12397	11701	seeds	Kaiser et al. (2006), calib 5.0.1 (2005)			12049	±348
AD-1	between AD1-2 & -3	Poz-2212	10030	±200	11957	11253	remains of moss	Kaiser et al. (2006), calib 5.0.1 (2005)			11605	±352
SHB	between SHB-2 and SHB-3	HV-21250	10390	±315			charcoal	Schlaak (1998 b)	13017	11181	12099	±918

Appendix F: Location of study sites and comparison of analytical results The location of each sampling site is shown on topographic maps. The results of age calculation, equivalent dose estimation, dose rate calculation, and radionuclide analyses using neutron activation analysis (NAA) and/or high-resolution gamma-ray spectrometry are presented. The error bars represent the 1-sigma errors. Note, that the uncertainty in beta source calibration is not included in the equivalent dose errors shown in the graphs. The standard deviation of each D_e value is shown as horizontal error bar, whereas the standard error is indicated by the caps. The OSL ages presented here are calculated excluding the systematic errors of beta source calibration as well as the uncertainty in water content estimation. Here, the average water content with a relative analytical error of 10 % was taken into account. By that any outliers in the data set can be identified and illustrated much better. If the systematic errors are taken into account at this stage, the systematic errors would mask the inconsistencies in the data set. The final ages used for the chronostratigraphic interpretation of the dune development include all systematic errors and are illustrated in the context of the site descriptions in chapter 4 and summarised in Appendix E, Table E 1.

List of the topographic maps (1:50 000) used for the following figures (cartography by U. Beha):

site 'Neuhaus': L 2730 Boizenburg

site 'Schletau': L 3134 Arendsee, L 2934 Lenzen

site 'Glashütte': L 3946 Baruth

site 'Cottbus': L 4352 Cottbus-Ost

site 'Jänschwalde': L 4152 Peitz

sites 'Jasien': M-33-6-D Lubsko, M-33-7-C Jasien

sites 'Rosenberg, Melchow, Finow, Spechthausen': L 3348 Werneuchen,
        L 3148 Eberswalde

sites 'Schorfheide': L 3146 Zehdenick, L 3148 Eberswalde

sites 'Ueckermünder Heide': L 2350 Ueckermünde, L 2550 Brüssow

sites 'Altdarss': L 1540 Prerow, L 1740 Ribnitz-Damgarten

Study area Elbe 'urstromtal'

Sampling sites: Location:

Neuhaus (N)   10°56'38" E, 53°16'35"N
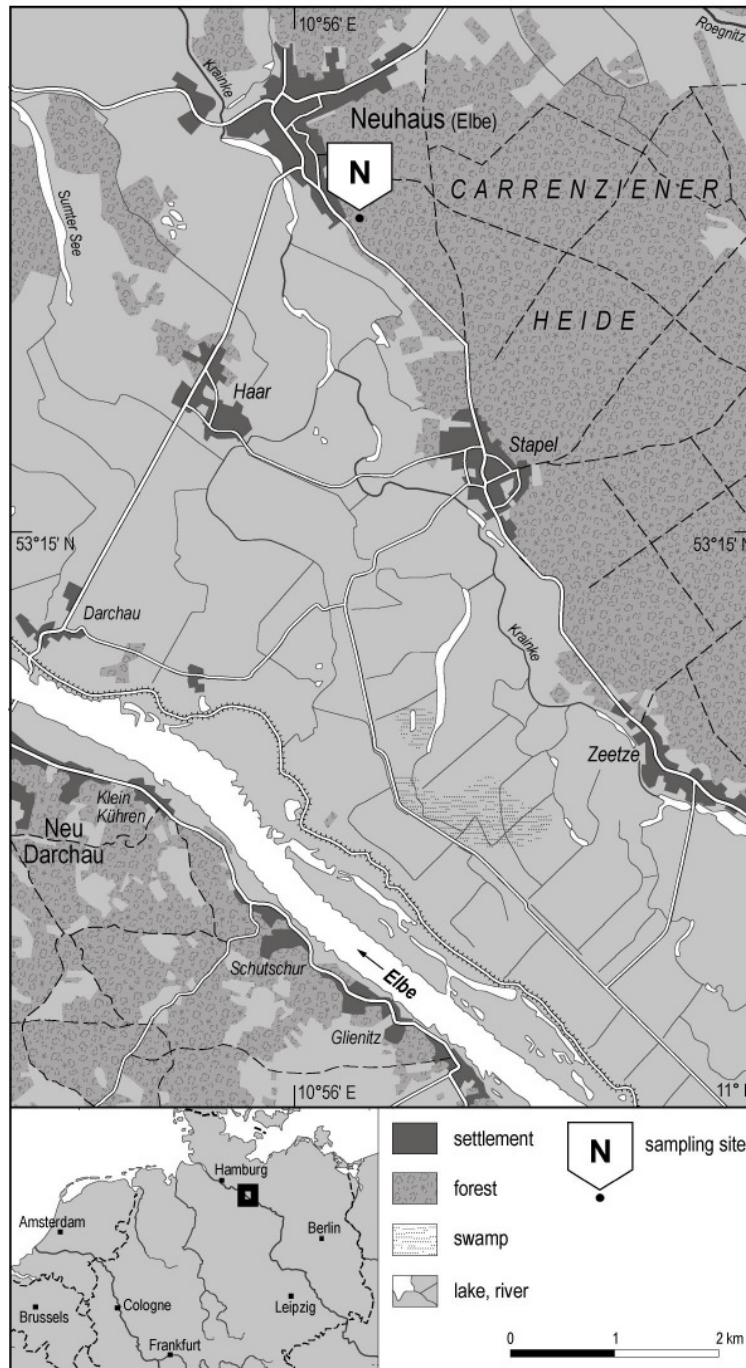
Site 'Neuhaus' (N)
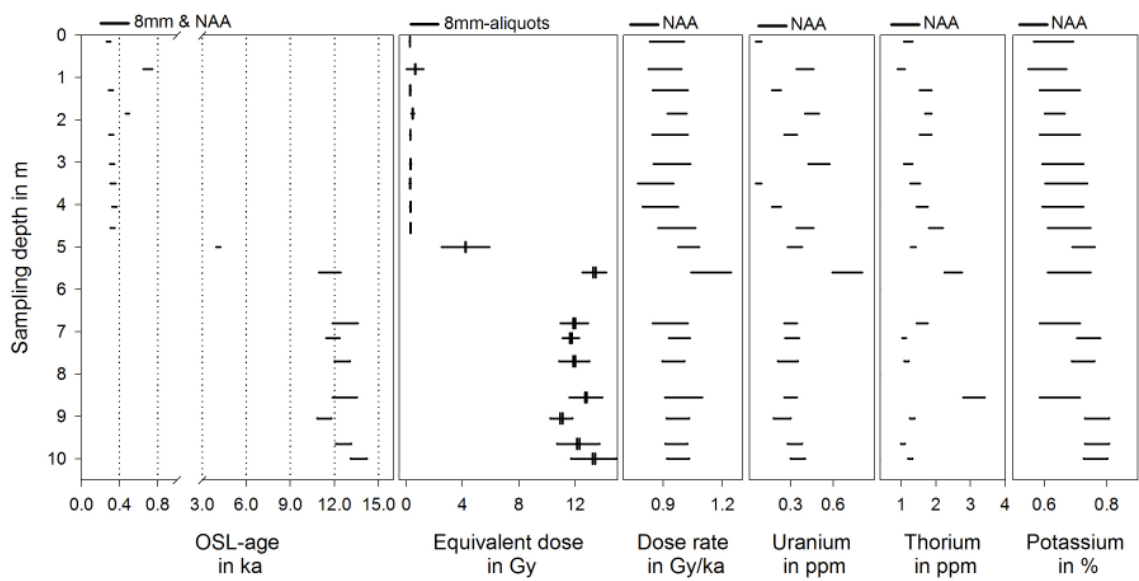
Study area Elbe 'urstromtal

Sampling sites: Location:

Schletau (STA)   11°21'14" E, 52°56'23" N

Site 'Schletau' (STA)
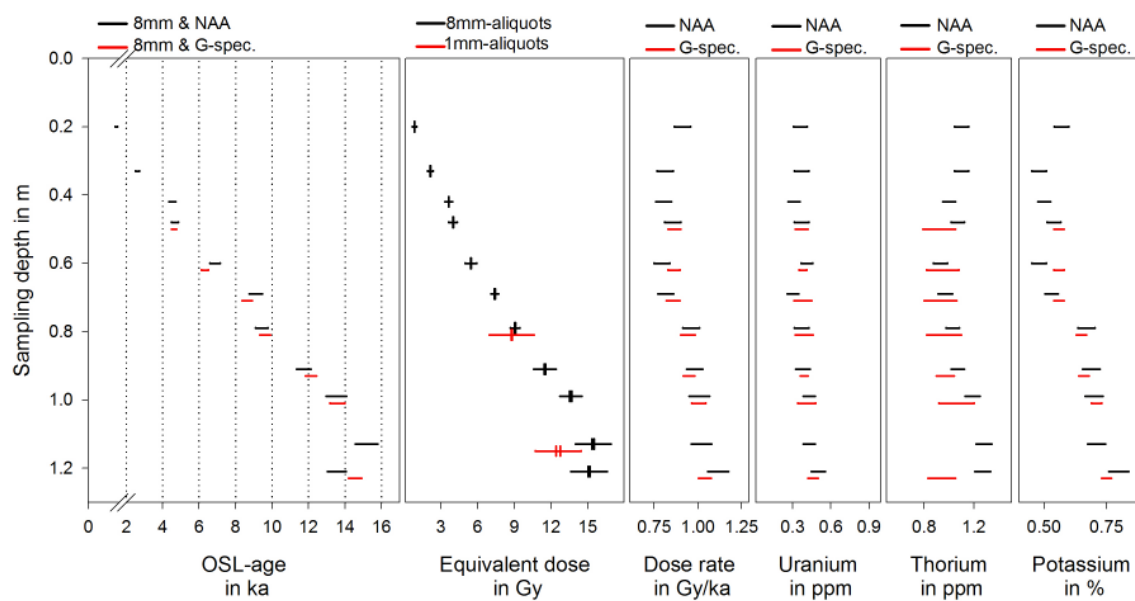
Study area Głogów-Baruth 'urstromtal'

Sampling sites: Location:

Glashütte (G)   13°33'38" E, 52°02'02" N
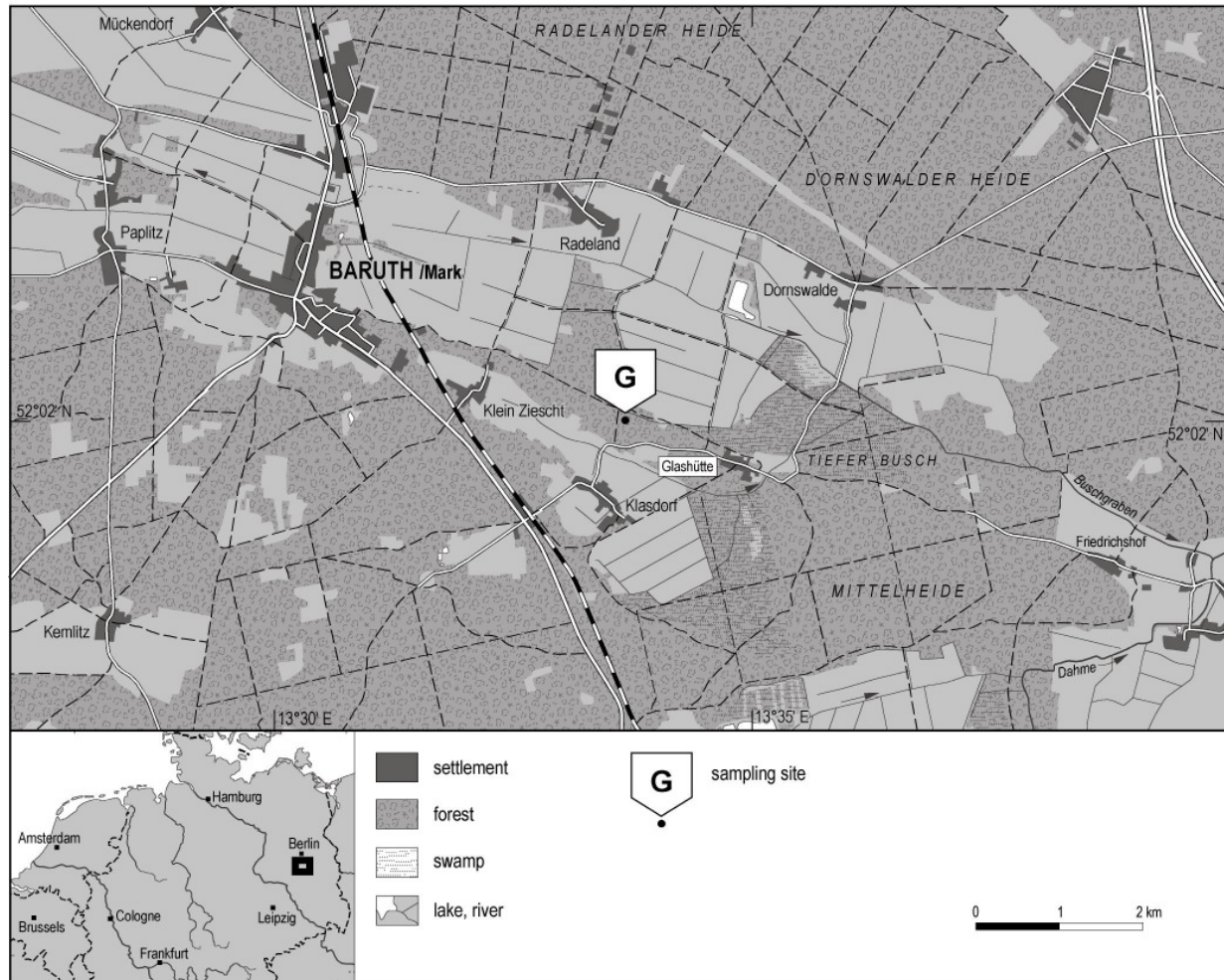
Site 'Glashütte' (G)
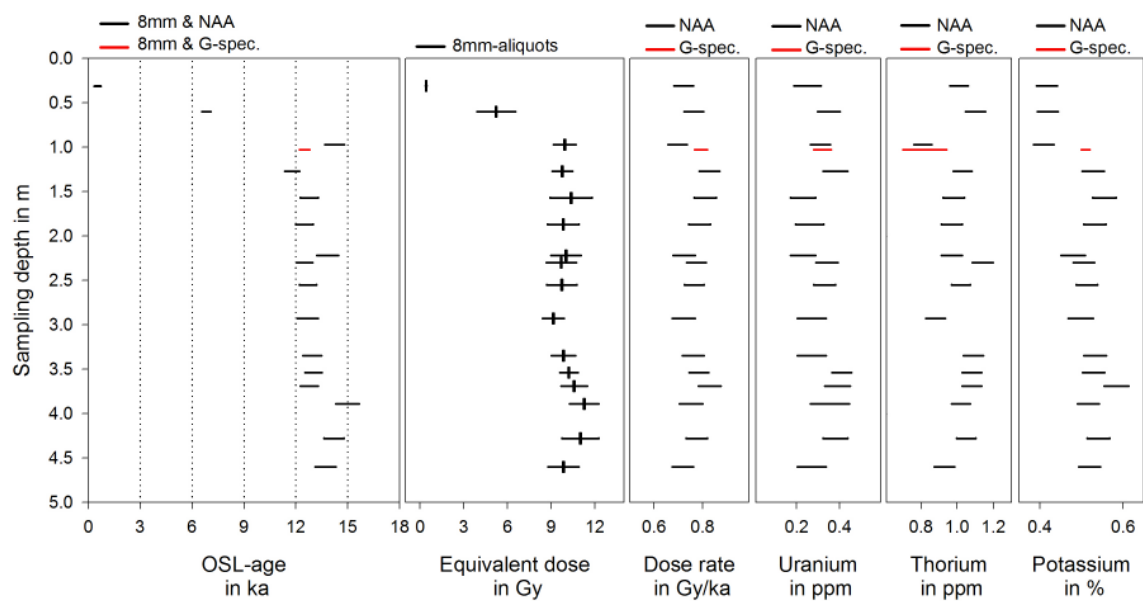
Study area Głogow-Baruth 'urstromtal'

Sampling sites: Location:

Cottbus (C)   14°24'48" E, 51°46'18" N

Jänschwalde (J)   14°33'51" E, 51°48'33" N
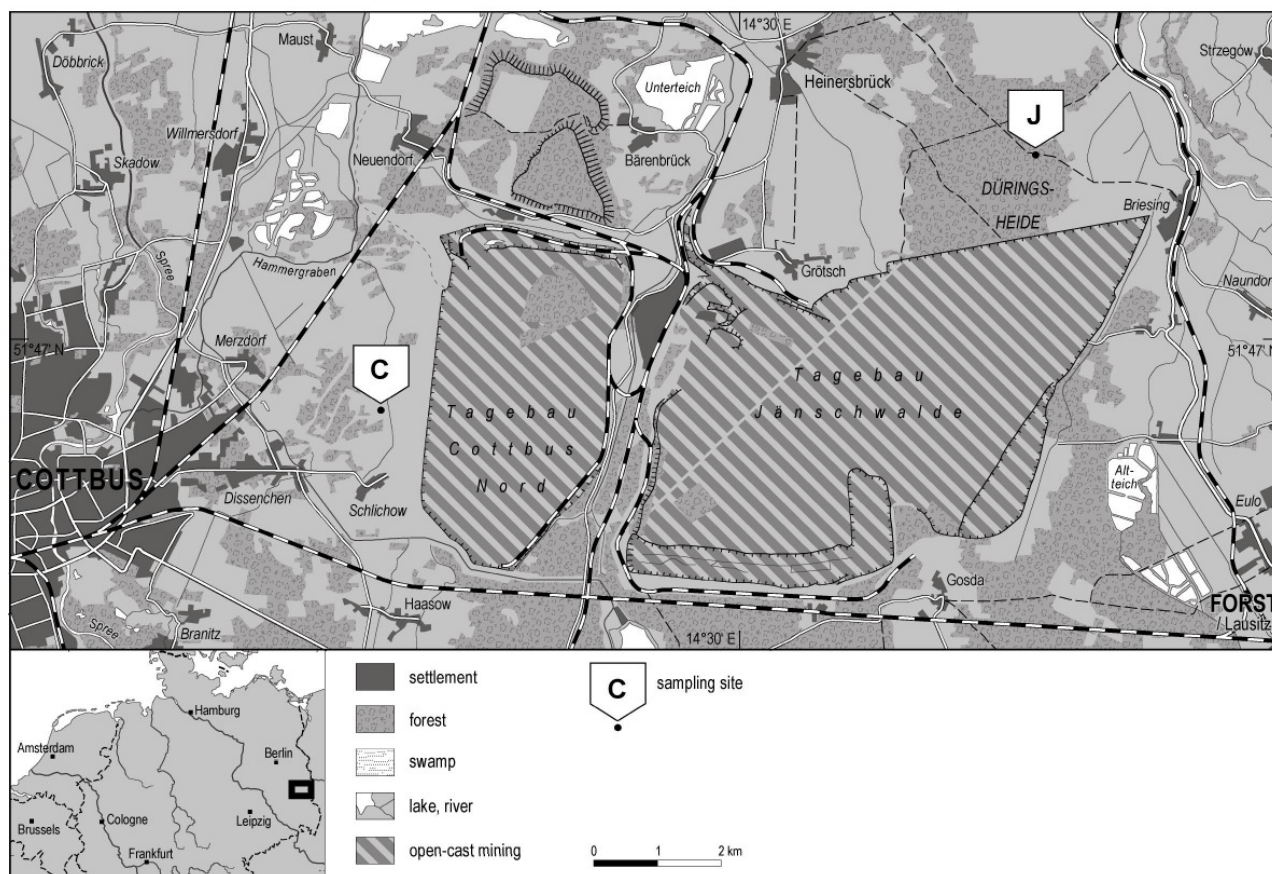
Site 'Cottbus' (C)
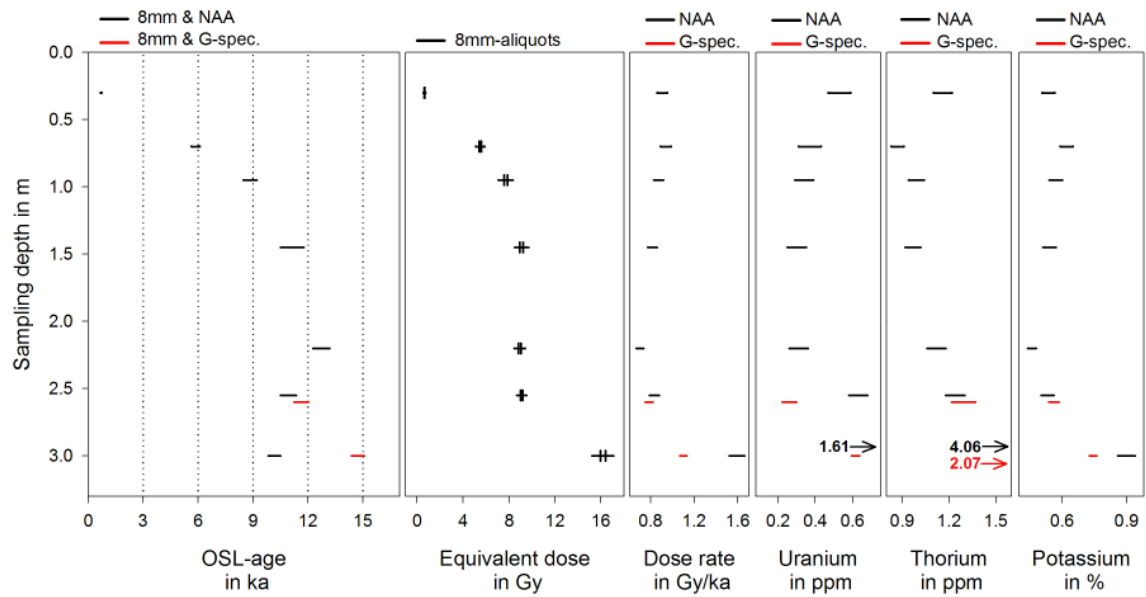
Site 'Jänschwalde' (J)
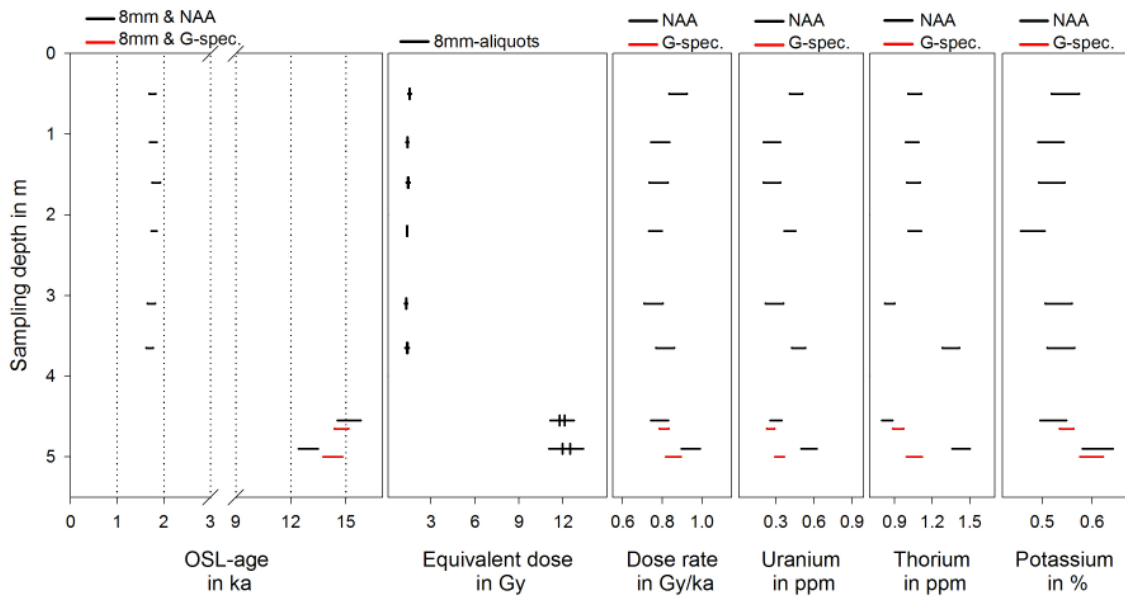
Study area Głogow-Baruth urstromtal

Sampling sites: Location:

Jasien-A (JA)   15°01'38" E, 51°45'18" N

Jasien-B (JB)   14°59'42" E, 51°45'08" N

Jasien-C (JC)   14°59'42" E, 51°45'08" N
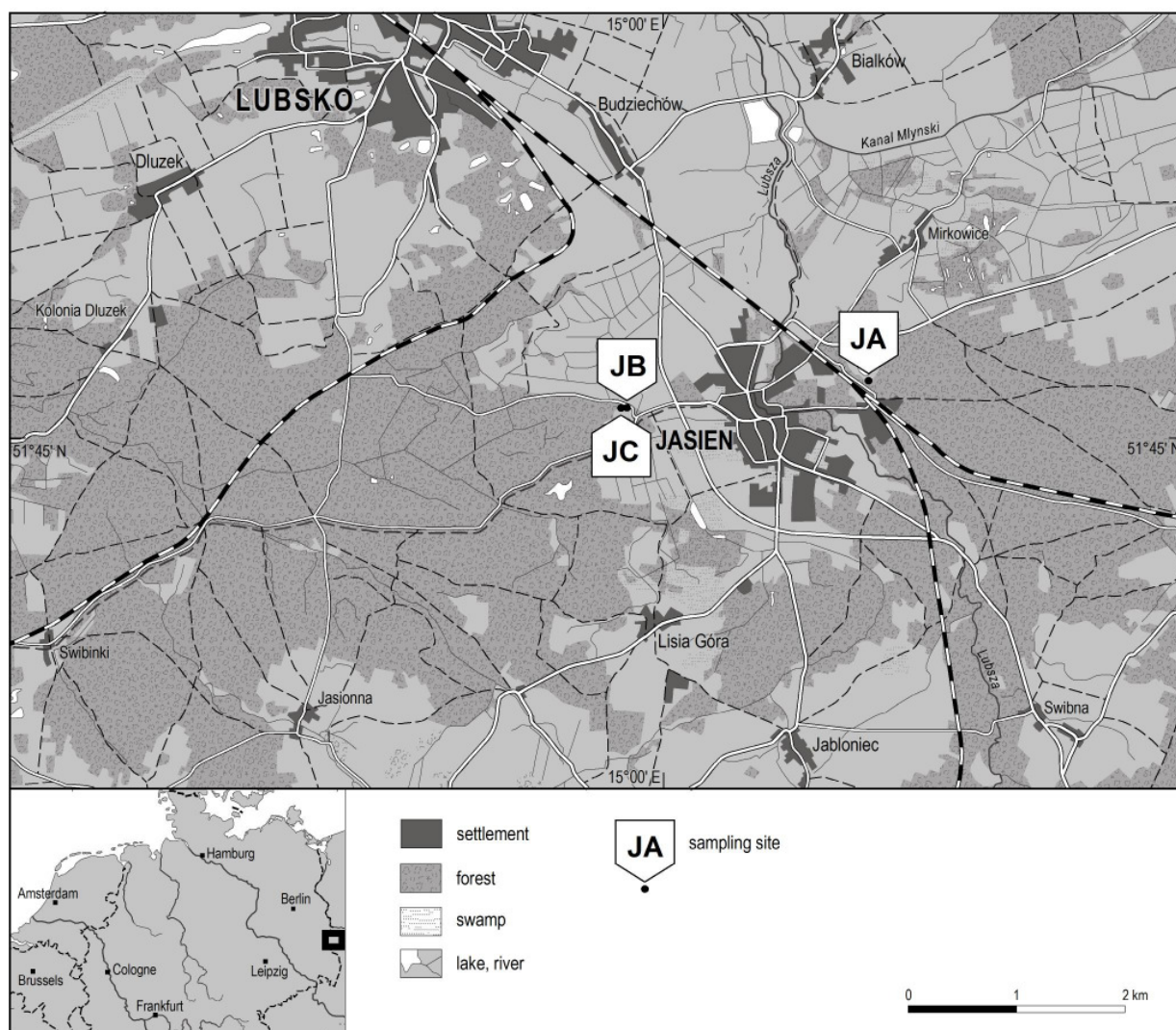
Site 'Jasien A' (JA)

Site 'Jasien-C' (JC)

Site 'Jasien B' (JB)

OSL-age
in ka

Equivalent dose
in Gy

Dose rate
in Gy/ka

Uranium
in ppm

Thorium
in ppm

Potassium
in %
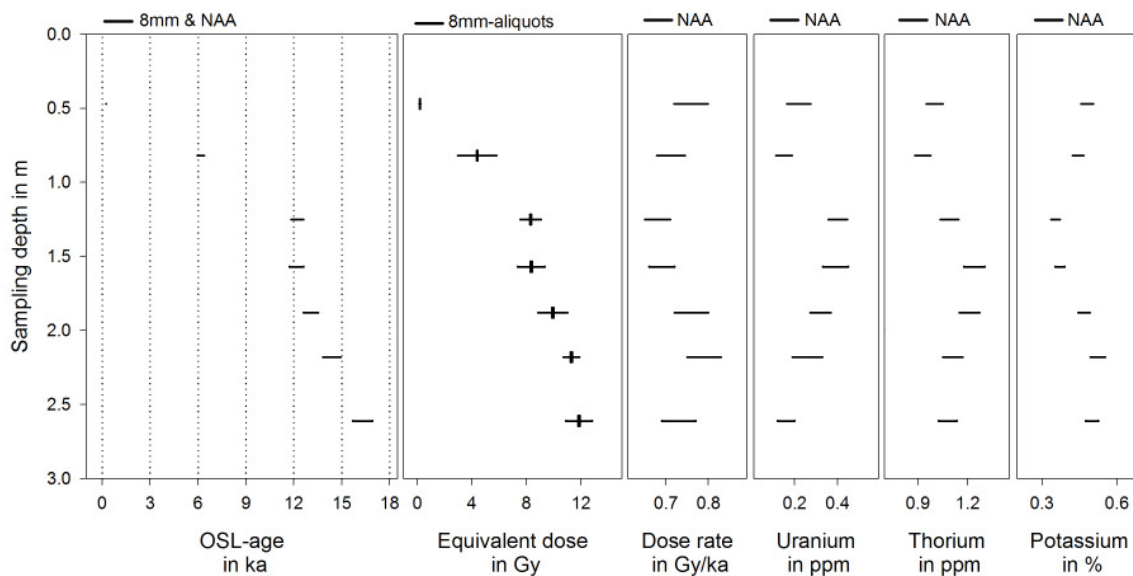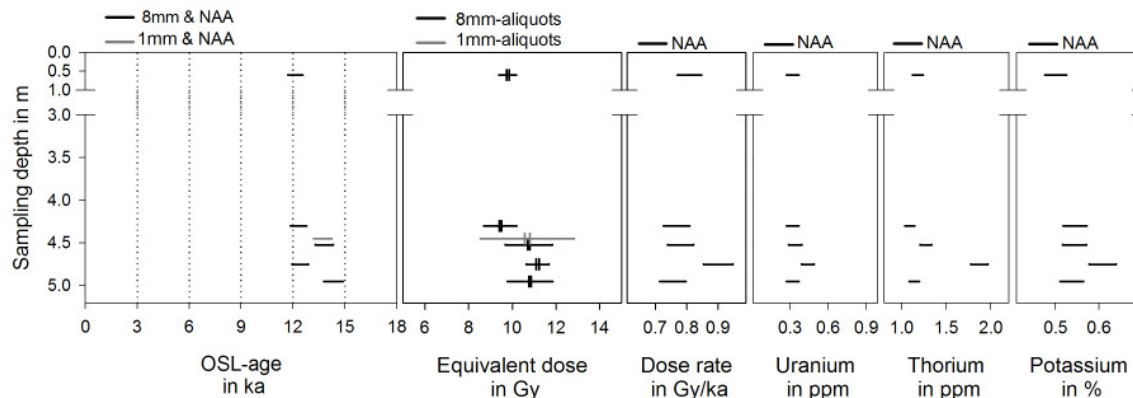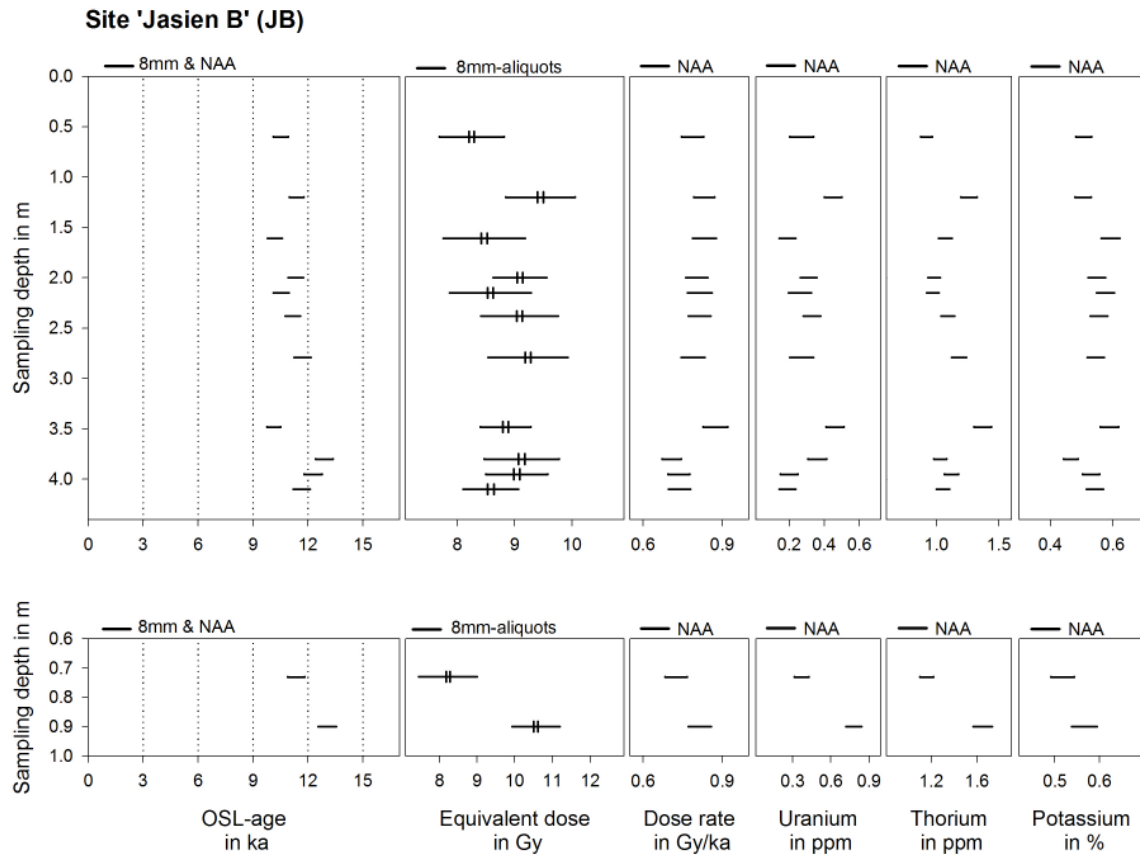
Study area Toruń-Eberswalde 'urstromtal'

Sampling sites: Location:

Rosenberg (R)   13°42'06" E, 52°47'08" N

Melchow (M)   13°42'24" E, 52°48'05" N

Finow (F)   13°41'43" E, 52°48'35" N

Spechthausen (S)   13°44'54" E, 52°48'54" N
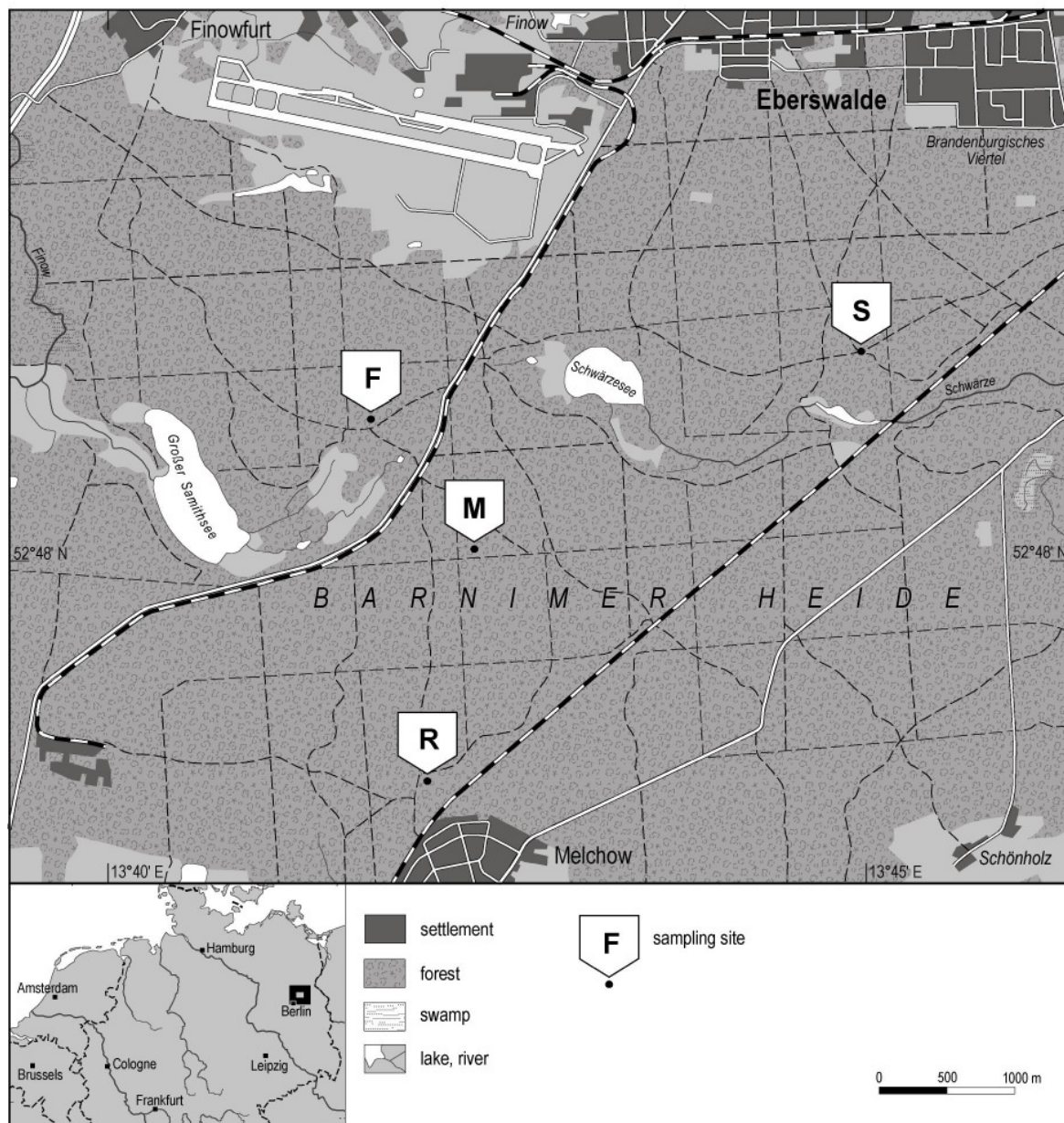
Site 'Rosenberg' (R)
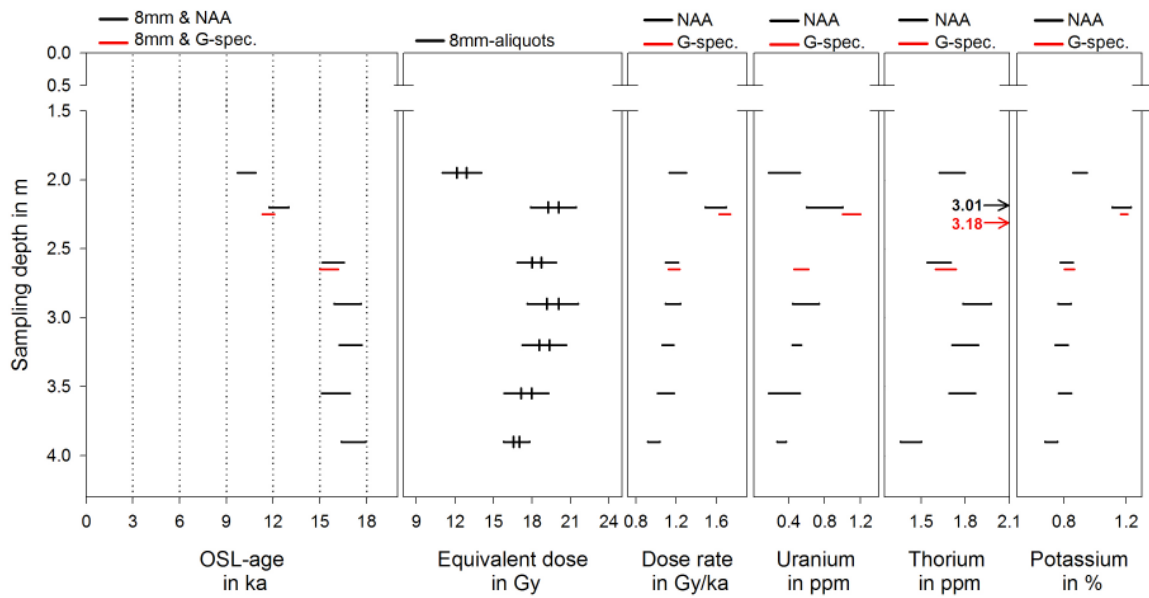
Site 'Melchow' (M)
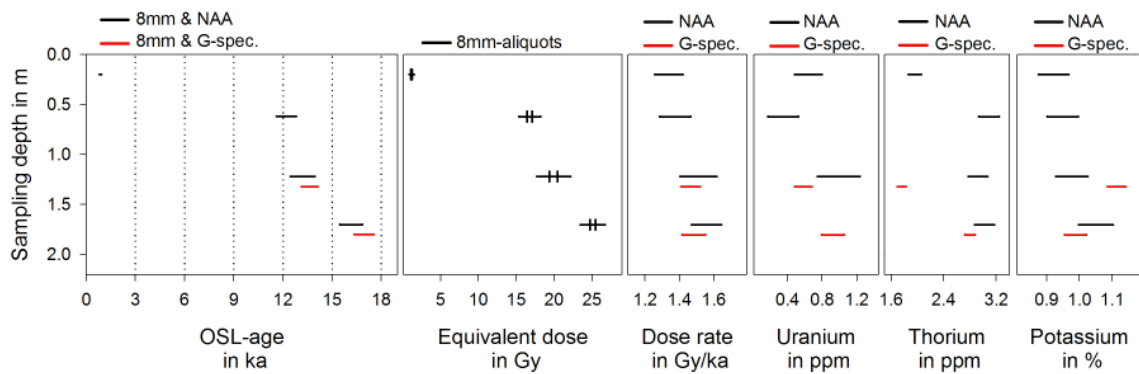
Site 'Spechthausen' (S)
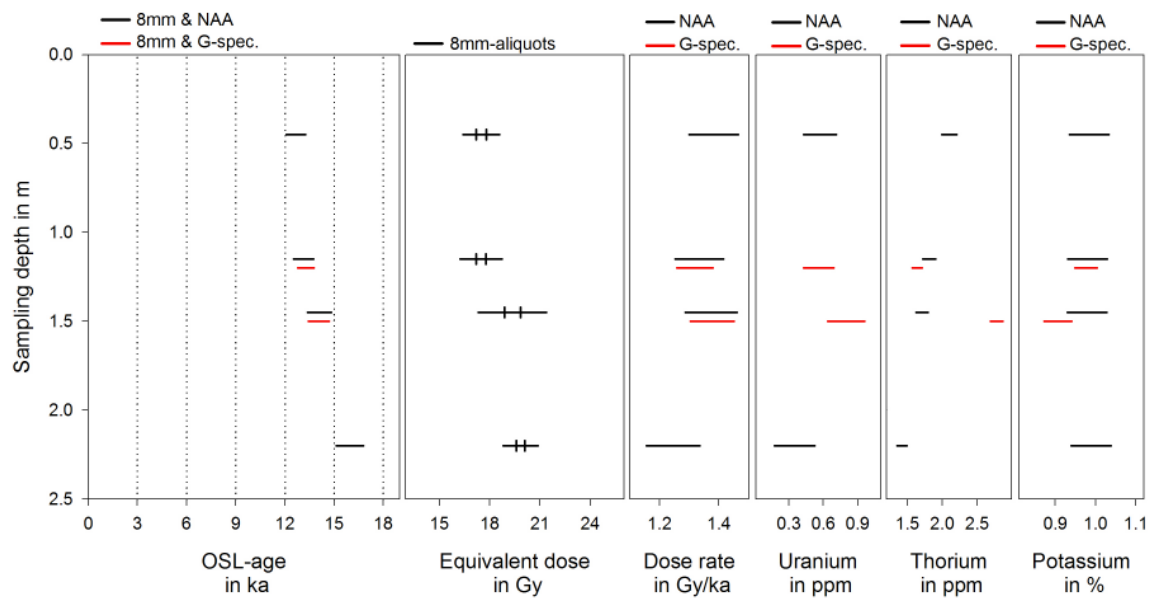
Site 'Finow A' (F)
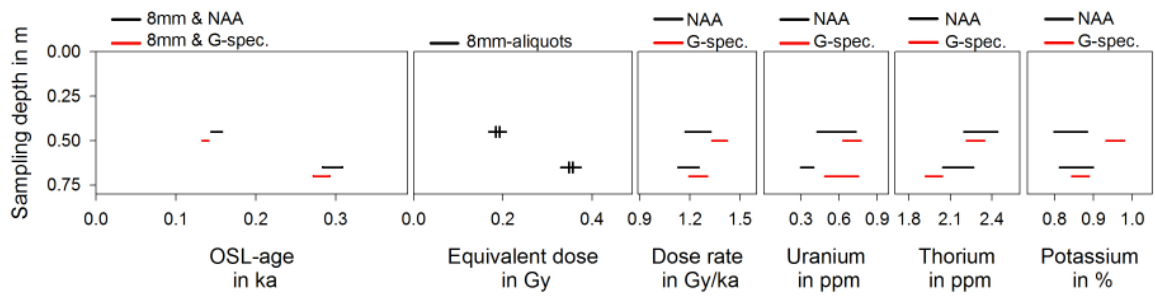
Site 'Finow B' (F)
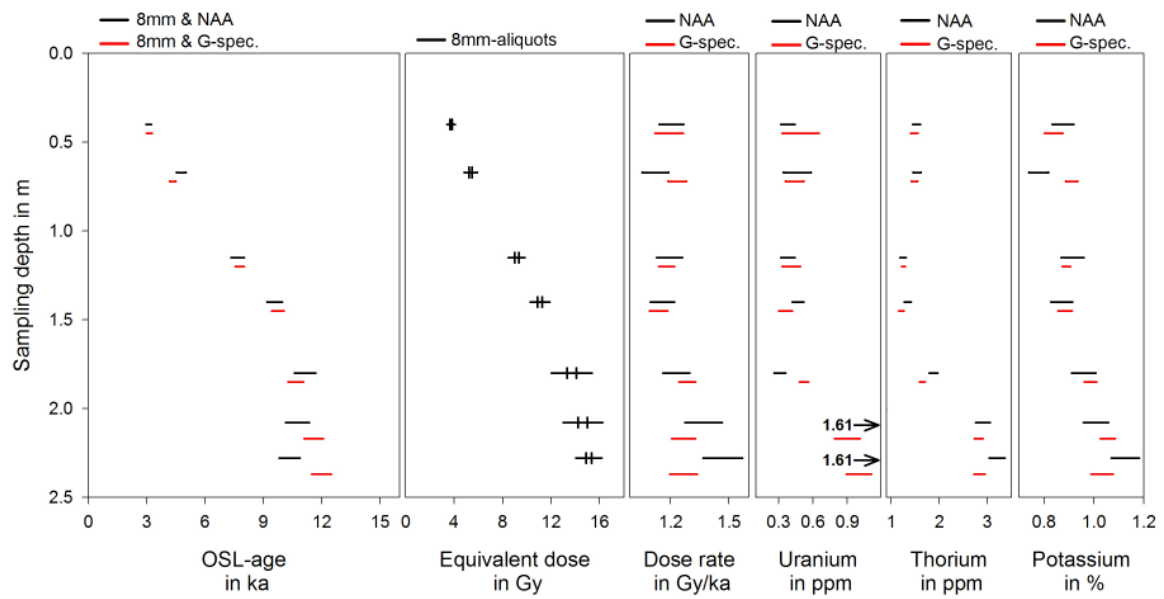
Site 'Finow C' (F)
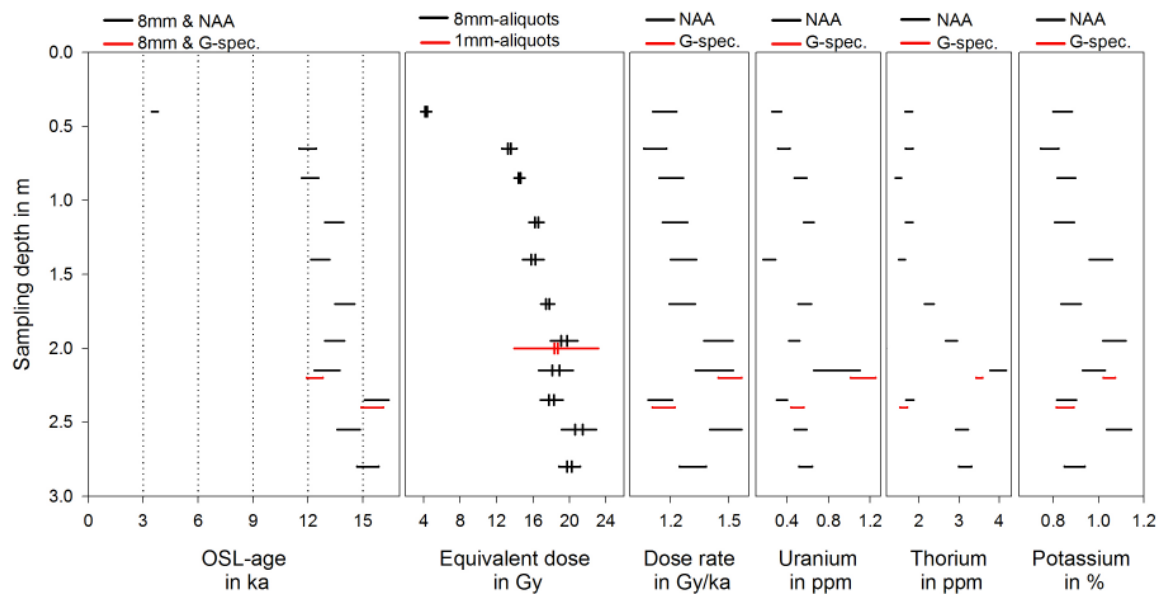
Study area Schorfheide sandur

Sampling sites: Location:

Schorfheide-A (SHA)   13°38'53" E, 52°58'25" N

Schorfheide-B (SHB)   13°40'06" E, 52°58'58" N
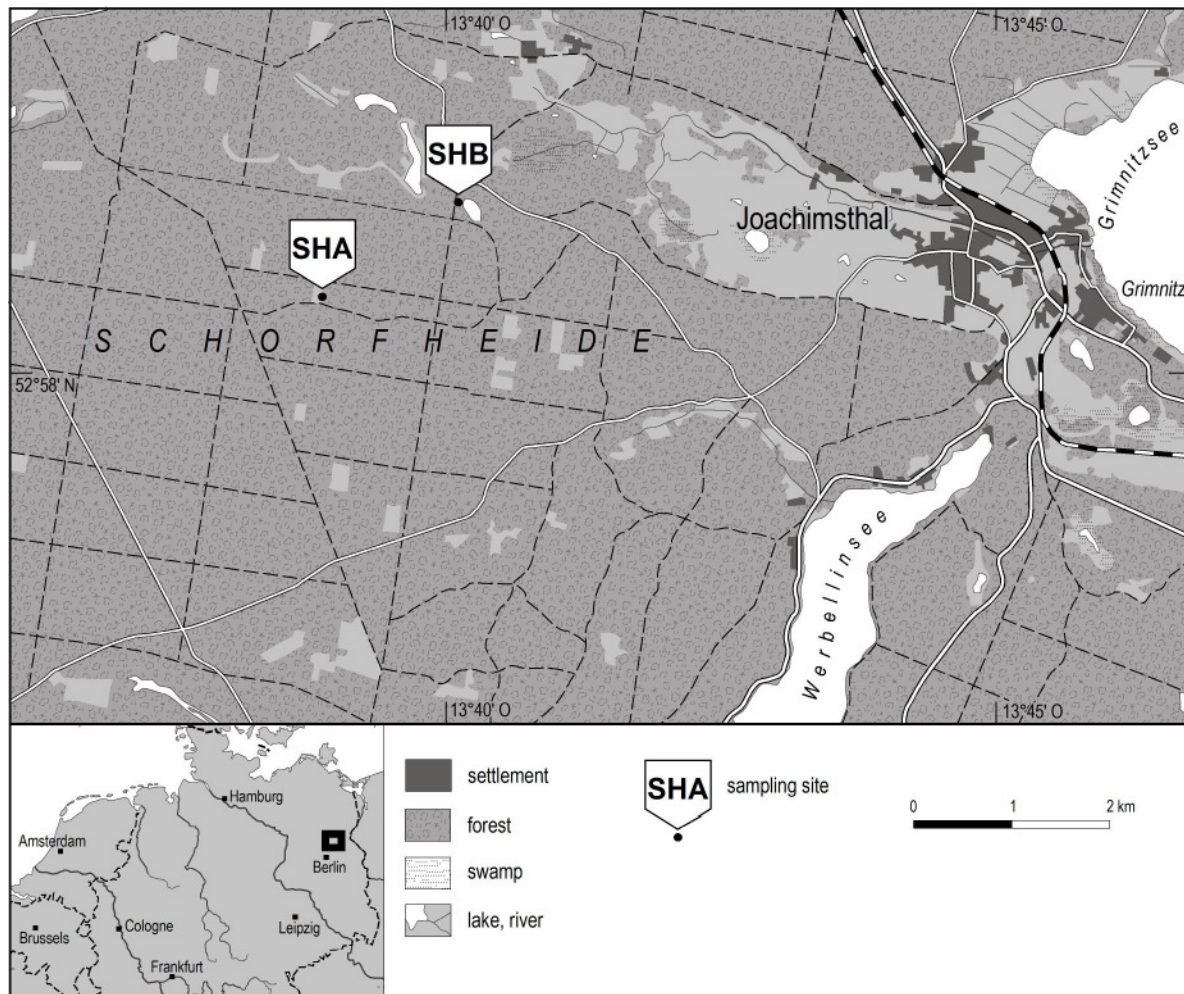
Site 'Schorfheide A' (SHA)
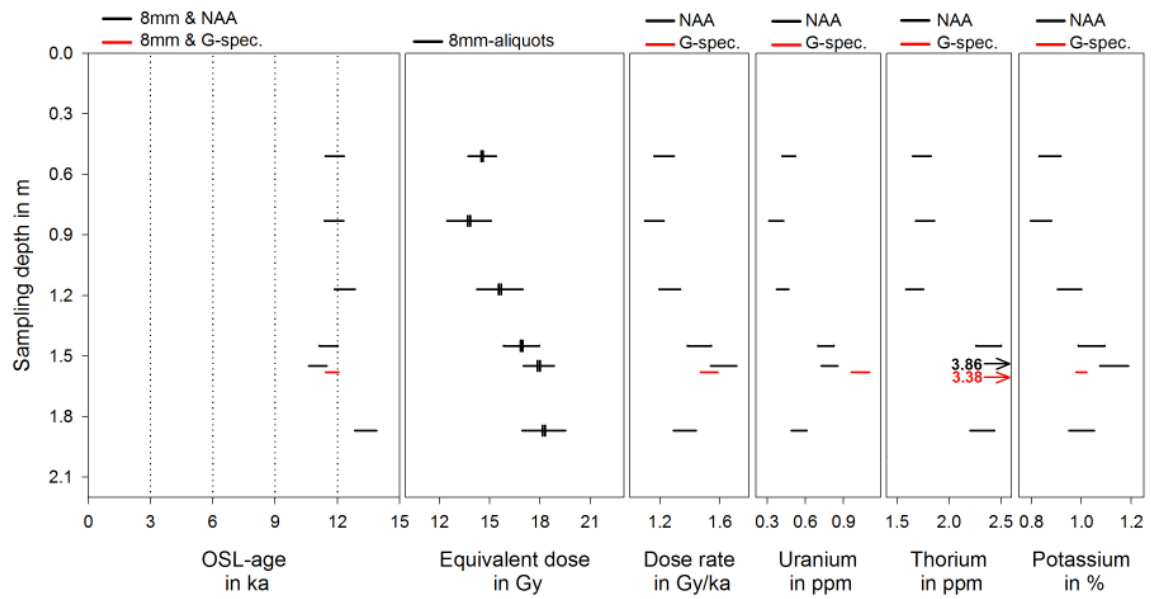
Site 'Schorfheide B' (SHB)
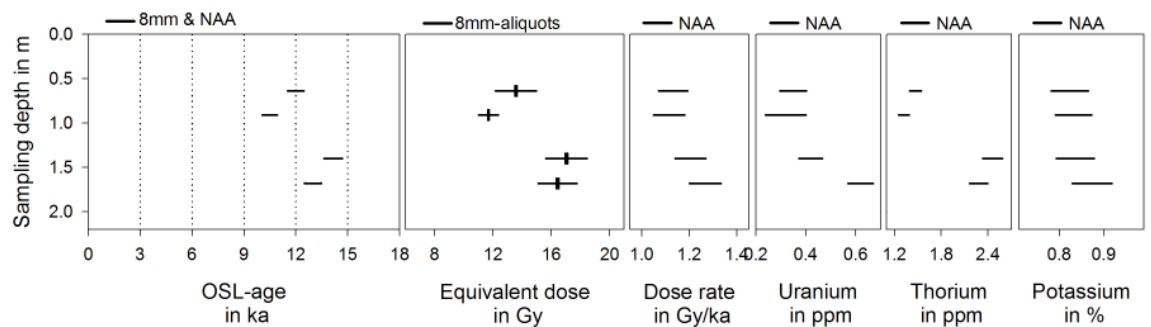
Study area Ueckermünder Heide

Sampling sites: Location:

Ueckermünde-A (UM-A)   14°16'41" E, 53°35'01" N

Ueckermünde-B (UM-B)   14°16'54" E, 53°35'04" N

Ueckermünde-C (UM-C)   14°16'40" E, 53°34'07" N

Ueckermünde-D (UM-D)   14°16'43" E, 53°36'52" N
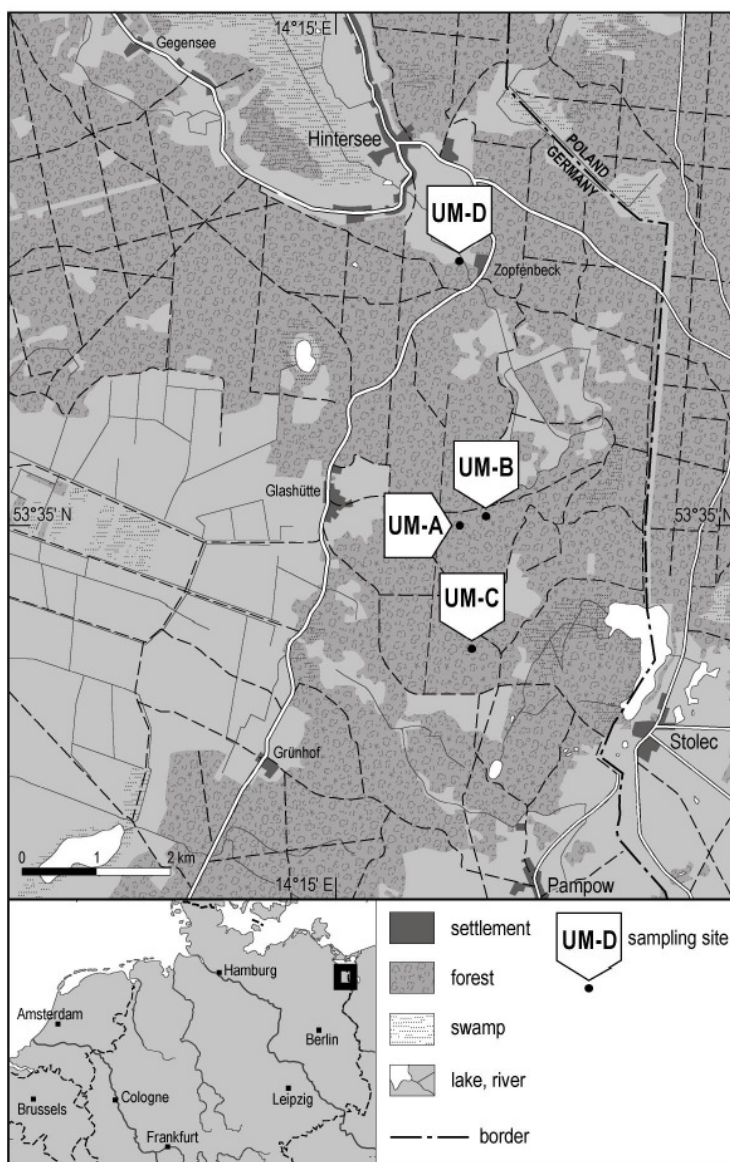
Site 'Ueckermünder Heide A' (UM-A)
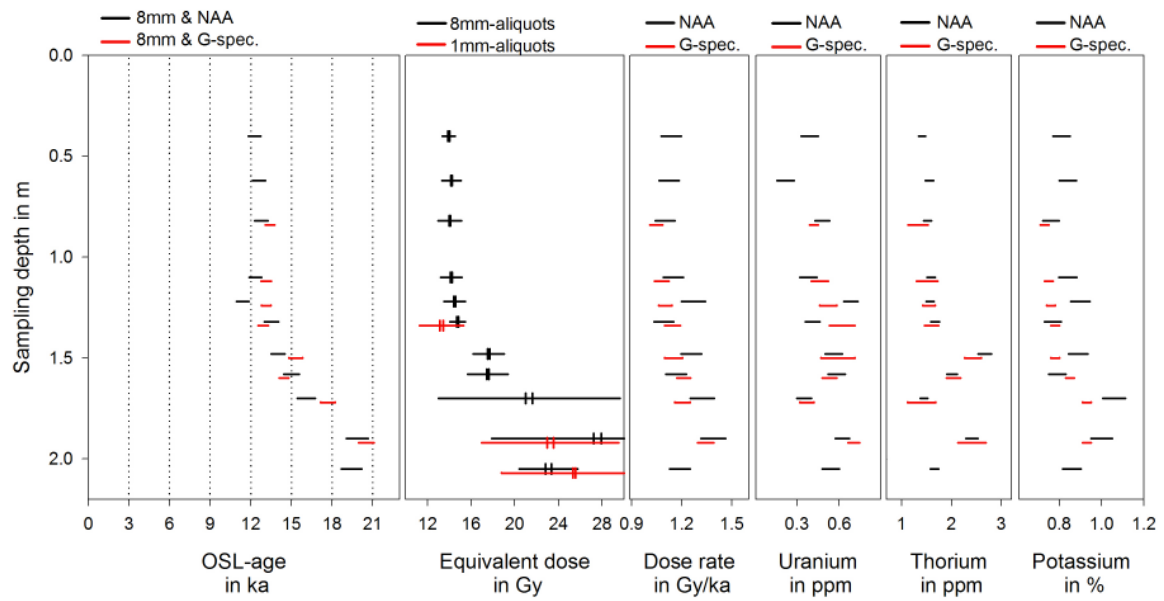
Site 'Ueckermünder Heide B' (UM-B)

Site 'Ueckermünder Heide C' (UM-C)
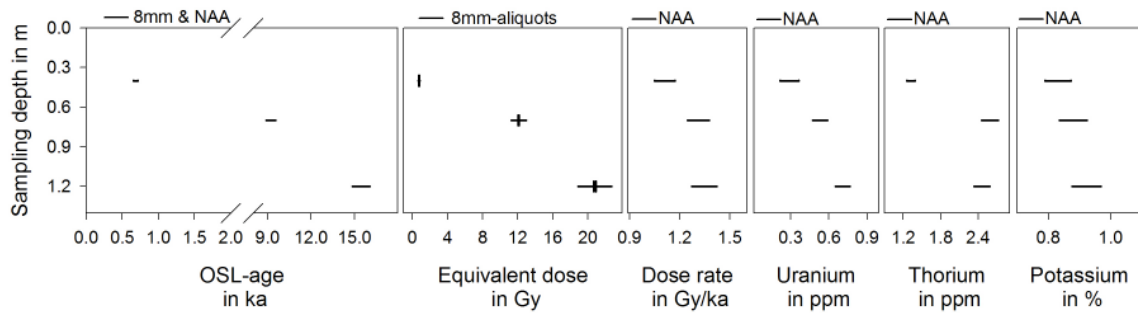
Site 'Ueckermünder Heide D' (UM-D)
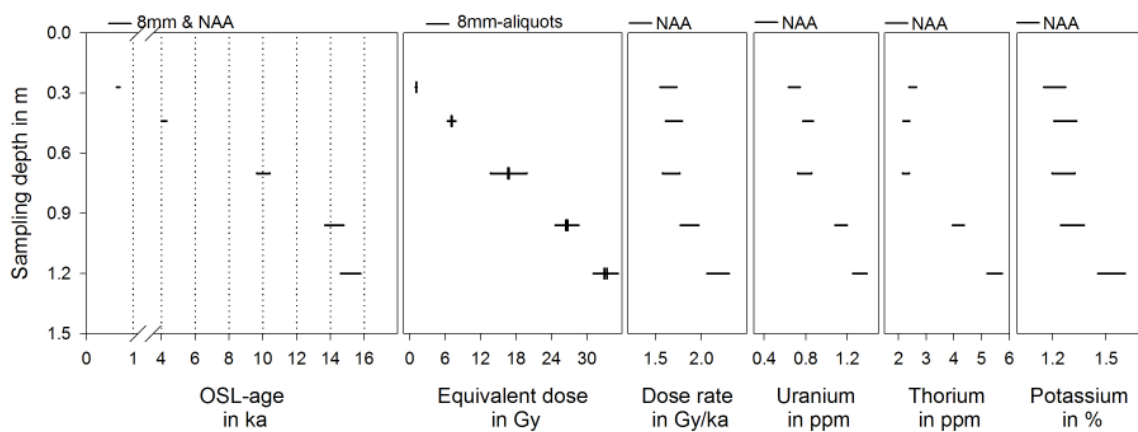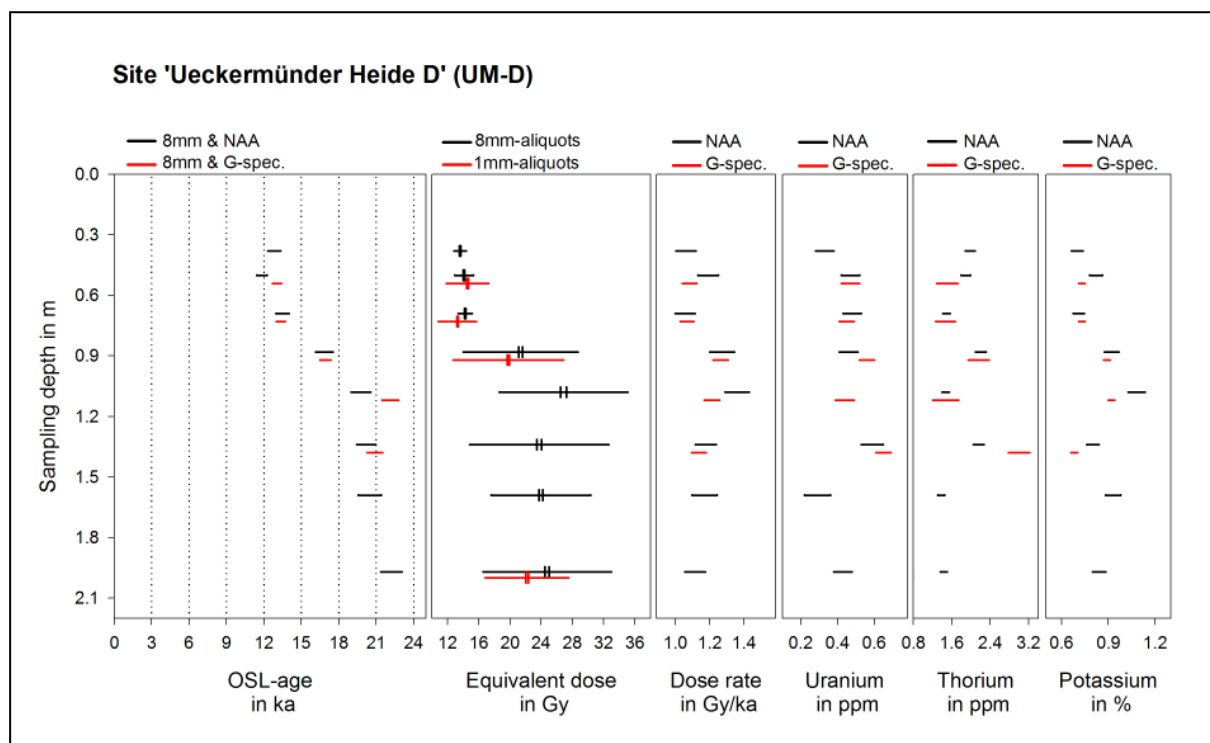
Study area Altdarss

Sampling sites: Location:

Altdarss-1 (AD1)   12°31'41" E, 54°24'07" N

Altdarss-4 (AD4)   12°32'05" E, 54°24'56" N
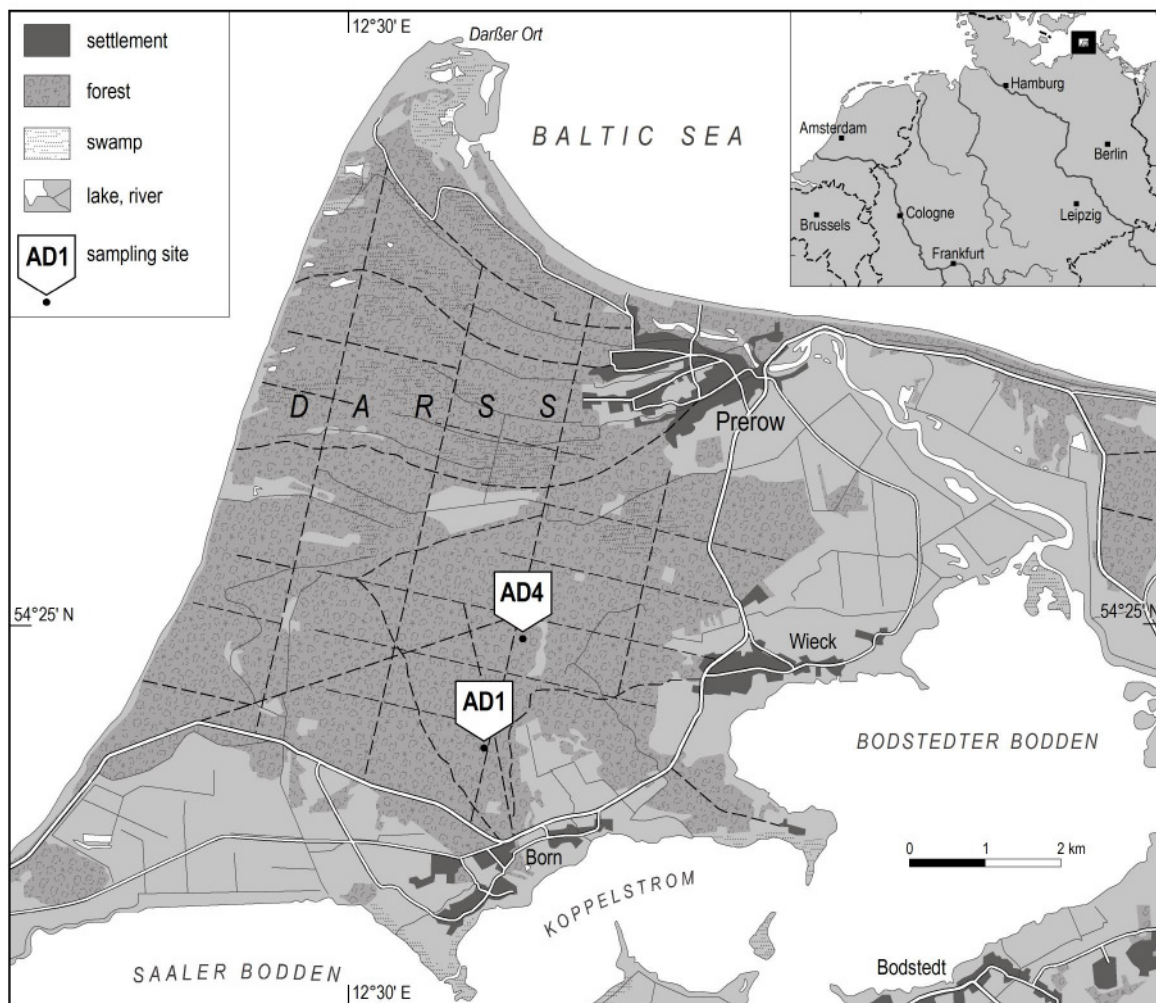
Site 'Altdarss-1' (AD-1)
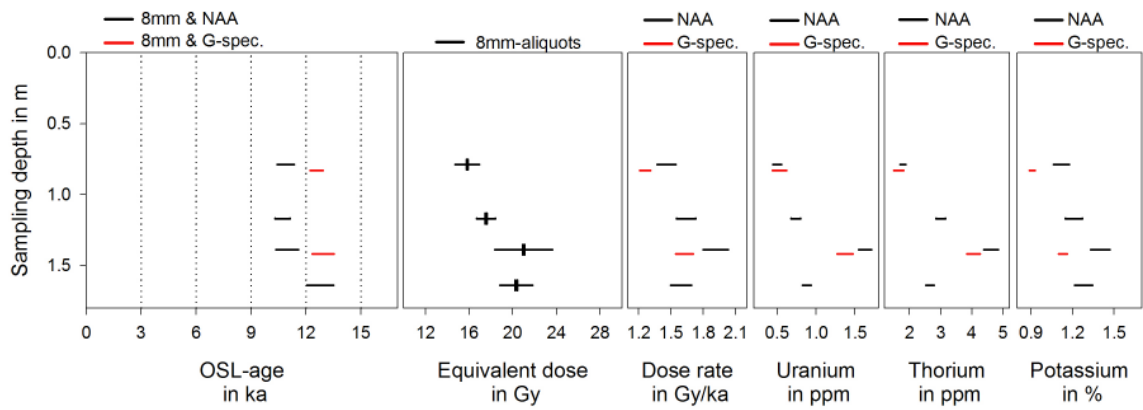
Site 'Altdarss-4' (AD-4)
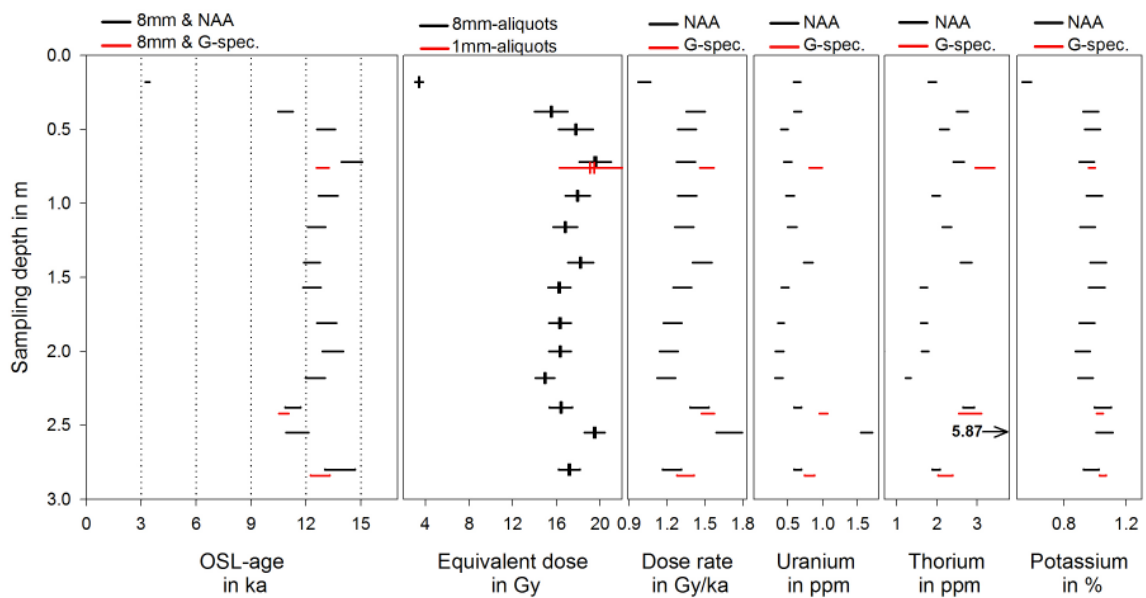
Danksagung/Acknowledgements

„Die Natur schafft ewig neue Gestalten;

was da ist, war noch nie,

was da war, kommt nicht wieder,

alles ist neu und doch immer das Alte."

<div align="right">

(J. W. von Goethe, Die Natur)

</div>

Als ich dieses Zitat vor einigen Jahren in einer Ausstellung auf dem Darss las, dachte ich, eine bessere Umschreibung meines Dissertationsthemas kann es eigentlich nicht geben. Mit Blick auf die teils intensiven jungen Dünenreaktivierungen erfasst dieses Zitat Goethes treffend eines der Ergebnisse der vorliegenden Arbeit. Der Sand bleibt als Medium in den Formungsprozessen der Landschaft, baut aber immer wieder neue Formen auf.

Mit der Thematik der spätglazialen und holozänen Dünenentwicklung im norddeutschen Tiefland haben sich in den vergangenen Jahrzehnten so viele Wissenschaftler auseinandergesetzt, dass es zuweilen schwierig ist, alle Arbeiten zu überblicken. Nicht selten wurde mir daher auch die Frage gestellt: *„Warum denn noch einmal die Dünengenese, dazu gibt es doch schon so viel?"*. Zurückblickend auf viele Jahre Arbeit und zahlreiche Ergebnisse kann ich die Antwort leicht formulieren: *„weil mit Anwendung neuer Verfahren neue Erkenntnisse gewonnen, Annahmen verifiziert und frühere Ergebnisse präzisiert werden können";* und nicht zuletzt auch *„weil es für mich als Geographin besonders interessant und spannend war, mich mit einem geomorphologischen Thema in seiner raum-zeitlichen Dimension zu beschäftigen"*.

Und so gilt an dieser Stelle mein ganz besonderer Dank meinem Doktorvater Universitätsprofessor Dr. Ulrich Radtke, für die Initiierung dieser Arbeit, seine stete Aufmunterung zum Weitermachen, seine Geduld und seinen Lesewillen, was die Betreuung dieser Arbeit angeht. Das Wissen, in allen Belangen stets auf seine Unterstützung zählen zu können, hat entscheidend zur Fertigstellung dieser Arbeit beigetragen. Für das mir in den vergangenen Jahren entgegen gebrachte Vertrauen und damit einhergehend die vielen Freiheiten und Gestaltungsmöglichkeiten was diese Arbeit anging, wie auch die Arbeiten im Lumineszenzlabor allgemein, möchte ich mich bedanken.

intensive Betreuung und Einführung in das ,Single Aliquot' Verfahren möchte ich Dr. Andrew Murray herzlich danken sowie für die gastfreundliche Aufnahme und gute Zusammenarbeit dem gesamten ,Risø-Team'.

Für die Einladung zu einem dreimonatigen Gastaufenthalt an der University of Adelaide und die freundliche Aufnahme dort möchte ich mich bei der „School of Earth and Environmental Sciences (Geology and Geophysics)" bedanken. Dank auch an die Leitung und die Mitbewohner des Kathleen Lumley College, Adelaide, die mir in dieser Zeit eine gute Lebens- und Arbeitsatmosphäre schufen.

Ganz besonders herzlich möchte ich Dr. Rowl Twidale und Dr. Jennie Bourne (beide Adelaide) danken. Sie haben nicht nur mit viel Engagement die Englischkorrektur weiter Teile der Dissertationsschrift übernommen, sondern mir durch viele inhaltliche Diskussionen, kritische Anmerkungen und zahlreiche Anregungen gerade in der schwierigen Endphase meiner Promotion weitergeholfen. Rowl, Jennie, I couldn't have wished for better critics and advisors! Thanks!

Abschließend möchte ich meiner Familie und meinen Freunden danken, für ihre Nachsicht, wenn wieder einmal zu wenig Zeit für sie übrig blieb, und für ihre unermüdliche Geduld, sich über die Jahre hinweg immer wieder mit dem Thema ,Doktorarbeit' konfrontiert zu sehen.

Danke Euch allen!
Was nun da ist, war noch nie, und was da war, kommt nicht wieder,
es ist endlich geschafft und ich bin immer noch die Alte!

Köln, Oktober 2007

Alexandra Hilgers

Erklärung gem. § 3, Abs. 10 der Promotionsordnung

Ich versichere, dass ich die von mir vorgelegte Dissertation selbstständig angefertigt, die benutzten Quellen und Hilfsmittel vollständig angegeben und die Stellen der Arbeit – einschließlich Tabellen, Karten und Abbildungen –, die anderen Werken im Wortlaut oder dem Sinn nach entnommen sind, in jedem Einzelfall als Entlehnung kenntlich gemacht habe; dass diese Dissertation noch keiner anderen Fakultät oder Universität zur Prüfung vorgelegen hat; dass sie – abgesehen von unten angegebenen Teilpublikationen – noch nicht veröffentlicht worden ist sowie, dass ich eine solche Veröffentlichung vor Abschluss des Promotionsverfahrens nicht vornehmen werde. Die Bestimmungen dieser Promotionsordnung sind mir bekannt. Die von mir vorgelegte Dissertation ist von Univ.-Prof. Dr. U. Radtke betreut worden.

Alexandra Hilgers

Teilpublikationen:

BOGEN, C., **HILGERS, A.**, KAISER, K., KÜHN, P. & LIDKE, G. (2003): Archäologie, Pedologie und Geochronologie spätpaläolithischer Fundplätze in der Ueckermünder Heide (Mecklenburg-Vorpommern). –Archäologisches Korrespondenzblatt, **33**: 1-20.

BREEST, K. & VEIL, S. (mit Beiträgen von Heinemann, B., **Hilgers, A.** & Willerding, U.) (2001): Die Ausgrabungen 2000 auf dem mesolithischen Dünenfundplatz Schletau, Ldkr. Lüchow Dannenberg. - Die Kunde, N.F., **52**: 239-254.

HILGERS, A., MURRAY, A. S., SCHLAAK, N. & RADTKE, U. (2001b): Comparison of Quartz OSL Protocols using Late Glacial and Holocene dune sands from Brandenburg, Germany. - Quaternary Science Reviews, **20**: 731-736.

KAISER, K., BARTHELMES, A., CZAKÓ PAP, S., **HILGERS, A.**, JANKE, W., KÜHN, P. & THEUERKAUF, M. (2006): A Lateglacial palaeosol cover in the Altdarss area, southern Baltic Sea coast (Northeast Germany): investigations on pedology, geochronology, and botany. - Netherlands Journal of Geosciences, **85**(3): 199-222.